

# Cooperative Intersection Collision Avoidance System Limited to Stop Sign and Traffic Signal Violations (CICAS-V)

## Subtask 3.2 Interim Report

### Naturalistic Infrastructure-Based Driving Data Collection and Intersection Collision Avoidance Algorithm Development

(Appendix A-2)

**April 30, 2008**



Crash Avoidance Metrics Partnership (CAMP) Produced  
In conjunction with Virginia Tech Transportation Institute for  
ITS Joint Program Office  
Research and Innovative Technology Administration  
U.S. Department of Transportation

CAMP Members:

Mercedes-Benz  
General Motors (GM)  
Toyota  
Honda  
Ford

## **Notice**

This document is disseminated under the sponsorship of the U.S. Department of Transportation in the interest of information exchange. The U.S. Government assumes no liability for the use of the information contained in this document. This report does not constitute a standard, specification, or regulation.

The U.S. Government does not endorse products or manufacturers. Trademarks or manufacturers' names appear in this report only because they are considered essential to the objective of the document.

### Form DOT F 1700.7 (8-72)

1. Report No.	2. Government Accession No.	3. Recipient's Catalog No.	
4. Title and Subtitle Cooperative Intersection Collision Avoidance System Limited to Stop Sign and Traffic Signal Violations (CICAS-V) – Phase I Final Report		5. Report Date April 30, 2008	
		6. Performing Organization Code:	
7. Author(s) Cooperative Intersection Collision Avoidance System Limited to Stop Sign and Traffic Signal Violations: Subtask 3.2 Interim Report		8. Performing Organization Report No.	
9. Performing Organization Name and Address Virginia Tech Transportation Institute 3500 Transportation Research Plaza (0536) Blacksburg, VA 24061 <i>In conjunction with:</i> Crash Avoidance Metrics Partnership on behalf of the Vehicle Safety Communications 2 Consortium 39255 Country Club Drive Suite B-40 Farmington Hills, MI 48331		10. Work Unit No.	
		11. Contract or Grant No.	
12. Sponsoring Agency Name and Address United States Department of Transportation, Federal Highway Administration 1200 New Jersey Ave, S.E. Washington, DC 20590		13. Type of Report and Period Covered	
		14. Sponsoring Agency Code	
15. Supplementary Notes			
16. Abstract <p>This report describes an experimental investigation performed at live intersections to gather naturalistic driver behavior. Data were collected and analyzed with the goal of understanding how drivers approach intersections at various speeds and environmental conditions. Analysis of these data focused on the development and evaluation of a threat assessment algorithm to predict impending violations of intersection control devices. Six stop-controlled intersection approaches and three signalized intersection approaches in the New River Valley region of Virginia were selected for data collection. The selection was based on the intersection characteristics, traffic volume, and crash statistics. Data were collected from each site for at least two consecutive months.</p> <p>The data analysis produced a working algorithm to predict human behavior at intersection approaches for the purpose of eventually providing a warning to a violating driver. From the raw data collected, driver approach behavior was dissected and analyzed for trends. Threat Assessment algorithms, based on kinematic equations and regression techniques, were designed to predict whether or not a driver would stop. These algorithms were then evaluated in a pseudo-real-time simulation using the raw data.</p> <p>The performance of each algorithm was based on its ability to predict a pending violation while minimizing false detections. In addition, other measures were considered: the location at which a violation warning was provided, the likelihood of annoyance, algorithm complexity, and data requirements. The best performing algorithms will be recommended for future system-level research. They will be tested for performance validation when integrated into the prototype hardware and warning interfaces.</p>			
17. Key Words Cooperative intersection collision avoidance, crash avoidance, intelligent transportation systems		18. Distribution Statement No restrictions. This document is available to the public through the National Technical Information Service, Springfield, VA 22161.	
19. Security Classif. (of this report) Unclassified	20. Security Classif. (of this page) Unclassified	21. No. of Pages 293	22. Price



## **Photos Credits**

**Photos and Illustration's courtesy of CAMP**

## Executive Summary

The Cooperative Intersection Collision Avoidance Systems for Violation (CICAS-V) project aims to develop and test a system to reduce the number of crashes at intersections due to violations of stop light and stop sign traffic control devices. These crashes account for thousands of injuries and fatalities in the United States every year (National Highway Traffic Safety Administration, 2006). To reduce these crashes, the CICAS-V presents a timely and salient in-vehicle warning to those drivers who are predicted to violate a stop light or a stop sign. The warning is designed to elicit behavior from the driver which will avoid a potential violation that could lead to an intersection crash.

CICAS-V monitors traffic approaching intersections through a network of in-vehicle and infrastructure sensors linked by 5.9 GHz DSRC wireless communication equipment. Using the sensor data as inputs, a threat-assessment algorithm performs computations to predict whether the driver will comply with the intersection stop sign or stop light. If the algorithm predicts a violation, the system delivers a warning by means of the driver-vehicle interface, with the aim of compelling the driver to stop.

To be effective, CICAS-V must present the warning to drivers who will benefit from it without inadvertently annoying the compliant drivers. Thus, the algorithm must correctly predict the driver's stopping decision at a distance that provides sufficient time for that driver to stop before entering conflicting traffic paths. Subtask 3.2 was created with the aim of developing and evaluating threat assessment algorithms for the CICAS-V prototype to meet this requirement.

The following report describes the work performed as part of Subtask 3.2. Under this Subtask, data collection efforts were undertaken at eight intersections in the New River Valley area of southwest Virginia. The intersections selected represented those that are expected to benefit from a CICAS-V system. Data collection equipment installed at these intersections recorded a variety of vehicle data. Detailed information was obtained for every vehicle approaching the instrumented stop-controlled and signalized approaches.

Analysis of the data focused on the development of a working algorithm that would predict driver stopping behavior at intersection approaches so that a warning would be provided to a violating driver. From the raw data collected, driver approach behavior was dissected and analyzed for trends. Threat assessment algorithms, designed to predict whether or not a driver will stop, were developed and then evaluated in a pseudo-real-time simulation using that raw data.

The performance of each potential algorithm was based on the effectiveness of a potential algorithm to predict a pending violation while minimizing false detections. In addition, other measures, such as the location at which a violation warning was provided, likelihood of annoyance, algorithm complexity, and data requirements, were also considered. Two algorithms for stop-controlled intersections and two algorithms for signalized intersections were recommended for the system-level tests of Subtask 3.4.

To obtain data for developing and testing the algorithms, data collection efforts focused on six approaches at five stop-controlled intersections and all approaches at three four-way signalized intersections. These sites were selected based upon intersection characteristics (e.g., representative posted speed limits), crash statistics, traffic volume, and recommendations by the Virginia Department of Transportation (VDOT). Selections were made to represent types of intersections that are expected to benefit from a CICAS-V system.

Custom, non-obtrusive data acquisition systems (DASs) were installed at the selected intersection approaches. The DASs consisted of three major subsystems: 1) sensing network, 2) processing stack, and 3) associated hardware enclosures and mounts. The sensing network consisted of a distributed subsystem of components that provided raw inputs to the processing stack at a rate of 20 Hz. The sensor suite consisted of the following:

1. Radar to provide parametric vehicle data.
2. Video cameras to collect the visual scene.
3. Weather stations (signalized intersections only).
4. Signal phase sniffer to provide the signal phase and timing at signalized intersections.
5. Global Positioning System to provide synchronized global time.

The processing stack pre-processed the sensor data and assembled the data set in real time while simultaneously archiving to binary data and compressed video files. The DAS was completely contained at the intersection sites and virtually invisible to drivers.

Data was transported at regular intervals to the Virginia Tech Transportation Institute, where it was uploaded to secure servers for storage. Post-processing of the stop-controlled and signalized data was performed; it consisted of a series of data filtering, extrapolation, and smoothing techniques to prepare the data set for analyses. These measures improved the quality of the raw data set and derived additional measurements that were used for the algorithm development and evaluation.

The first stage of data analysis included exploratory investigations of the stop-controlled and signalized data sets. When these investigations began, little was known about the trajectories of vehicles as they approached intersections. There was no consensus on which drivers should receive a warning or which metrics should be used in the threat assessment algorithm. The analyses included investigations of driver decisions at intersections regarding stopping, minimum stop-bar speed, brake onset, and overall vehicle trajectories. These exploratory analyses were performed with the goal of developing the CICAS-V algorithm.

After the exploratory analyses, a procedure was developed to test and evaluate the algorithm. Synthesis of the literature, engineering theory, and intersection-approach analysis generated data inputs for the algorithm development. The preliminary algorithms were tested in a pseudo-real-time simulation using the actual vehicle trajectory data collected for this study. This analysis generated a set of threat assessment algorithms that will be carried forward into the CICAS-V development and testing during subsequent tasks in the CICAS-V project.

Each algorithm was evaluated utilizing the theory of signal detection; extended to consider additional factors within the CICAS-V context. In addition to warning accuracy, the extended signal detection method also evaluated the algorithms in terms of the warning timing (i.e., required braking levels) and their anticipated level of nuisance. Analysis of the results determined possible regions for improvement based on the algorithm's classification of vehicle trajectories. Improvements were made and the iterations of the simulation cycle were conducted until additional revisions ceased to yield significant algorithm performance improvements.

All of the algorithms tested follow the same basic framework (Figure 1). An approaching vehicle first enters the monitored region of the intersection at time  $T_o$ . Once the vehicle enters the region of interest, its kinematic state is measured every 50 milliseconds. During the present research, the measurements were performed by the radar; in the CICAS-V application, these measures will be obtained from onboard sensors.

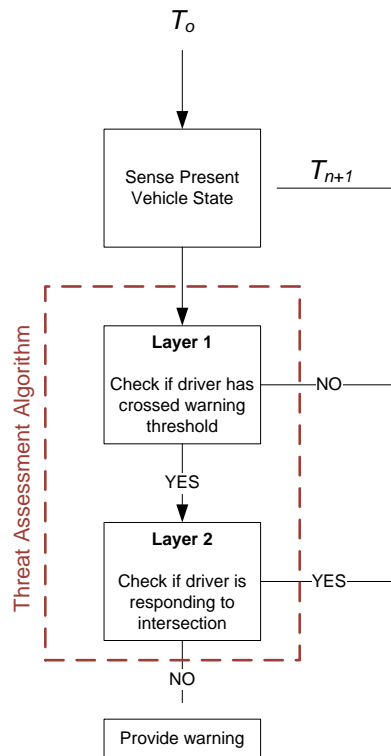


**Figure 1 Top-level algorithm architecture.**

Once the kinematic measures are evaluated, they are fed into the first layer of the algorithm. The first layer contains a computational component that evaluates whether or not the warning should be provided, based on the present kinematic state of the vehicle. This layer gathers together a variety of measures into a single metric, which is then compared to a prediction criterion. If the outcome of the comparison indicates driver compliance, the algorithm computations cease for that time frame. The evaluation process then starts over for the next time cycle. If the outcome of the comparison predicts a violation, the present vehicle kinematics are passed to the second layer of the algorithm.



The second layer of the algorithm was added to reduce the number of false alerts that were being produced by the first layer. The second layer evaluates the present state of the vehicle to predict whether the driver is attentive to the intersection. If the driver appears to be attentive (e.g., has started braking or is below a set speed), the warning is suppressed. If the driver is not attentive, the warning is set to active and the algorithm is terminated for the remainder of the intersection approach trajectory. If the warning is suppressed, the entire process begins again with the next time window and is repeated through the entire intersection approach trajectory unless a warning is presented.

Overall, more than 160 individual algorithms were tested with more than 7,000 unique parameter combinations. Some of the algorithms were based on the laws of physics and used standard kinematic equations, while other algorithms were based on regression techniques. An example of the regression-based threat assessment algorithm is provided in the figure below. This algorithm is based on regression of velocity as a function of distance from the intersection. Each line represents one permutation of the algorithm and is based on the percentile of the distribution fit by the regression analysis.

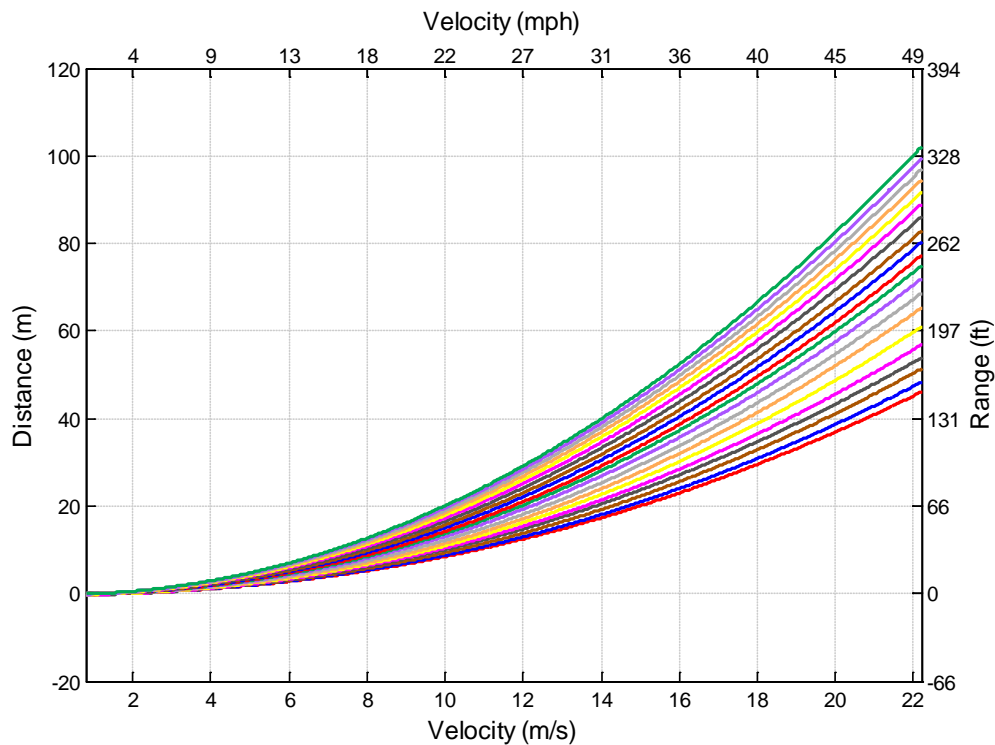


**Figure 2** The series of curves used to calculate the warning distance as a function of velocity at stop-controlled intersections for the piecewise distributions fit with a power function.

The algorithm analysis process generated a series of graphical outputs. They represented the accuracy of the algorithm, the timing of the produced warnings, and the anticipated level of nuisance that may result from the associated false warnings. Interpretation of these outputs would require a detailed explanation too long to be appropriate for an executive summary. The reader is encouraged to refer to the main report for details on the graphical analysis. The most notable trends included:

- The highest performing algorithms at stop-controlled intersections are not typically the highest performing algorithms for signalized intersections.
- At stop-controlled intersections, the braking criterion for warning suppression (located in the second layer of the algorithm) tends to provide the best results if braking effort (i.e., braking at 0.1 g or higher) rather than brake status (i.e., brake pressed) is used. This trend was not observed at signalized intersections.
- The low-speed cutoff in the second layer of the algorithm tends to provide the best results if it is set above 4.4 m/s (10 mph) at both stop-controlled and signalized intersections.
- The violation threshold represents the stop-bar speed used to classify compliant and violation intersection approaches. Drivers who roll through a stop sign or a signalized intersection in the red phase at a speed below the violation threshold are not considered violators. The results of the simulation show that algorithms discriminate better between compliant and violation approaches when higher violation thresholds are selected.

Although graphical analysis was very useful for identifying trends across the algorithms, it did not provide a reliable way to identify the best algorithms. A heuristic search procedure was developed to identify and evaluate the best algorithm based on the results of the pseudo-real-time simulation.

Three heuristics were used to rank-order the algorithms in terms of differing performance criteria. There is an inherent trade-off between providing the most overall true positives (warning a driver who violated), appropriately timed warnings (warning early enough for the driver to react and stop the vehicle), and minimizing the number of false positives (warning a compliant driver that is approaching a stop sign or traffic light in a yellow or red state). The preferred heuristic provided a compromise by simultaneously performing the following:

1. Allowing no more than either five percent or one percent false positives.
2. Maximizing the overall number of total true positives.
3. Maximizing the number of appropriately timed warnings (which allows sufficient braking distance).
4. Minimizing the number of false positives likely to be perceived as nuisance.

Presently, the driver's tolerance for false positives is not known. It is possible that some of the false positives will not be perceived as annoying. For instance, although a driver may have complied with the TCD, he or she may have braked late due to inattention or misjudgment, and may have appreciated, or at least tolerated, a warning if it was provided. By executing the heuristic while allowing either a five percent or a one percent false positive rate, two sets of algorithms were identified. The five percent algorithm results in more situations in which the CICAS-V system correctly warns violating drivers than the one percent algorithm; thus, it should be selected initially. If compliant become annoyed at the rate of inappropriate CICAS-V warnings, the one percent algorithm should provide viable alternative (at the cost of reducing the number of appropriately timed CICAS-V warnings for violating drivers).

The final set of recommended algorithms are predicted to provide an appropriately timed warning to 68 percent of the violating drivers at stop-controlled intersections and 82 percent of violating drivers at signalized intersections with five percent false positive rate. Nearly all of the remaining violators will eventually be identified by the algorithm; however, the warning will not be provided sufficiently early for these drivers to stop.

With a one percent false positive rate, 56 percent and 68 percent of the violating drivers are predicted to be correctly warned at stop-controlled and signalized intersections, respectively. Additional algorithms were identified that improved the performance rates, particularly at stop-controlled intersections; however, these additional algorithms use a “braking effort” criterion that could not be feasibly integrated into the current CICAS-V prototype. Thus, they are recommended for future CICAS-V hardware.

The algorithms developed during this subtask, along with the Driver Vehicle Interface (DVI) identified in Subtask 3.3, will be integrated for CICAS-V on-road testing during Subtask 3.4, a pilot test of the system. The on-road testing will provide the first system-level test with naive drivers. Data from the on-road testing will be analyzed during the collection period to monitor the algorithm performance. As appropriate during Subtask 3.4, the CICAS-V algorithm will be iteratively updated. At the end of Subtask 3.4, a threat assessment algorithm will be identified to carry forward into a Field Operation Test of the CICAS-V project.

## **ACKNOWLEDGMENTS**

The Subtask 3.2 effort of the CICAS-V project was conducted by the Virginia Tech Transportation Institute (VTTI) under contract to the Crash Avoidance Metrics Partnership Vehicle Safety Communications II (CAMP VSC2). VTTI would like to acknowledge the very valuable contributions made to the algorithm development process by the CAMP VSC2 CICAS-V Algorithm Subcommittee. The members of the subcommittee are listed in alphabetical order: Carol Flannagan (Independent Consultant), Raymond Kiefer (General Motors, Corp.), Michael Losh (General Motors, Corp.), Michael Maile (Mercedes-Benz Research and Development North America, Inc.), David Masselink (Toyota Motor Engineering and Manufacturing), Chuck Pall (Honda Research and Development), Joseph Stinnett (Ford Motor, Corp.), and Steve VanSickle (Danlaw, Inc.).

# Table of Contents

<b>1</b>	<b>Introduction.....</b>	<b>1</b>
1.1	Subtask 3.2 Overview .....	1
1.2	Background .....	2
1.2.1	Intersection Crash Problem Overview .....	3
1.2.2	Intersection Crash Taxonomy .....	3
1.2.3	Intersection Violation Causation.....	5
1.2.4	CICAS-V Warning Systems .....	7
1.2.5	Prior Algorithm Development.....	9
<b>2</b>	<b>Data Collection Sites and Apparatus.....</b>	<b>11</b>
2.1	Site Selection.....	11
2.1.1	Stop-Controlled Intersection Test Sites .....	13
2.1.2	Signalized Intersection Test Sites .....	24
2.2	Data Acquisition Systems .....	30
2.2.1	Stop-Controlled Intersection Data Acquisition.....	30
2.2.2	Signalized Intersection Data Acquisition.....	33
2.3	Test Site Installation.....	37
2.4	Data Retrieval and Management.....	39
2.5	Approvals .....	39
<b>3</b>	<b>Post-Processing.....</b>	<b>41</b>
3.1	First-Pass Filtering and Derivation of Unique Vehicle ID .....	41
3.2	Lane ID.....	42
3.3	Smoothed Kinematic Variables.....	44
3.4	Brake Status.....	46
3.5	System and Post-Processing Validation.....	47
3.6	Event Validation and Video Reduction .....	51
3.6.1	Data Reduction Reliability Assessments .....	52
<b>4</b>	<b>Exploratory Analyses of Vehicle Approaches at Stop- Controlled Intersections.....</b>	<b>55</b>
4.1	Stop-Controlled Intersection Approach Trends .....	55
4.1.1	Stop-Bar Speed Analysis at Stop-Controlled Intersections .....	60
4.2	Brake Onset Analysis at Stop-Controlled Intersections.....	62

4.3	Graphical Vehicle Trajectory Analysis at Stop-Controlled Intersections .....	66
<b>5</b>	<b>Exploratory Analysis of Vehicle Approaches at Signalized Intersections.....</b>	<b>72</b>
5.1	Signalized Violations by Maneuver Type.....	72
5.2	Time After Red for Signalized Violations .....	73
5.3	Stop bar Velocity for Violations at Signalized Intersections.....	76
<b>6</b>	<b>CICAS-V Algorithm Testing and Evaluation Procedure.....</b>	<b>78</b>
6.1	Application and Extension of SDT Method to the CICAS Context 78	
6.2	Algorithm Assessment Procedure.....	83
<b>7</b>	<b>Generated CICAS-V Threat Assessment Algorithms.....</b>	<b>88</b>
7.1	Variable Definitions .....	88
7.2	Top-Level Architecture .....	88
7.3	Layer 1 Algorithm Component .....	90
7.3.1	Algorithm 1: Static TTI.....	90
7.3.2	Algorithm 2: Static RDP .....	91
7.3.3	Algorithms 3 and 4: Static RDP with an Assumed PRT.....	92
7.3.4	Algorithm 5: Warning Range as a Function of TTI.....	92
7.3.5	Algorithm 6: Warning Range as a Function of Velocity .....	96
7.3.6	Algorithm 7: Warning Range as a Function of Velocity Based on Truncated Data	98
7.3.7	Algorithm 8: RDP as a Function of Range .....	99
7.3.8	Other Algorithms Developed and Tested but Not Presented .....	100
7.4	Layer 2 Algorithm Component .....	101
7.5	Algorithm Naming Convention .....	102
<b>8</b>	<b>Results of the Algorithm Evaluation.....</b>	<b>104</b>
8.1	ROC Curve Graphical Analysis Results .....	104
8.2	Algorithm Recommendations for CICAS-V.....	111
8.2.1	Procedure to Identify the Best Performing Algorithms .....	111
8.2.2	Results of the Algorithm Search Procedure .....	113
8.2.3	Figures of the Best Performing Algorithms .....	117
8.2.4	Implications of the Algorithm Results .....	119
<b>9</b>	<b>Recommendations, Limitations, and Future Research.....</b>	<b>1228</b>

9.1	Recommendations .....	122
9.1.1	Continue Research and Development of CICAS-V .....	122
9.1.2	Determine Who Should Receive a Warning .....	122
9.1.3	Warning Suppression Should Be Part of the Algorithm .....	122
9.1.4	Algorithms for Use in CICAS-V Prototype Tests .....	123
9.2	Limitations .....	124
9.3	Future Research Opportunities.....	124
9.3.1	Extensions of the Subtask 3.2 Analyses.....	124
9.3.2	Re-Analyzing the Subtask 3.2 Results Using Future Data Collections 125	
9.3.3	Additional Analyses Using the Subtask 3.2 Data .....	126
<b>10</b>	<b>References.....</b>	<b>1284</b>
<b>11</b>	<b>Appendices.....</b>	<b>134</b>
<b>9</b>		
11.1	Appendix A: Internal Review Board Authorization to Proceed..	1349
11.2	Appendix B: Deceleration Threshold and Driver Reaction Time .....	135
	30	
11.2.1	Introduction.....	13530
11.2.2	Methods.....	13530
11.2.3	Results.....	136
11.2.4	Conclusion .....	1372
11.3	Appendix C: Vehicle Data Acquisition .....	1394
11.4	Appendix D: Violation Trigger Development Process.....	1416
11.5	Appendix E: Post-Processing and Radar-Induced Error.....	1461
11.6	Appendix F: Summary of Results for the Cluster Analysis.....	1472
11.7	Appendix G: Summary Table of Results for the GEV Fits and the Kolmogorov-Smirnov Goodness of Fit Test.....	1483
11.8	Appendix H: Stop Bar Velocity Fit Information .....	1494
11.9	Appendix I: Brake Onset Fit Information .....	1505
11.10	Appendix J: Warning Timing Model.....	1516
11.11	Appendix K: Regression of Minimum RDP as a Function of Minimum Stop Bar Velocity .....	1527
11.12	Appendix L: Regression-Based Algorithm Fit Information .....	1538

11.13	Appendix M: Beta Permutation Values for Tested Algorithms	1592
11.14	Appendix N: ROC Curves for Stop-Controlled Algorithms ....	1667
11.15	Appendix O: Stop Controlled Warning Timing Distributions.	1833
11.16	Appendix P: Stop-Controlled Nuisance Distributions.....	2171
11.17	Appendix Q: ROC Curves for Signalized Algorithms .....	2499
11.18	Appendix R: Signalized Warning Timing Distributions .....	2598
11.19	Appendix S: Signalized Nuisance Distributions.....	2936
11.20	Appendix T: Algorithm Simulation Results Summary.....	3274
11.21	Appendix U: Plots of the Best Overall Algorithms .....	3317
11.22	Appendix V: Base Rate Data for the Best Overall and Best Applicable Algorithms Across the Tested Violation Thresholds and Maximum False Positive Rates .....	3328
11.23	Appendix W: System Latency Investigation .....	160
11.24	Appendix X: Approach Analysis of Violating and Nearly Violating Approaches at Stop-Controlled Intersections.....	42



# List of Figures

Figure 1 Top-level algorithm architecture. ....	iii
Figure 2 Intersection straight crossing path (SCP). ....	4
Figure 3 Left turn across path (LTAP). ....	4
Figure 4 Turn into path (TIP) – merge conflict: a) right – RTIP, b) left – LTIP.....	5
Figure 5 Diagram of Clubhouse & Lusters Gate intersection.....	13
Figure 6 Aerial view of Lusters Gate & Clubhouse intersection [image obtained through Microsoft® (2008)]......	14
Figure 7 Ground images of Clubhouse & Lusters Gate intersection. ....	14
Figure 8 Diagram of Plank & Lusters Gate intersection.....	15
Figure 9 Aerial view of Plank & Lusters Gate intersection [image obtained through Microsoft® (2008)]......	16
Figure 10 Ground images of Plank & Lusters Gate intersection. ....	16
Figure 11 Diagram of Nellies Cave & Woodland Hills intersection. ....	17
Figure 12 Aerial view of Nellies Cave & Woodland Hills intersection [image obtained through Microsoft® (2008)]. ....	18
Figure 13 Ground images of Nellies Cave & Woodland Hills intersection. ....	18
Figure 14 Diagram of Fairview Church & HW8 intersection. ....	19
Figure 15 Aerial view of the Fairview Church & HW8 intersection [image obtained through Microsoft® (2008)]. ....	20
Figure 16 Ground images from Fairview Church & HW8 intersection. ....	21
Figure 17 Diagram of Meadow Creek & Childress intersection. ....	22
Figure 18 Aerial view of the Meadow Creek & Childress intersection [image obtained through Microsoft® (2008)]. ....	23
Figure 19 Ground images from Meadow Creek & Childress intersection. ....	23
Figure 20 Diagram of Franklin, Elm & Independence intersection.....	24
Figure 21 Aerial view Franklin, Elm & Independence intersection [image obtained through Microsoft® (2008)]. ....	25
Figure 22 Ground images from Franklin, Elm & Independence intersection.....	25
Figure 23 Diagram of Depot & Franklin intersection.....	26
Figure 24 Aerial view of Depot & Franklin intersection [image obtained through Microsoft® (2008)]......	27
Figure 25 Ground images from Depot & Franklin intersection.....	27

Figure 26 Diagram of Peppers Ferry (VA-114) & Franklin (Bus460) intersection. ....	28
Figure 27 Aerial view of Peppers Ferry (VA-114) & Franklin (Bus460) intersection [image obtained through Microsoft® (2008)]. .....	29
Figure 28 Ground images from Peppers Ferry (VA-114) & Franklin (Bus460) intersection.....	29
Figure 29 Diagram of stop-controlled DAS.....	31
Figure 30 Stop-controlled DAS. ....	31
Figure 31 Video from stop-controlled camera unit.....	32
Figure 32 Diagram of signalized DAS.....	34
Figure 33 Video quadrants from camera units mounted on intersection mast arms.....	35
Figure 34 Camera and radar unit mounted on a single intersection arm mast, along with instrumentation inside traffic signal controller cabinet. ....	36
Figure 35 DSP tracking processors.....	36
Figure 36 VTTI processing stack.....	37
Figure 37 VTTI workers installing radar and camera unit at stop-controlled intersection. ....	38
Figure 38 VDOT workers mounting camera and radar unit to intersection mast arm. ....	38
Figure 39 Raw data collected by the DAS with the smoothing spline fit to the range and velocity data. The acceleration was then derived based on the data fit. Residuals for the velocity fit are also provided to convey the typical quality of the fitting procedure. ....	45
Figure 40 Example of an intersection approach showing the derived brake onset point for range, velocity, and acceleration kinematic measures. ....	47
Figure 41 Stop-controlled infrastructure and vehicle DAS measurements. ....	49
Figure 42 Signalized infrastructure and vehicle DAS measurements. ....	50
Figure 43 Data analysis and reduction software developed by VTTI. ....	52
Figure 44 Average RDP and the 5% and 95% population estimates show as error bars for each of the four assigned clusters describing different types of stop sign approach behavior.....	58
Figure 45 Cumulative distribution for the overall max RDP exhibited by drivers as they approached the stop bar. ....	59
Figure 46 Cumulative distribution for maximum RDP within each of the clusters signifying differing group stopping behaviors.....	60
Figure 47 Empirical cumulative probability of minimum stop-bar speed at stop-controlled intersections. ....	61
Figure 48 Distribution of stop-bar speed partitioned by cluster. Curve fits for clusters 1 and 4 are for exploratory purposes only. ....	62

Figure 49 Box plot for brake onset. ....	64
Figure 50 Cumulative distribution of brake onset as a function of distance to the intersection.....	65
Figure 51 Cumulative distribution of brake onset as a function of TTI. ....	65
Figure 52 Mean velocity trajectory of vehicles partitioned by the stopping behavior cluster.....	67
Figure 53 Mean acceleration trajectory of vehicles partitioned by the stopping behavior cluster.....	68
Figure 54 Mean RDP trajectory of vehicles partitioned by the stopping behavior cluster. ....	69
Figure 55 Mean TTI trajectory of vehicles partitioned by the stopping behavior cluster.	70
Figure 56 Total signalized violations broken down by turn maneuver for 4,924,267 total approaches across three signalized intersections. ....	73
Figure 57 Frequency distribution for signalized violations over time after onset of red phase. ....	74
Figure 58 Percentage of signalized violations that occurred within maneuver. The proportion of violations from each maneuver sum to 100 percent. ....	74
Figure 59 Stop-bar velocity at signalized intersections partitioned by maneuver type ...	77
Figure 60 Theoretical representation of the SDT signal (violation) and noise (compliant) distributions. The distance between the peaks of the two distributions represents the sensitivity of a given algorithm. The overlapping regions of the two curves that lie on the incorrect side of the decision criteria line represent misclassifications performed by the algorithm. ....	79
Figure 61 Example ROC curves. Each curve represents the hit and false alarm rates for a particular threat assessment algorithm across a variety of decision criteria (Beta). The larger the area under the curve, the better an algorithm is at discriminating violators from compliant drivers. ....	80
Figure 62 Example warning timing distribution for true positives using the algorithms depicted in Figure 61 evaluated at the Beta value corresponding to a false positive rate of 0.01.....	82
Figure 63 Example stop bar velocity distribution for false positives using the algorithms depicted in Figure 61 evaluated at the Beta value corresponding to a false positive rate of 0.01.....	83
Figure 64 Example vehicle trajectories that produced false negatives for one of the algorithm iterations. ....	86
Figure 65 Intersection scenario and variables used for algorithm development. ....	88
Figure 66 Top-level algorithm architecture. ....	89
Figure 67 Piecewise empirical percentiles across which the linear regression was performed for the stop-controlled intersection distribution. ....	93

Figure 68 The series of curves used to calculate the warning TTI as a function of range at stop-controlled intersections for the piecewise distributions fit with a power function. ..	94
Figure 69 The series of curves used to calculate the warning TTI as a function of range at signalized intersections for the piecewise distributions fit with a power function. ....	95
Figure 70 The series of curves used to calculate the warning distance as a function of velocity at stop-controlled intersections for the piecewise distributions fit with a power function. ....	97
Figure 71 The series of curves used to calculate the warning distance as a function of velocity at signalized intersections for the piecewise distributions fit with a power function. ....	97
Figure 72 The series of curves used to calculate the warning distance as a function of velocity at stop-controlled intersections for the piecewise distributions fit with a power function based on truncated data.....	98
Figure 73 The series of curves used to calculate the warning RDP as a function of range at stop-controlled intersections for the piecewise distributions fit with a power function. ....	99
Figure 74 The series of curves used to calculate the warning RDP as a function of range at signalized intersections for the piecewise distributions fit with a power function. ....	100
Figure 75 Diagram depicting the three-digit code used to name each of the algorithms described in this report.....	102
Figure 76 ROC curve for the stop-controlled 600 series algorithm family using a violation threshold of 5 mph.....	105
Figure 77 ROC curve for the stop-controlled 600 series algorithm family using a violation threshold of 10 mph.....	106
Figure 78 ROC curve for the signalized 600 series algorithm family using a violation threshold of 10 mph. ....	107
Figure 79 ROC curve for the stop-controlled 600 series algorithm family using a violation threshold of 15 mph.....	108
Figure 80 ROC curve for the signalized 600 series algorithm family using a violation threshold of 15 mph. ....	109
Figure 81 ROC curve for the stop-controlled 600 series algorithm family using a violation threshold of 20 mph.....	110
Figure 82 ROC curve for the signalized 600 series algorithm family using a violation threshold of 20 mph. ....	111
Figure 83 Points on the warning distribution (left) and the nuisance distribution (right) that were evaluated to support the heuristic used to select the highest performing algorithms. ....	112
Figure 84 Stop bar velocity versus warning distance for the best applicable algorithms identified in the stop-controlled intersection simulation. ....	118

Figure 85 Stop bar velocity versus warning distance for the best applicable algorithms identified in the signalized intersection simulation. ....	119
Figure 86 Experimental vehicle, 2006 Cadillac STS.....	139
Figure 87 Data acquisition system, installed in the vehicle trunk underneath the rear shelf. ....	139
Figure 88 Number of events that would be reduced as a function of the RDP threshold selected.....	143
Figure 89 Average minimum velocity for vehicles near the stop bar.....	144
Figure 90 Empirical cumulative probability distribution for RDP.....	145
Figure 91 Model of the probability of stopping by the stop bar based on the required constant deceleration at the warning onset. ....	151
Figure 92 Regression line relating the maximum stop bar RDP to the minimum stop-bar speed. ....	152
Figure 93 ROC curve for the 100 series algorithm family using a violation threshold of 5 mph. ....	166
Figure 94 ROC curve for the 200 series algorithm family using a violation threshold of 5 mph. ....	167
Figure 95 ROC curve for the 300 series algorithm family using a violation threshold of 5 mph. ....	167
Figure 96 ROC curve for the 400 series algorithm family using a violation threshold of 5 mph. ....	168
Figure 97 ROC curve for the 500 series algorithm family using a violation threshold of 5 mph. ....	168
Figure 98 ROC curve for the 600 series algorithm family using a violation threshold of 5 mph. ....	169
Figure 99 ROC curve for the 700 series algorithm family using a violation threshold of 5 mph. ....	169
Figure 100 ROC curve for the 800 series algorithm family using a violation threshold of 5 mph. ....	170
Figure 101 ROC curve for the 100 series algorithm family using a violation threshold of 10 mph. ....	171
Figure 102 ROC curve for the 200 series algorithm family using a violation threshold of 10 mph. ....	171
Figure 103 ROC curve for the 300 series algorithm family using a violation threshold of 10 mph. ....	172
Figure 104 ROC curve for the 400 series algorithm family using a violation threshold of 10 mph. ....	172

Figure 105 ROC curve for the 500 series algorithm family using a violation threshold of 10 mph. ....	173
Figure 106 ROC curve for the 600 series algorithm family using a violation threshold of 10 mph. ....	173
Figure 107 ROC curve for the 700 series algorithm family using a violation threshold of 10 mph. ....	174
Figure 108 ROC curve for the 800 series algorithm family using a violation threshold of 10 mph. ....	174
Figure 109 ROC curve for the 100 series algorithm family using a violation threshold of 15 mph. ....	175
Figure 110 ROC curve for the 200 series algorithm family using a violation threshold of 15 mph. ....	175
Figure 111 ROC curve for the 300 series algorithm family using a violation threshold of 15 mph. ....	176
Figure 112 ROC curve for the 400 series algorithm family using a violation threshold of 15 mph. ....	176
Figure 113 ROC curve for the 500 series algorithm family using a violation threshold of 15 mph. ....	177
Figure 114 ROC curve for the 600 series algorithm family using a violation threshold of 15 mph. ....	177
Figure 115 ROC curve for the 700 series algorithm family using a violation threshold of 15 mph. ....	178
Figure 116 ROC curve for the 800 series algorithm family using a violation threshold of 15 mph. ....	178
Figure 117 ROC curve for the 100 series algorithm family using a violation threshold of 20 mph. ....	179
Figure 118 ROC curve for the 200 series algorithm family using a violation threshold of 20 mph. ....	179
Figure 119 ROC curve for the 300 series algorithm family using a violation threshold of 20 mph. ....	180
Figure 120 ROC curve for the 400 series algorithm family using a violation threshold of 20 mph. ....	180
Figure 121 ROC curve for the 500 series algorithm family using a violation threshold of 20 mph. ....	181
Figure 122 ROC curve for the 600 series algorithm family using a violation threshold of 20 mph. ....	181
Figure 123 ROC curve for the 700 series algorithm family using a violation threshold of 20 mph. ....	182

Figure 124 ROC curve for the 800 series algorithm family using a violation threshold of 20 mph. ....	182
Figure 125 Cumulative distribution of the warning timing for true positives produced by the 100 series algorithm at a false positive rate of 0.01 using a violation threshold of 15 mph. ....	183
Figure 126 Cumulative distribution of the warning timing for true positives produced by the 200 series algorithm at a false positive rate of 0.01 using a violation threshold of 15 mph. ....	184
Figure 127 Cumulative distribution of the warning timing for true positives produced by the 300 series algorithm at a false positive rate of 0.01 using a violation threshold of 15 mph. ....	185
Figure 128 Cumulative distribution of the warning timing for true positives produced by the 400 series algorithm at a false positive rate of 0.01 using a violation threshold of 15 mph. ....	186
Figure 129 Cumulative distribution of the warning timing for true positives produced by the 600 series algorithm at a false positive rate of 0.01 using a violation threshold of 15 mph. ....	187
Figure 130 Cumulative distribution of the warning timing for true positives produced by the 700 series algorithm at a false positive rate of 0.01 using a violation threshold of 15 mph. ....	188
Figure 131 Cumulative distribution of the warning timing for true positives produced by the 800 series algorithm at a false positive rate of 0.01 using a violation threshold of 15 mph. ....	189
Figure 132 Cumulative distribution of the warning timing for true positives produced by the 100 series algorithm at a false positive rate of 0.01 using a violation threshold of 20 mph. ....	190
Figure 133 Cumulative distribution of the warning timing for true positives produced by the 200 series algorithm at a false positive rate of 0.01 using a violation threshold of 20 mph. ....	191
Figure 134 Cumulative distribution of the warning timing for true positives produced by the 300 series algorithm at a false positive rate of 0.01 using a violation threshold of 20 mph. ....	192
Figure 135 Cumulative distribution of the warning timing for true positives produced by the 400 series algorithm at a false positive rate of 0.01 using a violation threshold of 20 mph. ....	193
Figure 136 Cumulative distribution of the warning timing for true positives produced by the 500 series algorithm at a false positive rate of 0.01 using a violation threshold of 20 mph. ....	194
Figure 137 Cumulative distribution of the warning timing for true positives produced by the 600 series algorithm at a false positive rate of 0.01 using a violation threshold of 20 mph. ....	195

Figure 138 Cumulative distribution of the warning timing for true positives produced by the 700 series algorithm at a false positive rate of 0.01 using a violation threshold of 20 mph. ....	196
Figure 139 Cumulative distribution of the warning timing for true positives produced by the 800 series algorithm at a false positive rate of 0.01 using a violation threshold of 20 mph. ....	197
Figure 140 Cumulative distribution of the warning timing for true positives produced by the 200 series algorithm at a false positive rate of 0.05 using a violation threshold of 10 mph. ....	198
Figure 141 Cumulative distribution of the warning timing for true positives produced by the 600 series algorithm at a false positive rate of 0.05 using a violation threshold of 10 mph. ....	199
Figure 142 Cumulative distribution of the warning timing for true positives produced by the 800 series algorithm at a false positive rate of 0.05 using a violation threshold of 10 mph. ....	200
Figure 143 Cumulative distribution of the warning timing for true positives produced by the 100 series algorithm at a false positive rate of 0.05 using a violation threshold of 15 mph. ....	201
Figure 144 Cumulative distribution of the warning timing for true positives produced by the 200 series algorithm at a false positive rate of 0.05 using a violation threshold of 15 mph. ....	202
Figure 145 Cumulative distribution of the warning timing for true positives produced by the 300 series algorithm at a false positive rate of 0.05 using a violation threshold of 15 mph. ....	203
Figure 146 Cumulative distribution of the warning timing for true positives produced by the 400 series algorithm at a false positive rate of 0.05 using a violation threshold of 15 mph. ....	204
Figure 147 Cumulative distribution of the warning timing for true positives produced by the 500 series algorithm at a false positive rate of 0.05 using a violation threshold of 15 mph. ....	205
Figure 148 Cumulative distribution of the warning timing for true positives produced by the 600 series algorithm at a false positive rate of 0.05 using a violation threshold of 15 mph. ....	206
Figure 149 Cumulative distribution of the warning timing for true positives produced by the 700 series algorithm at a false positive rate of 0.05 using a violation threshold of 15 mph. ....	207
Figure 150 Cumulative distribution of the warning timing for true positives produced by the 800 series algorithm at a false positive rate of 0.05 using a violation threshold of 15 mph. ....	208



Figure 151 Cumulative distribution of the warning timing for true positives produced by the 100 series algorithm at a false positive rate of 0.05 using a violation threshold of 20 mph. ....	209
Figure 152 Cumulative distribution of the warning timing for true positives produced by the 200 series algorithm at a false positive rate of 0.05 using a violation threshold of 20 mph. ....	210
Figure 153 Cumulative distribution of the warning timing for true positives produced by the 300 series algorithm at a false positive rate of 0.05 using a violation threshold of 20 mph. ....	211
Figure 154 Cumulative distribution of the warning timing for true positives produced by the 400 series algorithm at a false positive rate of 0.05 using a violation threshold of 20 mph. ....	212
Figure 155 Cumulative distribution of the warning timing for true positives produced by the 500 series algorithm at a false positive rate of 0.05 using a violation threshold of 20 mph. ....	213
Figure 156 Cumulative distribution of the warning timing for true positives produced by the 600 series algorithm at a false positive rate of 0.05 using a violation threshold of 20 mph. ....	214
Figure 157 Cumulative distribution of the warning timing for true positives produced by the 700 series algorithm at a false positive rate of 0.05 using a violation threshold of 20 mph. ....	215
Figure 158 Cumulative distribution of the warning timing for true positives produced by the 800 series algorithm at a false positive rate of 0.05 using a violation threshold of 20 mph. ....	216
Figure 159 Cumulative distribution of the stop-bar speed for false positives produced by the 100 series algorithm at a false positive rate of 0.01 using a violation threshold of 15 mph. ....	217
Figure 160 Cumulative distribution of the stop-bar speed for false positives produced by the 200 series algorithm at a false positive rate of 0.01 using a violation threshold of 15 mph. ....	218
Figure 161 Cumulative distribution of the stop-bar speed for false positives produced by the 300 series algorithm at a false positive rate of 0.01 using a violation threshold of 15 mph. ....	219
Figure 162 Cumulative distribution of the stop-bar speed for false positives produced by the 400 series algorithm at a false positive rate of 0.01 using a violation threshold of 15 mph. ....	219
Figure 163 Cumulative distribution of the stop-bar speed for false positives produced by the 600 series algorithm at a false positive rate of 0.01 using a violation threshold of 15 mph. ....	220

Figure 164 Cumulative distribution of the stop-bar speed for false positives produced by the 700 series algorithm at a false positive rate of 0.01 using a violation threshold of 15 mph. ....	221
Figure 165 Cumulative distribution of the stop-bar speed for false positives produced by the 800 series algorithm at a false positive rate of 0.01 using a violation threshold of 15 mph. ....	222
Figure 166 Cumulative distribution of the stop-bar speed for false positives produced by the 100 series algorithm at a false positive rate of 0.01 using a violation threshold of 20 mph. ....	223
Figure 167 Cumulative distribution of the stop-bar speed for false positives produced by the 200 series algorithm at a false positive rate of 0.01 using a violation threshold of 20 mph. ....	224
Figure 168 Cumulative distribution of the stop-bar speed for false positives produced by the 300 series algorithm at a false positive rate of 0.01 using a violation threshold of 20 mph. ....	225
Figure 169 Cumulative distribution of the stop-bar speed for false positives produced by the 400 series algorithm at a false positive rate of 0.01 using a violation threshold of 20 mph. ....	226
Figure 170 Cumulative distribution of the stop-bar speed for false positives produced by the 500 series algorithm at a false positive rate of 0.01 using a violation threshold of 20 mph. ....	227
Figure 171 Cumulative distribution of the stop-bar speed for false positives produced by the 600 series algorithm at a false positive rate of 0.01 using a violation threshold of 20 mph. ....	228
Figure 172 Cumulative distribution of the stop-bar speed for false positives produced by the 700 series algorithm at a false positive rate of 0.01 using a violation threshold of 20 mph. ....	229
Figure 173 Cumulative distribution of the stop-bar speed for false positives produced by the 800 series algorithm at a false positive rate of 0.01 using a violation threshold of 20 mph. ....	230
Figure 174 Cumulative distribution of the stop-bar speed for false positives produced by the 200 series algorithm at a false positive rate of 0.05 using a violation threshold of 10 mph. ....	231
Figure 175 Cumulative distribution of the stop-bar speed for false positives produced by the 600 series algorithm at a false positive rate of 0.05 using a violation threshold of 10 mph. ....	232
Figure 176 Cumulative distribution of the stop-bar speed for false positives produced by the 800 series algorithm at a false positive rate of 0.05 using a violation threshold of 10 mph. ....	233

Figure 177 Cumulative distribution of the stop-bar speed for false positives produced by the 100 series algorithm at a false positive rate of 0.05 using a violation threshold of 15 mph. ....	234
Figure 178 Cumulative distribution of the stop-bar speed for false positives produced by the 200 series algorithm at a false positive rate of 0.05 using a violation threshold of 15 mph. ....	235
Figure 179 Cumulative distribution of the stop-bar speed for false positives produced by the 300 series algorithm at a false positive rate of 0.05 using a violation threshold of 15 mph. ....	236
Figure 180 Cumulative distribution of the stop-bar speed for false positives produced by the 400 series algorithm at a false positive rate of 0.05 using a violation threshold of 15 mph. ....	237
Figure 181 Cumulative distribution of the stop-bar speed for false positives produced by the 500 series algorithm at a false positive rate of 0.05 using a violation threshold of 15 mph. ....	238
Figure 182 Cumulative distribution of the stop-bar speed for false positives produced by the 600 series algorithm at a false positive rate of 0.05 using a violation threshold of 15 mph. ....	239
Figure 183 Cumulative distribution of the stop-bar speed for false positives produced by the 700 series algorithm at a false positive rate of 0.05 using a violation threshold of 15 mph. ....	240
Figure 184 Cumulative distribution of the stop-bar speed for false positives produced by the 800 series algorithm at a false positive rate of 0.05 using a violation threshold of 15 mph. ....	241
Figure 185 Cumulative distribution of the stop-bar speed for false positives produced by the 100 series algorithm at a false positive rate of 0.05 using a violation threshold of 20 mph. ....	242
Figure 186 Cumulative distribution of the stop-bar speed for false positives produced by the 200 series algorithm at a false positive rate of 0.05 using a violation threshold of 20 mph. ....	243
Figure 187 Cumulative distribution of the stop-bar speed for false positives produced by the 300 series algorithm at a false positive rate of 0.05 using a violation threshold of 20 mph. ....	244
Figure 188 Cumulative distribution of the stop-bar speed for false positives produced by the 400 series algorithm at a false positive rate of 0.05 using a violation threshold of 20 mph. ....	245
Figure 189 Cumulative distribution of the stop-bar speed for false positives produced by the 500 series algorithm at a false positive rate of 0.05 using a violation threshold of 20 mph. ....	246

Figure 190 Cumulative distribution of the stop-bar speed for false positives produced by the 600 series algorithm at a false positive rate of 0.05 using a violation threshold of 20 mph. ....	247
Figure 191 Cumulative distribution of the stop-bar speed for false positives produced by the 700 series algorithm at a false positive rate of 0.05 using a violation threshold of 20 mph. ....	247
Figure 192 Cumulative distribution of the stop-bar speed for false positives produced by the 800 series algorithm at a false positive rate of 0.05 using a violation threshold of 20 mph. ....	248
Figure 193 ROC curve for the 100 series algorithm family using a violation threshold of 10 mph. ....	249
Figure 194 ROC curve for the 200 series algorithm family using a violation threshold of 10 mph. ....	250
Figure 195 ROC curve for the 300 series algorithm family using a violation threshold of 10 mph. ....	250
Figure 196 ROC curve for the 400 series algorithm family using a violation threshold of 10 mph. ....	251
Figure 197 ROC curve for the 600 series algorithm family using a violation threshold of 10 mph. ....	251
Figure 198 ROC curve for 800 series algorithm family using a violation threshold of 10 mph. ....	252
Figure 199 ROC curve for 100 series algorithm family using a violation threshold of 15 mph. ....	253
Figure 200 ROC curve for 200 series algorithm family using a violation threshold of 15 mph. ....	253
Figure 201 ROC curve for 300 series algorithm family using a violation threshold of 15 mph. ....	254
Figure 202 ROC curve for 400 series algorithm family using a violation threshold of 15 mph. ....	254
Figure 203 ROC curve for 600 series algorithm family using a violation threshold of 15 mph. ....	255
Figure 204 ROC curve for 800 series algorithm family using a violation threshold of 15 mph. ....	255
Figure 205 ROC curve for 100 series algorithm family using a violation threshold of 20 mph. ....	256
Figure 206 ROC curve for 200 series algorithm family using a violation threshold of 20 mph. ....	256
Figure 207 ROC curve for 300 series algorithm family using a violation threshold of 20 mph. ....	257

Figure 208 ROC curve for 400 series algorithm family using a violation threshold of 20 mph. ....	257
Figure 209 ROC curve for 600 series algorithm family using a violation threshold of 20 mph. ....	258
Figure 210 ROC curve for 800 series algorithm family using a violation threshold of 20 mph. ....	258
Figure 211 Cumulative distribution of the warning timing for true positives produced by the 200 series algorithm at a false positive rate of 0.01 using a violation threshold of 10 mph. ....	259
Figure 212 Cumulative distribution of the warning timing for true positives produced by the 300 series algorithm at a false positive rate of 0.01 using a violation threshold of 10 mph. ....	260
Figure 213 Cumulative distribution of the warning timing for true positives produced by the 400 series algorithm at a false positive rate of 0.01 using a violation threshold of 10 mph. ....	261
Figure 214 Cumulative distribution of the warning timing for true positives produced by the 600 series algorithm at a false positive rate of 0.01 using a violation threshold of 10 mph. ....	262
Figure 215 Cumulative distribution of the warning timing for true positives produced by the 100 series algorithm at a false positive rate of 0.01 using a violation threshold of 15 mph. ....	263
Figure 216 Cumulative distribution of the warning timing for true positives produced by the 200 series algorithm at a false positive rate of 0.01 using a violation threshold of 15 mph. ....	264
Figure 217 Cumulative distribution of the warning timing for true positives produced by the 300 series algorithm at a false positive rate of 0.01 using a violation threshold of 15 mph. ....	265
Figure 218 Cumulative distribution of the warning timing for true positives produced by the 400 series algorithm at a false positive rate of 0.01 using a violation threshold of 15 mph. ....	266
Figure 219 Cumulative distribution of the warning timing for true positives produced by the 600 series algorithm at a false positive rate of 0.01 using a violation threshold of 15 mph. ....	267
Figure 220 Cumulative distribution of the warning timing for true positives produced by the 800 series algorithm at a false positive rate of 0.01 using a violation threshold of 15 mph. ....	268
Figure 221 Cumulative distribution of the warning timing for true positives produced by the 100 series algorithm at a false positive rate of 0.01 using a violation threshold of 20 mph. ....	269

Figure 222 Cumulative distribution of the warning timing for true positives produced by the 200 series algorithm at a false positive rate of 0.01 using a violation threshold of 20 mph. ....	270
Figure 223 Cumulative distribution of the warning timing for true positives produced by the 300 series algorithm at a false positive rate of 0.01 using a violation threshold of 20 mph. ....	271
Figure 224 Cumulative distribution of the warning timing for true positives produced by the 400 series algorithm at a false positive rate of 0.01 using a violation threshold of 20 mph. ....	272
Figure 225 Cumulative distribution of the warning timing for true positives produced by the 600 series algorithm at a false positive rate of 0.01 using a violation threshold of 20 mph. ....	273
Figure 226 Cumulative distribution of the warning timing for true positives produced by the 800 series algorithm at a false positive rate of 0.01 using a violation threshold of 20 mph. ....	274
Figure 227 Cumulative distribution of the warning timing for true positives produced by the 100 series algorithm at a false positive rate of 0.05 using a violation threshold of 10 mph. ....	275
Figure 228 Cumulative distribution of the warning timing for true positives produced by the 200 series algorithm at a false positive rate of 0.05 using a violation threshold of 10 mph. ....	276
Figure 229 Cumulative distribution of the warning timing for true positives produced by the 300 series algorithm at a false positive rate of 0.05 using a violation threshold of 10 mph. ....	277
Figure 230 Cumulative distribution of the warning timing for true positives produced by the 400 series algorithm at a false positive rate of 0.05 using a violation threshold of 10 mph. ....	278
Figure 231 Cumulative distribution of the warning timing for true positives produced by the 600 series algorithm at a false positive rate of 0.05 using a violation threshold of 10 mph. ....	279
Figure 232 Cumulative distribution of the warning timing for true positives produced by the 800 series algorithm at a false positive rate of 0.05 using a violation threshold of 10 mph. ....	280
Figure 233 Cumulative distribution of the warning timing for true positives produced by the 100 series algorithm at a false positive rate of 0.05 using a violation threshold of 15 mph. ....	281
Figure 234 Cumulative distribution of the warning timing for true positives produced by the 200 series algorithm at a false positive rate of 0.05 using a violation threshold of 15 mph. ....	282

Figure 235 Cumulative distribution of the warning timing for true positives produced by the 300 series algorithm at a false positive rate of 0.05 using a violation threshold of 15 mph. ....	283
Figure 236 Cumulative distribution of the warning timing for true positives produced by the 400 series algorithm at a false positive rate of 0.05 using a violation threshold of 15 mph. ....	284
Figure 237 Cumulative distribution of the warning timing for true positives produced by the 600 series algorithm at a false positive rate of 0.05 using a violation threshold of 15 mph. ....	285
Figure 238 Cumulative distribution of the warning timing for true positives produced by the 800 series algorithm at a false positive rate of 0.05 using a violation threshold of 15 mph. ....	286
Figure 239 Cumulative distribution of the warning timing for true positives produced by the 100 series algorithm at a false positive rate of 0.05 using a violation threshold of 20 mph. ....	287
Figure 240 Cumulative distribution of the warning timing for true positives produced by the 200 series algorithm at a false positive rate of 0.05 using a violation threshold of 20 mph. ....	288
Figure 241 Cumulative distribution of the warning timing for true positives produced by the 300 series algorithm at a false positive rate of 0.05 using a violation threshold of 20 mph. ....	289
Figure 242 Cumulative distribution of the warning timing for true positives produced by the 400 series algorithm at a false positive rate of 0.05 using a violation threshold of 20 mph. ....	290
Figure 243 Cumulative distribution of the warning timing for true positives produced by the 600 series algorithm at a false positive rate of 0.05 using a violation threshold of 20 mph. ....	291
Figure 244 Cumulative distribution of the warning timing for true positives produced by the 800 series algorithm at a false positive rate of 0.05 using a violation threshold of 20 mph. ....	292
Figure 245 Cumulative distribution of the stop-bar speed for false positives produced by the 200 series algorithm at a false positive rate of 0.01 using a violation threshold of 10 mph. ....	293
Figure 246 Cumulative distribution of the stop-bar speed for false positives produced by the 300 series algorithm at a false positive rate of 0.01 using a violation threshold of 10 mph. ....	294
Figure 247 Cumulative distribution of the stop-bar speed for false positives produced by the 400 series.....	295
Figure 248 Cumulative distribution of the stop-bar speed for false positives produced by the 600 series algorithm at a false positive rate of 0.01 using a violation threshold of 10 mph. ....	296

Figure 249 Cumulative distribution of the stop-bar speed for false positives produced by the 100 series algorithm at a false positive rate of 0.01 using a violation threshold of 15 mph. ....	297
Figure 250 Cumulative distribution of the stop-bar speed for false positives produced by the 200 series algorithm at a false positive rate of 0.01 using a violation threshold of 15 mph. ....	298
Figure 251 Cumulative distribution of the stop-bar speed for false positives produced by the 300 series algorithm at a false positive rate of 0.01 using a violation threshold of 15 mph. ....	299
Figure 252 Cumulative distribution of the stop-bar speed for false positives produced by the 400 series algorithm at a false positive rate of 0.01 using a violation threshold of 15 mph. ....	300
Figure 253 Cumulative distribution of the stop-bar speed for false positives produced by the 600 series algorithm at a false positive rate of 0.01 using a violation threshold of 15 mph. ....	301
Figure 254 Cumulative distribution of the stop-bar speed for false positives produced by the 800 series algorithm at a false positive rate of 0.01 using a violation threshold of 15 mph. ....	302
Figure 255 Cumulative distribution of the stop-bar speed for false positives produced by the 100 series algorithm at a false positive rate of 0.01 using a violation threshold of 20 mph. ....	303
Figure 256 Cumulative distribution of the stop-bar speed for false positives produced by the 200 series algorithm at a false positive rate of 0.01 using a violation threshold of 20 mph. ....	304
Figure 257 Cumulative distribution of the stop-bar speed for false positives produced by the 300 series algorithm at a false positive rate of 0.01 using a violation threshold of 20 mph. ....	305
Figure 258 Cumulative distribution of the stop-bar speed for false positives produced by the 400 series algorithm at a false positive rate of 0.01 using a violation threshold of 20 mph. ....	306
Figure 259 Cumulative distribution of the stop-bar speed for false positives produced by the 600 series algorithm at a false positive rate of 0.01 using a violation threshold of 20 mph. ....	307
Figure 260 Cumulative distribution of the stop-bar speed for false positives produced by the 800 series algorithm at a false positive rate of 0.01 using a violation threshold of 20 mph. ....	308
Figure 261 Cumulative distribution of the stop-bar speed for false positives produced by the 100 series algorithm at a false positive rate of 0.05 using a violation threshold of 10 mph. ....	309



Figure 262 Cumulative distribution of the stop-bar speed for false positives produced by the 200 series algorithm at a false positive rate of 0.05 using a violation threshold of 10 mph. ....	310
Figure 263 Cumulative distribution of the stop-bar speed for false positives produced by the 300 series algorithm at a false positive rate of 0.05 using a violation threshold of 10 mph. ....	311
Figure 264 Cumulative distribution of the stop-bar speed for false positives produced by the 400 series algorithm at a false positive rate of 0.05 using a violation threshold of 10 mph. ....	312
Figure 265 Cumulative distribution of the stop-bar speed for false positives produced by the 600 series algorithm at a false positive rate of 0.05 using a violation threshold of 10 mph. ....	313
Figure 266 Cumulative distribution of the stop-bar speed for false positives produced by the 800 series algorithm at a false positive rate of 0.05 using a violation threshold of 10 mph. ....	314
Figure 267 Cumulative distribution of the stop-bar speed for false positives produced by the 100 series algorithm at a false positive rate of 0.05 using a violation threshold of 15 mph. ....	315
Figure 268 Cumulative distribution of the stop-bar speed for false positives produced by the 200 series algorithm at a false positive rate of 0.05 using a violation threshold of 15 mph. ....	316
Figure 269 Cumulative distribution of the stop-bar speed for false positives produced by the 300 series algorithm at a false positive rate of 0.05 using a violation threshold of 15 mph. ....	317
Figure 270 Cumulative distribution of the stop-bar speed for false positives produced by the 400 series algorithm at a false positive rate of 0.05 using a violation threshold of 15 mph. ....	318
Figure 271 Cumulative distribution of the stop-bar speed for false positives produced by the 600 series algorithm at a false positive rate of 0.05 using a violation threshold of 15 mph. ....	319
Figure 272 Cumulative distribution of the stop-bar speed for false positives produced by the 800 series algorithm at a false positive rate of 0.05 using a violation threshold of 15 mph. ....	320
Figure 273 Cumulative distribution of the stop-bar speed for false positives produced by the 100 series algorithm at a false positive rate of 0.05 using a violation threshold of 20 mph. ....	321
Figure 274 Cumulative distribution of the stop-bar speed for false positives produced by the 200 series algorithm at a false positive rate of 0.05 using a violation threshold of 20 mph. ....	322

Figure 275 Cumulative distribution of the stop-bar speed for false positives produced by the 300 series algorithm at a false positive rate of 0.05 using a violation threshold of 20 mph. .... 323

Figure 276 Cumulative distribution of the stop-bar speed for false positives produced by the 400 series algorithm at a false positive rate of 0.05 using a violation threshold of 20 mph. .... 324

Figure 277 Cumulative distribution of the stop-bar speed for false positives produced by the 600 series algorithm at a false positive rate of 0.05 using a violation threshold of 20 mph. .... 325

Figure 278 Cumulative distribution of the stop-bar speed for false positives produced by the 800 series algorithm at a false positive rate of 0.05 using a violation threshold of 20 mph. .... 326

Figure 279 Stop bar velocity versus warning distance for the best overall algorithms identified in the stop-controlled intersection simulation. .... 331

Figure 280 Stop bar velocity versus warning distance for the best overall algorithms identified in the signalized intersection simulation. .... 331

Figure 281 The algorithm impact resulting from system latencies for the 634 algorithm. 2

## List of Tables

Table 1 Summary of taxonomy of intersection violations.....	6
Table 2 Summary of results for CICAS-V Subtask 3.3 study.....	8
Table 3 Stop-controlled intersections.....	12
Table 4 Signalized intersections.....	12
Table 5 ICAV Task 5 accuracy guidelines.....	51
Table 6 Stop-controlled DAS system error relative to the validation vehicle's high-accuracy DAS.....	51
Table 7 Signalized DAS system error relative to the vehicle's high-accuracy DAS.....	51
Table 8 Inter-rater test scores for stop-controlled violation reduction.....	53
Table 9 Inter-rater test scores for signalized violation reduction.....	53
Table 10 Potential cluster groupings.....	57
Table 11 Exploratory violation analysis for drivers turning left for the indicated seconds after the light turned red.....	76
Table 12 Possible outcomes of the threat assessment.....	79
Table 13 The selected violation threshold criteria tested at stop-controlled intersections and the resulting violation samples. Total number of samples in the data set was 30,458.....	85
Table 14 The selected violation threshold criteria tested at signalized intersections and the resulting violation samples. Total number of samples in the data set was 2,105,961.....	85
Table 15 First-layer algorithms presented in this report.....	90
Table 16 Stop-controlled intersection algorithms identified by the three heuristics for 0.05 and 0.01 allowable false positive rates at a violation threshold of 15 mph. The cell values represent the true positive rate and false positive rate evaluated at the point shown in Figure 83.....	114
Table 17 Signalized intersection algorithms identified by the three heuristics for 0.05 and 0.01 allowable false positive rates at a violation threshold of 15 mph. The cell values represent the true positive rate and false positive rate evaluated at the point shown in Figure 83.....	115
Table 18 Sample size and the resulting violation frequency for stop-controlled and signalized intersections. At signalized intersections, the sample only includes vehicles that approached the intersection while the signal phase was either yellow or red.....	119
Table 19 Stop-controlled intersection frequency table for the best algorithms identified by the heuristic designed to compromise between providing timely warnings and maximizing the overall number of true positives using a violation threshold of 15 mph (none of the algorithms could meet the minimum specification [true positive rate of at least 0.5] at 10-mph violation threshold for a false positive rate of 0.01).....	120

Table 20 Signalized intersection frequency table for the best algorithms identified by the heuristic designed to compromise between providing timely warnings and maximizing the overall number of true positives using a violation threshold of 15 mph. ....	120
Table 21 Deceleration thresholds and pre-determined deceleration values from 100-car data..	136
Table 22 Deceleration thresholds and pre-determined deceleration values from 100-car data (signalized data).....	137
Table 23 Stop-controlled post processing and radar-induced error.....	146
Table 24 Signalized post processing and radar-induced error.....	146
Table 25 Results from the performed cluster analysis.....	147
Table 26 Summary of GEV fits and the KS test.....	148
Table 27 Summary of GEV fit and KS test for Cluster 1.....	149
Table 28 Summary of Normal Fits and KS test for Cluster 2 through Cluster 4.....	149
Table 29 Summary of normal fit and KS test for brake onset at stop-controlled intersections..	150
Table 30 Summary of fits used in the regression-based threat assessment algorithms for stop-controlled intersections.....	153
Table 31 Summary of fits used in the regression based threat assessment algorithms for signalized intersections.....	157
Table 32 Beta permutation values for 100 series algorithms used at stop-controlled and signalized intersections.....	159
Table 33 Beta permutation values for 200 series algorithms used at stop-controlled and signalized intersections.....	159
Table 34 Beta permutations values for 300 and 400 series algorithms used at stop-controlled and signalized intersections. Algorithms were based on static RDP as a function of reaction time. 300 series algorithms assumed a PRT of 1.01, and 400 series algorithms assumed a PRT of 0.78. ....	161
Table 35 Beta permutation values for 500 series algorithms used at stop-controlled intersections. The algorithm compared the vehicle's TTI to a warning TTI, calculated using a regression of velocity.....	162
Table 36 Beta permutation values for 600 series algorithms used at stop-controlled intersections. The algorithm uses the vehicle's velocity to predict the minimum.....	162
Table 37 Beta permutation values for 700 series algorithms used at stop-controlled intersections. The algorithm used the same measures as the 600 series, but the data sample was truncated by removing velocities greater than 18 m/s (40 mph). ....	164
Table 38 Beta permutation values for 800 series algorithms used at stop-controlled intersections. The algorithm used the same strategy as the 500 series, however this regression equation used range to predict warning RDP.....	164

Table 39 Beta permutation values for 600 series algorithms used at signalized intersections. The algorithm uses the vehicle's velocity to predict the minimum range a warning must be presented to induce a successful stop.....	165
Table 40 Best stop-controlled algorithms for 10 mph. ....	327
Table 41 Best stop-controlled algorithms for 20 mph. ....	327
Table 42 Best signalized algorithms for 10 mph. ....	328
Table 43 Best signalized algorithms for 20 mph. ....	330
Table 44 Stop-controlled data. ....	332
Table 45 Signalized algorithm base rate results. ....	332
Table 46 Odds ratios for environmental variables. ....	5

## Acronyms

ACC: Adaptive cruise control

ADT: Average daily traffic

ANN: Artificial neural network

CAN: Controller area network

CCD: Charge coupled device

CICAS: Cooperative Intersection Collision Avoidance System

CICAS-V: Cooperative Intersection Collision Avoidance System for Violations

CP: Crossing path

DART: Data Analysis and Reduction Tool

DAS: Data acquisition system

DGPS: Differential Global Positioning System

DSP: Digital signal processor

DVI: Diver-vehicle interface

DVR: Digital video recorder

FCC: Federal Communications Commission

FN: False negative

FNR: False negative rate

FOT: Field operation test

FP: False positive

FPR: False positive rate

GES: General estimates system

GEV: Generalized extreme value

GPS: Global Positioning System

ICAS: Intersection Collision Avoidance System

ICAS-V: Intersection Collision Avoidance System for Violations

ICAV: Intersection Collision Avoidance for Violations

ICP: Intersection crossing path

IDS: Intersection decision support

IRB: Institutional Review Board

ITE: Institute of Transportation Engineers

KS: Kolmogorov-Smirnov

LTAP: Left turn across path

LTAP/LD: Left turn across path – lateral direction

LTAP/OD: Left turn into path – opposite direction  
LTIP: Left turn into path  
NHTSA: National Highway Traffic Safety Administration  
NTSC: National Television System Committee  
POV: Principal other vehicle  
PRT: Perception reaction time  
RDP: Required deceleration parameter  
ROC: Receiver operation characteristics  
RTIP: Right turn into path  
SCP: Straight crossing path  
VTTI: Virginia Tech Transportation Institute  
SDT: Signal detection theory  
SV: Subject vehicle  
TCD: Traffic control device  
TIP: Turn into path  
TN: True negative  
TNR: True negative rate  
TP: True positive  
TPR: True positive rate  
TTI: Time to intersection  
USDOT: United States Department of Transportation  
VDOT: Virginia Department of Transportation

## Introduction

The Cooperative Intersection Collision Avoidance Systems for Violation (CICAS-V) project aims to develop and test a cooperative system based on 5.9 GHz DSRC to reduce the number of crashes in intersections due to violations of stop light and stop sign traffic control devices. These crashes account for thousands of injuries and fatalities in the United States every year (National Highway Traffic Safety Administration, 2006). To reduce these crashes, the CICAS-V presents a timely and salient in-vehicle warning to those drivers who are predicted to violate a stop light or a stop sign. The warning is intended to elicit a behavior from the driver that will cause him or her to avoid a potential violation which could lead to an intersection crash.

### 1.1 Subtask 3.2 Overview

The CICAS-V project involves numerous tasks. The overall goal is to design, develop, and evaluate a warning system to assist drivers in avoiding intersection crashes that result from a driver either violating a stop sign or stop light traffic control device. Task 3 of the CICAS-V project is primarily concerned with the human-machine interaction of the CICAS-V system. Within Task 3, four Subtasks were created to address the following system design inputs:

- Subtask 3.1 – Mine the 100-Car database to
  - Determine which drivers should receive a warning.
  - Determine preliminary driver vehicle interface (DVI) arrangement.
- Subtask 3.2 – Collect and analyze a large sample of intersection approaches to
  - Determine appropriate warning timing to maximize system effectiveness while minimizing false warnings.
  - Develop and evaluate threat assessment algorithms.
  - Recommend a set of algorithms for system-level testing in Subtask 3.4
- Subtask 3.3 – Conduct test-track experiments to
  - Determine the best DVI for the CICAS-V system.
  - Provide appropriate warning timing for drivers receiving a warning.
  - Recommend DVI for system-level testing in Subtask 3.4
- Subtask 3.4 – Perform a pilot test of the CICAS-V system to
  - Test the system and driver under live-traffic conditions.
  - Evaluate driver acceptance and unintended consequences.

The following report describes the work performed as part of Subtask 3.2. Data were collected at eight intersections in the New River Valley area of southwest Virginia. The intersections were selected as representative of those that are expected to benefit from a CICAS-V system. Data collection equipment was installed at the designated intersections, and vehicle data were obtained for every vehicle approaching these stop-controlled and signalized approaches.

Data analysis focused on developing a working algorithm to predict driver stopping behavior at intersection approaches, for the purpose of providing a warning to a violating driver. From the raw data collected, driver approach behavior was dissected and analyzed for trends. Threat assessment algorithms designed to predict whether or not a driver would stop were developed and then evaluated in a pseudo-real-time simulation using this data.



The performance of each potential algorithm was based on its effectiveness to predict a pending violation while minimizing false detections. In addition, other measures were considered: the location at which a violation warning was provided, likelihood of annoyance, algorithm complexity, and data requirements. Two algorithms for stop-controlled intersections and two algorithms for signalized intersections were recommended for the system-level tests of Subtask 3.4. In addition, this research project will feed into a growing body of knowledge regarding intersection approach behavior and, in particular, intersection collision avoidance.

## 1.2 Background

Intersection crashes constitute over 35 percent of the nation's traffic-related fatalities (NHTSA, 2005). Currently, there is a major federal/industry initiative underway to determine the efficacy of Intersection Collision Avoidance Systems (ICAS). One objective of an ICAS is to mitigate crashes by providing warnings to drivers who might otherwise violate a signalized or stop-controlled intersection. This report presents the results of an effort to determine driver approach behavior at intersections. Its purpose is to support the development of the threat assessment algorithm component of a stop-controlled and signalized CICAS-V.

To provide an effective violation warning to a driver, the CICAS-V must discriminate between compliant and non-compliant stopping behavior. This discrimination must be performed significantly upstream from the intersection so that drivers have sufficient time to perceive the warning, react, and stop their vehicles if necessary. Drivers with varying levels of experience, judgment, cognitive state, and risk tolerance will respond differently as they approach an intersection. As a result, the behavior of a compliant driver may overlap with that of a violating driver at locations where a countermeasure should be deployed. This could lead to cases in which a driver who did not need a warning receives one or vice versa. Thus, engineers and designers must work to construct a threat assessment algorithm that enhances safety while avoiding unnecessary alarms.

Over the past four years, a significant volume of test-track research has been completed on ICAS (e.g., Lee et al. , 2005; Neale, Perez, Doerzaph, & Stone, 2005). From this project, a substantial amount of knowledge has been acquired about driver response to various ICAS countermeasure types. Subtask 3.3 of the CICAS-V project further enhances this research by focusing on deployable warnings and by further refining the driver-vehicle interface (DVI) (Perez, Neale, Kiefer, Viita, Wiegand, in review). The test-track environment has worked well for making relative comparisons between countermeasure options and determining at what point an inattentive driver must receive a warning in order to stop. Nonetheless, test-track data are limited when applied to algorithm design. This is due to the complex and dynamic nature of real-world intersection approaches, the rarity of violations, possible experimental effects, and the complexity of driver behavior (e.g., distractions, motivations, etc.).

Infrastructure-based data at live intersections across a variety of driving conditions provides additional information to tackle the multifaceted problem of algorithm development. From this data, an algorithm has been created to better represent actual driver behavior as an intersection is approached. The algorithm developed under Subtask 3.2 will be combined with the outputs of the other human factors and system development tasks to provide proof of the CICAS-V concept.

The warning timing, coupled with the DVI, will ultimately determine the effectiveness of CICAS-V. Alarms that sound too early will likely deflate the safety benefits of collision avoidance systems because of annoyance and loss of user trust in the system (Neale and Dingus, 2006). Warnings that are too late will fail to prevent a potential intersection collision. Thus, it is imperative that researchers and engineers thoroughly investigate driver behavior at intersections. In particular, the detailed analyses of trajectories of the intersection approaches must be analyzed to better understand how and when to warn appropriately.

This report describes an experimental investigation performed at live stop-controlled and signalized intersections to gather naturalistic driver approach behavior. Five stop-controlled and three signalized intersections in the New River Valley area of Virginia were selected for data collection. The sites were selected based on their intersection characteristics, traffic volume, and crash statistics. Data were collected from each site for at least two consecutive months and were analyzed to determine how drivers approach intersections at various speeds and under differing environmental conditions. Further, they were used to explore the feasibility of providing warnings to drivers who would otherwise violate the traffic control device.

Previous ICAS and general intersection research has provided a substantial amount of preliminary knowledge regarding appropriate warning timing. The following sections introduce the work completed to date. Numerous studies, consisting primarily of database analyses, have been conducted in order to examine factors that may be involved in intersection control device violations and crashes. A review of these studies provides numerous scenarios, environmental factors, and driver characteristics that were found to contribute to the large number of intersection crashes each year. This ICAS background was used as a foundation for the experimental design and site selection presented in the methods section.

### **1.2.1 Intersection Crash Problem Overview**

The CICAS-V system in development is designed primarily to address crossing path (CP) crashes that result from a violation of the stop-sign or stop-light Traffic Control Device (TCD). Violation-related CP maneuvers account for 393,000 annual crashes at a cost of 39 billion dollars (Lee et al., 2005). In 2000, there were approximately 162,000 CP crashes occurring at intersections in which a stop sign was present and where one driver was charged with a violation (Lee et al., 2005). Additionally, approximately 99,000 crashes involving a signalized intersection violation were reported in 2000 (Lee et al., 2005).

The purpose of the following section is to deconstruct the intersection CP crash problem. The discussion will begin with an introduction to terminology, followed by a review of the factors that influence intersection crashes. Next, the typical vehicle intersection approach will be dissected by considering environmental factors and required driver decisions with respect to human capabilities and limitations. The focus of this discussion is to understand and to attempt to predict the factors leading to intersection CP crashes.

### **1.2.2 Intersection Crash Taxonomy**

Because the incidence and severity of intersection-related crashes vary with, among other factors, the relative positions and travel directions of the vehicles involved, researchers have created different taxonomies of intersections and intersection crash types. These classifications are based on the various combinations of vehicle conflicts that can occur when the paths of two cars intersect in a traffic-controlled setting. Using these systems allows researchers to gather

statistics on, re-create, analyze, experiment with, and communicate particular intersection-crash situations in a repeatable manner. For this study, these taxonomies were used to select intersections, identify maneuvers for study, and communicate the results throughout this report.

Crash taxonomies consider the two different vehicles that must be present for an intersection crash to occur: the subject vehicle (SV) and the principal other vehicle (POV). The vehicle of interest is the SV; its travel path is intersected by the POV. The actions of the SV initiate the conflict sequence because it is a violating vehicle. The POV has the right of way in these crash sequences. Combining taxonomies from several sources (Ferlis, 2001b; Wang & Knipling, 1994; Najm, Mironer, Koziol, Wang, & Knipling, 1995; Pierowicz, Jocoy, Lloyd, Bittner, & Pirson, 2000), three primary classifications are presented below in a graphical format (Figure 3, Figure 4, Figure 5).

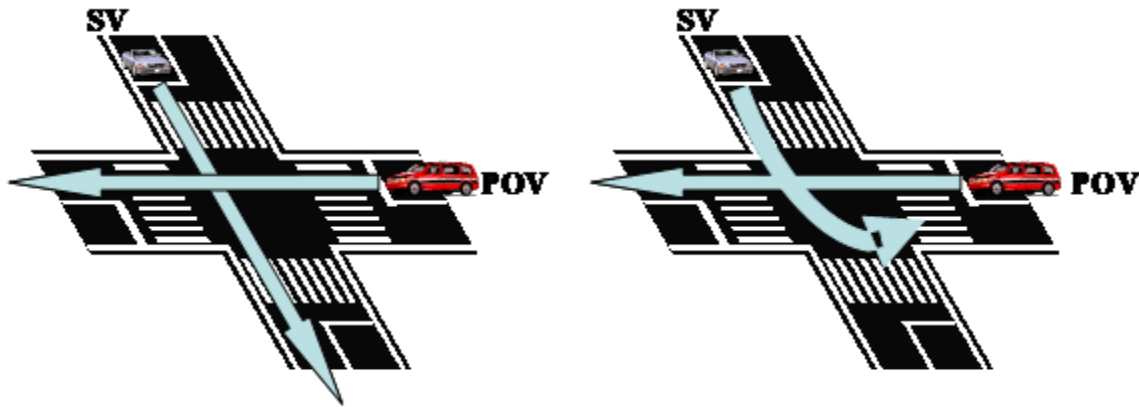


**Figure 3 Intersection straight crossing path (SCP).**



**Figure 4 Left turn across path (LTAP).**

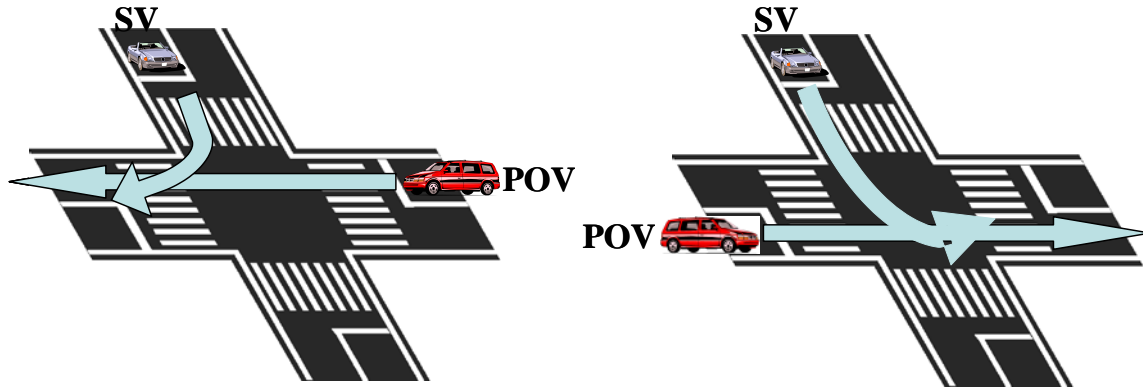


**Figure 5 Turn into path (TIP) – merge conflict: a) right – RTIP, b) left – LTIP.**

Intersections are a type of junction that do not include driveway or alley access and that are contained within the boundary lines of the roadway (Zabyszny & Ragland, 2003). Nearly 60 percent of U.S. crashes occur in the presence of a junction. Intersection crashes represent the largest contributor to the problem, comprising 44 percent. Other junction crashes include driveway/alley access (10.6 percent), entrance/exit ramp (2.6 percent), rail grade crossing (0.9 percent), and other (1.7 percent) (Zabyszny & Ragland, 2003).

Crash incidence data, segregated by classification, indicate the largest proportion of intersection crashes are classified as Straight Crossing Path (SCP) (Ferlis, 1999). General Estimates System (GES) data from 1998 also indicated the prevalence of SCP crashes in the distribution shown below (Smith & Najm, 1999). These results are supported by Wang and Knipling (1994), as well as Zabyszny and Ragland (2003), who demonstrated similar distributions of crossing path crashes.

- Straight crossing path (SCP) 36.6%
- Left turn across path/opposite dir. (LTAP/OD) 27.3%
- Left turn across path/lateral dir. (LTAP/LD) 15.9%
- Left turn in path (LTIP) 4.7%
- Right turn in path (RTIP) 4.7%

### 1.2.3 Intersection Violation Causation

Violations occur frequently (up to 20 per hour) for both signalized and stop-controlled intersections (Wierwille et al., 2000; Wierwille et al., 2001); however, not every TCD violation results in a crash. Crashes result when the timing of the violation aligns with the presence of a conflicting vehicle(s) or other object. Identifying when a crash will occur, based on the interactions of multiple vehicles, is a difficult problem. An alternative method for preventing intersection crashes due to violations is to mitigate the violations themselves. As such, characteristics of violation approaches contribute to the design of the threat assessment algorithm. The purpose of this section is to determine factors that contribute to drivers violating a TCD.

CICAS-V is intended to mitigate intersection crashes by preventing violations. As such, it is productive to review the types and causes of intersection violations. Fakhry and Salaita (2002) have provided some definitions of intersection violations. These classifications, provided below in Table 1, categorize the vehicle as either “at speed,” “rolling stop,” or “stop and go.” These particular classifications do not provide a breakdown of the speed at which the driver is moving through the intersection under each classification.

**Table 1 Summary of taxonomy of intersection violations.**

Intersection Type	Violation	Definition
Stop-Controlled Intersection	At Speed	Vehicle does not slow down and proceeds through the intersection. Also included are vehicles that “barely slowed” as they approached the intersection.
Stop-Controlled Intersection	Rolling Stop	Wheels of a vehicle are slowing but not stopping and the vehicle continues through the intersection.
Signalized Intersection	At Speed	No attempt is made to stop when proceeding through the intersection during the red cycle.
Signalized Intersection	Rolling Stop	Driver makes a right-hand turn during the red cycle without coming to a complete stop and proceeds through the intersection.
Signalized Intersection	Stop and Go	Driver stops, then proceeds without waiting for the signal to turn green.

As cited in Fakhry and Salaita, 2002.

Direct observations of violations provide some insight into the extensive issue of intersection violations. Fakhry and Salaita (2002) reported that at-speed violations occurring at stop-controlled intersections were recorded approximately 20 times more often than at signalized intersections. They also reported that, out of 1,000 intersection approaches, 17.5 vehicles committed stop-controlled violations, while only 1.5 committed signalized violations. Overall, rolling-stop violations greatly exceeded at-speed violations at both signalized and stop-controlled intersections. As will be demonstrated in the results section, the high prevalence of rolling stops suggests targeting the CICAS-V warning to at-speed violations.

In Subtask 3.1 of the CICAS-V project, Sudweeks et al. (in review) conducted an analysis of stop-controlled and signalized violations and near violations. This analysis used data collected in the 100-Car Naturalistic Driving Study (Dingus et al., 2006), in which 100 vehicles were instrumented to collect behavioral and environmental data in a naturalistic driving setting. The study identified violations and near violations for 77 primary drivers at the 143 stop-controlled and 168 signalized intersections analyzed. Sudweeks et al. (in review) found that 61 percent of stop-controlled violations occurred at stop-bar speeds greater than 10 mph, while 39 percent occurred between 6 and 10 mph. Roughly 50 percent of violating drivers at stop-controlled intersections crossed straight through the intersection, 27 percent of violators performed left-turn maneuvers, and 23 percent performed right-turn maneuvers. Sudweeks et al. (in review) also reported that approximately 96 percent of violations at signalized intersections involved a right-turn maneuver. The average stop-bar speed of signalized intersection straight crossing violations was 40 mph.

As reported by ITE (2003) one survey presented drivers with a scenario in which they were approaching an intersection that had been in the yellow light stage for several seconds. Drivers were asked if they would either slow down to stop at the red light or speed up in order to make it through the intersection before the red light. Twenty-nine percent of the drivers indicated they would have sped up in order to beat the red light. Of those drivers, 69 percent indicated that their motivation was due to being in a rush or to save time, and 12 percent reported doing it out of frustration.

The decision to run or attempt to beat a traffic signal is due to a belief that a collision can be avoided. This belief could be based upon the failure to see cross traffic, misjudgment of the velocity, distance, or direction associated with perceived traffic, or the assumption that other vehicles will yield to the violating vehicle. Although 99 percent of surveyed drivers acknowledged the dangers of red light running, they also perceived a low likelihood of receiving a ticket for the infraction (ITE, 2003).

Drivers who tend to run red lights are a population that is more likely to be driving while impaired by alcohol, have invalid driver's licenses, and have prior infractions (particularly prior intersection violation citations) (ITE, 2003; Retting et al., 1999). In a survey, 55.8 percent of the respondents self-reported running red lights (ITE, 2003). Those who admitted to intentional red light running tended to be younger drivers without children who were driving without passengers, unemployed, or in a job requiring less education, and rushing to work or school.

Driver behavior is a large area of interest in determining the cause of violations. Sudweeks et al. (in review) found that driving-related inattention (i.e., driving-related task that diverts the driver's attention from the forward roadway [Klauer, Dingus, Neale, Sudweeks & Ramsey, 2006]), coupled with secondary tasks, resulted in the largest number of stop-controlled violations. The most frequently observed secondary tasks were talking on a cell phone, passenger distraction, and talking or singing with no obvious passenger. The most frequent secondary tasks reported in signalized violations and near violations were talking or singing with no obvious passenger, passenger distraction, and cell phone usage.

For more information regarding violation type and prevalence, refer to the CICAS Subtask 3.1 report (Sudweeks et al., in review).

#### **1.2.4 CICAS-V Warning Systems**

A CICAS-V warning should be timed so as to provide the driver ample time to recognize the alarm, react, and stop before committing a violation. In addition, a warning system should be able to recognize a compliant driver versus a non-compliant driver in order to reduce nuisance alarms.

Maltz and Shinar (2004) conducted a simulator study in which participants were presented with various warning interfaces to study the effects of false alarms on driver response. A warning was given to the participant when the participant's vehicle was too close to the lead vehicle. Drivers were given both true and false alarms over the course of the study. The results demonstrate that drivers who received a warning spent less time in the danger zone (i.e., when the participant's vehicle had less than 2 seconds temporal headway from the lead vehicle). It was also reported that drivers responded quicker to true alarms and were also able to differentiate between true and false alarms. When responding to false alarms, drivers were more likely to

respond to situational context as opposed to relying solely on the warning. As a result, drivers did not become overly dependent on the warning system.

Driver reliance depends on the alarm's credibility and tends to decrease as the system proves to be ineffective (i.e., presents false alarms). As a result, driver response may decrease or drivers may begin to discount the warning system. Conversely, if drivers become too reliant on the warning system, they may begin to disregard important stimuli in the surrounding environment (Yamada & Kuchar, 2006). For these reasons, the CICAS-V warning must accurately identify violators while providing a warning that discourages abuse (e.g., provide the warning late so that it is uncomfortable to use it as a decision aid).

The Intersection Collision Avoidance-Violation (ICAV) study (Lee et al., 2005) examined varying DVIs that would assist drivers and prevent intersection violations. The ICAV project studied the required deceleration of vehicles at varying speeds in order to determine the correct timing of the warning. ICAV ran multiple groups of participants, for both too late and too early warnings, until a warning timing was found in which 100 percent of the participants stopped before committing a violation. The "STOP" [auditory] + stop sign [visual] warning provided a high percentage of compliant drivers (i.e., drivers who stopped within the "No Violation" zone). A haptic brake pulse was also tested and provided the same percentage of compliance as the "STOP" + stop sign warning. The warning onset for the selected DVI was 2.65 s time to intersection (TTI) for a vehicle travelling 35 mph and 3.32 s TTI for a vehicle travelling 45 mph.

As previously mentioned, CICAS-V Subtask 3.3 (Perez et al., in review) conducted research to determine the most effective DVI to present to drivers in order to prevent intersection violations. The study was conducted on Virginia Department of Transportation's Smart Road Test Track and presented naive participants with various DVIs, including a visual warning, an auditory warning, and a single brake pulse. After collecting data from 172 participants through 11 studies, researchers suggested that a DVI with a combination visual, auditory (spoken), and brake pulse warning would provide the most effective results. Table 2 provides information for each of the naturalistic DVIs tested in Subtask 3.3 (Perez, Neale, Viita, & Wiegand, in review). The warning timing and reaction time of participants to these DVIs provided inputs to a number of the tested algorithms (see Section 7).

**Table 2 Summary of results for CICAS-V Subtask 3.3 study.**

<b>DVI*</b>	<b>TTI (s)</b>	<b>Number of drivers who complied</b>	<b>Number of drivers who did not comply</b>
CAMP Tone	2.44	7 (39%)	11 (61%)
Speech	2.44	7 (39%)	11 (61%)
CAMP Tone with Brake Pulse	2.44	14 (78%)	4 (22%)
<b>Speech with Brake Pulse</b>	<b>2.44</b>	<b>17 (94%)</b>	<b>1 (6%)</b>
Beep Tone with Brake Pulse and PBA	2.24	5 (50%)	5 (50%)

<b>Speech with Brake Pulse and PBA</b>	<b>2.24</b>	<b>16 (89%)</b>	<b>2 (11%)</b>
Speech with Brake Pulse and PBA	2.04	7 (78%)	2 (22%)
<b>Speech with Brake Pulse and PBA</b>	<b>1.84</b>	<b>3 (33%)</b>	<b>6 (67%)</b>

All of these studies featured a visual display that performed both advisory and warning functions (only the advisory function of this display was used in Study 11).

Studies in bold used the warning recommended based on the results presented in this report.

### 1.2.5 Prior Algorithm Development

Most human factors research is concerned with how a typical person responds under a given set of circumstances. Often, human factors engineers design a system for use by most people by considering the majority of the population (Sanders & McCormick, 1993). In contrast, a collision avoidance system is specifically designed to address uncommon driver decisions. To minimize nuisance alarms, the CICAS-V algorithm must distinguish between compliant drivers and violators, so that a countermeasure is directed to those drivers who need it.

Certain types of intersection approaches present a significant challenge for a threat assessment algorithm. The vehicle of a driver who performs a late aggressive stopping maneuver will demonstrate similar kinematic signatures to violating vehicles. Furthermore, rolling stops present a challenge at stop-controlled intersections and during right-turn maneuvers at signalized intersections. Presumably, rolling stops are performed by a driver who is aware of the TCD but feels it is safe to proceed. A driver rolling past a stop bar may be a violator; however, because this driver is aware and likely making a safe maneuver, the question arises of whether it is appropriate to issue a warning. The presence of these challenges has led to some previous investigations of CICAS-V algorithms.

Support for the feasibility of a CICAS-V algorithm at live intersections is provided by White and Ferlis (2004), in which a hand-held radar gun was used to collect the intersection approach behavior of drivers at four intersections. The researchers collected data for two groups of drivers: those who were stopping for a red light and those who were going through a green light. It was presumed that drivers who went through a green signal would act identically to an inattentive violator. Drivers who received the phase change were not included in the sample, so the scenario is similar to a stop-controlled approach (approaching a red light should be similar to approaching a stop sign).

The data set consisted of 270 samples taken at the four intersections. Only approaches in which the subject vehicle was alone were included. The speed and acceleration profiles of vehicles were then used to graphically distinguish the groups prior to reaching the intersection. The initial speeds of both groups overlapped considerably. As drivers approached the intersection, those who intended to go would exhibit a relatively constant speed profile. The drivers who intended to stop would exhibit decreasing speed. At some point, the two curves would completely diverge, which was thought to indicate a location at which the threat assessment can be made.

The study by White and Ferlis (2004) provides proof-of-concept for a CICAS-V algorithm in a simplified scenario; however, the assumption that drivers going through a green light are



identical to inattentive violators must be validated. An inattentive violator may attend to the TCD at some point prior to entering the intersection. This could result in many different driver actions, such as acceleration or heavy and/or late braking, which may influence the threat assessment.

The ICAS-V work performed by VTTI under the IDS contract performed a preliminary algorithm development (Neale, Perez, Doerzaph & Stone, 2005). Three general types of algorithms were constructed, based on three types of potential sensing equipment used in the ICAS: single point (vehicle data were measured at a single point on the approach); multi-point (vehicle data were measured at several discrete points on the approach); and continuous (vehicle data measured at all points on the approach). A comparison of the schemes clearly showed that an algorithm based on continuous detection performed more accurately than the other two options. In addition, the ongoing CICAS-V project indicates that the continuous detection scheme is the most likely deployment architecture. Therefore, only the algorithms based on continuous detection will be discussed further.

Seven continuous detection algorithms in all were tested during the IDS project. These relevant seven will be discussed further in the algorithm development section of the results chapter. The curious reader should refer to Neale et al., 2005 for more information regarding them. The data used to test these algorithms had limitations. In particular, these data were based on a small sample of drivers who approached a signalized intersection on a test track. A small sample of drivers cannot capture the range of possible intersection approaches. Furthermore, the study did not account for the variety of factors that can affect the intersection approach trajectory (i.e., distractions, individual motivations, and weather).

Despite these limitations, the preliminary IDS algorithm work guided the initial methods that were expanded and refined during this subtask. The results of the IDS analysis lead to conclusions regarding the usefulness and applicability of the various algorithm options. The tests eliminated some basic algorithms, based on high rates of false alarms when compared with other options. Five algorithms were recommended in the IDS report (Neale et al., 2005) for future consideration. These algorithms were reviewed during the algorithm development, and three were included in the algorithm evaluation analyses.

## 2 Data Collection Sites and Apparatus

The following sections describe the methods used to generate a database of stop-controlled and signalized intersection approaches. The sections describe the process of selecting the test sites, development of the data acquisition system (DAS), test site installation, data management methods, and approvals.

### Site Selection

Located in the New River Valley area of southwest Virginia, six stop-controlled approaches across five intersections and every approach at three four-way signalized intersections were selected for data collection. While considering the literature described previously, these sites were selected based on intersection characteristics (e.g., roadway design speed, number of lanes, protected and unprotected turn lanes, intersection box size, geometry of approaches), crash statistics, traffic volume, and recommendations by the Virginia Department of Transportation (VDOT).

The selection process began by gathering detailed information about the intersections with the assistance of representatives from the Salem District VDOT, the Blacksburg Police Department, and the Christiansburg Police Department. The information provided crash and violation data, as well as anecdotal data, on intersections in the region. From these data, several intersections were chosen for site visits, during which further information regarding geometry, signage, locality, and intersection type was gathered.

Site visit information was added to a database and compared to a list of selection criteria. Sites meeting the selection criteria were kept for further consideration. These criteria are listed below, and were established based on literature reviewed, the requirements of the study, the collection apparatus, and the feasibility of implementation.

Selected stop-controlled intersections must:

- Represent intersections of the configuration found across the United States.
- Contain a balanced set of posted approach speeds (25 mph, 35 mph, and 45 mph)
- Be free from obstructions to install and operate the DAS
- Be equipped with sufficient shoulders to allow for safe DAS access
- Have a location reasonably close to VTTI for data retrieval
- Be located within VDOT's Southwest Region for installation assistance and approval
- Be in range of differential global positioning system (DGPS) corrections for calibration/validation
- Have a minimum of 150 meter radar sight distance

Selected signalized intersections must:

- Have mast-arm mounted signals
- Have load carrying ability to support the radar antenna and camera
- Have line of site to radar antenna location for at least 150 m
- Have suitable location to mount DAS
- Have power capability to house DAS
- Be located within VDOT's Southwest Region for installation assistance and approval

- Have standard (ITE-recommended) signal phase timing
- Not have parked cars or other radar obstructions.

A pool of candidate intersections was selected based upon these criteria, the probability of obtaining relevant data, and the crash and average daily traffic (ADT) statistics. To make the final selection, representatives of the USDOT visited the remaining test sites. Six stop-controlled approaches at five intersections and three signalized intersections were selected. Table 3 and Table 4 below provide a list of all the selected intersections and the corresponding speed limits. The following pages provide images depicting a map that details measurements of each of the selected stop-controlled intersections, an aerial view, and ground images of each site. Ground images were captured from site visits and aerial images later extracted from <http://maps.live.com> (Microsoft®, 2008).

**Table 3 Stop-controlled intersections.**

<b>Intersection</b>	<b>Posted Speed Limit</b>
Clubhouse & Lusters Gate	25 mph
Plank & Lusters Gate	25 mph
Nellies Cave & Woodland Hills	35 mph
Fairview Church & HW8	35 mph
Meadow Creek & Childress Eastbound	45 mph
Meadow Creek & Childress Westbound	45 mph

**Table 4 Signalized intersections.**

<b>Intersection</b>	<b>Posted Speed Limit</b>
Franklin & Elm & Independence	25 mph, 35 mph, & 45 mph
Depot & Franklin	25 mph & 35 mph
Bus460 & VA-114	35 mph & 45 mph

### Stop-Controlled Intersection Test Sites

The intersection of Clubhouse Road and Lusters Gate Road is a three-way intersection with a single stop sign for vehicles traveling west on Clubhouse (Figure 6, Figure 7, Figure 8). A driveway opposite to the clubhouse approach may appear to some drivers as a fourth leg of the intersection. The posted speed limit on Clubhouse is 25 mph and the posted speed limit for traffic traveling on Lusters Gate is 45 mph. The entering ADT for this intersection is 2,084 and typically has less than one accident per year.

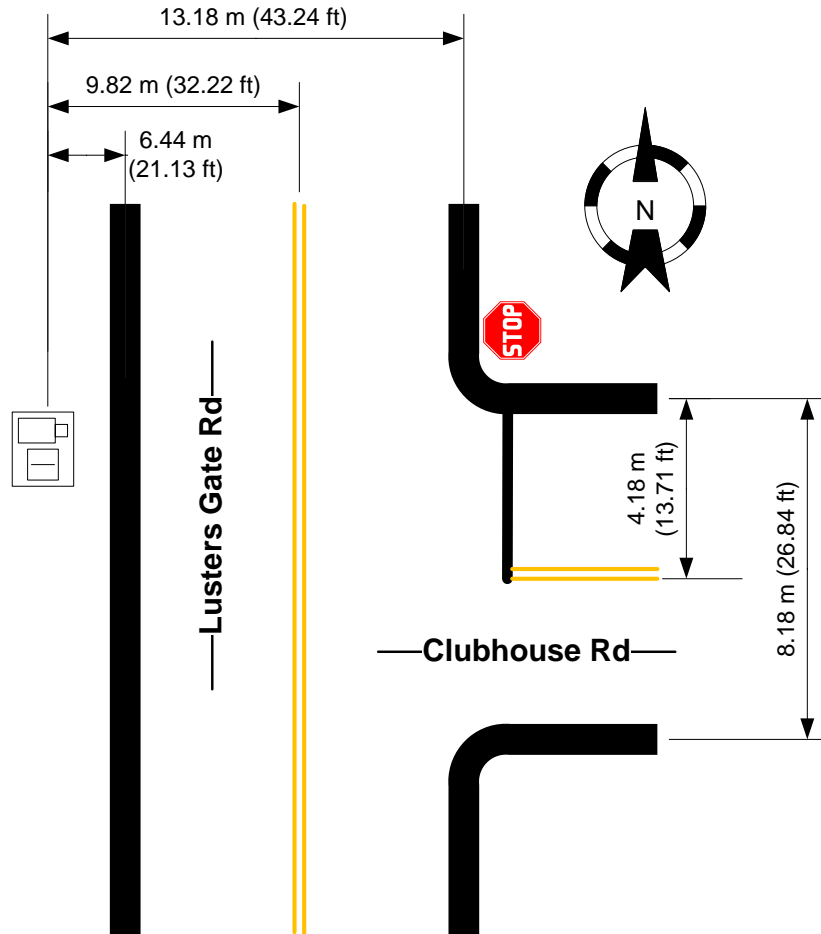


Figure 6 Diagram of Clubhouse & Lusters Gate intersection.



Image is the copyrighted work of Microsoft® and subject to the terms and conditions of the Microsoft® license agreement.

Figure 7 Aerial view of Lusters Gate & Clubhouse intersection [image obtained through Microsoft® (2008)].



Figure 8 Ground images of Clubhouse & Lusters Gate intersection.

The intersection of Plank Drive and Lusters Gate Road is a three-way stop-controlled intersection with a single stop sign for vehicles traveling west on Plank (Figure 9, Figure 10, Figure 11). The speed limit approaching the stop sign is 25 mph, and traffic traveling on Lusters Gate has a posted speed limit of 45 mph. VDOT records show the entering ADT at 1,794 and a typical crash rate of less than one per year.

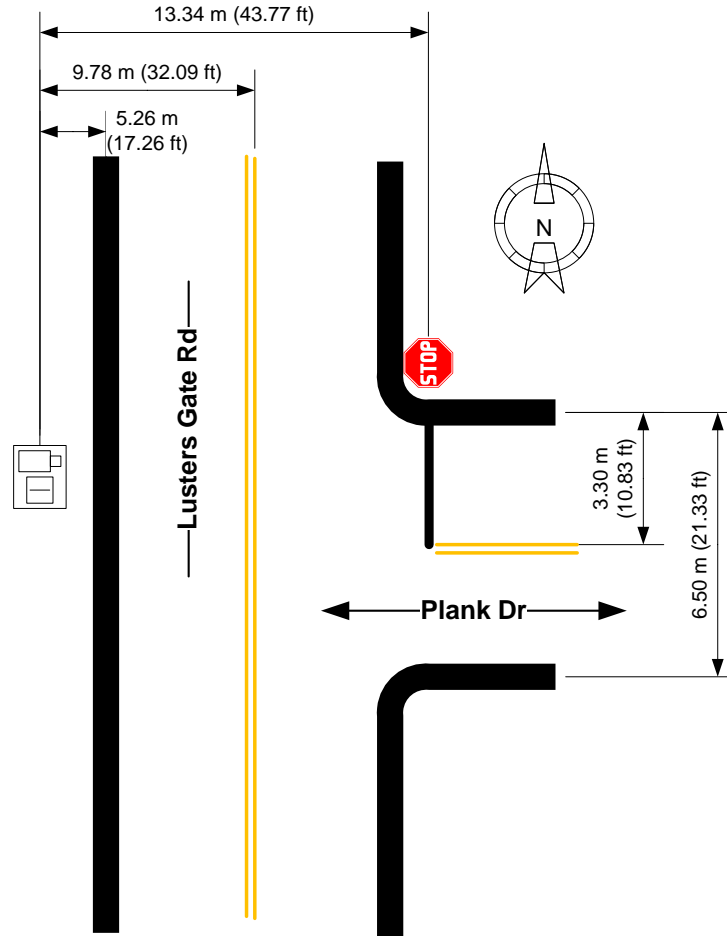


Figure 9 Diagram of Plank & Lusters Gate intersection.



Image is the copyrighted work of Microsoft® and subject to the terms and conditions of the Microsoft® license agreement.

**Figure 10 Aerial view of Plank & Lusters Gate intersection [image obtained through Microsoft® (2008)].**



**Figure 11 Ground images of Plank & Lusters Gate intersection.**

The intersection at Nellies Cave Road and Woodland Hills is a three-way intersection with a single stop sign for vehicles traveling north on Nellies Cave (Figure 12, Figure 13, Figure 14). Vehicles traveling through the Nellies Cave and Woodland Hills intersection have a posted speed limit of 35 mph. The entering ADT for this intersection is 1,674 and there was an average of one accident per year reported at this intersection.

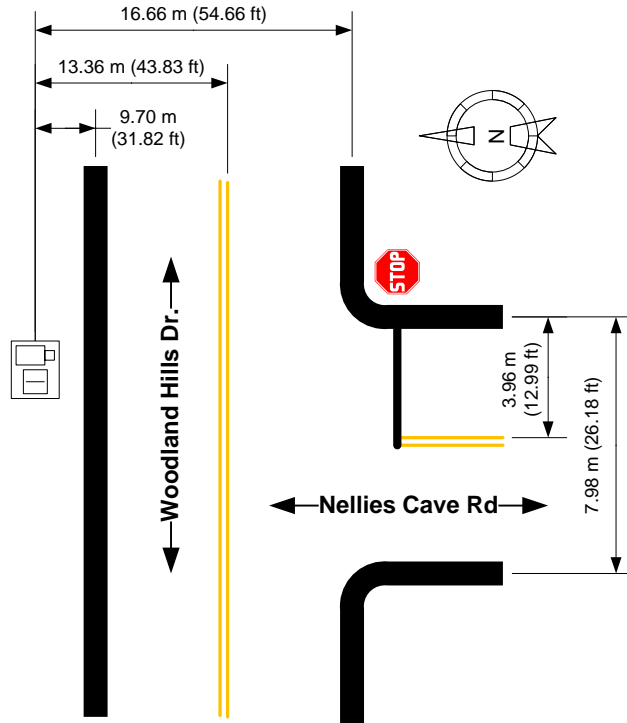


Figure 12 Diagram of Nellies Cave & Woodland Hills intersection.





Image is the copyrighted work of Microsoft® and subject to the terms and conditions of the Microsoft® license agreement.

**Figure 13 Aerial view of Nellies Cave & Woodland Hills intersection [image obtained through Microsoft® (2008)].**



**Figure 14 Ground images of Nellies Cave & Woodland Hills intersection.**

The intersection of Fairview Church Road and Highway 8 is a four-way intersection with stop signs presented to traffic traveling both directions on Fairview Church Road (Figure 15, Figure 16, Figure 17). The posted speed limit for traffic traveling through this intersection is 35 mph. The entering ADT for this intersection is 8,110 and there is an average of four annual crashes at this intersection.

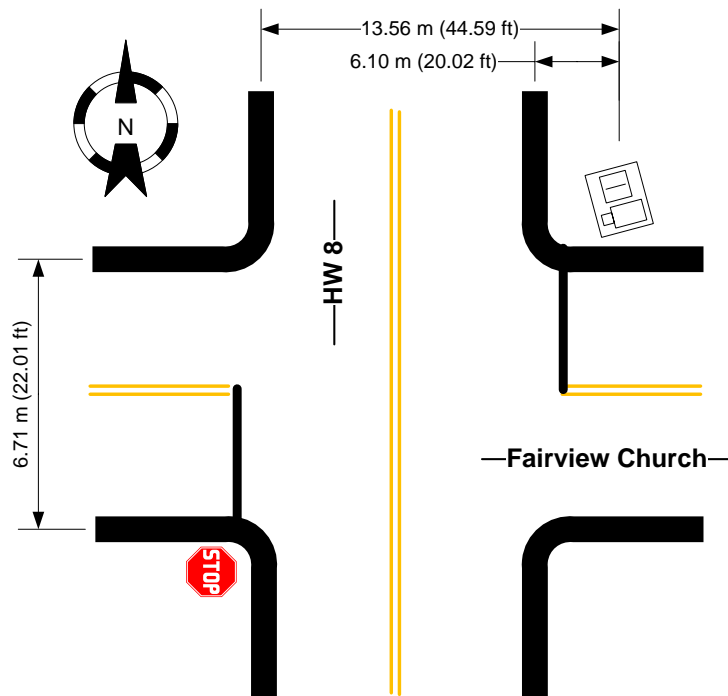


Figure 15 Diagram of Fairview Church & HW8 intersection.

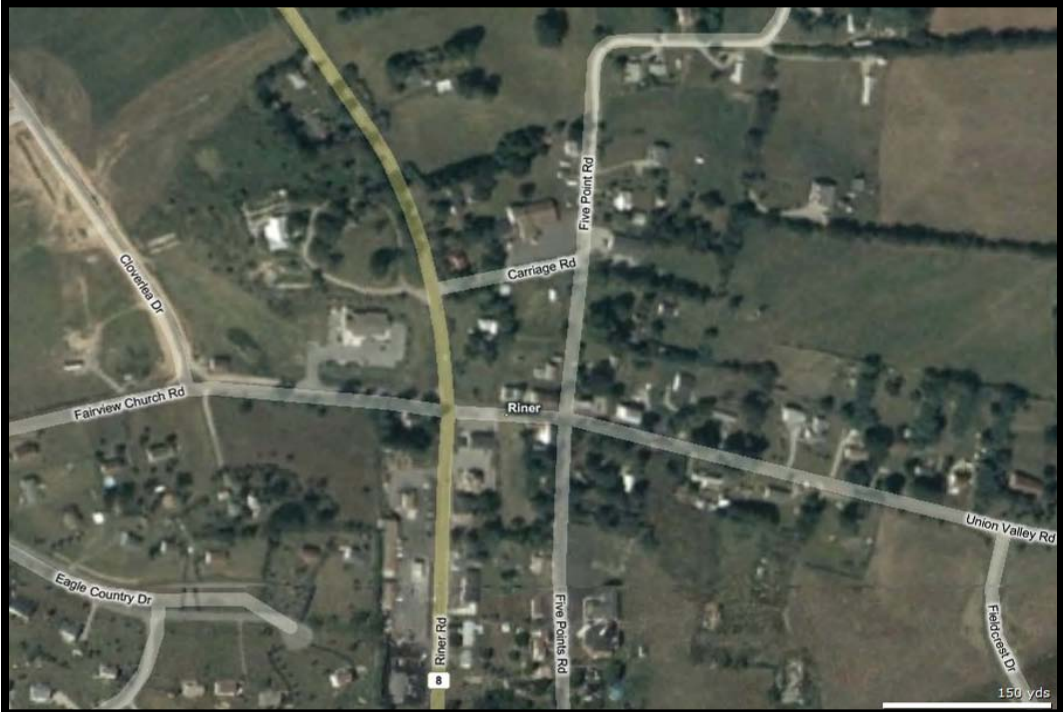


Image is the copyrighted work of Microsoft® and subject to the terms and conditions of the Microsoft® license agreement.

Figure 16 Aerial view of the Fairview Church & HW8 intersection [image obtained through Microsoft® (2008)].



**Figure 17 Ground images from Fairview Church & HW8 intersection.**

The intersection of Meadow Creek and Childress is a four-way intersection. A dual set of stop signs (two stop signs at each pole) are located in each direction on Meadow Creek (Figure 18, Figure 19, Figure 20). The posted speed limit for traffic on both Meadow Creek and Childress is 45 mph. The entering ADT for this intersection is 3,010 and there is an average of five annual crashes at this intersection. This intersection is listed in VDOT's 2006 Critical Rate Report, which identifies intersections in the state with high crash statistics.

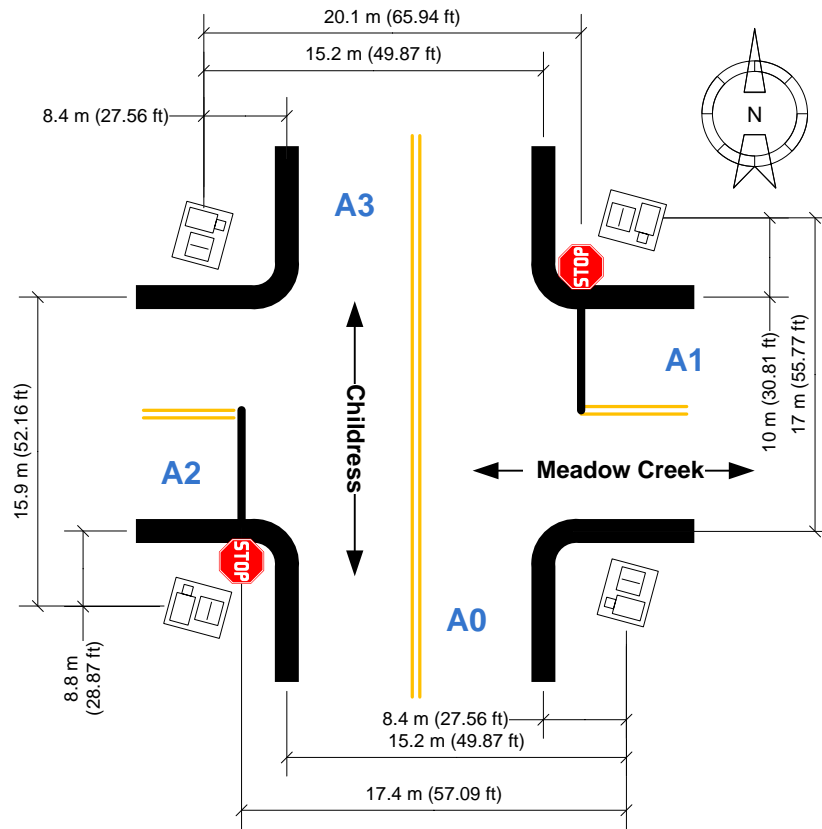


Figure 18 Diagram of Meadow Creek & Childress intersection.





Image is the copyrighted work of Microsoft® and subject to the terms and conditions of the Microsoft® license agreement.

**Figure 19** Aerial view of the Meadow Creek & Childress intersection [image obtained through Microsoft® (2008)].



**Figure 20** Ground images from Meadow Creek & Childress intersection.

### Signalized Intersection Test Sites

The intersection of Franklin Street, Elm Street, and Independence Boulevard is a signalized intersection (Figure 21, Figure 22, Figure 23). The posted speed limits for Franklin Street, Independence, and Elm are 45 mph, 35 mph, and 25 mph, respectively. VDOT records show the entering ADT at 25,975. There has been an average of 21 annual crashes reported at this intersection.

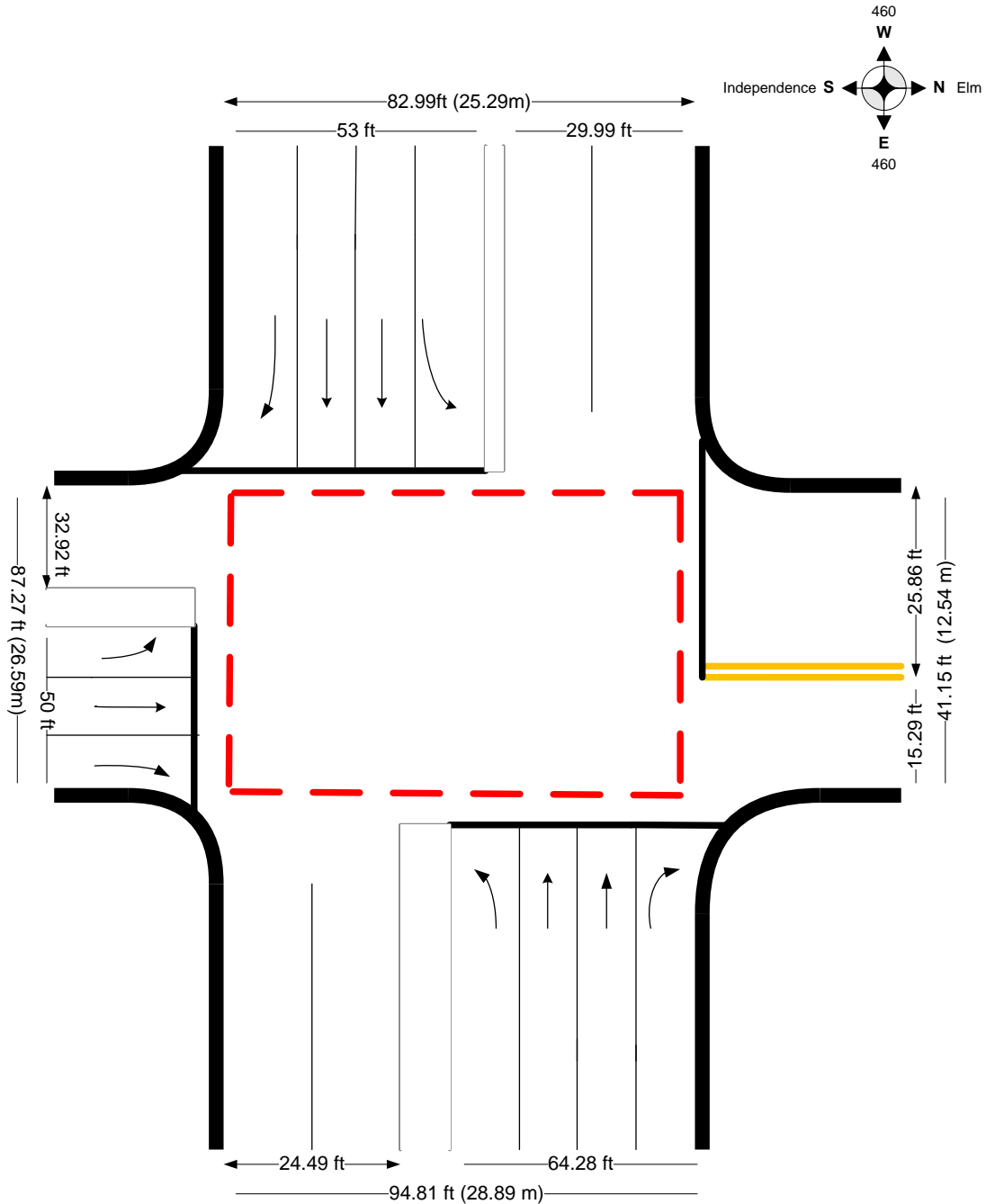


Figure 21 Diagram of Franklin, Elm & Independence intersection.



Image is the copyrighted work of Microsoft® and subject to the terms and conditions of the Microsoft® license agreement.

Figure 22 Aerial view Franklin, Elm & Independence intersection [image obtained through Microsoft® (2008)].



Figure 23 Ground images from Franklin, Elm & Independence intersection.



The intersection of Franklin Street and Depot Street is a signalized intersection (Figure 24, Figure 25, Figure 26). The Franklin Street eastbound intersection approach has a 35 mph posted speed limit, while the westbound intersection approach has a 25 mph posted speed limit. The Depot Street intersection approach has a 25 mph posted speed limit going southbound and a 35 mph posted speed limit going northbound. The entering ADT for this intersection is 26,671 and there were an average of 11 accidents per year reported at this intersection.

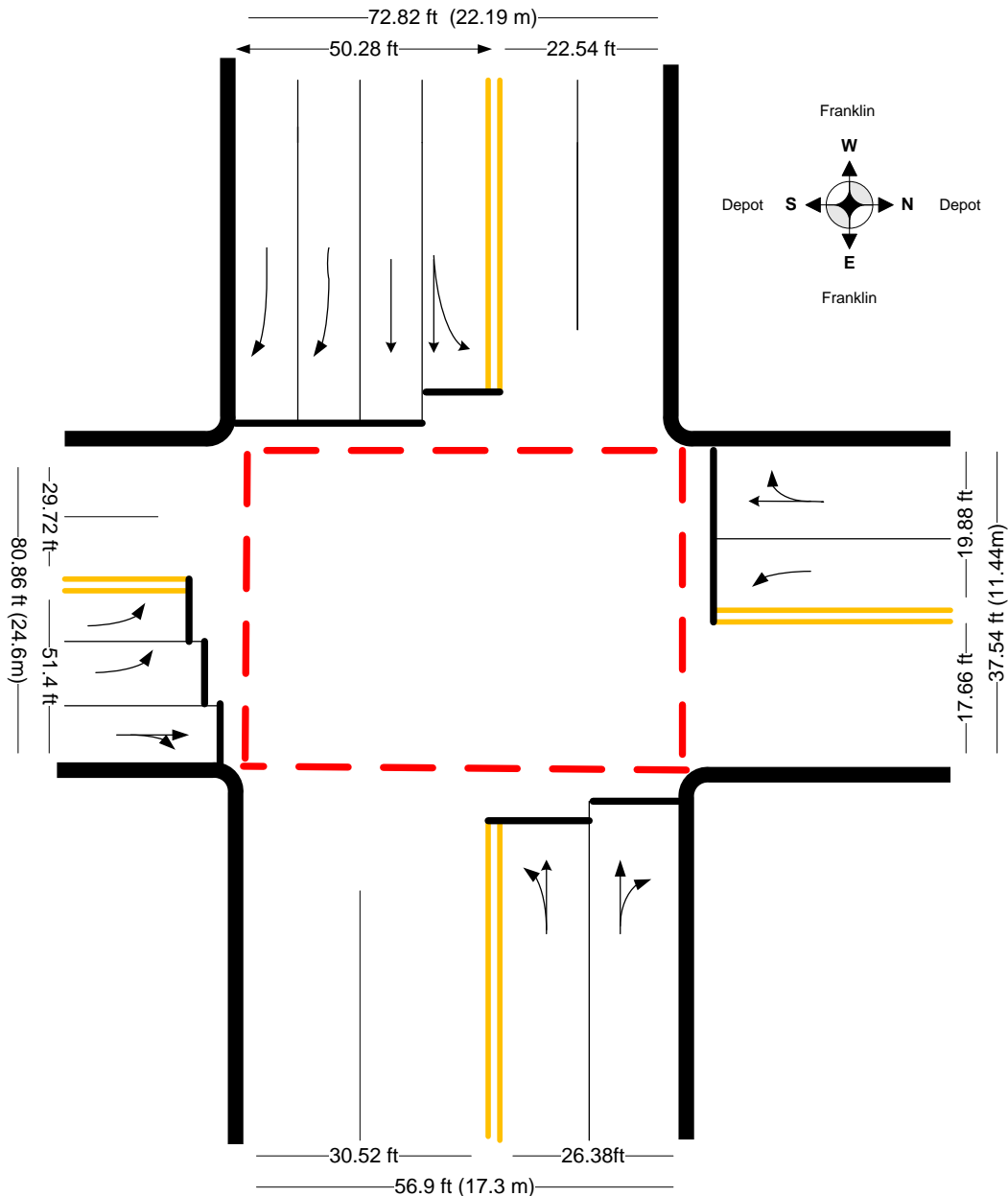


Figure 24 Diagram of Depot & Franklin intersection.



Image is the copyrighted work of Microsoft® and subject to the terms and conditions of the Microsoft® license agreement.

Figure 25 Aerial view of Depot & Franklin intersection [image obtained through Microsoft® (2008)].



Figure 26 Ground images from Depot & Franklin intersection.

The intersection of Peppers Ferry (VA-114) and Franklin (HW-460) is a signalized intersection (Figure 27, Figure 28, Figure 29). The Peppers Ferry intersection approach has a 35 mph posted speed limit in both westbound and eastbound directions. On Franklin there is a 45 mph posted speed limit in both northbound and southbound directions. The entering ADT for this intersection is 31,905 and there have been an average of 23 accidents per year reported at this intersection.

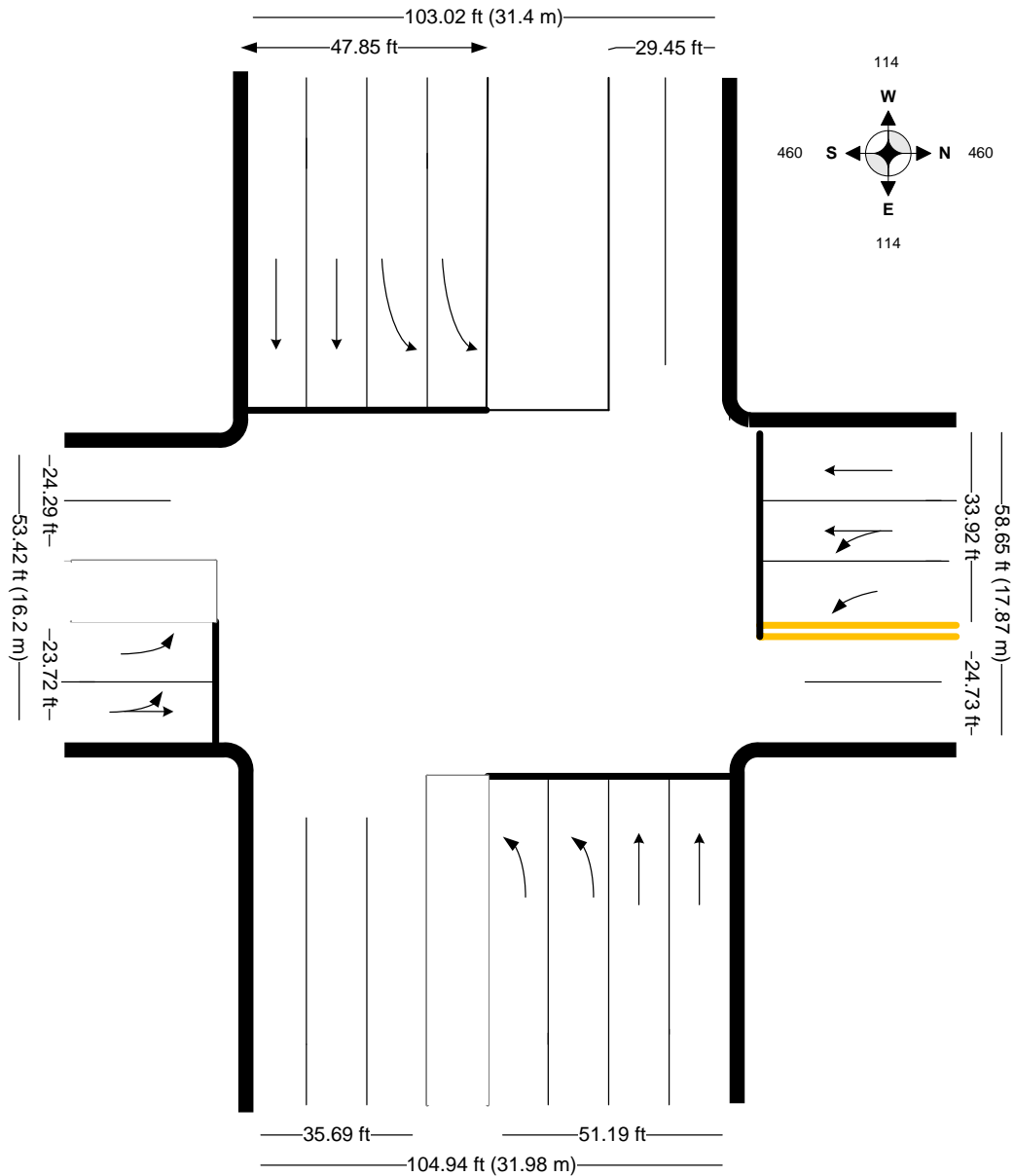


Figure 27 Diagram of Peppers Ferry (VA-114) & Franklin (Bus460) intersection.



Image is the copyrighted work of Microsoft® and subject to the terms and conditions of the Microsoft® license agreement.

**Figure 28 Aerial view of Peppers Ferry (VA-114) & Franklin (Bus460) intersection [image obtained through Microsoft® (2008)].**



**Figure 29 Ground images from Peppers Ferry (VA-114) & Franklin (Bus460) intersection.**

## 2.1 Data Acquisition Systems

The Center for Technology Development at VTTI designed, developed, and installed the DAS for this study. The DAS employed a suite of hardware and software to record information about vehicles that approached the test sites. The following two sections describe the DAS developed, first for the stop-controlled intersections and then for the signalized intersections.

### Stop-Controlled Intersection Data Acquisition

A custom, non-obtrusive DAS installed at the selected intersection approaches acquired data at the stop-controlled intersections. The characteristics of the stop-controlled intersections created some unusual requirements for the DAS. In particular, the rural nature of some sites meant the DAS would not have access to power or communication lines. Therefore, it was designed to be completely self-contained and self-powered. Furthermore, the relatively short data collection period suggested that tunneling under the roadway should be avoided. To provide instrumentation on the multiple approaches at the Meadow Creek intersection, four independent DAS units were installed. The data from these four DASs were synchronized post-hoc, based on the GPS time.

The apparatus consisted of a sensing network, a custom digital signal processor (DSP) circuit board, a digital video recorder (DVR), and an enclosure with a power source. The sensing network measured raw inputs and provided the measures to the DSP at 20 Hz. The DSP pre-processed the inputs and assembled the data set while archiving digital data files on the DVR. This system was completely contained at the intersection site and virtually invisible to drivers. The DAS time stamped the vehicle data acquired from automotive radar with millisecond time provided by the GPS. These parametric data were accompanied by an MPEG 4 video stream obtained from a charge coupled device (CCD) camera focused in the same orientation as the radar. To avoid tunneling below the roadway, each approach of the intersection was monitored by an independent system. The DAS is illustrated in Figure 30, with pictures provided in Figure 31, and the subsequent sections containing detailed descriptions of each component.



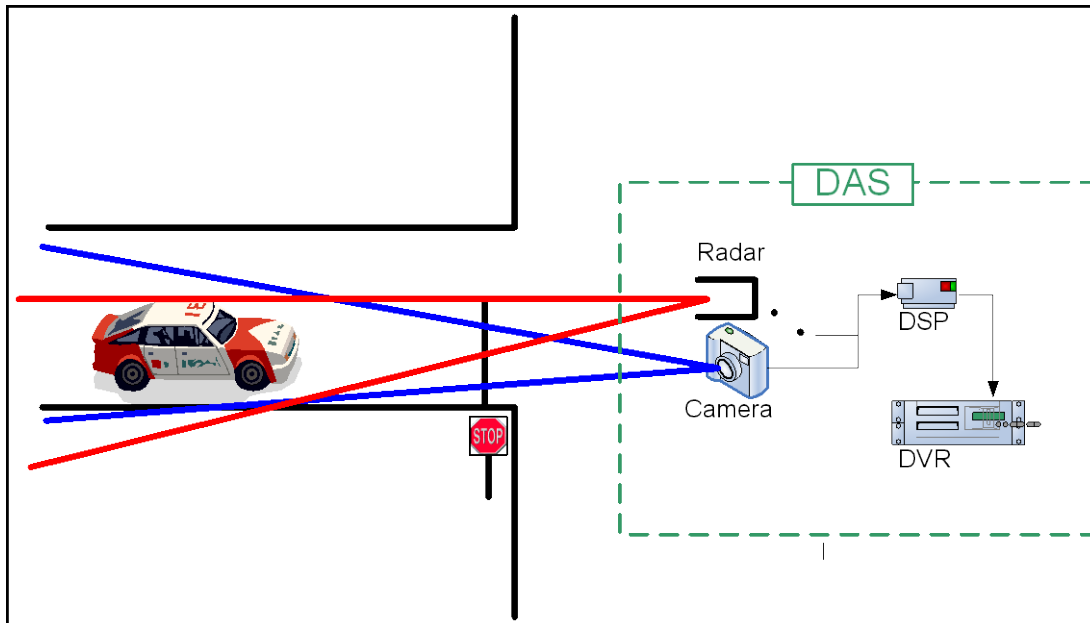


Figure 30 Diagram of stop-controlled DAS.



Figure 31 Stop-controlled DAS.

### *Sensing Network*

The sensing network consisted of two major components: vehicle sensing and uncompressed video. A thorough investigation of current sensing technology identified radar as the most promising technology for obtaining vehicle kinematic information from the roadside (Neale et al., 2005). Previous research indicated that a minimum range of 150 m with an accuracy of plus/minus 3 m and a range-rate accuracy of plus/minus 1 km/h is sufficient for ICAS operation (Neale et al., 2005). The radar must also be relatively inexpensive, weatherproof, and have Federal Communications Commission (FCC) approval. The AC20 Autocruise radar from TRW is an adaptive cruise control (ACC) radar that exceeded the requirements for this study.

The second raw data input provided by the sensing network is uncompressed video. This video was later used to derive measures via manual reduction techniques. The video was recorded using a robust all-weather National Television System Committee (NTSC) video camera, mounted in an inconspicuous location that provided a view of the desired approach. The camera selected for this study was a SuperCircuits PC219ZWPH.

The NTSC signal provided by the camera was attached to the DVR for compression, as choreographed by the DSP. The compressed video (Figure 32), along with the other raw data from the sensing network, was transmitted to the data DSP for pre-processing.



**Figure 32 Video from stop-controlled camera unit.**

### *Digital Signal Processor Circuit*

The DSP, housed on a proprietary circuit board with hardware and firmware, was designed specifically for this study. This processor detects inputs from the sensing network and pre-processes, aligns in time, integrates, and transfers them to the DVR and solid state memory for storage.

In addition to the data collection tasks, the DSP board housed the power management system and sampling scheme. The power management system controlled the on/off state of the sensing network and DVR. Battery voltage was monitored. In the event voltage dropped below a

specified threshold, the entire DAS would systematically shut down to prevent data loss. Furthermore, to maximize battery life, the DSP would switch the sensing components and the DVR off when vehicles were not present at the approach. Data from the sensing network were sent to two separate locations by the DSP. Parametric data were processed by the DSP, time stamped, and sent to a 2 GB solid state memory card. Video data were time stamped and sent to the 100 GB DVR for compression and storage.

#### *Digital Video Recorder*

An Archos AV 500 was selected for compressing and storing the video collected by the DAS. This highly portable DVR uses an extremely efficient MPEG 4 compression algorithm for reducing video file size. The hardware-based compression system is configurable such that the balance between file size and quality can be manipulated. For the purpose of this study, a high compression was selected to minimize file size and reduce the possibility of attaining personal information (e.g., license plate number, discussed further in the approvals section of this chapter).

The compressed video was written to a 100 GB hard drive housed within the DVR. The storage space needed to be capable of collecting over a week of uninterrupted video. This hard drive was retrieved as needed and transported to VTTI for storage.

#### *Enclosure and Power Source*

To minimize behavioral adaptation by the driver, it was essential for the DAS to be as unobtrusive as possible. The sensing network was mounted inside a standard telecommunications box frequently seen on roadsides. These boxes were buried approximately 0.5 m underground with roughly 1 m protruding above the surface. The above-ground portion included a lid that was field-removable and was secured with a tamper-resistant bolt. The telecommunications box was constructed from thin uniform plastic which was easily penetrated by the radar without any cutting, making it completely invisible to drivers. A small hole was drilled for the camera, which provided a clear image of the intersection. Finally, a small box was mounted inside the enclosure that contained the DSP board and the DVR. The telecommunications box located the sensing equipment at the recommended heights while protecting them from direct moisture and ultraviolet rays.

In addition to the above-ground sensing enclosure, a second enclosure resided underground near the telecommunications box. The second enclosure was a Pelican® waterproof high-impact case with security lock. The enclosure provided storage for the power source. The enclosure was buried in order to be inconspicuous and to provide temperature stability for the power source.

The DAS was designed to operate at low voltage for at least six days, at which time the batteries (two large capacity 12-V gel-cells built by MK, part number VRLA-Gel 8G31) would need to be exchanged for a freshly-charged cell. At the time of the battery exchange, the DVR was also swapped for an empty unit. Data from the test site was transported back to VTTI and uploaded to a secure fiber channel server for long-term storage.

## **Signalized Intersection Data Acquisition**

Similar to the stop-controlled data collection system, the signalized DAS was responsible for sensing, pre-processing, and recording data. The apparatus consisted of three major subsystems:



1) sensing network, 2) processing stack, and 3) associated hardware enclosures and mounts. The sensing network was a distributed subsystem of components that provided raw inputs to the processing stack at a rate of 20 Hz. The processing stack pre-processed these inputs and assembled the data set in real time while archiving to binary data files. This system was completely contained at the intersection site and virtually invisible to drivers. The DAS was installed at each site in approximately four working days without affecting intersection operations. A description of the DAS hardware will be presented in this section, and a diagram is presented below (Figure 33).

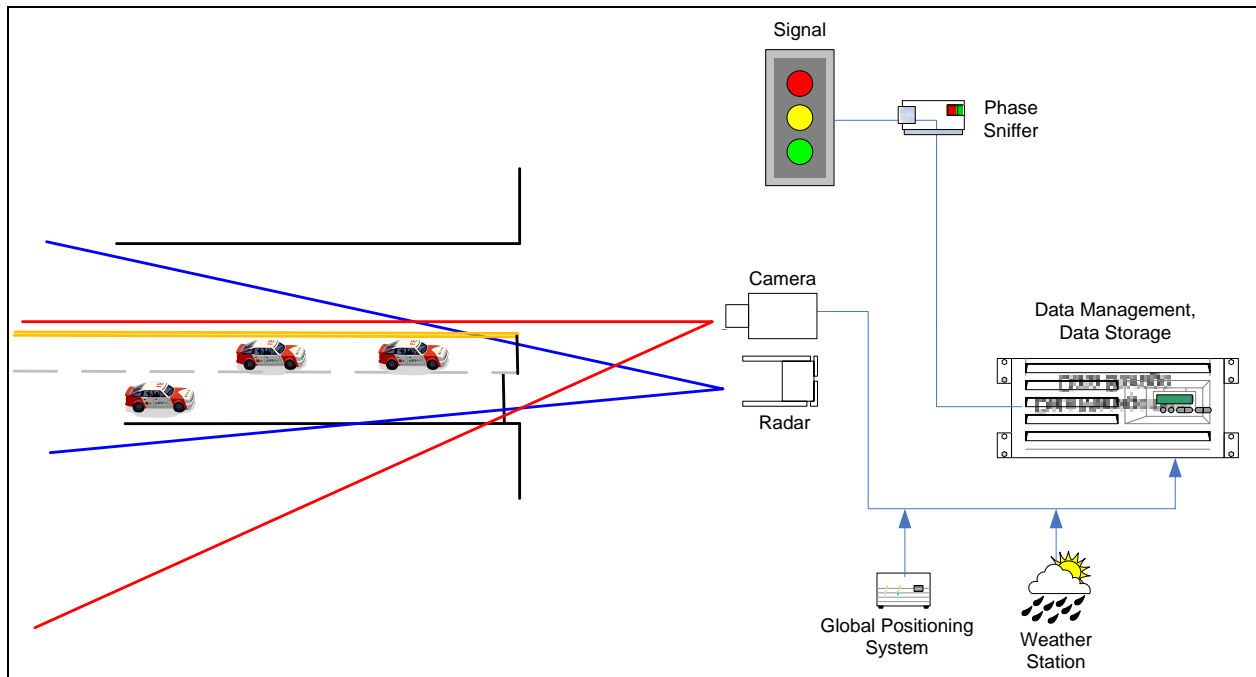


Figure 33 Diagram of signalized DAS.

### Sensing Network

The sensing network was distributed throughout the intersection with equipment located on all four signal mast arms as well as inside the traffic signal controller cabinet. The sensing network consisted of five major components: GPS, weather station, signal phase sniffer, video array, and radar array.

A basic GPS system was employed at the intersection primarily for acquiring an accurate global time. This time information was used to stamp the data to enable analysis related to time of day, day of week, etc. In addition, the accurate time base allowed multiple data acquisition systems to be aligned. This alignment was important for the system validation process. Discussed in a subsequent section, the data validation process was comprised of performing a series of controlled approaches to the intersection in an instrumented vehicle. The data sets from the intersection and the vehicle were merged to validate the accuracy of the intersection-based DAS.

The second component of the sensing network was the weather station. This station provided weather information once each minute. The collected data included long-term rain fall, daily rain fall, wind direction, wind speed, average wind speed, temperature, barometric pressure, and

humidity. These weather-related data allowed researchers to investigate weather-related changes in traffic patterns without employing manual reduction techniques.

The third component of the sensing network is a device referred to as the signal phase sniffer. The signal sniffer is a custom digital signal processor developed at VTTI. This board uses inductive loops to measure the electrical current flowing to the traffic signal heads. Using the loops, the sniffer monitors the current phase of every signal at the intersection. This method results in a completely unobtrusive system for monitoring the signal phase and timing. It does not require any direct connections to the signal controller; the intersection's signal operation was not interrupted during installation. In addition, the sniffer learned the yellow phase lengths at the intersection. This learning process took place over the first few phase cycles, after which the sniffer provided a countdown of remaining yellow time until red.

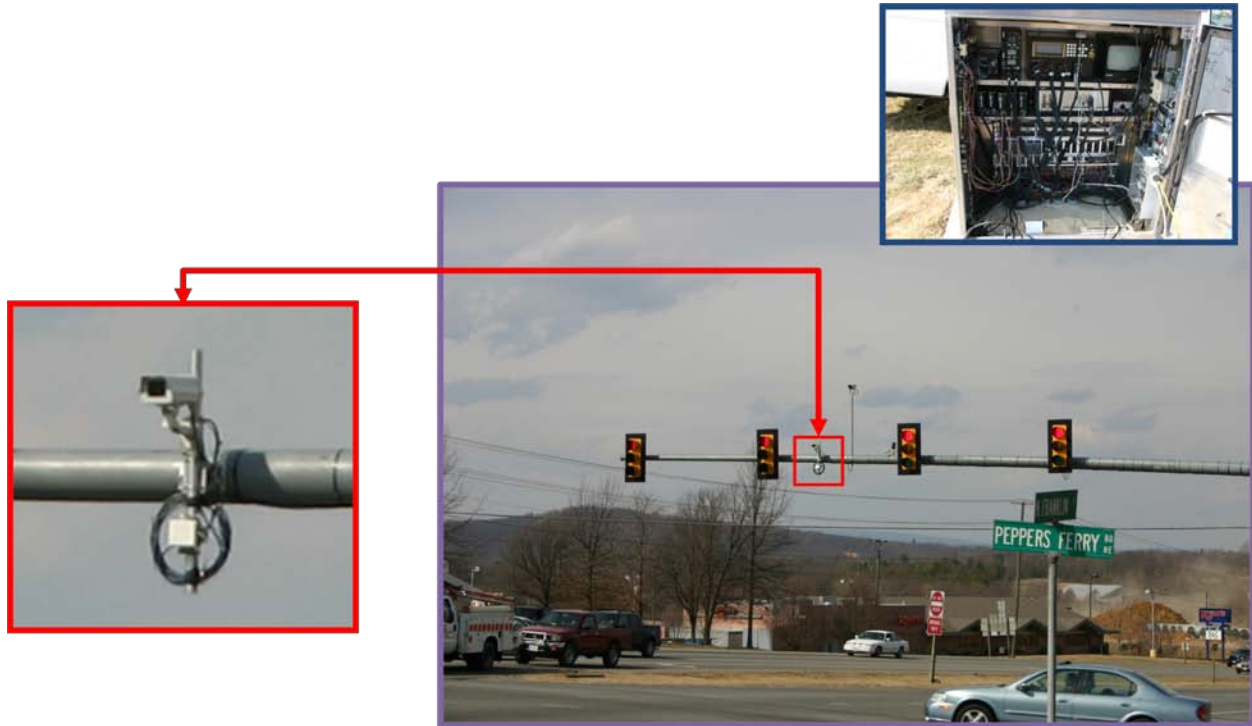
The fourth element, a video camera, was installed on each of the four traffic signal mast arms to provide an image of the entire intersection environment (Figure 34). The video was streamed to the DAS using a NTSC format over a coaxial line. The selected cameras are intended for outdoor use and have special features designed for vehicle environments including headlight bloom reduction and a wide-range iris. The cameras were housed inside heated and power-vented water resistant enclosures to ensure consistently high video quality.



Figure 34 Video quadrants from camera units mounted on intersection mast arms.

The final component in the sensing network was the high-performance radar designed and developed for the CICAS-V team by Smart Micro Systems. The custom radar underwent extensive lab testing and on-site tuning to ensure a high level of data quality. The radars operate in the 24 GHz band with a transmit power of less than 20 dBm. Advertised position accuracy is better than 0.5 m with a range of 0.5 m to more than 200 m. Speed accuracy is advertised at

better than 1 percent. A single radar was mounted on each of the four mast arms below the camera and aimed directly at the approaching traffic (Figure 35).



**Figure 35** Camera and radar unit mounted on a single intersection arm mast, along with instrumentation inside traffic signal controller cabinet.

Each of the four sensors returned raw radar data over a Controller Area Network (CAN) interface to DSP tracking processors located in the traffic signal controller cabinet (Figure 36). A separate DSP performed the tracking computations for each of the four radars. The tracking DPSs then provided the position, velocity, acceleration, length, and proprietary credibility statistics for up to 32 vehicles simultaneously (a maximum of 128 vehicles approaching the intersection at a given instant in time).



**Figure 36** DSP tracking processors.

As discussed in a subsequent section, the data provided by the radar network were independently validated using a highly capable instrumented vehicle.

### Processing Stack

The processing stack installed at the intersections was a high-performance computational subsystem developed by VTTI over the past decade. The system is built on a PC104 backbone with a custom interface capable of accepting and transmitting information to a variety of sensing components. This system of distributed data acquisition provides a flexible solution for obtaining data from a variety of sources. Each of the distributed sensors described above connects to the processing stack via custom interface boards located on the internal system bus (Figure 37). A custom motherboard provides the interconnections and passes data to the PC104 where the parametric data source integration is choreographed via a proprietary VTTI software package running on the real-time Linux operating system. The software time stamps and aligns the various incoming messages and compresses them into a binary file, which is then written to a removable hard drive in real time.



Figure 37 VTTI processing stack.

The parametric data are accompanied by an MPEG 4 file containing digitized video from the four cameras. The four individual NTSC camera signals are multiplexed into a single video stream and digitally compressed to the MPEG 4 format via hardware compression in real time. This provides a full 30-Hz video stream at a highly efficient data rate.

### Test Site Installation

Sites were sequentially outfitted with the DAS. The installation, calibration, and validation process took approximately two days for each stop-controlled site and four days for each signalized intersection. VDOT assisted in the installation by providing the necessary signage and equipment support. In order to decrease the interruption of traffic flow, each intersection was equipped during daytime hours when traffic volume was considered to be at a minimum.

For the stop-controlled intersections, the enclosures were mounted first, followed by the installation of the DAS hardware and cabling. The battery pack, used to provide power at each site, was buried in order to remain as unobtrusive to traffic as possible. At the signalized intersections, cabling was first pulled through the existing conduit at the intersections. This was followed by installation of the equipment on the mast arms and the controller cabinet. Figure 38 and Figure 39 provide images of the installation process at a selected stop-controlled intersection and signalized intersection, respectively.





Figure 38 VTTI workers installing radar and camera unit at stop-controlled intersection.



Figure 39 VDOT workers mounting camera and radar unit to intersection mast arm.

VTTI and VDOT workers were responsible for mounting the camera, radar units, and enclosures. The camera and radar units placed at each intersection were designed and mounted so as to not attract the attention of motorists. Following the installation of the equipment, each of the radars was aligned. The alignment was achieved using a laser distance finder, which measured the distance of the stop bar from the radar. Additional fine adjustments regarding positioning and focus were made once the installation was completed and the systems were brought online.

A calibration procedure was initiated once the hardware was installed and powered up. During calibration, the camera focal length and zoom were set to obtain the desired image. This image captured the entire vehicle approach into the intersection. The radar aim was finalized via visualization software to ensure data was recorded for vehicles beginning at a range of at least 150 m continuously through the stop bar.

## Data Retrieval and Management

Data retrieval at stop-controlled intersections was somewhat different than at signalized intersections. As with most stop-controlled intersections, traffic volume at the test sites would decrease substantially during non-peak hours. Collecting data when vehicles were not present on the intersection approach would be inefficient. The battery-based power supply would drain faster, and the storage devices would reach capacity sooner. Thus, a triggering scheme was used at stop-controlled intersections. Data were only written to the storage devices when a vehicle was present on the intersection approach. When no vehicles were sensed, the DAS entered a low-power mode in which the camera and assorted other components were powered off or put into a standby mode. With the higher traffic volumes at the signalized intersections, at least one vehicle was likely to be present at a given time. Furthermore, power was not limited by battery capacity at the signalized intersections, and the storage space within the DAS was larger. As such, a triggered approach to data collection was not used at the signalized intersections.

The frequency with which data were collected from the stop-controlled intersections was dependent on the traffic volume at a given site. Sites with higher traffic volumes placed higher demands on the DAS, consuming battery life and data storage at a higher rate. On average, data retrieval occurred every five (Meadow Creek intersection) to seven (Nellies Cave intersection) days. Data accumulated much faster at signalized intersections, where the DAS recorded additional variables in all four directions. This required bi-weekly data retrievals at all three sites.

Trained data retrievers maintained each of the sites to eliminate down time during which data were not collected. The system was temporarily shut down for approximately two minutes to replace the data storage and to replace the battery array when applicable. During this time, a health check was performed on the system to ensure data quality was being maintained.

Following data retrieval, the files were transported to VTTI and uploaded onto the VTTI data storage servers. Each of the files was named based on the intersection, day, and time at which they were retrieved. This process was completed automatically using a custom software program written for this purpose. The data servers reside on a secure network in which daily incremental and full weekly offset backups are performed.

## Approvals

To collect data on human participants, approval from the Virginia Tech Institutional Review Board (IRB) was obtained (Appendix A). This research project collected infrastructure-based data, including video, of thousands of participants in a naturalistic intersection environment. It was neither feasible to control who entered the test sites nor was it possible to obtain an informed consent from drivers passing through the test sites. For this reason, the IRB approvals were obtained early in the process to ensure the proposed work could be carried out. As part of this approval, the participant's anonymity was protected by reducing the quality of the video to make

it impossible to read the license plate numbers or identify the vehicle occupants. Other measures, such as secure data storage, analyst authentication, and breakaway roadside equipment also protected participants in the study.

A second approval by VDOT permitted the installation of the DAS at the test locations. As discussed earlier in this chapter, these installations were nearly transparent to the driver and did not affect the safety of participants at the test sites.

### 3 Post-Processing

Post-processing of the stop-controlled and signalized data was conducted to apply a series of data cleansing, extrapolation, and smoothing techniques in order to prepare the data set for analysis. The following sections describe the validation procedure and subsequent analysis to validate the DAS and post-processing method. These processed data sets were used for the remaining analyses described in subsequent sections.

Post-processing performed on the raw data improved quality and derived additional measures that were used for the algorithm development and evaluation. The following sections discuss each of the post-processing steps and the data set on which they were performed.

#### First-Pass Filtering and Derivation of Unique Vehicle ID

This section provides information regarding the assignment of unique vehicle IDs. A unique vehicle ID was required to individually address each independent vehicle that approached the intersection. Derivation of a unique vehicle ID proved significantly more challenging for the stop-controlled database than the signalized database.

The Autocruise model AC20 radar was used to collect vehicle data at the stop-controlled intersections. The AC20 was developed for adaptive cruise control (ACC) systems that place the radar on the front of a vehicle. The AC20 performance was disappointing when it was placed at the intersection. Although the radar returned accurate measurements of range and velocity, it did not reliably return these measures for a given vehicle for every frame.

The erroneous radar returns (e.g., reflection shadows, trees, deer, and so forth) were first cleaned from the database. This process was primarily performed by a filter that passed data based on a metric computed from several quality measures calculated by the sensor. The filter was iteratively developed to remove invalid data points while passing the valid data. Although this process provided a cleaner dataset, it did not address the largest deficiencies of the sensor. Data drop-outs and incomplete tracks were commonly reported by the radar. Furthermore, the radar did not provide a unique ID to group data points from each vehicle. These data limitations required that a substantial effort be undertaken to improve the raw data used for algorithm development.

Instead of providing each vehicle with a unique ID, the track ID variable reported by the sensor repeated as soon as the vehicle with a given ID was no longer visible. For example, three vehicles approaching the intersection can be assigned IDs one through three. If a fourth vehicle were to enter the field of view of the sensor just after vehicle two exited the view, the new vehicle can now be designated as vehicle two. In addition, as a vehicle approached the stop-controlled intersection, it was not uncommon for the track ID to change (track switching). For the analysis, it was imperative that each vehicle be indexed individually so the algorithm could be executed independently on each vehicle trajectory. Data provided by each vehicle needed to be continuous in order for the algorithm to be functional on each data frame.

To develop the unique ID and mitigate the track switching problem, a post-hoc tracking algorithm was developed to enhance the radar tracking. This was accomplished by software scripts that crawled through the data, frame by frame. For each frame, the associated radar returns were compared to the returns in the previous points in time at which the subject vehicle



was believed to exist in the data. Thus, even if a vehicle dropped out for a period of time, the program would hold information about that vehicle's prior dynamic state while waiting for it to reappear.

The tracking algorithm required a series of criteria to be met in order for a point to be assigned the current vehicle ID. The criteria were based on a dynamic prediction of the vehicle's location in the current frame, based on the dynamic state of the vehicle during its previous incarnation in the data. This prediction was made using the fundamental kinematic equations of motion. In addition, the time between returns, overall distance traveled for the vehicle, and overall number of points returned was also part of the comparison. For the derived unique vehicle ID, the assigned track could not last more than 15 s, had to contain at least two data points, must have reported ranges greater than zero, and must have traveled at least 1 m. The resulting vehicle ID was a database-wide unique ID associated with each vehicle that approached the intersection. Thus, all of the data points returned from a single vehicle were assigned the same ID.

In conjunction with the vehicle ID, a fit ID was also created. The fit ID served as a more stringent version of vehicle ID. Where vehicle ID contained all the data points from one vehicle, the fit ID contained only series of points that included sufficient information for repairing broken tracks and deriving the acceleration measure. For a set of points to be assigned this ID, it was required to contain at least 10 data points, cover at least 2 m, and drop out for no more than 4 s.

It was possible for a single vehicle ID to have multiple associated fit IDs. For instance, consider a vehicle track that was returned by the radar at a long range, disappeared for some time, and then reappeared later. If that dropout was less than 4 s, a single fit ID would have been created; however, if that dropout lasted more than 4 s, a second fit ID would have been assigned to the second collection of points within that vehicle ID. The resulting fit ID grouped sets of points together so it was feasible to perform additional post-processing to improve the data. These additional post-processing steps, discussed in subsequent sections, utilized fitting procedures to improve the continuity of the reported kinematic data where possible.

At the signalized intersections, the parametric vehicle data was collected by a sophisticated sensor suite (Section 2.2.2) utilizing the Smart Micro Systems radar. This suite underwent extensive design, lab testing, and on-site tuning to provide high-quality radar data at intersections. As a result, the custom sensors provided data more consistently and without the level of noise present in the stop-controlled data. Therefore, signalized data did not require the first-pass filtering process.

An additional benefit of this system was an object ID that only recycled every 255 objects. To develop a unique vehicle ID, the object ID was converted to a non-repeating counter. The additional logic used in the stop-controlled collection to mitigate track switching and to identify groups of data for fitting was not required for the signalized data.

## Lane ID

At signalized intersections, the travel lane was important as it influenced the relative location of the stop bar and identified the corresponding signal phase. A lane ID was not necessary at the stop-controlled intersections because these all contained single-lane approaches.

The first step in creating lane IDs was to collect information on the geometry of lane markings and stop bars at the signalized intersections. Anderson and Associates of Blacksburg, Virginia, was contracted to survey the three signalized intersections to be used for this study. All markings for through lanes, turn lanes, merge lanes, and stop bars were surveyed up to 305 m (1,000 ft) in approaching lanes and 50 m (165 ft) in departing lanes. Information was collected at increments of 31 m (100 ft) or less. Points were shot at tighter increments when required to accurately represent lane geometry. Horizontal mast arms (on which the radars were mounted) were also located at each intersection.

An adaptive artificial neural network (ANN) was then developed to determine the travel lane for each vehicle, which was recorded at every time step during an intersection approach. The ANN is a non-linear statistical modeling tool that can be used to find patterns in data. The ANN was used to learn the patterns of the lateral and longitudinal position of vehicles; thus defining the location of the lanes in the radar data stream. The first step of this process was to translate the radar-reported coordinates to an overall intersection coordinate system that could be correlated with the survey data collected for this purpose. The equations for this transformation are provided below (Equation 1, Equation 2, and Equation 3).

**Equation 1**

$$X = (D_o + R) \left( \cos \left[ A_o + a \cos \left( \frac{R_x}{R} \right) \right] \right)$$

**Equation 2**

$$Y = (D_o + R) \left( \sin \left[ A_o + a \cos \left( \frac{R_y}{R} \right) \right] \right)$$

**Equation 3**

$$R = (R_x^2 + R_y^2)^{1/2}$$

Where:

$R$  = Range

$D_o$  = Distance offset

$A_o$  = Angle offset

For the next step, researchers created a cascade-correlation neural network. Cascade-correlation is an architecture and supervised learning algorithm developed by Fahlman and Lebiere (1991). As previously discussed, the ANN begins with a minimal network, then automatically trains and adds new hidden units one by one, creating a multi-layer structure. The cascade-correlation architecture can quickly learn, determine its own size and topology, and retain the structures it has built even if the training set changes. Using the x and y coordinates calculated above, the following inputs was provided to the network (Equation 4).

**Equation 4**

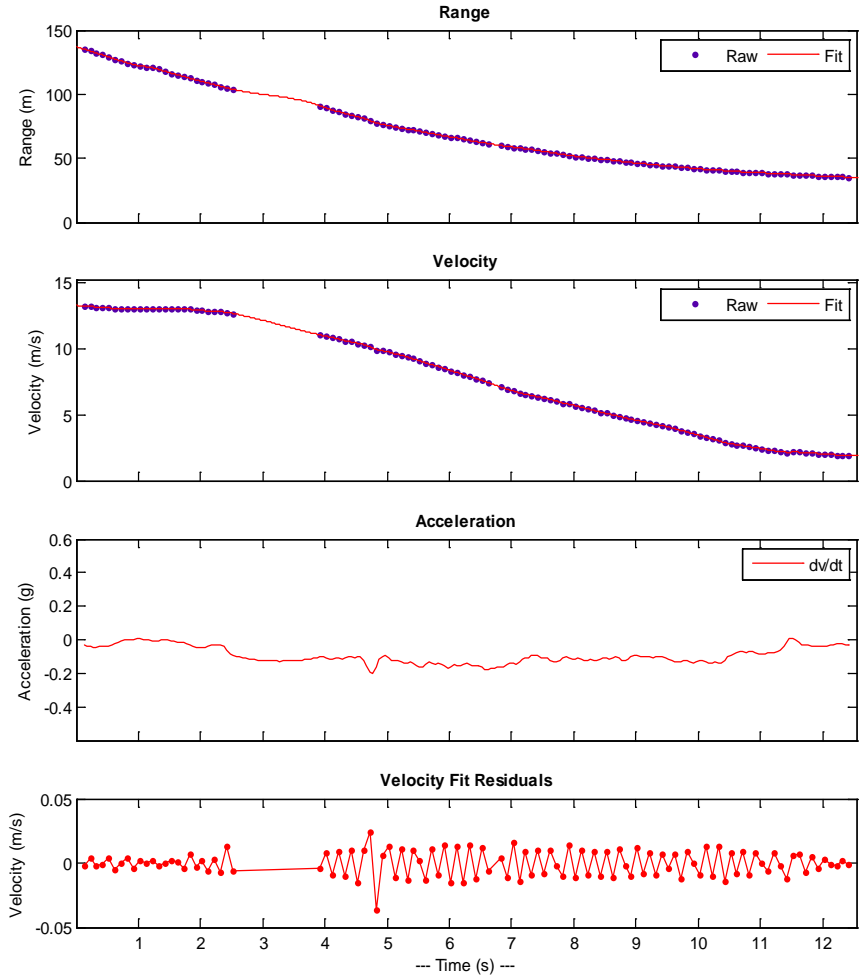
$$X, Y, X^2, Y^2, X * Y, X^3, Y^3$$

The ANN used a sigmoid transfer function with weights created through supervised training. The learning procedure compared the ANN's predicted lane to the lane identified in the survey for 30 to 90 discrete locations (depending on geometry) along each approach. After each training session, researchers manually compared the calculated lane ID with the video data to validate the ANN for at least 10 random vehicle approaches across 10 random files for each of the 36 lanes. Training of the ANN continued until all 10 vehicles were correctly placed in the each lane throughout their approach to the intersection. Once the ANN was completed, the calculation was programmed into the data analysis scripts to determine the vehicles lane position at every time frame.

**Smoothed Kinematic Variables**

As previously mentioned, the data sets (particularly the stop-controlled data set) contained dropouts in which the radar would stop providing updates for a brief period of time. In addition, the radar sensors performed real-time smoothing; however, this smoothing of radar data is challenging. With a complete trace of the vehicle, post-hoc smoothing can alleviate much of the noise induced from the vehicle's changing radar reflection, thus improving accuracy of the parametric data. It is particularly important to smooth this data prior to deriving acceleration, which is sensitive to noise-induced dither. Thus, a non-parametric smoothing spline (Figure 40) was fit to each vehicle trace. The smoothing spline was a knotted piecewise polynomial that responded very quickly to changes in the underlying form of the data. No latency was introduced though the use of this fitting technique.

The polynomial produced by the smoothing spline was used to repair tracks with short dropouts. A repaired dropout is depicted in the range and velocity traces shown in Figure 40. In addition, the derivative of the polynomial function created by the spline was used to calculate the vehicle acceleration. (The derived acceleration and the velocity fit residuals are also depicted in Figure 40). The smoothing procedure shown below was carefully selected from a variety of other techniques because it bridged data dropouts with polynomials of varying order that tended to accurately represent the missing data (see Section 3.5 for validation). Unlike parametric techniques or linear interplants, the smoothing spline does not require any distribution assumptions.



Data Source: File =121212 Approach =21 StartFrame =20872

**Figure 40** Raw data collected by the DAS with the smoothing spline fit to the range and velocity data. The acceleration was then derived based on the data fit. Residuals for the velocity fit are also provided to convey the typical quality of the fitting procedure.

In addition to acceleration, two other continuous measures were also calculated from the smoothed parametric data. These included the time to intersection (TTI) and required constant deceleration parameter (RDP). TTI is a calculated value based on the current distance to the intersection and speed of the vehicle. TTI is believed to be a good approximation of the measure used by the human visual system to judge whether or not to stop (Horst, 1990). It combines the effects of speed and distance into a single measure (Equation 5).

**Equation 5**

$$TTI = \frac{D_s}{V}$$

Where:

VSC2 Consortium Proprietary - For USDOT Internal Review Only

V = Vehicle speed at the point when driver initiated braking (m/s)  
 $D_s$  = Distance to the trailing edge of the stop bar or start of perpendicular roadway when a stop bar was not present (m)

RDP represents the calculated constant acceleration required to stop at the stop bar, based on the vehicle's current speed and distance from the intersection. RDP is an easily- interpreted variable that represents the braking effort required to stop at any point during the intersection approach. This equation is provided below (Equation 6).

#### Equation 6

$$RDP = \frac{V^2}{2 \cdot D_s \cdot g}$$

Where:

RDP = Required deceleration parameter (g)  
 V = Vehicle speed at the point when driver initiated braking (m/s)  
 $D_s$  = Distance to stop bar when driver initiated braking (m)  
 g = gravitational acceleration constant (9.81 m/s<sup>2</sup>)

## Brake Status

Brake status is a binary indication of whether or not the driver is pressing the brake pedal. The brake status provides a clue to driver intent and is often monitored in vehicle collision warning systems to determine if a warning should be provided. As such, brake status was included in the evaluation as a potential method to surpass a warning to attentive drivers. While this variable cannot be directly measured with the radar, it can be approximated. To approximate brake status, an algorithm was devised to monitor the acceleration rate throughout each vehicle's intersection approach. The algorithm first used a 10-point zero-phase-shift moving-average-filter to smooth the acceleration. The smoothed acceleration was monitored for a change point that dropped below a set deceleration level. Searching for this change point allowed vehicles to coast, slowing through engine braking, without actively pressing the brake. This threshold was selected through a controlled investigation of a naturalistic driver performance database housed at VTTI.

First, the data used for the validation procedure (Section 3.5) were analyzed to determine the threshold at which the radar would reliably show braking. This was accomplished by comparing data collected within the vehicle to data collected by the radar. This study indicated that a deceleration rate greater than 0.05 g could be reliably identified from the radar data.

Next, an examination of stop-controlled and signalized intersection approaches extracted from the 100-Car database (Dingus et al., 2004) during Subtask 3.1 (Sudweeks et al., in review) was performed. The intersection approach data extracted were analyzed to determine how to predict brake status, based on deceleration (Appendix B). The results of the study were entered into a brake-status algorithm to predict brake activation from radar data.

The brake status algorithm monitored the vehicle's deceleration rate. From the study described in Appendix B, braking was known to occur at a deceleration rate greater than 0.075 g. The study also indicated that actual brake onset was occurred 1.6 s prior to exceeding the 0.075-g threshold. Thus, a brake-active status was indicated 1.6 s before a vehicle exceeded a 0.075-g

deceleration rate. An example of the predicted brake onset point for an intersection approach is depicted below (Figure 41).

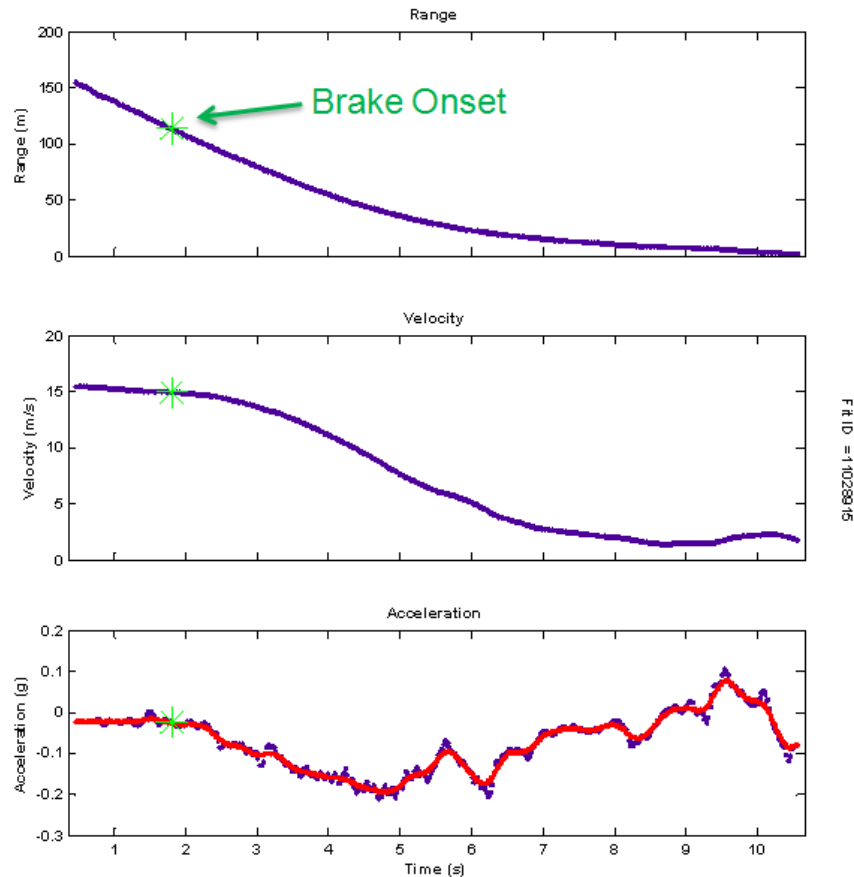


**Figure 41** Example of an intersection approach showing the derived brake onset point for range, velocity, and acceleration kinematic measures.

After initial brake activation, the brake flag remained on until the deceleration dropped back below 0.05 g. If the deceleration rate dropped below 0.05 g it was assumed that the driver had stopped braking. After initial braking, 0.05 g was used as the threshold for determining ongoing brake status throughout the remainder of the approach. As described above, this value was selected because it could be reliably detected by the radar and represented a threshold that was in excess of most vehicles' engine braking rate.

## System and Post-Processing Validation

System validations were performed to ensure accuracy of the stop-controlled and signalized DAS and post-processing methods. The validation procedure began by driving an instrumented vehicle at a signalized and a stop-controlled intersection in a series of test trials while simultaneously recording data using the intersection and vehicle DAS (see Appendix C for a description of the vehicle DAS). Data from the two sources were then compared post-hoc to evaluate the accuracy of reported measures.

The vehicle used for this experiment was a highly capable test vehicle initially set up for Subtask 3.1 of the CICAS-V project (Sudweeks et al., in review). The measures reported by the two DASs were compared using the vehicle DAS as the true measure. Any deviation of the infrastructure DAS from the vehicle DAS was considered an error. These errors were evaluated to develop an overall estimate of system accuracy.

To evaluate the infrastructure DAS accuracy over a range of realistic scenarios, a set of intersection approaches were performed using three initial speeds and three initial braking rates. These runs included 25-mph, 35-mph, and 45-mph stop approaches with soft (~0.2 g), medium (~0.4 g), and hard (~0.6 g) average braking rates. In addition, violation runs were simulated (performed on the green phase) at the signalized intersection and performed with caution (when no traffic was in the vicinity) at the stop-controlled intersection.

Figure 42 and Figure 43 depict exemplar vehicle approach trajectory as measured by the vehicle and infrastructure DAS. Each subplot contains a line series for the post-processed radar data, a scatter plot of the raw radar data, and a line series for the vehicle data, as appropriate. Note that a stop-controlled approach with sparse raw radar data was intentionally selected to demonstrate the effectiveness of the post-processing for a worst-case scenario.

The top subplot in each figure depicts the range as reported from the two data sources. The second subplot shows the vehicle's velocity during the approach. The third subplot depicts the acceleration as measured by an accelerometer inside the vehicle and the acceleration that was computed as the first derivative of the post-processed radar velocity. Finally, the bottom subplot depicts the error between the radar-derived acceleration and directly measured acceleration. Because the radar-based acceleration is the derivative of the measured velocity, the bottom subplot is the most sensitive to errors in the radar data. As depicted in the two figures below, the acceleration error was usually less than 0.05 g.

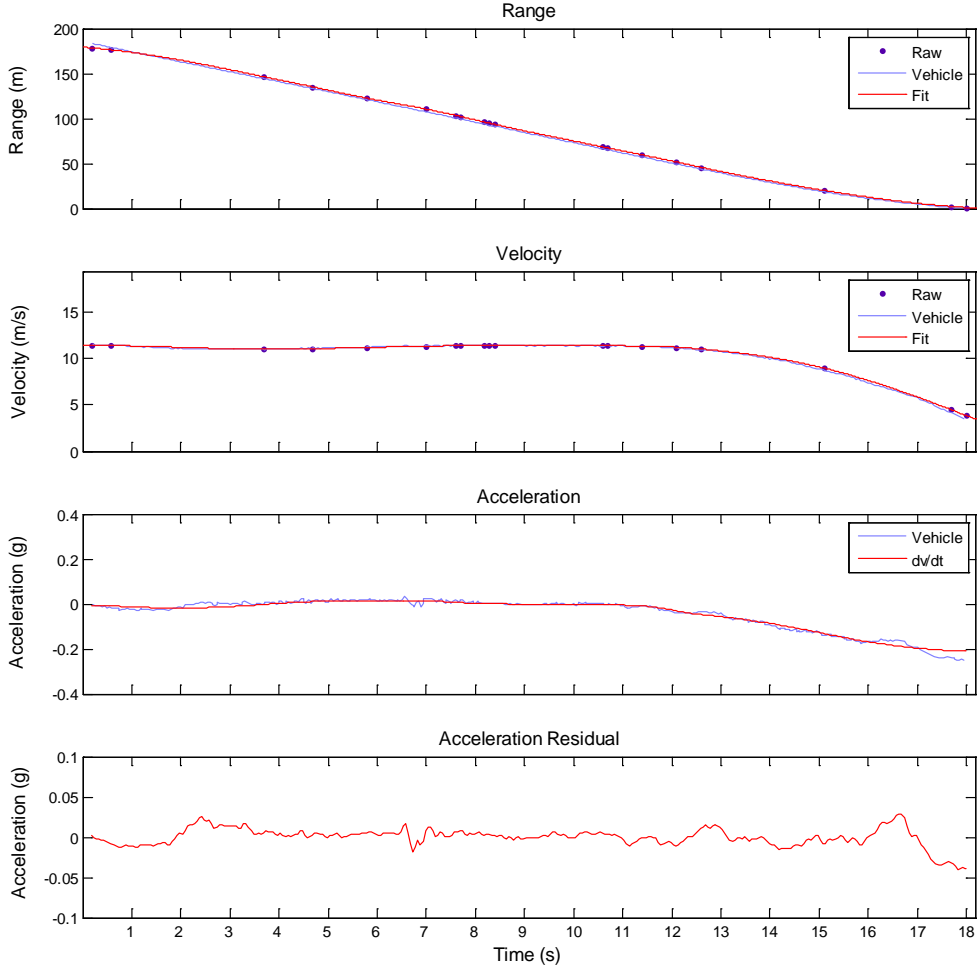
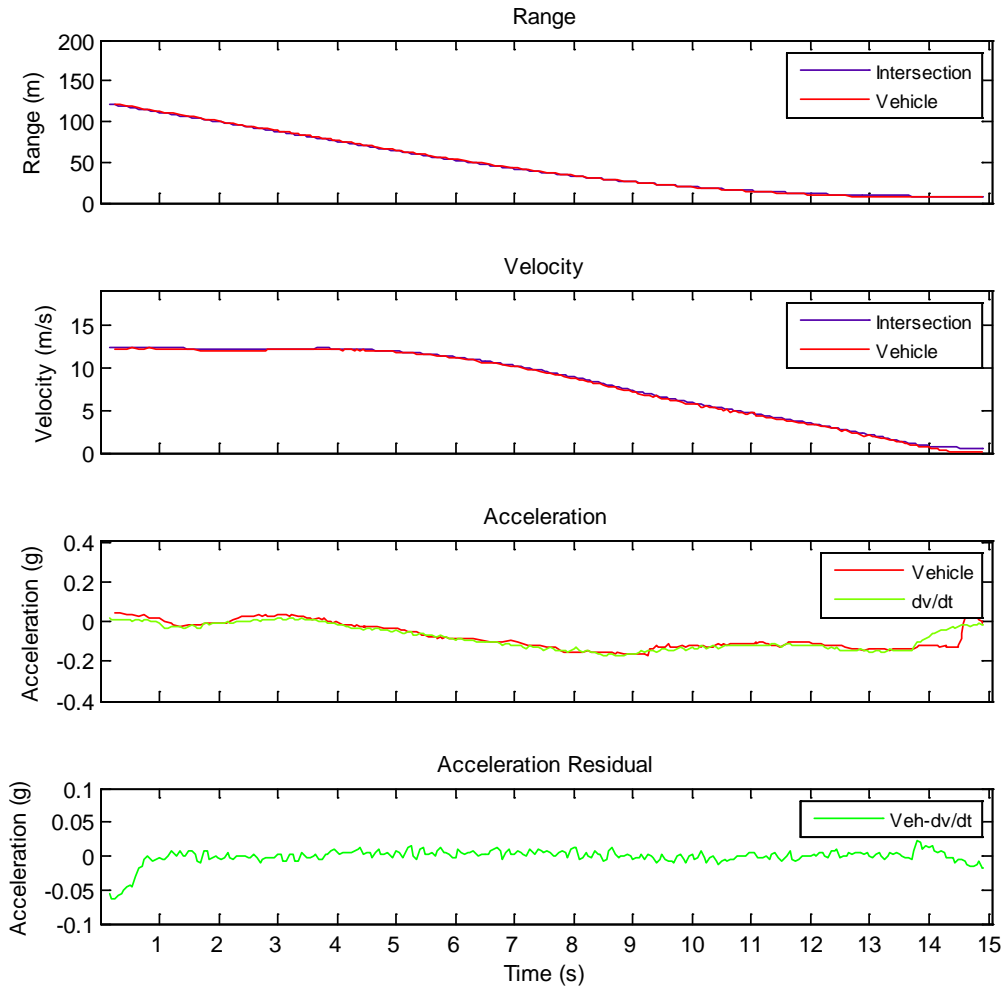


Figure 42 Stop-controlled infrastructure and vehicle DAS measurements.





**Figure 43** Signalized infrastructure and vehicle DAS measurements.

Based on the results (Table 6, Table 7, and Appendix E), the final data sets were deemed sufficient for the purposes of the intended analyses. The overall accuracy levels demonstrated through the validation met or exceeded the accuracy guidelines presented in the ICAV Task 5 report (Lee et al., 2005).

These values are provided in the table below (Table 5). No speed- or approach-type bias was observed in the error data; thus, the radar error should be consistent across a variety of intersection approach types. There are some occasional large errors produced by the radar; however, these events are relatively rare and will be mitigated through the statistical techniques used in the subsequent analyses. Given the moderate quality of the initial stop-controlled data, the relatively high accuracy of the final data set demonstrates a successful post-processing method.

Table 5 ICAV Task 5 accuracy guidelines.

	Range	Speed
ICAV Task 5 Guidelines	1.75 m	±0.447 m/s

Table 6 Stop-controlled DAS system error relative to the validation vehicle's high-accuracy DAS.

	Range	Speed	Acceleration
Mean	0.829 m	0.062 m/s	-0.002 g
Standard Deviation	2.401 m	0.151 m/s	0.026 g

Table 7 Signalized DAS system error relative to the vehicle's high-accuracy DAS.

	Range	Speed	Acceleration
Mean	-1.08 m	0.06 m/s	0.001 g
Standard Deviation	1.40 m	0.28 m/s	0.035 g

## Event Validation and Video Reduction

The data collected for this study were obtained primarily from an infrastructure-mounted radar sensor. Radar has some limitations relative to in-vehicle sensors. While the measurements of speed and range are accurate, it is the association of those measures with a particular vehicle that is prone to error. This means that a vehicle reported by the radar is not necessarily a valid vehicle. The quintessential example of this behavior occurs with large vehicles and trailers. The radar used for this study would frequently treat a large vehicle as two separate targets, particularly if a trailer was in tow. As a result, the subject vehicle may have completed a stop at a stop-controlled intersection; however, the secondary false target located at the rear of the vehicle would appear to violate as it was pulled through the intersection at speed.

The primary purpose of the video reduction was to validate the events of interest. It was important to ensure that false targets were not inadvertently being included in the sample of violating and aggressive driver approaches. In addition to false triggers, other invalid events also needed to be removed from the data set. These included violations that were a result of atypical scenarios such as a funeral procession and the crossing of in-service emergency vehicles. Therefore, it was necessary to mark and remove invalid events from the analysis.

The data set contained over 2 million unique vehicle trajectories. The time for a typical validation was a few minutes per event. While reducing all of the events would provide an excellent data set for investigation, this simply was not possible to perform within the time and budget constraints of this study.

Consequently, a strategy was devised to methodically select approaches of interest for reduction. The selection process occurred through the development of a trigger that swept through the

parametric data and flagged events requiring attention. The flagged events were automatically collected for easy retrieval and accessible to the data reductionists. A detailed discussion of the method used to identify validation events is available in Appendix D.

The validation process required a reductionist to view each event. Once the event was opened and viewed, it was logical to collect a few additional measures that were not available natively in the data collection system. These measures included environmental data (such as surface condition) as well as information about the adjacent and conflicting vehicles. Most of these reduced measures were not used as part of the analyses described in this report and represent an avenue for future research.

The Data Analysis and Reduction Tool (DART) software package was used by data reductionists to validate the events. DART is the result of over six years of software development at VTTI. DART provides a user interface for the viewing and reducing of digital data (Figure 44). It contains user-configurable video and graphical interfaces to aid in manual reduction, and allows users to simultaneously view synchronized video and graphical data streams frame by frame.

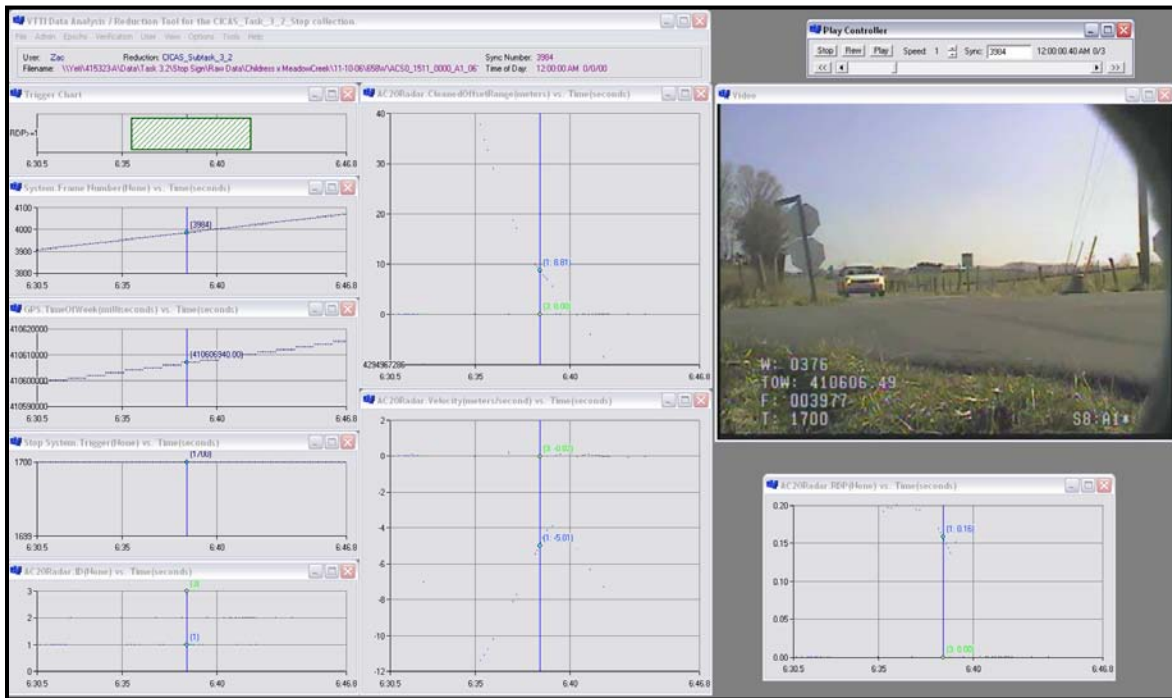


Figure 44 Data analysis and reduction software developed by VTTI.

### Data Reduction Reliability Assessments

Two measures of rater reliability were conducted on the trigger validations. First, reductionists performed 30 minutes of spot checking (of their own or other reductionists' work) during each 4-hour shift. Any disagreements were flagged for review by the data reduction manager. Approximately 20 percent of all data points were spot checked. Any errors noted were addressed with the data reductionists.

The second measure was an inter-rater reliability test administered to each reductionist. The test contained 30 stop-controlled and 13 signalized triggers representing a variety of scenarios and a range of interpretation complexity. The test included both valid and invalid events, as well as violations, near violations, and non-violations. Triggers were first evaluated by the project manager and a gold standard was developed against which rater tests were scored. Test scores are reported below (Table 8 and Table 9).

Stop-controlled test scores (Table 8) were based on overall scores (average across all events), subject driver stopping behavior (percent correct out of 30 events), and event classification (percent correct out of 30 events). Average overall scores were all over 95 percent. In general, stopping behavior was assessed correctly 80.7 percent of the time. Over half (65.6 percent) of the errors in assessing subject stopping behavior were due to the subjectivity of discriminating between a “Rolling violation” and a “Violation with caution,” 27.6 percent were due to “Violation with caution” versus “Violation without caution” disagreements, and 6.9 percent were due to “No Violation” versus “Rolling Violation” disagreements. Errors occurred in event classification only 3.3 percent of the time, including two disagreements in “Non-crash” versus “Near crash” and two disagreements in “Non-crash” versus “Non-conflict.”

**Table 8 Inter-rater test scores for stop-controlled violation reduction.**

Rater	Test Score: Average all Events	Test Score: Driver Stopping Behavior	Test Score: Event Classification
1	95.8%	80.0%	96.7%
2	97.3%	90.0%	96.7%
3	95.8%	76.7%	96.7%
4	95.1%	83.3%	96.7%
5	96.1%	73.3%	100.0%

Signalized test scores (Table 9) were based on event validity (percent correct out of 13 events), radar target crossing behavior (percent correct out of all valid events), and radar target stopping behavior (percent correct out of all valid events). Average scores for each column in the table were all greater than or equal to 90 percent. All of the errors in assessing event validity were due to the subjectivity of discriminating between a “Valid” event and an “Incorrect Vehicle Position Prediction.” All errors in assessing crossing behavior involved violation/near violation and near violation/compliant decisions. The one error noted in stopping behavior was a “Stopped in Protrusion Zone” versus a “Stopped in Intrusion Zone” error.

**Table 9 Inter-rater test scores for signalized violation reduction.**

Rater	Test Score: Event Validity	Test Score: Crossing Behavior	Test Score: Stopping Behavior
1	92%	100%	100%
2	92%	92%	91%
3	77%	100%	100%

<b>4</b>	92%	82%	100%
<b>5</b>	92%	82%	100%
<b>6</b>	92%	82%	100%
<b>Average</b>	90%	90%	98%

## 4 Exploratory Analyses of Vehicle Approaches at Stop-Controlled Intersections

The purpose of this chapter is to describe exploratory analyses of drivers' intersection approach trajectories at the stop-controlled test sites. This investigation was an initial step toward determining which drivers should receive a warning and what metrics should be used in the threat assessment algorithm. The analyses included investigations of driver decisions at stop-controlled intersections with regard to stopping, minimum stop-bar speed, brake onset, and overall vehicle trajectories. These analyses were performed with the goal of assisting the development of the CICAS-V algorithm presented in Section 7.

A CICAS-V algorithm must be capable of predicting the driver's stopping decision at a distance that provides sufficient time for the driver to stop before entering the path of conflicting traffic. The analysis reported in this section has three purposes. The first is to investigate attributes of the vehicle's intersection approach that indicate a target driver population for CICAS-V. The second purpose is to investigate the different types of stopping maneuvers performed by drivers as they approach stop-controlled intersections. Finally, the third purpose is to identify trends in the approach trajectories that could be leveraged by a CICAS-V algorithm.

### Stop-Controlled Intersection Approach Trends

Good driving practice and traffic laws dictate that drivers are expected to perform a complete stop each and every time they approach a stop-controlled intersection. In practice, however, drivers frequently cross stop-controlled intersections without completely stopping. For this report, these slow-moving violations are referred to as rolling violations.

Consider a driver approaching a stop-controlled intersection at the posted speed limit. This driver may slow the vehicle at a sufficient rate to stop at the stop bar; however, if visibility of the adjacent traffic lanes is good near the intersection box, the driver may cease braking and perform a rolling violation. While this is technically illegal, if the driver is cognizant and prepared to stop, it is unlikely that this behavior contributes to the target population (i.e., drivers involved in stop-sign violation-related crashes).

From the analyses performed for Subtask 3.1 and an evaluation of the stop-controlled data, it is clear that rolling violation behavior is very common. If a warning is provided to all drivers performing a rolling violation, a nuisance alarm problem is likely to result. Thus, a binary discrimination based on traffic laws is insufficient for determining algorithm effectiveness. Rather, a stopping behavior classification scheme is required to differentiate the infrequent unsafe behaviors from the numerous safe behaviors. This section describes the determination of the classification system, based on driver behavior at the collection sites. (This classification system was later used to develop and evaluate the performance of candidate algorithms).

A cluster analysis was performed to objectively explore and categorize stopping behavior. Cluster analysis is a statistical method designed to partition data into subsets so that data within each subset shares some common trait. In the present context, the clusters represent different driver behavior groups.

There are several potential measures by which the driver's stopping behavior may be classified. For instance, the speed at the stop bar may be one indicator of this behavior (i.e., a violator

would have a higher speed than a compliant driver). Other possible measures include minimum TTI or average deceleration.

The variable selected for classifying driver stopping behaviors was the maximum RDP. As discussed in Section 3.3, RDP is the required constant deceleration to stop at the stopbar. This measure was selected because the value has a direct relationship to the ability of the vehicle to stop, and is therefore easily interpreted. For instance, if the maximum RDP is 0.3 g, the driver could have easily stopped by the stop bar. On the other hand, a driver with a maximum RDP of 4.0 g would not have been able to stop by the stop bar and is committed to the violation. The maximum RDP was calculated only for ranges greater than 2 m from the stop bar.

A 2-m cutoff was selected because of the behavior of RDP near the stop bar. As a vehicle draws near to the stop bar, RDP will tend toward infinity regardless of travel speed. By only considering RDP values that occur at a range greater than 2 m, the remaining portion of the trajectory is not considered, making the measure sensitive to differences in approach behavior.

The non-parametric kmeans (MacQueen, 1967) method of clustering was selected for this analysis. Kmeans is a partitional unsupervised learning algorithm that minimizes the distance between each data point and the center of the corresponding cluster. The optimization occurs in an iterative process that moves the cluster center and recalculates the distances until a minimum is obtained. Kmeans was selected for this large dataset because it is a common and well understood clustering method (Davidson, 2002) that is computationally efficient (Matlab, 2007) and sensitive to rare observations (Haukrecht, 2003), such as violations in the presence of compliant approaches.

The cluster analysis was performed on a subset of the data that contained a sample of complete vehicle approaches. As discussed in the post-processing section, it was not unusual for a new vehicle track to be generated when vehicles deployed from a standing queue. Thus, only vehicle approaches in which the vehicle remained present from 100 m to 2 m were included in the analysis. The 100-m cutoff also ensured that the vehicle was present for the entire warning region, which became important when the clusters generated during this analysis were used for algorithm development. This resulted in a sample size of 30,623 observations.

The kmeans procedure requires prior selection of the distance measure used for optimization, initial locations for the clusters' centers (seeds), and the number of clusters to partition the data. The squared Euclidian distance was used as the distance metric over which the optimization was performed. It was preferred because of the low dimensionality of the clustering measure and ease of interpretation.

To mitigate the chance of a local optimization, the seed locations were determined using three methods. First, the seeds were allowed to be selected at random. Next, the seeds were selected based on the expected cluster groupings. These seed values were selected using expert knowledge of vehicle deceleration kinematics. The last method selected seeds by evenly distributing them across the range of the cluster variable. For each of the three seed selection methods, the kmeans optimization was allowed 100 iterations for convergence and was replicated 10 times. For all seeds and replications, convergence was obtained and resulted in the same total sum of distances. Therefore, local minimums did not appear to exist in the clustering variable, and thus seed selection strategy did not influence the resulting clusters.

Selection of the number of clusters was based on the stopping behavior groups described in the literature review (Section 1.2). In general, the previous research and experimenter experience suggested a range of potential groupings from a simple two-cluster to a more comprehensive five-cluster grouping scheme. The potential groups are provided below (Table 10). From these groupings, a rolling violation is defined as a driver who nearly stops at the intersection. The attentive violation is a driver who violates the intersection but demonstrates some slowing before reaching the stop bar. The inattentive violation group represents drivers who demonstrate little or no slowing during the approach.

**Table 10 Potential cluster groupings.**

2-Level Clustering	3-Level Clustering	4-Level Clustering	5-Level Clustering
No violation	Stop	Stop	Conservative stop
Violation	Rolling violation	Rolling violation	Normal stop
	Violation	Attentive violation	Rolling violation
		Inattentive violation	Attentive violation
			Inattentive violation

To evaluate the appropriate number of clusters, the kmeans analysis was repeated for two, three, four, and five cluster groups. The quality of the clusters was evaluated through the overall- and within-cluster silhouette widths (Rousseeuw, 1987) and the functional implications of the cluster thresholds. The silhouette width is based on the proximity of an observation to other observations in its cluster versus the proximity to observations assigned to its brother cluster; the width ranges from -1 to 1. A positive silhouette width indicates an observation that belongs in the assigned cluster; the higher the value, the stronger the association. Negative values represent likely misclassifications.

Considering the cluster analysis results (Appendix F), the four-cluster classification scheme was selected. Although the two-cluster scheme resulted in the highest overall silhouette width (0.9924), the groupings were too coarse to segregate the desired behaviors. For instance, the first group contained drivers who demonstrated a maximum RDP of up to 2.23 g. It is desirable to break this group down further as a driver with a very low RDP should not be grouped together with a driver with a 2-g or greater RDP. On the other hand, the five-cluster model contained too much resolution, with partitions in the data that were not necessary for the algorithm to discriminate. In addition, the five-cluster models failed to converge in 100 iterations for a few of the replications. This may indicate over-partitioning of the data, which could lead to lower repeatability in future investigations.

The three- and four-cluster models performed nearly identically when the overall silhouette widths were compared. However, the within-cluster silhouette widths tended to be better for the four-cluster model. In addition, the clusters created (Figure 45) generate logical partitions of RDP. Cluster 1 consists of the normal driver approach containing nearly 25,000 approaches with an average RDP of 0.25 g. Cluster 2 contained 5,573 drivers with an average RDP of 0.75 g and likely contains most safe rolling violations. Cluster 3 contained 51 drivers with an average RDP of 3.15 g, representing violations. Cluster 4 contained the violations with the highest required deceleration with only four drivers and an average RDP of 9.8 g. The error bars displayed in the figure represent the 5 percent and 95 percent of the population determined by a distribution fit, discussed below.



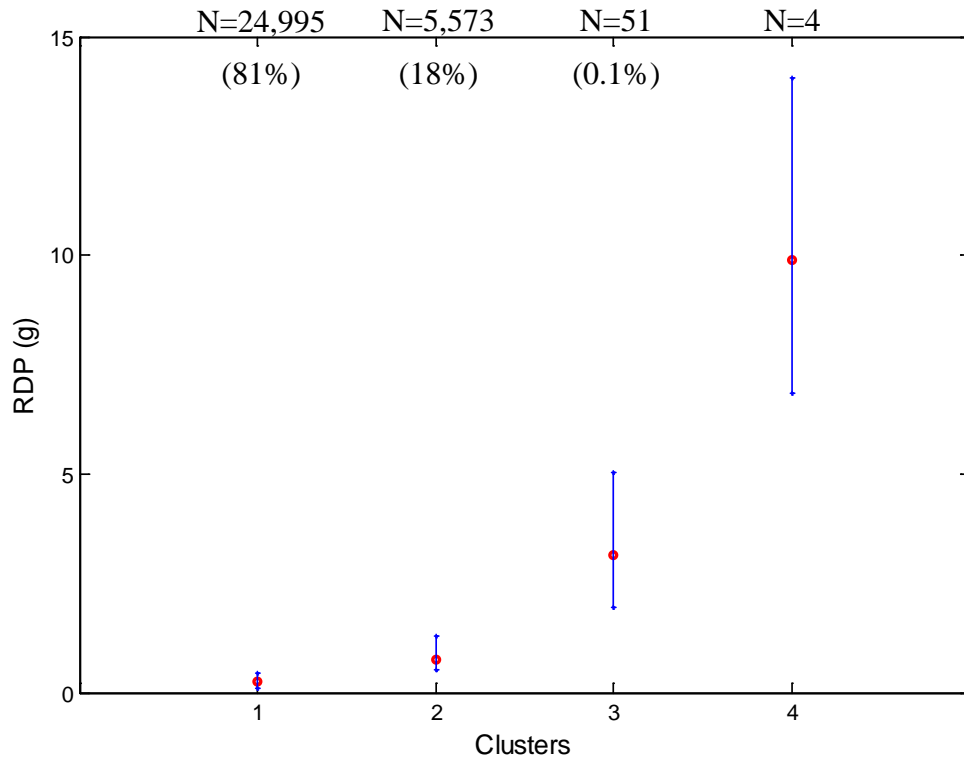


**Figure 45 Average RDP and the 5% and 95% population estimates show as error bars for each of the four assigned clusters describing different types of stop sign approach behavior.**

The cluster analysis provided a partitioning scheme to describe stopping behavior within the sample provided. However, clustering in itself did not describe how the population is distributed into the partitions. To obtain this information, a distribution fit was performed to the overall max RDP measure and within cluster groups. A variety of distributions were considered including normal, exponential, inverse Gaussian, Generalized Pareto, Rayleigh, Birnbaum-Sanders, and Gamma. However, the best performing and most applicable distribution for the measure was the Generalized Extreme Value (GEV) distribution.

The GEV distribution is a family of continuous probability distributions that are well suited for modeling the tails of other distributions (Kotz & Nadarajah, 2001). As such, it is particularly well suited for the max RDP measure that was used as the clustering measure. In addition, the GEV is good for capturing skewed data. These data include unusual events which are of particular interest in this application (e.g., serious violations that are uncommon). Finally, when graphically comparing the GEV to the other potential distributions listed above, the GEV was superior at capturing the empirical distribution of the data.

To ensure that the GEV was appropriate, a one sample Kolmogorov-Smirnov (KS) goodness-of-fit test was performed. The KS test is a statistical comparison between the empirical distribution function of the data and the theoretical underlying population distribution (Chakravart, Laha, & Roy, 1967). The KS test can be sensitive to large data samples, thus the data sets were ordered and down-sampled to 50 equally- distributed observations. These 50 observations were used to

construct the cumulative distribution function, which was then compared to the GEV using the KS test. The KS test was not significant (which indicates a good model) at a 0.05 alpha for the overall max RDP ( $p=0.195$ ) as well as for each of the within-cluster groups (Appendix G). Thus, the GEV distribution may be used to model driver stopping behavior at stop-controlled intersections. The resulting cumulative distributions are provided below (Figure 46) with the parameter estimates provided in Appendix G.

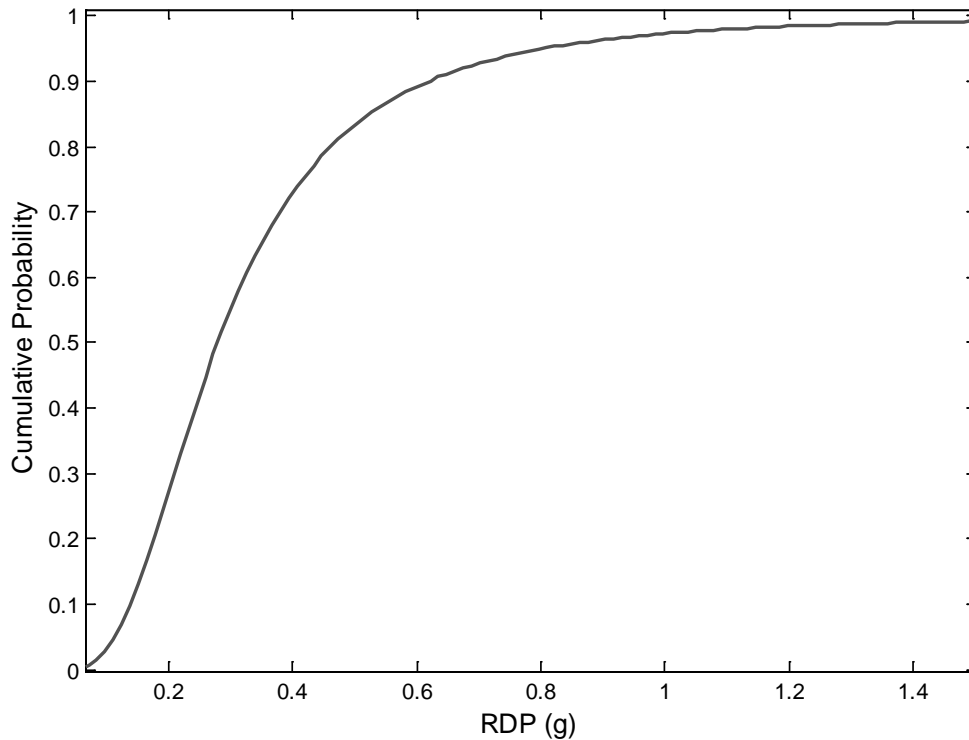


**Figure 46 Cumulative distribution for the overall max RDP exhibited by drivers as they approached the stop bar.**

For the overall distribution, the average maximum RDP across all stop-sign approaches was 0.35 g, which is consistent with typical driver braking levels. Ninety-five percent of the population will approach the stop bar with an RDP of 0.8 g or less. Since most vehicles are capable of a  $\sim 0.9g$ , this suggests that most drivers approach the stop bar with an RDP that allows them to come to a complete stop if required. However, as will be demonstrated in the subsequent section, most of these drivers will roll through the intersection without bringing their vehicle to a complete stop. These rolling violations result in the seemingly high RDP values, representing deceleration rates at which most drivers would not intentionally brake.

The GEV fit also works well for describing the distribution of drivers within each of the cluster groups created (Figure 47). These GEV fits were used to calculate the error bars displayed in Figure 45. While the first cluster contains considerably more data than any of the other three clusters, it is also substantially more compact. As the clusters' average RDP increases, the number of observations decreases and the variance increases. The fourth-cluster fit is based on only a few data points and is therefore exploratory in nature. Considering the four-cluster

scheme and the data reduction results described in a previous section, it appears that the target groups are primarily contained in the third and fourth clusters. These two clusters represent drivers who violate at speeds that do not permit them to come to a complete stop prior to entering adjacent traffic.

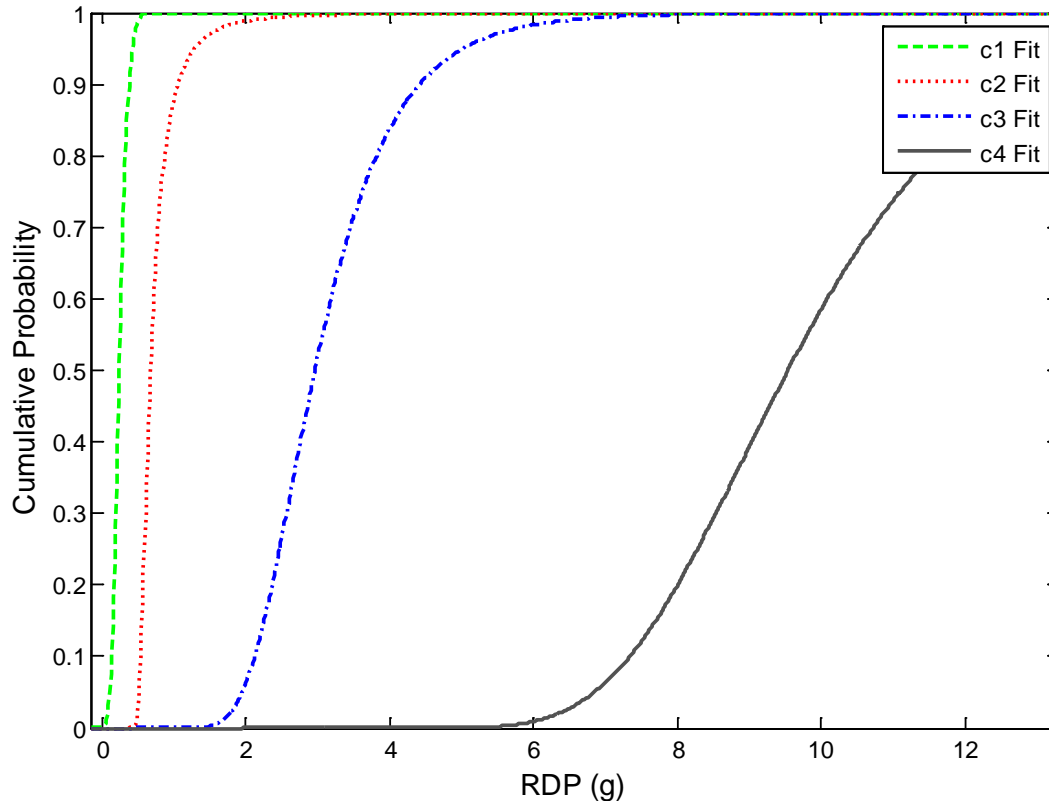


Figure 47 Cumulative distribution for maximum RDP within each of the clusters signifying differing group stopping behaviors.

## Stop-Bar Speed Analysis at Stop-Controlled Intersections

The average RDPs found for the cluster analysis suggested that a large portion of drivers do not completely stop at the stop bar. These drivers are performing a rolling stop, a low-speed violation that is commonly performed by attentive drivers who do not want to completely stop. If a warning is issued to attentive drivers, it will likely be considered a nuisance. Such nuisance alarms will have a negative impact on driver acceptance, which may reduce the effectiveness of an alert issued during a crash threat scenario.

To investigate the stop-bar speed of drivers at stop-controlled intersections, the distribution of minimum speed (from 2 m prior to the stop bar up to 1 m over the stop bar) was evaluated (Figure 48). This region was selected because it allows for variations in the location drivers stop. Only approaches in which the vehicle was reported by the radar through the stop-bar region were included in the analysis; this yielded a total sample of 28,880 observations. As expected, a significant number of drivers failed to fully stop their vehicles. Half of the drivers maintained a

speed of 2 m/s (4 mph) or more as they crossed the intersection. However, 90 percent of the drivers exhibited a minimum stop-bar speed at less than 4 m/s (9 mph).

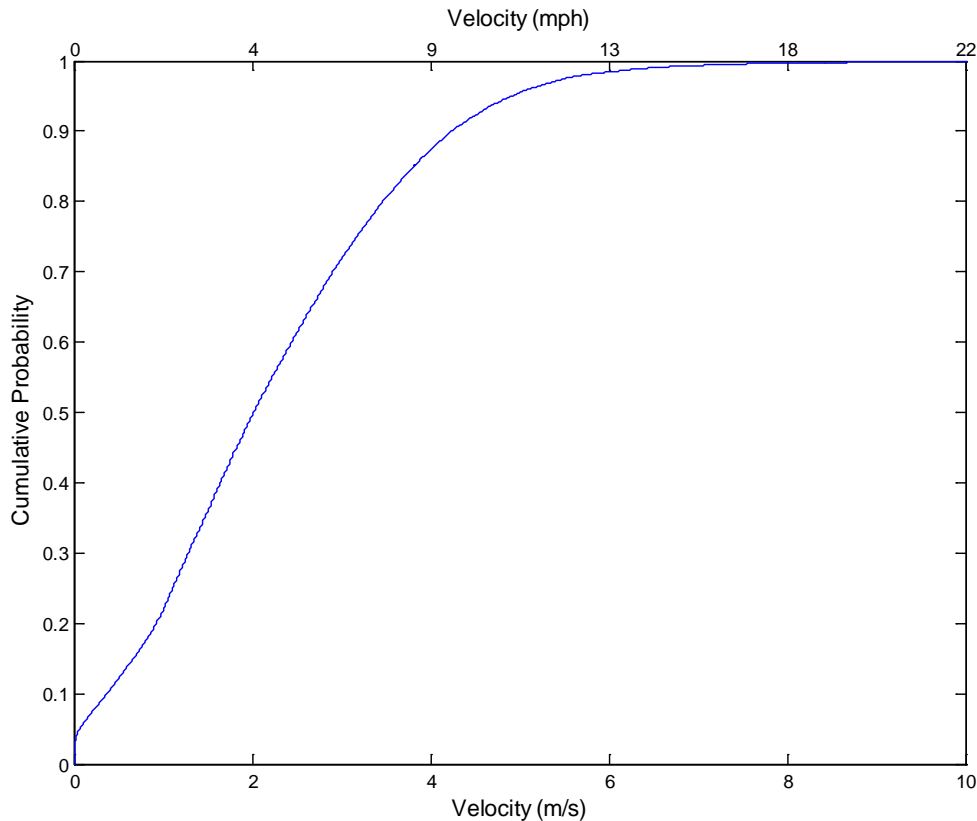


**Figure 48 Empirical cumulative probability of minimum stop-bar speed at stop-controlled intersections.**

This overall distribution can be partitioned into the driver stopping groups defined by the cluster analysis. The behavior grouping provides insight into the relationship between the maximum RDP measure of stopping behavior and the driver's corresponding stop-bar speed. Figure 49 depicts the distribution for stop-bar velocity for each of the clusters. A GEV distribution was fit to cluster 1, while normal distributions were fit to clusters 2, 3 and 4 (parameters are provided in Appendix H). The distribution fits for clusters 1 and 4 are for exploratory purposes only. Cluster 4 contains only four observations that are not sufficient for modeling the population. Cluster 1 exhibited a mixed distribution with a substantial number of drivers completing a full stop; only the drivers who did not stop are modeled by the depicted fit.

As expected, stop-bar speed tends to increase with the stopping behavior group. The cluster analysis suggested that the goal should be to warn all drivers in clusters 3 and 4. It also suggested that a warning to drivers in the right tail of the cluster 2 distributions would not be considered a false alarm. This logic suggests that a minimum speed threshold of 4.4 m/s (10 mph) may be appropriate as a warning criterion; that way any driver traveling slower than this speed threshold would not be warned. As illustrated in Figure 49, a speed threshold of 5 m/s

(11 mph) is predicted to warn over 99.9 percent of the drivers in the third and fourth cluster, while providing alerts to only 20 percent of the cluster 2 drivers.

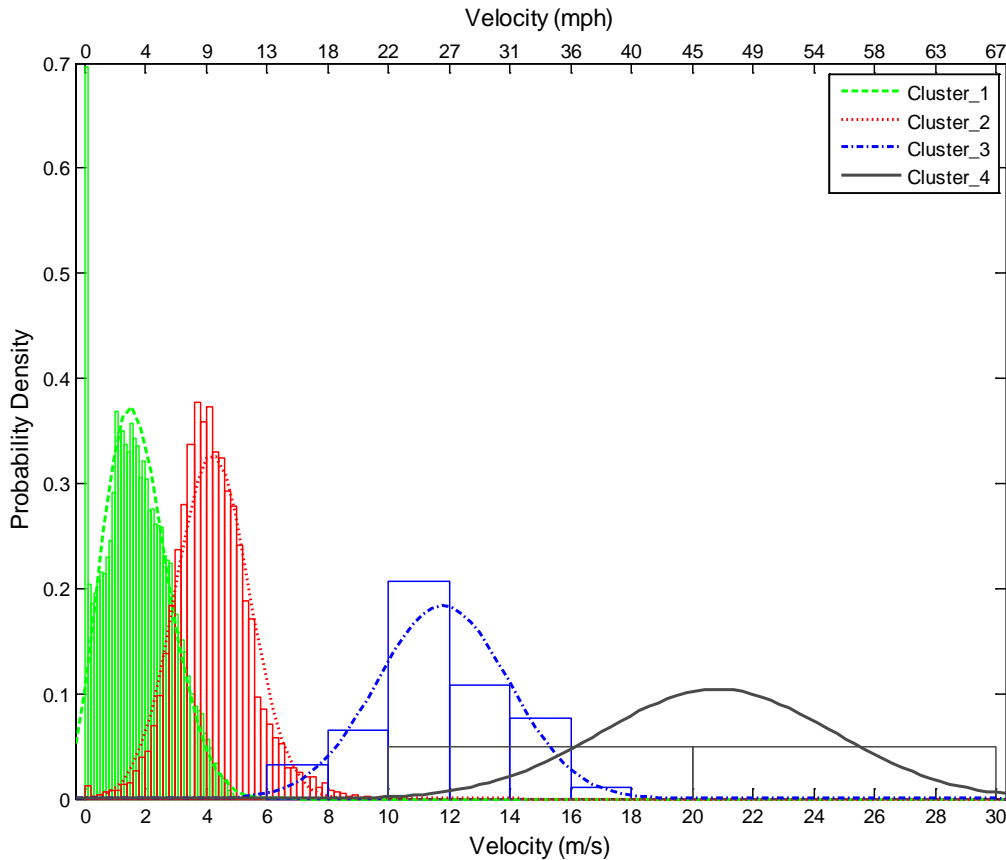


Figure 49 Distribution of stop-bar speed partitioned by cluster. Curve fits for clusters 1 and 4 are for exploratory purposes only.

### Brake Onset Analysis at Stop-Controlled Intersections

The literature reviewed in the introduction suggested that nuisance alarms should be minimized to ensure warning acceptance and effectiveness. One potential method to avoid alerting an attentive driver is to monitor brake status. If the driver is braking, it may be reasonable to assume that he or she is aware of the intersection and does not require an alert. Thus, when the driver is actively braking, an CICAS-V algorithm would suppress the warning without regard to the vehicle’s other kinematic measures.

To study the use of brake status as a component of the algorithm, a box plot of brake onset for clusters 1 through 3 was drawn (Figure 50). A box plot for the fourth cluster was not included because only one driver in this group applied the brakes during the approach. Cluster 3 included only 10 observations because the rest of this group also did not apply the brake during approach. Thus, the box plot was exploratory.

A box plot is a statistical method that visually shows the empirical distributions of different populations without any assumptions of the underlying distribution. Most of the data within a group are contained inside the box bounded by the first and third quartile. The line within the

box represents the median. The whiskers depict the regions that lie within 1.5 times the corresponding quartile. Values outside the whisker are unusual observations and may be treated as outliers.

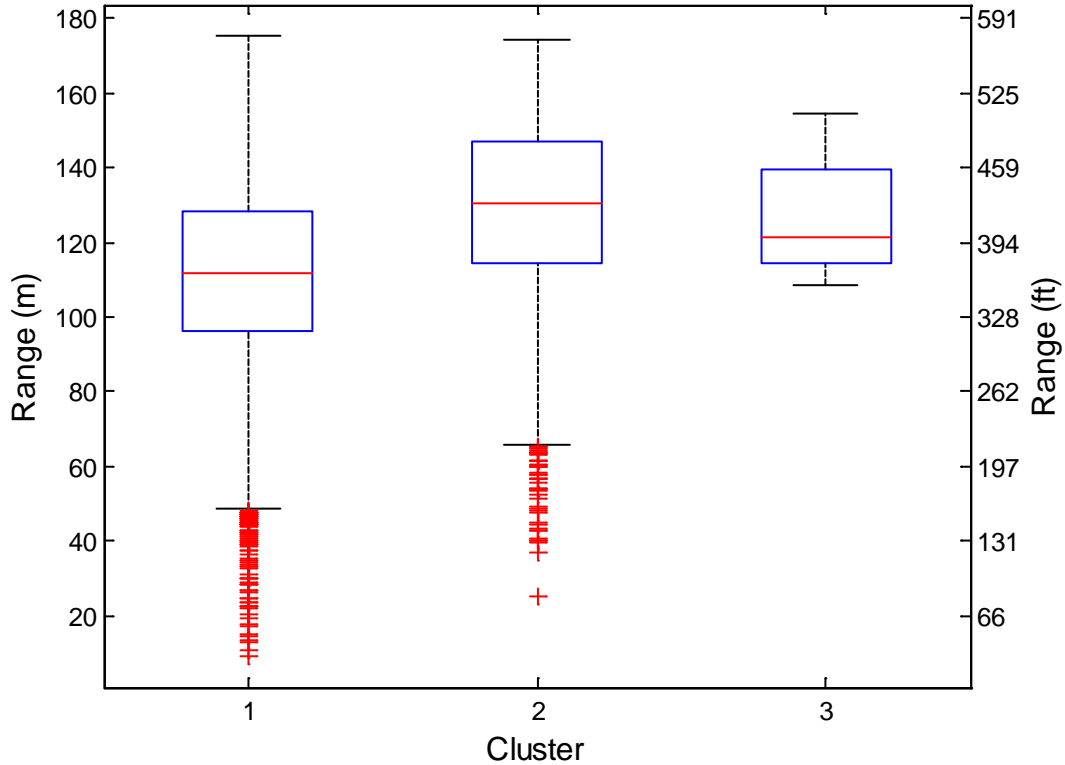


Figure 50 Box plot for brake onset.

The overlapping boxes indicate that a statistical difference for the onset of braking is unlikely. It is interesting to note that the conservative drivers of cluster 1 appear to brake closer to the intersection. This result was initially unexpected, but may be explained by the approach style of the conservative drivers. As discussed later, drivers in cluster 1 tended to initiate slowing earlier by coasting, thus taking advantage of engine braking without actually applying the brake. At some point closer to the intersection, an increase in slowing is required such that the brake is eventually applied.

The primary lesson of this plot is that conservative drivers do not necessarily brake further from the intersection than do aggressive drivers. Thus, algorithm designers should not assume that a braking criterion alone will prevent warning compliant drivers. Many of the compliant drivers brake as late as the more aggressive drivers. It may, however, help suppress the warning for aggressive drivers who will perform a compliant stop. These drivers have to brake earlier in order to slow from their increased initial travel speed.

Group differences for drivers who apply the brake do not appear to exist, so the groups were collapsed while the distribution of brake onset was evaluated. Brake onset followed a normal

distribution (Figure 51, Figure 52) (parameters are listed in Appendix I). The distribution of braking was calculated using both distance and TTI as the dependent measures.

TTI is an interesting measure for representing variables such as brake onset because it is a construct that has been shown to be used by drivers when making last-second braking judgments of vehicles ahead (Kiefer et al., 1999) as well as in other traffic situations (Horst, 1990).

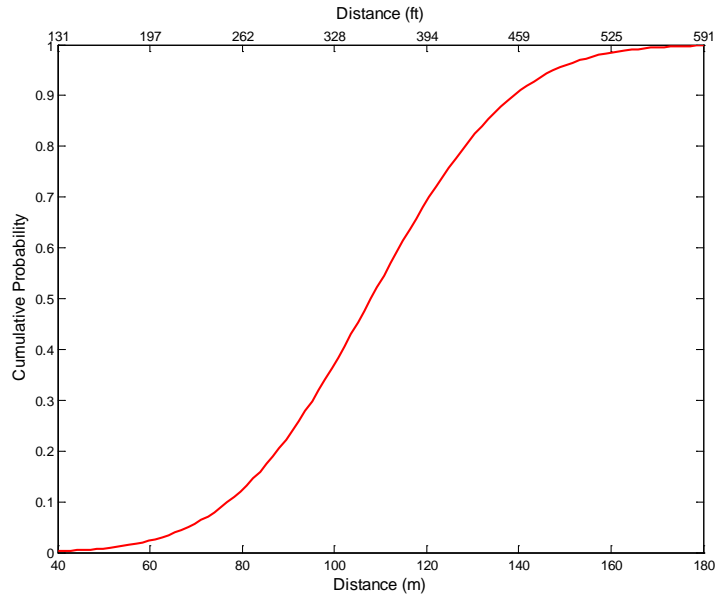


**Figure 51 Cumulative distribution of brake onset as a function of distance to the intersection.**

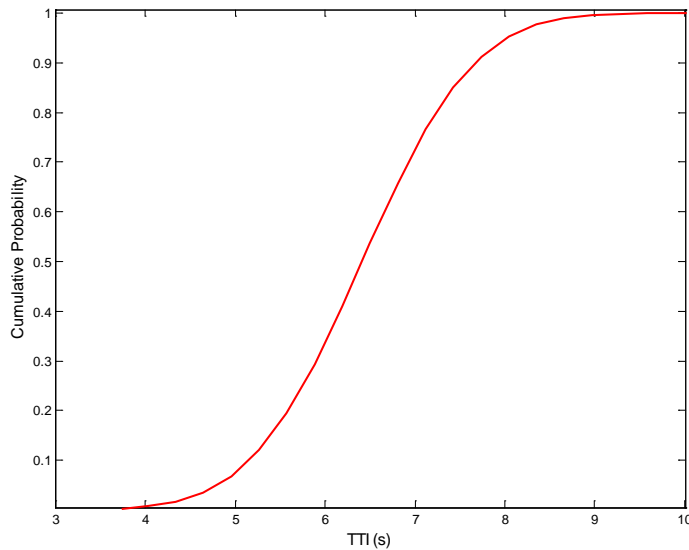


**Figure 52 Cumulative distribution of brake onset as a function of TTI.**

As indicated in the plots, only one percent of the drivers have not pressed the brake at 51 m (or a TTI of 4.3 s). Therefore, ninety-nine percent of the drivers applied the brakes at distance greater



than 51 m or at a TTI greater than 4.3 s. This distribution supports the use of a brake onset component in a CICAS-V algorithm. Smart Road experiments performed in Subtask 3.3 suggested a warning timing of 2.44 s TTI to obtain a high compliance rate. Based on the data above, nearly all drivers would have applied the brake prior to this warning range.

## **Graphical Vehicle Trajectory Analysis at Stop-Controlled Intersections**

Moving beyond driver behaviors at a specified point, it is important for a CICAS-V algorithm to consider measures across the entire intersection approach (e.g., certain trajectory patterns may reflect inattentive driver behavior). The algorithm will need to operate on a continuous basis to provide a timely warning to the violating driver (Neale et al., 2005). Considering the exploratory nature of this project, the vehicle trajectories will be graphically analyzed for trends that may be exploited during future statistical analysis. It is beyond the scope of the present work to develop statistical methods to fully characterize the trajectory data.

Plots of the vehicle kinematic measures provide insight into the differences between driver groups that may be used for threat assessment. A figure for each kinematic variable used in this study is provided below, along with a discussion of the characteristics of the plot. Each plot was created by calculating the average of the depicted kinematic measure (every 2 m from the stop bar to 100 m from the intersection) across all of the test sites. These observations are the same sample that was described in the driver stopping behavior section. For the sake of clarity, the figures in this section depict only the mean of each measure. When applicable, the confidence intervals for the data will be described.

The velocity trajectory plot (Figure 53) demonstrates the large separation between the cluster 4 stopping behaviors. Drivers in this group tend to exhibit higher velocities that demonstrate a minimal decrease over the entire intersection approach. Cluster 1 also tends to exhibit a different approach than the other clusters. As described in the brake onset results, drivers in cluster 1 brake earlier, resulting in a lower velocity at the maximum range reliably measured by the radar (100 m).

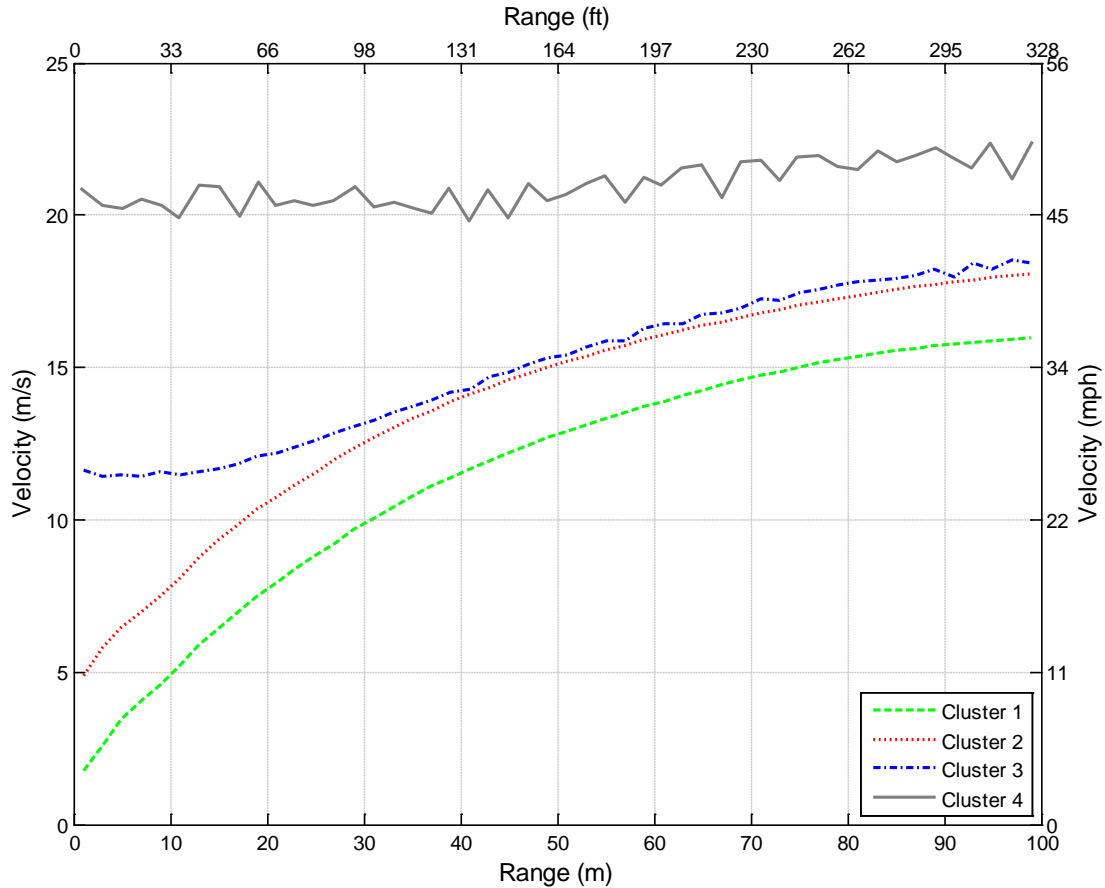


**Figure 53 Mean velocity trajectory of vehicles partitioned by the stopping behavior cluster.**

The second cluster parallels the velocity trajectory exhibited by the first cluster. It appears that drivers in clusters 1 and 2 are similar except in their desired stop-bar speed. Functionally, their velocity patterns are identical, except cluster 2 drivers appear to brake later; thus they carry more velocity into the intersection and demonstrate the rolling stop behavior.

Clusters 3 and 2 are extremely similar at longer distances from the stop bar. As each cluster group approaches the intersection, the two curves deviate, and cluster 3 drivers carry much higher speeds into the intersection than those in cluster 2. Partitioning drivers from clusters 2 and 3 will be the challenge for an ICAS algorithm. For the mean velocity depicted, the curves for these two groups diverge around 33 m. This distance from the intersection is likely sufficient for providing a warning to drivers. However, when the confidence intervals are considered, the point of separation (between the 15 percent and 85 percent confidence limits) is reduced to just 10 m. This distance may not provide sufficient warning time for higher-speed approaches.

Like the velocity trajectory plots, the acceleration plots also provide substantial insight into the differences among the driver stopping behavior clusters (Figure 54). Drivers in the fourth cluster exhibit a minimal amount of braking early in the approach, which tends to drop off to nearly no braking after that point. It is doubtful that this mild acceleration is indicative of an intentional violation. None of the intersections have sight distances that would permit drivers to see the

adjacent traffic at the speeds exhibited by this group. It is possible that this early acceleration was the result of some other intersection characteristics (e.g., the incline present at the Nellies Cave intersection).

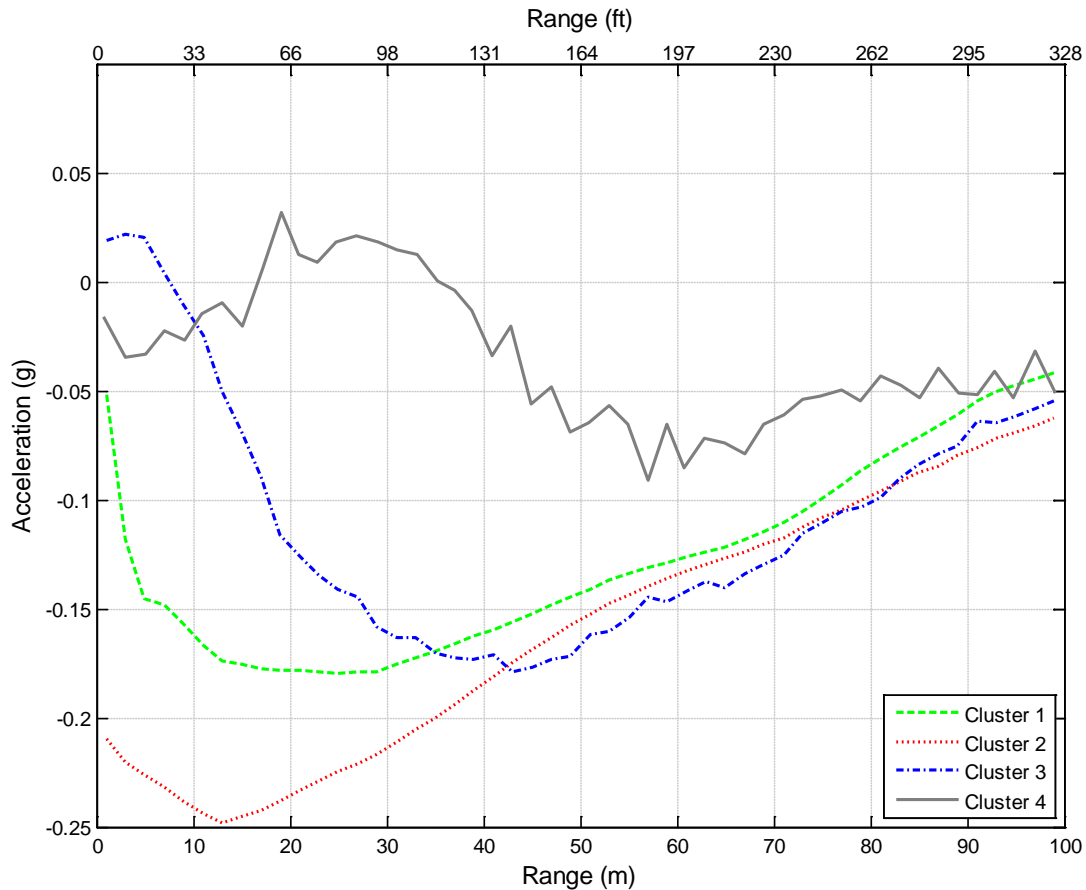


**Figure 54 Mean acceleration trajectory of vehicles partitioned by the stopping behavior cluster.**

Clusters 1, 2, and 3 all exhibited similar decelerations for the first 50 m of the approach. Cluster 1 drivers demonstrate the lowest acceleration initially, likely because they press the brake farthest from the intersection. This provides them more time in which they can decrease their speed. Interestingly, the cluster 2 drivers appear to brake harder toward the end of the intersection approach. This may indicate that this group of drivers is more aggressive with their approach behavior. These drivers are aware of the intersection and initiate braking fairly early, but carry more speed further into the intersection and brake harder and later than cluster 1 drivers. Drivers in cluster 3 may initiate braking so that they can stop if cross traffic is present. However, it appears that, at around 40 m, these drivers may feel confident enough that cross traffic is not present so that they cease braking.

The velocity plots indicated that it would be difficult to discriminate between clusters 2 and 3. This discrimination may actually be somewhat more sensitive for acceleration. In particular, the cluster 3 group appears to stop braking earlier in the approach than cluster group 2. This behavior may indicate an intentional violation of the stop-controlled intersection. However,

clusters 1 and 2 are actually more similar in their acceleration patterns. Perhaps the algorithm will be most effective if it considers a combination of speed and acceleration, which will take advantage of the strengths of each measure.

In terms of algorithm assessment, RDP appears to have some significant advantages over the other kinematic measures (Figure 55). In particular, the confidence intervals for clusters 1 and 4 (not shown in figure) never overlap at any point during the entire intersection approach. This indicates that discrimination between these groups will be more effective than for any other kinematic measure.

The cluster 1 and 4 groups, in general, are substantially more divergent from every other group, as demonstrated by the additional kinematic measures. It is difficult to discriminate between clusters 2 and 3 when comparing their data. The confidence limits of these two groups do not completely diverge until the intersection stop bar is within 10 m. It is likely that some drivers in cluster 2 will be warned in order to catch most of the drivers in cluster 3. However, the drivers on the tail of cluster 2 will have relatively aggressive approaches and will contribute to roughly less than 5 percent of the overall population (based on the models presented in the cluster analysis).

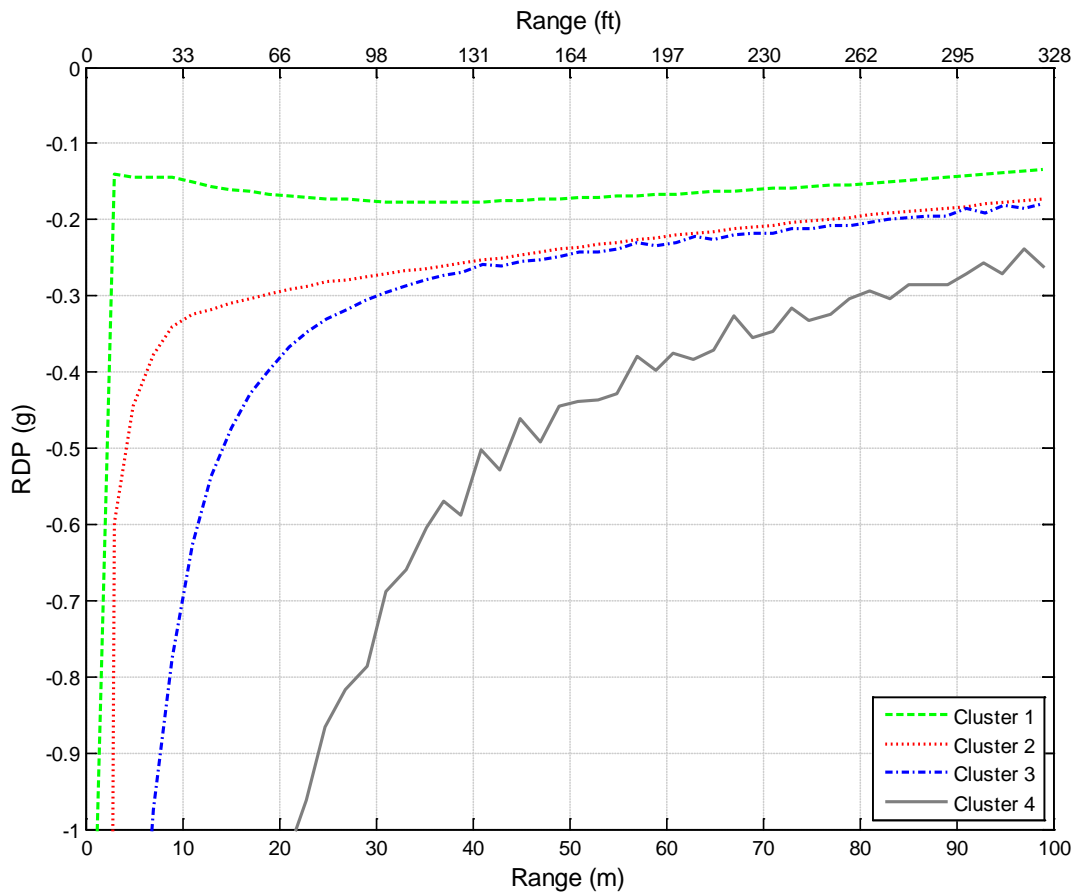
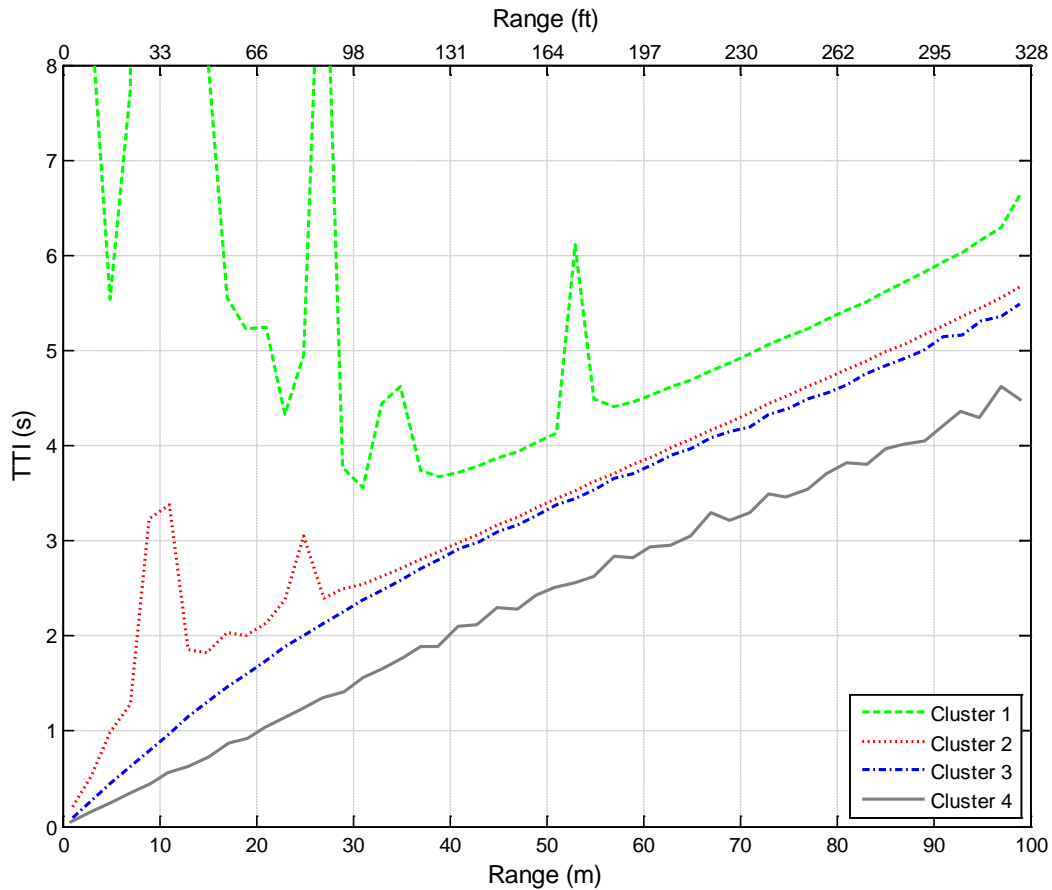


Figure 55 Mean RDP trajectory of vehicles partitioned by the stopping behavior cluster.

The TTI trajectories contain the largest variability of any kinematic measure (Figure 56). The spikes present in the data represent locations in which vehicles began to enter queues at the intersection. When a vehicle slows, the velocity approaches zero, which in turn causes TTI to approach infinity. Thus, the TTI for any given vehicle may tend toward infinity at a variety of locations, depending on the queue length at a specific stop-controlled intersection. However, this behavior is one-sided, so TTI could make an effective algorithm component if the algorithm looks for values below a set value. This value, however, must be dependent on the distance to the intersection because TTI will always approach zero as the intersection stop bar draws nearer.



**Figure 56 Mean TTI trajectory of vehicles partitioned by the stopping behavior cluster.**

The figure above demonstrates that only clusters 1 and 2 regularly approach the intersection with a queue. Drivers in cluster 1 tend to encounter queues more frequently and at greater distances than cluster 2. If the cluster 2 TTI trajectory is projected for cases in which the queue is not present, it does not appear substantially different than cluster 3. This may indicate that TTI is not the optimal measure for determining when the warning should be initiated.

Overall, the analyses described in this section provided the foundation on which the algorithm development process will be built. The cluster analysis provided insight into how drivers should be classified based on their behavior at the stop bar. The subsequent stop-bar speed, braking onset, and trajectory analyses provided data leading to the derivation of the threat assessment algorithms developed and tested in Section 8.

## 5 Exploratory Analysis of Vehicle Approaches at Signalized Intersections

An exploratory analysis of the signalized intersection approaches was performed. This analysis was conducted differently than that for its stop-controlled counterpart. This was due largely to the high frequency of rolling stops at stop-controlled intersections, which created difficulty in classifying compliant versus violating drivers. For this reason, the bulk of the stop-controlled exploratory analysis focused on determining the criteria that would constitute a violation and therefore dictate the need for a CICAS-V warning. This was not necessary at signalized intersections because the signal phase provided clear indication of a violating versus compliant approach.

The signalized exploratory analysis focused on violations and the conditions under which they occurred. Rather than examining vehicle trajectories (as for the stop-controlled intersection approach), this analysis examined signal violations based on maneuver type, time after onset of the red phase, and velocity of the vehicle at the stop bar. This knowledge was applied to the algorithm development and the evaluation procedure discussed in subsequent sections.

### 5.1 Signalized Violations by Maneuver Type

Out of 4,924,267 total approaches, 7,654 violations were identified across the three instrumented signalized intersections. For the analyses described, a violation was defined as any vehicle that crossed the stop bar after the presentation of the red phase and continued through the intersection; drivers that abruptly stopped over the stop bar were not considered violations. In addition, violations for this study do not include all violations as defined by traffic law, which requires that all vehicles come to a complete stop prior to performing a right turn maneuver on a red phase. A high prevalence of vehicles rolled through a right turn during red phase, so only vehicles that maintained velocity of at least 3.6 m/s (8 mph) during the first 2 m after the stop bar were included in the sample. The reduction procedure to validate violations would have been cost- and time-prohibitive if all the rolling violation were analyzed.

A breakdown of the maneuvers performed by violating drivers is illustrated in Figure 57. A majority of violations (54 percent) occurred while drivers were attempting a right-turn maneuver, while smaller percentages of violations were observed for straight-crossing and left-turn maneuvers (36 percent and 10 percent, respectively).

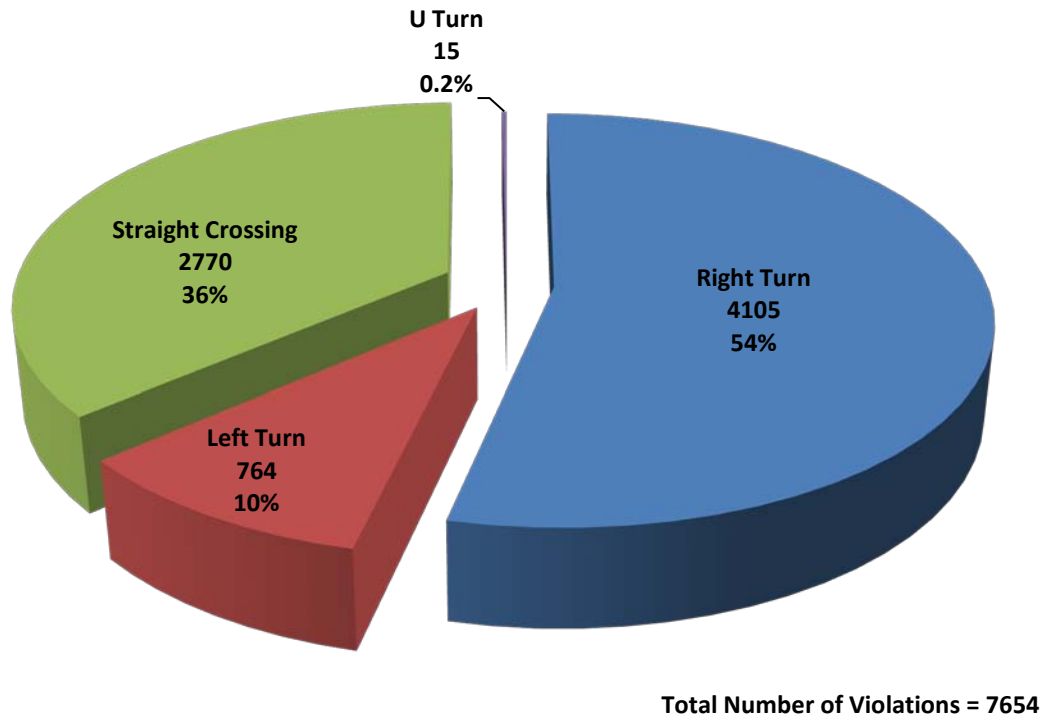


Figure 57 Total signaled violations broken down by turn maneuver for 4,924,267 total approaches across three signaled intersections.

Video- based observations of randomly selected violation events indicated that most of the right-turn maneuvers observed were made by drivers performing a rolling right turn on red. Most of the straight-crossing and left-turn maneuvers were made by drivers attempting to beat the light. These observations are supported by the evidence presented in the next two sections.

## 5.2 Time After Red for Signalized Violations

For straight-crossing maneuvers (which are of primary interest here), most violations occurred in the first second following the red light onset (Figure 58 and Figure 59), indicating that drivers may have been trying to beat the onset of the red phase (Zimmerman & Bonneson, 2005). Although not as prominent, violations occurring during left-turn maneuvers also indicated that drivers trying to beat the onset of a red phase interval. Conversely, most violations arising during right-turn maneuvers occurred more than 5 s after the presentation of the red phase, suggesting that drivers were making rolling violations while making a right-on-red maneuver.



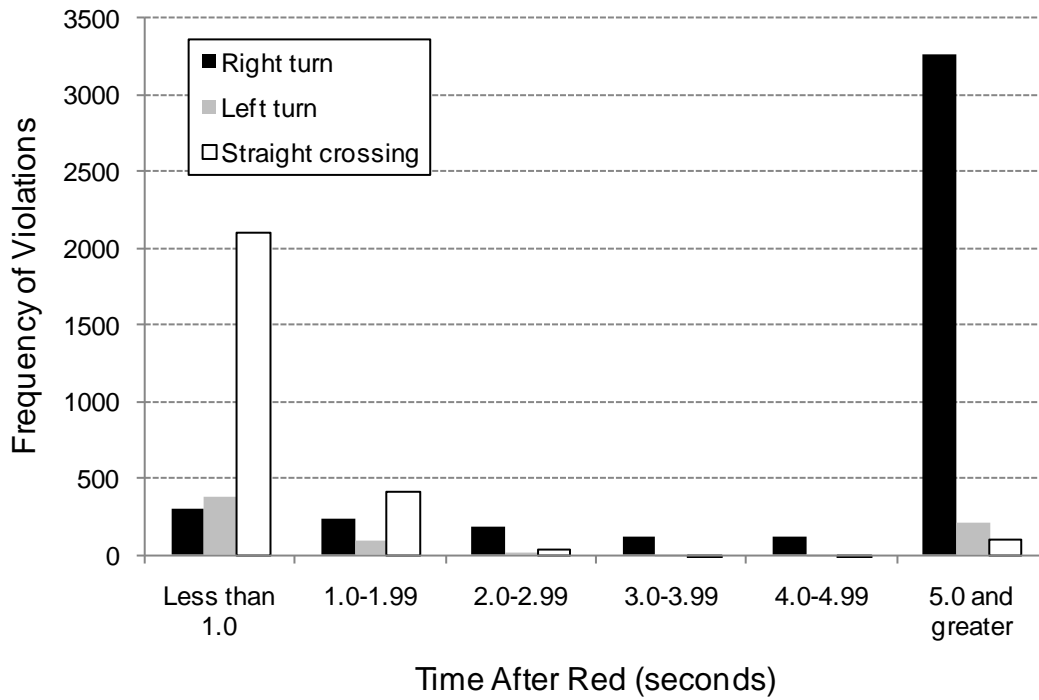


Figure 58 Frequency distribution for signaled violations over time after onset of red phase.

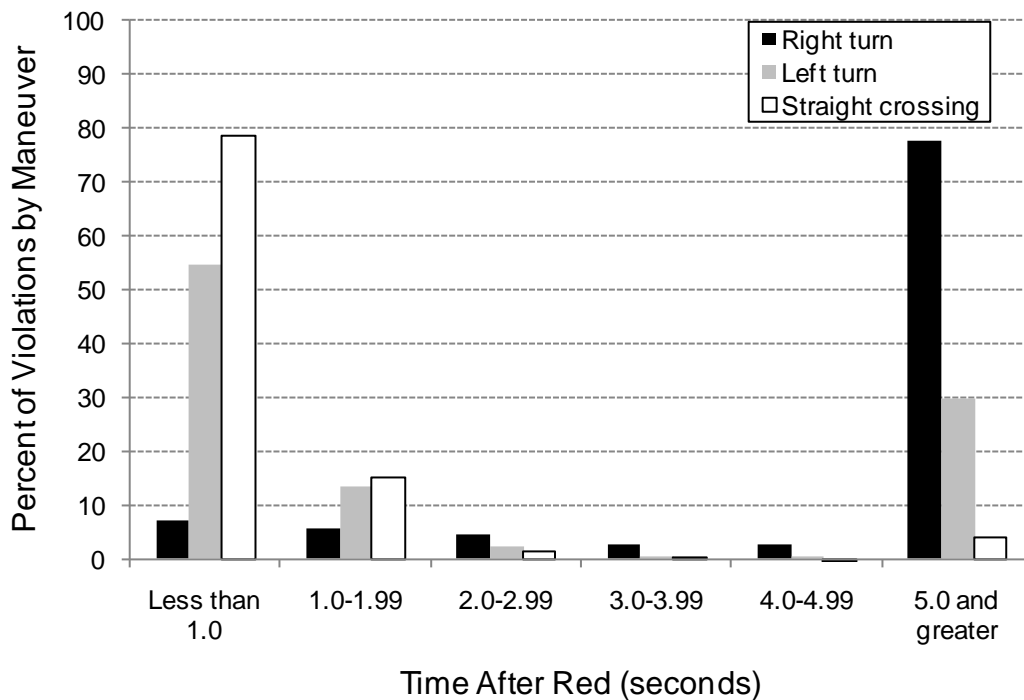


Figure 59 Percentage of signaled violations that occurred within maneuver. The proportion of violations from each maneuver sum to 100 percent.

Eighty percent of the violations performed during a right-turn maneuver occurred more than 5 s after the presentation of red. These violations resulted primarily from drivers who did not completely stop while performing a right-turn-on-red. This effect highlights the similarity between right-turn approaches performed on the red phase at signalized intersections and approaches made to stop-controlled intersections (Section 4). In both cases it is likely that a large portion of drivers are attentive to the intersection control device and surrounding traffic. As these drivers approach the intersection, they slow their vehicle such that a stop would be possible; however, at some point near the stop bar they note the absence of conflicting traffic and choose to proceed without coming to a complete stop.

The analysis performed under Subtask 3.1 (Sudweeks et al., in review) also found that nearly all violations performed while making a right turn during a red phase were performed by drivers who appeared to be attentive. It is hypothesized that providing warnings to these attentive drivers will be perceived as nuisance. Such nuisance alarms will have a negative impact on driver acceptance, which may reduce the effectiveness of an alert issued under crash threat conditions.

The straight-crossing maneuver violations that occurred in the first few seconds of red are most likely to result in a crash with a vehicle performing a left-turn maneuver from an opposing lane (Zimmerman & Bonneson, 2005). This type of crash (LTAP) tends to occur during the termination of green at intersections without left-turn protection. As the phase turns red, the driver performing a left turn attempts to clear the intersection while incorrectly assuming that the opposing straight-crossing vehicle will stop. The violations that occur in the first few seconds of red may result primarily from drivers who misjudge the length of the yellow phase. To elicit a change in the intended behavior of these drivers, the CICAS-V warning will need to convey stopping as the prudent choice.

Violations that occurred more than 4 s after the red are likely to result in a straight-crossing-path (SCP) crash (Zimmerman & Bonneson, 2005). An SCP crash involves a violating vehicle that is either performing a straight-crossing or a left-turn maneuver and collides with a vehicle arriving from one of the perpendicular approaches. Subtask 3.1 (Sudweeks et al., in review) and Zimmerman and Bonneson (2005) suggest that drivers who violate several seconds after the presentation are likely to be distracted. For these drivers the CICAS-V warning will need to direct the driver's attention to the traffic control device and convey stopping as the prudent choice.

While analyzing Figure 59 it was noted that a large portion of the left-turn violations were occurring more than 5 s after presentation of red. A small informal investigation was performed in an attempt to better understand this finding. Thirty left-turn violation approaches with a time after red greater than 1 s were analyzed. The violations were randomly selected within time after red bins of 1 to 5 s, 5 to 20 s, and 20 s or more (10 approaches from each bin).

The analysis indicated that the left turn violations were valid. Overall, most of the violations observed occurred without any phase change, without traffic, and during the day (Table 11). Violations more than 5 s after the presentation of red tended to occur when the adjacent signal turned green. This may indicate that some drivers adhered to the incorrect signal indication. In addition, with increasing time after red, more of the violating drivers may have been predicting their phase change would soon be green. For these drivers, the traffic signal changed to green

after they crossed the stop bar but before they exited the intersection. Finally, the violating drivers observed within the shorter time-after-red bin appeared to be attempting to beat the arrival of the red phase where neither signal turned green, as some increase in speed was often observed.

**Table 11 Exploratory violation analysis for drivers turning left for the indicated seconds after the light turned red**

\*Sample size was 30 (10 approaches from each time-after-red bin)

Time After Red	Adjacent Signal Turned Green	Signal Turned Green After Vehicle Entered Intersection	Neither Signal Turned Green	Traffic Present	Night
1-5 s	0	1	9	7	1
5-20 s	4	2	4	1	3
20+ s	4	4	2	1	6
<b>Total</b>	8	7	15	8	10

### 5.3 Stop bar Velocity for Violations at Signalized Intersections

The stop bar velocity during violations is an important consideration when determining the target population for CICAS-V. As discussed in the stop-controlled section, many of the low-speed violations are likely performed intentionally by drivers who are attentive to the intersection and surrounding traffic. At signalized intersections, most of these slow-speed intentional violations are performed during right-turn maneuvers (Figure 60).

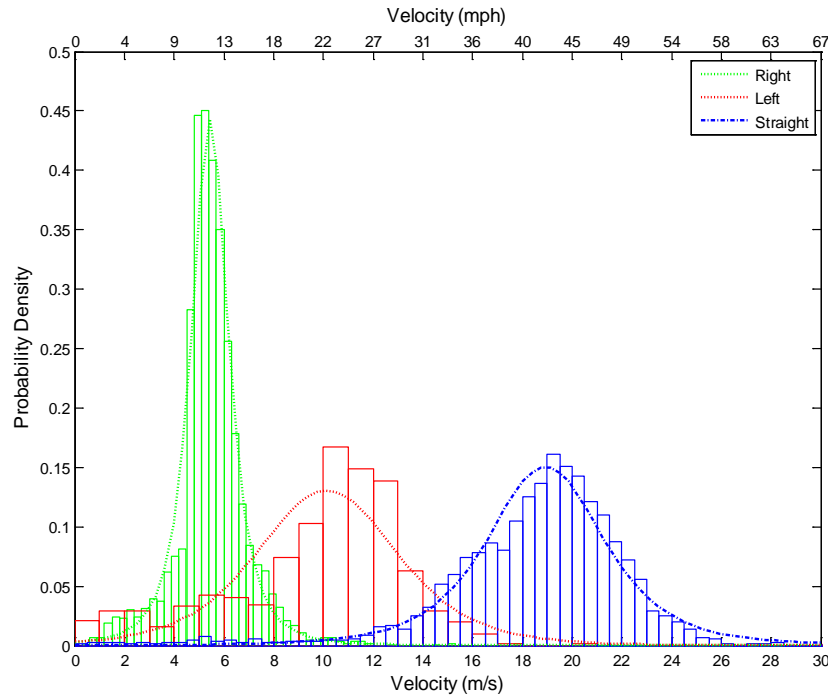


**Figure 60 Stop-bar velocity at signalized intersections partitioned by maneuver type**

The relative location of the three curves in Figure 60 indicates the differences in approach trajectories for these three types of violations. Drivers who perform a right turn typically have to slow substantially to perform the maneuver. Similarly, drivers also have to slow their vehicle to perform a left turn though not by the same magnitude. Finally, drivers who perform straight crossings tend to maintain higher speeds with few approaches below the minimum speed limit found at the test sites (11.6 m/s, 25 mph).

An attempted model of the stop-bar speed distributions is indicated by the lines displayed in Figure 60. The best fit identified across the distributions was a t-location scale. The t-location scale uses the student's t distribution and is better than a normal curve for fitting data with heavier tails. While the curves appear to provide good approximations of stop bar velocity for the different maneuvers, a Kolmogorov-Smirnov Test (Appendix H) indicated that the fit was significant (indicating an inappropriate model).

Overall the analyses described in this section provided the foundation on which to develop the signalized intersection approach algorithm. Investigation of the violations built an understanding of the types of vehicle approaches that must be addressed by the algorithm. Based on the frequency of right turn violations, the time after red at which they occur, and their associated stop-bar speeds, it appears that drivers performing right turns on red are similar to drivers at stop signs. In both cases, many of the drivers appear to intentionally roll through the intersection without performing a complete stop. As suggested previously, these drivers are likely to perceive a warning as nuisance, potentially undermining the effectiveness of the CICAS-V during crash threat conditions.

## 6 CICAS-V Algorithm Testing and Evaluation Procedure

The work described thus far has provided the foundation for the threat assessment algorithm development and analysis procedures. Synthesis of the literature described in Section 1.2, engineering theory, and the intersection approach analysis described in Sections 4 and 5 generated data inputs for algorithm analyses. Algorithms were assembled from interpretations of the synthesized data and based on principles of human factors and physics. The devised algorithms were tested in a pseudo-real-time simulation using the actual vehicle trajectory data collected for this study. The primary output of this analysis is a set of threat assessment algorithms that will be carried forward into the CICAS-V development and testing in subsequent tasks of the CICAS-V project.

Each algorithm was evaluated using the theory of signal detection to compare the sensitivity, specificity and nature of the predicted outcome (e.g. alert timeliness and predicted level of nuisance). Results were analyzed to determine possible regions for improvement based on the classification of vehicle trajectories. Improvements were made and the simulation cycle was conducted iteratively until additional revisions did not yield significant algorithm performance improvements (for clarity in presentation of the material, most of the iteration cycles are not reported here).

Signal detection theory (SDT) provides a general framework to describe and study outcomes that are made in uncertain or ambiguous situations. Developed by Tanner and Swets (1953), SDT is an established statistical method. It has been applied in a variety of contexts across a variety of disciplines; from air traffic control to medical diagnostics (Parasurman, Hancock & Olofinboba, 1997; Swets, 1996; Wickens, 2002). The method defines a signal that represents the true state of the world. There is a desire to evaluate this signal; however, the signal is masked by the presence of noise in the environment. This makes discrimination of the true state of the signal a probabilistic process based primarily on the ratio of the signal-to-noise.

### Application and Extension of SDT Method to the CICAS Context

In the context of CICAS-V, the threat assessment algorithm must predict a violation well before the driver crosses the stop bar in the presence of an extremely high proportion compliant intersection approaches. This prediction is difficult because it must be made without direct knowledge of the driver's intent; rather, it is inferred through the vehicle trajectory information.

Drivers exhibit differing driving styles, which introduces dynamic noise into the prediction process. In particular, the approach characteristics that would indicate a violation for one driver may be another driver's typical driving style. In SDT, it is assumed that the true state of the signal is unknown to the detector. In the present context, the threat assessment algorithm does not know whether or not the driver will violate. This scenario results in four possible outcomes of the threat assessment (Table 12). The number of outcomes that fall into each of the four categories depends on the threat assessment algorithm and its associated algorithm-specific parameter settings.

Table 12 Possible outcomes of the threat assessment.

		True State	
		Violation	Compliant
Algorithm Response	Violation	True Positive	False Positive
	Compliant	False Negative	True Negative

This phenomenon is demonstrated in the theoretical distributions below (Figure 61). The figure depicts two normal probability distributions: one for the violating drivers and the other for the compliant drivers. The horizontal axis represents a hypothetical dimension used by the algorithm to predict the outcome.

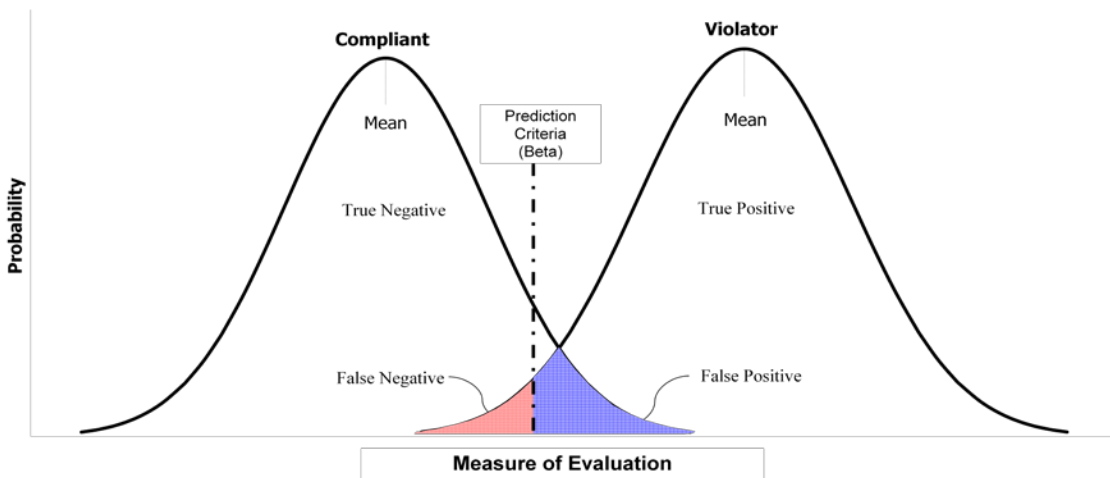


Figure 61 Theoretical representation of the SDT signal (violation) and noise (compliant) distributions. The distance between the peaks of the two distributions represents the sensitivity of a given algorithm. The overlapping regions of the two curves that lie on the incorrect side of the decision criteria line represent misclassifications performed by the algorithm.

The location and shape of the two distributions will depend on the measure evaluated by the threat assessment algorithm. If a particular measure is more sensitive, the two curves will exhibit less overlap. The vertical line in Figure 61 represents the prediction criteria as defined by SDT and is typically referred to as Beta. Beta is used by the threat assessment algorithm to place the current driver in the compliant or violation category. If the prediction of the current vehicle trajectory falls to the left of Beta, it will be categorized as a compliant approach. If it falls to the right, it will be categorized as a violation.

Depending on the driver’s true stopping behavior, the prediction would result in one of the four outcomes in Table 12. False negatives (often referred to as misses) and false positives (often referred to as false alarms) are the result of the prediction falling on the incorrect side of the decision criteria, while true positives and true negatives indicate a correct assessment. The true positive and false positive rates are typically used to describe the performance of an algorithm.

In considering the cost and benefits for CICAS-V, it is clear that the true positive rate should be maximized since a violation that is not identified is more likely to lead to a crash. However, it is also important that false positives are minimized. As discussed in the literature review, an

abundance of false positives will result in annoyance and distrust which can ultimately lead to a decrease in system effectiveness.

The receiver operation characteristic (ROC) curve is a tool for evaluating the discriminability of an algorithm through a range of Beta combinations. The ROC curve plots the combination of true positive and false positive rates as Beta is varied within a given algorithm. In the present context, the area under the curve represents the sensitivity of a given threat assessment algorithm. The larger the area, the better the algorithm will discriminate between violators and compliant intersection approaches.

An example ROC curve is provided below in Figure 62 for one of the algorithms analyzed as part of this project. This ROC curve represents a simple RDP algorithm in which the vehicle’s instantaneous RDP is compared to a warning RDP over each frame of the intersection approach trajectory. The warning RDP value, which represents Beta, is set at a value while a simulation is performed. The resulting number of false positives and true positives are recorded and then plotted as a single point on the ROC plot (see figure annotation). This process is repeated for various values of the warning RDP (Beta) until a curve is created across the plot space.

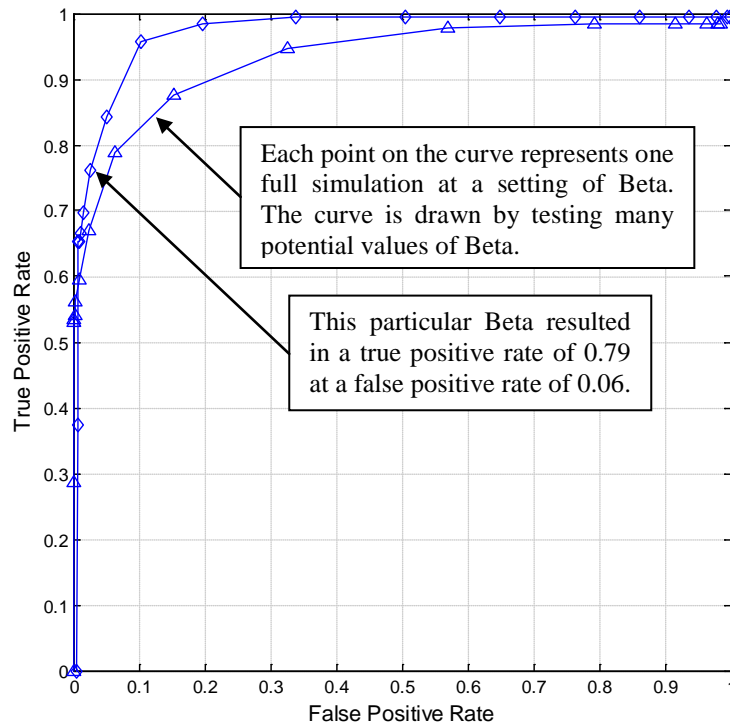


**Figure 62 Example ROC curves. Each curve represents the hit and false alarm rates for a particular threat assessment algorithm across a variety of decision criteria (Beta). The larger the area under the curve, the better an algorithm is at discriminating violators from compliant drivers.**

There is an important distinction from many classical SDT problems that must be made when applying the technique to a time-critical system such as CICAS-V. Consider that a driver must receive the warning at a sufficient distance to allow time for perception, reaction, and vehicle braking before the intersection stop bar is crossed. Classic SDT would indicate that an algorithm

performed perfectly, even if every warning was provided 1 m before the vehicle crossed stop bar. Clearly, none of the drivers receiving the warning would have sufficient time to stop, thus negating the safety benefit of CICAS-V.

Unfortunately, there is no single point on the intersection approach at which a warning becomes too late. Rather, as a warning is provided later in the approach a decreasing number of drivers will be able to stop. During Subtask 3.3, a substantial volume of test-track research was performed to determine the optimal CICAS-V warning (Perez et. al, in review). These test-track experiments were primarily focused on comparing the effectiveness of a variety of warning modalities; however, warning timing was sometimes used as an independent variable. An auxiliary analysis of the warning timing results for the best warnings tested during these studies was performed (Appendix J).

The auxiliary analysis developed a model to describe the distribution of warning effectiveness as a function of the RDP at which a warning was provided. Two points on the distribution were extracted for use in the SDT analysis. First, the too-late point was defined as the location after which a warning would have very low utility. If the violating drivers do not receive a warning prior to the too-late point, at least 95% will not be able to stop in response to the warning. Based on the model, the too-late point for the most effective warnings tested to date corresponds to a warning RDP of 0.49 g. Any warning presented such that an RDP higher than 0.49 g would be required to stop is not considered a true positive during this analysis.

If an algorithm correctly identifies a violator after the too-late point, the event is counted as a false negative. Thus, the true positive axis on the ROC plot contains only those warnings that were provided to the correct group of drivers and before the too-late point was reached. The result is substantially lower true positive rates; however, these rates better reflect the anticipated actual effectiveness of the warning.

The second point extracted from the warning effectiveness distribution is the favorable warning point. This warning point represents the location at which nearly 100% of the drivers are predicted to stop when a warning is received. A preferred algorithm will provide all of the warnings at or before the favorable warning point (warning RDP  $\leq$  0.36 g). The favorable and too-late warning points allow relative comparisons between the timing of different algorithms.

To compare the warning timing for the various algorithms, the optimal Beta value for each algorithm must first be selected. Considering different Beta values corresponds to moving across the ROC curve depicted in Figure 62. Each permutation of Beta for a particular algorithm results in a corresponding true positive and false positive rate. Thus, there is an inherent trade-off between true positives and false positives that must be considered when selecting the optimal Beta. Selecting the highest possible true positive rate will result in an unacceptable number of false positives; whereas minimizing false positives reduces the true positives to an unacceptable level. Typically, when SDT is used, Beta is selected by setting the allowable false positive rate and then identifying the corresponding true positive rate.

Currently, it is unknown how many false positives drivers will tolerate from a CICAS-V or the relationship of false positives to system effectiveness. From other collision avoidance system research, it is clear that every effort must be made to minimize the number of false positives (Neale & Dingus, 2006; Kiefer et al., 1999; Dingus, et al., 1998). Rather than select a single false positive rate, two possible values were investigated and subsequently modeled during this



research. The 0.05 and 0.01 false positives rates bounded the problem space and allow comparisons to be made across a reasonable selection of Beta.

After identifying the allowable false positive rates, the associated Beta was selected to maximize the true positive rate for each algorithm. This process resulted in the selection of an optimal Beta for each algorithm used. The intersection approaches represented by the selected Beta were then further analyzed. First, the warning timing was investigated for the optimal Beta within each algorithm. This was accomplished by graphing the empirical cumulative probability across the warning RDP. The distributions included markers for the too-late and favorable warning points identified earlier. The example selected to draw the ROC curve in Figure 62 is used to illustrate the warning distribution investigation in Figure 63.

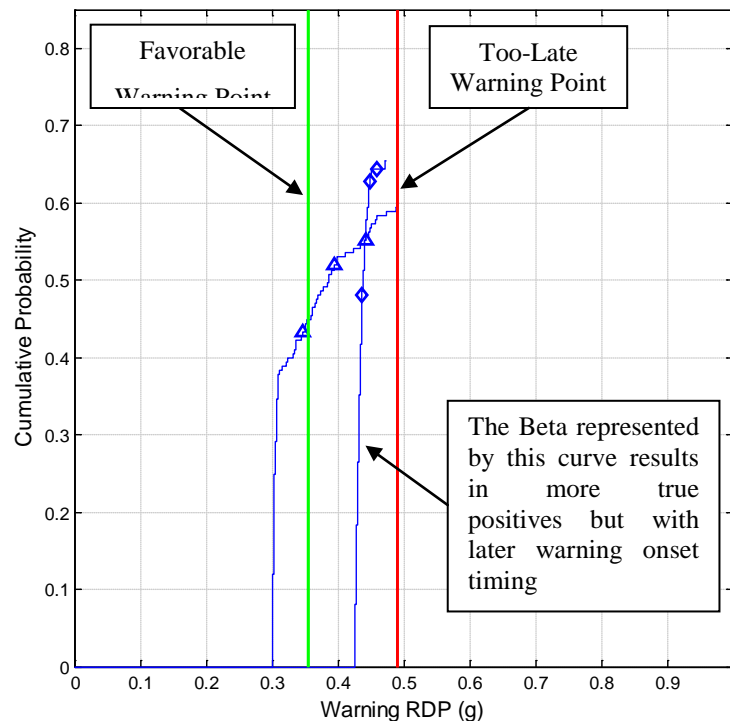


**Figure 63 Example warning timing distribution for true positives using the algorithms depicted in Figure 62 evaluated at the Beta value corresponding to a false positive rate of 0.01.**

Using the figure above, comparisons were made in terms of the maximum true positive rate obtained at both the too-late point and the favorable warning point. An algorithm that provides most of the warnings near the favorable warning point may be preferable to an algorithm that provides more true positives overall but provides them at warning timings near the too-late point.

In addition to warning timing, the distribution of the false positives was also evaluated. This evaluation is based on the principle that not all false positives are created equal. The effect of a false positive will be different depending on the experience of the driver. A driver who nearly violated may not consider the alert a nuisance and may even appreciate the warning (may also instill confidence in the systems credibility).

Thus, a false positive presented to a driver whose stopping maneuver is a near violation is considered less annoying than a false positive provided to a driver who had a mild, compliant intersection approach. To evaluate this effect, the distribution of the stop-bar speed for the false positive approaches was plotted relative to the violation criteria. Distributions that were skewed toward the violation threshold were preferred over those that occurred far from the criteria. The false positive distribution is demonstrated below (Figure 64) using the same example algorithm depicted in Figure 62 and Figure 63. The vertical marker is the violation threshold (15 mph in this example). A distribution in which most false positives occur close to the threshold is preferred over a distribution in which most of the false positives occur far from the threshold.

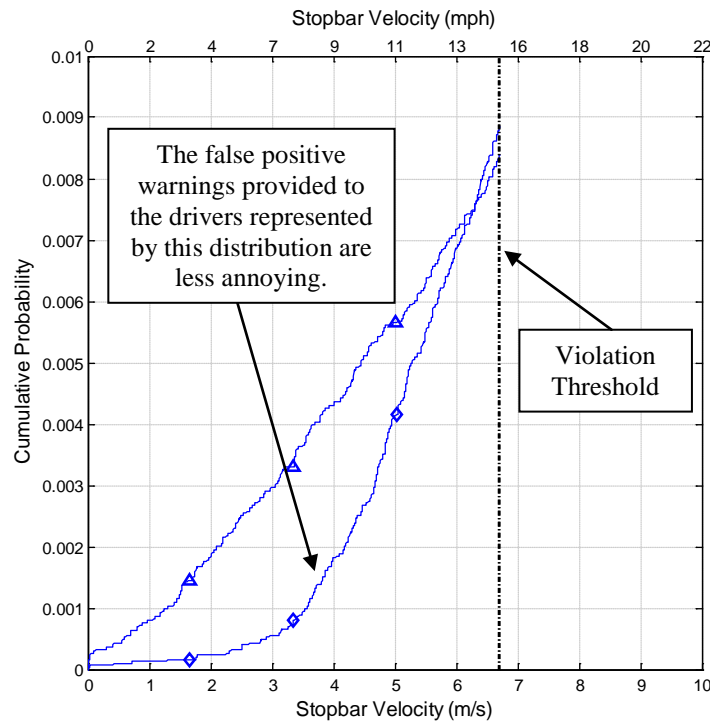


**Figure 64 Example stop bar velocity distribution for false positives using the algorithms depicted in Figure 62 evaluated at the Beta value corresponding to a false positive rate of 0.01.**

The SDT method described in this section was deployed to over 160 algorithm permutations to arrive at a recommended set of threat assessment algorithms. The procedure used to employ the SDT method on the collected data sets is described in the next section.

## Algorithm Assessment Procedure

A structured approach was devised to develop and test a variety of potential intersection CICAS-V threat assessment algorithms. This approach was highly iterative and is outlined below. With the exception of steps two and three, which will be discussed in detail in the following chapter, this section will describe each of the following steps:

1. Define the target warning group.
2. Generate prototype algorithms.

3. Define Beta ranges for each algorithm.
4. Run pseudo-real-time simulation for each algorithm/Beta combination to obtain true positives and false positive alerts.
5. Compare resulting ROC curves for each of the algorithm forms.
6. Select the best-performing algorithms, evaluate misclassifications, and improve algorithm.
7. Re-define all algorithms with the enhancements identified in step six.
8. Iterate steps three through seven until no further enhancements are realized.
9. Select the algorithms with the highest final sensitivity.
10. Compare the remaining algorithms in terms of the following:
  - a. The warning timing distribution relative to the required warning timing for drivers receiving a CICAS-V warning.
  - b. The distribution of false alerts relative to the violation criteria to understand the severity of the false alarms.
11. Provide recommendations for CICAS-V algorithm based on overall results.

A basic underlying assumption of SDT is a binary signal. The first step in applying SDT to the CICAS-V threat assessment context is to define the signal (violators) and the noise (compliant drivers). According to Virginia law, any driver who does not come to a complete stop at a stop-controlled intersection or during a red phase at a signalized intersection is a violator. However, in reality few drivers will receive a ticket while slowly rolling through a stop sign or right-on-red. Furthermore, based on the data presented previously in Figure 48, most drivers passing through the intersection would be classified as violators. If the warning criteria followed the law, most drivers would be violators, which will result in a false positive (nuisance alarm) problem.

It is beyond the scope of this report to strictly define the target violation population, since defining a violation is a political and safety-related issue. That said, the results presented earlier may be used to guide the decision process. In particular, the cluster analysis and subsequent graphical analysis demonstrated some natural groups in the data. These analyses suggested that clusters 3 and 4 appeared to represent the target population of violators, with some portion of cluster 2 representing less dangerous violations that may still benefit from a warning. Rather than assume a particular portion of the second cluster that should be warned, multiple thresholds were selected. This allowed interpretation of the results across a broad range of violation criteria. Results will show that lower speed violation (e.g. less than 10 mph) thresholds do not appear to be feasible.

Four violation criteria at stop-controlled intersections (Table 13) and three criteria at signalized intersections (Table 14) were tested as part of this investigation. The criteria were selected based primarily on the stop-controlled intersection analyses reported in Section 4. The lessons learned during the stop-controlled analyses were carried forward into the signalized analyses for drivers who performed right-on-red maneuvers (details regarding this decision are available in Section 5). The 5-mph stop bar velocity violation threshold was not tested at signalized intersections for two primary reasons. First, the stop-controlled analysis described in Sections 4 (and later in Section 8) clearly show the 5-mph violation threshold resulted in a very large number of nuisance alerts. Second, setting a violation threshold at 5 mph resulted in over 80,000 signalized

intersection triggers that 1) seemed highly unlikely and 2) could not be validated with reduction during the time frame of this project.

The violation thresholds span a range of logical choices for determining when an approach should become a target violation for the CICAS-V system. Stop-bar speed was selected to define the violation threshold because rolling stops are typically discussed in terms of the speed at which they occur. A regression was performed to relate stop-bar speed to minimum RDP (Appendix K). Using this regression, a span of stop-bar speeds was selected according to the distribution of clusters from Section 4. The values selected in Table 13 ensure that clusters 3 and 4 are violators, while cluster 2 ranges from just over one percent violators to 100 percent violators. A driver who never slowed below the cutoff was classified as a violator for purposes of algorithm evaluation.

**Table 13 The selected violation threshold criteria tested at stop-controlled intersections and the resulting violation samples. Total number of samples in the data set was 30,458.**

Stop Bar Velocity	Minimum RDP (g)	Number of Violators	Percent of Sample	Percent of Cluster 1	Percent of Cluster 2	Percent of Cluster 3	Percent of Cluster 4
2.2 m/s (5 mph)	0.34	10,808	35.5	17.6	100	100	100
4.52 m/s (10 mph)	0.80	1,673	5.5	0	27.7	100	100
6.72 m/s (15 mph)	1.36	185	0.6	0	4.2	99.9	100
8.92 m/s (20 mph)	2.00	49	0.2	0	1.2	93.8	100

**Table 14 The selected violation threshold criteria tested at signalized intersections and the resulting violation samples. Total number of samples in the data set was 2,105,961.**

Stop Bar Velocity	Minimum RDP (g)	Number of Violators	Percent of Sample
4.52 m/s (10 mph)	0.80	3,335	0.16
6.72 m/s (15 mph)	1.36	2,670	0.13
8.92 m/s (20 mph)	2.00	2,491	0.12

Pseudo-real-time simulation refers to the process of coding the algorithm into a program that loads each individual intersection vehicle approach trajectory through the algorithm in a frame-by-frame fashion. Thus, the method simulates the process under which the algorithm would

actually function if it was installed in every vehicle that approached the intersection during the data collection. For every vehicle approach, the algorithm predicted either a violation or compliant vehicle approach. The algorithm classifications were then compared to the true actions of the driver to compute the true positive and false positive rates.

Once algorithm performance was obtained, an ROC curve was plotted for each algorithm across its potential settings of Beta. Every algorithm family (described in the subsequent section) was plotted on a single ROC plot space. The best in-family and across-family algorithms were selected for further analysis. The follow-up analyses continued using graphical methods to investigate the misclassifications resulting from the algorithm simulation.

For example, trajectory plots such as the ones shown in Figure 65 were created for range, velocity, TTI, and RDP. These plots were viewed to determine trends in the trajectories that could be addressed by an algorithm enhancement. The approaches below resulted in false negatives for an algorithm that suppressed the warning if it detected that braking was active. For these approaches, violations resulted despite a mild level of braking. To address this, a new algorithm was developed that required the vehicle to be braking at a rate of at least 0.1 g before the warning would be suppressed. Many similar enhancements were made in an iterative fashion.

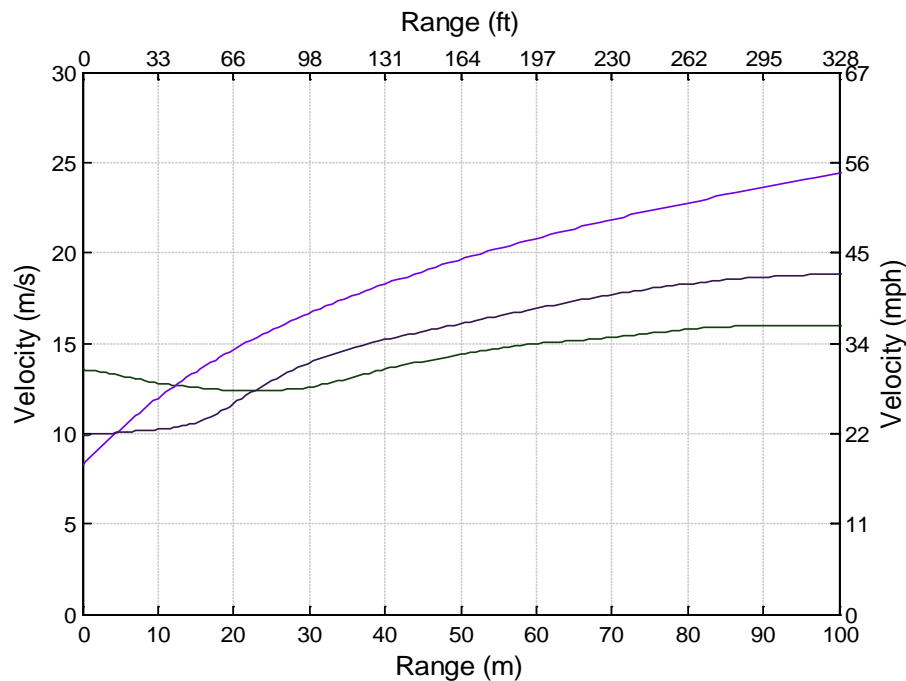


Figure 65 Example vehicle trajectories that produced false negatives for one of the algorithm iterations.

Each time an enhancement was developed for a particular algorithm, it was applied to all of the algorithms and the simulation cycle was iterated. This ensured that a poorly performing algorithm would not benefit greatly from an enhancement placed on an initially higher-performing algorithm. This cycle was repeated until no further algorithm enhancements were identified.

With each iteration cycle, the ROC curves were evaluated with all the potential algorithms and Beta criteria represented. The most sensitive algorithms were selected for the warning timing and false positive evaluations described in the previous section. Algorithms were preferred if:

- They provided the highest true positive rate
- At the lowest false positive rate
- With true positives that obtained warnings sufficiently early to allow a violating driver to stop
- While resulting in false positives with the lower level of nuisance

Over the course of the development and evaluation cycles, a few algorithms emerged as consistently high-performing predictors of stop-controlled intersection violations. These algorithms were identified using a search heuristic and subsequently recommended as the prototype algorithms for the CICAS-V system (Section 8).

## 7 Generated CICAS-V Threat Assessment Algorithms

The following discussion opens with some general definitions for the variables used in the algorithms. Next, the basic two-level architecture of the algorithm is described. This is followed by a detailed description of each layer and the algorithms contained within them. The section closes with a description of the naming convention that will be used for describing the algorithms throughout the subsequent evaluation results.

### Variable Definitions

This section provides definitions for the variables found in the various algorithms. The reader may find it useful to refer to Figure 66 for a visual representation.

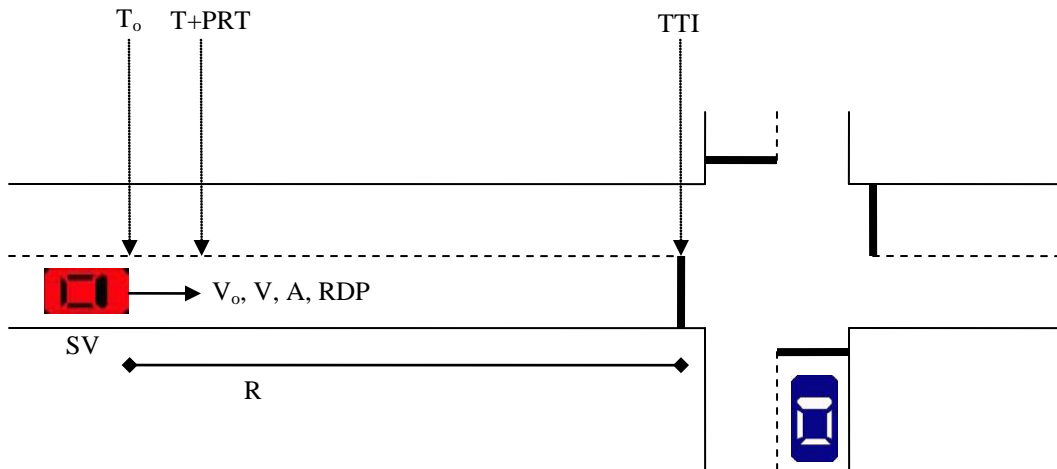


Figure 66 Intersection scenario and variables used for algorithm development.

SV	= Subject vehicle (the vehicle that is being evaluated by the algorithm)
$T_o$	= Initial time when vehicle enters the intersection communication region
R	= Instantaneous range from SV to stop bar
V	= Instantaneous velocity of SV
$V_o$	= Initial velocity of SV
$V_f$	= Final velocity of SV
A	= Instantaneous acceleration of SV
TTI	= Instantaneous time to intersection of SV
$TTI_{req}$	= TTI required for the driver to stop at the stop bar
RDP	= Constant deceleration required to stop at the stop bar
PRT	= Perception reaction time from warning presentation to the brake application
a,b,c	= Parameters used in the regression equations

### Top-Level Architecture

All of the algorithms tested in this research follow the same basic framework (Figure 67). An approaching vehicle first enters the monitored region of the intersection at time  $T_o$ . Once the

vehicle enters the region of interest, its kinematic state is measured every 50 milliseconds. For the present research, the measurements were performed by the radar; however, in the CICAS-V application, these measures are obtained from onboard sensors. The kinematic measures available to the algorithms include the vehicle's range to the intersection, velocity, and acceleration. From these measures, other composite measures such as TTI and RDP are frequently calculated (see Chapter 5 for derivations). Once the kinematic measures are evaluated, they are fed into the first layer of the algorithm.

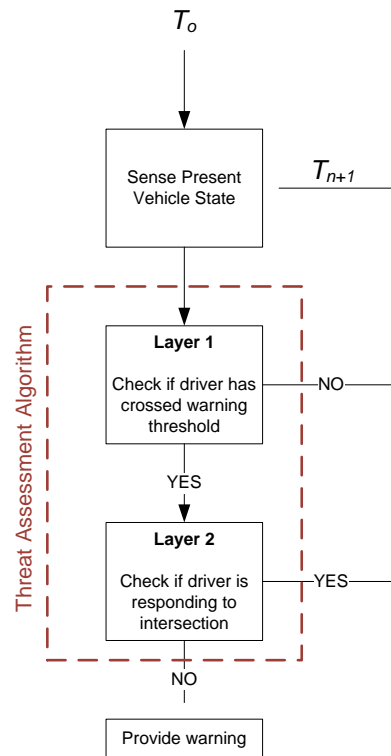


**Figure 67 Top-level algorithm architecture.**

The first layer contains a computational component that evaluates whether the warning should be provided, based on the present kinematic state of the vehicle. This layer gathers together a variety of measures into a single metric, which is then compared to the prediction criteria Beta. If the outcome of the comparison indicates compliance, the algorithm computations cease for the present time frame. The evaluation process then starts over the next time cycle. If the outcome of the comparison predicts a violation, the present vehicle kinematics are passed to the second layer of the algorithm.

The second layer of the algorithm was added to reduce the number of false alarms produced by the first layer. The second layer evaluates the present state of the vehicle to predict whether the driver is attentive to the intersection. If the driver is assumed to be attentive (e.g., has started braking or is below a set speed), the warning is suppressed. If the driver is not assumed to be attentive, the warning is set to active and the algorithm is terminated for the remainder of the intersection approach trajectory. If the warning is suppressed, the entire process begins again



with the next time window and is repeated through the entire intersection approach trajectory unless a warning is presented.

The remaining portion of this section will be devoted to describing the two major layers of the algorithm. These layers and their components were developed iteratively to address a variety of characteristics noted in the trajectory plots presented in the graphical analysis section of this report. The iterative development is not reflected in this discussion; only the fully developed algorithms are discussed.

## Layer 1 Algorithm Component

The first layer of the algorithm compares the vehicle's current dynamic state to decision criteria that will determine when a warning should be activated. Each of the layer 1 algorithms described in this section actually represents a family of algorithms when combined with the second layer. Combinations of the two layers represent the decision criteria (Beta) in the SDT process.

There are two broad categories of layer 1 algorithms: kinematic and empirical. Kinematic algorithms are constructed based on the laws of physics. The empirical algorithms were created through regression of sampled behaviors. The advantages of each class of algorithm were explored. For instance, the kinematic procedures have a foundation in physics, which provides an easily- interpreted and well- understood format.

The empirical methods often provided better performing algorithms but potentially at the cost of a decreased ability to generalize to other intersections. There are various issues surrounding a lack of acceptance in the engineering community, since these algorithms are more difficult to interpret. The following first-layer algorithms (Table 15) are described next. Additional algorithms were investigated but are not presented in detail; they are briefly discussed at the end of this section.

**Table 15 First-layer algorithms presented in this report.**

Algorithm Family	Description
100	Static TTI
200	Static RDP
300	Static RDP with an assumed 1.01-s PRT
400	Static RDP with an assumed 0.78-s PRT
500	Warning TTI as a function of range
600	Warning range as a function of velocity
700	Warning range as a function of velocity with truncated data
800	Warning RDP as a function of range

### Algorithm 1: Static TTI

The first algorithm uses a constant warning TTI that is compared to the driver's instantaneous TTI. A similar warning strategy has been examined in the past for forward collision avoidance

systems (Kiefer et al., 2000) and ICAS (Neale et al., 2005). Time-based measures, such as TTI, are thought to be a good representation of the metric used by the human visual system to judge whether or not to stop (Horst, 1990). With this algorithm, a warning is provided to a driver when the vehicle's instantaneous TTI is less than the required TTI ( $TTI_{req}$ ).

#### Equation 7

$$\text{Warn if: } TTI < TTI_{req}$$

The  $TTI_{req}$  represents the minimum TTI at which a driver must receive the warning in order to come to a complete stop before entering the intersection. The  $TTI_{req}$  is a composite of both the driver's reaction time and the time necessary for the driver to stop the vehicle. For this algorithm,  $TTI_{req}$  is the warning criteria Beta, over which the algorithm was simulated. Repetitions were made with a  $TTI_{req}$  ranging from 1 s to 5 s with a step size of 0.25 s.

#### Algorithm 2: Static RDP

The second algorithm resembles the first, except it uses a static level of required deceleration as the warning unit. This algorithm assumes that all drivers need a warning when the deceleration required to stop at the stop bar exceeds a pre-defined threshold. Research performed by Neale et al. (2005) indicated that the observed RDP needed by drivers to stop at intersections in response to a DVI was constant across speed. This relationship suggests that RDP is a good metric for representing the time when drivers begin responding to the traffic control device. The RDP equation is developed based on kinematic relationships which are defined by particle motion physics. For simplicity of explanation, the derivation is performed below, starting with the classical engineering kinematic equation rather than with a derivation starting from the underlying physical laws.

#### Equation 8

$$V_f^2 = V_o^2 + 2 * a * R$$

The goal is to get the driver to stop the vehicle at the stop bar, so the final velocity is set to zero. In addition, with that goal in mind,  $a$  is the constant acceleration required to stop, defined previously as RDP. The equation may then be re-organized as follows.

#### Equation 9

$$R_{warn} = \frac{V_o^2}{2RDP}$$

#### Equation 10

$$\text{Warn if: } R < R_{warn}$$

An alert is issued if a vehicle approaches the intersection in such a way that its instantaneous range is less than the warning range. The RDP in Equation 9 represents the maximum RDP at which a driver must receive the warning in order to come to a complete stop before entering the intersection. As with the static TTI algorithm, RDP for the static RDP algorithm is also a composite of both the driver's reaction time and the time necessary for the driver to stop the vehicle. For this algorithm, RDP is the adjustable warning criteria Beta. The simulation was performed for RDPs of 0.025 g through 0.5 g with a 0.25-g step size.

### Algorithms 3 and 4: Static RDP with an Assumed PRT

As with the previous two, the third and fourth algorithms assume a constant RDP at which a driver must respond to successfully stop at the intersection. They also explicitly consider the driver's reaction time. One advantage of these algorithms is the ease of interpretation of the parameters. The RDP value is the actual constant deceleration that the driver will need to perform, rather than a composite of the constant deceleration and the PRT values. The equation for the second algorithm is extended to consider the distance traveled while the driver is reacting to the warning:

#### Equation 11

$$R_{warn} = \frac{V_0^2}{2RDP} + V_0 * PRT$$

#### Equation 12

$$\text{Warn if: } R < R_{warn}$$

In this algorithm, PRT is defined as the time from presentation of the warning to the application of the brake. This includes the time required for the driver to perceive the warning, release the throttle, and transition to pressing the brake. The PRT value is selected based on the Subtask 3.3 DVI studies. The overall average PRT from these studies was 0.78 s (SD=0.10). Algorithm 3 uses the 0.78-s average as the PRT value. The fourth algorithm assumes that it is desirable for nearly all drivers to have sufficient time to stop. Thus, it assumes the 99th percentile PRT of 1.01.

### Algorithm 5: Warning Range as a Function of TTI

The next series of algorithms is based on models of vehicle trajectories developed as part of this investigation. The data for 30,000 compliant vehicle approaches from stop-controlled and signalized intersections were randomly selected (60,000 total approaches) for these algorithms. At signalized intersections, only vehicles approaching a yellow or red phase and performing a stop were considered. For each of the two intersection types, a linear regression was performed to define a set of empirical threat assessment algorithms.

The fifth algorithm compares the vehicle’s instantaneous TTI to a warning TTI. The warning TTI is calculated using an equation developed through a regression of velocity. The first step in this process was to place the TTI data into a series of velocity bins. For instance, the TTI for all the stop-controlled or signalized approaches that occurred between 0.5 m/s and 1.5 m/s were placed into the 1 m/s bin. This process was repeated for each 1 m/s (2 mph) increment from 0 to 22 m/s (49 mph, just beyond the speed limit at the highest-speed intersection). The data residing in each bin was modeled with an empirical cumulative distribution. Within the velocity bins, the distribution tails were selected to form a series across the velocity bins. For example, the top three points at each velocity bin on Figure 68 (shown in red) represent the 15th, 12th, and 10th percentile values from top to bottom for the stop-controlled intersection distribution.

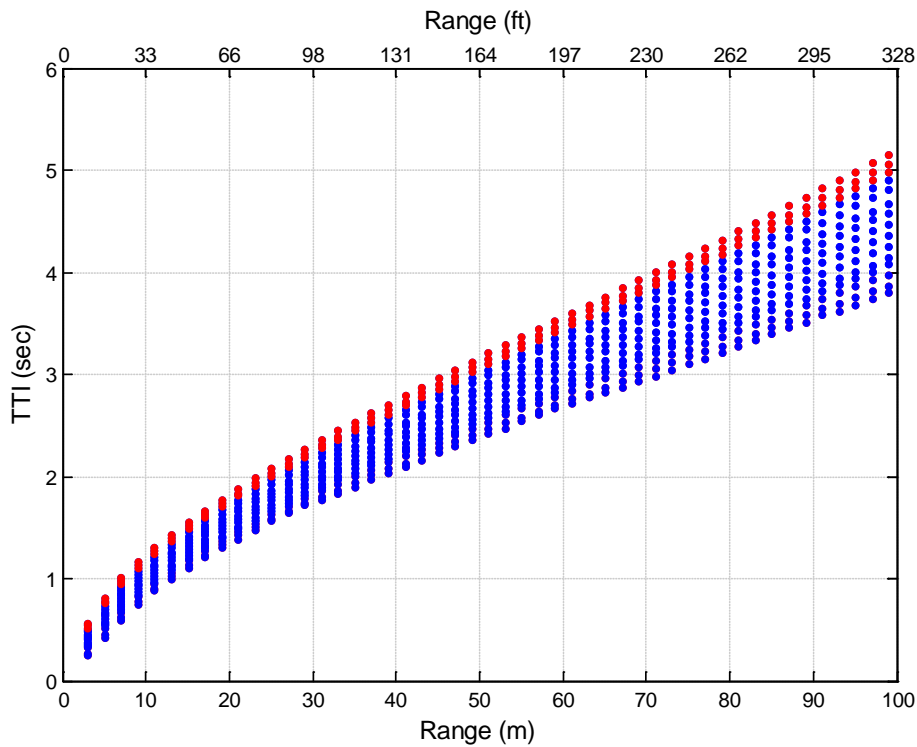


**Figure 68 Piecewise empirical percentiles across which the linear regression was performed for the stop-controlled intersection distribution.**

Each series of points represented by the percentiles was gathered and fit through a linear regression (where curves were fit for each percentile selected). Although several models would have been effective for fitting the data, a power function was selected (Figure 69 and Figure 70; fit information provided in Appendix L). The power function has some advantages over other equations such as polynomials, Gaussians, and exponentials for this data set. The power equation fits the data extremely well (typical  $R^2 \sim 0.98$ ) and has a stable nature when extrapolated beyond the data collected.

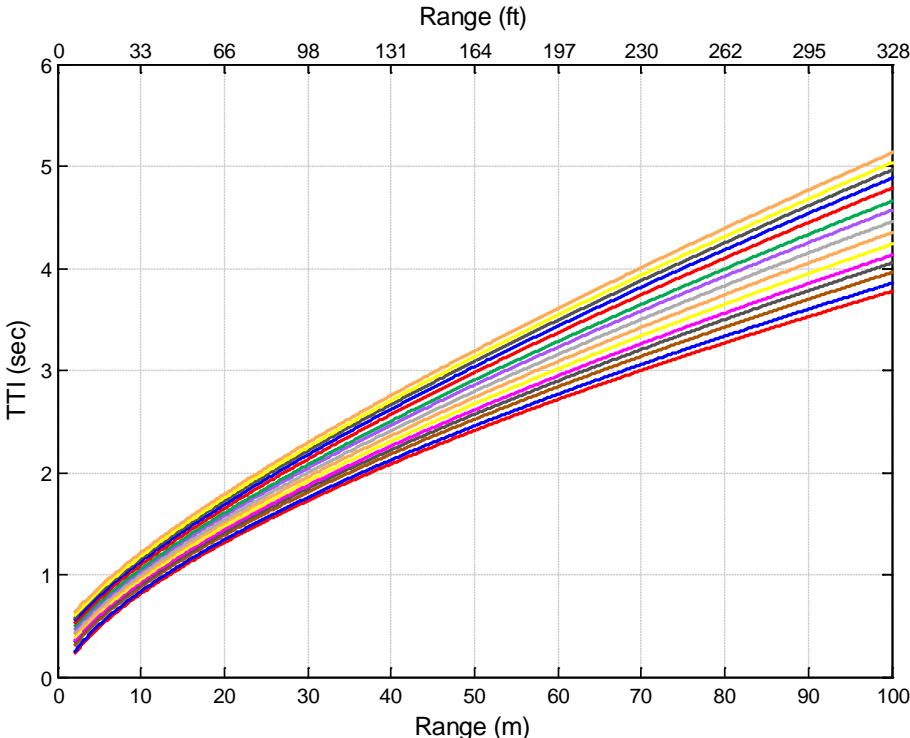


**Figure 69** The series of curves used to calculate the warning TTI as a function of range at stop-controlled intersections for the piecewise distributions fit with a power function.

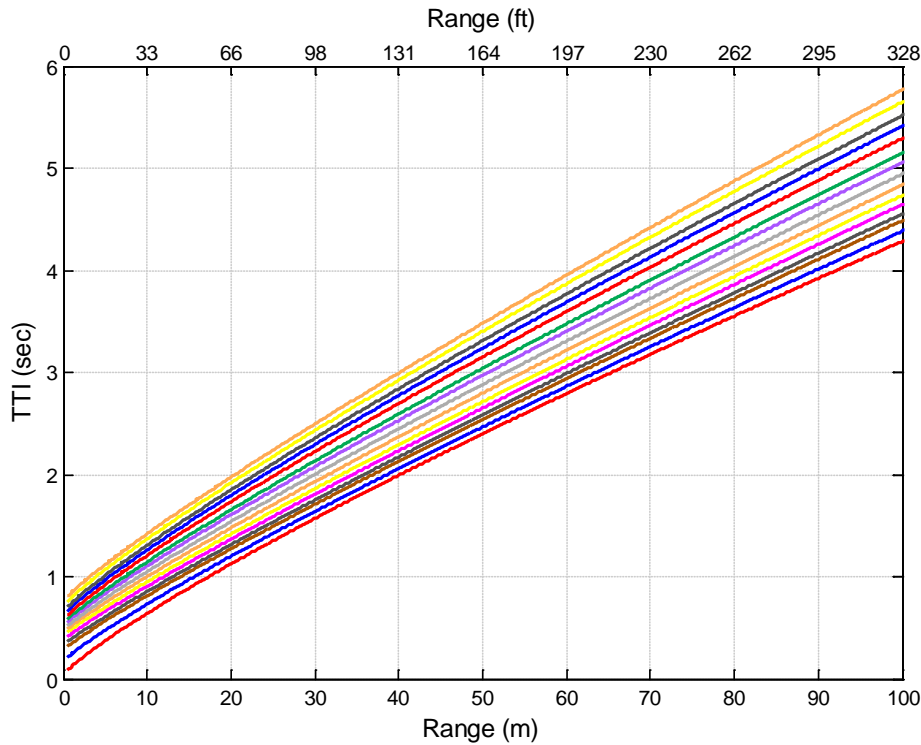


**Figure 70** The series of curves used to calculate the warning TTI as a function of range at signaled intersections for the piecewise distributions fit with a power function.

Extreme behaviors that would result in a low TTI at long ranges are too rare for distribution fitting. To avoid late or early warnings for some drivers, it is desirable for the algorithm to function across all foreseeable inputs. This means it must behave predictably beyond the data collected. Many fit types tended to behave erratically outside the range of data used during the regression. Second order polynomials, for instance, dive rapidly toward zero after fitting the data points. Using such a distribution could result in late warnings for drivers approaching the intersections at high speeds.

The power equation continues in a nearly linear form beyond the regression data. This trend matches the trend exhibited by the data points for nearly half of the distribution. Therefore, it likely provides a valid warning threshold outside the regression range. Using the regression function, the following warning equation was devised (parameters in Appendix L):

**Equation 13**

$$TTI_{warn} = a * V^b + c$$

**Equation 14**

Warn if:  $TTI < TTI_{warn}$

**Algorithm 6: Warning Range as a Function of Velocity**

The sixth algorithm uses the same basic framework as the fifth. The main difference between the two is the measurement used to differentiate between a violating and a compliant driving maneuver. The sixth algorithm takes advantage of the large separation between highly aggressive and compliant approaches when they are viewed in the velocity domain (see Figure 53 in Section 4).

This algorithm predicts the minimum distance at which a warning must be provided in order for the driver to successfully stop. A warning is issued if the driver's current range to the intersection is less than the warning range (Equation 15). The calculated warning distance is based on a piecewise regression and subsequent power equation fit of distance (as a function of the vehicle velocity trajectory). The basic method for developing the equation follows the method described in the fifth algorithm section above. The logic employed by the sixth algorithm is provided in Equation 15 and Equation 16. The functions tested are depicted in Figure 71 and Figure 72 with details of the fits provided in Appendix L.

**Equation 15**

$$R_{warn} = a * V^b + c$$

**Equation 16**

$$\text{Warn if: } R < R_{warn}$$

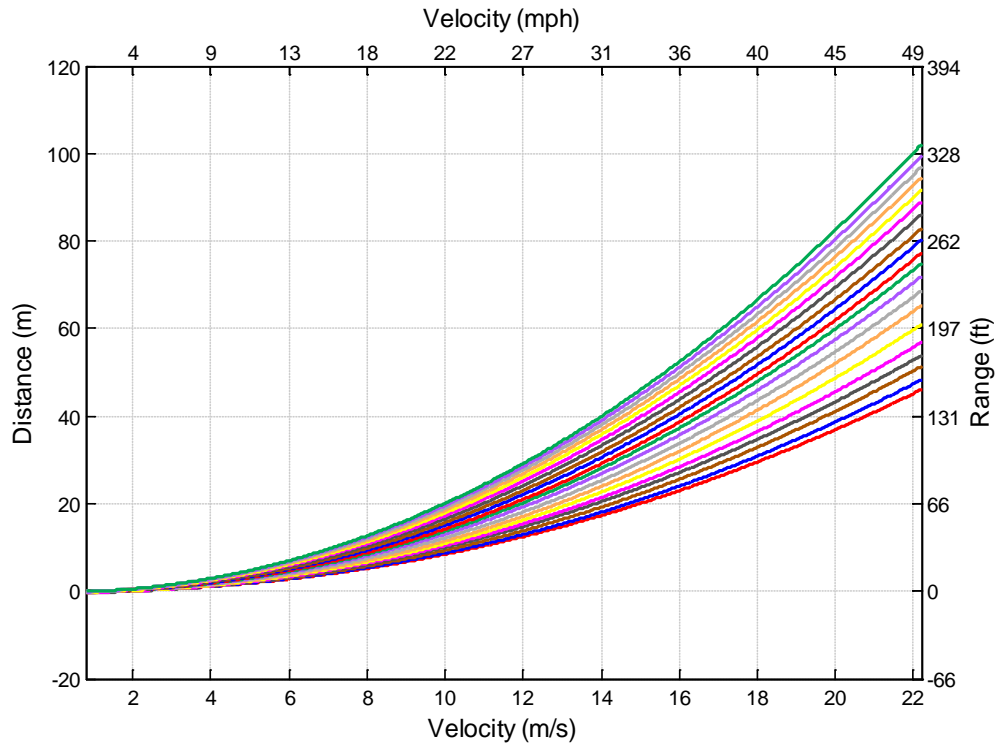


**Figure 71** The series of curves used to calculate the warning distance as a function of velocity at stop-controlled intersections for the piecewise distributions fit with a power function.

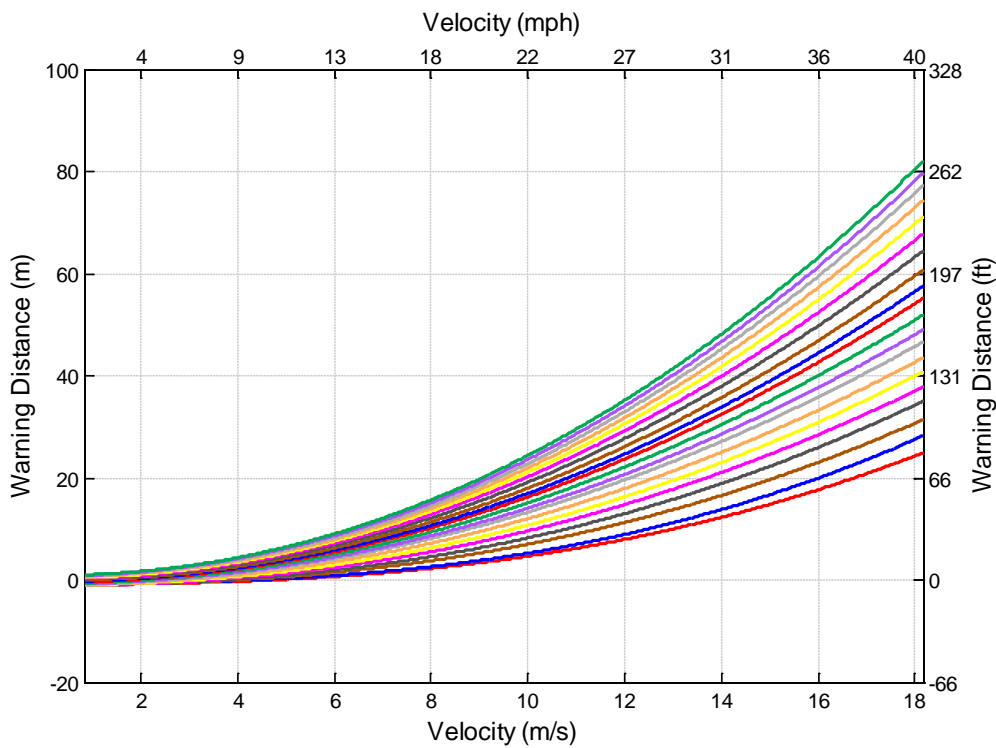


**Figure 72** The series of curves used to calculate the warning distance as a function of velocity at signalized intersections for the piecewise distributions fit with a power function.



### Algorithm 7: Warning Range as a Function of Velocity Based on Truncated Data

The seventh algorithm uses the same measures employed by the sixth algorithm. The difference between the two is in the data sample manipulated during the regression. While performing the regression on stop-controlled data, a plateau was noted at the higher velocities. Considering the implications of this trend, one possible concern was identified. The plateau occurred as the maximum speed limit across the intersection sample was approached. This plateau may be due to the maximum speed limit at the test sites rather than to a warning distance as a function of speed trend. To investigate this possibility, the data sample was truncated by removing velocities greater than 18 m/s (40 mph) before the regression was performed. This resulted in better regression fits that exhibited a somewhat steeper trend at higher velocities than found for algorithm 6. The array of fits used as the threat assessment algorithm is shown in Figure 73 (fit details are provided in Appendix L). The plateau trend was not noted at signalized intersections. As a result, algorithm seven was only applied to the stop-controlled data set.

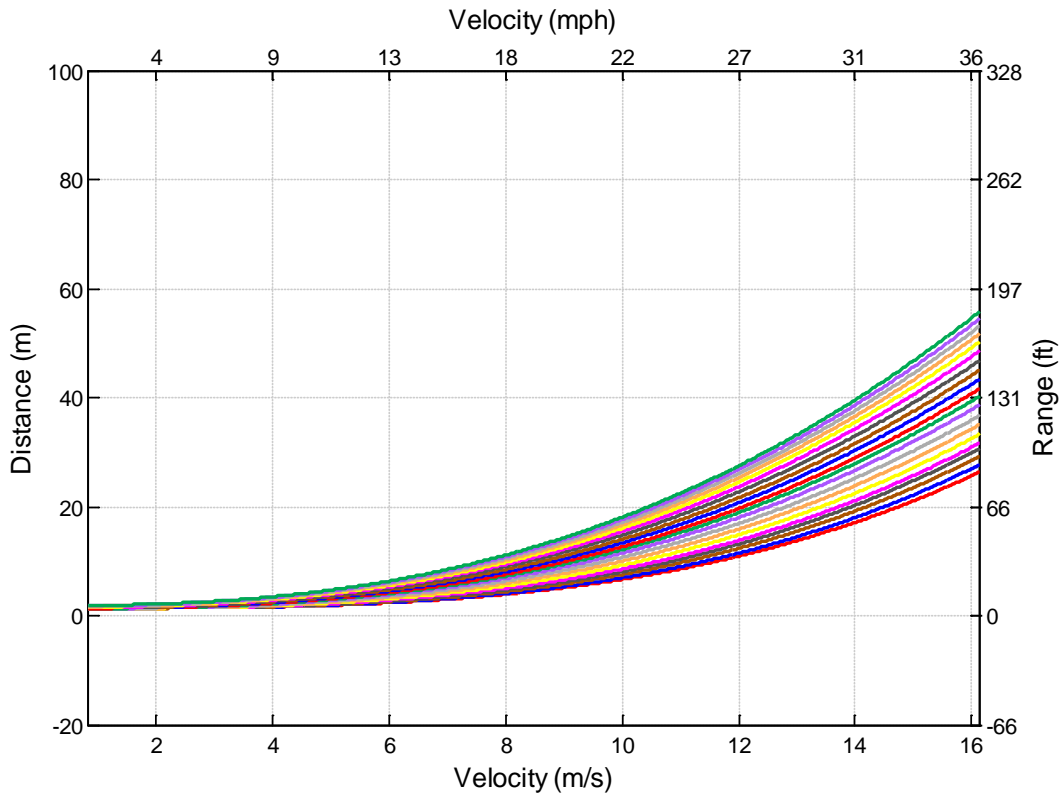


Figure 73 The series of curves used to calculate the warning distance as a function of velocity at stop-controlled intersections for the piecewise distributions fit with a power function based on truncated data.

**Algorithm 8: RDP as a Function of Range**

The eighth algorithm also follows the same basic strategy used for algorithm 5; however, the regression equation here uses range to predict the warning RDP. Using RDP as the predictor could take advantage of the earlier separation of stopping maneuvers found for RDP versus TTI during the graphical cluster analyses. The basic logic is shown in Equation 17, followed by the array of fits used as the threat assessment algorithm shown in Figure 74 and Figure 75. The reader is referred to Appendix L for fit details.

**Equation 17**

$$RDP_{warn} = a * R^b + c$$

**Equation 18**

Warn if:  $RDP > RDP_{warn}$

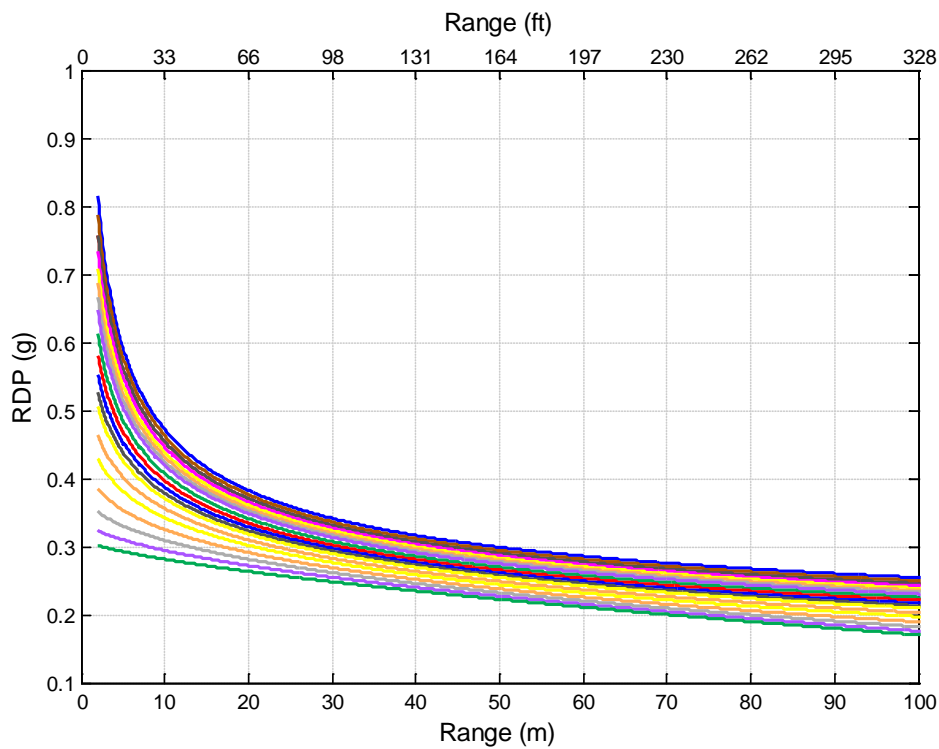


**Figure 74** The series of curves used to calculate the warning RDP as a function of range at stop-controlled intersections for the piecewise distributions fit with a power function.

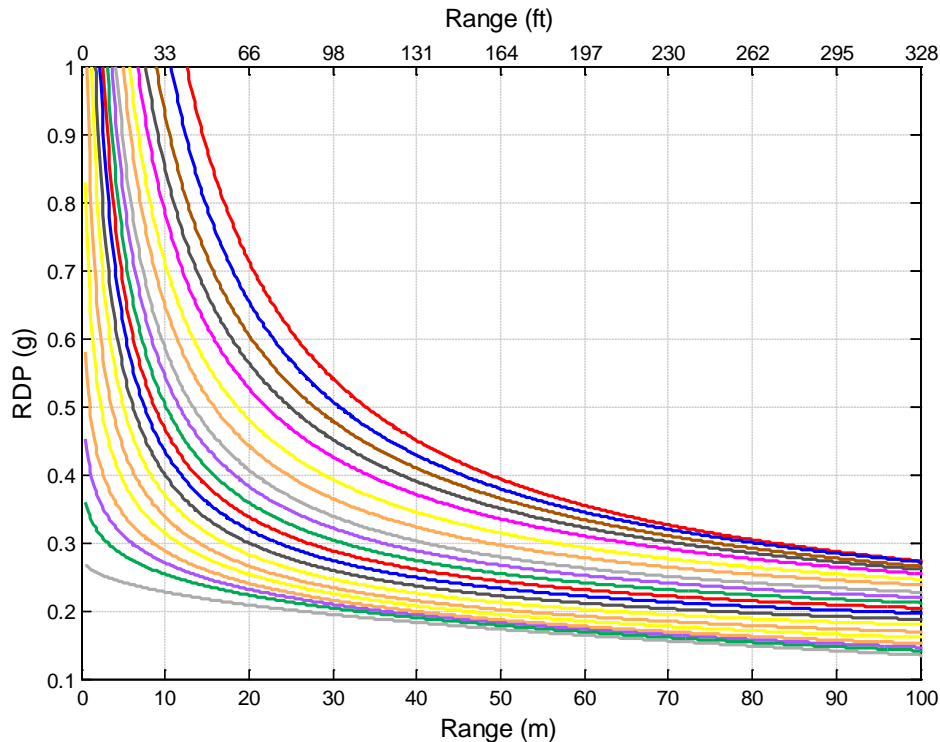


**Figure 75** The series of curves used to calculate the warning RDP as a function of range at signalized intersections for the piecewise distributions fit with a power function.

### Other Algorithms Developed and Tested but Not Presented

In addition to the layer 1 algorithms presented above, several other algorithms were developed and tested but are not represented in the results. These algorithms either performed very poorly or could not be fully developed without substantially extending the scope of this work. They are briefly discussed below.

There are several existing algorithms discussed in the literature review that was developed for applications such as forward collision warning. On first glance, these algorithms appeared to be applicable to the CICAS-V scenario. The algorithms were developed using empirical methods from data collected in a forward collision scenario. The ICAV project (Lee et al., 2005) compared the results of a study performed for both ICAS and forward collision scenarios. In the report, the authors concluded that drivers did not respond similarly in the two conditions. Since the equations were constructed from regression techniques, they did not transfer effectively to the CICAS-V. Some equations, such as the static RDP algorithm, did transfer effectively and were used as part of this investigation.

Other algorithms were initially developed but were eventually abandoned as well. A series of regression-based algorithms were developed using a piecewise method similar to the one described for algorithm 5. The main difference was that, rather than assume empirical distributions, the abandoned algorithms used a normal distribution for the piecewise fit. These included RDP as a function of range, RDP as a function of velocity, TTI as a function of range, TTI as a function of velocity, and warning range as a function of velocity. While some of the

algorithms performed decently, none of them performed as effectively as those using empirical distribution. There is an explanation for this effect.

First, consider the results presented in the cluster analysis and graphical analysis sections of Section 6. Many of the kinematic measures are normally distributed at long ranges from the intersection; however, as the measures are evaluated closer to the stop bar, the distributions take on a highly skewed shape. Therefore, representing the data as a series of piecewise normal distributions is not an accurate depiction of the underlying data.

Finally, two algorithms were not fully investigated because there were insufficient resources to fully explore their form. These two algorithms included the empirical regression of RDP as a function of velocity and TTI as a function of velocity. In both of these regressions, the underlying data exhibited a discontinuity. This discontinuity could not be fit effectively with a single equation and represented a challenging mixed distribution problem. The discontinuity could represent an undefined trend in the data that would naturally help discriminate violators. Unfortunately, investigating this possibility was beyond the scope of this effort.

In all, over 20 layer 1 algorithms were evaluated and/or considered. The eight best-performing layer 1 algorithms are presented in this report. When combined with the layer 2 algorithms, 160 algorithms are represented in the subsequent results.

## Layer 2 Algorithm Component

The first layer of the algorithm determines when a driver should receive the warning. The second layer of the algorithm infers the drivers' level of attentiveness toward the intersection. If input parameters suggest that a driver is responding to the intersection (e.g., vehicle kinematics indicate braking), the warning will be suppressed. The primary purpose is to reduce false positives (nuisance alerts) via assumptions as to whether the driver is responding to the intersection or not. Therefore, the layer two algorithm component determines whether or not the driver appears to be responding to the intersection and suppresses the warning if necessary. This occurs regardless of the layer 1 algorithm outcome.

The first input is the level of braking present during the given time frame. The data presented during the brake onset analysis and the graphical trajectory analysis were synthesized to develop five possible methods for investigation. The following different possible combinations of the driver braking component were tested for all of the algorithms:

- No braking assumption.
- Brake status was active.
- Braking detected at a rate of  $-0.1$  g or less.
- Braking detected at a rate of  $-0.2$  g or less.
- Braking detected equal to or lower than the current RDP.

A speed-based evaluation was also added into the second layer of the algorithm. The purpose of the minimum speed check was to reduce false positives that were occurring as a result of drivers who did not completely stop at the stop bar. As discussed in Section 4, rolling stops are extremely common. Furthermore, the algorithm does not contain any hysteresis. This means the

minimum speed threshold ensures that a driver who completely stops a short distance from the stop bar will not receive warning once they proceed through the intersection.

During an early iteration, the minimum speed cutoff was varied over a wide range of values for each of the algorithms. The results indicated that, in general, the number of false positives decreases with an increasing cutoff speed. The number of true positives is relatively stable until about 9 m/s (20 mph), at which point it tends to drop off rapidly.

Although it may seem that a minimum speed cutoff should simply be set around 9 m/s (20 mph), some implications of this cutoff must be considered. A high threshold resulted in missing some violations at low-speed intersections (where the speed limit was only a few meters per second higher than the minimum speed cutoff). In addition, setting the minimum speed cutoff at a single value did not provide information regarding the correlation between the algorithm minimum speed cutoff and the violation threshold defined previously. Therefore, it was decided to test minimum speed over the same range of speeds that was used to define the violation. Thus, four minimum speeds were tested: 2.2 m/s (5 mph), 4.52 m/s (10 mph), 6.72 m/s (15 mph), and 8.92 m/s (20 mph).

## Algorithm Naming Convention

A naming convention was devised to aid in interpreting the large number of algorithms represented in the subsequent sections. This naming convention uses a three-digit code to quickly identify the algorithm components. The first digit represents the layer 1 algorithm (often referred to as an algorithm “family”). Families of algorithms were typically plotted together on the ROC curve so that the best “in-family” curves could be identified. The second and third digits of the naming convention represent the second layer of the algorithm, specifically, the minimum speed cutoff and braking thresholds.

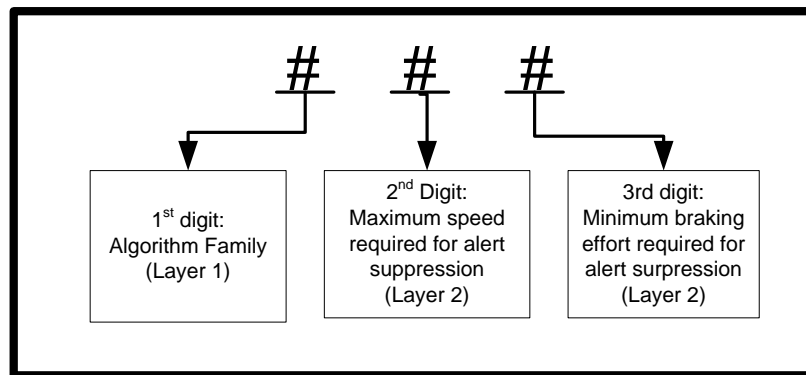


**Figure 76** Diagram depicting the three-digit code used to name each of the algorithms described in this report.

The algorithm component identified by the value of each digit is provided in the list below.

1. Basic Algorithms Tested (first digit)
  1. Static TTS
  2. Static RDP
  3. Static RDP with PRT

4. Variable RDP based on regression of velocity
  5. Variable TTI based on regression of range
  6. Variable warning distance based on regression of velocity
  7. Variable RDP based on regression of range
  8. Variable velocity based on regression of range
2. Speed Threshold (second digit)
    1. Suppress warning if current speed < 2.2 m/s (5 mph)
    2. Suppress warning if current speed < 4.52 m/s (10 mph)
    3. Suppress warning if current speed < 6.72 m/s (15 mph)
    4. Suppress warning if current speed < 8.92 m/s (20 mph)
  3. Braking Thresholds (third digit)
    1. Never suppress warning based on braking
    2. Suppress warning if brake status = on
    3. Suppress warning if present deceleration > 0.1 g
    4. Suppress warning if present deceleration > 0.2 g
    5. Suppress warning if present deceleration > RDP

As an example, if the algorithm code is 324, it is a static RDP algorithm family paired with a 10-mph minimum speed cutoff and a 0.2-g or higher braking level requirement. Furthermore, each algorithm contains parameters that were varied during the simulation. They represented the various settings of Beta, which created the ROC curve for each algorithm. A code was assigned to each unique combination of parameters tested; when applicable, the unique value is shown after a dash in the algorithm code. For instance, the algorithm incarnation 634-15 has a unique code of 15. A key for determining the parameter values based on the unique code is provided in Appendix M.

## 8 Results of the Algorithm Evaluation

The algorithm analysis process generated a series of graphical outputs (Appendix N and Appendix O). These outputs were methodically examined for trends across the violation thresholds and algorithm settings. This section will present the results from this graphical inspection process, as well as the output of a heuristic scheme devised to identify the best performing algorithms. The following phrases will be used throughout this section to describe the algorithms:

- **Violation threshold:** The violation threshold is the stop-bar speed used to define when a violation has occurred. The performance of the algorithm is determined by its ability to correctly predict a violation based on this threshold. The violation threshold values tested were discussed in Table 13 and Table 14.
- **Low-speed cutoff:** The low-speed cutoff is a component of the second algorithm layer (Section 7.4). A warning is suppressed if the vehicle's speed is below the cutoff.
- **Braking criterion:** The braking criterion is a component of the second algorithm layer (Section 7.4). A warning is suppressed if the braking criterion is satisfied.

### ROC Curve Graphical Analysis Results

This discussion opens with an exemplar inspection of the ROC curves. An individual ROC plot was created for each algorithm family under each defined violation threshold. Within an ROC plot, a color and marker scheme was used to identify the different components of the algorithms. For example, the cyan color always represented the 5-mph speed cutoff while the diamond marker always represented the 0.2-g braking criterion. This allowed quick assessments of the data trends within, as well as across, the ROC figures.

A comprehensive set of ROC curves is available in Appendix N and Appendix O. For the purpose of explaining the process, this discussion will use the 600 series algorithm family to describe the general trends noted in the ROC curves. This algorithm proved to be one of the best-performing algorithms at both stop-controlled and signalized intersections. It also exhibits many of the general trends noted across the other ROC curves, thus providing an excellent subject for demonstrating the analysis.

Recall from the literature review (Section 1.2) the determination that warning systems such as CICAS-V need to yield a very low false positive rate. To reduce the pool of candidate -algorithms, only those providing a true positive rate of at least 0.5 with a false positive rate below 0.05 were evaluated on an ROC curve. A good algorithm exceeded these minimum requirements. Since the focus of the ROC curves is on low false positive rates, the x-axes have been truncated at 0.35 to enhance legibility.

Figure 77 below depicts the ROC plot for the 600 series family of algorithms when the violation threshold is set at 5 mph at stop-controlled intersections. Considering the minimum performance specification set above, the performance of all of the algorithms tested at a violation threshold of 5 mph is disappointing because at a false positive rate of 0.05, the best true positive rate is just over 0.3. Recall that the 5-mph violation threshold was not tested at signalized intersections due to the unreasonable data reduction requirements and the low performance at stop-controlled intersections, demonstrated by Figure 77.

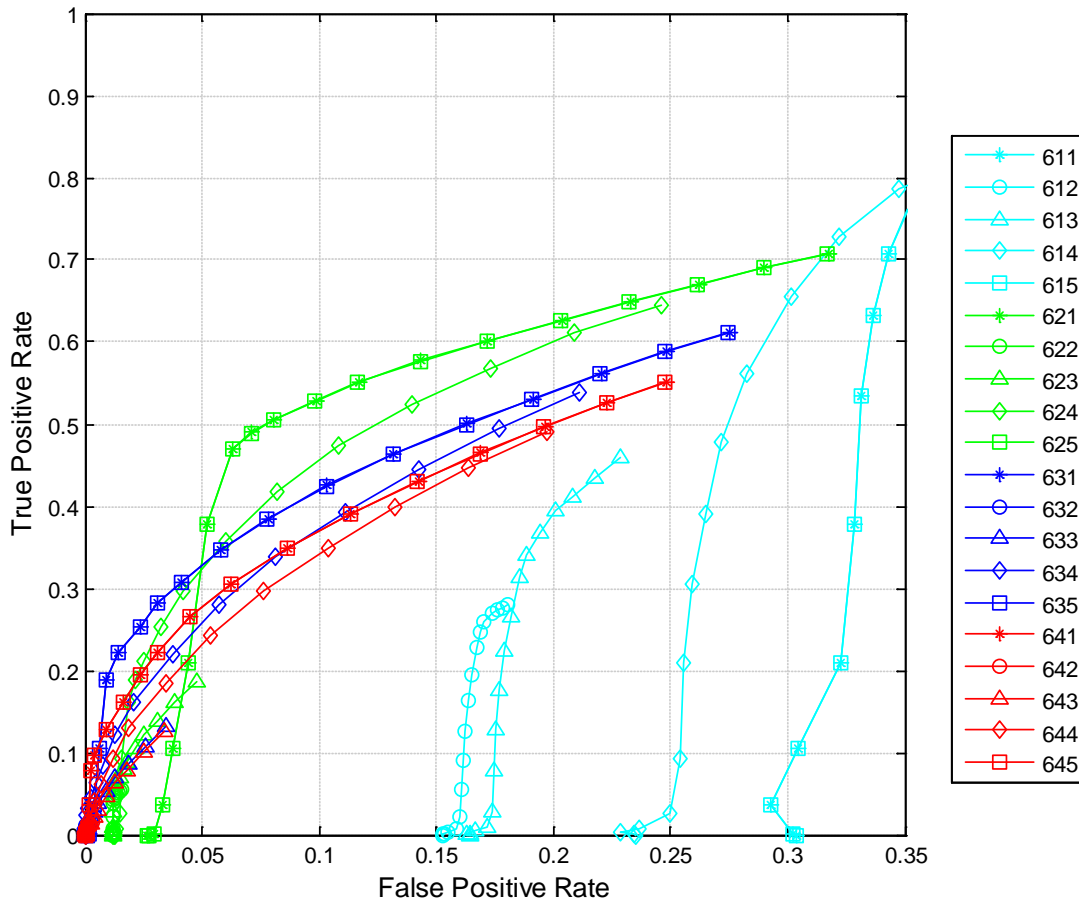


Figure 77 ROC curve for the stop-controlled 600 series algorithm family using a violation threshold of 5 mph.

It is reasonable to assume that a low-speed cutoff equivalent to the violation threshold would provide the best performance. Nonetheless, the figure above indicates a particularly poor ability to discriminate a violation for the 5-mph low-speed cutoff. Inspection across the ROC figures shows this to be a recurring phenomenon. The consistently high false positive rate produced by a 5-mph low-speed cutoff likely indicates the frequency at which compliant drivers exceed this speed threshold in the warning region. The clear suboptimal trend across all of the ROC curves indicates that a 5-mph low-speed cutoff should not be used in a CICAS-V threat assessment.

Figure 78 displays the ROC curves for the same 600 series algorithm family at stop-controlled intersections but with the 10-mph violation threshold. The ability to discriminate among all the algorithms is improved compared to a 5-mph violation threshold. Notice the 5-mph low-speed cutoff continues to perform poorly. In addition, the 10-mph low-speed cutoff does not perform as well as the 15-mph and 20-mph low-speed cutoffs. This trend is also noted across all of the ROC curves.



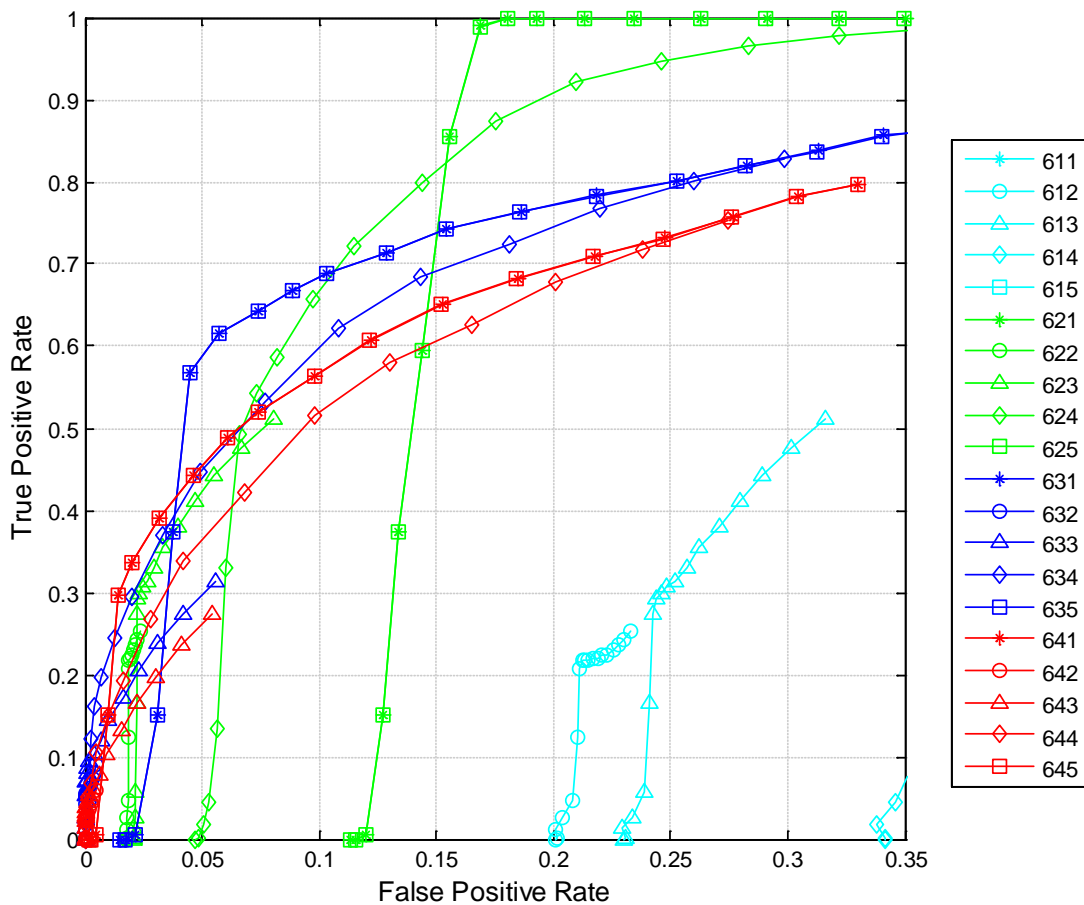


Figure 78 ROC curve for the stop-controlled 600 series algorithm family using a violation threshold of 10 mph.

Figure 79 indicates better performance for the same algorithms and violation threshold at signalized intersections. This performance difference decreases as the violation threshold increases. The difference may be attributed to the differences in the traffic control device between the two intersection types. At signalized intersections, a larger portion of the violations occur at high speeds (Figure 60), due to drivers’ attempts to beat the arrival of the red light. For this reason, violations that occur at high stop-bar speeds are not susceptible to altering the violation threshold; these vehicles are traveling at speeds above all the tested minimum speed thresholds.

The performance of the signalized algorithms, however, still improves as the violation threshold is raised. The performance improvement is attributed to drivers performing a right-turn-on-red maneuver. The right-turn-on-red maneuver is very similar to the approaches made at a stop sign; drivers are likely to intentionally perform rolling violations if they perceive it is a prudent choice.

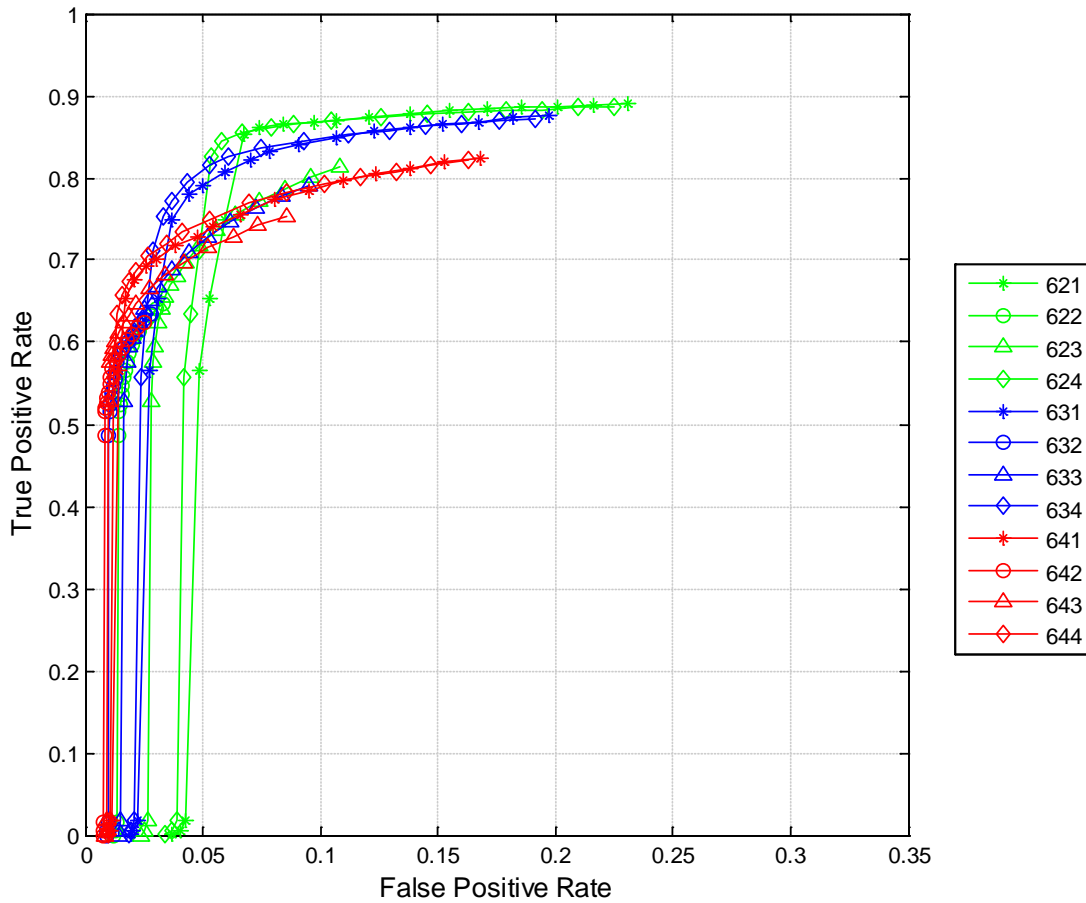


Figure 79 ROC curve for the signaled 600 series algorithm family using a violation threshold of 10 mph.

Further inspection of the low-speed cutoff in the ROC curves results in more notable trends. Although not consistent across all ROC curves, the general shape of each algorithm is retained across the low-speed cutoff. For instance, notice the similarity in the curves generated from the 10-mph and 15-mph low-speed cutoffs in Figure 79 and Figure 80. With the violation threshold set at 10 mph, the 15-mph and 20-mph low-speed cutoffs do not warn as many drivers as the 10-mph low-speed cutoff. The cost of obtaining these additional warnings with a 10-mph low cutoff speed is a higher false positive rate.

Without a large range of Beta parameters, the ROC curves do not always appear complete. Simulating the full range of Beta parameters would have required significantly more processing time without adding value to the analysis. Care was exercised to ensure the curves were inclusive in the region in which assessments were performed (e.g., false positive rate less than 0.05). In addition, the parameters were selected considering a reasonable range of driver or vehicle capabilities in response to the warning (i.e., RDP values greater than 1.0 g were not tested). Parameters extending beyond the values tested would be well outside the capabilities of all driver-vehicle systems.

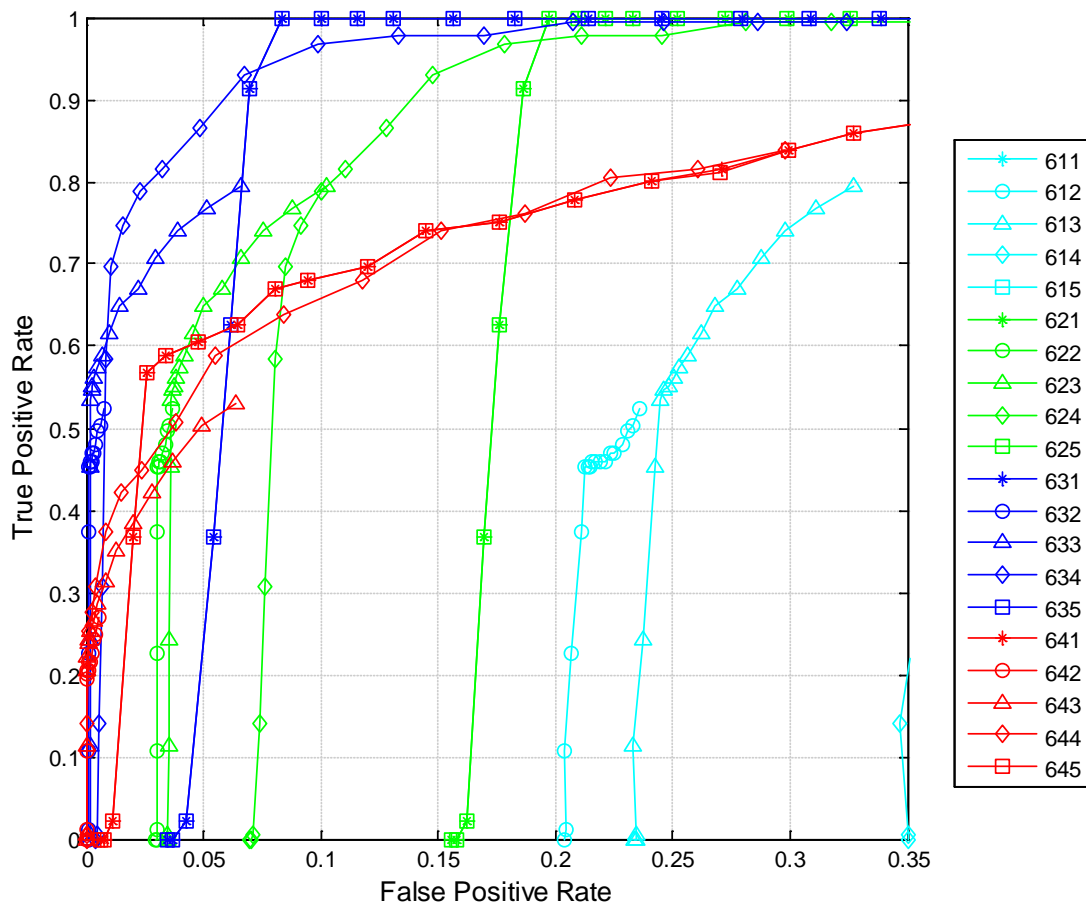


Figure 80 ROC curve for the stop-controlled 600 series algorithm family using a violation threshold of 15 mph.

As the violation threshold is increased, all of the algorithms demonstrate an improved ability to discriminate (Figure 80 and Figure 81). At a 15-mph violation threshold, some of the stop-controlled algorithms showed improved performance. As with the 10-mph violation threshold in Figure 78, the 15-mph low-speed cutoff also performs best when the violation threshold is 15 mph (Figure 80). In fact, across nearly all of the stop-controlled ROC curves, the 15-mph low-speed cutoff is typically the best performing speed criteria. This trend continues even at a 20-mph violation threshold. This may indicate that compliant drivers typically exhibit speeds slower than 15 mph in the warning region. A similar trend is not as salient on the signalized intersection ROC curves; the 15-mph and 20-mph speed cutoffs both tend to perform similarly. This is likely due to the higher typical violation speeds at traffic signals.

Consider the general trends exhibited by the braking criterion. The typical trend across many of the ROC figures indicates best performance for 0.1-g and 0.2-g braking criteria. The no-brake criterion and the braking at or above RDP criterion tend to perform very similarly in the stop-controlled ROC plots. Notice that the braking at or above RDP criterion is not represented in the signalized algorithms. After a pilot simulation on the signalized data set, the braking at or above

RDP criterion also performed similarly to the no brake criteria; thus, it was not considered in the full simulation.

The no brake criterion is occasionally represented in the best discriminating algorithms (particularly at signalized intersections). Finally, the on/off binary brake status requirement is rarely represented in the best algorithms at stop-controlled intersections. In general, brake status appears to reduce the number of true positives. Therefore, the brake status criterion appears to be suppressing the warning at stop-controlled intersections for drivers who will exceed the violation threshold.

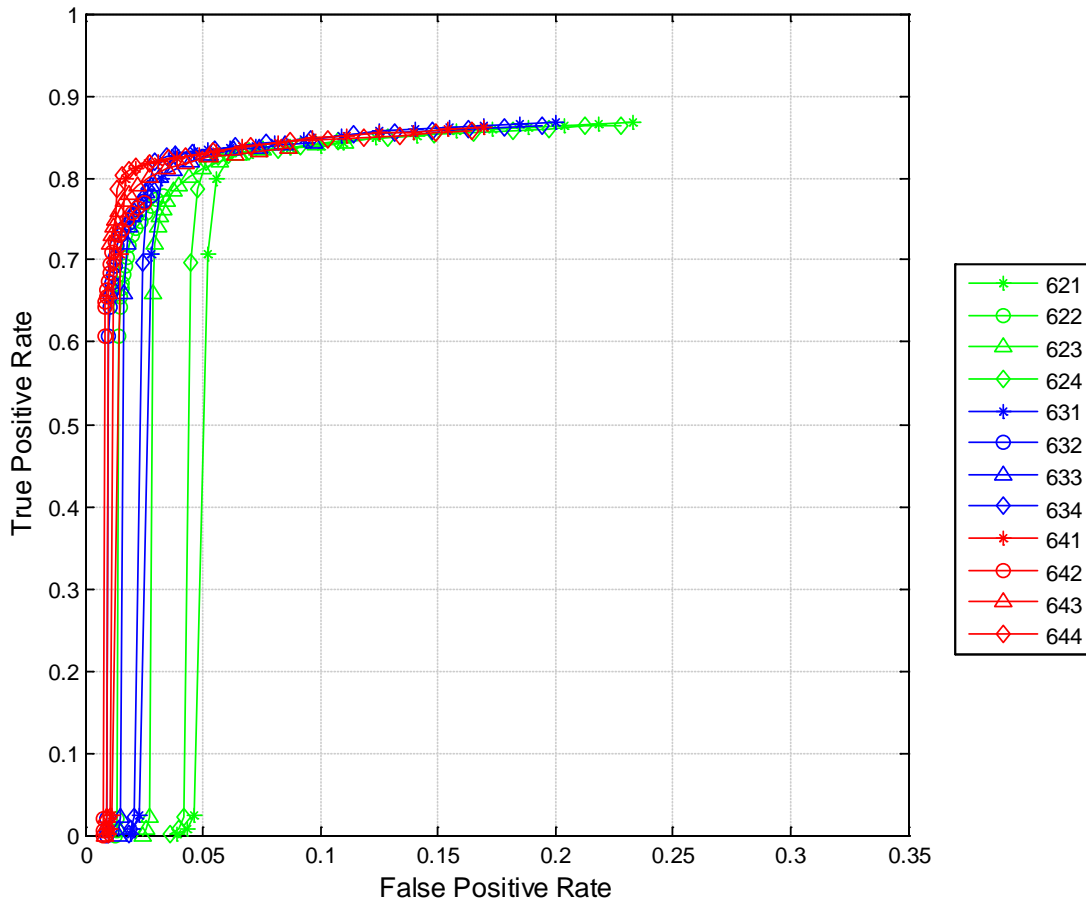


Figure 81 ROC curve for the signalized 600 series algorithm family using a violation threshold of 15 mph.

The final ROCs for the 600 series algorithm represent the increased ability to discriminate when a 20-mph violation threshold is used (Figure 82). Across all the ROC curves, the ability to discriminate improves as the violation threshold increases. This is likely due to the unusually high stop-bar velocity of the violators. As discussed during the cluster analysis, the higher stop-

bar velocity approaches are substantially different from compliant drivers and, therefore, easier to identify at both stop-controlled and signalized intersections.

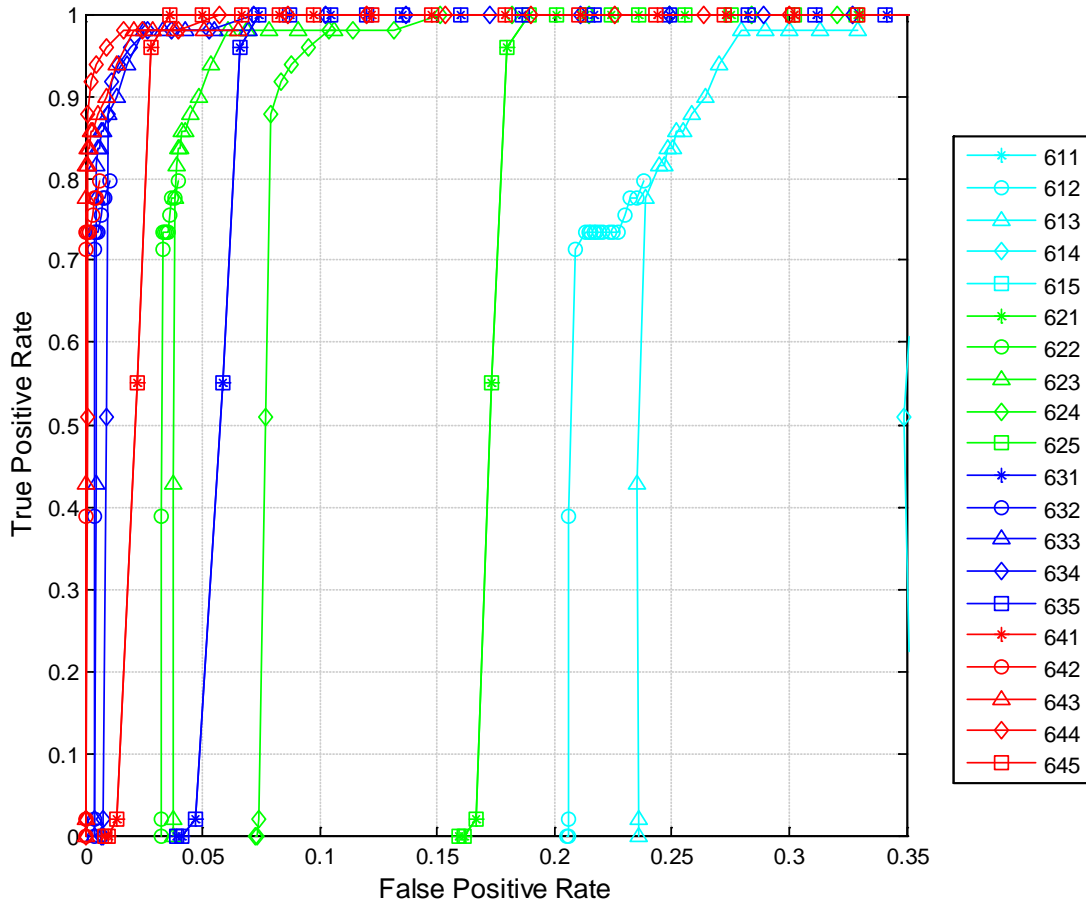


Figure 82 ROC curve for the stop-controlled 600 series algorithm family using a violation threshold of 20 mph.

There is an inherent trade-off in assuming a higher violation threshold. As the threshold is increased, there is an opportunity to miss some potentially dangerous violations. This is particularly true at low-speed intersections where the speed limit may only be 5 mph higher than the 20-mph violation threshold. For example, it is conceivable that a distracted driver may inadvertently travel at 5 mph below the threshold and not receive a warning despite showing no braking response in response to the intersection.

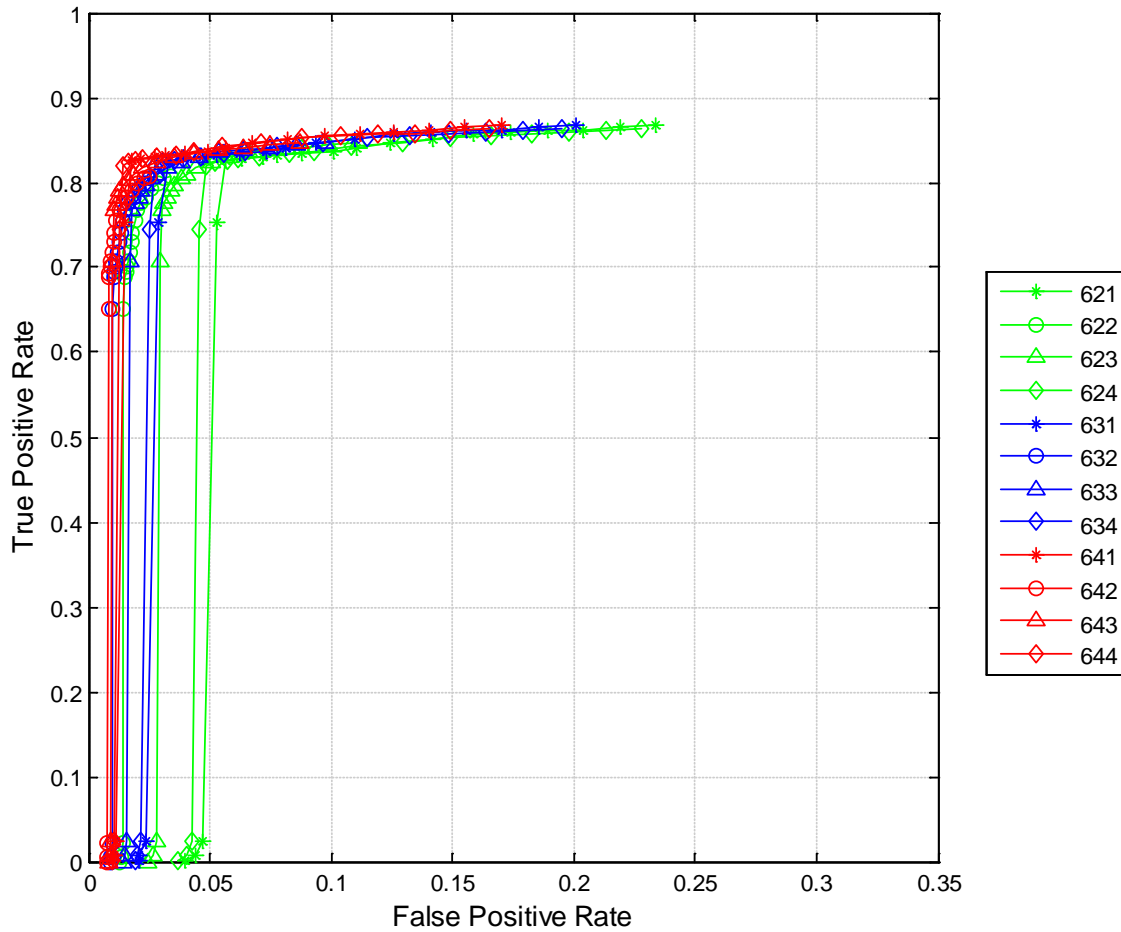


Figure 83 ROC curve for the signaled 600 series algorithm family using a violation threshold of 20 mph.

### Algorithm Recommendations for CICAS-V

The series of ROC, warning, and nuisance distributions provided in Appendix N and Appendix O are very useful for identifying trends. Simply viewing the numerous figures, however, does not provide an easy way to identify the optimal algorithms. Consequently, a heuristic search procedure was developed to identify and evaluate the best instantiations across the two intersection types, the 160 algorithms, and the four violation thresholds.

### Procedure to Identify the Best Performing Algorithms

The search heuristic began by setting a minimum performance specification to limit the pool of algorithms. To be considered for review, the algorithm had to result in a true positive rate of at least 0.5 while producing a false positive rate no higher than 0.05. These minimum criteria eliminated over half the potential algorithms and removed all those employing the 5-mph violation threshold.

Furthermore, the minimum false positive criteria of 0.05 may not be sufficiently stringent for a deployable CICAS-V from a customer acceptance perspective. To explore tighter requirements,

the highest performing algorithms with a minimum false positive criterion of 0.01 were identified. With this second set of minimum criteria, all algorithms employing the 10-mph violation threshold were removed from further consideration.

The remaining algorithms were rank-ordered in terms of a performance heuristic. For the first step in this process, performance measures were selected; are represented by the shape of the ROC, warning, and nuisance distributions (Appendix N and Appendix O). To capture their shape, these distributions were evaluated at multiple locations, as shown in Figure 84. The true positive rate was evaluated at several points on the warning distribution curve. The true positive rate that corresponded to the favorable (A) and too-late (E) warning points were evaluated. Furthermore, the true positive rate at the first quartile (B), second quartile (C), and third quartile (D) of the region between the favorable and too-late warning points was also obtained. The heuristic also used the false negative rate evaluated at the maximum true positive rate (G) and at a midway point between the zero and the maximum (F).

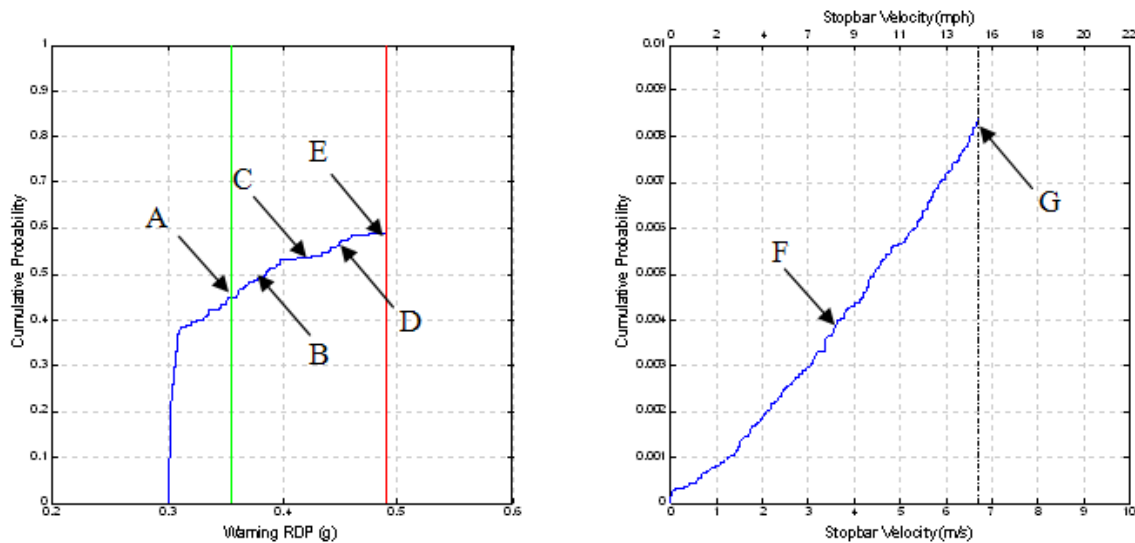


**Figure 84** Points on the warning distribution (left) and the nuisance distribution (right) that were evaluated to support the heuristic used to select the highest performing algorithms.

Once these points were evaluated, the next step was to decrease the precision of the resulting performance measure. For example, each ordering heuristic reduced the precision of the true positive and false positive rates to the second decimal place (i.e., a true positive rate of 0.79532 was rounded to 0.80). The decrease in precision allowed ordering of the data across multiple performance measures. Leaving the data at full precision would have resulted in ordering determined only by the first variable. After considering a variety of heuristics, the CICAS-V engineering team settled on three ordering schemes.

The first ordering scheme aims to maximize the number of true positives that occur at any time prior to the too-late point. To do this the measures of true positives and false positives at points E, D, F, and G were rounded to two decimal points. The algorithms were then sorted by the following criteria:

1. Descending by the true positive rate at point E

2. Ascending by the false positive rate at point F
3. Descending by the true positive rate at point D
4. Ascending by the false positive rate at point G

The second ordering scheme aims to maximize the number of warnings that occur at or before the favorable warning point. To do this the measures of true positives and false positives at points A, B, F, and G were rounded to two decimal points. The algorithms were then sorted by the following criteria:

1. Descending by the true positive rate at point A
2. Ascending by the false positive rate at point F
3. Descending by the true positive rate at point B
4. Ascending by the false positive rate at point G

The third ordering scheme compromises between maximizing the number of true positives and providing the warnings by the favorable warning point. To do this the true positives measured at points E and A were ordered at two levels of precision:

1. Descending by the true positive rate at point E with one decimal
2. Descending by the true positive rate at point A with one decimal point
3. Descending by the true positive rate at point E with two decimal points
4. Descending by the true positive rate at point A with two decimal points
5. Ascending by the false positive rate at point F with two decimal points

With each scheme above, all algorithms were placed in a unique order from highest performance to lowest performance. The ordering heuristics resulted in three substantially different algorithms that traded maximizing warnings for providing the warning as early as possible. There are other ordering heuristics that could be used, depending on the relative importance placed on each of the ordering variables. The schemes identified above were selected to best fulfill the needs of a CICAS-V based on the previous analyses, literature reviewed, outputs of other CICAS-V tasks, and the CICAS-V engineers' experience in this topic area. In general, the schemes aim to maximize the true positives that provide sufficient time for most drivers to stop while minimizing the number of nuisance false positives. This goal is implied or explicitly stated in most relevant CICAS-V documents (Kiefer, 1999; Lee et al., 2004; Neale et al., 2005; Ferlis, 1999).

## Results of the Algorithm Search Procedure

The selection heuristics yielded the following results for a violation threshold of 15 mph (Table 16 and Table 17). The 15-mph violation threshold became the focus of this analysis based on the results presented in Sections 4 and 5. These results indicated that a 15-mph threshold effectively segregated the target violations from rolling stop-controlled and signalized right-turn violations. This violation threshold is also supported by the results of Subtask 3.1, which found that drivers appeared to be intentionally violating at stop-bar speeds below 12 mph (Sudweeks et al., in review). The heuristic results for the 5-mph, 10-mph, and 20-mph violation thresholds are provided in Appendix P and will be discussed later in this section.



Table 16 and Table 17 summarize the results achieved by the top six performing algorithms for a 15-mph violation threshold within the heuristic and maximum false positive criteria partitions. In addition, the table provides the best overall and best applicable algorithms. As discussed previously, the layer 2 algorithms based on acceleration could not be feasibly implemented in the Phase I CICAS-V fleet (several vehicle platforms did not have acceleration measures on the network). Thus, for the purposes of CICAS-V Phase I, the best applicable set was limited to brake-status (on/off) and no-brake layer 2 algorithms. The best applicable algorithm set will be used in the Subtask 3.4 pilot FOT. The best overall set considered all possible algorithms and may be used to identify alternative algorithms in future CICAS-V efforts if accelerometers are available on the vehicle.

**Table 16 Stop-controlled intersection algorithms identified by the three heuristics for 0.05 and 0.01 allowable false positive rates at a violation threshold of 15 mph. The cell values represent the true positive rate and false positive rate evaluated at the point shown in Figure 84.**

Maximize True Positives									
	Algorithm	Point A	Point B	Point C	Point D	Point E	Point F	Point G	
Allowable FP=0.05	Best Overall	734 - 10	0.314	0.373	0.459	0.616	0.897	0.017	0.047
	Best Applicable	532 - 12	0.324	0.395	0.573	0.681	0.697	0.019	0.041
	Maximize Early Warnings								
		Algorithm	Point A	Point B	Point C	Point D	Point E	Point F	Point G
	Best Overall	633 - 18	0.616	0.676	0.703	0.724	0.741	0.020	0.039
	Best Applicable	232 - 8	0.514	0.578	0.622	0.659	0.676	0.029	0.048
	Compromise between Early Warnings and Maximum True Positives								
		Algorithm	Point A	Point B	Point C	Point D	Point E	Point F	Point G
	Best Overall	634 - 12	0.605	0.800	0.827	0.854	0.865	0.017	0.049
Best Applicable	232 - 8	0.514	0.578	0.622	0.659	0.676	0.029	0.048	

Maximize True Positives									
	Algorithm	Point A	Point B	Point C	Point D	Point E	Point F	Point G	
Allowable FP=0.01	Best Overall	234 - 17	0.011	0.011	0.011	0.643	0.654	0.001	0.009
	Best Applicable	732 - 14	0.222	0.438	0.492	0.535	0.562	0.004	0.009
	Maximize Early Warnings								
		Algorithm	Point A	Point B	Point C	Point D	Point E	Point F	Point G
	Best Overall	233 - 12	0.449	0.508	0.535	0.573	0.595	0.003	0.008
	Best Applicable	632 - 20	0.341	0.405	0.454	0.497	0.524	0.004	0.007
	Compromise between Early Warnings and Maximum True Positives								
		Algorithm	Point A	Point B	Point C	Point D	Point E	Point F	Point G
	Best Overall	234 - 17	0.011	0.011	0.011	0.643	0.654	0.001	0.009
Best Applicable	732 - 14	0.222	0.438	0.492	0.535	0.562	0.004	0.009	

The first heuristic scheme found that it is possible to correctly provide a warning to nearly 90% (point E) of the violating drivers at stop-controlled intersections if an allowable false positive rate of 0.05 is selected. A 0.05 false positive rate is recommended for further CICAS-V testing because it results in significantly more true positives. If future in-traffic testing with human

subjects finds that a 0.05 false positive rate creates customer acceptance issues, the allowable false positive rate of 0.01 can be selected, resulting in correctly warning 65 percent of the violating drivers.

Recall that some algorithms provide warnings earlier than others. It may be prudent to trade off a few true positives to maximize the number of warnings that are provided early enough to guarantee that nearly all drivers will stop. At an allowable false positive rate of 0.05, the heuristic to maximize early warnings increases the percentage of violating drivers who receive the warning by the favorable warning timing (point A) from 31 percent to 62 percent at the cost of decreasing the overall number of true positives (point E) from 90 percent to 74 percent.

Rather than focusing on either maximizing the number of overall true positives or early warnings, the third heuristic was aimed at compromising between these two goals. The compromise algorithm results in warning 87 percent of the violators (point E) while providing the warnings by the favorable warning point (point A) for 61 percent of the violating drivers. This is only 3 percent fewer total true positives than the first heuristic and only 1 percent fewer warnings by the favorable warning point than the second heuristic. This indicates that the compromise algorithm is the best selection for moving forward and is recommended for integration into the CICAS-V prototype equipment. Without a braking-effort-based algorithm, the best applicable compromise algorithm (232-8) results in 68 percent of the violating drivers (point E) receiving a warning. Based on these findings, the Phase II CICAS-V system should work toward integrating the brake effort criterion into the test vehicles.

**Table 17 Signalized intersection algorithms identified by the three heuristics for 0.05 and 0.01 allowable false positive rates at a violation threshold of 15 mph. The cell values represent the true positive rate and false positive rate evaluated at the point shown in Figure 84.**

Maximize True Positives									
	Algorithm	Point A	Point B	Point C	Point D	Point E	Point F	Point G	
Allowable FP=0.05	Best Overall	634 - 10	0.767	0.785	0.800	0.814	0.831	0.007	0.045
	Best Applicable	631 - 8	0.003	0.754	0.797	0.814	0.833	0.009	0.045
	Maximize Early Warnings								
		Algorithm	Point A	Point B	Point C	Point D	Point E	Point F	Point G
	Best Overall	433 - 3	0.794	0.799	0.806	0.814	0.824	0.014	0.046
	Best Applicable	322 - 3	0.778	0.781	0.786	0.792	0.799	0.013	0.044
	Compromise between Early Warnings and Maximum True Positives								
		Algorithm	Point A	Point B	Point C	Point D	Point E	Point F	Point G
	Best Overall	634 - 10	0.767	0.785	0.800	0.814	0.831	0.007	0.045
Best Applicable	641 - 11	0.769	0.783	0.797	0.810	0.828	0.018	0.047	

Maximize True Positives									
	Algorithm	Point A	Point B	Point C	Point D	Point E	Point F	Point G	
Allowable FP=0.01	Best Overall	442 - 6	0.634	0.644	0.654	0.667	0.678	0.001	0.010
	Best Applicable	442 - 6	0.634	0.644	0.654	0.667	0.678	0.001	0.010
	Maximize Early Warnings								
		Algorithm	Point A	Point B	Point C	Point D	Point E	Point F	Point G
	Best Overall	442 - 6	0.634	0.644	0.654	0.667	0.678	0.001	0.010
	Best Applicable	442 - 6	0.634	0.644	0.654	0.667	0.678	0.001	0.010
	Compromise between Early Warnings and Maximum True Positives								
		Algorithm	Point A	Point B	Point C	Point D	Point E	Point F	Point G
	Best Overall	442 - 6	0.634	0.644	0.654	0.667	0.678	0.001	0.010
Best Applicable	442 - 6	0.634	0.644	0.654	0.667	0.678	0.001	0.010	

The signalized results demonstrated some interesting findings. First, the 442-6 algorithm produced more total true positives (point E) and timely true positives (point A) than any other algorithm at a 0.01 false positive rate. Thus, the best algorithm at an allowable false positive rate of 0.01 is always 442-6, regardless of the heuristic applied. Secondly, the number of timely true positives (point A) for a 0.01 allowable false positive rate is much better at signalized intersections than at the stop-controlled intersections (63 percent vs. 22 percent). This indicates that the assessment of whether a driver will violate or not is made farther from the stop bar at signalized intersections than at stop-controlled intersections. The likely cause of this effect is the higher typical violation stop-bar speeds that occur at signalized intersections. By maintaining a higher speed throughout the violation, the trajectory of a violating driver versus that of a compliant driver diverge at a greater distance than at stop-controlled intersections (where the violating stop-bar speed was lower).

Also, the frequency of false positives assumed to be annoying (point F) is between 1 percent and 5 percent lower at signalized intersections than at stop-controlled intersections. This should indicate that drivers will find the false positives at the signalized intersections somewhat less annoying than the false positives at stop-controlled intersections.

At signalized intersections, the maximum number of true positives (point E) is 83 percent at an allowable false positive rate of 0.05. But at 83 percent, the best applicable algorithm only

provides timely warnings (point A) to 1.5 percent of the violating drivers. This can be seen by the warning distribution in Figure 229 in Appendix N, which shows the 231-16 algorithm providing nearly all of the warnings nearly halfway to the too-late warning distance.

The compromise algorithm (with a 0.05 false positive rate), as with the stop-controlled results, appears to be the best threat assessment metric to carry forward into the CICAS-V prototype system. The compromise heuristic indicated that the system could correctly warn 83 percent of the violating drivers (point E) while 77 percent of the violating drivers would receive the warning by the favorable warning point (point A). Notice that at signalized intersections the difference between the best applicable algorithm and the best overall algorithm is small. In fact, the best applicable algorithm obtains slightly higher true positive rates (point E) at full precision with the only downside being more potentially annoying false positives (point F). Overall, it appears little is lost by not supporting a braking effort criterion as signalized intersections.

As with the stop-controlled algorithm, if future testing (i.e., Subtask 3.4) indicates that drivers are annoyed by the false positives they receive, a false positive rate of 0.01 may be selected instead of 0.05. At signalized intersections, moving to the lower allowable false positive rate has a much lesser effect than it appears to have at stop-controlled intersections. Of the violating drivers, 63 percent would still receive the warning by the favorable warning point (point A) while nearly 70 percent will still receive a warning prior to the too-late warning point (point E).

### **Figures of the Best Performing Algorithms**

The best applicable performing algorithms identified in the previous section (compromise heuristic from Table 16 and Table 17) are graphically represented in Figure 85 and Figure 86 (figures for each of the best overall algorithms are available in Appendix Q). The figures are presented over the variables that are used by the CICAS-V warning logic. In the CICAS-V system, a table of warning distances as a function of current velocity is used to determine when a warning should be initiated. A warning is provided to the driver if the vehicle's distance to the stop bar is less than the warning distance indicated in the table.

When viewing the curves, care should be taken to consider the layer 2 components of the algorithm that are not represented in the figures. The kinematic curves displayed have an interaction with the braking and minimum speed checks that can affect the actual warning distance. Since this interaction cannot be depicted on the plot space, comparisons between algorithms should be made cautiously.

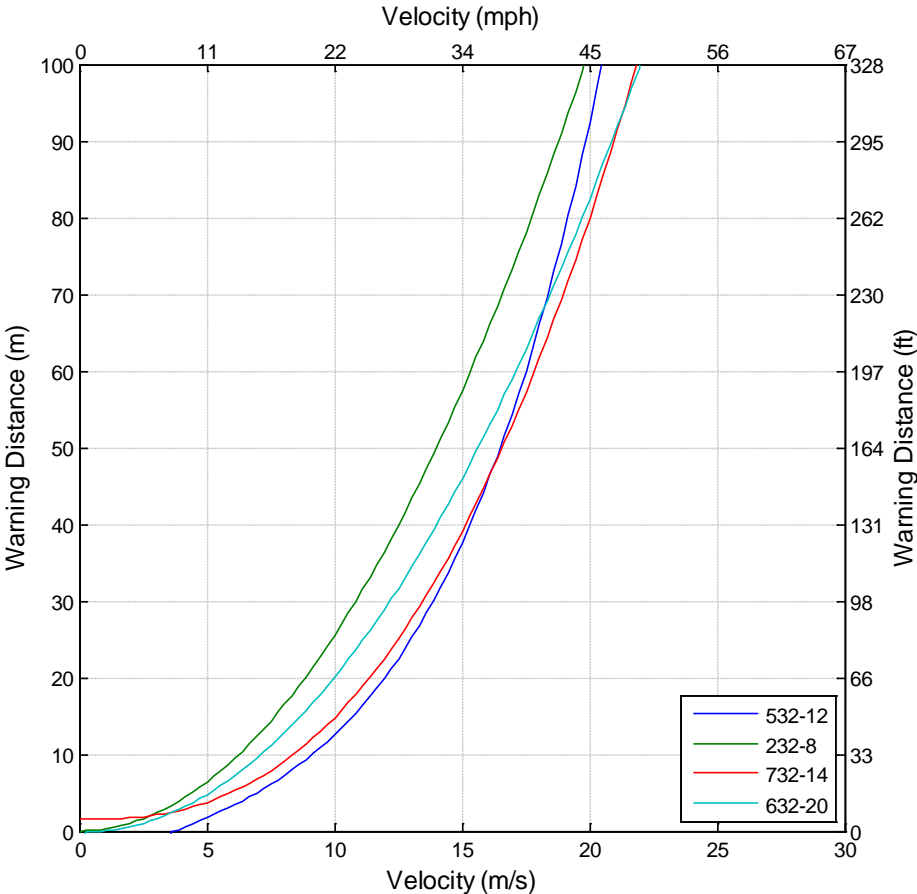


Figure 85 Stop bar velocity versus warning distance for the best applicable algorithms identified in the stop-controlled intersection simulation.

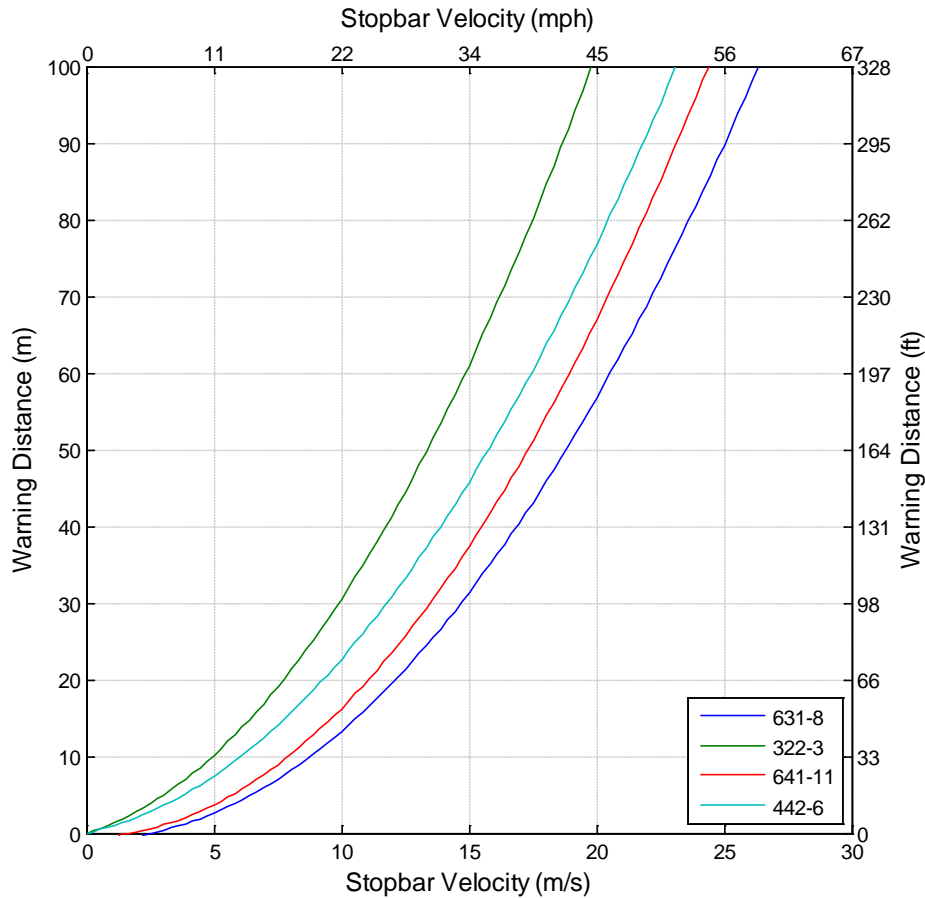


Figure 86 Stop bar velocity versus warning distance for the best applicable algorithms identified in the signalized intersection simulation.

### Implications of the Algorithm Results

While previous analyses provide a disciplined approach for making relative comparisons between algorithms, they do not fully represent their anticipated performance in terms of real-world driving. To better understand the implications, it is helpful to consider the base rates of occurrence for the false positive and true positive groups. The analyses described in Sections 4 and 5 indicated that opportunities for false positives occur more than opportunities for true positives by several orders of magnitude. For example, at signalized intersections there were 2,670 violations across 2.1 million crossings (Table 18, using a 15-mph violation threshold). Thus, on average, 789 compliant approaches occurred for every one violation for the sample of intersections.

Table 18 Sample size and the resulting violation frequency for stop-controlled and signalized intersections. At signalized intersections, the sample only includes vehicles that approached the intersection while the signal phase was either yellow or red.

Stop-Controlled Intersections				Signalized Intersections			
Violation Threshold	10 mph	15 mph	20 mph	Violation Threshold	10 mph	15 mph	20 mph
Sample Violations	1673	185	49	Sample Violations	3335	2670	2491
Sample Crossings	30,458			Sample Crossings	2,105,961		

From the algorithms presented in the previous section, it is possible to obtain a true positive rate as high as 80 percent (with a false positive rate as low as one percent); however, since there are more opportunities for false positives than true positives, the frequency of false positives will be much higher than that of true positives. This paradox highlights the importance of minimizing false positives as drivers will likely experience many false alerts for every valid warning.

Table 20 shows the base rate data for the best algorithms (identified by the heuristic) that were designed to compromise between providing timely warnings and maximizing true positives (tables for other algorithms presented in Appendix R). The tables convert the rate data that has been discussed up to this point into frequency counts for each of the possible algorithm outcomes. These frequency counts are provided as a count per 100,000 intersection crossings. In addition, the tables include ratios of false positives to true positives and true positives to false negatives.

**Table 19 Stop-controlled intersection frequency table for the best algorithms identified by the heuristic designed to compromise between providing timely warnings and maximizing the overall number of true positives using a violation threshold of 15 mph (none of the algorithms could meet the minimum specification [true positive rate of at least 0.5] at 10-mph violation threshold for a false positive rate of 0.01).**

		Per 100,000 Crossings										
		Algorithm	TPR	FNR	FPR	TNR	TP	FN	FP	TN	FP : TP	TP : FN
Maximum FPR = 0.05	Best Overall	634 - 12	0.86	0.14	0.05	0.95	525	82	4853	95118	9 : 1	6 : 1
	Best Applicable	232 - 8	0.68	0.32	0.05	0.95	410	197	4757	95214	12 : 1	2 : 1
Maximum FPR = 0.01	Best Overall	234 - 17	0.65	0.35	0.01	0.99	397	210	880	99115	2 : 1	2 : 1
	Best Applicable	732 - 14	0.56	0.44	0.01	0.99	341	266	929	99065	3 : 1	1 : 1

**Table 20 Signalized intersection frequency table for the best algorithms identified by the heuristic designed to compromise between providing timely warnings and maximizing the overall number of true positives using a violation threshold of 15 mph.**

		Per 100,000 Crossings										
		Algorithm	TPR	FNR	FPR	TNR	TP	FN	FP	TN	FP : TP	TP : FN
Maximum FPR = 0.05	Best Overall	634 - 10	0.83	0.17	0.04	0.96	105	21	4445	95549	42 : 1	5 : 1
	Best Applicable	641 - 11	0.83	0.17	0.05	0.95	105	22	4671	95323	44 : 1	5 : 1
Maximum FPR = 0.01	Best Overall	442 - 6	0.68	0.32	0.01	0.99	86	41	970	99028	11 : 1	2 : 1
	Best Applicable	442 - 6	0.68	0.32	0.01	0.99	86	41	970	99028	11 : 1	2 : 1

- TPR=True Positive Rate
- FNR=False Negative Rate
- TP=True Positive
- FN=False Negative

- FPR=False Positive Rate
- TNR=True Negative Rate
- FP=False Positive
- TN=True Negative

From the tables above, it can be seen that more false positives will be issued for every true positive at signalized intersections than there will at stop-controlled intersections. The true positive rates at the two intersection types are similar; however, there are more compliant approaches for every violation at signalized intersections than there are at stop-controlled intersections. In addition, notice that more warnings (both true positives and false positives) will be issued at stop-controlled intersections than at signalized intersections.

The effect of moving from a maximum false positive rate of 0.05 to 0.01 is a significant reduction in the ratio of false positives to true positives. The downside is that fewer true positives are generated for each false negative. Thus, the CICAS-V system should start testing at the higher false positive rate and move to the lower rate only if drivers do not tolerate the higher level of nuisance alerts.

Note the effect of limiting the applicable algorithms on the false positive to true positive ratio. At signalized intersections the effect is not very large; however, at stop-controlled intersections the effect is substantial, particularly at an allowable false positive rate of 0.05. This effect suggests that it may be worth integrating braking effort suppression into future CICAS-V prototypes rather than limiting the system to brake-status suppression.

Finally, it would be helpful to obtain a better understanding of the benefit provided by correct CICAS-V warnings. Some of the false negative rates (particularly at the 0.05 false positive rate) may not be acceptable. A compressive cost-benefit analysis needs to be performed to understand the implications of the algorithm performance.



## 9 Recommendations, Limitations, and Future Research

This final chapter extracts the most relevant outcomes of the previous analyses and summarizes the recommendations for CICAS-V, limitations of the methods employed, and suggestions for future research.

### 9.1 Recommendations

Based on the Subtask 3.2 analyses, a set of recommendations for CICAS-V are presented in this section. They will support the data requirements for the design, development, and deployment of the CICAS-V. In particular, these recommendations will be used as inputs into the design of the threat assessment algorithm that will be integrated into the prototype CICAS-V system; this will be tested in the remaining Phase I tasks of the CICAS-V project.

#### 9.1.1 Continue Research and Development of CICAS-V

The results of Subtask 3.2 suggest that CICAS-V systems can correctly identify most violations at low false positive rates (e.g. 0.05 and 0.01 false positive rates). This outcome provides support for the continued research and development of the CICAS-V.

#### 9.1.2 Determine Who Should Receive a Warning

The stop-bar speed analyses presented in Section 4 and Section 5 established the need for the CICAS-V to deviate from the standard legal definition of a violation. At stop-controlled intersections, for instance, this analysis demonstrated that 36 percent of the vehicles crossing through the intersections never slowed below 3.4 m/s (5 mph). Even with a higher 4.5 m/s (10 mph) criteria, nearly six percent of the vehicles violated. Events of this frequency suggested that drivers intentionally perform rolling stops and likely do not need or want a CICAS-V warning. Unwanted warnings presented to drivers will likely be perceived as a nuisance alert that will generate loss of user trust, potentially undermine the effectiveness of the CICAS-V system (Neale and Dingus, 2006).

A violation threshold of 6.7 m/s (15 mph) is recommended for CICAS-V, based on the analyses performed during this subtask. This threshold is supported by Subtask 3.1, which found that drivers performing violations at speeds below 4.9 m/s (11 mph) appeared to be doing so intentionally. If the ongoing CICAS-V tasks suggest that the 6.7-m/s violation threshold is inappropriate, the best algorithms for other violation thresholds are provided in Appendix P.

#### 9.1.3 Warning Suppression Should Be Part of the Algorithm

The threat assessment algorithm presented in this report contains a layer that suppresses the warning under certain circumstances. The layer is intended to suppress warnings if the behaviors of the driver suggest that they are attentive to the intersection and are highly likely to perform in a compliant manner. The two components of the suppression layer included a low-speed cutoff and a driver braking criterion.

The low-speed cutoff allows drivers to perform a rolling stop without receiving an alert. In addition, the low-speed cutoff also allows drivers to stop significantly behind the stop bar and accelerate through the intersection without receiving an alert. The selection of the best low-speed cutoff depends on the algorithm. Typically, the 6.7-m/s (15-mph) and 8.9-m/s (20-mph) low-speed cutoffs result in the best algorithm performance.

The brake criterion suppresses the warning if it determines that the driver is actively braking. This criterion reduces false positives by suppressing a warning to attentive drivers that respond late to the intersection and are likely to stop. The best algorithms typically use a 0.1-g or a 0.2-g minimum braking effort to suppress the warning.

The CICAS-V system available in Phase I can only support the brake status criterion. The effect of having only a brake status criterion is larger at stop-controlled intersections (~20 percent decrease in the total predicted number of false positives) than at signalized intersections, where the effect is minimal. The decrease in performance at stop-controlled intersections may justify enhancing future versions of the CICAS-V hardware to support the braking effort criterion.

#### **9.1.4 Algorithms for Use in CICAS-V Prototype Tests**

A systematic method was developed to simulate and subsequently evaluate the performance of over 160 unique algorithms with more than 7,000 unique parameter combinations. From these analyses, a set of the best performing algorithms were identified. One best algorithm was identified for each violation threshold (at allowable false positive rates of 0.01 and 0.05) within three distinct selection heuristics. In addition, the set of best applicable algorithms were also identified under the constraint that only the no-brake and brake status criterion could be supported by the present CICAS-V hardware. The recommendations below are based on these best applicable algorithms.

As discussed in Section 9.1.2, the algorithms identified by a 6.7-m/s (15-mph) violation threshold are recommended for use in the CICAS-V prototype. Furthermore, the allowable false positive rate of 0.05 is recommended as the starting point for the remaining CICAS-V project tasks. The algorithms at this false positive rate will result in higher levels of true positives at the expense of more nuisance alerts. If the future tasks indicate that drivers will not tolerate this level of false positives, an algorithm from the 0.01 allowable false positive category should be selected.

Finally, the three heuristics used to rank-order the algorithms were used to determine which algorithm is selected as the top-performer. One of the heuristics attempted to maximize the number of overall true positives while another maximized the number of warnings that were provided by the optimal warning timing. The third heuristic, which is presently recommended, seeks a compromise between these two competing goals.

From this set of recommendations, one algorithm was recommended for stop-controlled intersections and a second algorithm was recommended for signalized intersections. The recommended stop-controlled algorithm is 232-8, a constant-deceleration-based algorithm which uses a low-speed cutoff of 6.7 m/s (15 mph) and the brake status criterion. This algorithm is estimated to correctly warn 67 percent of the violating drivers while providing optimal warning timing to 51 percent of the violating drivers.

The recommended signalized algorithm is 641-11, a regression algorithm based on warning distance as a function of velocity. The algorithm uses an 8.9-m/s (20-mph) low-speed cutoff and does not require any braking criterion. It is estimated to provide correct warnings to 83 percent violating drivers while providing optimal warning timing to 78 percent of violating drivers.

## 9.2 Limitations

There are certain limitations that need to be considered when interpreting the results of this study. First, the geographic region was limited to southwest Virginia and urban corridor intersections. Drivers from different regions and across other roadway types may approach intersections differently. Furthermore, the data collection took place over two consecutive months during the spring season. Thus, the database collected may not necessarily reflect seasonal differences in intersection driving behavior.

Placing the DAS at the intersection was required to obtain the volume of data necessary to construct a valid CICAS-V algorithm; however, placing the data collection equipment at the intersection rather than in the vehicle has certain limitations. This study did not provide information about the driver actions that led up to the violation. For instance, it is not possible to know for certain whether a violation was intentional or unintentional. Furthermore, measures such as brake status and acceleration had to be inferred. While care was taken to validate these measures, there may be some situations (e.g., riding the brake) that are unaccounted for in the analyses. In addition, the CICAS-V system was intended to address light vehicle traffic control violations, while data that was not visually examined may have included other vehicle types with different approach and braking profiles.

Finally, the radar sometimes provided sparse data where continuous data should have been provided, especially the radar used for the stop-controlled intersection data collection. This required a post-processing effort to improve the data so that continuous algorithms could be evaluated. During this effort, only vehicle tracks that contained sufficient fidelity were carried through to the analysis portion of the study. While there was no direct evidence to suggest that this systematic selection confounded the data, it remains possible that certain types of vehicles or vehicle approach characteristics were prone to degraded radar performance. Thus, certain types of vehicles or approach types may be unknowingly underrepresented in the data set.

## 9.3 Future Research Opportunities

The research discussed is a key step in the development of the CICAS-V. Once combined with the other tasks from Phase I of the CICAS-V project, a fully functional prototype CICAS-V was produced and tested in a pilot FOT (Subtask 3.4), however at this time there are no plans to conduct a Phase II FOT for the CICAS-V prototype. The discussion below focuses on future research that is relevant to the threat assessment algorithm and is not currently part of the Phase I test plan.

### 9.3.1 Extensions of the Subtask 3.2 Analyses

While performing Subtask 3.2, several research questions arose outside the subtask's original scope of work. These questions extend the subtask analysis to further investigate the CICAS-V algorithm and potentially improve the threat assessment performance.

The Subtask 3.2 analyses simulated the CICAS-V system based on data collected from vehicles approaching instrumented intersections. These vehicles performed a variety of maneuvers across approaches of varying geometries, speed limits, traffic volumes, and environmental conditions. The analyses were only partitioned by the traffic control device and the outcome (violation versus compliant). Additional factors could be extracted from the analysis that should provide a better understanding of the algorithm performance.

For example, the analyses described in this report provide overall performance of each algorithm; however, they do not contain information about the strengths and weaknesses of each. There are probably instances in which one algorithm is better at predicting certain types of violation approaches but has poor overall performance. If other factors are considered in the analyses, the strengths of each algorithm can be identified. Based on those strengths, it may be possible to create new algorithms combining the best attributes of different algorithms, or suggest a parallel algorithm implementation. Some examples of intersection factors that could be considered include the phase timing, lane type, intersection type, and posted speed limit.

The algorithm performance can also be partitioned by the kinematic attributes of the vehicle approaches. In this case, performance would be analyzed in terms of the types of approaches the algorithm can correctly categorize versus those it cannot. For instance, to improve the algorithm's hit rate, comparisons between true positive and false negative vehicle trajectories could be made. Conversely, comparisons between true negatives and false positives may also be made. The comparisons would highlight the differences between cases of correct and incorrect approach classification by the algorithm. From these results, the algorithms could be modified to improve the incorrect classifications without inadvertently reducing the correct classifications.

The analyses performed can also be extended to include entirely new algorithms. The algorithms in this report were selected based on particle-motion engineering equations and linear regression techniques. There are a series of additional methods that could be applied to generate alternative algorithms, such as logistic regression and change point analysis.

Finally, threat assessment algorithms could benefit from considering additional measures that were not part of this analysis (e.g., drivers likely to perform different approach trajectories depending on when they receive a phase change). A driver who receives a yellow phase change near the intersection will slow the vehicle later and at a higher rate than a driver who approaches a red light from a long distance. An algorithm could use the phase timing information to provide earlier warnings to drivers as the time-after-red at which they are predicted to arrive at the stop bar increases. There are many other variables that can be part of the algorithm assessment as well. Some possible variables include the posted speed limit, lane type, vehicle type, and turn signal activation. Determining which variables to investigate further could be part of the additional analysis described in the next section.

### **9.3.2 Re-Analyzing the Subtask 3.2 Results Using Future Data Collections**

The CICAS-V project performed a few additional investigations before Phase I ended. In addition, future research concerning the CICAS-V can further enhance our understanding of violations and the ability of CICAS-V to mitigate them. The data from these additional studies could feed back into the Subtask 3.2 analyses to validate or improve some of the required assumptions. However, there are no plans at this time to conduct the second phase of the CICAS-V project.

Algorithm recommendations were made based on assumptions regarding the permissible levels of false positives (0.01 and 0.05 rates). These assumed rates should be supported with research that studies the allowable types and frequency of nuisance alerts. It is possible that drivers are willing to tolerate more false positives than expected, which would increase the allowable false positive range. Phase I, Subtask 3.4 provided an initial understanding of drivers' tolerance for false positives. If the assumed rates are not appropriate they can be adjusted, and the Subtask 3.2 analysis can be re-evaluated to suggest a new set of algorithms for testing. Future research

could provide refined estimates of the permissible levels of false alarms that would help further determine the algorithm that should be carried forward to deployment.

There is another important assumption on the distribution of warning timing created from Subtask 3.3 data. The warning timing model was used to determine which algorithms provided warnings at a sufficient distance for drivers to stop. This model can be refined as additional data are collected from drivers who receive a warning. In particular, Subtask 3.4 and a FOT (should one be performed in the future) should provide information regarding the timeliness of the warning across a wider range of speeds than were tested during Subtask 3.3 (Perez et al., in review).

Finally, the definition of a target violation for the CICAS-V system was an important assumption of the Subtask 3.2 analyses. Several definitions were studied to allow researchers and engineers to understand algorithm performance as a function of the selected target population. It was clear from the results that the formal definition (all vehicles must complete a full stop at a red light or stop sign) is not a practical way to define the CICAS-V target population. A data-driven violation definition was suggested based on the results of Subtask 3.1 (Sudweeks et al., in review) and Subtask 3.2; however, it would be prudent to investigate the violation definition through an independent evaluation. This investigation should focus on the connection between the violation definition and crash risk. A definition should be selected based on the anticipated crashes prevented, and the CICAS-V team could work to maximize system performance based on that definition.

### 9.3.3 Additional Analyses Using the Subtask 3.2 Data

The database obtained while satisfying the requirements of Subtask 3.2 enables a large number of future studies to be performed. Many of these future studies include more traditional civil engineering investigations. For instance, the data could be used to improve the intersection components of simulation models or to study signal timing paradigms. While studies such as these are beneficial, they are beyond the scope of this effort. This section will focus on the analyses relevant to CICAS-V.

For the Subtask 3.2 analysis, potential violation approaches were flagged through an automated process. Once flagged, data reductionists evaluated the data relevant to each flag and visually determined whether or not the event was valid based on video data and graphs of the parametric data. For valid events, the data were reviewed to gather additional data regarding the violation. This information included the following:

- Information about the violating vehicle:
  - Vehicle type
  - Maneuver performed
  - Legality of the maneuver performed
- Information about other vehicles on the same approach:
  - Forward vehicle presence and crossing type
  - Rearward vehicle presence and crossing type
  - Adjacent vehicle presence and crossing type
- Information about traffic that will next legally occupy the intersection box:
  - Conflicting traffic behavior (no movement, entered intersection, etc.)
  - Event classification (non-conflict, near crash, etc.)

- Information about the environment:
  - Sky cover and precipitation
  - Roadway surface condition
  - Ambient lighting

Using this additional information, a variety of future analyses could be performed to learn more about violators. An example analysis using the data above was performed to investigate factors that differentiate between violations and near violations at stop-controlled intersections (Appendix T). This analysis was limited because it only considered approaches where the automated process predicted a violation. More useful analyses could be performed if a baseline data reduction effort was undertaken to collect the measures for compliant vehicle approaches. Such an effort would allow investigation into the factors that lead to violations. These factors could then be used integrated into new algorithms, as described in the previous section, possibly improving their ability to predict violations.

A handful of interesting violations showed up during data reduction. It may be productive to revisit some of these violations using a case-study method. As an example, there were 27 near crashes (events requiring an evasive maneuver) identified by the data reductionists. These near crashes approximate the target population of the CICAS-V. It would be interesting to investigate these 27 cases to determine what may have led to the violation. Another possible selection includes violations that occur more than a few seconds after the red light is presented. Such late violations have been shown to lead to straight-crossing-path crashes (Zimmerman & Bonneson, 2005). Case studies could provide insights into violation scenarios that are central to the purpose of CICAS-V. These insights may suggest enhancements to the threat assessment algorithms that could be incorporated into the additional algorithms discussed in the previous section.

## 10 References

- Brewer, M.A., Bonneson, J., & Zimmerman, K. (2002). *Engineering countermeasures to red-light-running*. Paper presented at the Proceedings of the ITE 2002 Spring Conference and Exhibit (CD-ROM), Washington, D.C.
- Campbell, B., Smith, J., & Wassim, N. (2004). *Analysis of Fatal Crashes Due to Signal and Stop Sign Violations*. (Report No. DOT HS 809 779). Washington, D.C.: National Highway Traffic Safety Administration.
- Chang, M. S., Messer, C. J., & Santiago, A. J. (1985). Timing traffic signal change intervals based on driver behavior. *Transportation Research Record*, 1027, 20-30.
1. Chakravart, Laha, & Roy. (1967). *Handbook of Methods of Applied Statistics: Volume I*. New York: John Wiley and Sons, pp. 392-394.
  2. Chovan, J., Tijerina, L., Pierowicz, J., & Hendricks, D. (1994). *Examination of unsignalized intersection, straight crossing path crashes, and potential IVHS countermeasures* (Report No. DOT-HS-808 152). Washington, D.C.: National Highway Traffic Safety Administration.
  3. Davidson, I. *Understanding K-Means Non-hierarchical Clustering*. Albany, New York: State University of New York, 2002.
  4. Dingus, T. A., Jahns, S. K., Horowitz, A. D., & Knipling, R. (1998). Human factors design issues for crash avoidance systems. In: W. Barfield and T.A. Dingus, Editors, *Human Factors in Intelligent Transportation Systems*, Lawrence Erlbaum Associates, New Jersey, pp. 55-93.
- Dingus, T. A., Klauer, S.G., Neale, V. L., Petersen, A., Lee, S. E., Sudweeks, J., Perez, M. A., Hankey, J., Ramsey, D., Gupta, S., Bucher, C., Doerzaph, Z. R., & Jermeland, J. (2004). *The 100-car naturalistic driving study; Phase II- Results of the 100-car field experiment*. Contract No. DTNH22-00-C-07007 (Task Order No. 06). Blacksburg, VA: Virginia Tech Transportation Institute.
- Dingus, T. A., Klauer, S. G., Neale, V. L., Petersen, A., Lee, S. E., Sudweeks, J., Prez, M. A., Hankey, J., Ramsey, D., Gupta, S., Bucher, C., Doerzaph, Z. R., Jermeland, J., & Knipling, R. R. (2006). *The 100-car naturalistic driving study, Phase II – Results of the 100-car field experiment*. (Contract No. DTNH22-00-C-07007). Washington, D.C.: National Highway Traffic Safety Administration.

- Doerzaph, Z. (2004). *Intersection stopping behavior as influenced by driver state: Implications for intersection decision support systems*. (Contract No. 02-1635-02). Washington, D.C.: Federal Highway Administration.
- Doerzaph, Z. (November 2007). *Development of a Threat Assessment Algorithm for Intersection Collision Avoidance Systems*. Unpublished doctoral dissertation, Virginia Tech, Blacksburg, VA.
- Fahlman, S. E., & Lebiere, C. (1991). The Cascade-Correlation Learning Architecture. National Science Foundation and Defense Advanced Research Projects Agency.
- Fakhry, S. M., & Salaita, K. (2002). Aggressive driving: A preliminary analysis of a serious threat to motorists in a large metropolitan area. *Journal of Trauma*, 52(2), 217-224.
- Ferlis, R. (1999). *Intelligent transportation systems, analysis of infrastructure-based system concepts, intersection collision avoidance problem area*. Washington, D.C.: Federal Highway Administration.
- Ferlis, R. (2001). *Infrastructure systems for intersection collision avoidance*. Paper presented at the Proceedings of the First International Driving Symposium on Human Factors in Driver Assessment, Training, and Vehicle Design, Aspen, CO.
- 5.
6. Hauskrecht, M. Clustering. Presentation for CS2750 Machine Learning. Pittsburgh, Pennsylvania: University of Pittsburgh, 2003.
- Hendricks, D. L., Fell, J. C., & Freedman, M. (1999). *The relative frequency of unsafe driving acts in serious traffic crashes*. (Contract No. DTNH22-94-C-05020). Washington, D.C.: National Highway Traffic Safety Administration.
- Horst. (1990). A Time-Based Analysis of Road User Behavior in Normal and Critical Encounters. Soesterberg: TNO Institute for Perception.
- ITE. (2003). *Making Intersections Safer: A Toolbox of Engineering Countermeasures to Reduce Red-Light Running*. Washington, D.C.: Institute of Transportation Engineers, 74.
- Johnson, D. E. (1998). *Applied Multivariate Methods for Data Analysts*. Duxbury Press: Pacific Grove.



- Kiefer, R., LeBlanc, D., Palmer, M., Salinger, J., Deering, R., & Shulman, M. (1999). *Development and validation of functional definitions and evaluation procedures for collision warning/avoidance systems* (Report No. DOT HS 808 964). Washington, D.C.: National Highway Traffic Safety Administration.
- Klauer, S. G., Dingus, T. A., Neale, V. L., Sudweeks, J. D., & Ramsey, D. J. (2006). The impact of driver inattention on near-crash/crash risk: an analysis using the 100-car naturalistic driving study data. Report no. DOT HS 810 594. Washington, D.C.: National Highway Transportation Safety Administration.
- 7.
8. Kotz, S., & Nadarajah, S. (2001). *Extreme value distributions: Theory and applications*. River Edge, NJ: World Scientific Publishing.
- Lee, S. E., Knipling, R. R., DeHart, M. C., Perez, M., Holbrook, T., Brown, S., Stone, S., & Olson, R. (2004). *Task 1 & 2 of the Intersection Collision Avoidance - Violation Project: Intersection Control Violation Crash Analysis and Top-Level System and Human Factors Requirements*. Blacksburg: Virginia Tech Transportation Institute.
- Lee, S. E., Perez, M. A., Doerzaph, Z. R., Stone, S. R., Brown, S. B., Neale, V. L., Knipling, R.R., & Holbrook, G.T. (2005). *Task 5 of the Intersection Collision Avoidance - Violation Project: Final Project Report*. Blacksburg: Virginia Tech Transportation Institute.
- Liu, B. S. (2007). Association of intersection approach speed with driver characteristics, vehicle type and traffic conditions comparing urban and suburban areas. *Accident Analysis and Prevention*, 39, 216-223.
9. MacQueen, J. B. (1967). Some methods for classification and analysis of multivariate observations. *Proceedings of 5th Berkeley Symposium on Mathematical Statistics and Probability*. Berkeley: University of California Press, 1, 281-297.
10. Matlab. (2007). *Statistics Toolbox 6: Users Guide*. Natick, MA: The Mathworks, Inc.
- Maltz, M., & Shinar, D. (2004). Imperfect in-vehicle collision avoidance warning systems can aid drivers. *Human Factors*, 46, 357-366.
- Microsoft®. (2008). Images are the copyrighted works of Microsoft® and subject to the terms and conditions of the Microsoft® License Agreement. Images retrieved from <http://maps.live.com>.
- Najm, W., Mironer, M., Koziol, J., Wang, J. S., & Knipling, R. R. (1995). *Synthesis report: Examination of target vehicular crashes and potential ITS countermeasures* (Report No. DOT HIS 808 263). Washington, D.C.: National Traffic Highway Safety Administration.

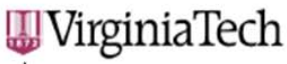

- Neale, V. L., Perez, M. A., Doerzaph, Z. R., & Stone, S. R. (2005). *Intersection Decision Support Final Report*. Blacksburg: Virginia Tech Transportation Institute.
- Neale, V. & Dingus, T. (2006). Motor vehicle warnings. *Handbook of Warnings*. M. Wogalter. Mahwah, Lawrence Erlbaum.
- NHTSA. (2005). *Traffic Safety Facts 2005*. (Report No. DOT HS 810 631). Washington, D.C.: National Highway Traffic Safety Administration.
- Parasuraman, R., Hancock, P. A., & Olofinboba, O. (1997). Alarm effectiveness in driver centered collision warning systems. *Ergonomics*, 39, 390-399.
- Perez, M. A., Neale, V. L., Kiefer, R. J., Viita, D., Wiegand, K., and Maile, M. (In Print). *Cooperative Intersection Collision Avoidance Systems Limited to Stop Sign and Traffic Signal Violations (CICAS-V) Subtask 3.3 Interim Report: Test of Alternative Driver-Vehicle Interfaces on the Smart Road*. Washington, DC: National Highway Traffic Safety Administration.
- Pierowicz, J., Jocoy, E., Lloyd, M., Bittner, A., & Pirson, B. (2000). *Intersection Collision Avoidance Using ITS Countermeasures: Task 9 Final Report – Intersection Collision Avoidance System Performance Guidelines*. (Contract No. DTNH22-93-C- 07024). Seattle, WA: Battelle Human Factors Transportation.
- Retting, R. A., Ulmer, R. G., & Williams, A. F. (1999). Prevalence and characteristics of red light running crashes in the United States. *Accident Analysis and Prevention*, 31, 687-694.
11. Rousseeuw, P. J. (1987). Silhouette: A graphical aid to the interpretation and validation of cluster analysis. *J. Computational Applied. Mathematics*, 20, 53-65.
- Sanders, M. S., & McCormick, E. J. (1993). *Human Factors in Engineering and Design*. New York: McGraw-Hill.
- Sharma, A., Bullock, D., & Peeta, S. (2005). *Limitations of Simultaneous Gap Out Logic*. Paper presented at the Proceeding of the Transportation Research Board 85<sup>th</sup> Annual Meeting, Washington, D.C.
- Smith, D. L., & Najm, W. (1999). *Analysis of crossing path crashes* (Report No. DOT-VNTSC-HS019-PM-99-01). Cambridge, MA: Volpe National Transportation Systems Center.
- Stimpson, W. A., Zador, P. L., & Tarnoff, P. J. (1980). The influence of the time duration of yellow traffic signals on driver response. *ITE Journal*, 50, 22-29.

- Sudweeks, J., Neale, V. L., Wiegand, K., Bowman, J., Perez, M. and Maile, M. (In Print). *Cooperative Intersection Collision Avoidance Systems Limited to Stop Sign and Traffic Signal Violations (CICAS-V) Subtask 3.1 Report: Mining of the 100-Car Naturalistic Database to Determine Factors Related to Intersection Violations and Near Violations*. Washington, DC: National Highway Traffic Safety Administration.
- Swets, J. A. (1996). *Signal detection theory and ROC analysis in psychology and diagnostics: Collected papers*. Mahwah, NJ: Erlbaum.
- Tanner, W. P., & Swets, J. A. (1953). *A New Theory of Visual Detection* (Technical Report No. 18). University of Michigan, Ann Arbor, MI: Electronic Defense Group.
- Tijerina, L., Chovan, J., Pierowicz, J., & Hendricks, D. (1994). *Examination of signalized intersection, straight crossing path crashes, and potential IVHS countermeasures* (Report No. DOT-HS-808 143). Washington, D.C.: National Highway Traffic Safety Administration.
- Van der Horst, R. (1988). Driver decision making at traffic signals. *Transportation Research Record*, 1172, 93-97.
- VDOT. (2005). *Average daily traffic volumes with vehicle classification data of interstate, arterial, and primary routes*. Washington, D.C.: Federal Highway Administration.
- Wang, J. S., & Knipling, R. R. (1994). *Intersection crossing path crashes: Problem size assessment and statistical description* (Report No. DOT HS 808 190). Washington, D.C.: National Highway Traffic Safety Administration.
- White, B., & Ferlis, B. (2004). *Algorithm for determining inattentive signal violators to be used in infrastructure-based intelligent system for signal violation prevention*. Paper presented at the 83rd annual meeting of the Transportation Research Board, Washington, D.C.
- Wierwille, W. W., Keiliszewski, D. A., Hanowski, J. J., Keisler, A. S., & Olsen, E. C. B. (2000). *Identification and evaluation of driver errors: Task E report – Investigation of critical incidents* (Interim Report for Federal Highway Administration Contract No. DTHF-61-97-C-00051). Washington, D.C.: Federal Highway Administration.
- Wierwille, W. W., R. J. Hanowski, et al. (2001). *Identification and evaluation of driver errors: Overview and recommendations*. Washington, D.C., Federal Highway Administration.

- Wickens, T. D. (2002). *Elementary signal detection theory*. Oxford University Press.
- Yamada, K., & Kuchar, J. K. (2006). Preliminary study of behavioral and safety effects of driver dependence on a warning system in a driving simulator. *IEEE Transactions on Systems, Man, and Cybernetics – Part A: Systems and Humans*, 36:3, 602-610.
- Yan, X., Radwan, E., & Abdel-Aty, M. (2005). Characteristics of rear-end accidents at signalized intersections using multiple logistic regression model. *Accident Analysis and Prevention*, 37, 983-995.
- Yang, David C. Y. & Najm, W. G. (2006). *Analysis of Red Light Violation Data Collected from Intersections Equipped with Red Light Photo Enforcement Cameras* (Report No. DOT HS 810 580). Washington, D.C.: National Highway Traffic Safety Administration.
- Zabyshny, A. A., & Ragland, D. R. (2003). *False Alarms and Human-Machine Warning Systems*. Berkeley, California: University of California, Berkeley, U.C. Berkeley Traffic Safety Center.
- Zimmerman, K. and J. A. Bonneson (2005). Investigation of the time-into-red for red-light-related crashes. 84th Annual Meeting of the Transportation Research Board, Washington, D.C.

# 11 Appendices

## 11.1 Appendix A: Internal Review Board Authorization to Proceed

		Office of Research Compliance Institutional Review Board 1880 Fran Drive (0497) Blacksburg, Virginia 24061 [Redacted] [Redacted] <a href="http://www.irb.vt.edu">www.irb.vt.edu</a> <small>FINA000005721 expires 7/20/07          IRB # is IRB0000667.</small>
DATE:	July 25, 2006	
MEMORANDUM		
TO:	Vicki Neale Zachary Doerzaph Tia Tucker	Approval date: 7/25/2006 Continuing Review Due Date: 7/10/2007 Expiration Date: 7/24/2007
FROM:	David M. Moore 	
SUBJECT:	IRB Expedited Approval: "Cooperative Intersection Collision Avoidance Systems: Task 3, 2, Live Data Collection", IRB # 06-405	
<p>This memo is regarding the above-mentioned protocol. The proposed research is eligible for expedited review according to the specifications authorized by 45 CFR 46.110 and 21 CFR 56.110. As Chair of the Virginia Tech Institutional Review Board, I have granted approval to the study for a period of 12 months, effective July 25, 2006.</p> <p>As an investigator of human subjects, your responsibilities include the following:</p> <ol style="list-style-type: none"> <li>1. Report promptly proposed changes in previously approved human subject research activities to the IRB, including changes to your study forms, procedures and investigators, regardless of how minor. The proposed changes must not be initiated without IRB review and approval, except where necessary to eliminate apparent immediate hazards to the subjects.</li> <li>2. Report promptly to the IRB any injuries or other unanticipated or adverse events involving risks or harms to human research subjects or others.</li> <li>3. Report promptly to the IRB of the study's closing (i.e., data collecting and data analysis complete at Virginia Tech). If the study is to continue past the expiration date (listed above), investigators must submit a request for continuing review prior to the continuing review due date (listed above). It is the researcher's responsibility to obtain re-approval from the IRB before the study's expiration date.</li> <li>4. If re-approval is not obtained (unless the study has been reported to the IRB as closed) prior to the expiration date, all activities involving human subjects and data analysis must cease immediately, except where necessary to eliminate apparent immediate hazards to the subjects.</li> </ol> <p><b>Important:</b>          If you are conducting federally funded non-exempt research, this approval letter must state that the IRB has compared the OSP grant application and IRB application and found the documents to be consistent. Otherwise, this approval letter is invalid for OSP to release funds. Visit our website at <a href="http://www.irb.vt.edu/pages/newstudy.htm#OSP">http://www.irb.vt.edu/pages/newstudy.htm#OSP</a> for further information.</p> <p>As indicated on the IRB application, this study is receiving federal funds. The approved IRB application has been compared to the OSP proposal listed above and found to be consistent. Funds involving procedures relating to human subjects may be released. Visit our website at <a href="http://www.irb.vt.edu">www.irb.vt.edu</a> for further information</p> <p>cc: File          Department Reviewer: Suzanne E. Lee</p>		

*Invent the Future*

VIRGINIA POLYTECHNIC INSTITUTE UNIVERSITY AND STATE UNIVERSITY  
 An equal opportunity, affirmative action institution

## 11.2 Appendix B: Deceleration Threshold and Driver Reaction Time

### 11.2.1 Introduction

The following study was performed to determine the relationship between brake pedal status and acceleration for drivers approaching stop-controlled and signalized intersections. The goal of the analysis was to predict driver-induced brake status (on/off), based on the vehicle's instantaneous rate of deceleration. This relationship was used to infer brake status using radar data, which does not natively contain brake information. The primary measures evaluated in this study included the deceleration level at which the brake was initially pressed, and the time from brake press to various pre-determined deceleration levels. The outputs of this task included a threshold below which the brakes will be considered active and the corresponding delay to determine the initial point at which the brakes were applied. This information was used to determine the point of brake activation.

### 11.2.2 Methods

The 100-car database (Dingus et al., 2006) was mined during Subtask 3.1 (Sudweeks et al., in review) to study driver approaches to stop-controlled and signalized intersections. For the purpose of this analysis, a balanced set of intersections approaches was randomly selected to collect the desired braking information. The Subtask 3.1 database includes continuous naturalistic in-vehicle data for over 100 participants who drove a personal or leased vehicle for one full year. The parametric data included a variety of kinematic and environmental variables collected at 10 Hz. This parametric data were accompanied by a digital video feed containing images of the driver and vehicle environment collected at 30 Hz.

To extract the relevant data samples, a query for each intersection type was created to randomly select 10 approaches within six vehicle platforms, providing a total of 120 observations. Only intersection approaches that contained straight, flat geometry were considered in the evaluation. The task was to determine the threshold values and time offsets for each of the approaches. The parameters that were collected from the database were:

- Trigger ID for each vehicle
- Vehicle type (e.g., Ford Explorer, Ford Taurus, Chevy Malibu, etc.)
- Deceleration values when the driver initiated braking
- Deceleration values when the car reached -0.05 g, -0.075 g, -0.10 g, -0.12 g.
- Time elapsed between brake activation and the abovementioned deceleration values

### 11.2.3 Results

Based on the method described above, Table 21 and Table 22 provide the average deceleration thresholds determined for each vehicle. The table also contains the time it took each vehicle to reach pre-determined deceleration values.

**Table 21 Deceleration thresholds and pre-determined deceleration values from 100-car data (stop-controlled data).**

Threshold deceleration when braking starts(g)		CAR TYPE						
		Chevy Malibu	Toyota Corolla	Toyota Camry	Leased Cavalier	Ford Taurus	Ford Explorer	
Threshold deceleration when braking starts(g)	Average	-0.042	-0.040	-0.012	-0.025	-0.052	-0.007	
	Std Dev	0.034	0.038	0.022	0.034	0.022	0.017	
	Min	-0.11	-0.05	-0.04	-0.07	-0.04	-0.04	
	Max	0.01	0.07	0.03	0.04	0.03	0.02	
Time taken to reach pre-determined deceleration value (seconds)	-0.05 g	Average	0.257	0.600	1.450	0.778	1.778	0.840
		Std dev	0.257	0.644	2.514	1.180	1.300	0.609
		Min	0	0	0.1	0	0.6	0.1
		Max	0.6	2.1	8.5	2.9	4	1.7
	-0.075 g	Average	1.600	1.230	2.180	1.200	2.289	1.120
		Std dev	3.090	0.979	2.785	1.217	1.274	0.890
		Min	0.1	0.5	0.2	0.1	0.8	0.3
		Max	9.8	3.4	9.3	3.4	4.2	3.1
	-0.10 g	Average	1.840	1.730	2.520	1.290	2.844	1.3
		Std dev	3.769	1.636	3.134	1.251	1.455	0.885
		Min	0	0.6	0.3	0.1	1.3	0.5
		Max	12.5	6	10.7	3.7	4.9	3.1
	-0.12 g	Average	2.660	2.440	2.810	1.640	3.712	1.460
		Std dev	4.884	2.872	3.252	1.510	1.726	0.916
		Min	0.1	0.7	0.4	0.2	1.7	0.6
		Max	16.2	10.3	11.3	4.1	6.2	3.2

#### 11.2.3.1.1.1.1.1

Table 22 Deceleration thresholds and pre-determined deceleration values from 100-car data (signalized data).

Threshold deceleration when braking starts(g)	CAR TYPE							
	Chevy Malibu	Toyota Corolla	Toyota Camry	Leased Cavalier	Ford Taurus	Ford Explorer		
Average	-0.047	-0.019	-0.003	-0.02	-0.008	-0.017		
Std Dev	0.024	0.034	0.037	0.043	0.335	0.062		
Min	0.01	-0.06	-0.08	-0.08	-0.06	-0.09		
Max	-0.08	0.05	0.04	0.06	0.05	0.11		
Time taken to reach pre-determined deceleration value (seconds)	-0.05 g	Average	0.284	0.712	0.56	0.625	1.69	0.937
		Std dev	0.299	1.03	0.384	0.762	1.859	0.988
		Min	0	0	0	0	0	0
		Max	0.9	3.1	1.3	2.2	4.9	2.9
	-0.075 g	Average	1.18	1.056	1.12	0.71	2.52	1.19
		Std dev	2.458	1.11	1.381	0.970	2.148	1.182
		Min	0	0.1	0	0	0.2	0
		Max	8.1	3.4	4.9	3	6.2	3.1
	-0.10 g	Average	1.812	1.3	1.27	1.46	3.2	1.14
		Std dev	2.630	1.18	1.34	1.50	2.155	1.145
		Min	0.2	0.2	0.4	0.3	0.8	0.1
		Max	8.2	3.6	5.0	4.3	6.4	3.4
	-0.12 g	Average	1.91	1.5	1.62	1.81	4.94	2.23
		Std dev	2.387	1.19	1.282	1.563	4.303	2.08
		Min	0.3	0.3	0.7	0.5	0.9	0.2
		Max	8.3	3.9	5.1	4.4	14.2	5.4

### 11.2.4 Conclusion

The purpose of this study was to determine: 1) the deceleration threshold at which it may be stated that a vehicle is actively braking; and 2) the corresponding time from initiation of braking to the selected threshold deceleration value. Rather than selecting an average threshold deceleration value, the 95 percent value was selected for three primary reasons:

1. The vehicle data collected for this study were measured by radar. As radar does not directly measure acceleration, the acceleration had to be derived from the velocity. As a derivative, any noise inherent in the velocity data was amplified in the acceleration data. Thus, a more strident threshold would minimize early identification of braking.
2. Drivers initiate braking at a variety of initial levels of acceleration. It was not unusual for the acceleration at the brake onset to be positive (i.e., driver accelerating just prior to pressing the brakes). This explains a number of the low average threshold values



displayed in the table above. Given the safety application of an ICAS system, it is desirable to select a threshold in which a majority of drivers will have applied the brake.

3. The braking points were determined by identifying the threshold deceleration level and subsequently subtracting the average time elapsed from the onset of braking until the threshold is reached. Thus, the time measure will take into account the differences in the actual brake onset described in the table above.

The overall average threshold value for the 60 observations was  $-0.015$  g with a standard deviation of  $-0.031$  g. Thus, the 95th percentile driver has initiated braking at a threshold of approximately  $-0.077$  g. From the table above, this corresponds closely to the  $-0.075$ -g threshold suggesting an average response time value of  $1.60$  s with a standard deviation of  $1.89$  s. Thus, the brake onset will be identified at  $1.60$  s before the vehicle acceleration reaches  $-0.075$  g.

### 11.3 Appendix C: Vehicle Data Acquisition

In order to verify radar data at instrumented intersections, an experimental vehicle was used to collect redundant speed, acceleration, and braking data. The vehicle was a 2006 Cadillac STS (Figure 87), used as part of the Smart Road study for Subtask 3.3 (Perez et al., in press).



Figure 87 Experimental vehicle, 2006 Cadillac STS.

The vehicle was outfitted with a data acquisition system (DAS), custom-built by VTTI, and contained within the trunk of the vehicle (Figure 88). Attached to the system DAS was a series of custom-designed circuit boards that controlled the various functions of the acquisition device. This system included an accelerometer/gyroscope, a vehicle network sniffer (to pull variables from the vehicle network), and power management boards. The alignment and time stamping data retrieved from these boards was choreographed by a customized VTTI proprietary software package, which collected data at 100 Hz. Hardware was contained in a custom-mounting case designed to affix instrumentation in orientations necessary for accurate measurement and durability.



Figure 88 Data acquisition system, installed in the vehicle trunk underneath the rear shelf.

Each component of the DAS network provided information to the DAS for recording. The distributed DAS network included two important components: 1) three-axis accelerometer; and 2) Differential Global Positioning System (DGPS). The accelerometer box was located near the vehicle pitch-center to minimize pitch-induced acceleration noise. A Crossbow VG400 was used to provide acceleration data. Specifications for this device follow:

- Update rate: 70 Hz
- Latency: 0.01 s
- Reliability: 99%
- Accuracy:
  - Longitudinal: 0.6 mg @ 70 Hz
  - Lateral: 0.6 mg @ 70 Hz
- Power requirement: 9V @ <250 mA

The DGPS subsystem provided vehicle position and speed for data collection. A Novatel OEM4-G2L DGPS unit was used to provide position and speed data. This unit received differential corrections from a base unit with an antenna on the roof of the VTTI building. The corrections were transmitted via a Pacific Crest RFM96W radio unit operating at 35 W. Specifications for this DGPS system were as follows:

- Update rate: 20 Hz maximum
- Latency: 0.05 s
- Reliability: 99%
- Accuracy:
  - Longitudinal: Position – 1 cm, Speed – 0.03 m/s
  - Lateral: Position – 1 cm, Speed – 0.03m/s
  - Heading: Not available
- Power requirement: 2 W

## 11.4 Appendix D: Violation Trigger Development Process

The data requirements identified in the Section 5 needed the validation of aggressive intersection approaches. In particular, it was necessary to identify approaches in which drivers either committed a violation, or performed a stop (or near stop) in such a way that their behavior would make it difficult for the algorithm to discriminate. Thus, the trigger development focused on finding a metric that would identify aggressive stopping behaviors.

In addition, a second important criterion was to identify a trigger that functioned on sparsely populated data. As discussed in the methods and results section, the radar used for this study did not reliably return a measurement for every collection frame. Thus, the trigger could not operate at a single location, as it would miss vehicles that were not reported by the radar in that location.

Several possible trigger strategies were considered in order to identify violations. In particular, triggers evaluating the stop-bar speed, average deceleration, peak deceleration, and minimum speed were assessed. However, a measure of the average deceleration required to stop at the stop bar was identified as the appropriate triggering variable.

The required deceleration parameter (RDP) is a calculated value computed at each frame of data. RDP is the kinematic relationship between instantaneous velocity and distance to the stop bar as described by Equation 19.

### Equation 19

$$RDP = \frac{V^2}{2 * R * g}$$

Where:

V = Instantaneous velocity

R = Instantaneous range from stop bar

G = Gravitational constant

RDP has several advantageous characteristics that make it a particularly good metric for triggering the data reduction. First, RDP uses velocity and range which are frequently measured by the radar. This has the advantage of not relying on a derived measure such as acceleration, which is prone to amplified noise. Second, RDP is easily interpreted in the context of stopping behavior. A driver who performs an aggressive intersection approach would have to brake hard to stop before the stop bar. Thus, this driver would also exhibit a high RDP.

If that driver did not stop, the RDP would likely exceed the capabilities of the vehicle as the stop bar neared. On the other hand, a conservative driver would exhibit a low required deceleration. Furthermore, unlike evaluating velocity at a particular point, RDP can be evaluated at any point along the intersection approach and remain valid. For instance, a driver who initially approached the intersection at a high speed followed by a hard brake will be missed by a stop-bar speed trigger. A RDP trigger, on the other hand, will catch the high deceleration that was required to slow that vehicle upstream of the stop bar.

To develop an effective trigger, there were some additional criteria that had to be considered during the RDP computation. First, RDP tends towards infinity as the vehicle nears the stop bar. This tendency would have a negative impact on the sensitivity of the measure to segregate stopping behaviors. Investigation of RDP indicated that the tendency did not exist for typical approaches until the vehicle was within 1 m from the stop bar. Thus, RDP was only evaluated at distances greater than 1 m.

RDP provided a continuous measure over the entire time period in which the vehicle was tracked. Thus, to enable a simple trigger comparison the maximum RDP was extrapolated and compared to a trigger threshold. The maximum RDP over the entire vehicle approach represented the highest rate at which the driver would have needed to stop. For a violating driver, the maximum RDP would exist near the stop bar. However, for an aggressive driver who stops rapidly, the maximum RDP may exist at some point upstream prior to the high deceleration stop. This made the trigger particularly advantageous because it was sensitive to violators and aggressive drivers; these were the groups of primary interest for the algorithm.

With the triggering metric identified, the next step was to set a threshold for separating the reduction events from the non-reduction events. To identify the trigger threshold, the maximum RDP was calculated for each vehicle approach in the data set. The distribution of maximum RDP was then analyzed to determine an appropriate threshold. This analysis will be described through the subsequent figures.

First, in light of time and budget constraints, it was important to select a threshold that provided a reasonable number of reducible events. The number of events was evaluated as a function of the threshold selected (Figure 89). As the RDP threshold was lowered, the number of events rose sharply. Based on the constraints, a cap was set at 10,000 events, with a desire to reduce the number of events to a lower number, if possible. This criterion suggested a threshold in the region of 0.8 g to 1.2 g. Initially, while these values may appear high, they are actually well within the region that provides the data of interest. Additional details will be provided with the figures below as well as during the stopping behavior analysis discussed in the results section.

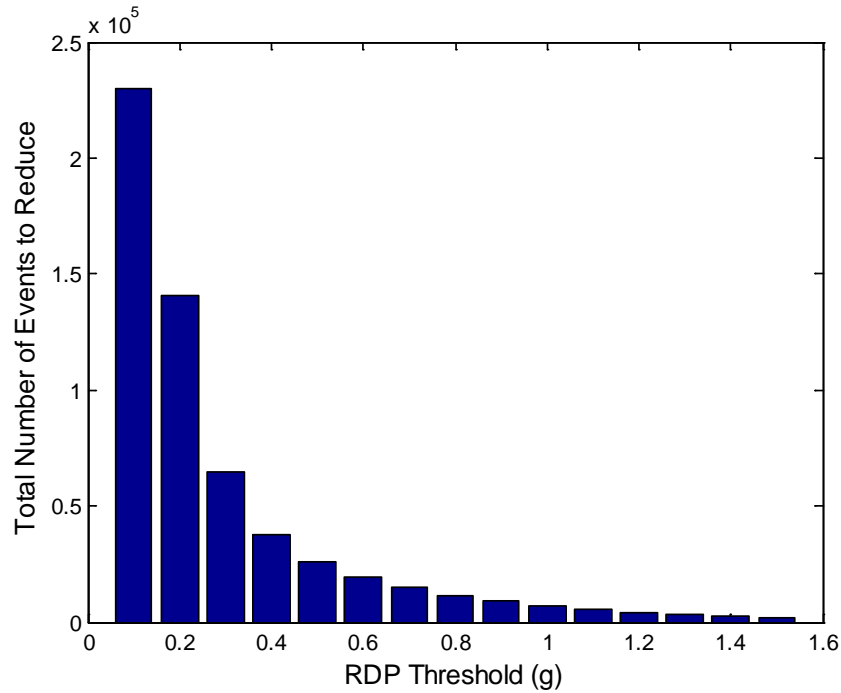


**Figure 89** Number of events that would be reduced as a function of the RDP threshold selected.

In conjunction with the results shown above, the average stop-bar speed (as a function of the RDP threshold) was also considered (Figure 90). Stop-bar speed provided an indication of the severity of a violation that could be readily understood. Furthermore, results discussed during the introduction indicated that a stop-bar speed of 4.47 m/s (10 mph) appeared to separate intentional rolling stops from a violation resulting from some form of inattention. Considering the stop-bar speed, it appeared that an RDP threshold of approximately 1.2 g was appropriate as it corresponded to a stop-bar speed of 4.47 m/s (10 mph). To ensure that these approaches were obtained, a cutoff closer to 1 g looked more feasible.

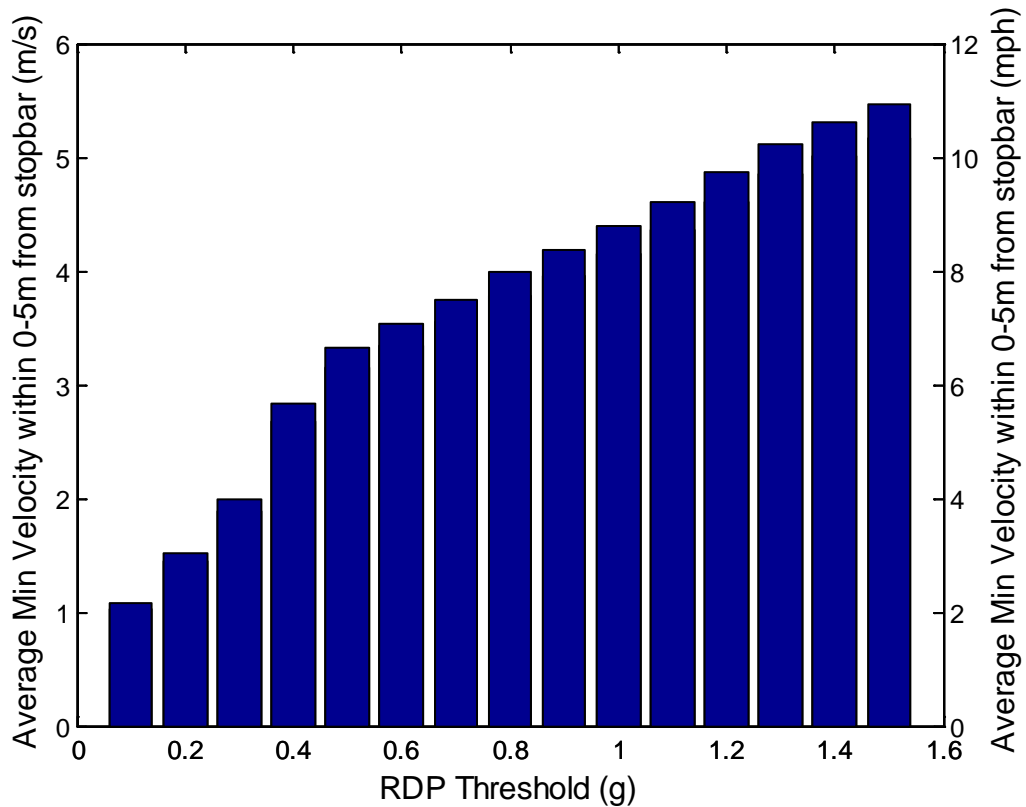


**Figure 90 Average minimum velocity for vehicles near the stop bar.**

Finally, the team evaluated the empirical distribution of RDP across the entire sample of drivers. (Figure 91). With warning systems such as the ICAS, researchers are interested primarily in the tail of a distribution that represents uncommon behavior. In this context, these behaviors belong to dangerous violators. Considering the distribution, a 1-g RDP threshold addresses 5% of the sample. Focusing on the top 5% of the population provides a convenient and logical cutoff for investigation. Furthermore, this cutoff should be conservative, as ICAS developers are aiming for warning rates significantly lower than 5% to avoid excessive nuisance alarms. Setting the reduction threshold for RDP at 1 g provides a conservative cutoff that will include nearly all of the severe violations, as well as a sample of the more aggressive intersection approaches.

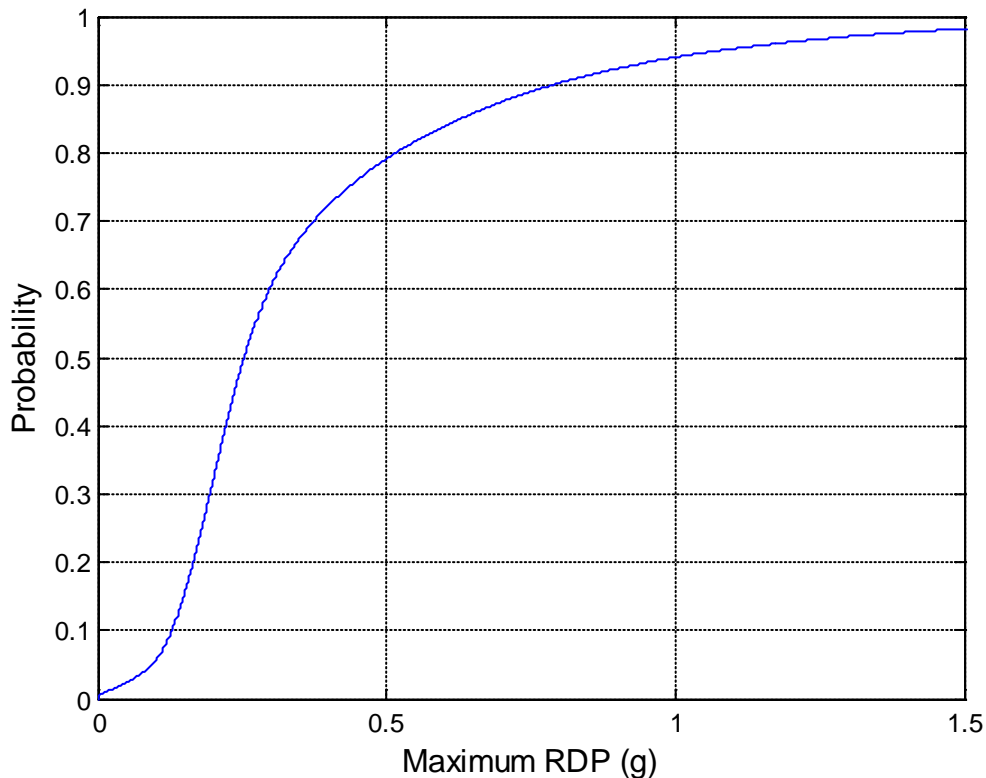


**Figure 91 Empirical cumulative probability distribution for RDP.**

Based on the data presented above, a trigger threshold of 1 g was selected for identifying the approaches for reduction. This resulted in the reduction of 6,171 events. Considering that a typical braking maneuver occurs around 0.3 g, the 1-g threshold may appear larger than one might expect.

The reasons for this include:

First, most drivers do not come to a complete stop. Thus, even the drivers performing a slow rolling stop will exhibit an elevated RDP. However, these slow rolling cases occur with such frequency that it would be a mistake to issue a warning. Secondly, such a low threshold warning system would have an impact on driver acceptance and would not be implemented by the automotive manufacturers. Finally, the purpose of the ICAS system is to mitigate crashes through a violation warning. In general, drivers who perform a slow rolling stop are as attentive as a driver that completely stops. This suggests no increase in crash likelihood.



## 11.5 Appendix E: Post-Processing and Radar-Induced Error

Table 23 Stop-controlled post processing and radar-induced error.

		Range	Speed	Acceleration
45 mph	Mean	0.506	0.164	-0.013
	Standard Deviation	2.154	0.245	0.054
	Min	-6.579	-0.095	-0.318
	Max	2.446	1.520	0.076
35 mph	Mean	1.061	0.076	-0.003
	Standard Deviation	2.200	0.159	0.023
	Min	-6.207	-0.085	-0.140
	Max	4.247	0.934	0.047
25 mph	Mean	0.833	0.034	0.000
	Standard Deviation	2.505	0.102	0.014
	Min	-6.292	-0.278	-0.115
	Max	5.562	0.690	0.029
Overall	Mean	0.829	0.062	-0.003
	Standard Deviation	2.401	0.151	0.026
	Min	-6.579	-0.278	-0.318
	Max	5.562	1.520	0.076

Table 24 Signalized post processing and radar-induced error.

		Range	Speed	Acceleration
45 mph	Mean	-1.760	-0.026	0.003
	Standard Deviation	2.143	0.341	0.035
	Min	-6.669	-0.728	-0.094
	Max	1.517	1.022	0.187
35 mph	Mean	-1.627	0.072	-0.003
	Standard Deviation	1.247	0.279	0.046
	Min	-3.471	-0.826	-0.208
	Max	1.458	1.205	0.403
25 mph	Mean	-0.743	0.096	-0.001
	Standard Deviation	1.174	0.308	0.038
	Min	-2.137	-0.417	-0.190
	Max	1.864	1.530	0.225
Overall	Mean	-1.342	0.045	-0.001
	Standard Deviation	1.352	0.287	0.038
	Min	-6.669	-0.826	-0.208
	Max	1.864	1.530	0.403

### 11.6 Appendix F: Summary of Results for the Cluster Analysis

Table 25 Results from the performed cluster analysis.

		Within Cluster Information					Overall Cluster Information			
		Cluster 1	Cluster 2	Cluster 3	Cluster 4	Cluster 5	Clusters	Silhouette Width	Sum of Differences	
Cluster	Count	30581	42				2	0.9924	1896.82	
	Centroid	0.34418	4.1308							
	Standard Deviation	0.23626	2.152							
	Min	0.000339	2.4224							
	Max	2.2254	13.1572							
	Silhouette Width	0.99328	0.35142							
Cluster	Count	25083	5499	41			3	0.8453	740.833	
	Centroid	0.25316	0.75972	4.1724						
	Standard Deviation	0.098582	0.23753	2.1615						
	Min	0.000339	0.50647	2.4885						
	Max	0.506337	2.42239	13.1572						
	Silhouette Width	0.9221	0.49996	0.1854						
Cluster	Count	24995	5573	51	4			4	0.84656	590.728
	Centroid	0.25228	0.75228	3.1587	9.8971					
	Standard Deviation	0.09762	0.22803	0.93244	2.5392					
	Min	0.000339	0.5023	1.9724	7.2506					
	Max	0.502221	1.93996	5.15076	13.1572					
	Silhouette Width	0.92056	0.51739	0.56914	0.62755					
Cluster	Count	21494	6784	2303	38	4	5	0.79096	576.093	
	Centroid	0.22356	0.51428	0.96885	3.5238	9.8971				
	Standard Deviation	0.070347	0.10409	0.22779	0.79739	2.5392				
	Min	0.000339	0.36893	0.74161	2.4224	7.2506				
	Max	0.368885	0.741524	2.2254	5.15076	13.1572				
	Silhouette Width	0.8716	0.64893	0.45761	0.76373	0.56416				

### 11.7 Appendix G: Summary Table of Results for the GEV Fits and the Kolmogorov-Smirnov Goodness of Fit Test

Table 26 Summary of GEV fits and the KS test.

Generalized Extremely Value Fit Information								
Overall Max RDP GEV Fit	Results	Centroid		0.3494				
		95%		0.8017				
		5%		0.1142				
	Fit	Quality	H		0			
			P		0.1946			
			KSTAT		0.1497			
			CV		0.1884			
		Parameters	K		0.2787			
			k_95% LC		0.2701			
			k_95% UC		0.2874			
			Sigma		0.1235			
			Sigma_95% LC		0.1223			
			Sigma_95% UC		0.1248			
			Mu		0.2309			
Mu_95% LC		0.2294						
Mu_95% UC		0.2325						
Four Partition Within Cluster GEV Fit	Group			Cluster 1	Cluster 2	Cluster 3	Cluster 4	
	Results	Centroid		0.25228	0.75228	3.1587	9.8971	
		95%		0.426	1.2885	5.0285	14.0513	
		5%		0.11	0.5187	1.9494	6.8464	
	Fit	Quality	H		0	0	0	0
			P		0.4678	0.7098	0.1571	0.9994
			KSTAT		0.1177	0.0973	0.2152	0.1665
			CV		0.1884	0.1884	0.2591	0.6239
		Parameters	K		-0.1249	0.3677	0.0674	-0.0279
			k_95% LC		-0.1343	0.3339	-0.3048	-1.6251
			k_95% UC		-0.1155	0.4016	0.4396	1.5693
			Sigma		0.0864	0.1224	0.7085	1.8173
			Sigma_95% LC		0.0855	0.1189	0.5351	0.6093
			Sigma_95% UC		0.0872	0.1259	0.9382	5.4205
Mu			0.2116	0.6292	2.6987	8.8712		
Mu_95% LC		0.2104	0.6252	2.4492	6.4333			
Mu_95% UC		0.2128	0.6332	2.9481	11.3091			

### 11.8 Appendix H: Stop Bar Velocity Fit Information

Table 27 Summary of GEV fit and KS test for Cluster 1.

GEV Fit Information			
			Cluster 1
Fit	Quality	H	0
		p	0.2708
		KSTAT	0.0444
		CV	0.0604
	Parameters	k	-0.1392
		k_95% LC	-0.1506
		k_95% UC	-0.1279
		Sigma	0.9756
		Sigma_95% LC	0.9653
		Sigma_95% UC	0.986
		Mu	1.203
		Mu_95% LC	1.189
		Mu_95% UC	1.2171

Table 28 Summary of Normal Fits and KS test for Cluster 2 through Cluster 4.

Normal Fit Information					
			Cluster 2	Cluster 3	Cluster 4
Fit	Quality	H	0	0	0
		P	0.1894	0.796	0.9526
		KSTAT	0.05	0.089	0.2373
		CV	0.0626	0.1866	0.6239
	Parameters	Mu	3.8542	11.6836	20.7889
		Mu_95% LC	3.8168	11.0576	14.6622
		Mu_95% UC	3.8917	12.3096	26.9155
		Sigma	1.4254	2.2258	3.8503
		Sigma_95% LC	1.3994	1.8623	2.1811
		Sigma_95% UC	1.4523	2.7668	14.356

## 11.9 Appendix I: Brake Onset Fit Information

Table 29 Summary of normal fit and KS test for brake onset at stop-controlled intersections.

Normal Fit Information				
			Range	TTI
Fit	Quality	H	0	0
		p	0.7886	0.0761
		KSTAT	0.0295	0.0569
		CV	0.0614	0.0604
	Parameters	Mu	115.6876	6.4111
		Mu_95% LC	115.1761	6.3985
		Mu_95% UC	116.1991	6.4237
		Sigma	26.2639	0.9767
		Sigma_95% LC	25.9071	0.9679
		Sigma_95% UC	26.6306	0.9858

### 11.10 Appendix J: Warning Timing Model

Warning timing is an important consideration in the development of the threat assessment algorithm. The likelihood of a driver stopping in response to a CICAS-V warning decreases as the required deceleration to stop increases. Subtask 3.3 developed the DVI as part of the CICAS-V project. During the DVI development, several potential warning timings were investigated.

The probability of stopping is plotted below (Figure 92) for each of the warning timings tested during Subtask 3.3. A normal probability function was assumed, which allowed a sigmoid curve fit to the data. The following equation was used in the model:

**Equation 20**

Where:

$$a = -0.417$$

$$b = 0.025$$

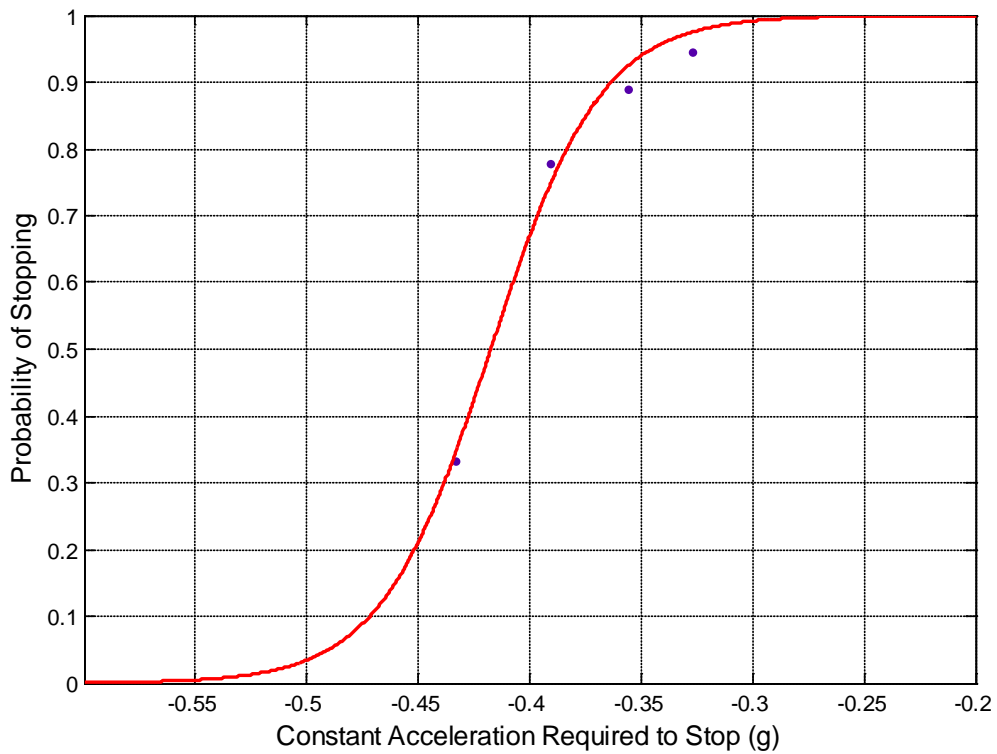


**Figure 92 Model of the probability of stopping by the stop bar based on the required constant deceleration at the warning onset.**

### 11.11 Appendix K: Regression of Minimum RDP as a Function of Minimum Stop Bar Velocity

To relate the minimum RDP to stop bar velocity a series of regression fits were performed. For the purpose of the analysis, a fourth- order polynomial fit was found to produce the best regression of stop bar velocity as a function of RDP. This regression resulted in the following:

$$\text{Velocity} = \text{RDP}^a + \text{RDP}^b + \text{RDP}^c + \text{RDP}^d + e$$

Coefficients:	Goodness of fit
a= -0.0012	sse = 25571
b= 0.0506	rsquare = 0.6403
c= -0.7336	dfe = 30437
d= 5.4488	adjrsquare = 0.6403
e= 0.5191	rmse = 0.9166

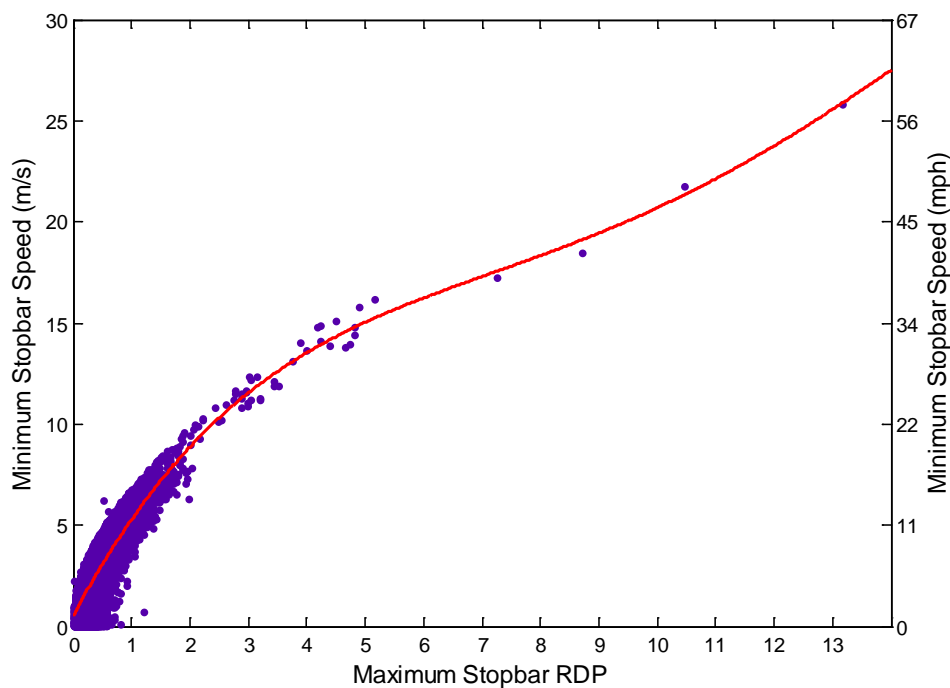


Figure 93 Regression line relating the maximum stop bar RDP to the minimum stop-bar speed.

### 11.12 Appendix L: Regression-Based Algorithm Fit Information

Table 30 Summary of fits used in the regression-based threat assessment algorithms for stop-controlled intersections.

	Percentile	a	b	c	SSE	Rsquare	dfe	adjRsquare	RSME
500 Algorithm Family TTI as a function of Range	0.0008	0.2251	0.6192	-0.1266	0.0476	0.9990	47	0.9989	0.0318
	0.0011	0.2164	0.6301	-0.0901	0.0476	0.9990	47	0.9989	0.0318
	0.0020	0.2020	0.6470	-0.0180	0.0476	0.9990	47	0.9989	0.0318
	0.0033	0.1906	0.6622	0.0279	0.0476	0.9990	47	0.9989	0.0318
	0.0050	0.1861	0.6700	0.0541	0.0476	0.9990	47	0.9989	0.0318
	0.0080	0.1776	0.6838	0.0936	0.0476	0.9990	47	0.9989	0.0318
	0.0130	0.1725	0.6943	0.1259	0.0476	0.9990	47	0.9989	0.0318
	0.0200	0.1666	0.7056	0.1591	0.0476	0.9990	47	0.9989	0.0318
	0.0300	0.1634	0.7141	0.1870	0.0476	0.9990	47	0.9989	0.0318
	0.0400	0.1581	0.7240	0.2179	0.0476	0.9990	47	0.9989	0.0318
	0.0600	0.1542	0.7337	0.2578	0.0604	0.9992	47	0.9991	0.0359
	0.0800	0.1508	0.7415	0.2938	0.0694	0.9991	47	0.9990	0.0384
	0.1000	0.1502	0.7450	0.3184	0.0710	0.9991	47	0.9990	0.0389
	0.1200	0.1495	0.7483	0.3410	0.0725	0.9991	47	0.9990	0.0393
0.1500	0.1458	0.7564	0.3807	0.0820	0.9990	47	0.9989	0.0418	
600 Algorithm Family Range as a Function of Velocity All Data (Percentile based)	0.0008	0.0656	2.1145	-0.0892	81.3590	0.9816	19	0.9796	2.0693
	0.0011	0.0660	2.1279	-0.1004	70.5930	0.9854	19	0.9839	1.9275
	0.0020	0.0715	2.1219	-0.1428	66.4230	0.9878	19	0.9865	1.8698
	0.0033	0.0715	2.1219	-0.1428	66.4230	0.9878	19	0.9865	1.8698
	0.0050	0.0845	2.1013	-0.2795	81.5690	0.9879	19	0.9866	2.0720
	0.0080	0.0822	2.1322	-0.2109	69.8650	0.9909	19	0.9899	1.9176
	0.0130	0.0775	2.1730	-0.0661	47.5540	0.9945	19	0.9940	1.5820
	0.0200	0.0851	2.1584	-0.0792	45.8210	0.9952	19	0.9947	1.5529
	0.0300	0.0973	2.1310	-0.1486	51.5450	0.9951	19	0.9946	1.6471
	0.0400	0.1054	2.1181	-0.1750	53.1400	0.9954	19	0.9949	1.6724
	0.0500	0.1127	2.1067	-0.1909	54.4930	0.9956	19	0.9951	1.6935
	0.0650	0.1256	2.0844	-0.2432	61.1170	0.9954	19	0.9949	1.7935



	0.0800	0.1372	2.0660	-0.2732	63.9880	0.9955	19	0.9950	1.8352
	0.1000	0.1484	2.0533	-0.2784	68.9140	0.9955	19	0.9950	1.9045
	0.1200	0.1603	2.0389	-0.3065	74.3750	0.9954	19	0.9950	1.9785
	0.1400	0.1702	2.0292	-0.3193	79.4170	0.9954	19	0.9949	2.0445
	0.1600	0.1745	2.0308	-0.2731	76.7420	0.9958	19	0.9954	2.0097
	0.1800	0.1820	2.0256	-0.2743	83.6960	0.9957	19	0.9952	2.0988
	0.2000	0.1883	2.0227	-0.2691	89.5390	0.9956	19	0.9951	2.1709
	0.2200	0.1898	2.0285	-0.2202	89.8380	0.9958	19	0.9954	2.1745

	Percentile	a	b	c	SSE	Rsquare	dfc	adjRsquare	RSME
<b>700 Algorithm Family</b> Range as a Function of Velocity part data (Percentile based)	0.0008	0.0030	3.2428	1.3828	8.4489	0.9906	13	0.9892	0.8062
	0.0011	0.0033	3.2295	1.3644	8.4727	0.9916	13	0.9903	0.8073
	0.0020	0.0046	3.1320	1.3380	8.1537	0.9928	13	0.9917	0.7920
	0.0033	0.0046	3.1320	1.3380	8.1537	0.9928	13	0.9917	0.7920
	0.0050	0.0072	2.9989	1.3411	6.3113	0.9953	13	0.9946	0.6968
	0.0080	0.0098	2.9073	1.3027	6.5355	0.9957	13	0.9950	0.7090
	0.0130	0.0128	2.8338	1.2859	6.3718	0.9962	13	0.9957	0.7001
	0.0200	0.0161	2.7668	1.2857	5.8580	0.9969	13	0.9964	0.6713
	0.0300	0.0190	2.7258	1.3202	4.8019	0.9977	13	0.9973	0.6078
	0.0400	0.0222	2.6848	1.3276	4.4091	0.9981	13	0.9978	0.5824
	0.0500	0.0248	2.6585	1.3491	3.9315	0.9984	13	0.9981	0.5499
	0.0650	0.0283	2.6254	1.3916	3.1954	0.9988	13	0.9986	0.4958
	0.0800	0.0318	2.5971	1.4254	2.7186	0.9991	13	0.9989	0.4573
	0.1000	0.0366	2.5602	1.4671	2.1952	0.9993	13	0.9992	0.4109
	0.1200	0.0394	2.5471	1.5313	1.6759	0.9995	13	0.9994	0.3591
	0.1400	0.0418	2.5377	1.5993	1.2379	0.9997	13	0.9996	0.3086
	0.1600	0.0448	2.5235	1.6493	0.9750	0.9997	13	0.9997	0.2739
	0.1800	0.0465	2.5189	1.7230	0.6848	0.9998	13	0.9998	0.2295
0.2000	0.0484	2.5141	1.7886	0.4933	0.9999	13	0.9999	0.1948	
0.2200	0.0499	2.5110	1.8492	0.3703	0.9999	13	0.9999	0.1688	
<b>800 Algorithm Family</b> RDP as a Function of Range (percentile based)	0.0300	0.9838	-0.4567	0.1396	0.0115	0.9752	47	0.9741	0.0157
	0.0350	0.9321	-0.4312	0.1265	0.0115	0.9752	47	0.9741	0.0157
	0.0400	0.8979	-0.4127	0.1158	0.0115	0.9752	47	0.9741	0.0157
	0.0450	0.8623	-0.3891	0.1020	0.0115	0.9752	47	0.9741	0.0157
	0.0500	0.8341	-0.3701	0.0904	0.0115	0.9752	47	0.9741	0.0157
	0.0550	0.8073	-0.3462	0.0749	0.0115	0.9752	47	0.9741	0.0157
	0.0600	0.7871	-0.3266	0.0609	0.0115	0.9752	47	0.9741	0.0157
	0.0650	0.7699	-0.3086	0.0472	0.0115	0.9752	47	0.9741	0.0157
	0.0700	0.7568	-0.2863	0.0278	0.0115	0.9752	47	0.9741	0.0157
	0.0800	0.7394	-0.2501	-0.0082	0.0115	0.9752	47	0.9741	0.0157
	0.0900	0.7416	-0.2124	-0.0577	0.0082	0.9650	47	0.9636	0.0132

	0.1000	0.7768	-0.1710	-0.1364	0.0076	0.9643	47	0.9628	0.0128
	0.1100	0.8744	-0.1270	-0.2741	0.0070	0.9644	47	0.9629	0.0122
	0.1200	1.0366	-0.0929	-0.4662	0.0068	0.9629	47	0.9613	0.0120
	0.1400	15.8370	-0.0043	-15.3260	0.0058	0.9630	47	0.9614	0.0111
	0.1600	-0.5642	0.0838	1.0272	0.0048	0.9643	47	0.9628	0.0101
	0.1900	-0.1217	0.2223	0.5282	0.0038	0.9662	47	0.9648	0.0089
	0.2200	-0.0407	0.3684	0.4044	0.0028	0.9701	47	0.9688	0.0077
	0.2500	-0.0158	0.5172	0.3465	0.0019	0.9755	47	0.9745	0.0064
	0.2800	-0.0068	0.6610	0.3126	0.0012	0.9813	47	0.9805	0.0051

**Table 31 Summary of fits used in the regression based threat assessment algorithms for signalized intersections.**

	Percentile	a	b	c	SSE	Rsquare	dfe	adjRsqure	RSME
<b>600 Algorithm Family Range as a Function of Velocity All Data (Percentile based)</b>	0.0010	0.0135	2.6045	-0.7519	21.4858	0.9807	15	0.9781	1.1968
	0.0015	0.0128	2.6610	-0.6339	8.7801	0.9936	15	0.9928	0.7651
	0.0030	0.0348	2.3566	-0.8976	13.1285	0.9926	15	0.9916	0.9355
	0.0050	0.0348	2.3566	-0.8976	13.1285	0.9926	15	0.9916	0.9355
	0.0080	0.0731	2.1640	-1.0494	10.4789	0.9959	15	0.9954	0.8358
	0.0120	0.0874	2.1275	-0.9884	8.0076	0.9973	15	0.9969	0.7306
	0.0180	0.1126	2.0618	-0.9787	7.9744	0.9976	15	0.9973	0.7291
	0.0260	0.1331	2.0267	-0.8966	7.6260	0.9980	15	0.9977	0.7130
	0.0320	0.1389	2.0280	-0.7803	6.6618	0.9984	15	0.9982	0.6664
	0.0420	0.1524	2.0146	-0.6565	6.1405	0.9987	15	0.9985	0.6398
	0.0550	0.1627	2.0121	-0.4910	5.9754	0.9989	15	0.9987	0.6312
	0.0650	0.1638	2.0232	-0.3317	5.0018	0.9991	15	0.9990	0.5775
	0.0800	0.1705	2.0270	-0.1836	5.3685	0.9991	15	0.9990	0.5982
	0.1000	0.1762	2.0352	0.0084	4.7173	0.9993	15	0.9992	0.5608
	0.1200	0.1843	2.0363	0.1427	5.7552	0.9993	15	0.9992	0.6194
	0.1400	0.1833	2.0538	0.3417	5.9246	0.9993	15	0.9992	0.6285
	0.1600	0.1796	2.0755	0.5495	5.2842	0.9994	15	0.9994	0.5935
	0.1800	0.1816	2.0843	0.6932	5.5546	0.9994	15	0.9994	0.6085
0.2000	0.1902	2.0782	0.7862	6.3641	0.9994	15	0.9993	0.6514	
0.2200	0.1981	2.0741	0.8736	7.3731	0.9993	15	0.9993	0.7011	

	Percentile	a	b	c	SSE	Rsquare	dfe	adjRsqure	RSME
<b>800 Algorithm Family</b> <b>RDP as a Function of Range (percentile based)</b>	0.9990	7.5594	-0.8512	0.1230	0.0809	0.9967	72	0.9966	0.0335
	0.9987	5.9481	-0.8108	0.1297	0.0809	0.9967	72	0.9966	0.0335
	0.9980	4.3884	-0.7315	0.1140	0.0809	0.9967	72	0.9966	0.0335
	0.9972	3.8260	-0.7214	0.1227	0.0809	0.9967	72	0.9966	0.0335
	0.9950	3.4279	-0.7203	0.1302	0.0809	0.9967	72	0.9966	0.0335
	0.9935	3.1797	-0.7513	0.1459	0.0809	0.9967	72	0.9966	0.0335
	0.9900	2.9639	-0.7812	0.1568	0.0809	0.9967	72	0.9966	0.0335
	0.9840	2.5404	-0.7705	0.1542	0.0809	0.9967	72	0.9966	0.0335
	0.9780	2.2555	-0.7603	0.1515	0.0809	0.9967	72	0.9966	0.0335
	0.9700	1.9829	-0.7492	0.1487	0.0809	0.9967	72	0.9966	0.0335
	0.9600	1.7431	-0.7341	0.1446	0.0691	0.9587	72	0.9576	0.0310
	0.9480	1.5267	-0.7161	0.1400	0.0627	0.9530	72	0.9517	0.0295
	0.9300	1.2379	-0.6595	0.1279	0.0539	0.9447	72	0.9431	0.0274
	0.9100	1.0167	-0.6034	0.1160	0.0474	0.9349	72	0.9331	0.0256
	0.8800	0.7719	-0.4915	0.0888	0.0383	0.9228	72	0.9207	0.0231
	0.8500	0.6217	-0.3598	0.0423	0.0310	0.9133	72	0.9109	0.0208
	0.8100	0.5911	-0.1928	-0.0914	0.0242	0.9045	72	0.9018	0.0183
	0.7000	-0.0208	0.4266	0.2832	0.0105	0.9110	72	0.9085	0.0121
0.7800	1.2556	-0.0512	-0.8456	0.0196	0.9022	72	0.8994	0.0165	
0.7500	-0.2723	0.1186	0.6115	0.0158	0.9027	72	0.9000	0.0148	

### 11.13 Appendix M: Beta Permutation Values for Tested Algorithms

**Table 32 Beta permutation values for 100 series algorithms used at stop-controlled and signalized intersections.**

Beta Permutation	Static TTI
1	1
2	1.25
3	1.5
4	1.75
5	2
6	2.25
7	2.5
8	2.75
9	3
10	3.25
11	3.5
12	3.75
13	4
14	4.25
15	4.5
16	4.75
17	5

**Table 33 Beta permutation values for 200 series algorithms used at stop-controlled and signalized intersections.**

Beta Permutation	Static RDP
1	0.025
2	0.05
3	0.075
4	0.1
5	0.125
6	0.15
7	0.175
8	0.2
9	0.225
10	0.25
11	0.275
12	0.3
13	0.325
14	0.35
15	0.375
16	0.4
17	0.425
18	0.45
19	0.475
20	0.5
21	0.525
22	0.55
23	0.575

24	0.6
----	-----

**Table 34 Beta permutations values for 300 and 400 series algorithms used at stop-controlled and signalized intersections. Algorithms were based on static RDP as a function of reaction time. 300 series algorithms assumed a PRT of 1.01, and 400 series algorithms assumed a PRT of 0.78.**

Beta Permutation	Static RDP
1	0.2
2	0.225
3	0.25
4	0.275
5	0.3
6	0.325
7	0.35
8	0.375
9	0.4
10	0.425
11	0.45
12	0.475
13	0.5
14	0.525
15	0.55
16	0.575
17	0.6
18	0.625
19	0.65
20	0.675
21	0.7

Beta Permutation	Static RDP
22	0.725
23	0.75
24	0.775
25	0.8
26	0.825
27	0.85
28	0.875
29	0.9
30	0.925
31	0.95
32	0.975
33	1
34	1.025
35	1.05
36	1.075
37	1.1
38	1.125
39	1.15
40	1.175
41	1.2



**Table 35 Beta permutation values for 500 series algorithms used at stop-controlled intersections. The algorithm compared the vehicle's TTI to a warning TTI, calculated using a regression of velocity.**

Beta Permutation	Constant A	Constant B	Constant C
1	0.225	0.619	-0.127
2	0.216	0.630	-0.090
3	0.202	0.647	-0.018
4	0.191	0.662	0.028
5	0.186	0.670	0.054
6	0.178	0.684	0.094
7	0.172	0.694	0.126
8	0.167	0.706	0.159
9	0.163	0.714	0.187
10	0.158	0.724	0.218
11	0.154	0.734	0.258
12	0.151	0.742	0.294
13	0.150	0.745	0.318
14	0.150	0.748	0.341
15	0.146	0.756	0.381

**Table 36 Beta permutation values for 600 series algorithms used at stop-controlled intersections. The algorithm uses the vehicle's velocity to predict the minimum**

**range a warning must be presented to induce a successful stop.**

Beta Permutation	Constant A	Constant B	Constant C
1	0.066	2.115	-0.089
2	0.066	2.128	-0.100
3	0.072	2.122	-0.143
4	0.072	2.122	-0.143
5	0.085	2.101	-0.280
6	0.082	2.132	-0.211
7	0.077	2.173	-0.066
8	0.085	2.158	-0.079
9	0.097	2.131	-0.149
10	0.105	2.118	-0.175
11	0.113	2.107	-0.191
12	0.126	2.084	-0.243
13	0.137	2.066	-0.273
14	0.148	2.053	-0.278
15	0.160	2.039	-0.306
16	0.170	2.029	-0.319
17	0.175	2.031	-0.273
18	0.182	2.026	-0.274
19	0.188	2.023	-0.269
20	0.190	2.029	-0.220



**Table 37 Beta permutation values for 700 series algorithms used at stop-controlled intersections. The algorithm used the same measures as the 600 series, but the data sample was truncated by removing velocities greater than 18 m/s (40 mph).**

Beta Permutation	Constant A	Constant B	Constant C
1	0.003	3.243	1.383
2	0.003	3.230	1.364
3	0.005	3.132	1.338
4	0.005	3.132	1.338
5	0.007	2.999	1.341
6	0.010	2.907	1.303
7	0.013	2.834	1.286
8	0.016	2.767	1.286
9	0.019	2.726	1.320
10	0.022	2.685	1.328
11	0.025	2.659	1.349
12	0.028	2.625	1.392
13	0.032	2.597	1.425
14	0.037	2.560	1.467
15	0.039	2.547	1.531
16	0.042	2.538	1.599
17	0.045	2.524	1.649
18	0.047	2.519	1.723
19	0.048	2.514	1.789
20	0.050	2.511	1.849

**Table 38 Beta permutation values for 800 series algorithms used at stop-controlled intersections. The algorithm used the same strategy as the 500 series, however this regression equation used range to predict warning RDP.**

Beta Permutation	Constant A	Constant B	Constant C
1	0.984	-0.457	0.140
2	0.932	-0.431	0.127
3	0.898	-0.413	0.116
4	0.862	-0.389	0.102
5	0.834	-0.370	0.090
6	0.807	-0.346	0.075
7	0.787	-0.327	0.061
8	0.770	-0.309	0.047
9	0.757	-0.286	0.028
10	0.739	-0.250	-0.008
11	0.742	-0.212	-0.058
12	0.777	-0.171	-0.136
13	0.874	-0.127	-0.274
14	1.037	-0.093	-0.466
15	15.837	-0.004	-15.326
16	-0.564	0.084	1.027
17	-0.122	0.222	0.528
18	-0.041	0.368	0.404
19	-0.016	0.517	0.346
20	-0.007	0.661	0.313

**Table 39 Beta permutation values for 600 series algorithms used at signalized intersections. The algorithm uses the vehicle's velocity to predict the minimum range a warning must be presented to induce a successful stop.**

Beta Permutation	Constant A	Constant B	Constant C
1	0.014	2.605	-0.752
2	0.013	2.661	-0.634
3	0.035	2.357	-0.898
4	0.035	2.357	-0.898
5	0.073	2.164	-1.049
6	0.087	2.128	-0.988
7	0.113	2.062	-0.979
8	0.133	2.027	-0.897
9	0.139	2.028	-0.780
10	0.152	2.015	-0.657
11	0.163	2.012	-0.491
12	0.164	2.023	-0.332
13	0.171	2.027	-0.184
14	0.176	2.035	0.008
15	0.184	2.036	0.143
16	0.183	2.054	0.342
17	0.180	2.076	0.550
18	0.182	2.084	0.693
19	0.190	2.078	0.786
20	0.198	2.074	0.874

### 11.14 Appendix N: ROC Curves for Stop-Controlled Algorithms

ROC Curves for Stop-Controlled Intersections Using the 5-mph Violation Threshold

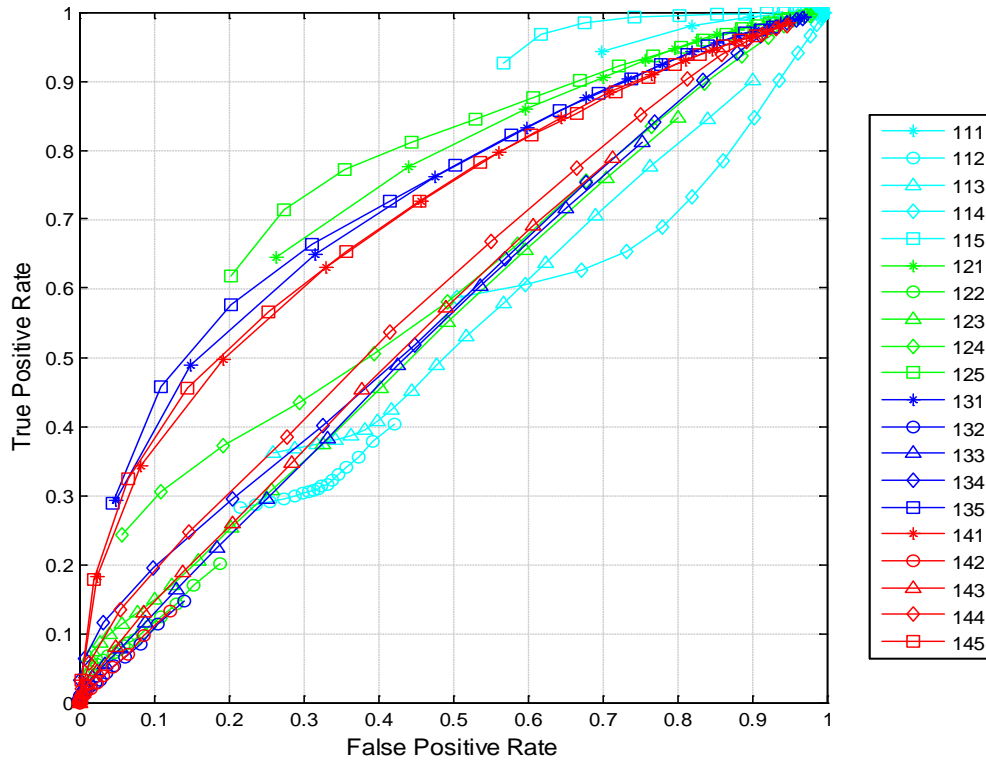


Figure 94 ROC curve for the 100 series algorithm family using a violation threshold of 5 mph.

ROC Curves for Stop-Controlled Intersections Using the 5-mph Violation Threshold

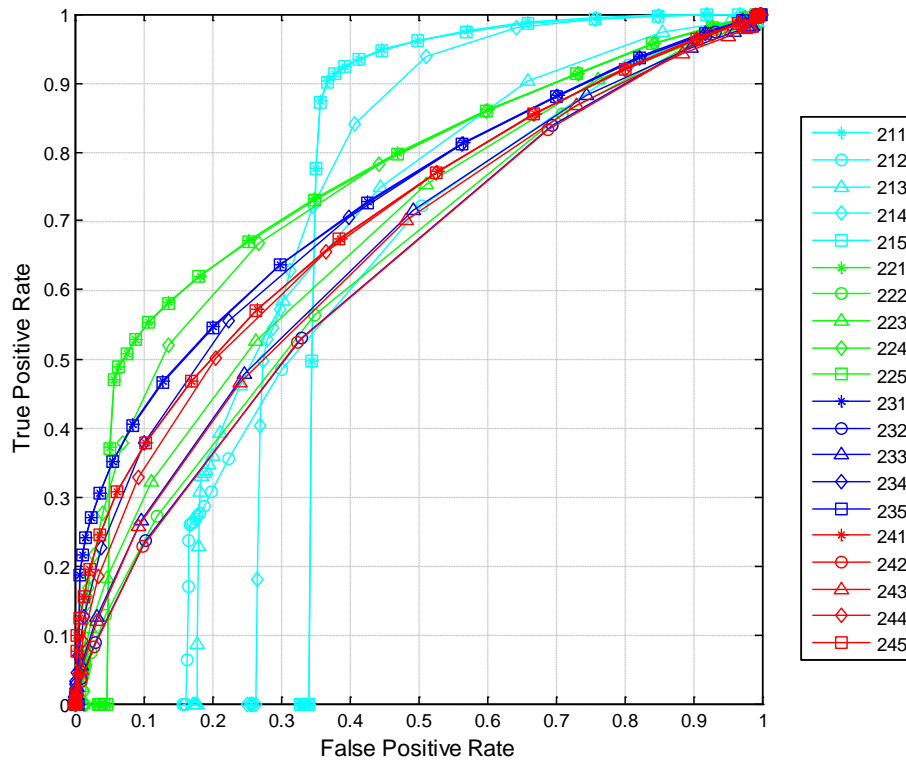


Figure 95 ROC curve for the 200 series algorithm family using a violation threshold of 5 mph.

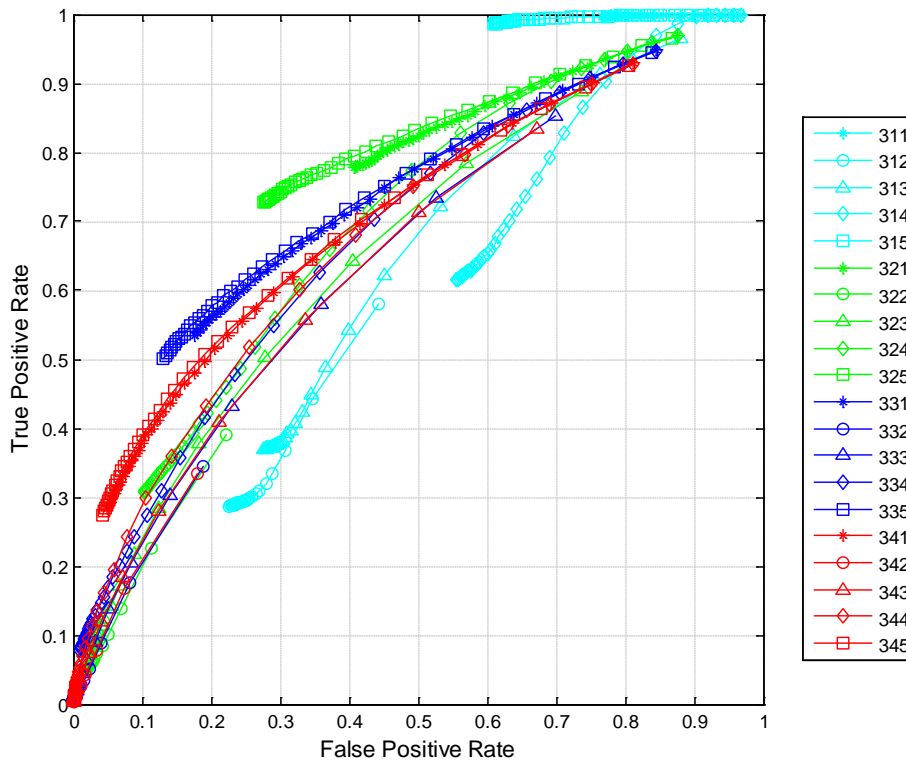


Figure 96 ROC curve for the 300 series algorithm family using a violation threshold of 5 mph.

ROC Curves for Stop-Controlled Intersections Using the 5-mph Violation Threshold

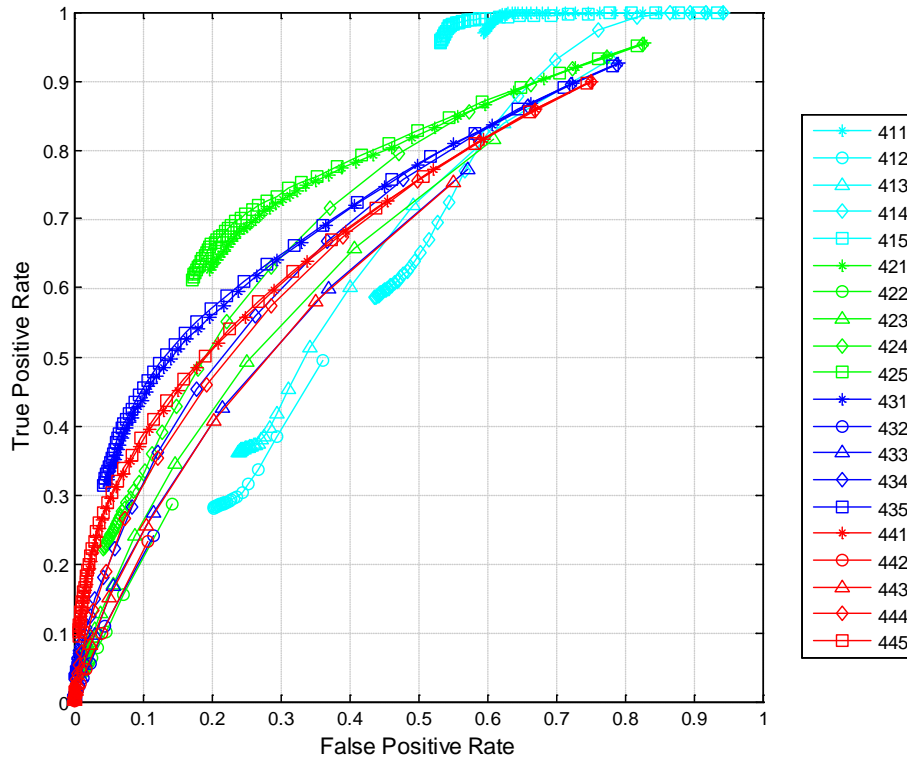


Figure 97 ROC curve for the 400 series algorithm family using a violation threshold of 5 mph.

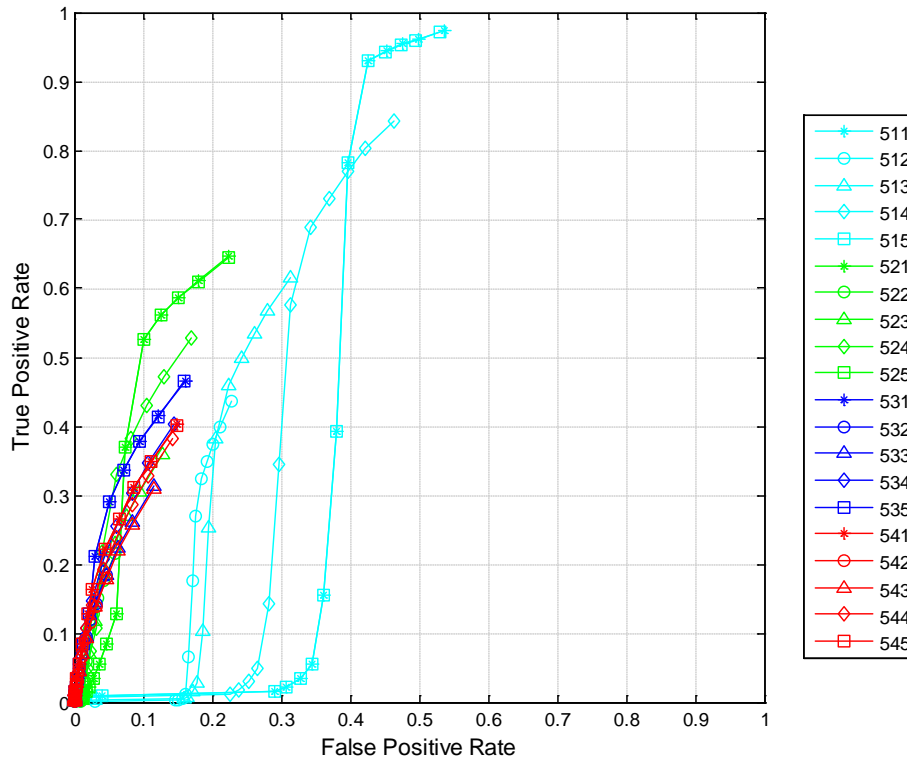


Figure 98 ROC curve for the 500 series algorithm family using a violation threshold of 5 mph.

ROC Curves for Stop-Controlled Intersections Using the 5-mph Violation Threshold

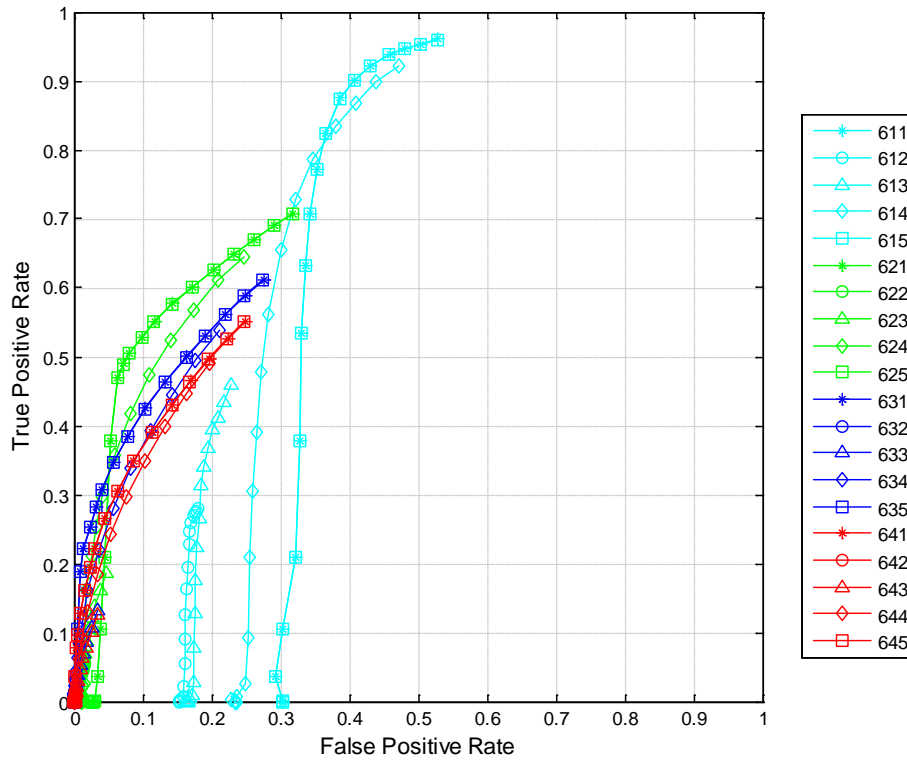


Figure 99 ROC curve for the 600 series algorithm family using a violation threshold of 5 mph.

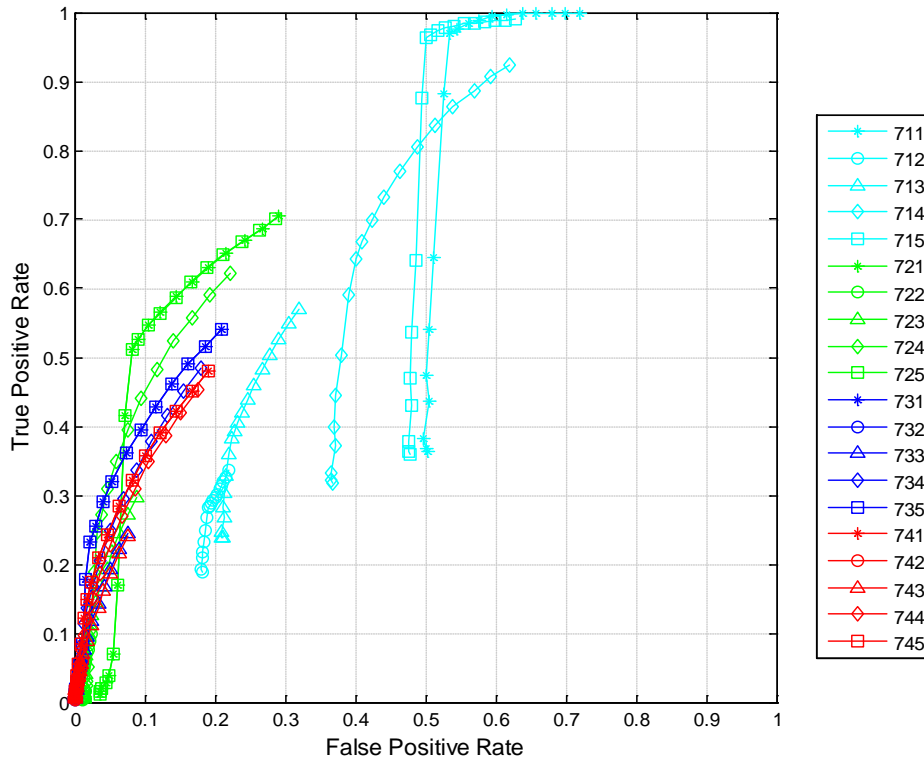


Figure 100 ROC curve for the 700 series algorithm family using a violation threshold of 5 mph.



ROC Curves for Stop-Controlled Intersections Using the 5-mph Violation Threshold

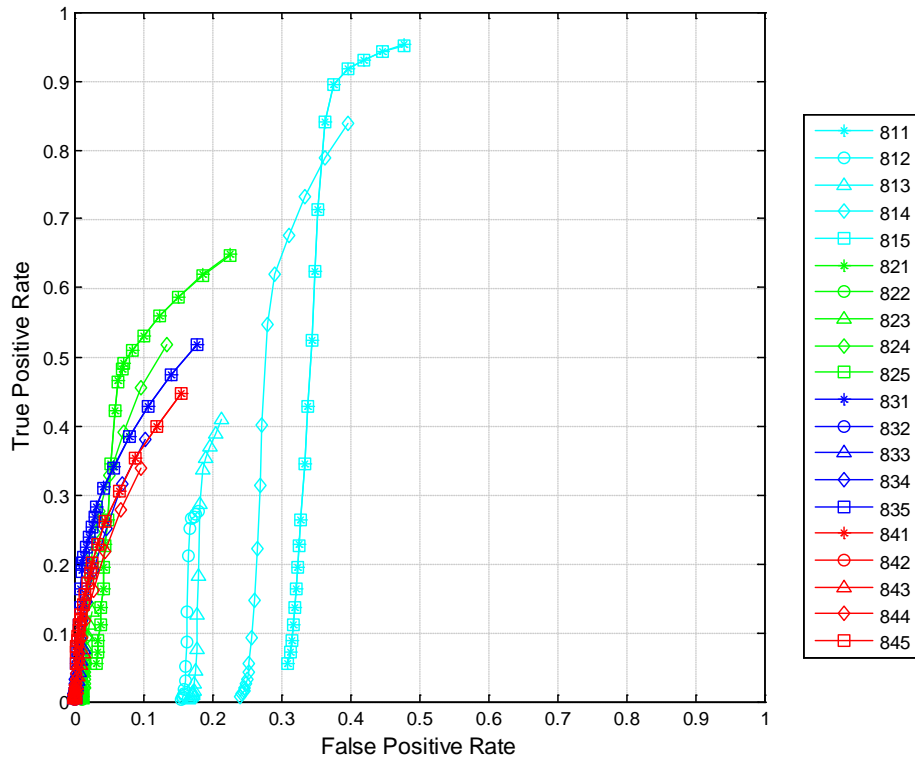


Figure 101 ROC curve for the 800 series algorithm family using a violation threshold of 5 mph.

ROC Curves for Stop-Controlled Intersections Using the 10-mph Violation Threshold

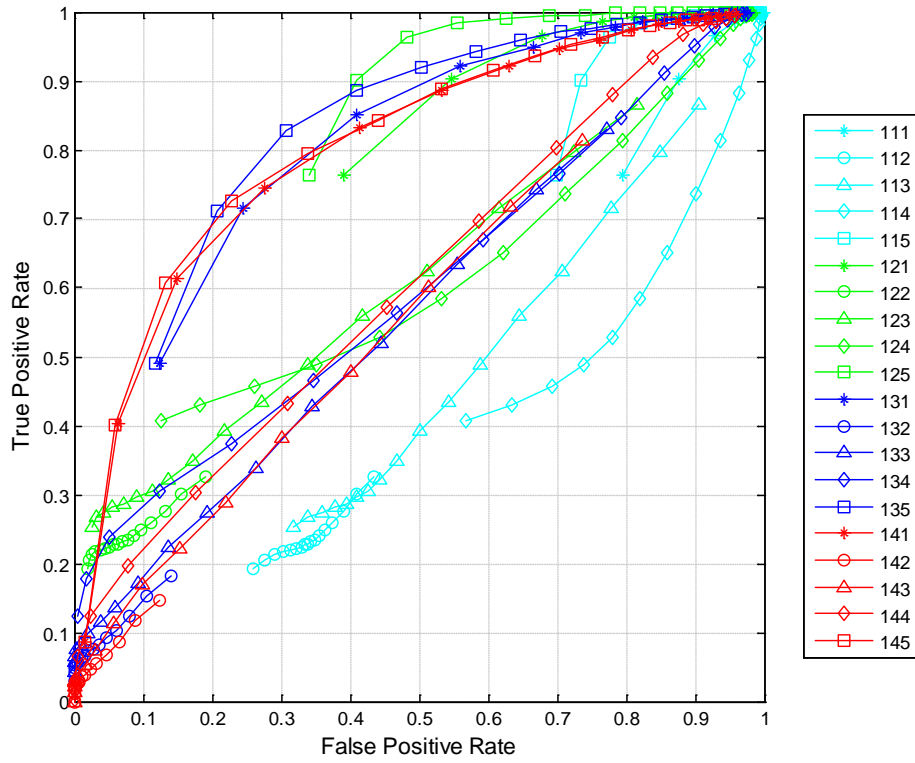


Figure 102 ROC curve for the 100 series algorithm family using a violation threshold of 10 mph.

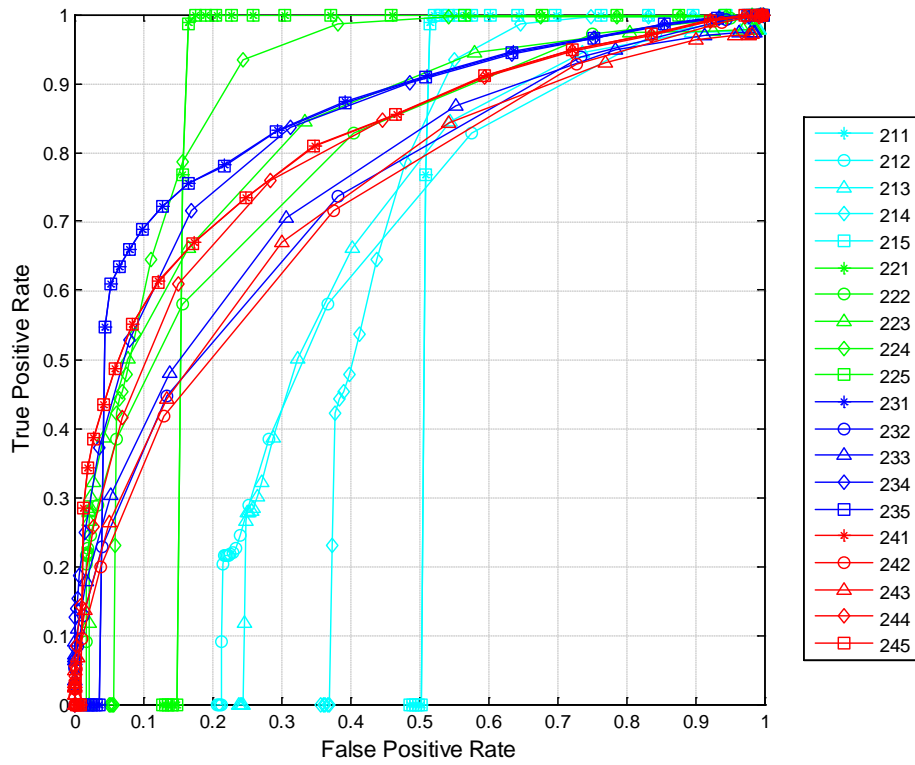


Figure 103 ROC curve for the 200 series algorithm family using a violation threshold of 10 mph.

ROC Curves for Stop-Controlled Intersections Using the 10-mph Violation Threshold

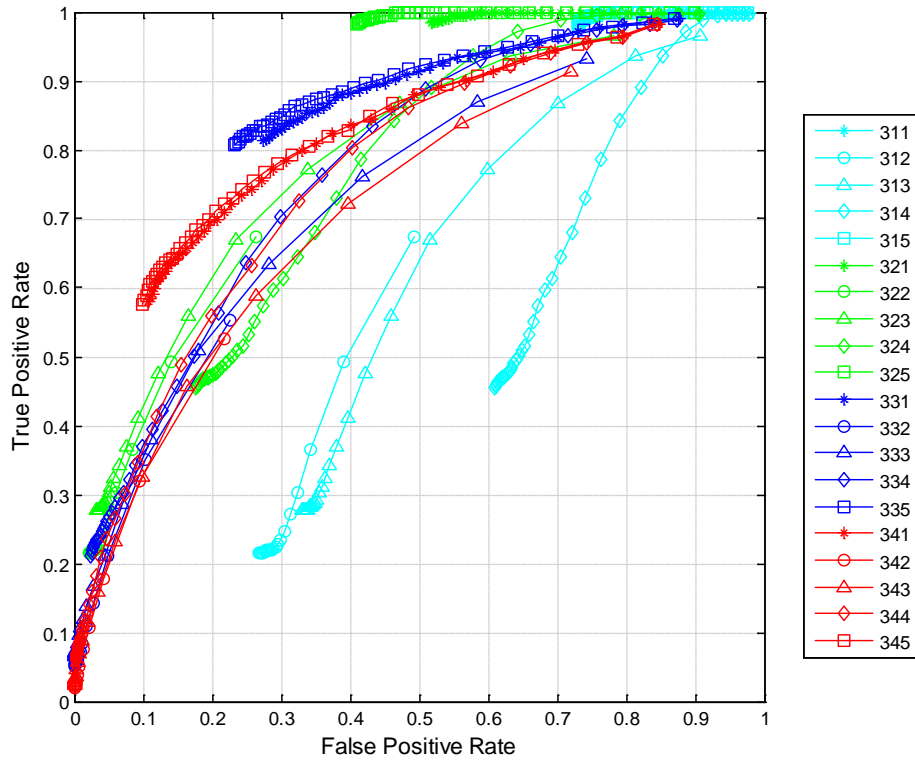


Figure 104 ROC curve for the 300 series algorithm family using a violation threshold of 10 mph.

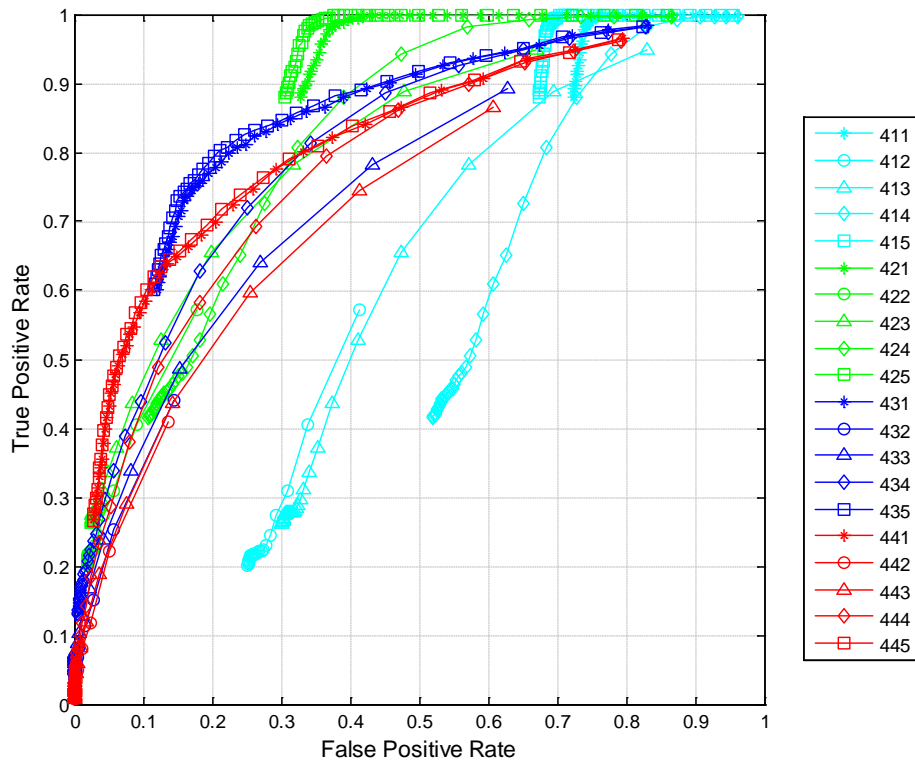


Figure 105 ROC curve for the 400 series algorithm family using a violation threshold of 10 mph.

ROC Curves for Stop-Controlled Intersections Using the 10-mph Violation Threshold

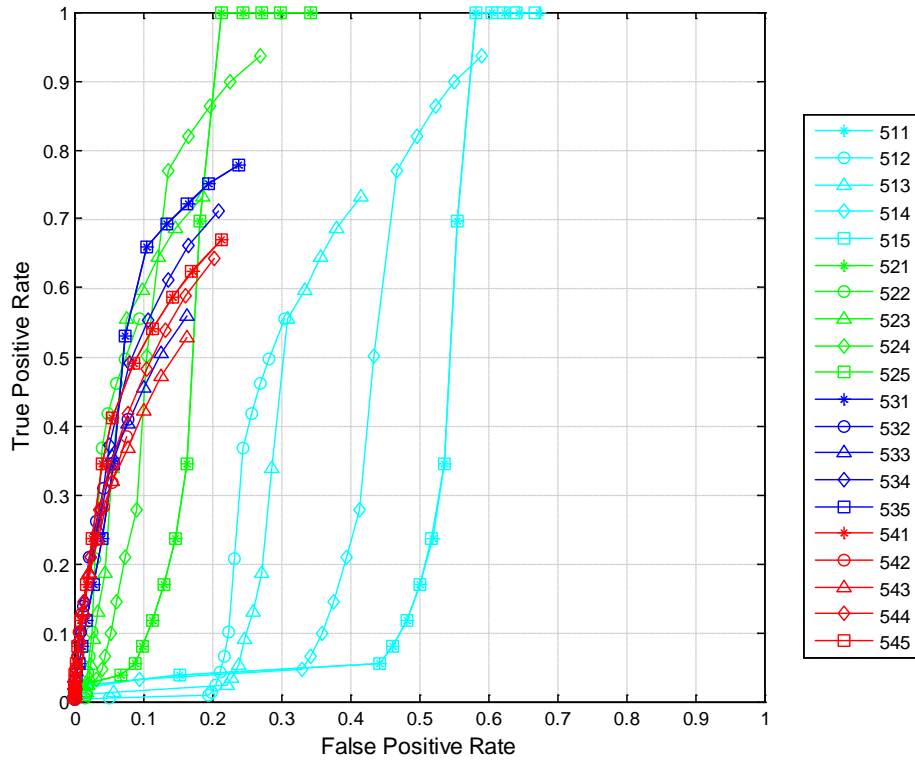


Figure 106 ROC curve for the 500 series algorithm family using a violation threshold of 10 mph.

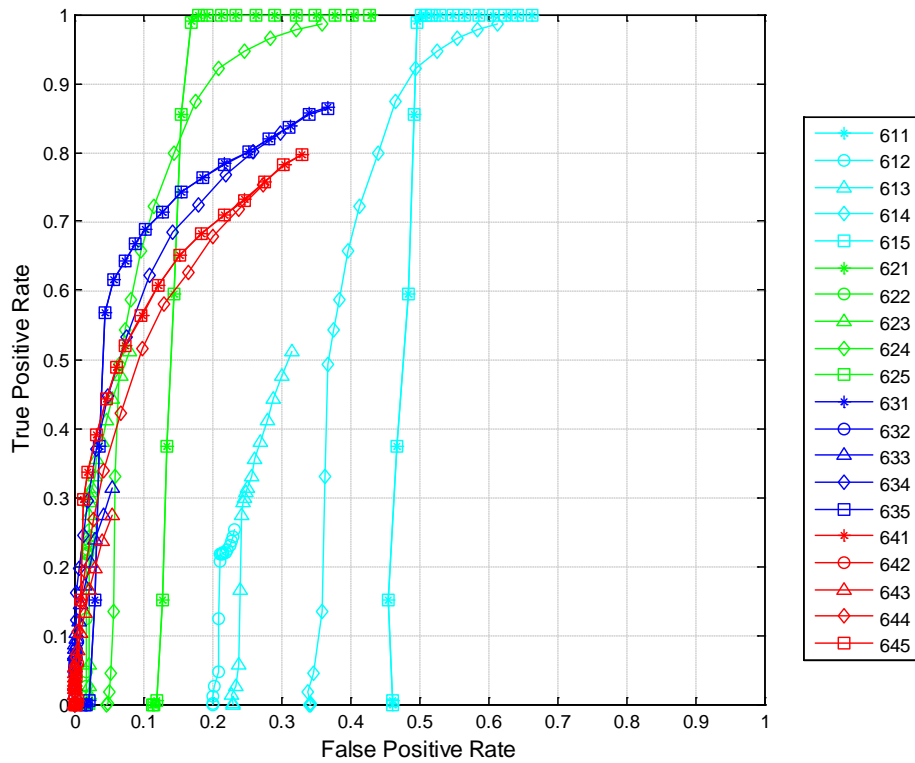


Figure 107 ROC curve for the 600 series algorithm family using a violation threshold of 10 mph.

ROC Curves for Stop-Controlled Intersections Using the 10-mph Violation Threshold

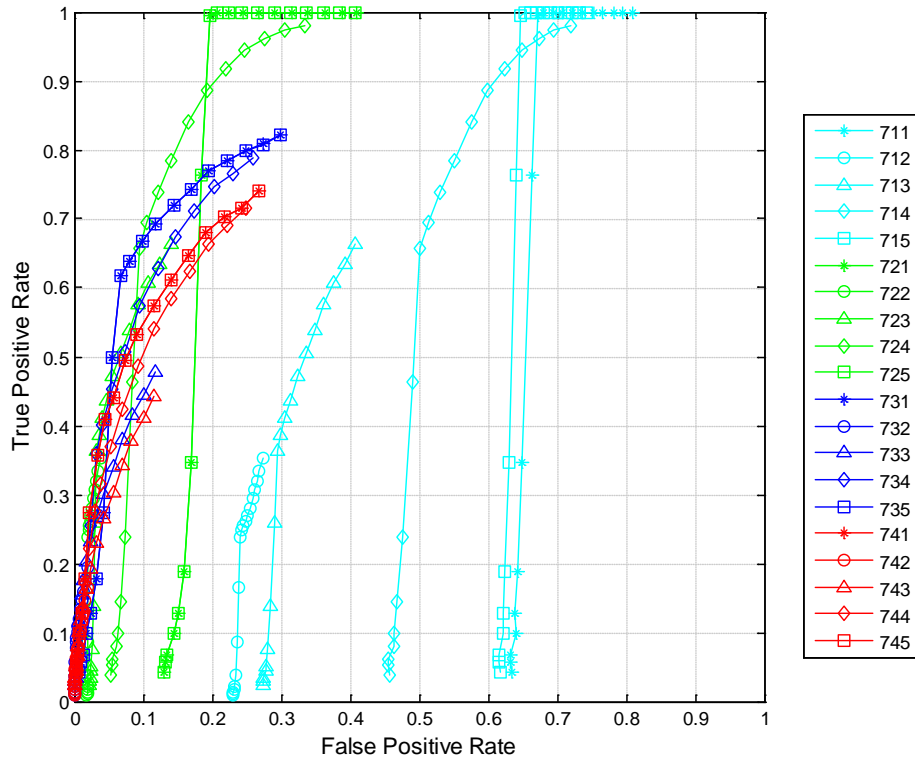


Figure 108 ROC curve for the 700 series algorithm family using a violation threshold of 10 mph.

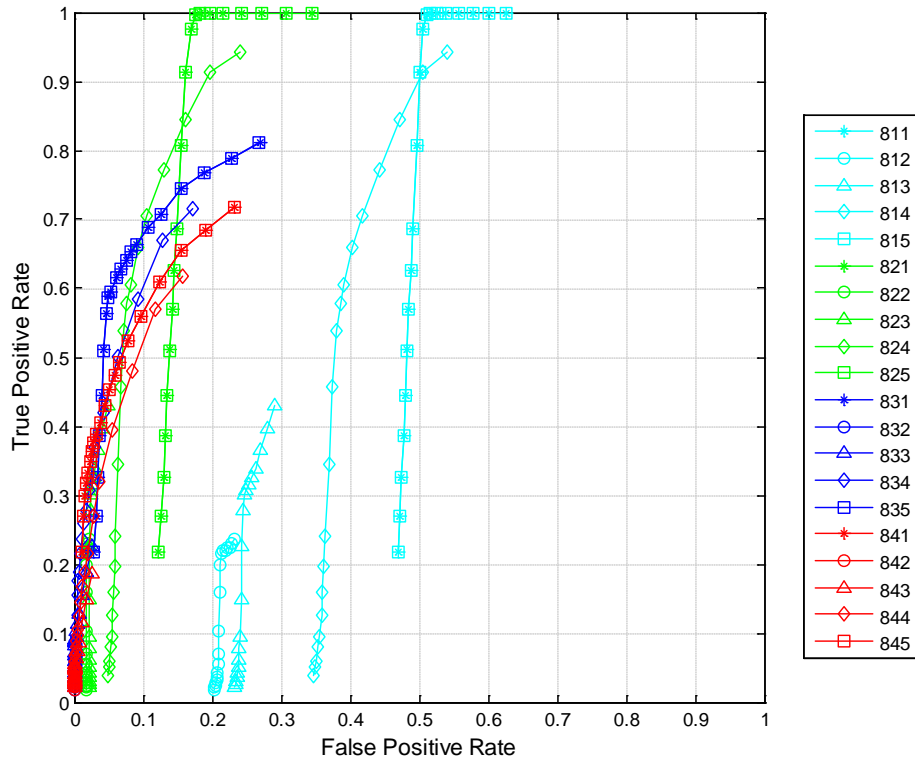


Figure 109 ROC curve for the 800 series algorithm family using a violation threshold of 10 mph.

ROC Curves for Stop-Controlled Intersections Using the 15-mph Violation Threshold

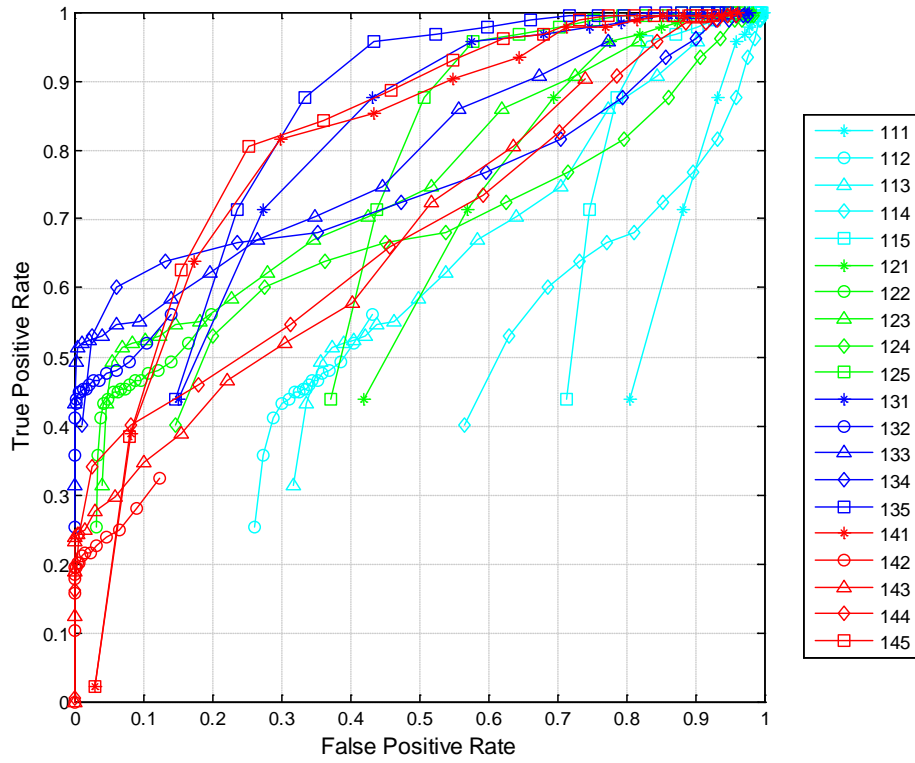


Figure 110 ROC curve for the 100 series algorithm family using a violation threshold of 15 mph.

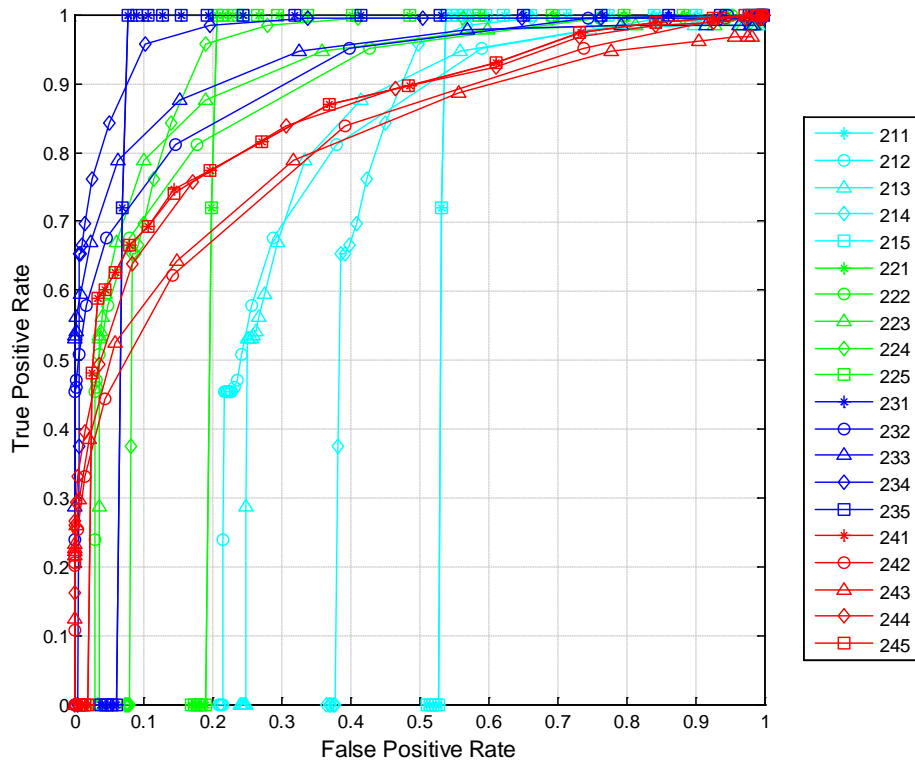


Figure 111 ROC curve for the 200 series algorithm family using a violation threshold of 15 mph.

ROC Curves for Stop-Controlled Intersections Using the 15-mph Violation Threshold

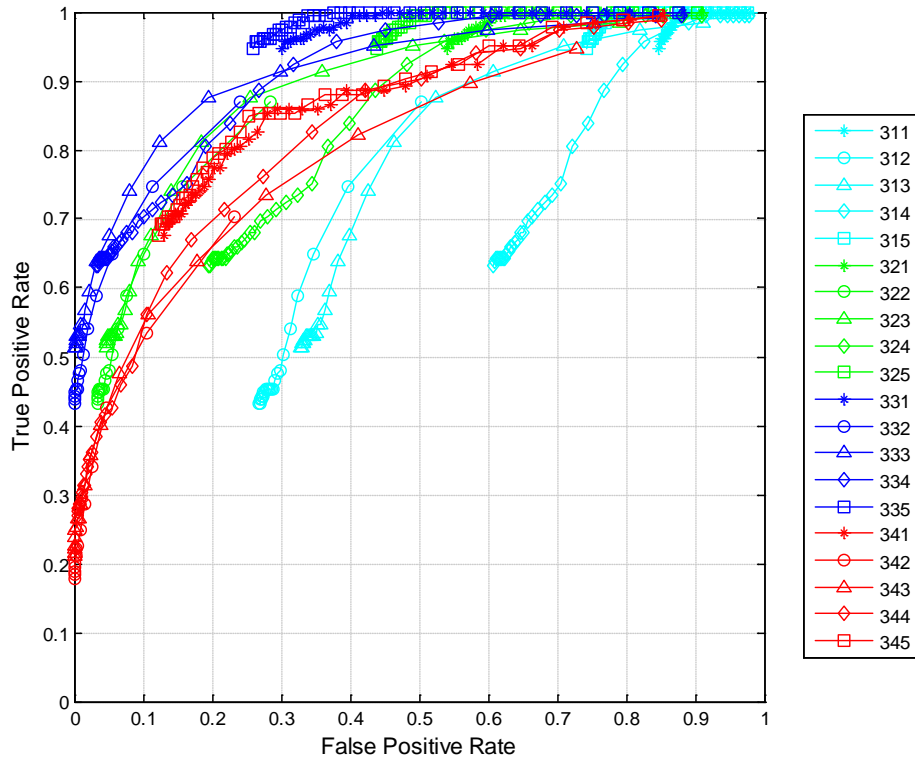


Figure 112 ROC curve for the 300 series algorithm family using a violation threshold of 15 mph.

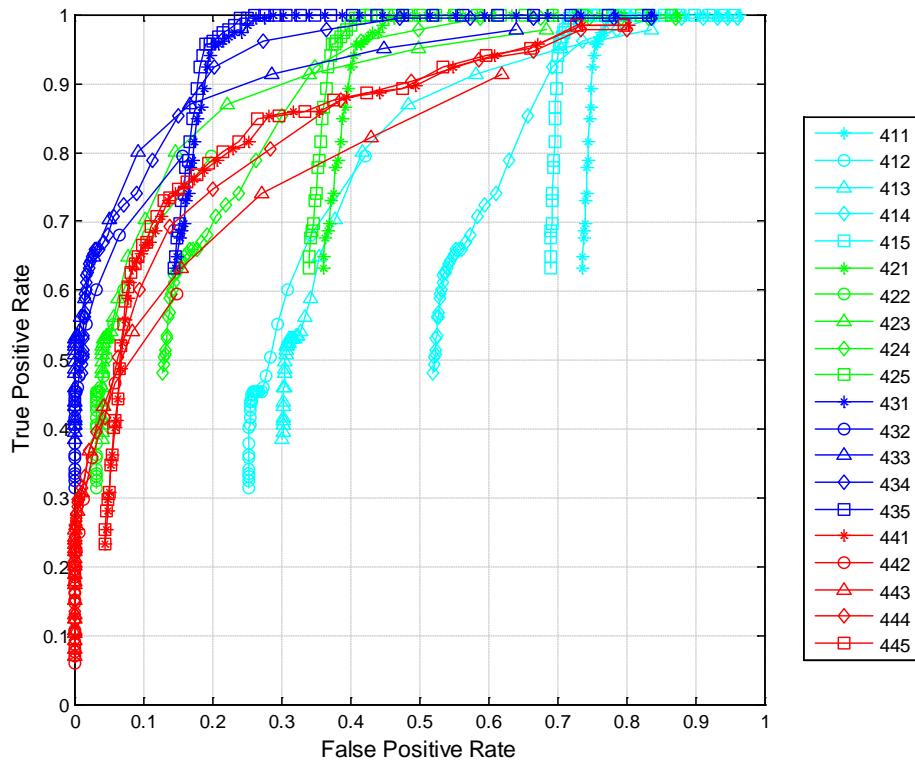


Figure 113 ROC curve for the 400 series algorithm family using a violation threshold of 15 mph.

ROC Curves for Stop-Controlled Intersections Using the 15-mph Violation Threshold

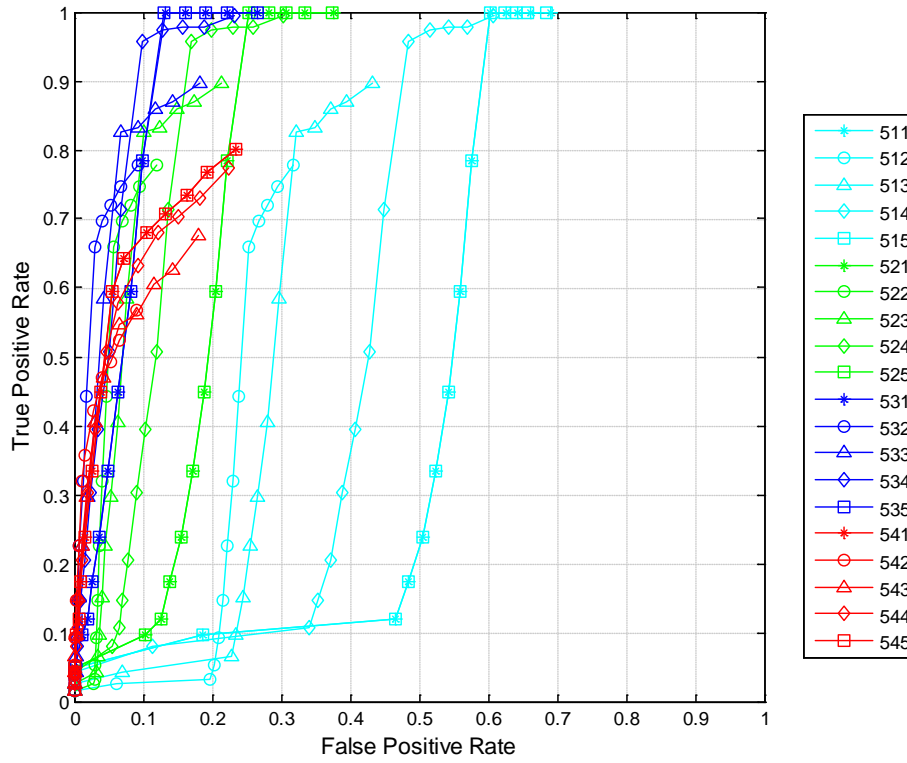


Figure 114 ROC curve for the 500 series algorithm family using a violation threshold of 15 mph.

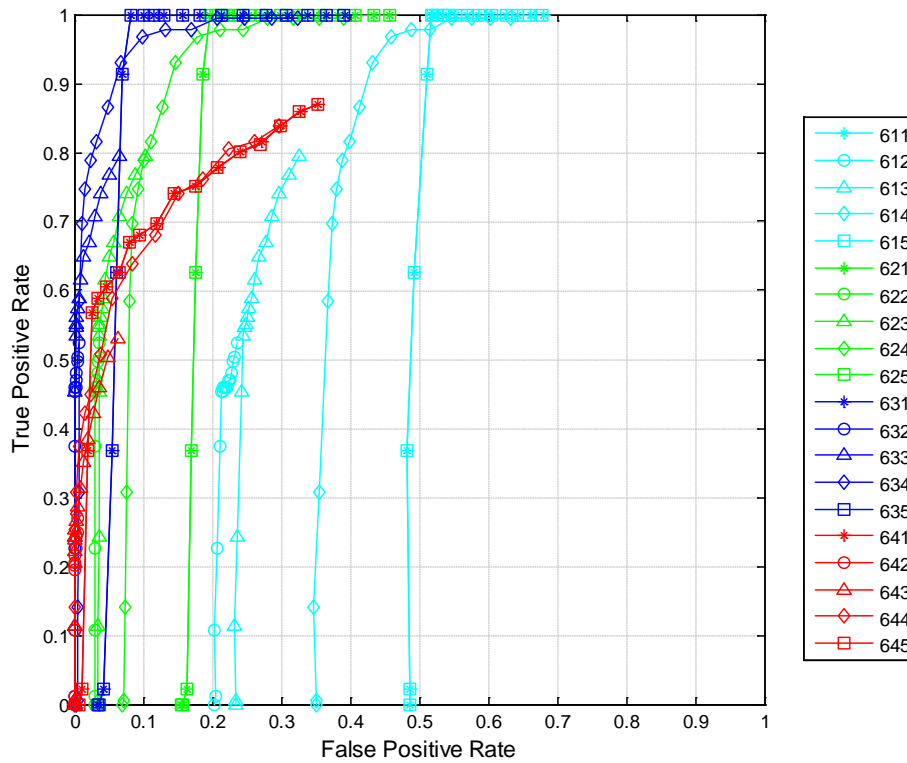


Figure 115 ROC curve for the 600 series algorithm family using a violation threshold of 15 mph.



ROC Curves for Stop-Controlled Intersections Using the 15-mph Violation Threshold

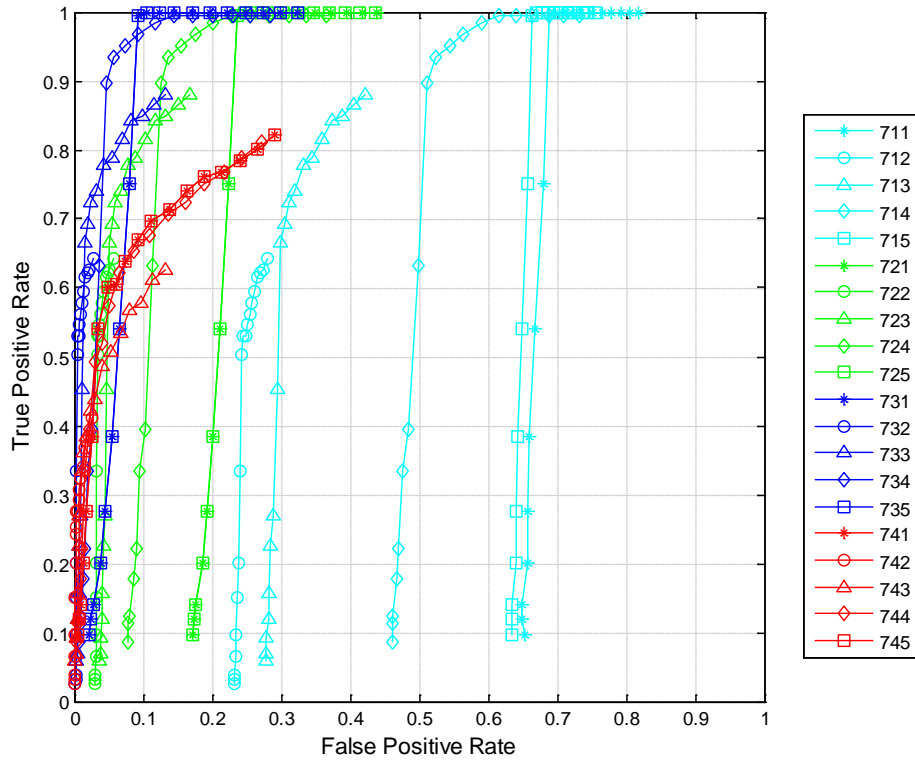


Figure 116 ROC curve for the 700 series algorithm family using a violation threshold of 15 mph.

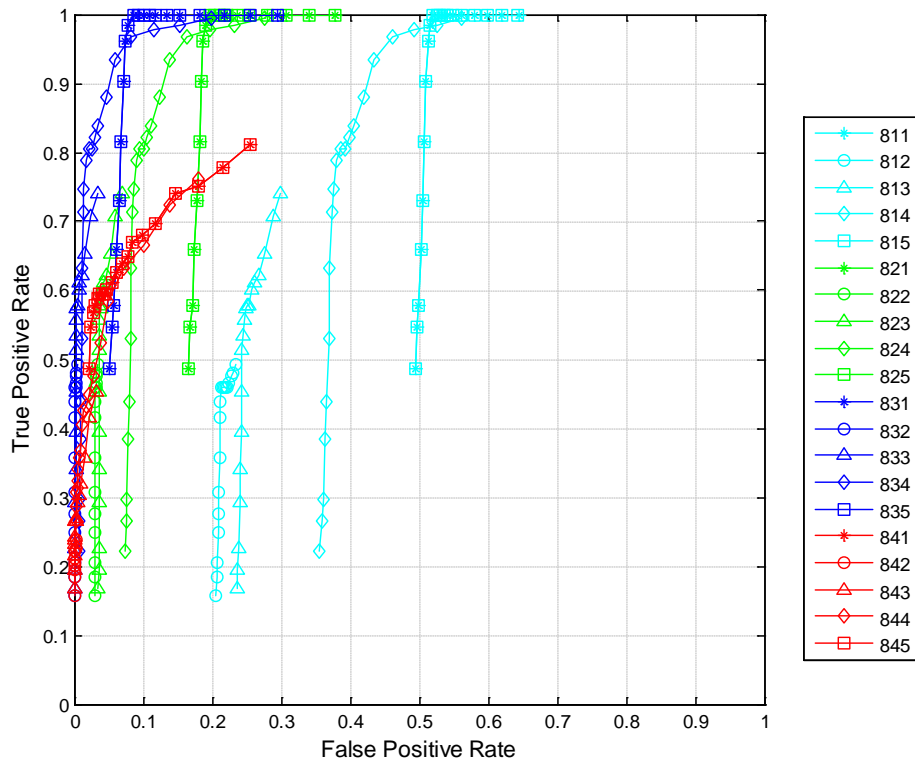


Figure 117 ROC curve for the 800 series algorithm family using a violation threshold of 15 mph.

ROC Curves for Stop-Controlled Intersections Using the 20-mph Violation Threshold

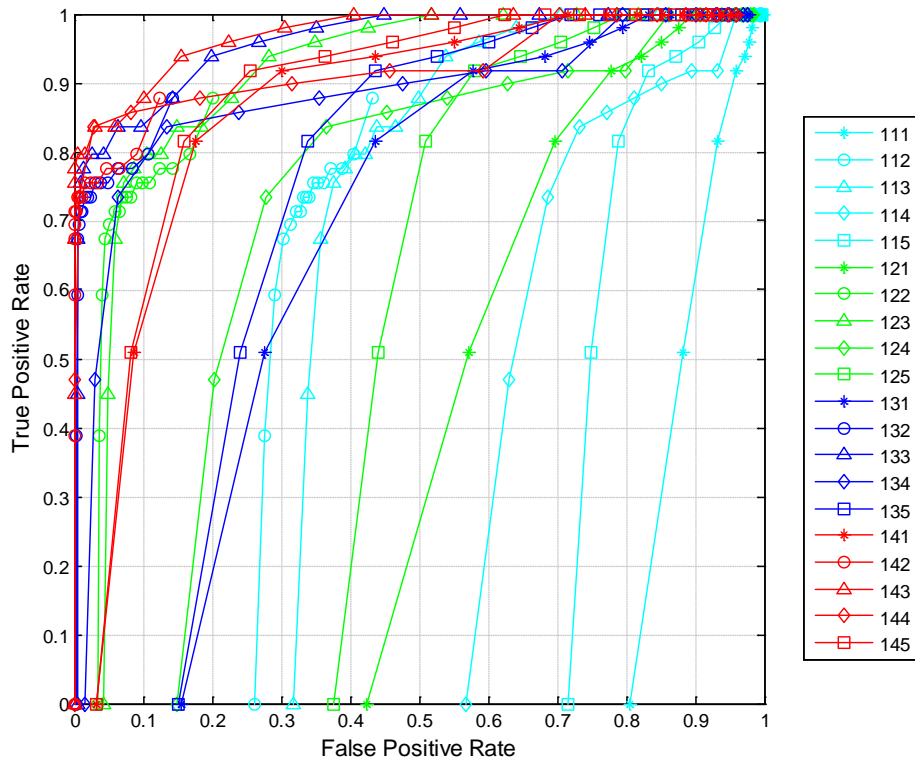


Figure 118 ROC curve for the 100 series algorithm family using a violation threshold of 20 mph.

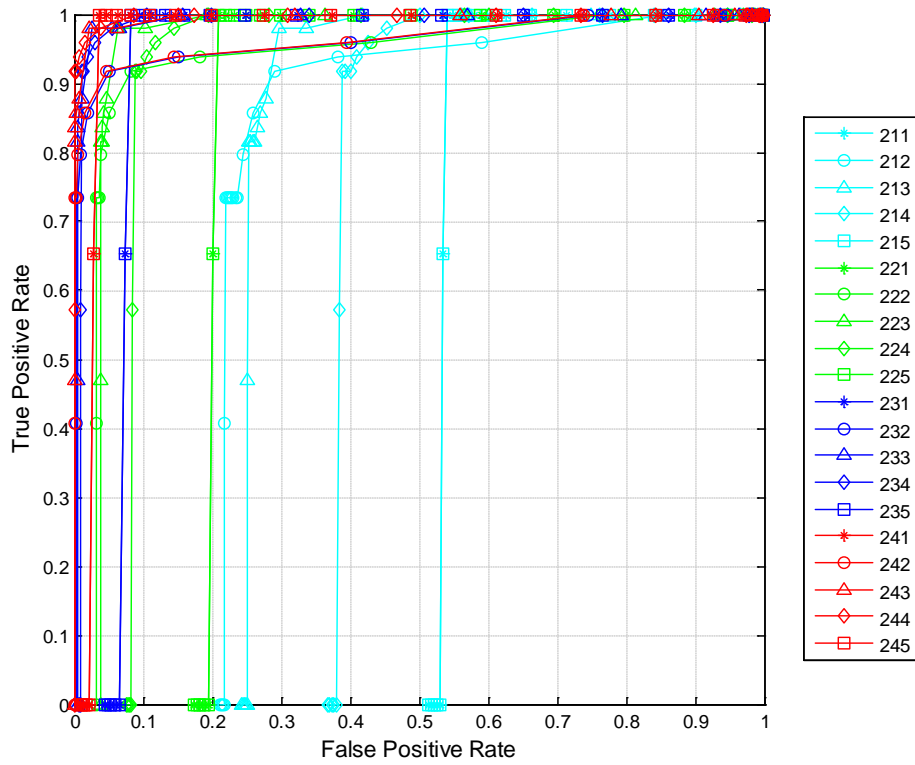


Figure 119 ROC curve for the 200 series algorithm family using a violation threshold of 20 mph.

ROC Curves for Stop-Controlled Intersections Using the 20-mph Violation Threshold

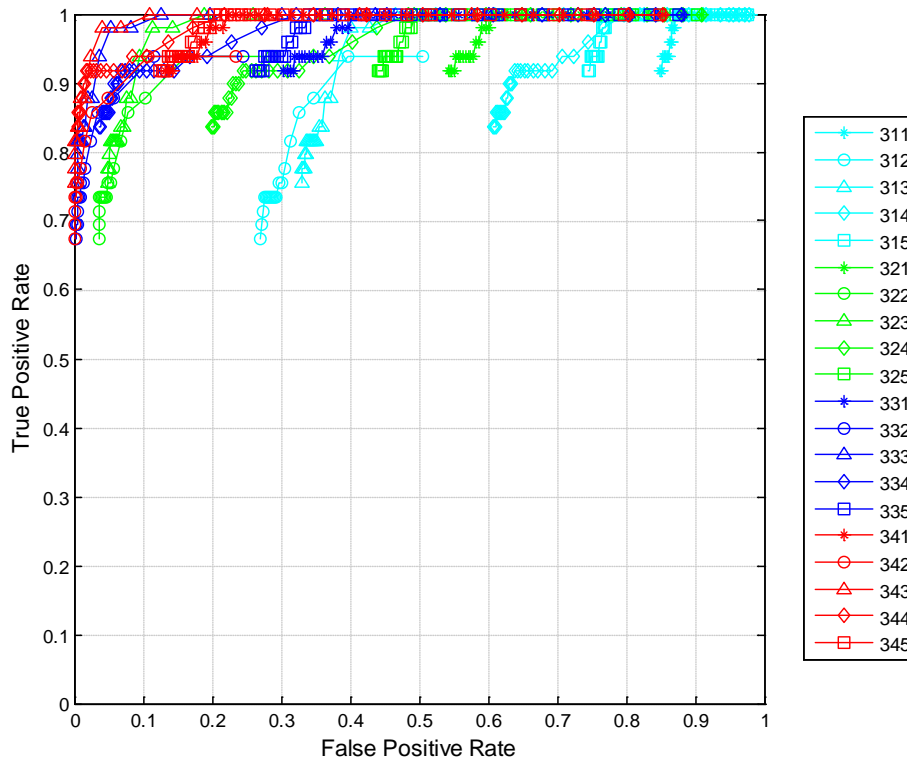


Figure 120 ROC curve for the 300 series algorithm family using a violation threshold of 20 mph.

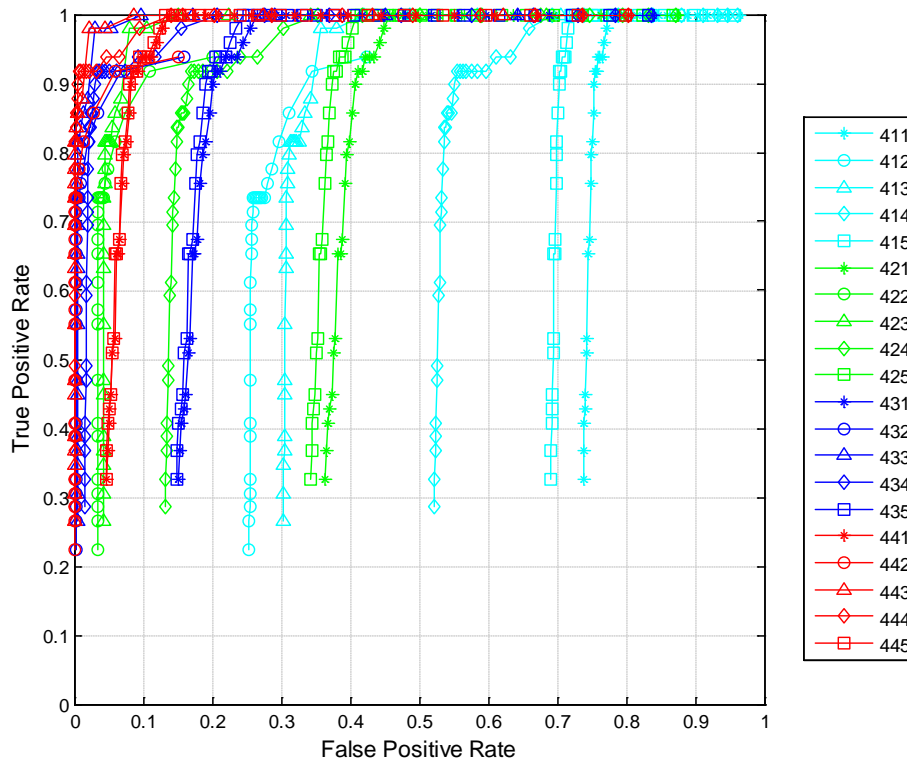


Figure 121 ROC curve for the 400 series algorithm family using a violation threshold of 20 mph.

ROC Curves for Stop-Controlled Intersections Using the 20-mph Violation Threshold

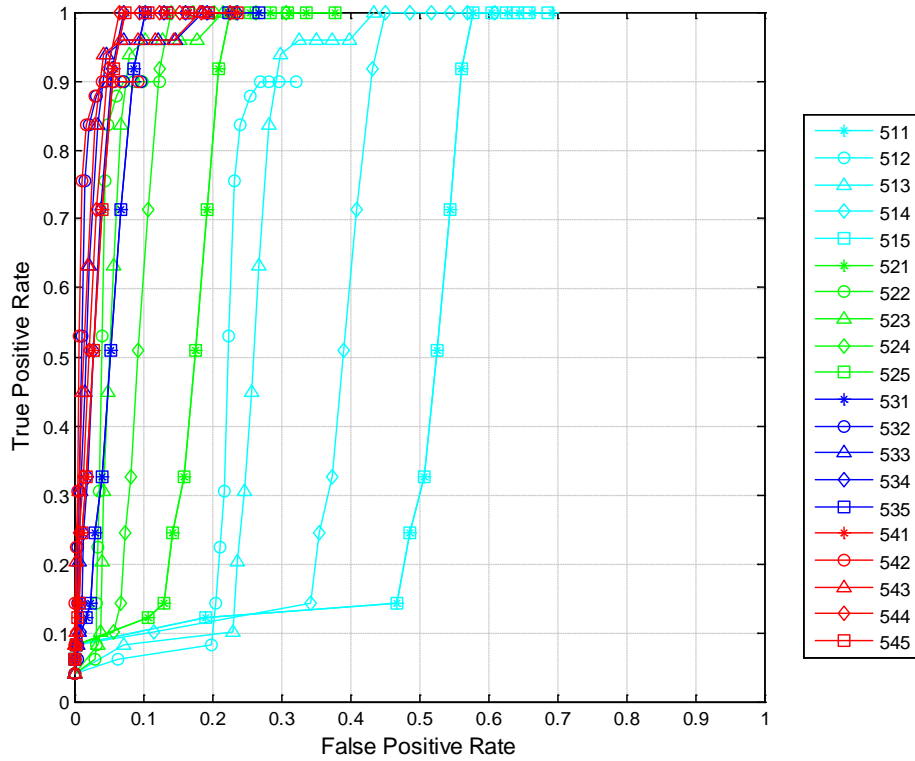


Figure 122 ROC curve for the 500 series algorithm family using a violation threshold of 20 mph.

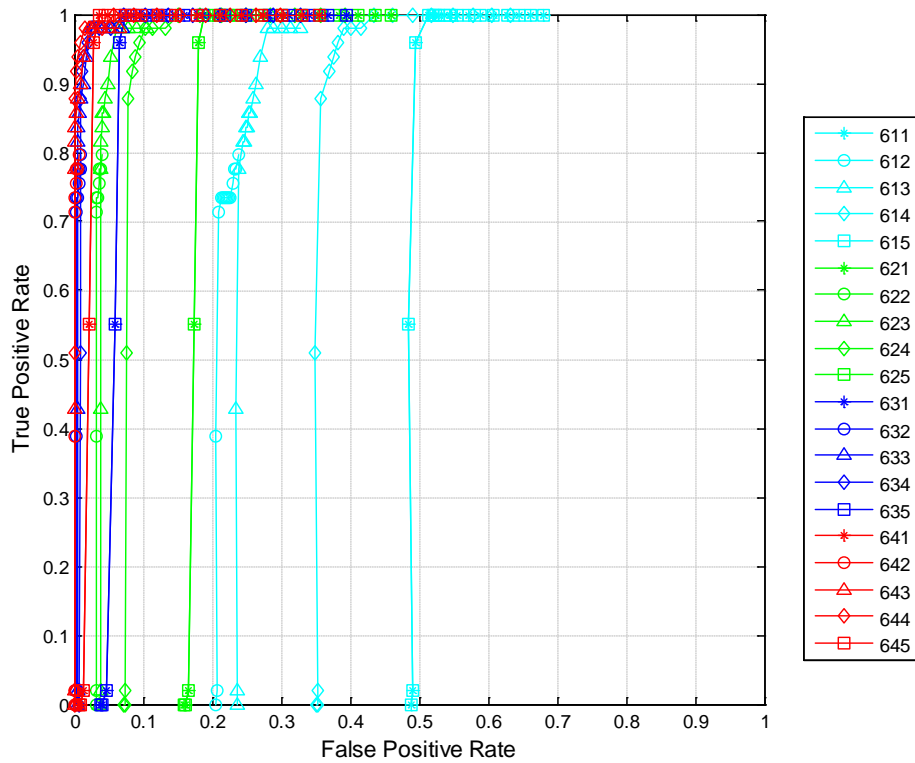


Figure 123 ROC curve for the 600 series algorithm family using a violation threshold of 20 mph.

ROC Curves for Stop-Controlled Intersections Using the 20-mph Violation Threshold

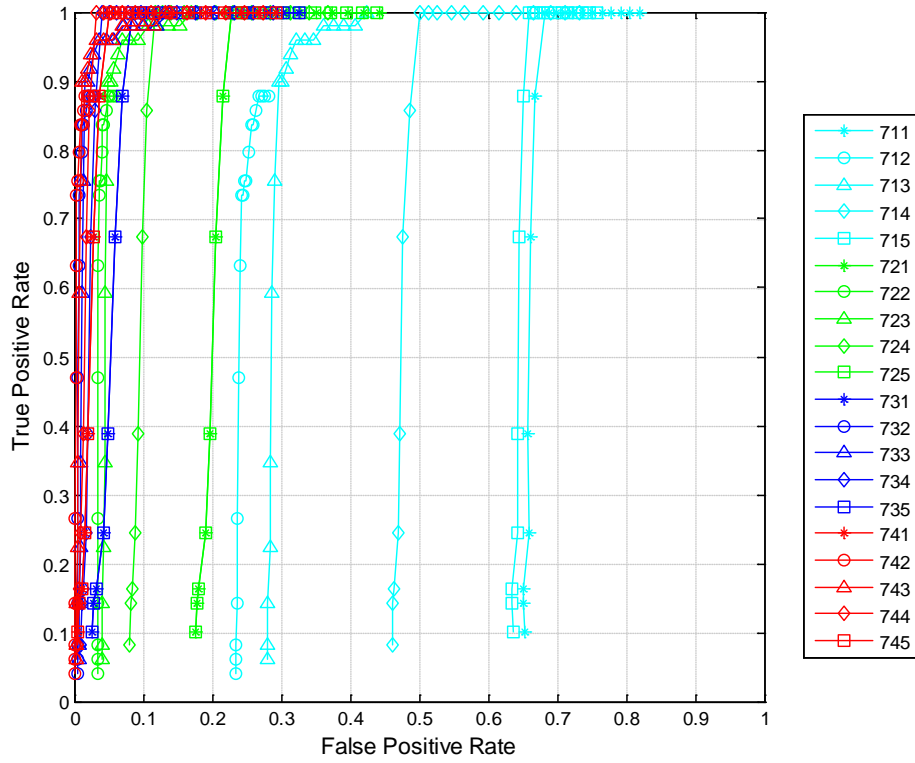


Figure 124 ROC curve for the 700 series algorithm family using a violation threshold of 20 mph.

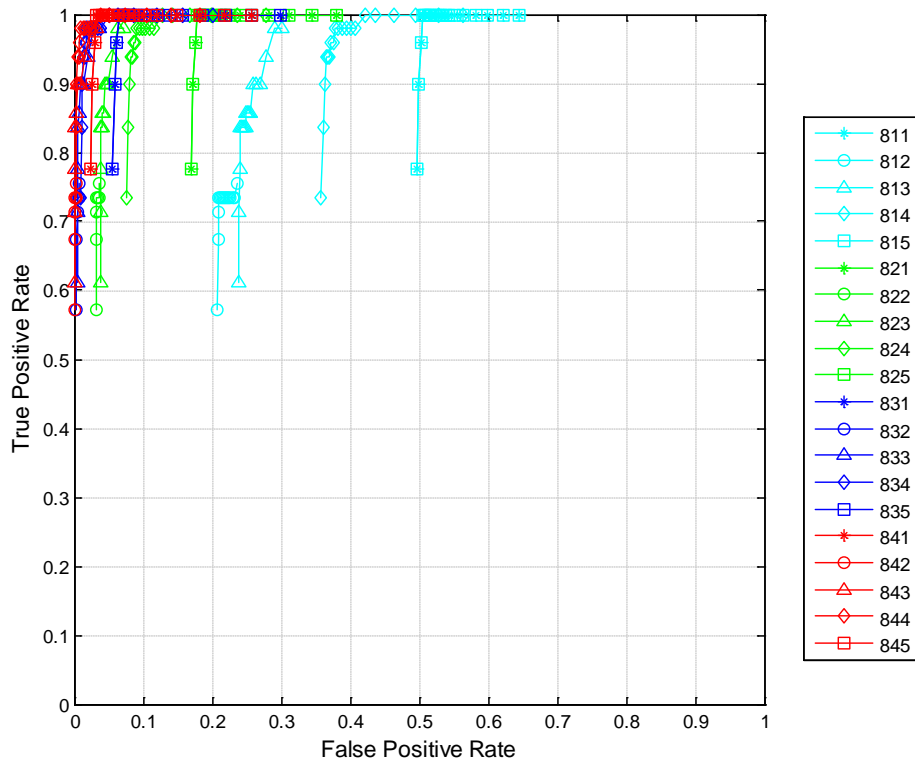


Figure 125 ROC curve for the 800 series algorithm family using a violation threshold of 20 mph.

### 11.15 Appendix O: Stop Controlled Warning Timing Distributions

Warning Timing Distributions for Stop-Controlled Intersections Using an FPR of 0.01 and a 15-mph Violation Threshold

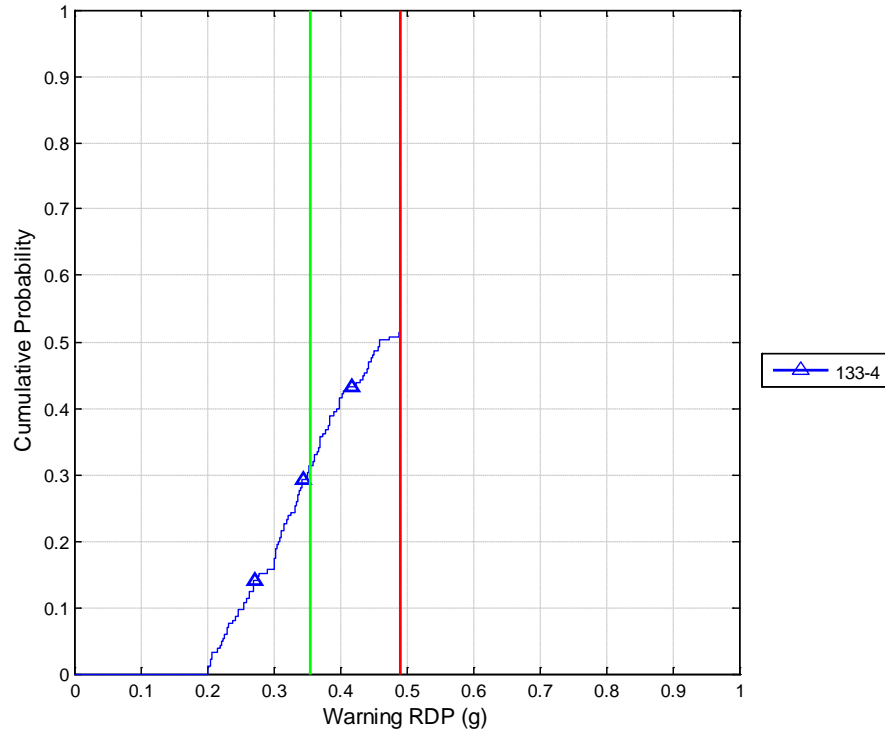


Figure 126 Cumulative distribution of the warning timing for true positives produced by the 100 series algorithm at a false positive rate of 0.01 using a violation threshold of 15 mph.

Warning Timing Distributions for Stop-Controlled Intersections Using an FPR of 0.01 and a 15-mph Violation Threshold

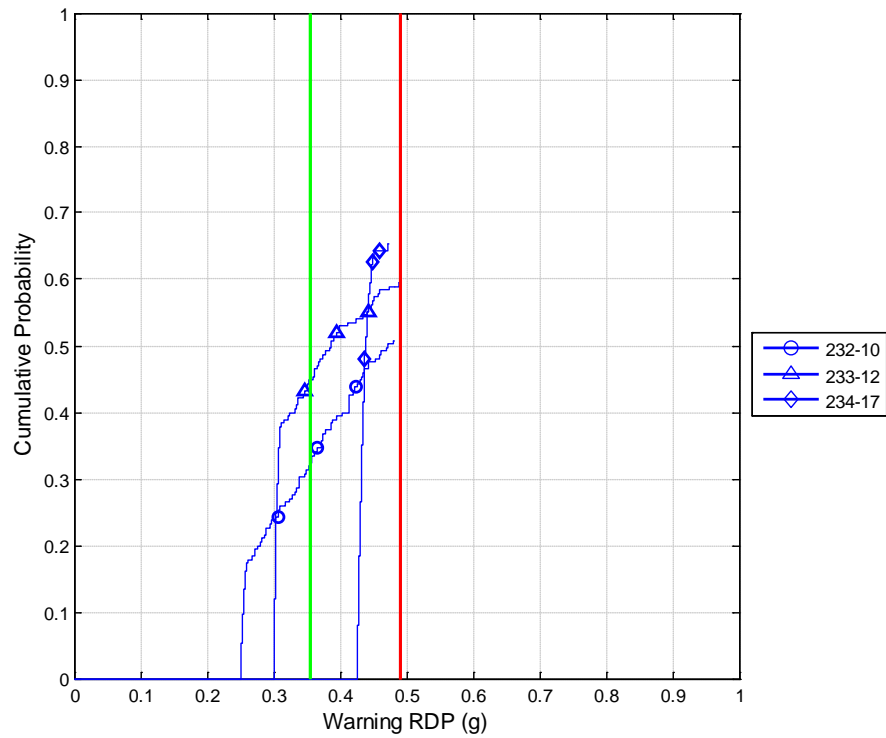


Figure 127 Cumulative distribution of the warning timing for true positives produced by the 200 series algorithm at a false positive rate of 0.01 using a violation threshold of 15 mph.

Warning Timing Distributions for Stop-Controlled Intersections Using an FPR of 0.01 and a 15-mph Violation Threshold

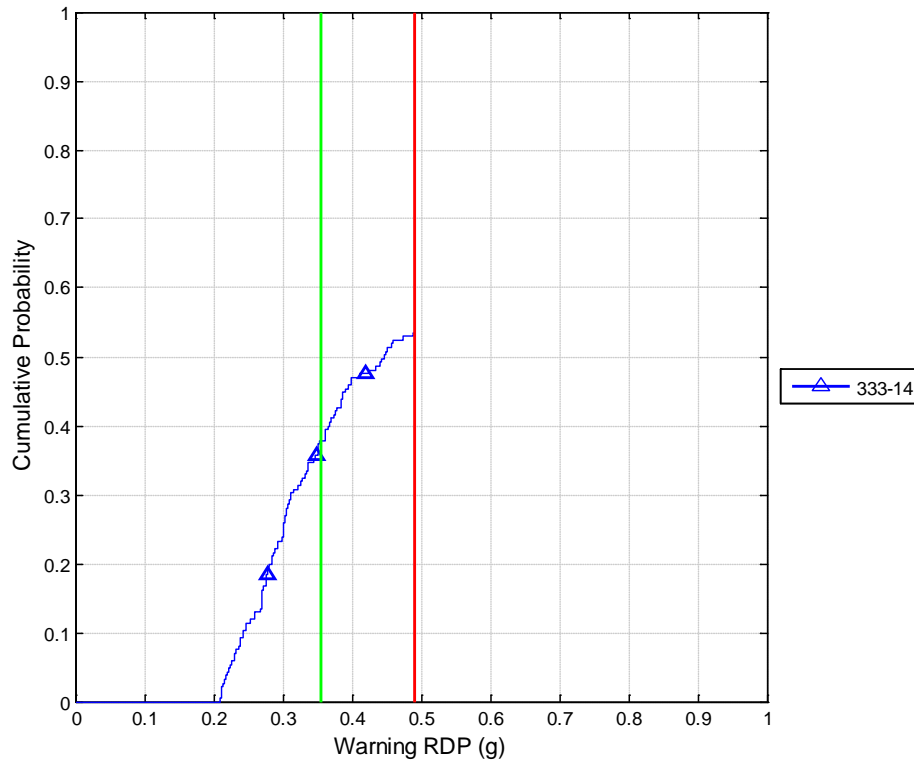


Figure 128 Cumulative distribution of the warning timing for true positives produced by the 300 series algorithm at a false positive rate of 0.01 using a violation threshold of 15 mph.



Warning Timing Distributions for Stop-Controlled Intersections Using an FPR of 0.01 and a 15-mph Violation Threshold

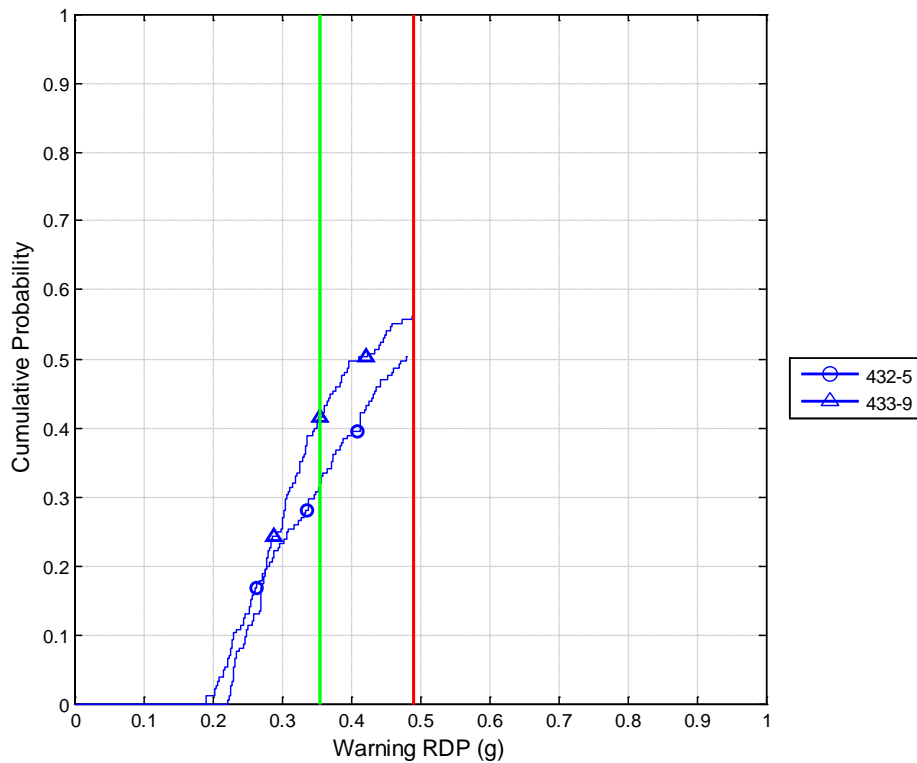


Figure 129 Cumulative distribution of the warning timing for true positives produced by the 400 series algorithm at a false positive rate of 0.01 using a violation threshold of 15 mph.

Warning Timing Distributions for Stop-Controlled Intersections Using an FPR of 0.01 and a 15-mph Violation Threshold

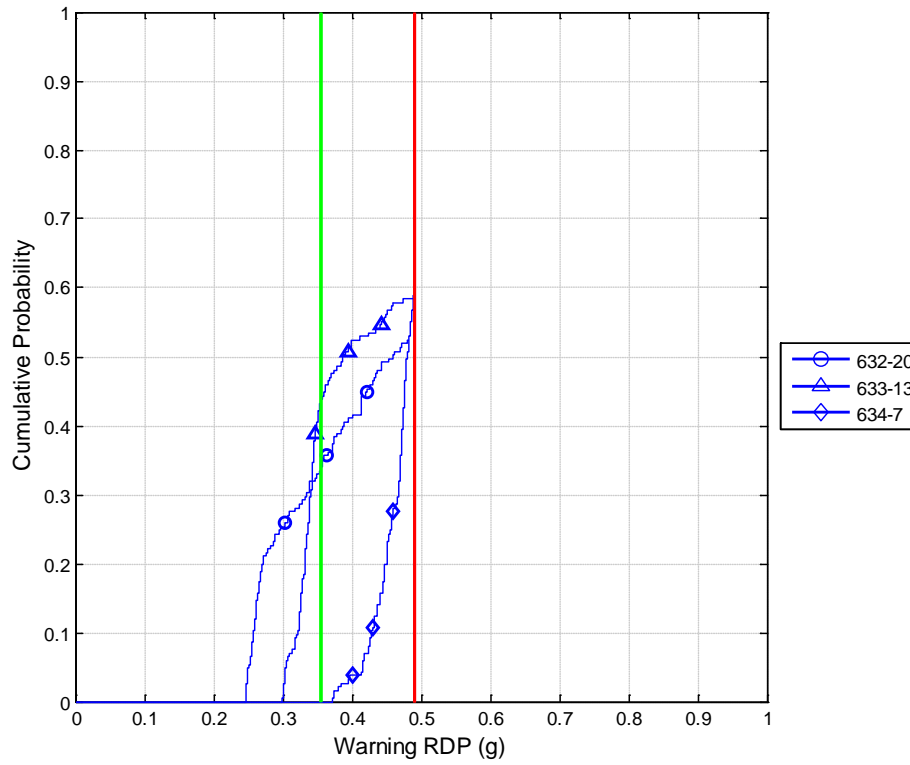


Figure 130 Cumulative distribution of the warning timing for true positives produced by the 600 series algorithm at a false positive rate of 0.01 using a violation threshold of 15 mph.

Warning Timing Distributions for Stop-Controlled Intersections Using an FPR of 0.01 and a 15-mph Violation Threshold

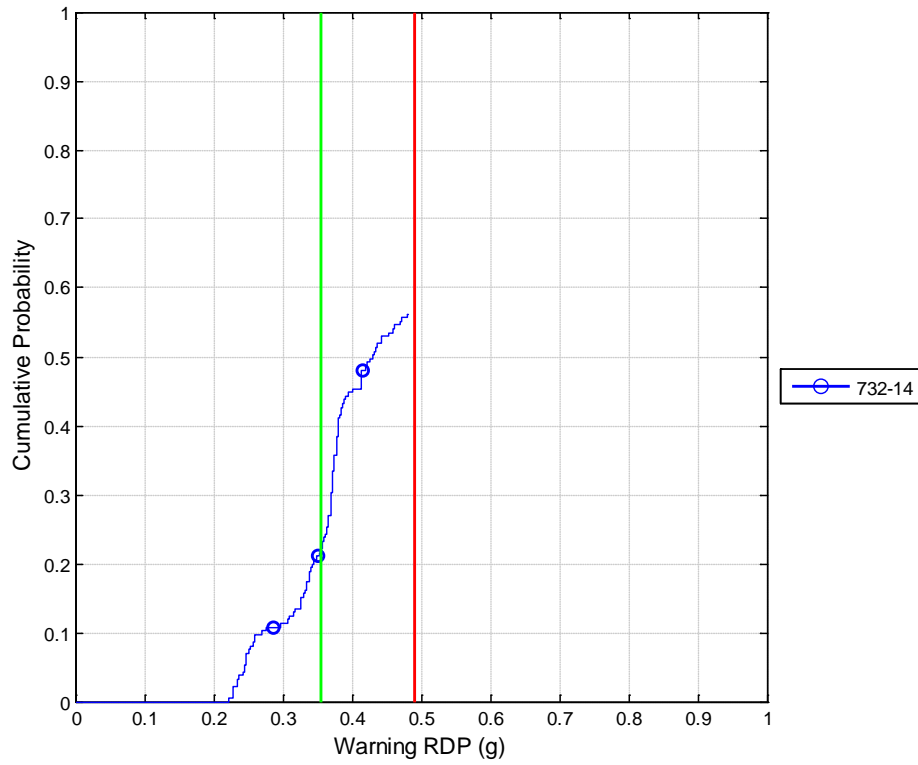


Figure 131 Cumulative distribution of the warning timing for true positives produced by the 700 series algorithm at a false positive rate of 0.01 using a violation threshold of 15 mph.

Warning Timing Distributions for Stop-Controlled Intersections Using an FPR of 0.01 and a 15-mph Violation Threshold

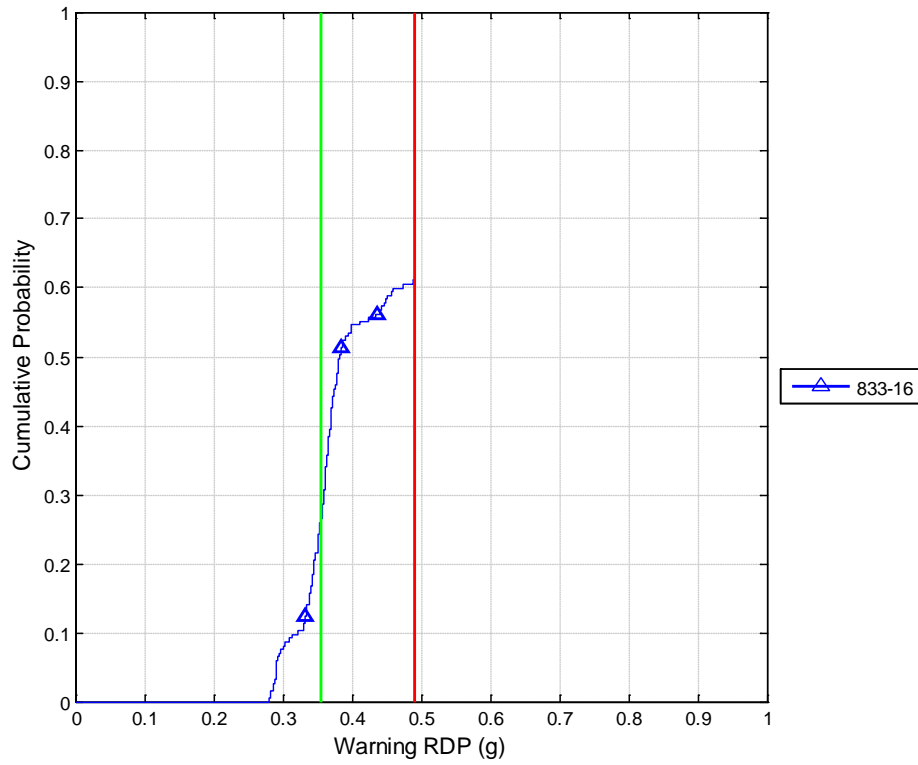


Figure 132 Cumulative distribution of the warning timing for true positives produced by the 800 series algorithm at a false positive rate of 0.01 using a violation threshold of 15 mph.

Warning Timing Distributions for Stop-Controlled Intersections Using an FPR of 0.01 and a 20-mph Violation Threshold

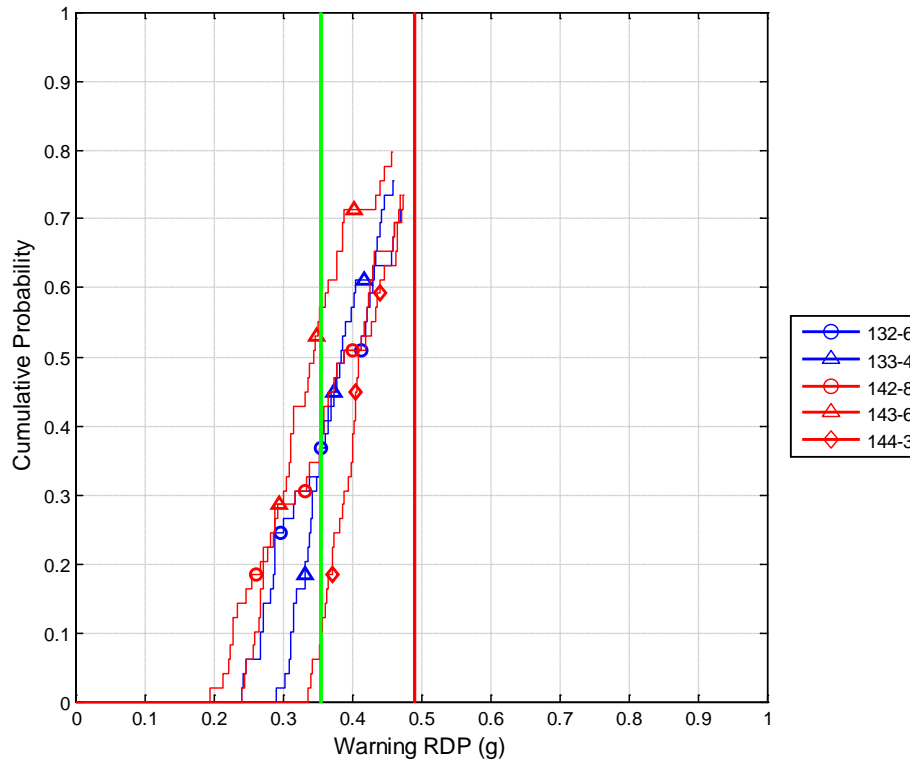


Figure 133 Cumulative distribution of the warning timing for true positives produced by the 100 series algorithm at a false positive rate of 0.01 using a violation threshold of 20 mph.

Warning Timing Distributions for Stop-Controlled Intersections Using an FPR of 0.01 and a 20-mph Violation Threshold

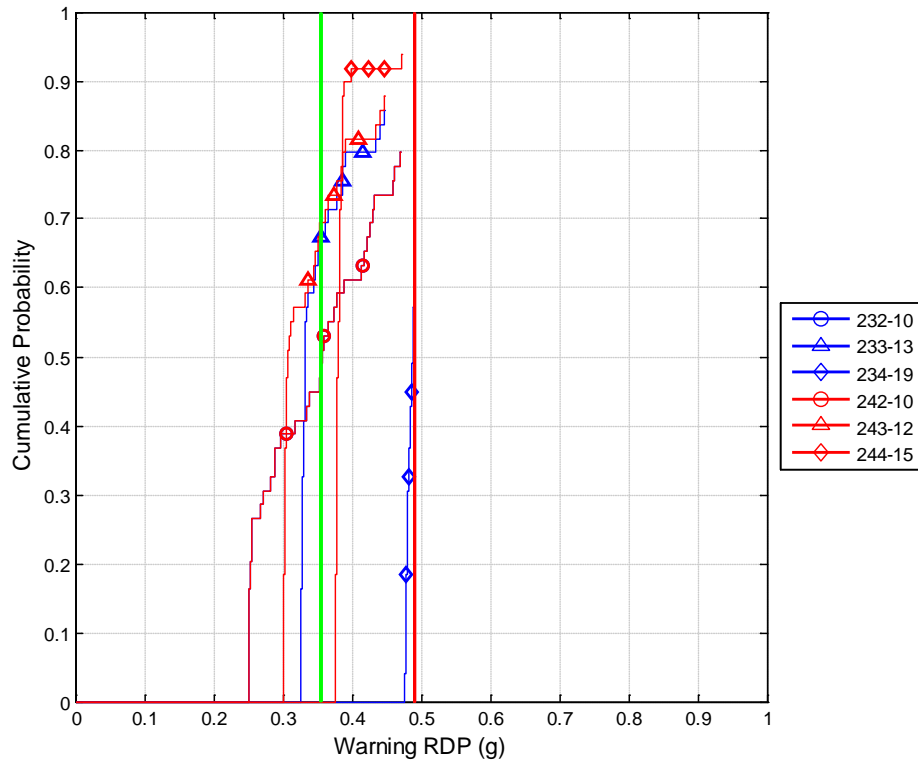


Figure 134 Cumulative distribution of the warning timing for true positives produced by the 200 series algorithm at a false positive rate of 0.01 using a violation threshold of 20 mph.

Warning Timing Distributions for Stop-Controlled Intersections Using an FPR of 0.01 and a 20-mph Violation Threshold

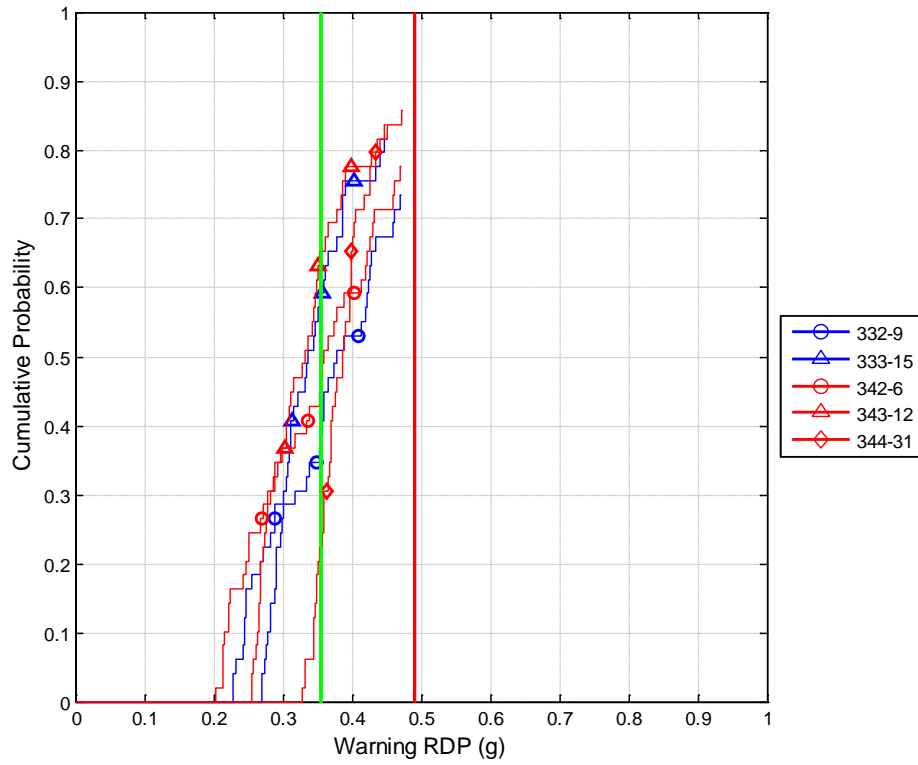


Figure 135 Cumulative distribution of the warning timing for true positives produced by the 300 series algorithm at a false positive rate of 0.01 using a violation threshold of 20 mph.

Warning Timing Distributions for Stop-Controlled Intersections Using an FPR of 0.01 and a 20-mph Violation Threshold

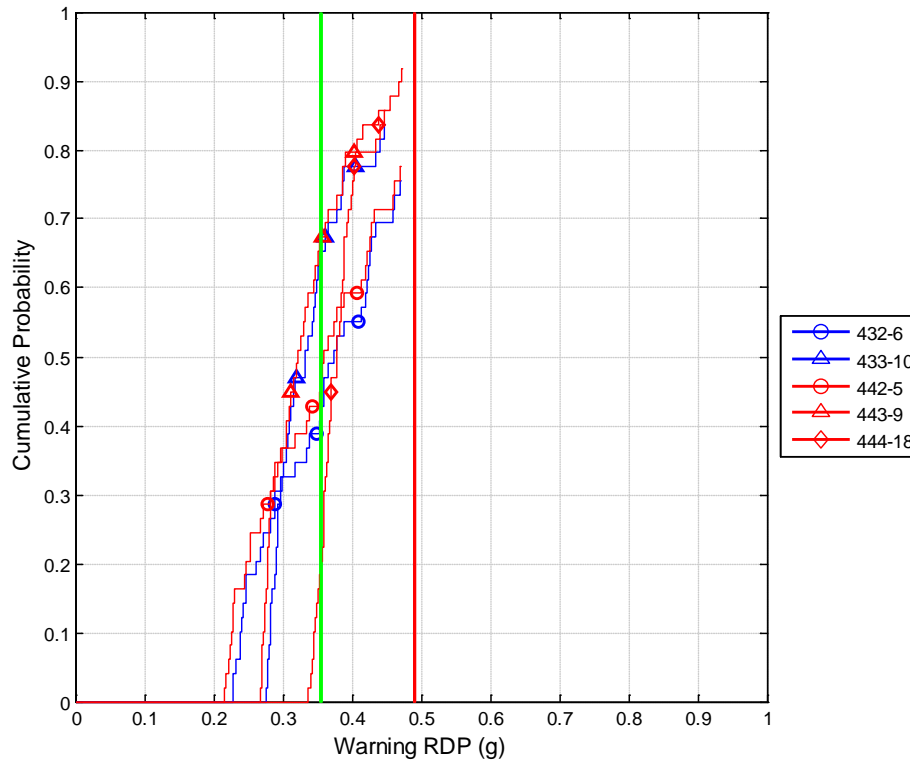


Figure 136 Cumulative distribution of the warning timing for true positives produced by the 400 series algorithm at a false positive rate of 0.01 using a violation threshold of 20 mph.



Warning Timing Distributions for Stop-Controlled Intersections Using an FPR of 0.01 and a 20-mph Violation Threshold

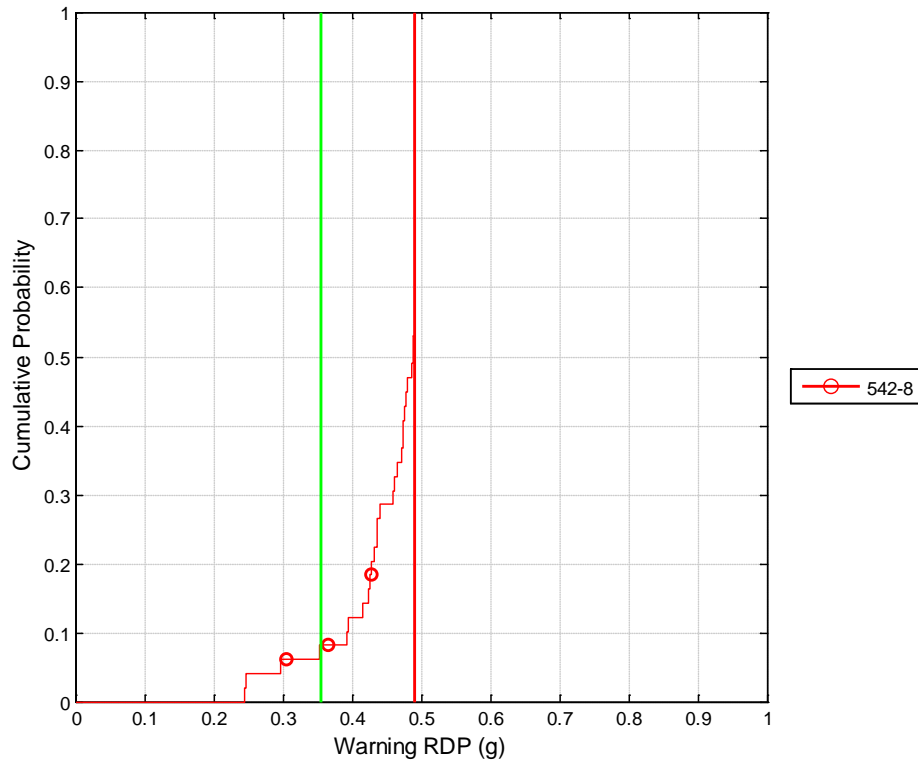


Figure 137 Cumulative distribution of the warning timing for true positives produced by the 500 series algorithm at a false positive rate of 0.01 using a violation threshold of 20 mph.

Warning Timing Distributions for Stop-Controlled Intersections Using an FPR of 0.01 and a 20-mph Violation Threshold

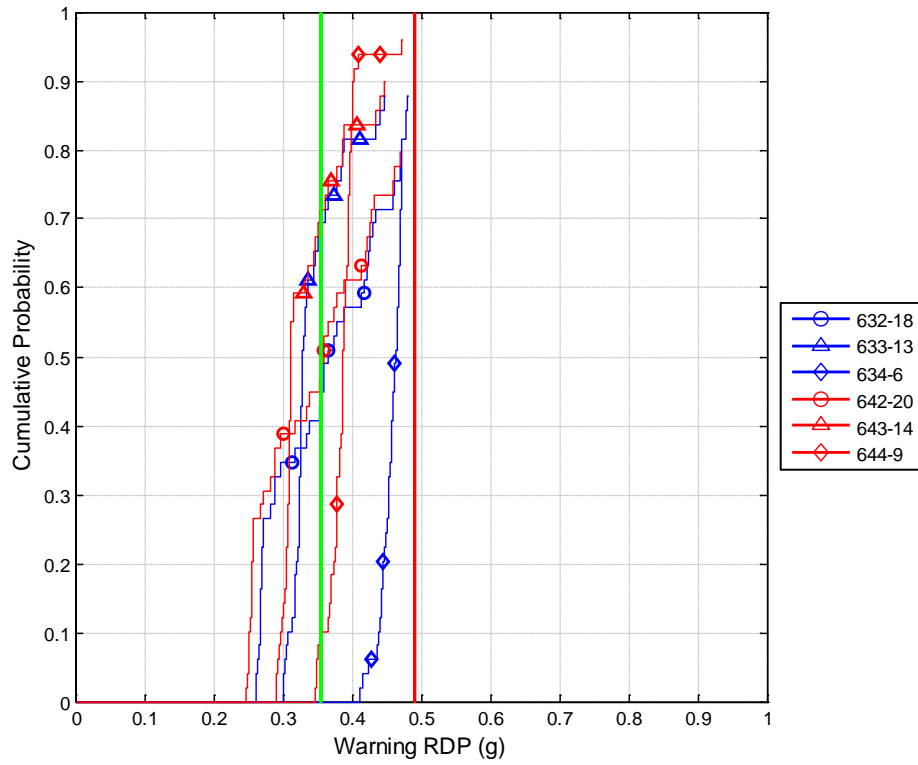


Figure 138 Cumulative distribution of the warning timing for true positives produced by the 600 series algorithm at a false positive rate of 0.01 using a violation threshold of 20 mph.

Warning Timing Distributions for Stop-Controlled Intersections Using an FPR of 0.01 and a 20-mph Violation Threshold

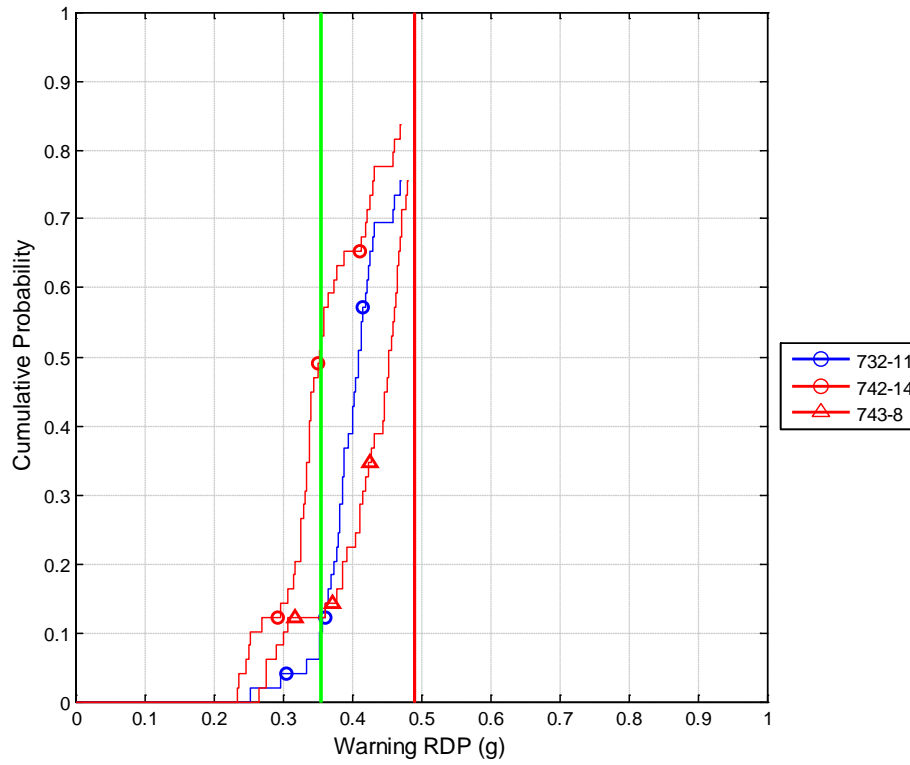


Figure 139 Cumulative distribution of the warning timing for true positives produced by the 700 series algorithm at a false positive rate of 0.01 using a violation threshold of 20 mph.

Warning Timing Distributions for Stop-Controlled Intersections Using an FPR of 0.01 and a 20-mph Violation Threshold

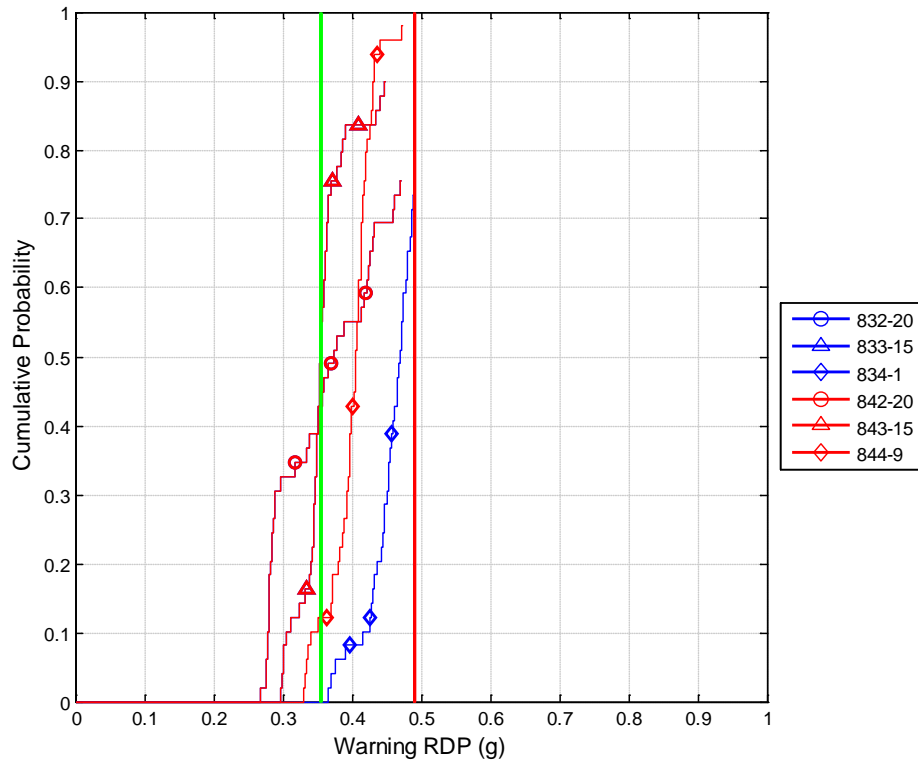


Figure 140 Cumulative distribution of the warning timing for true positives produced by the 800 series algorithm at a false positive rate of 0.01 using a violation threshold of 20 mph.

Warning Timing Distributions for Stop-Controlled Intersections Using an FPR of 0.05 and a 10-mph Violation Threshold

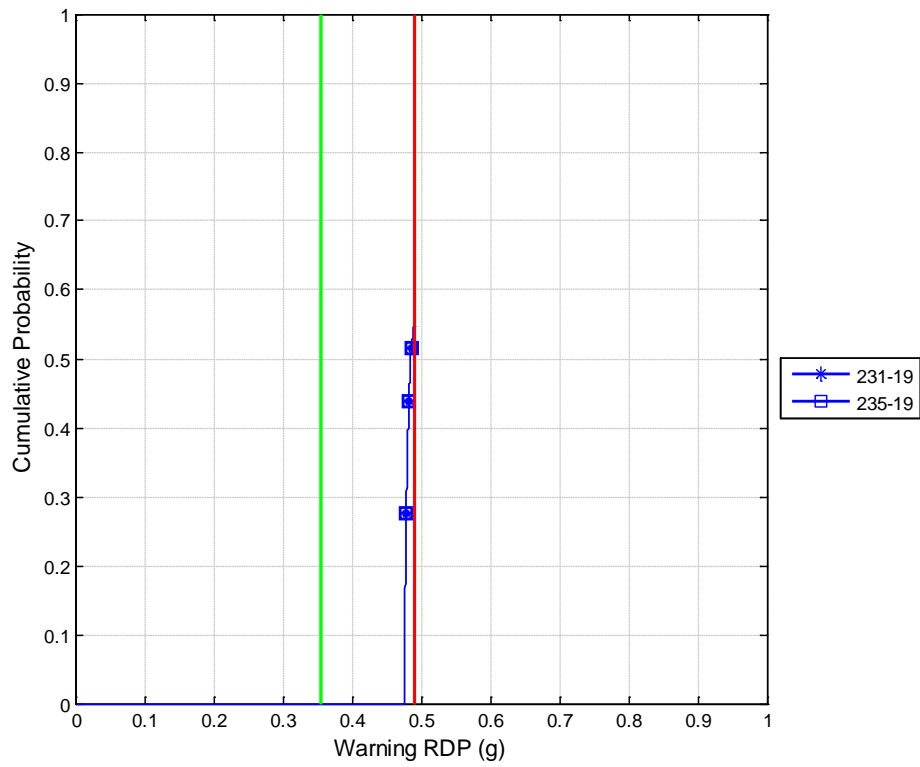


Figure 141 Cumulative distribution of the warning timing for true positives produced by the 200 series algorithm at a false positive rate of 0.05 using a violation threshold of 10 mph.

Warning Timing Distributions for Stop-Controlled Intersections Using an FPR of 0.05 and a 10-mph Violation Threshold

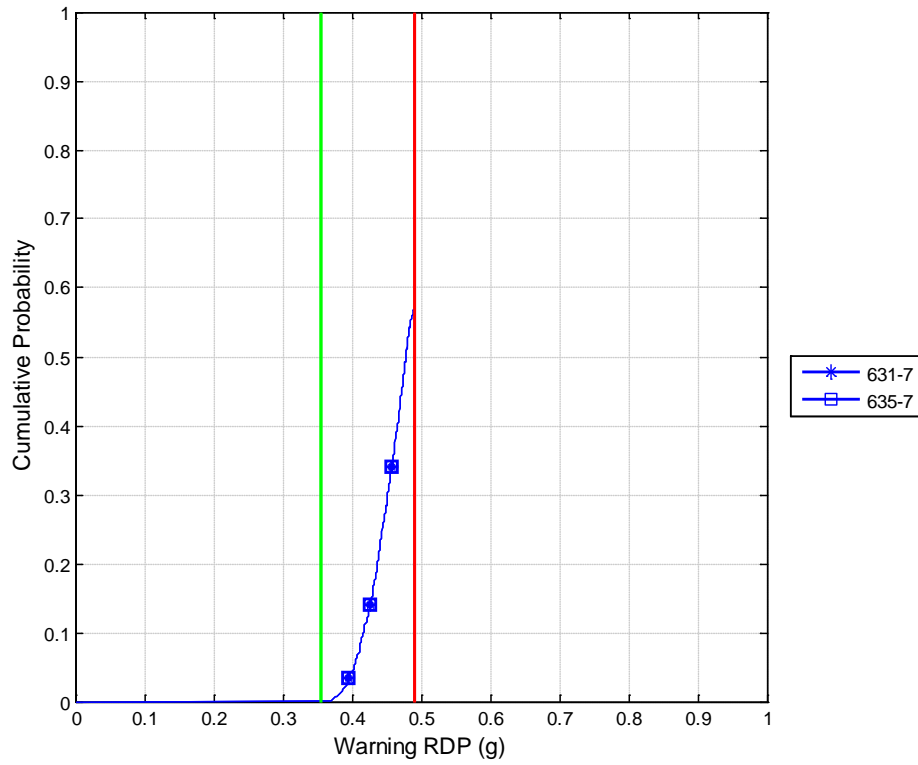


Figure 142 Cumulative distribution of the warning timing for true positives produced by the 600 series algorithm at a false positive rate of 0.05 using a violation threshold of 10 mph.

Warning Timing Distributions for Stop-Controlled Intersections Using an FPR of 0.05 and a 10-mph Violation Threshold

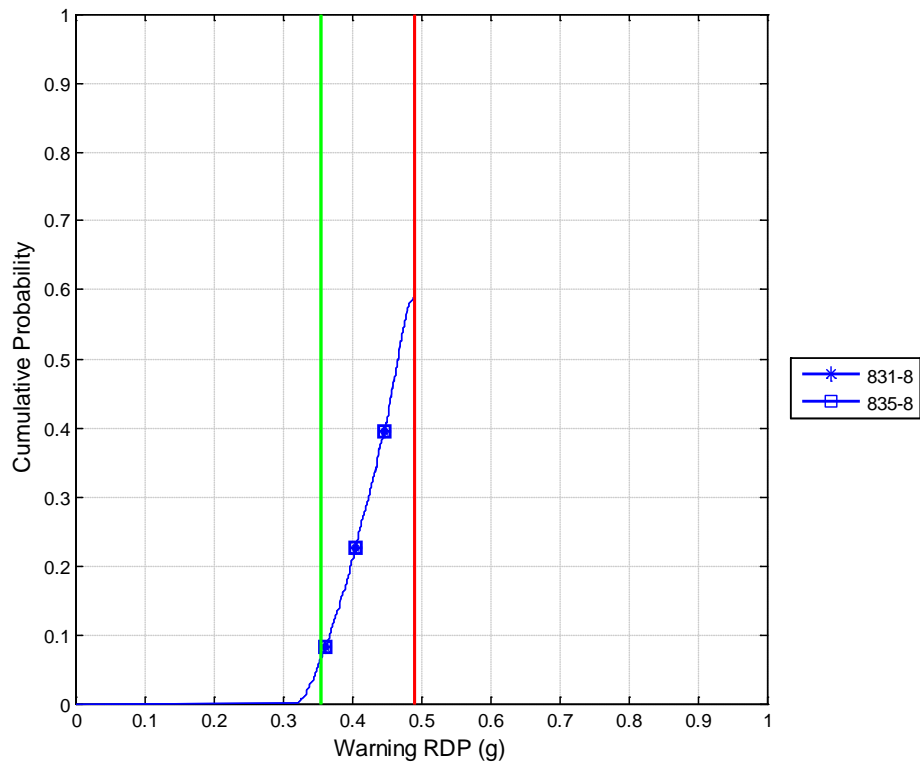


Figure 143 Cumulative distribution of the warning timing for true positives produced by the 800 series algorithm at a false positive rate of 0.05 using a violation threshold of 10 mph.

Warning Timing Distributions for Stop-Controlled Intersections Using an FPR of 0.05 and a 15-mph Violation Threshold

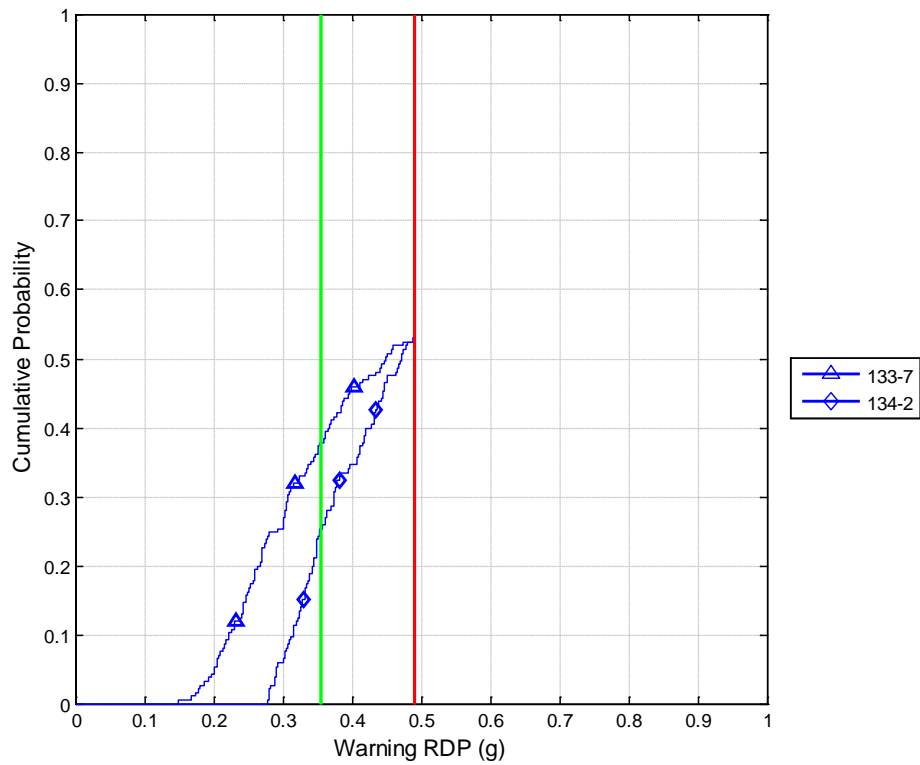


Figure 144 Cumulative distribution of the warning timing for true positives produced by the 100 series algorithm at a false positive rate of 0.05 using a violation threshold of 15 mph.



Warning Timing Distributions for Stop-Controlled Intersections Using an FPR of 0.05 and a 15-mph Violation Threshold

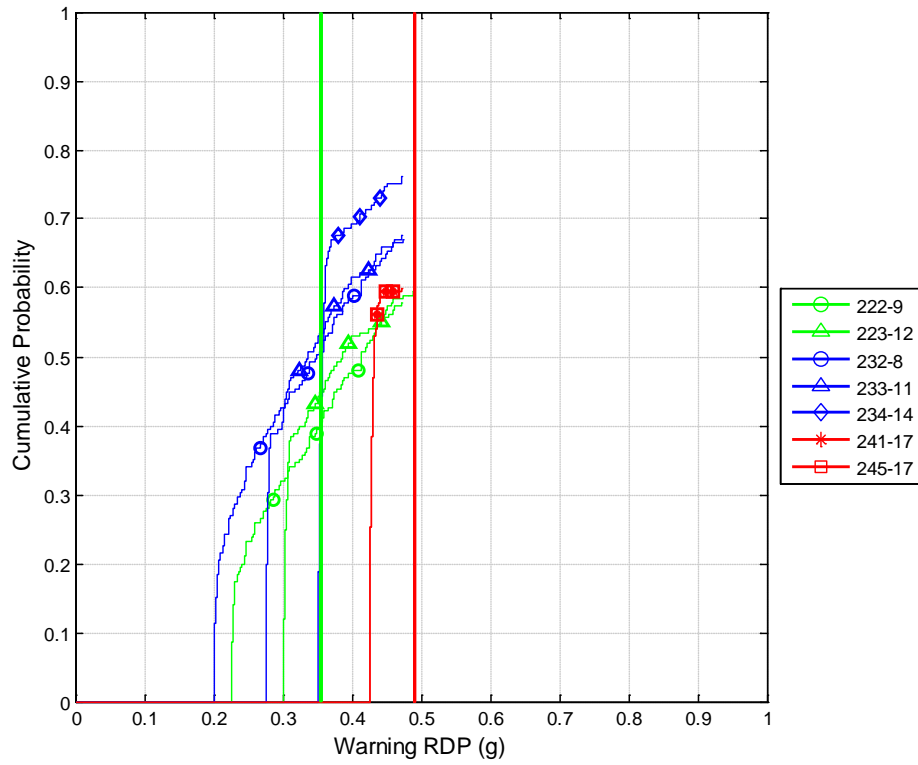


Figure 145 Cumulative distribution of the warning timing for true positives produced by the 200 series algorithm at a false positive rate of 0.05 using a violation threshold of 15 mph.

Warning Timing Distributions for Stop-Controlled Intersections Using an FPR of 0.05 and a 15-mph Violation Threshold

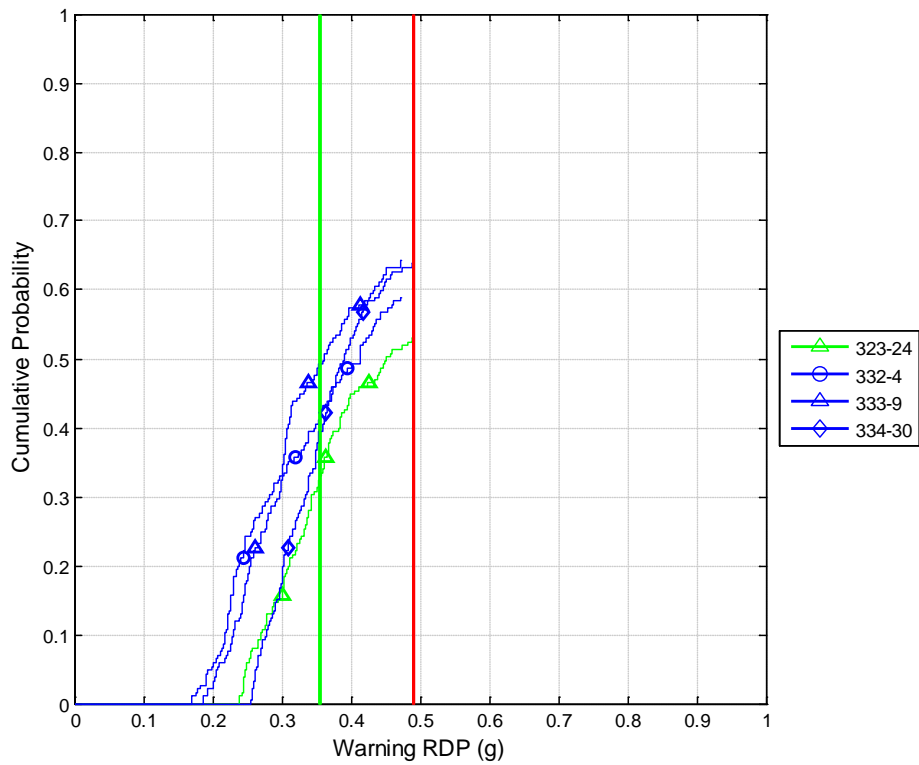


Figure 146 Cumulative distribution of the warning timing for true positives produced by the 300 series algorithm at a false positive rate of 0.05 using a violation threshold of 15 mph.

Warning Timing Distributions for Stop-Controlled Intersections Using an FPR of 0.05 and a 15-mph Violation Threshold

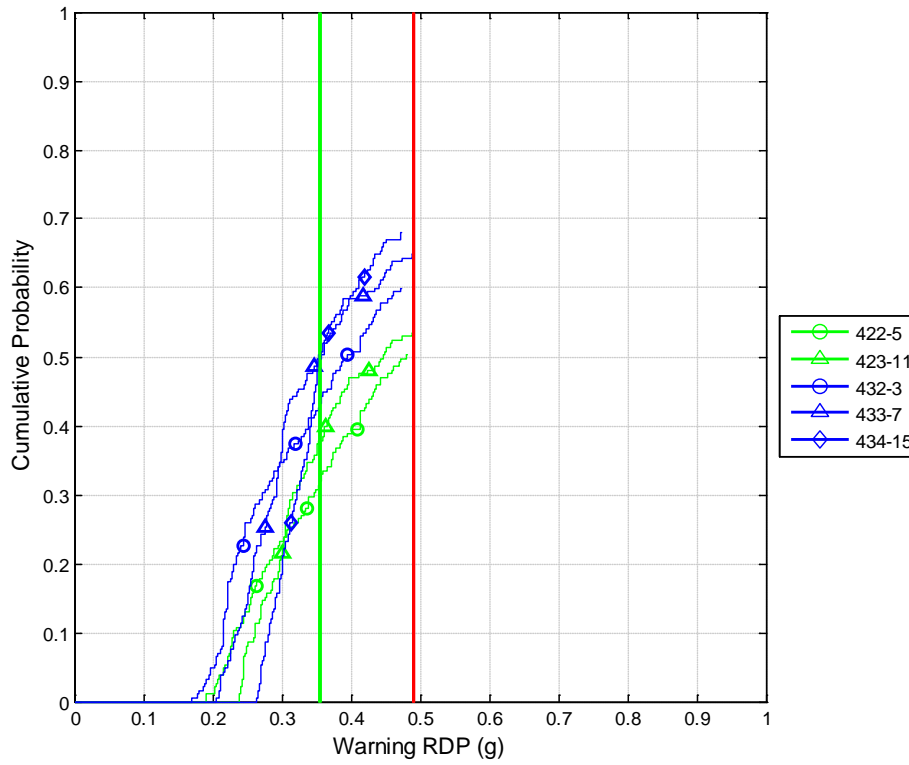


Figure 147 Cumulative distribution of the warning timing for true positives produced by the 400 series algorithm at a false positive rate of 0.05 using a violation threshold of 15 mph.

Warning Timing Distributions for Stop-Controlled Intersections Using an FPR of 0.05 and a 15-mph Violation Threshold

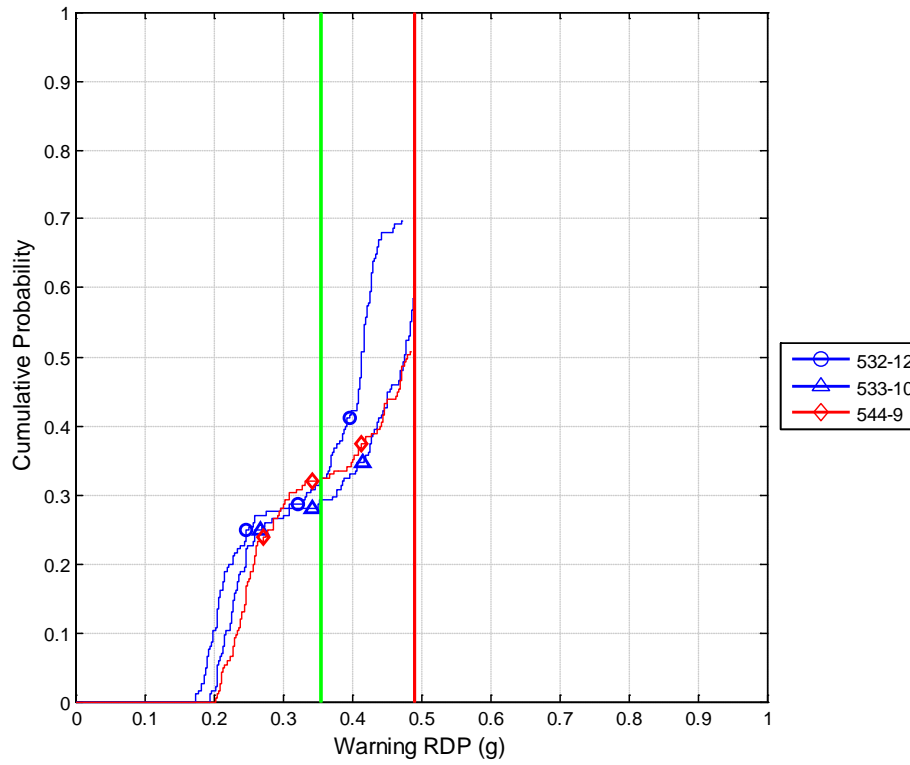


Figure 148 Cumulative distribution of the warning timing for true positives produced by the 500 series algorithm at a false positive rate of 0.05 using a violation threshold of 15 mph.

Warning Timing Distributions for Stop-Controlled Intersections Using an FPR of 0.05 and a 15-mph Violation Threshold

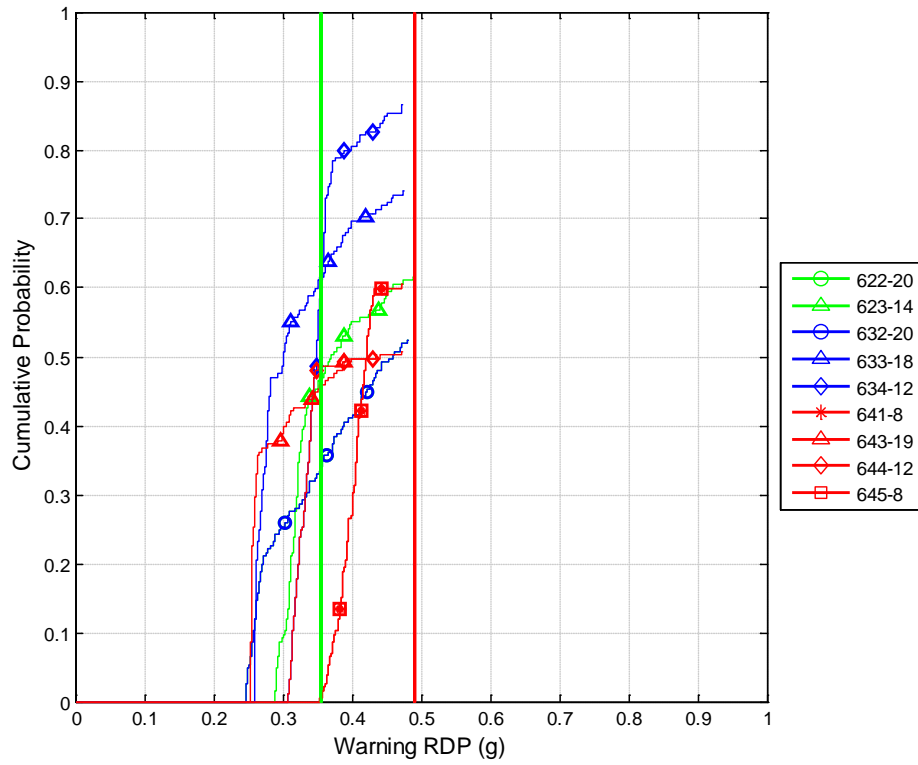


Figure 149 Cumulative distribution of the warning timing for true positives produced by the 600 series algorithm at a false positive rate of 0.05 using a violation threshold of 15 mph.

Warning Timing Distributions for Stop-Controlled Intersections Using an FPR of 0.05 and a 15-mph Violation Threshold

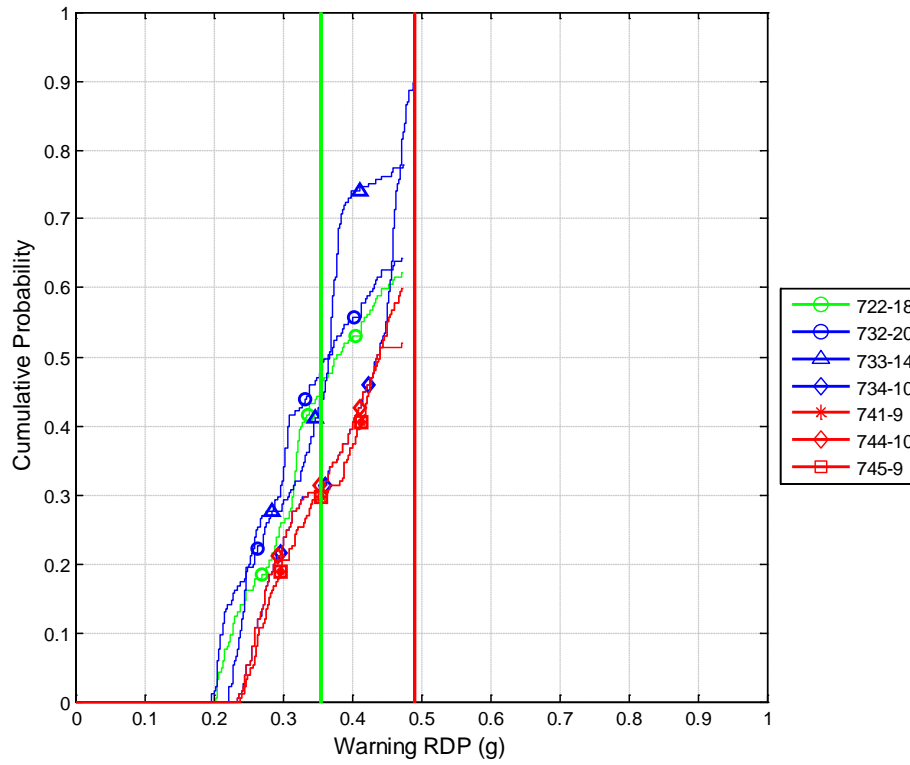


Figure 150 Cumulative distribution of the warning timing for true positives produced by the 700 series algorithm at a false positive rate of 0.05 using a violation threshold of 15 mph.

Warning Timing Distributions for Stop-Controlled Intersections Using an FPR of 0.05 and a 15-mph Violation Threshold

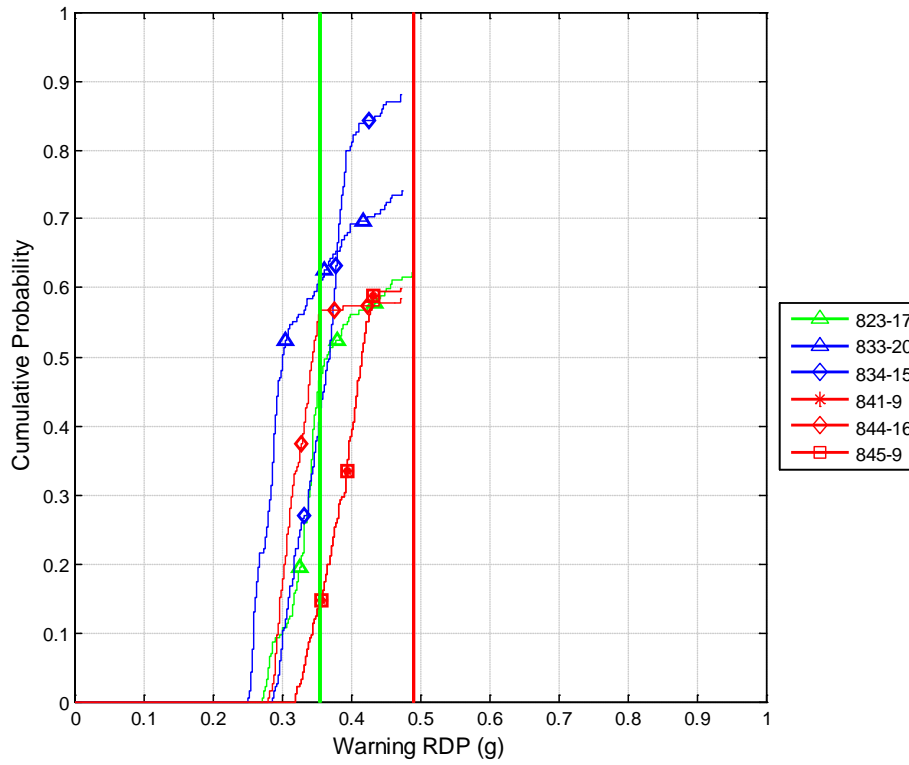


Figure 151 Cumulative distribution of the warning timing for true positives produced by the 800 series algorithm at a false positive rate of 0.05 using a violation threshold of 15 mph.

Warning Timing Distributions for Stop-Controlled Intersections Using an FPR of 0.05 and a 20-mph Violation Threshold

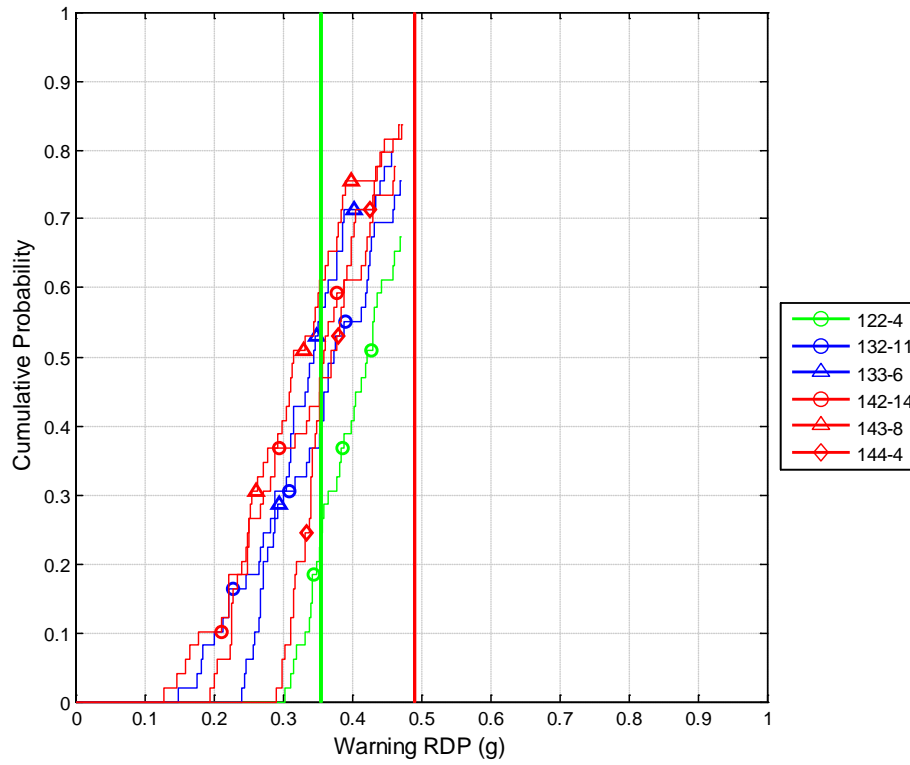


Figure 152 Cumulative distribution of the warning timing for true positives produced by the 100 series algorithm at a false positive rate of 0.05 using a violation threshold of 20 mph.



Warning Timing Distributions for Stop-Controlled Intersections Using an FPR of 0.05 and a 20-mph Violation Threshold

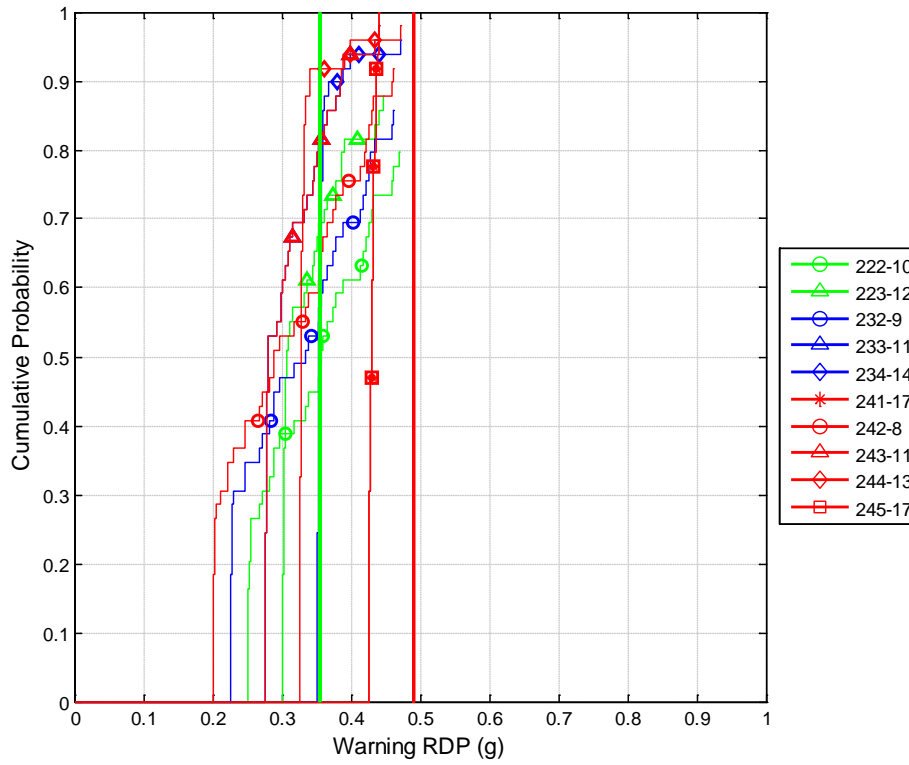


Figure 153 Cumulative distribution of the warning timing for true positives produced by the 200 series algorithm at a false positive rate of 0.05 using a violation threshold of 20 mph.

Warning Timing Distributions for Stop-Controlled Intersections Using an FPR of 0.05 and a 20-mph Violation Threshold

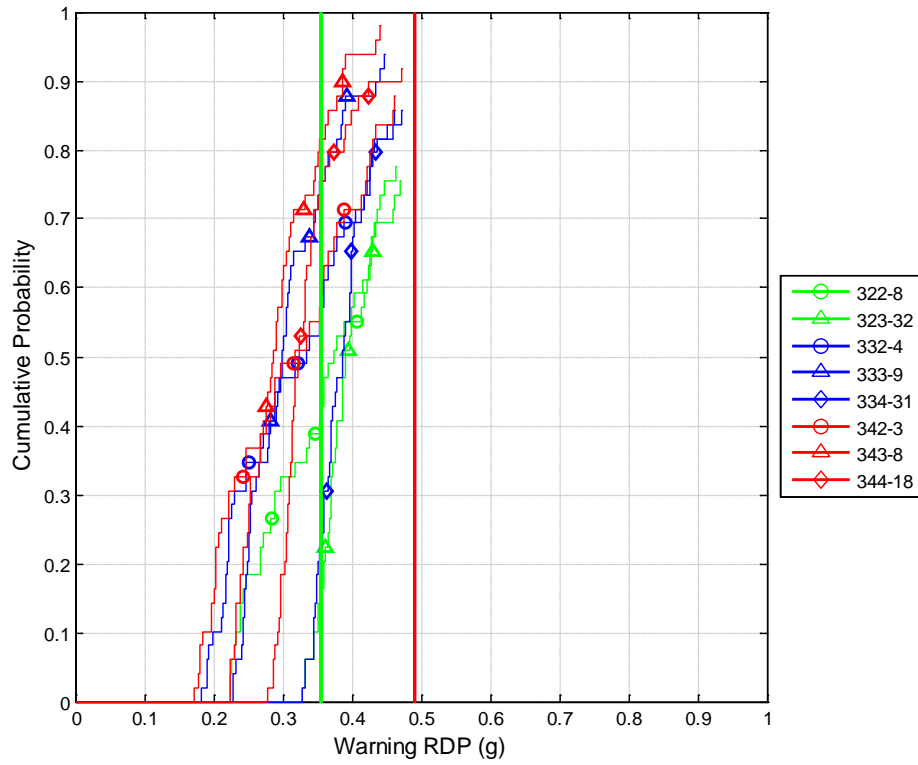


Figure 154 Cumulative distribution of the warning timing for true positives produced by the 300 series algorithm at a false positive rate of 0.05 using a violation threshold of 20 mph.

Warning Timing Distributions for Stop-Controlled Intersections Using an FPR of 0.05 and a 20-mph Violation Threshold

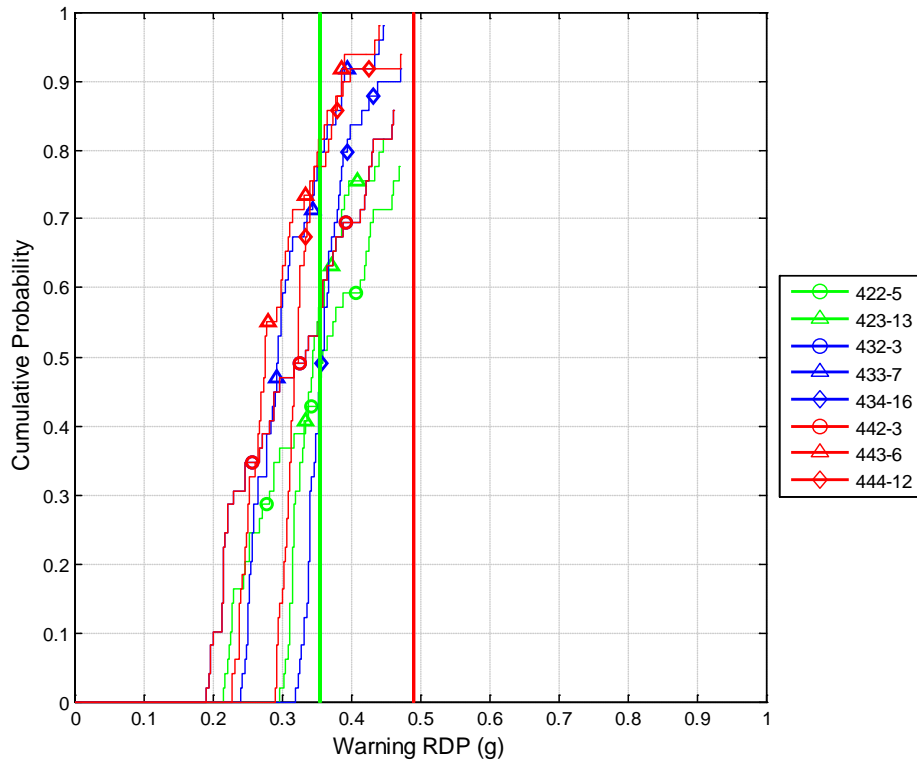


Figure 155 Cumulative distribution of the warning timing for true positives produced by the 400 series algorithm at a false positive rate of 0.05 using a violation threshold of 20 mph.

Warning Timing Distributions for Stop-Controlled Intersections Using an FPR of 0.05 and a 20-mph Violation Threshold

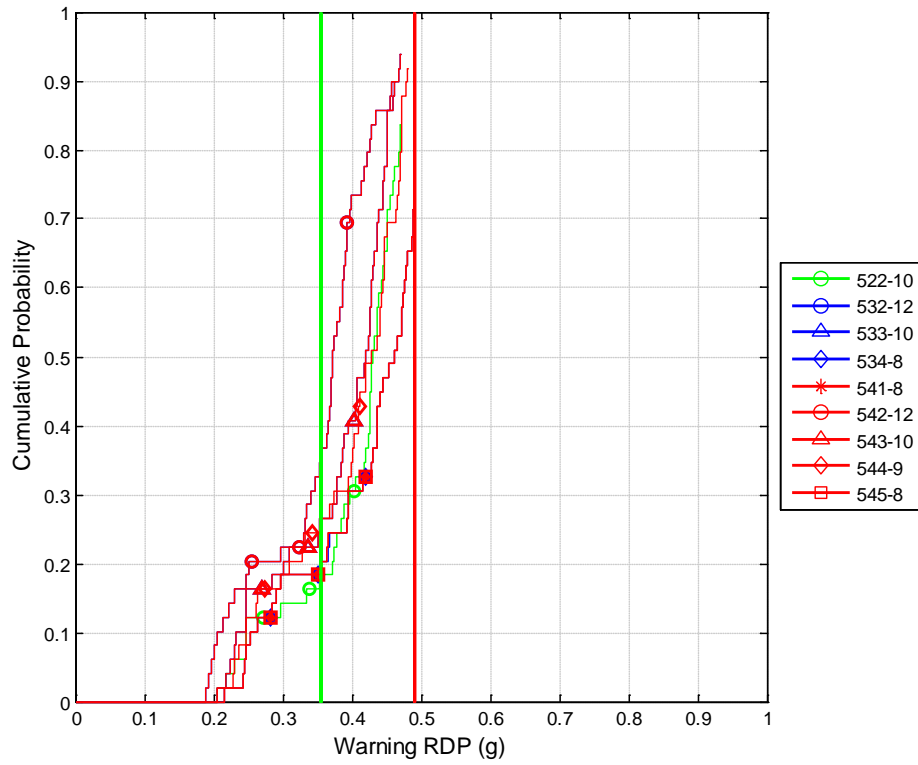


Figure 156 Cumulative distribution of the warning timing for true positives produced by the 500 series algorithm at a false positive rate of 0.05 using a violation threshold of 20 mph.

Warning Timing Distributions for Stop-Controlled Intersections Using an FPR of 0.05 and a 20-mph Violation Threshold

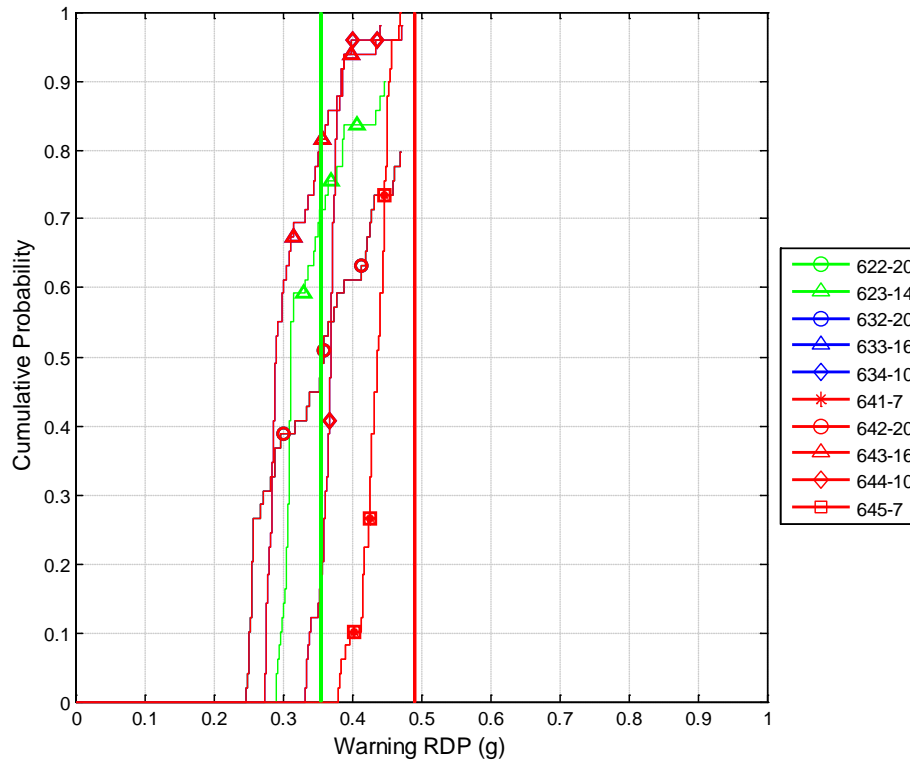


Figure 157 Cumulative distribution of the warning timing for true positives produced by the 600 series algorithm at a false positive rate of 0.05 using a violation threshold of 20 mph.

Warning Timing Distributions for Stop-Controlled Intersections Using an FPR of 0.05 and a 20-mph Violation Threshold

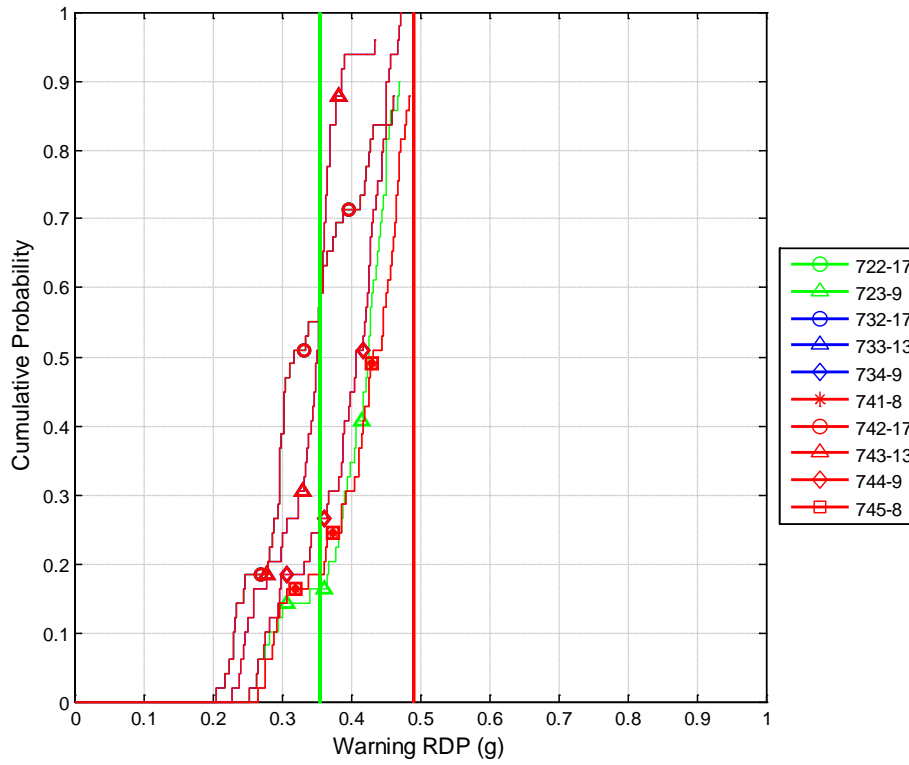


Figure 158 Cumulative distribution of the warning timing for true positives produced by the 700 series algorithm at a false positive rate of 0.05 using a violation threshold of 20 mph.

Warning Timing Distributions for Stop-Controlled Intersections Using an FPR of 0.05 and a 20-mph Violation Threshold

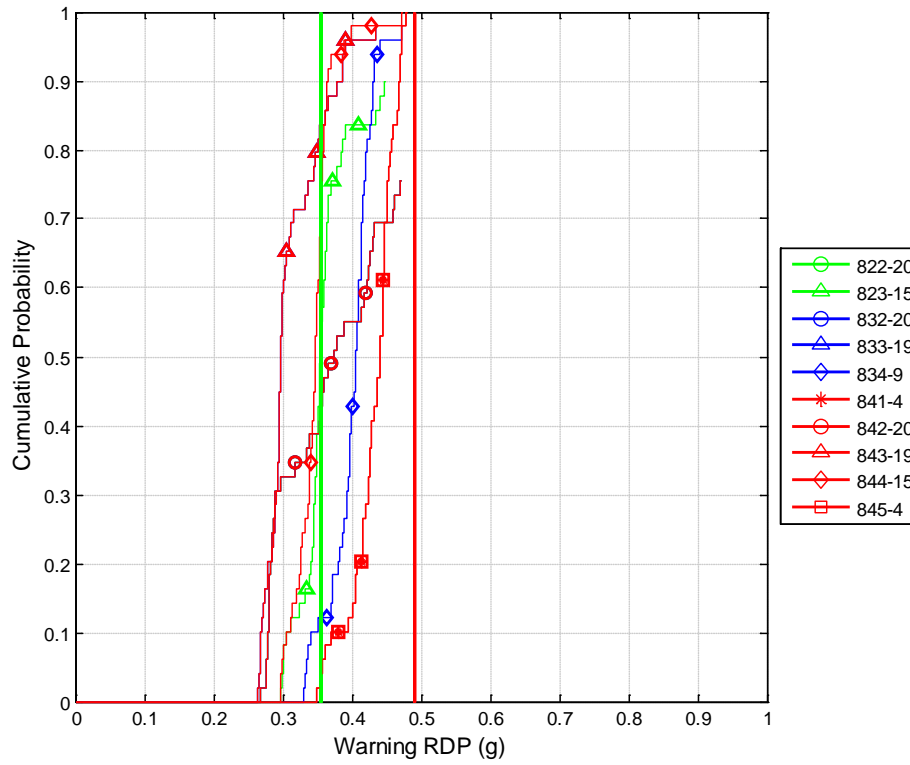


Figure 159 Cumulative distribution of the warning timing for true positives produced by the 800 series algorithm at a false positive rate of 0.05 using a violation threshold of 20 mph.

### 11.16 Appendix P: Stop-Controlled Nuisance Distributions

Stopbar Velocity Distributions for Stop-Controlled Intersections Using an FPR of 0.01 and a 15-mph Violation Threshold

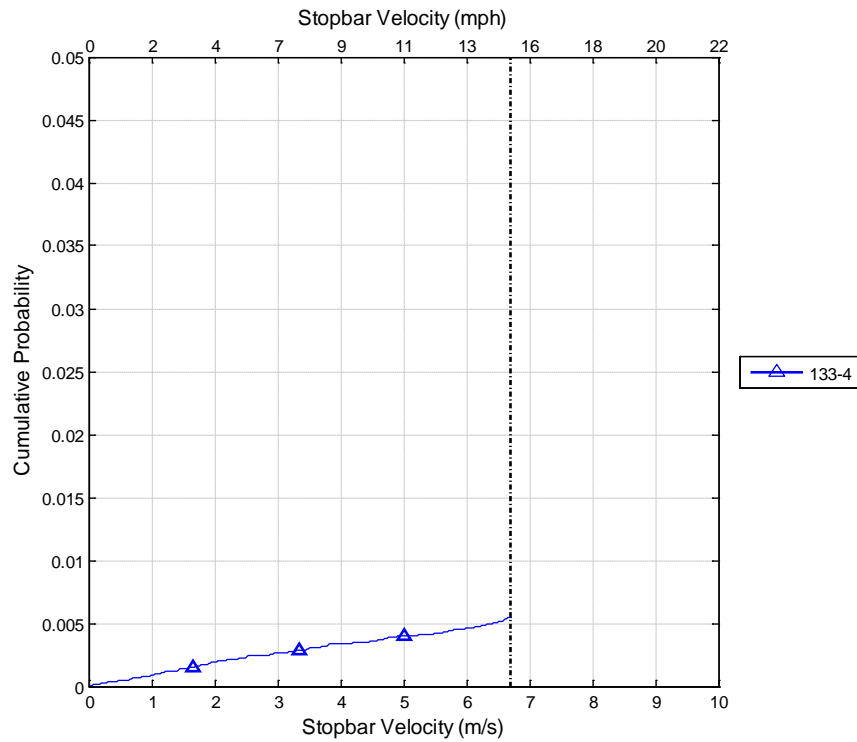


Figure 160 Cumulative distribution of the stop-bar speed for false positives produced by the 100 series algorithm at a false positive rate of 0.01 using a violation threshold of 15 mph.



Stopbar Velocity Distributions for Stop-Controlled Intersections Using an FPR of 0.01 and a 15-mph Violation Threshold

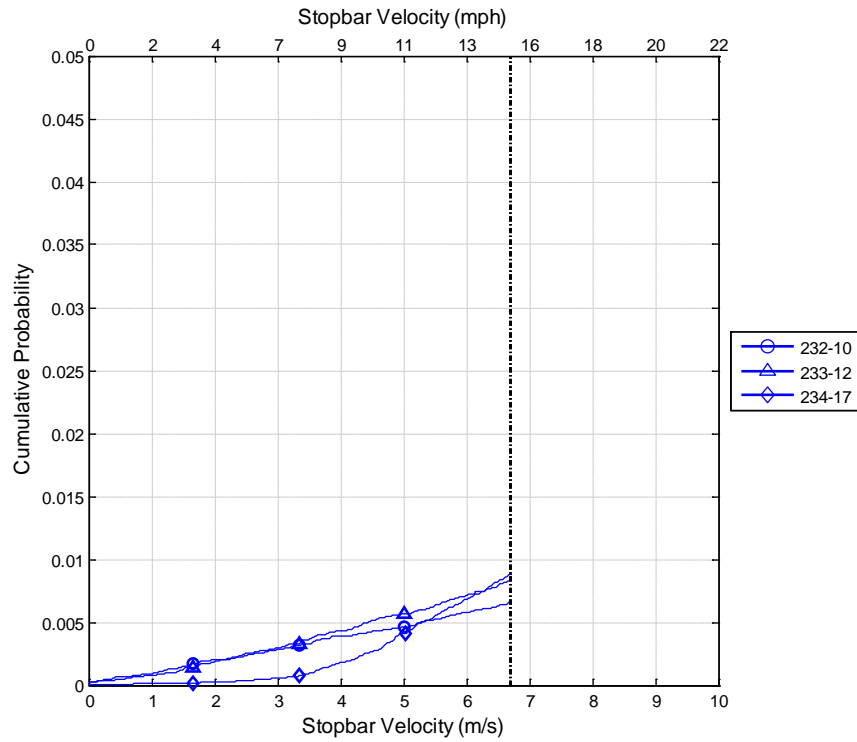
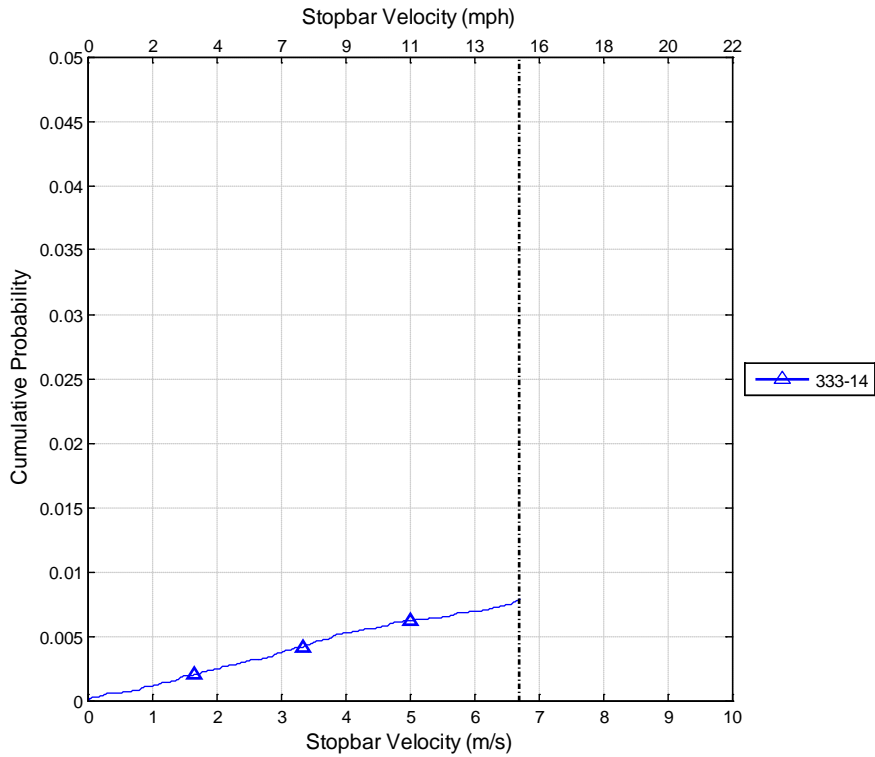


Figure 161 Cumulative distribution of the stop-bar speed for false positives produced by the 200 series algorithm at a false positive rate of 0.01 using a violation threshold of 15 mph.



Stopbar Velocity Distributions for Stop-Controlled Intersections Using an FPR of 0.01 and a 15-mph Violation Threshold

Figure 162 Cumulative distribution of the stop-bar speed for false positives produced by the 300 series algorithm at a false positive rate of 0.01 using a violation threshold of 15 mph.

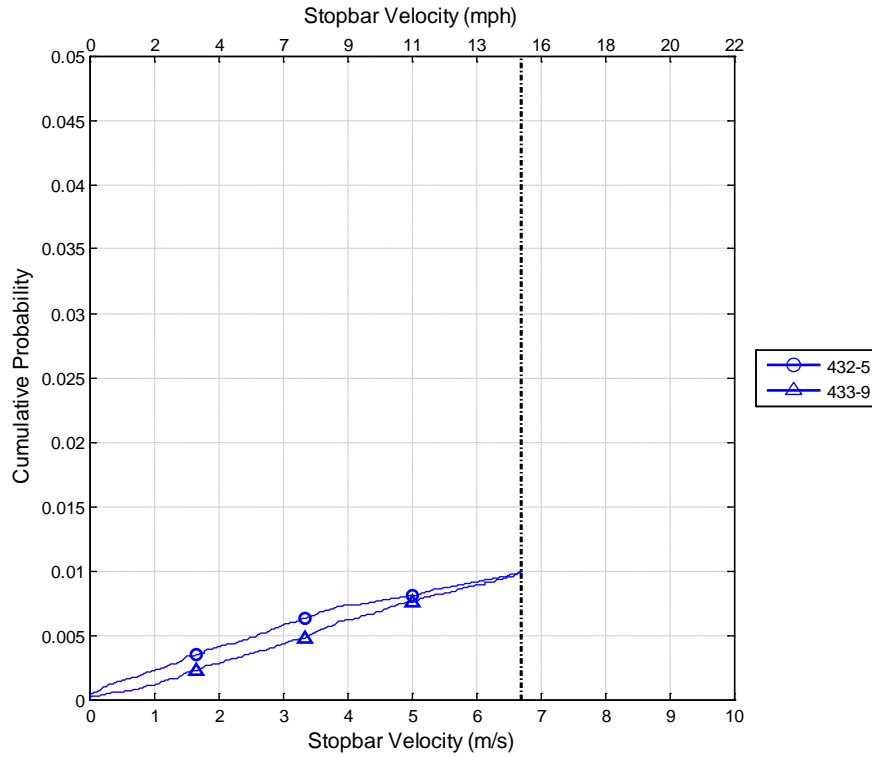


Figure 163 Cumulative distribution of the stop-bar speed for false positives produced by the 400 series algorithm at a false positive rate of 0.01 using a violation threshold of 15 mph.

Stopbar Velocity Distributions for Stop-Controlled Intersections Using an FPR of 0.01 and a 15-mph Violation Threshold

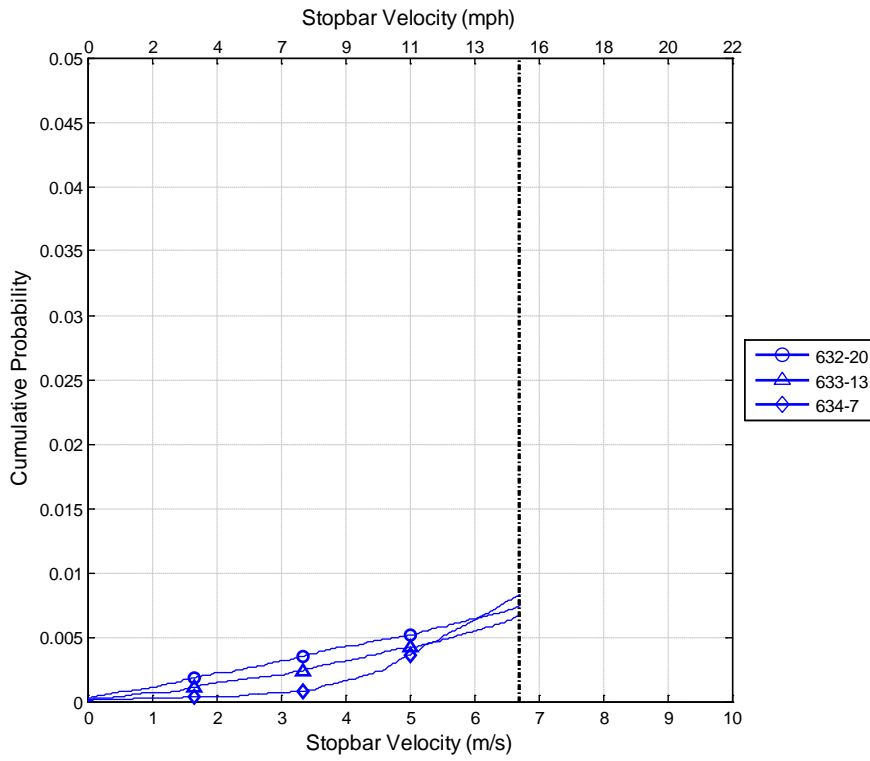


Figure 164 Cumulative distribution of the stop-bar speed for false positives produced by the 600 series algorithm at a false positive rate of 0.01 using a violation threshold of 15 mph.

Stopbar Velocity Distributions for Stop-Controlled Intersections Using an FPR of 0.01 and a 15-mph Violation Threshold

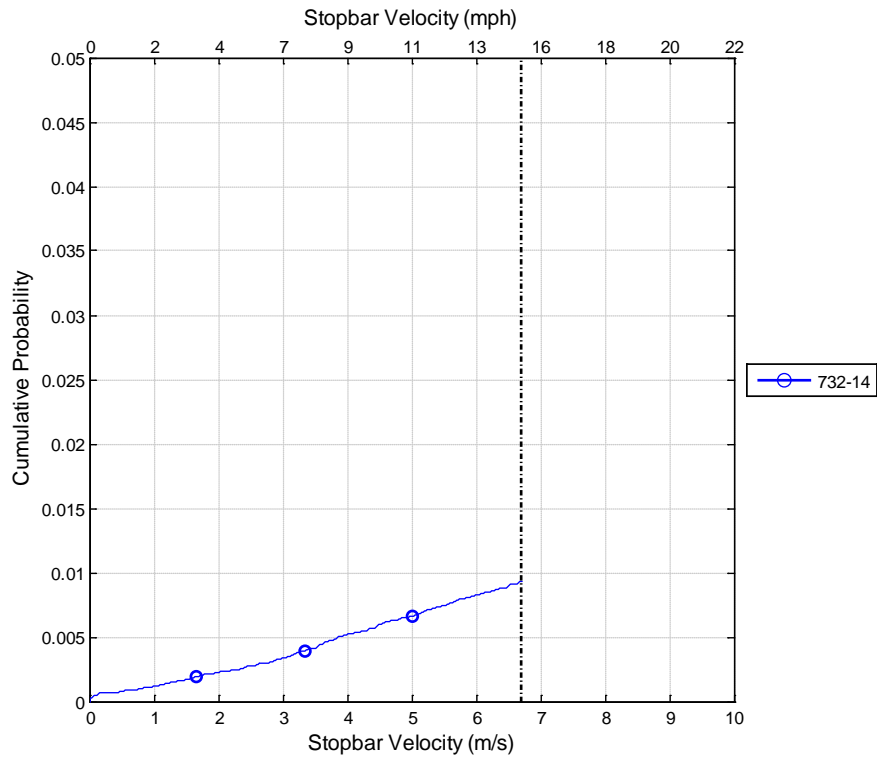


Figure 165 Cumulative distribution of the stop-bar speed for false positives produced by the 700 series algorithm at a false positive rate of 0.01 using a violation threshold of 15 mph.

Stopbar Velocity Distributions for Stop-Controlled Intersections Using an FPR of 0.01 and a 15-mph Violation Threshold

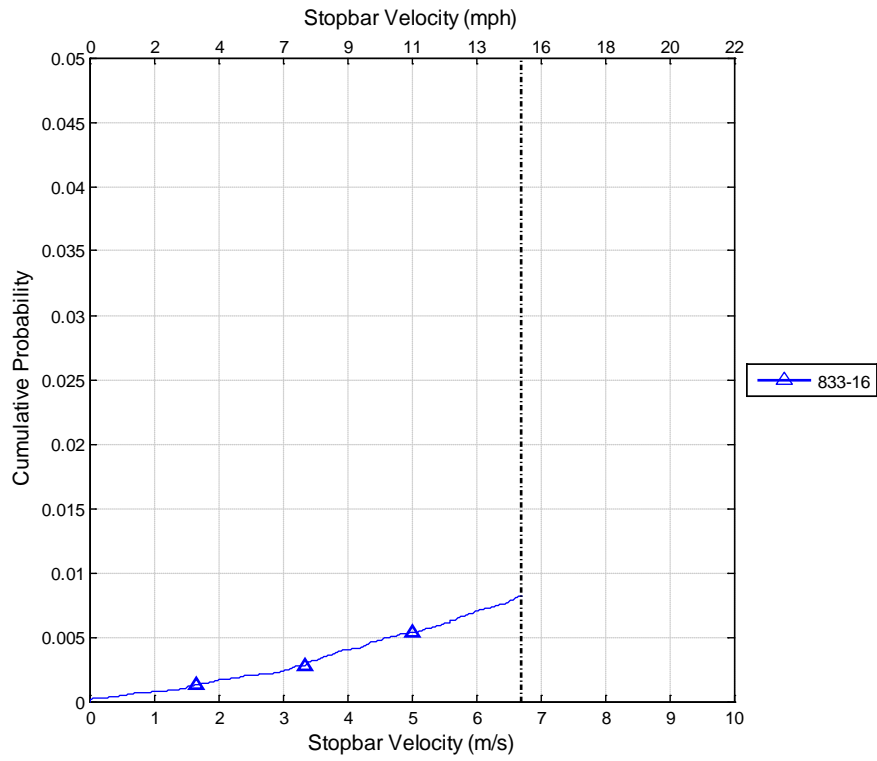


Figure 166 Cumulative distribution of the stop-bar speed for false positives produced by the 800 series algorithm at a false positive rate of 0.01 using a violation threshold of 15 mph.

Stopbar Velocity Distributions for Stop-Controlled Intersections Using an FPR of 0.01 and a 20-mph Violation Threshold

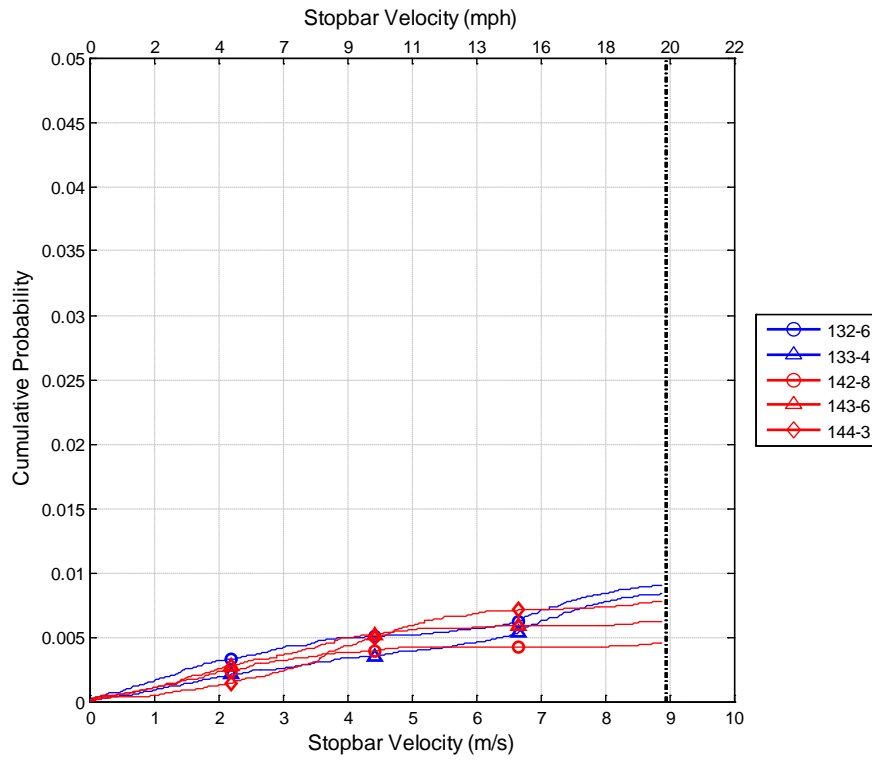


Figure 167 Cumulative distribution of the stop-bar speed for false positives produced by the 100 series algorithm at a false positive rate of 0.01 using a violation threshold of 20 mph.

Stopbar Velocity Distributions for Stop-Controlled Intersections Using an FPR of 0.01 and a 20-mph Violation Threshold

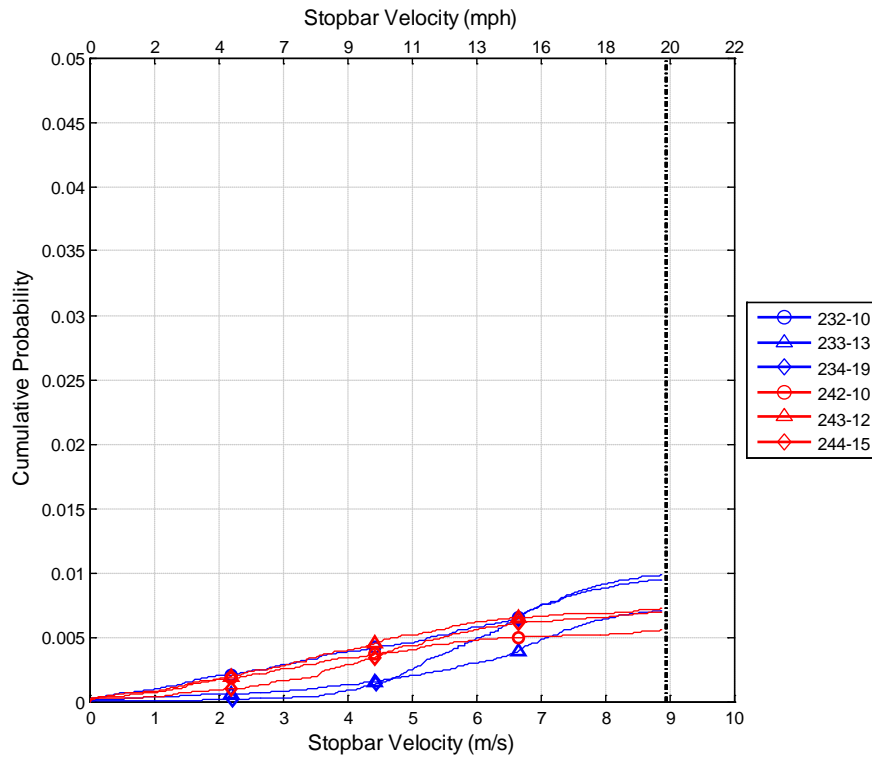


Figure 168 Cumulative distribution of the stop-bar speed for false positives produced by the 200 series algorithm at a false positive rate of 0.01 using a violation threshold of 20 mph.

Stopbar Velocity Distributions for Stop-Controlled Intersections Using an FPR of 0.01 and a 20-mph Violation Threshold

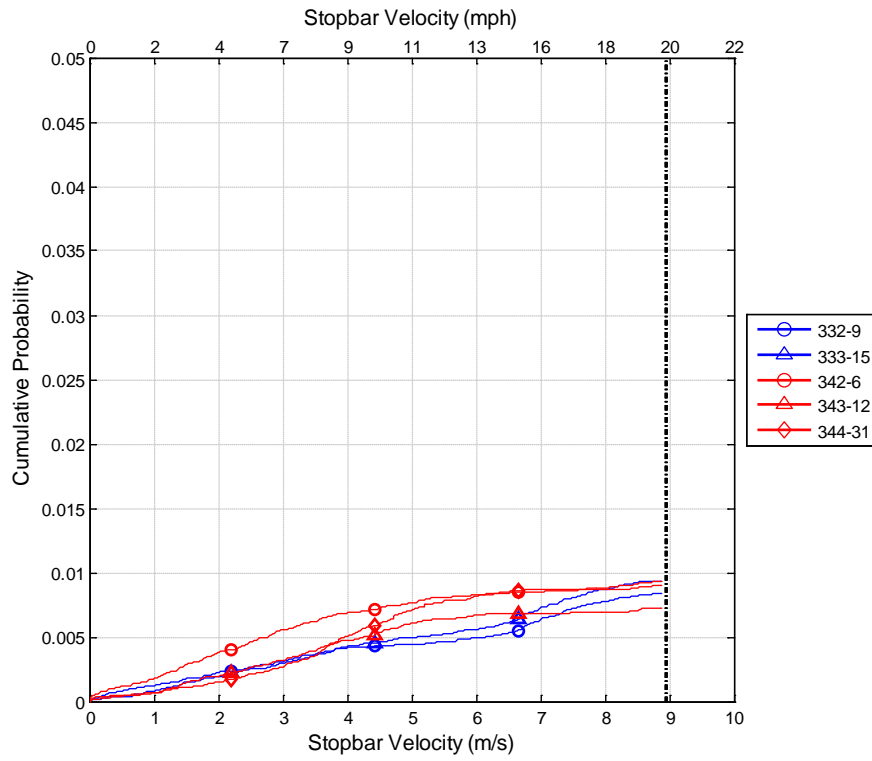


Figure 169 Cumulative distribution of the stop-bar speed for false positives produced by the 300 series algorithm at a false positive rate of 0.01 using a violation threshold of 20 mph.



Stopbar Velocity Distributions for Stop-Controlled Intersections Using an FPR of 0.01 and a 20-mph Violation Threshold

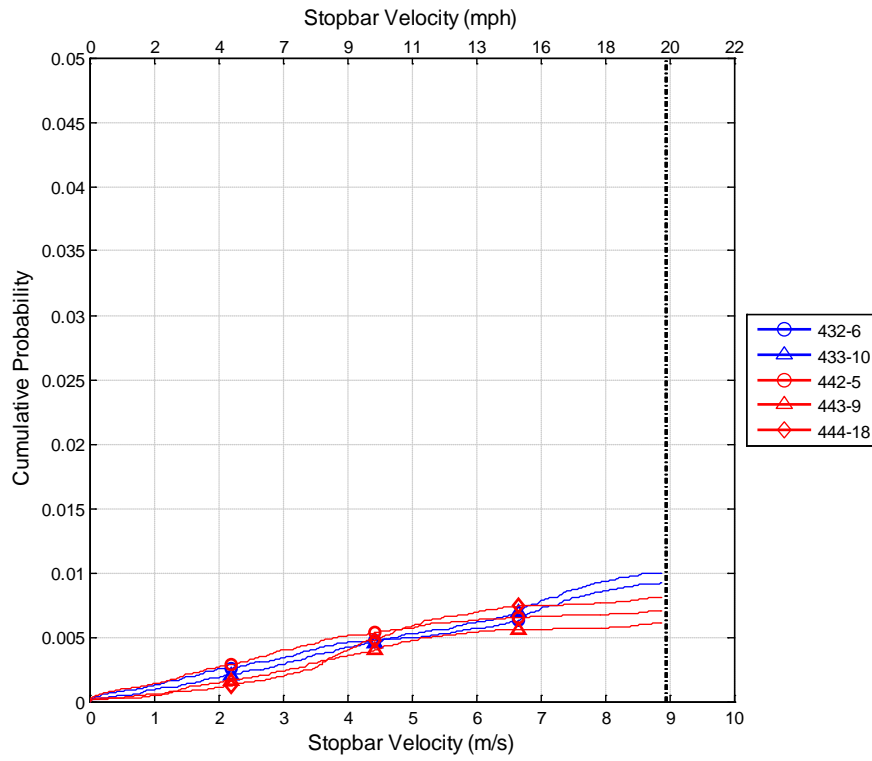


Figure 170 Cumulative distribution of the stop-bar speed for false positives produced by the 400 series algorithm at a false positive rate of 0.01 using a violation threshold of 20 mph.

Stopbar Velocity Distributions for Stop-Controlled Intersections Using an FPR of 0.01 and a 20-mph Violation Threshold

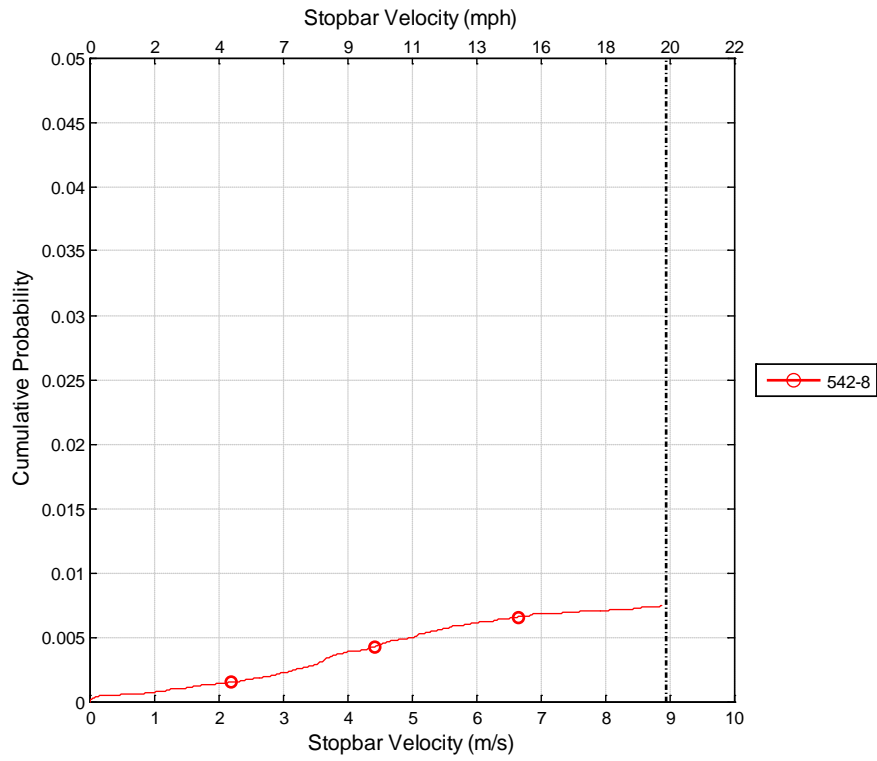


Figure 171 Cumulative distribution of the stop-bar speed for false positives produced by the 500 series algorithm at a false positive rate of 0.01 using a violation threshold of 20 mph.

Stopbar Velocity Distributions for Stop-Controlled Intersections Using an FPR of 0.01 and a 20-mph Violation Threshold

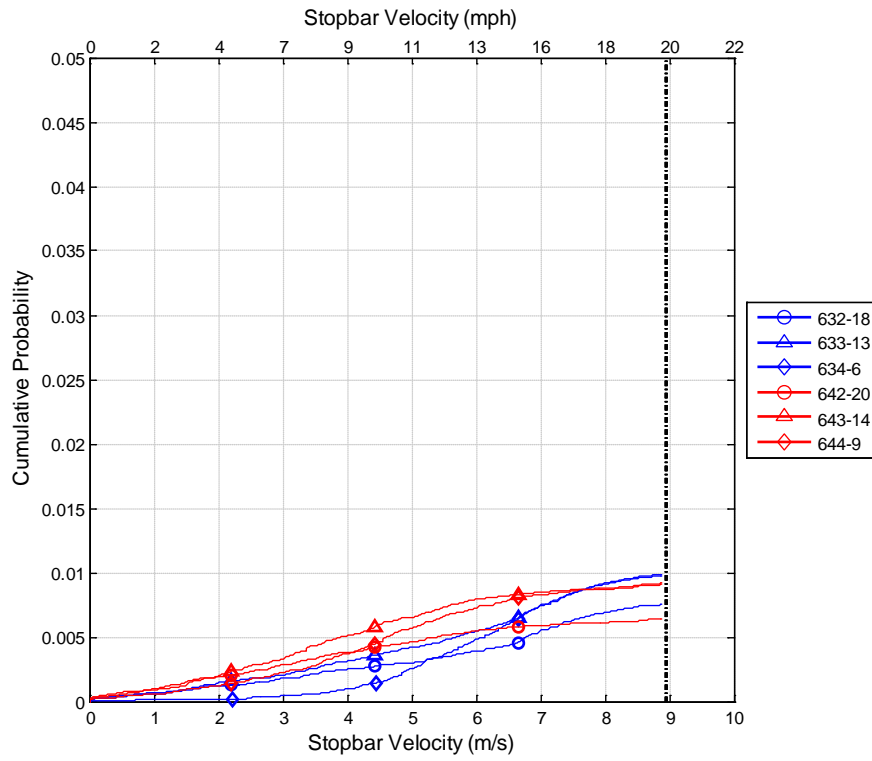


Figure 172 Cumulative distribution of the stop-bar speed for false positives produced by the 600 series algorithm at a false positive rate of 0.01 using a violation threshold of 20 mph.

Stopbar Velocity Distributions for Stop-Controlled Intersections Using an FPR of 0.01 and a 20-mph Violation Threshold

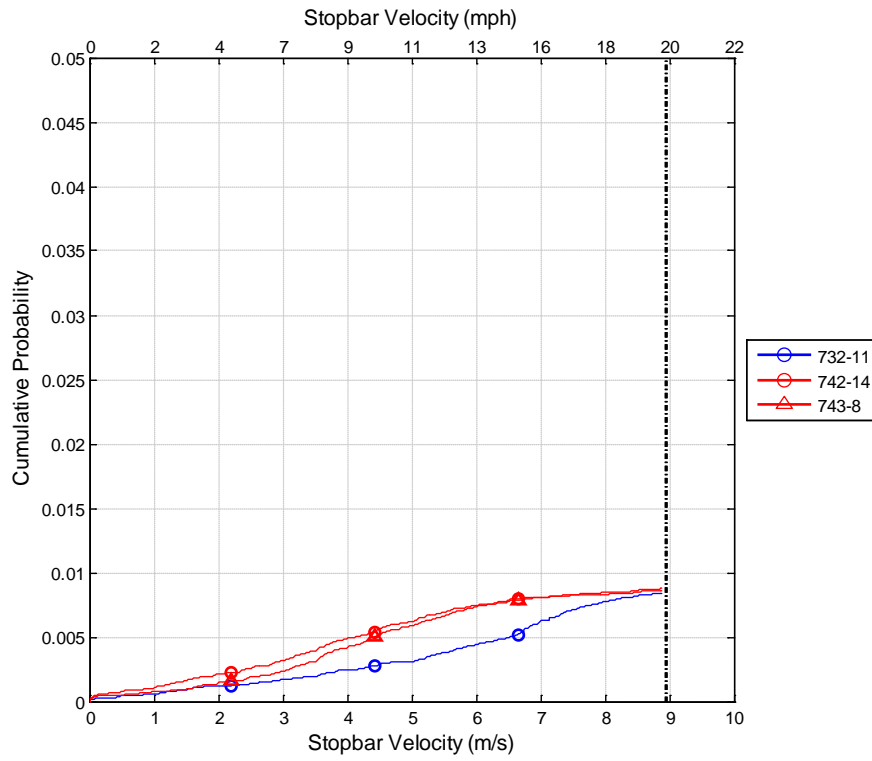


Figure 173 Cumulative distribution of the stop-bar speed for false positives produced by the 700 series algorithm at a false positive rate of 0.01 using a violation threshold of 20 mph.

Stopbar Velocity Distributions for Stop-Controlled Intersections Using an FPR of 0.01 and a 20-mph Violation Threshold

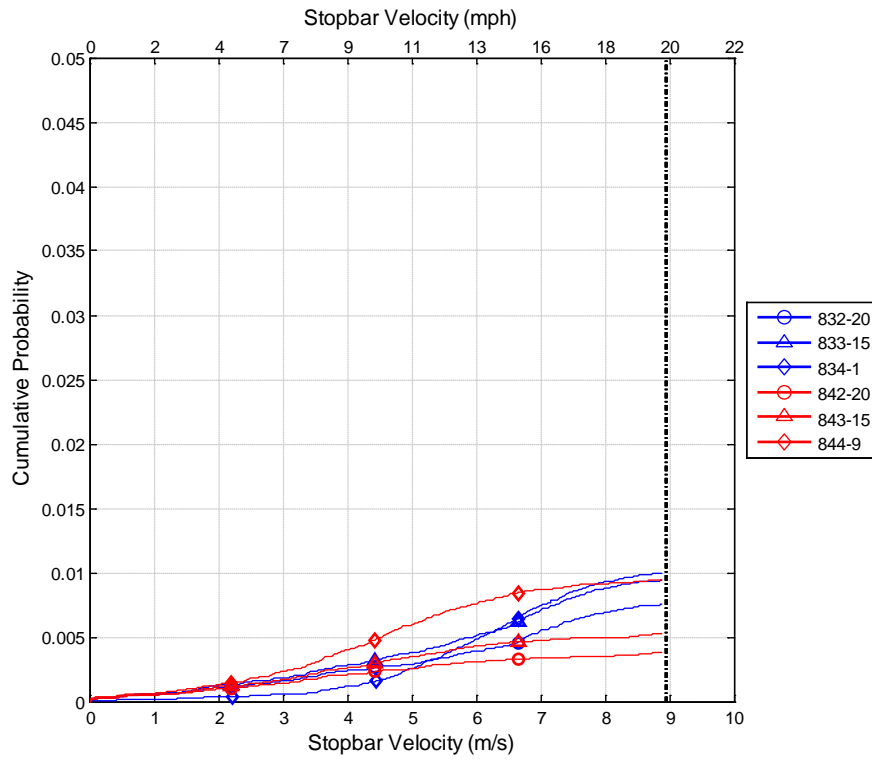


Figure 174 Cumulative distribution of the stop-bar speed for false positives produced by the 800 series algorithm at a false positive rate of 0.01 using a violation threshold of 20 mph.

Stopbar Velocity Distributions for Stop-Controlled Intersections Using an FPR of 0.05 and a 10-mph Violation Threshold

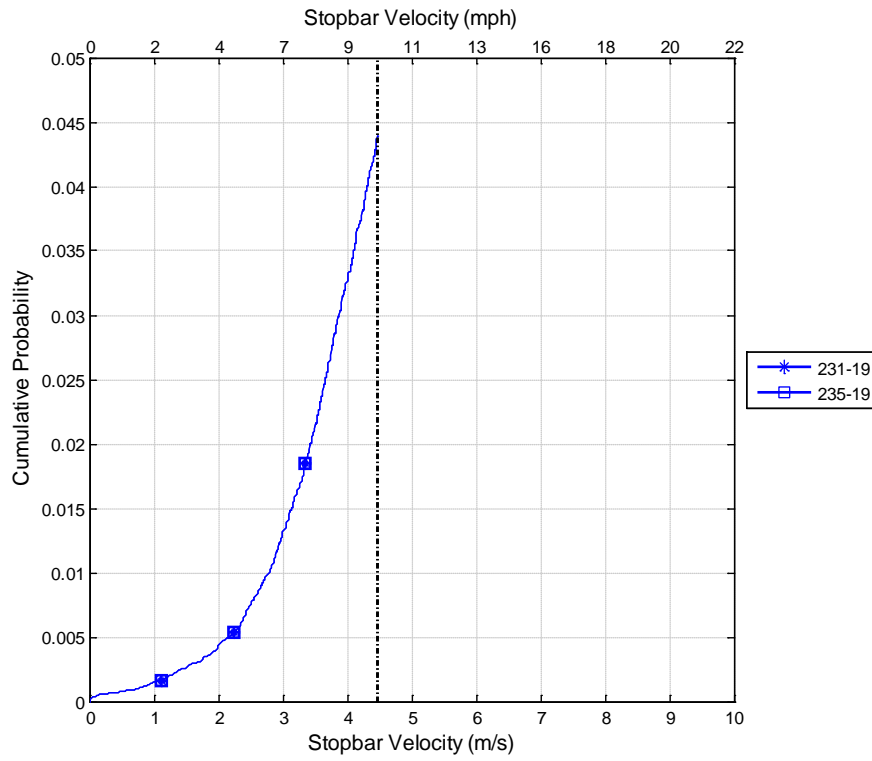


Figure 175 Cumulative distribution of the stop-bar speed for false positives produced by the 200 series algorithm at a false positive rate of 0.05 using a violation threshold of 10 mph.

Stopbar Velocity Distributions for Stop-Controlled Intersections Using an FPR of 0.05 and a 10-mph Violation Threshold

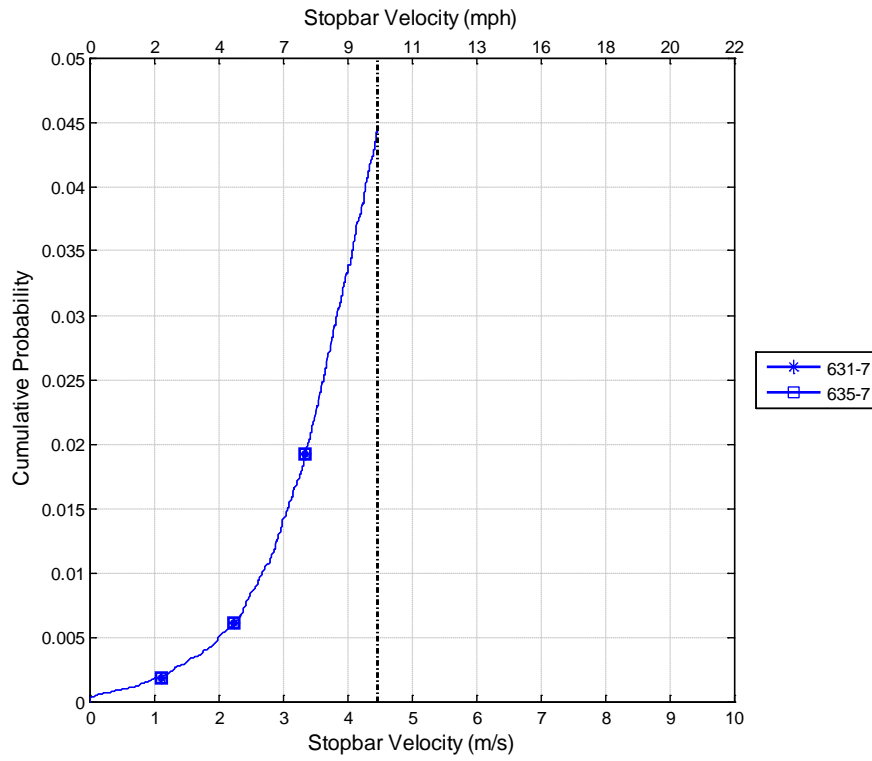


Figure 176 Cumulative distribution of the stop-bar speed for false positives produced by the 600 series algorithm at a false positive rate of 0.05 using a violation threshold of 10 mph.

Stopbar Velocity Distributions for Stop-Controlled Intersections Using an FPR of 0.05 and a 10-mph Violation Threshold

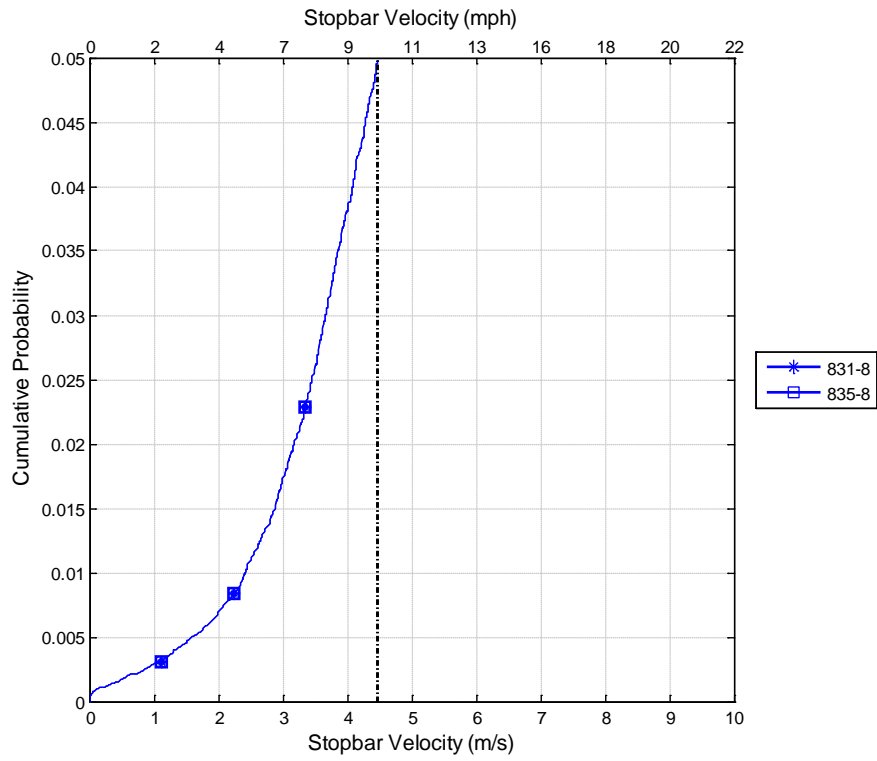


Figure 177 Cumulative distribution of the stop-bar speed for false positives produced by the 800 series algorithm at a false positive rate of 0.05 using a violation threshold of 10 mph.



Stopbar Velocity Distributions for Stop-Controlled Intersections Using an FPR of 0.05 and a 15-mph Violation Threshold

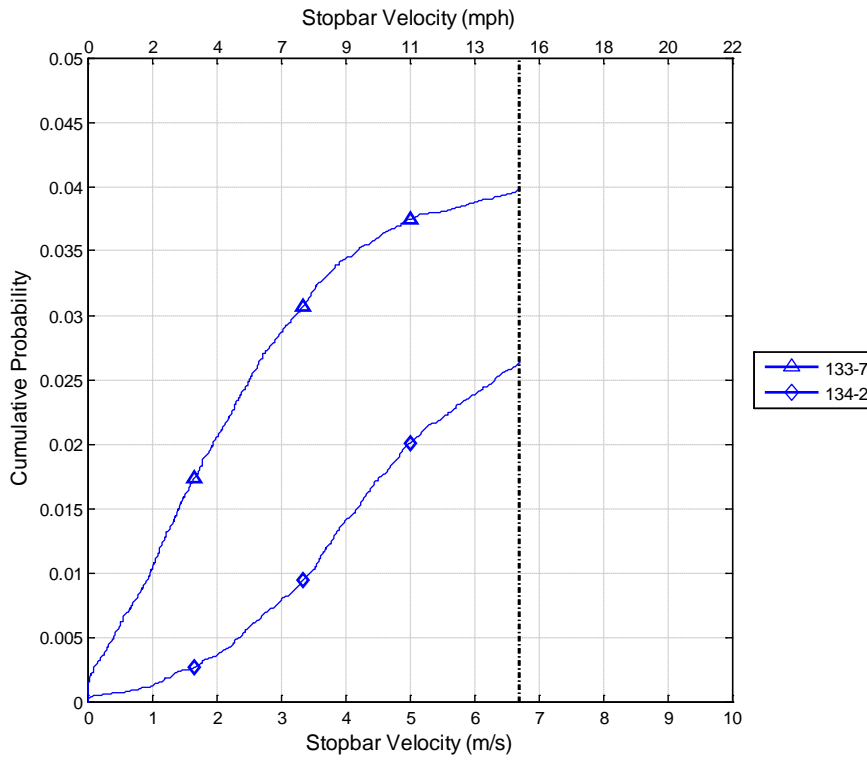


Figure 178 Cumulative distribution of the stop-bar speed for false positives produced by the 100 series algorithm at a false positive rate of 0.05 using a violation threshold of 15 mph.

Stopbar Velocity Distributions for Stop-Controlled Intersections Using an FPR of 0.05 and a 15-mph Violation Threshold

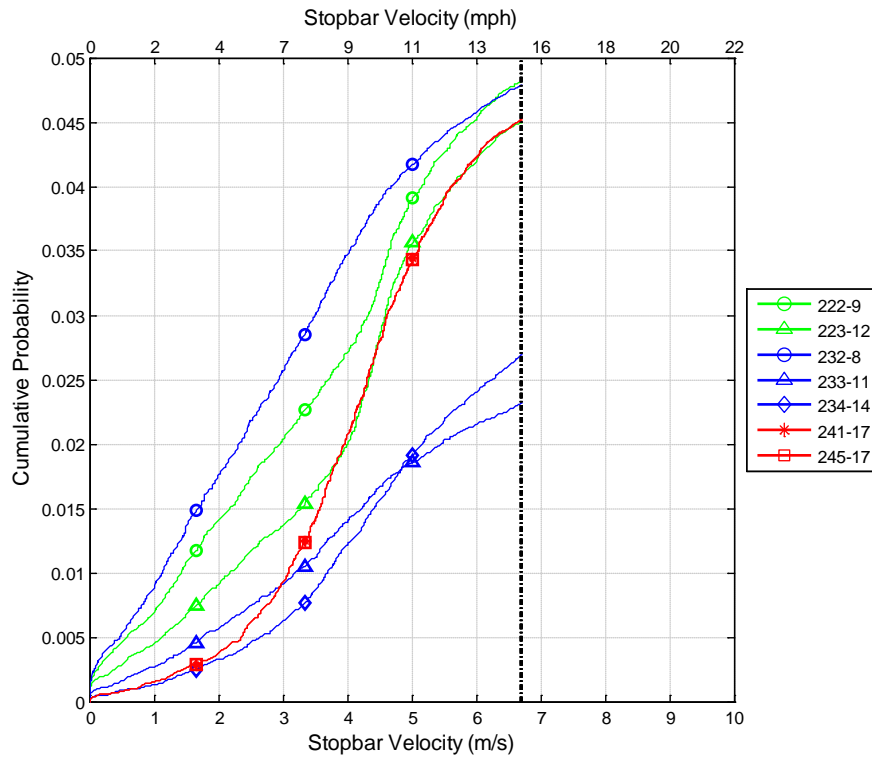


Figure 179 Cumulative distribution of the stop-bar speed for false positives produced by the 200 series algorithm at a false positive rate of 0.05 using a violation threshold of 15 mph.

Stopbar Velocity Distributions for Stop-Controlled Intersections Using an FPR of 0.05 and a 15-mph Violation Threshold

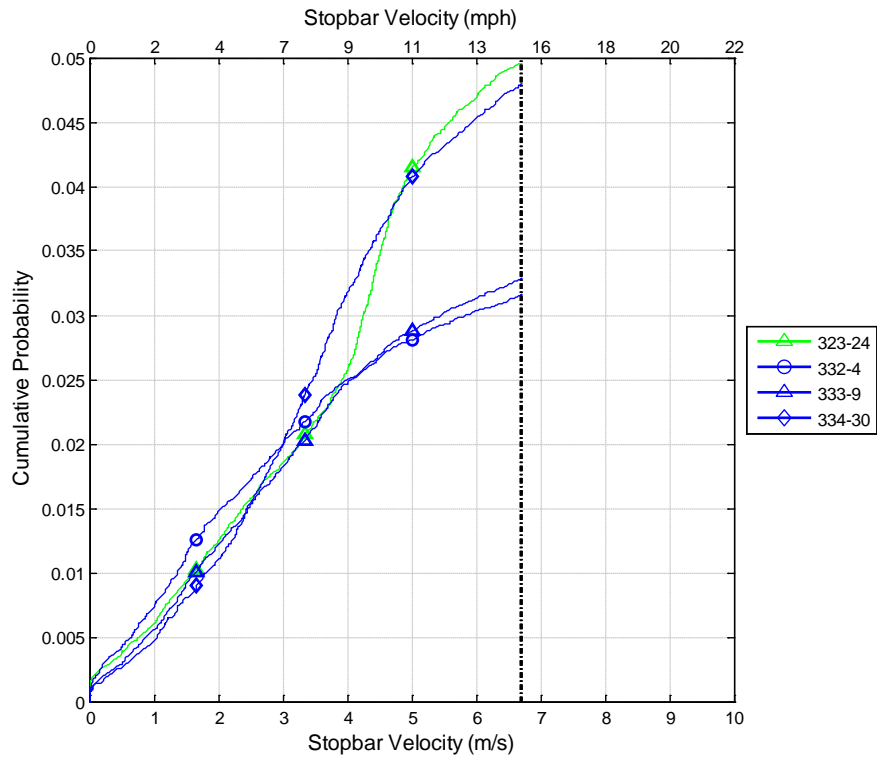


Figure 180 Cumulative distribution of the stop-bar speed for false positives produced by the 300 series algorithm at a false positive rate of 0.05 using a violation threshold of 15 mph.

Stopbar Velocity Distributions for Stop-Controlled Intersections Using an FPR of 0.05 and a 15-mph Violation Threshold

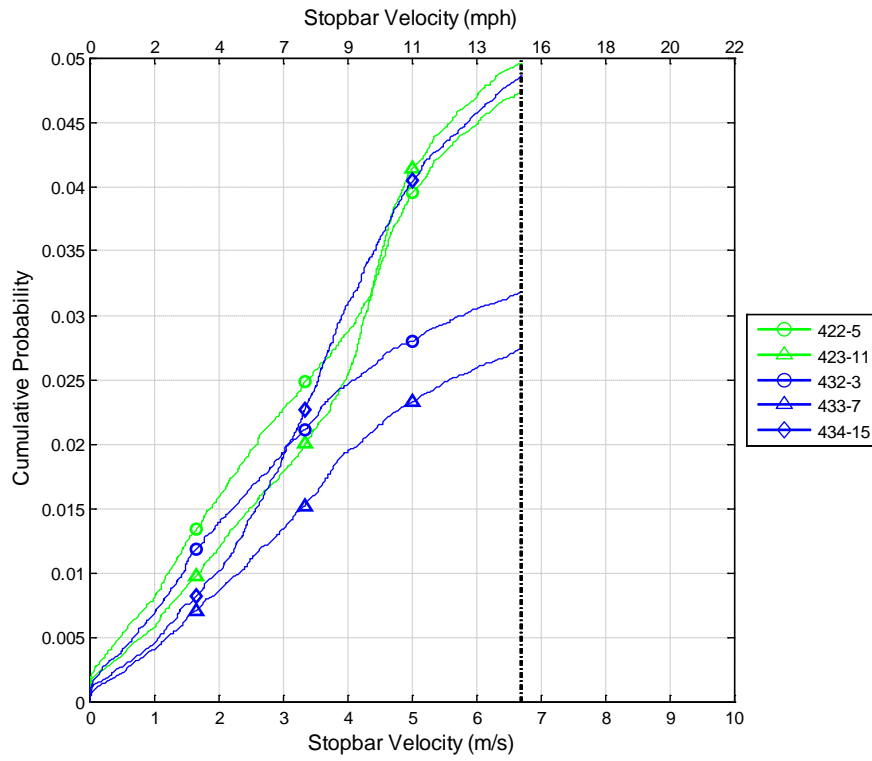


Figure 181 Cumulative distribution of the stop-bar speed for false positives produced by the 400 series algorithm at a false positive rate of 0.05 using a violation threshold of 15 mph.

Stopbar Velocity Distributions for Stop-Controlled Intersections Using an FPR of 0.05 and a 15-mph Violation Threshold

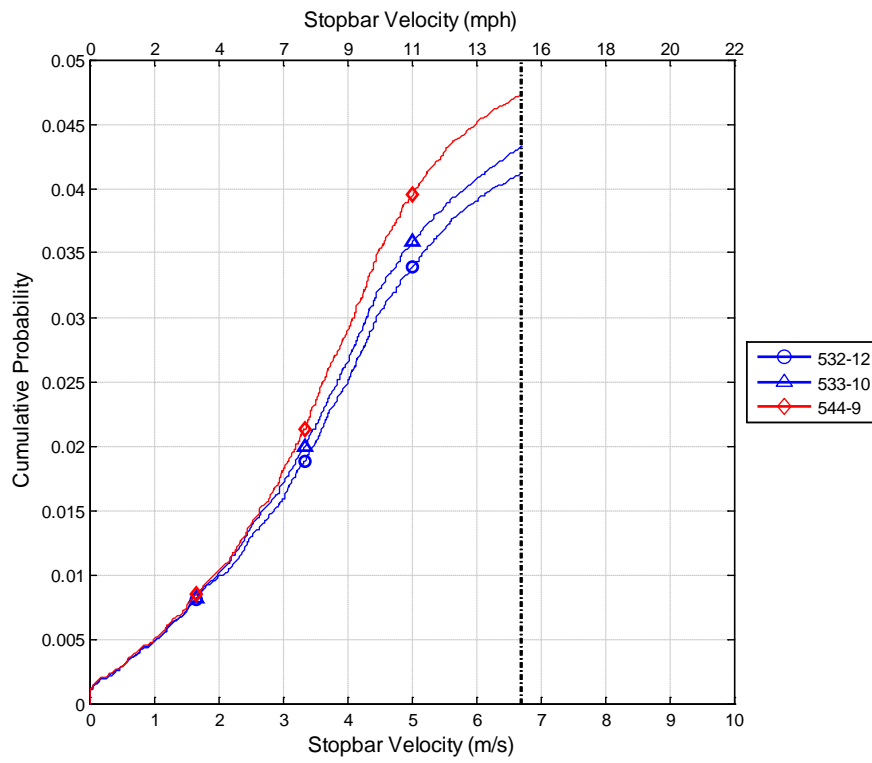


Figure 182 Cumulative distribution of the stop-bar speed for false positives produced by the 500 series algorithm at a false positive rate of 0.05 using a violation threshold of 15 mph.

Stopbar Velocity Distributions for Stop-Controlled Intersections Using an FPR of 0.05 and a 15-mph Violation Threshold

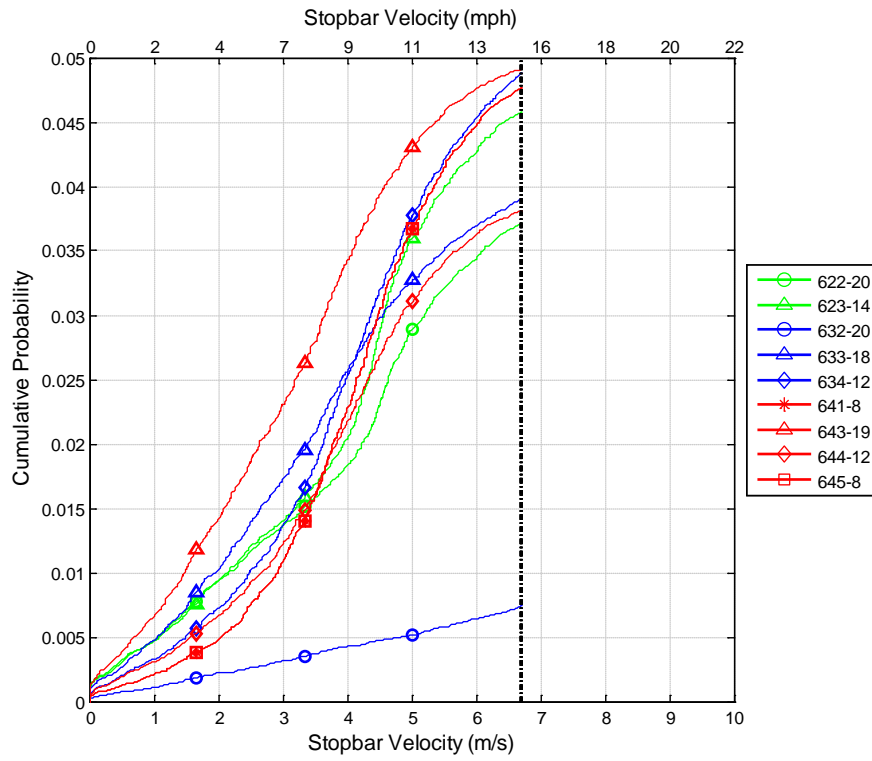


Figure 183 Cumulative distribution of the stop-bar speed for false positives produced by the 600 series algorithm at a false positive rate of 0.05 using a violation threshold of 15 mph.

Stopbar Velocity Distributions for Stop-Controlled Intersections Using an FPR of 0.05 and a 15-mph Violation Threshold

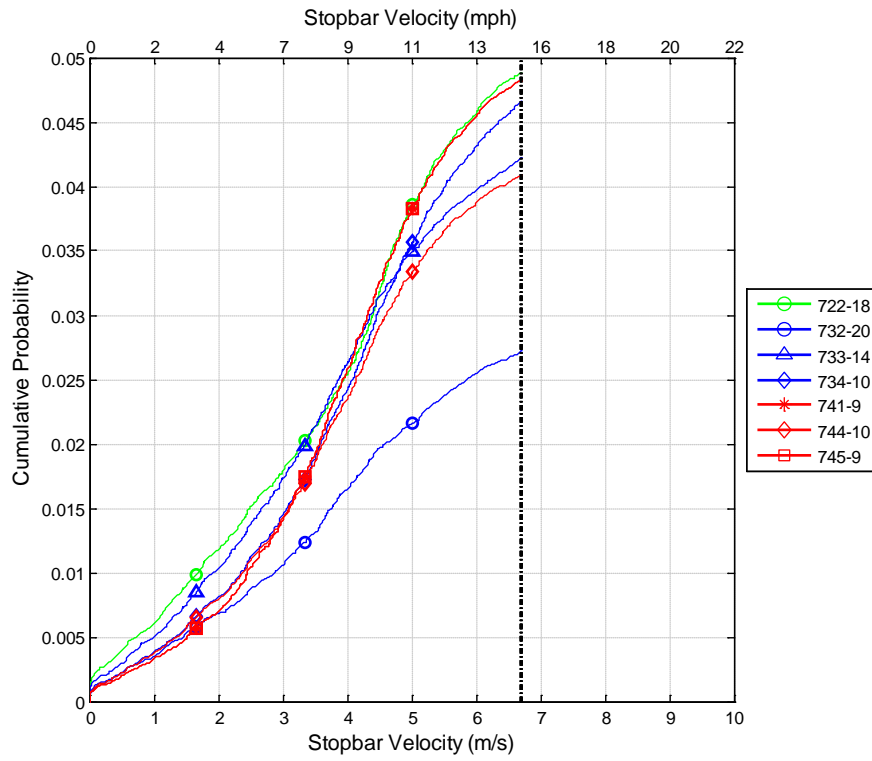


Figure 184 Cumulative distribution of the stop-bar speed for false positives produced by the 700 series algorithm at a false positive rate of 0.05 using a violation threshold of 15 mph.

Stopbar Velocity Distributions for Stop-Controlled Intersections Using an FPR of 0.05 and a 15-mph Violation Threshold

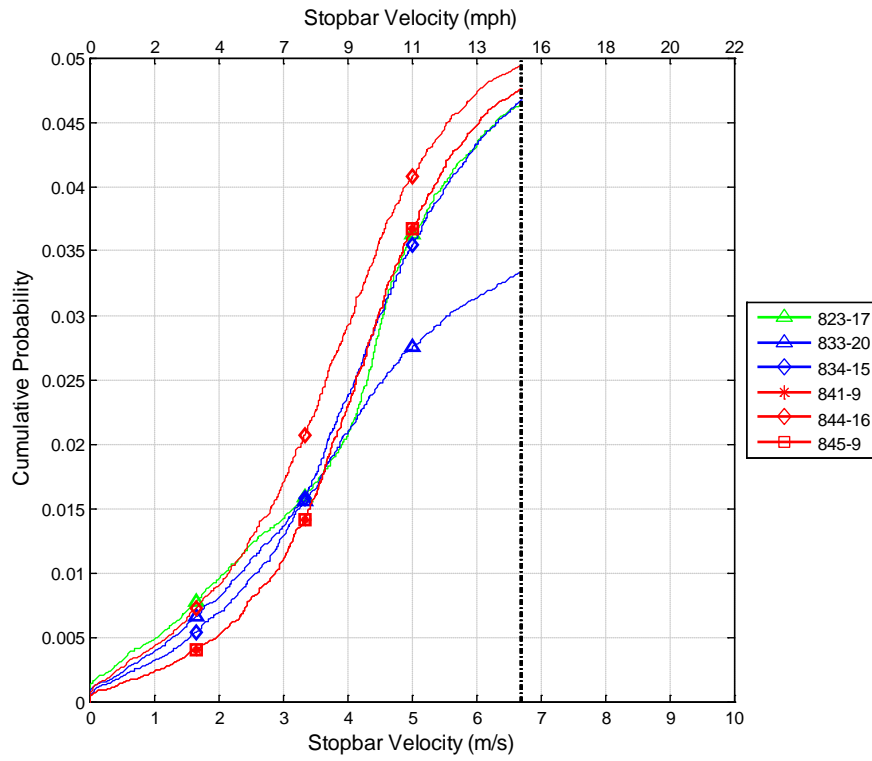


Figure 185 Cumulative distribution of the stop-bar speed for false positives produced by the 800 series algorithm at a false positive rate of 0.05 using a violation threshold of 15 mph.



Stopbar Velocity Distributions for Stop-Controlled Intersections Using an FPR of 0.05 and a 20-mph Violation Threshold

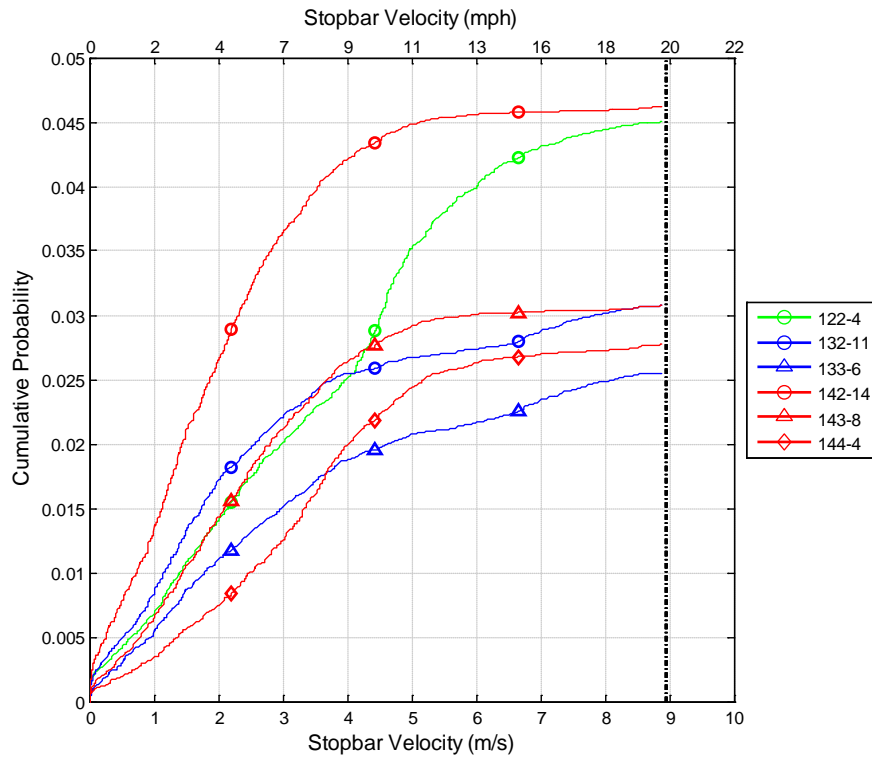


Figure 186 Cumulative distribution of the stop-bar speed for false positives produced by the 100 series algorithm at a false positive rate of 0.05 using a violation threshold of 20 mph.

Stopbar Velocity Distributions for Stop-Controlled Intersections Using an FPR of 0.05 and a 20-mph Violation Threshold

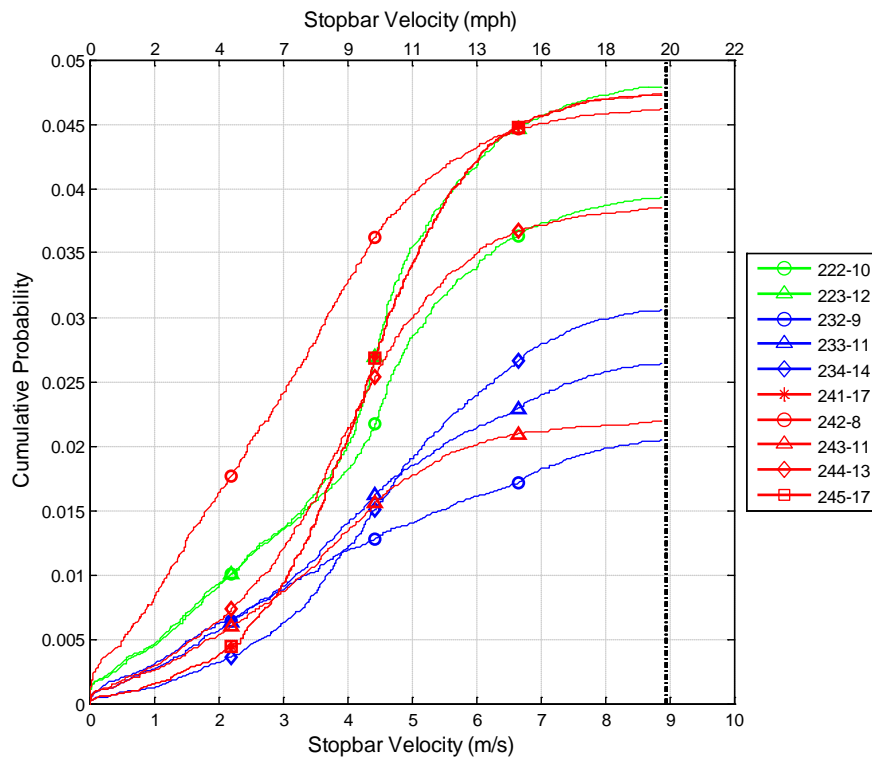


Figure 187 Cumulative distribution of the stop-bar speed for false positives produced by the 200 series algorithm at a false positive rate of 0.05 using a violation threshold of 20 mph.

Stopbar Velocity Distributions for Stop-Controlled Intersections Using an FPR of 0.05 and a 20-mph Violation Threshold

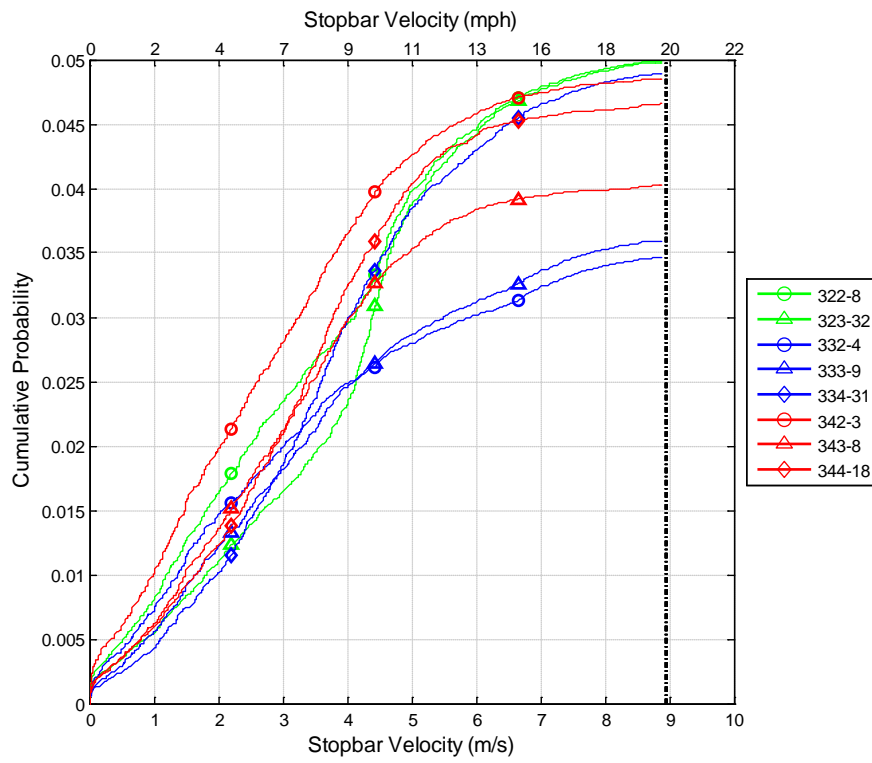


Figure 188 Cumulative distribution of the stop-bar speed for false positives produced by the 300 series algorithm at a false positive rate of 0.05 using a violation threshold of 20 mph.

Stopbar Velocity Distributions for Stop-Controlled Intersections Using an FPR of 0.05 and a 20-mph Violation Threshold

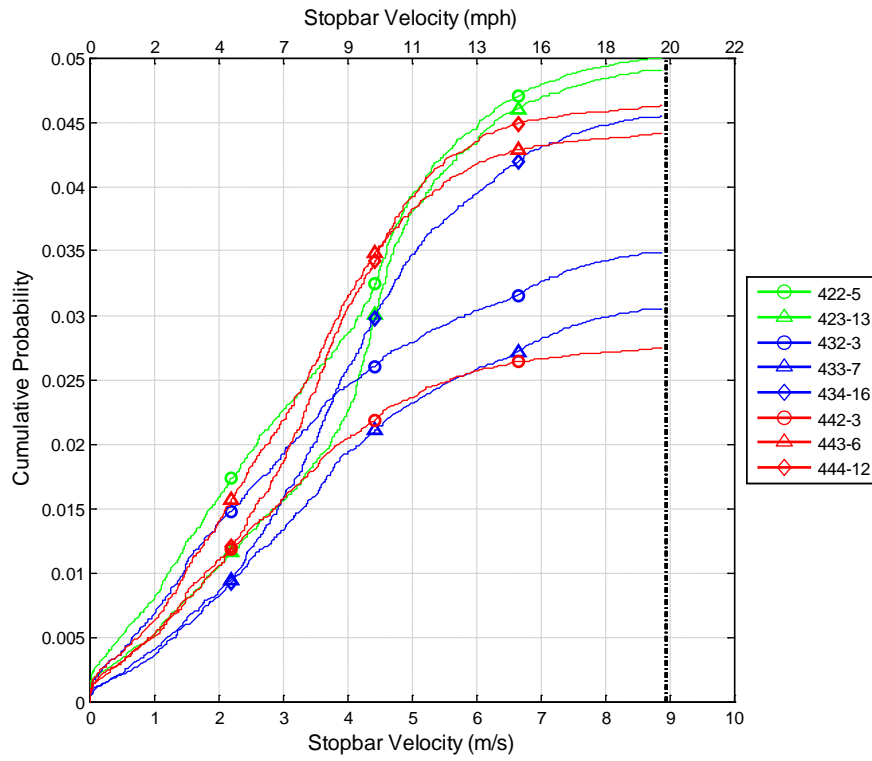


Figure 189 Cumulative distribution of the stop-bar speed for false positives produced by the 400 series algorithm at a false positive rate of 0.05 using a violation threshold of 20 mph.

Stopbar Velocity Distributions for Stop-Controlled Intersections Using an FPR of 0.05 and a 20-mph Violation Threshold

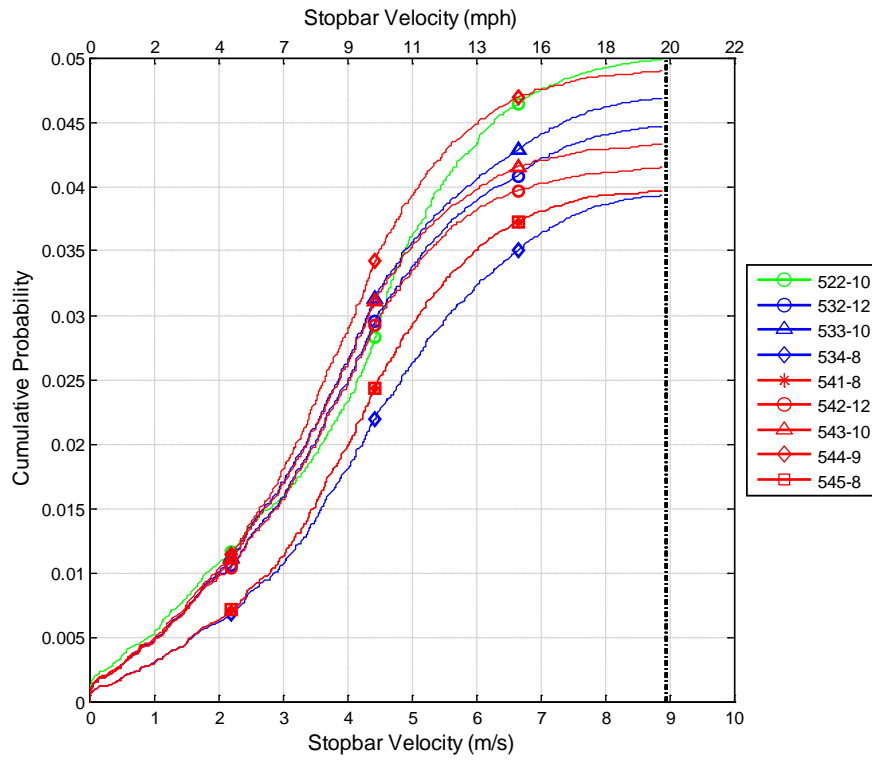
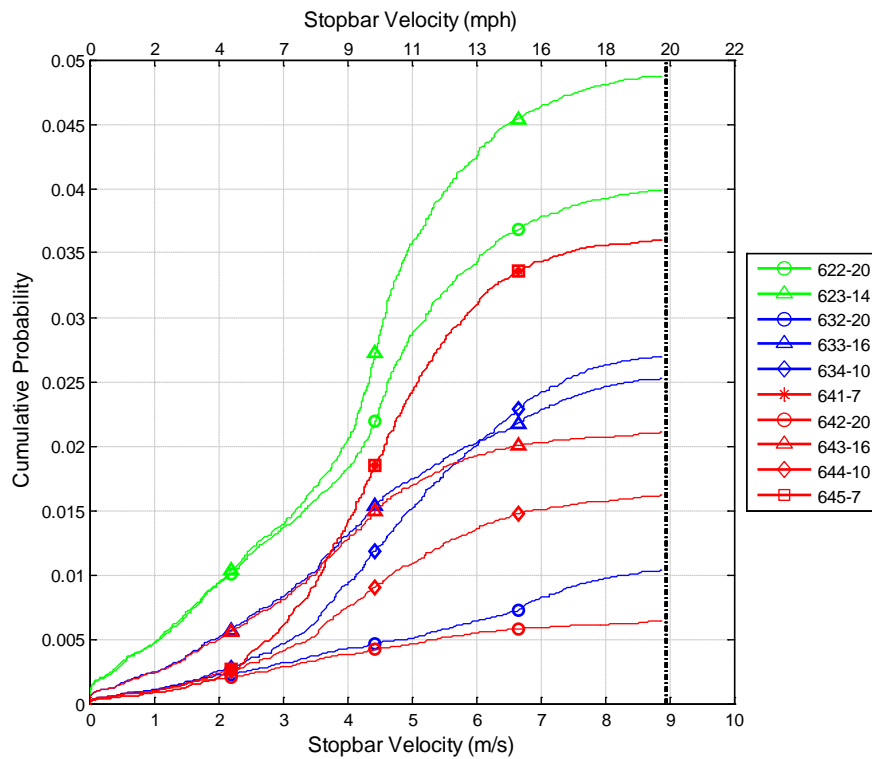


Figure 190 Cumulative distribution of the stop-bar speed for false positives produced by the 500 series algorithm at a false positive rate of 0.05 using a violation threshold of 20 mph.



Stopbar Velocity Distributions for Stop-Controlled Intersections Using an FPR of 0.05 and a 20-mph Violation Threshold

Figure 191 Cumulative distribution of the stop-bar speed for false positives produced by the 600 series algorithm at a false positive rate of 0.05 using a violation threshold of 20 mph.

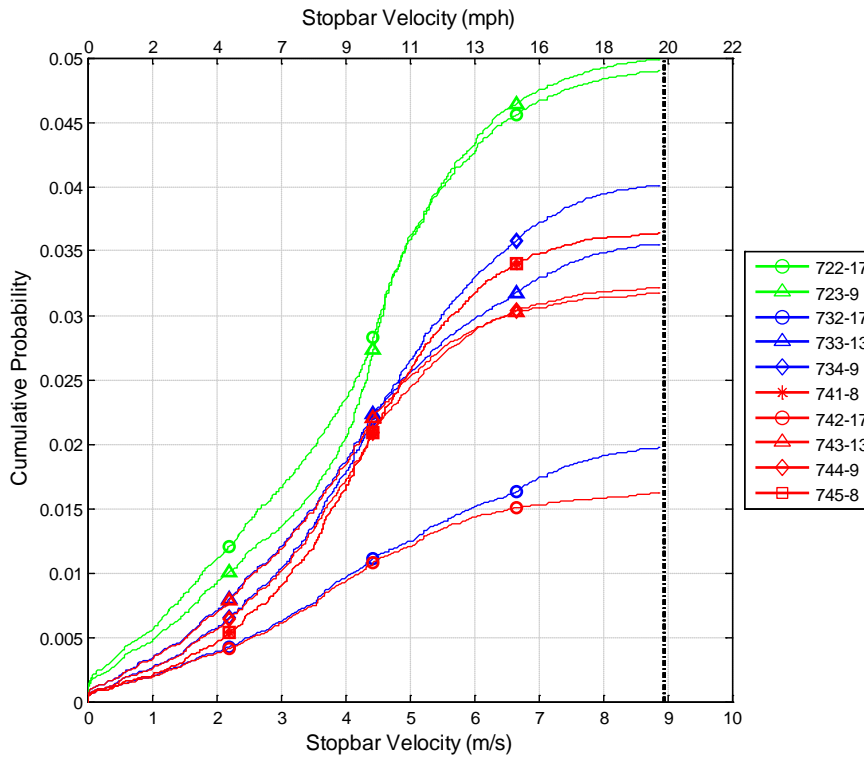


Figure 192 Cumulative distribution of the stop-bar speed for false positives produced by the 700 series algorithm at a false positive rate of 0.05 using a violation threshold of 20 mph.

Stopbar Velocity Distributions for Stop-Controlled Intersections Using an FPR of 0.05 and a 20-mph Violation Threshold

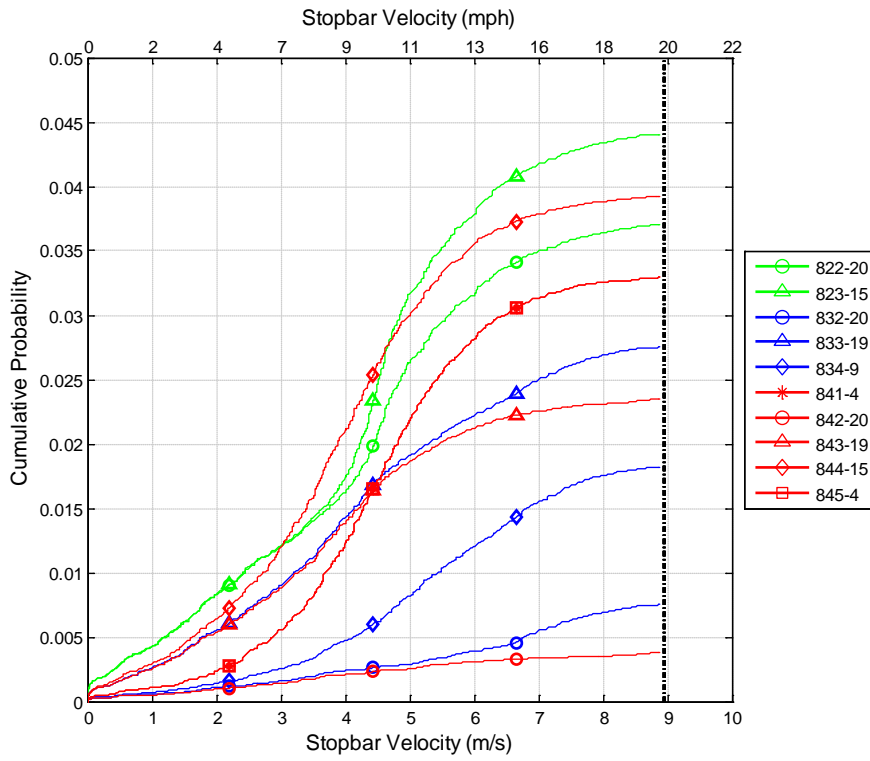


Figure 193 Cumulative distribution of the stop-bar speed for false positives produced by the 800 series algorithm at a false positive rate of 0.05 using a violation threshold of 20 mph.

### 11.17 Appendix Q: ROC Curves for Signalized Algorithms

ROC Curves for Signalized Intersections Using the 10-mph Violation Threshold

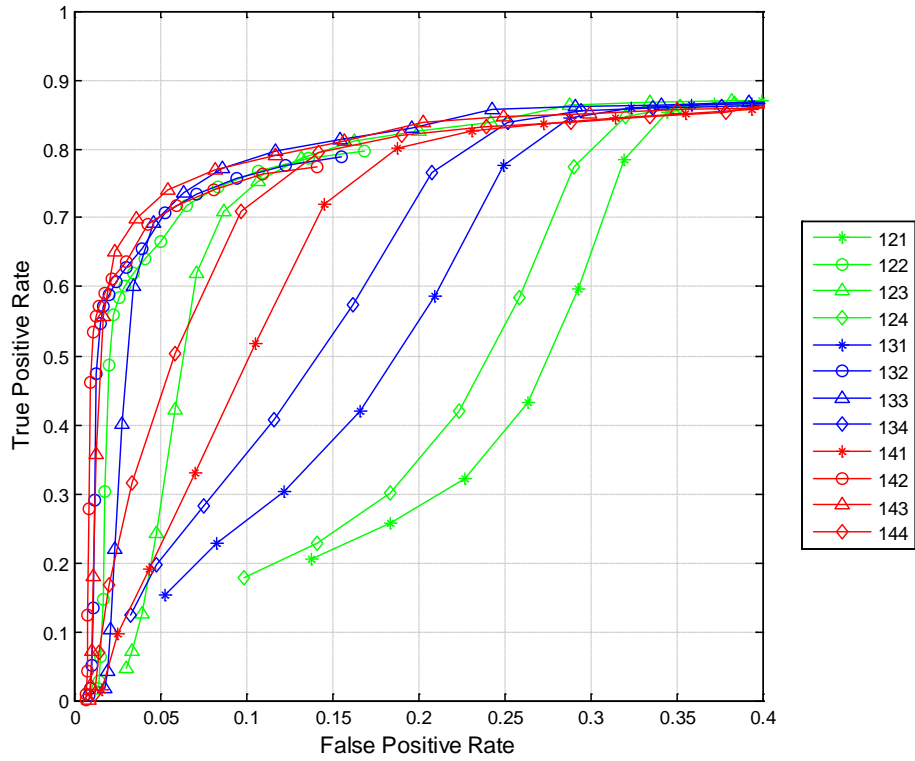


Figure 194 ROC curve for the 100 series algorithm family using a violation threshold of 10 mph.



ROC Curves for Signalized Intersections Using the 10-mph Violation Threshold

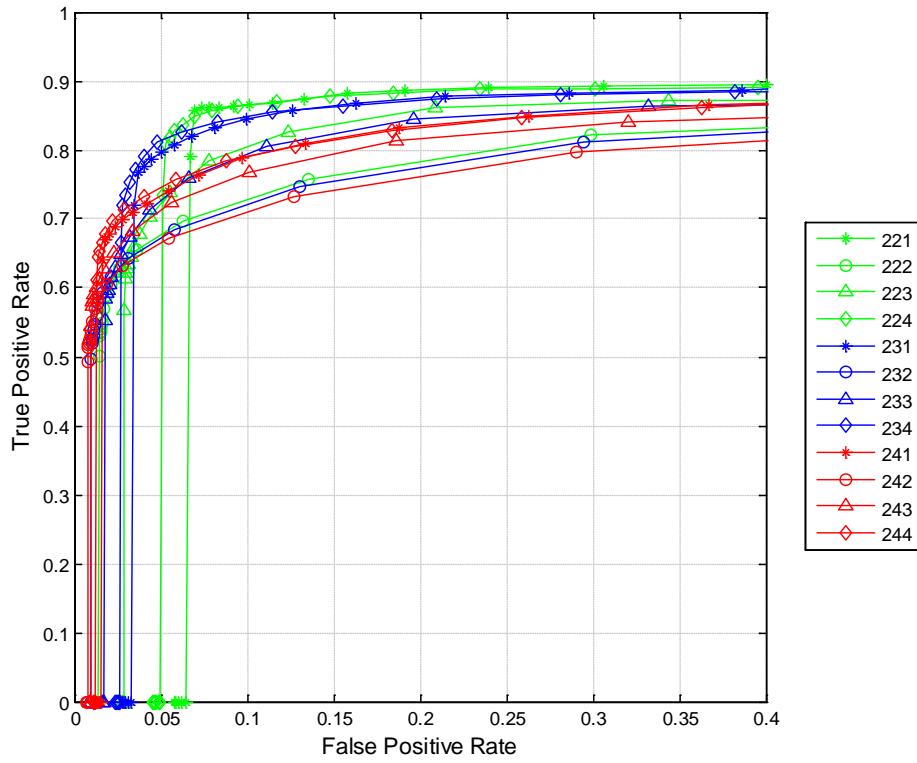


Figure 195 ROC curve for the 200 series algorithm family using a violation threshold of 10 mph.

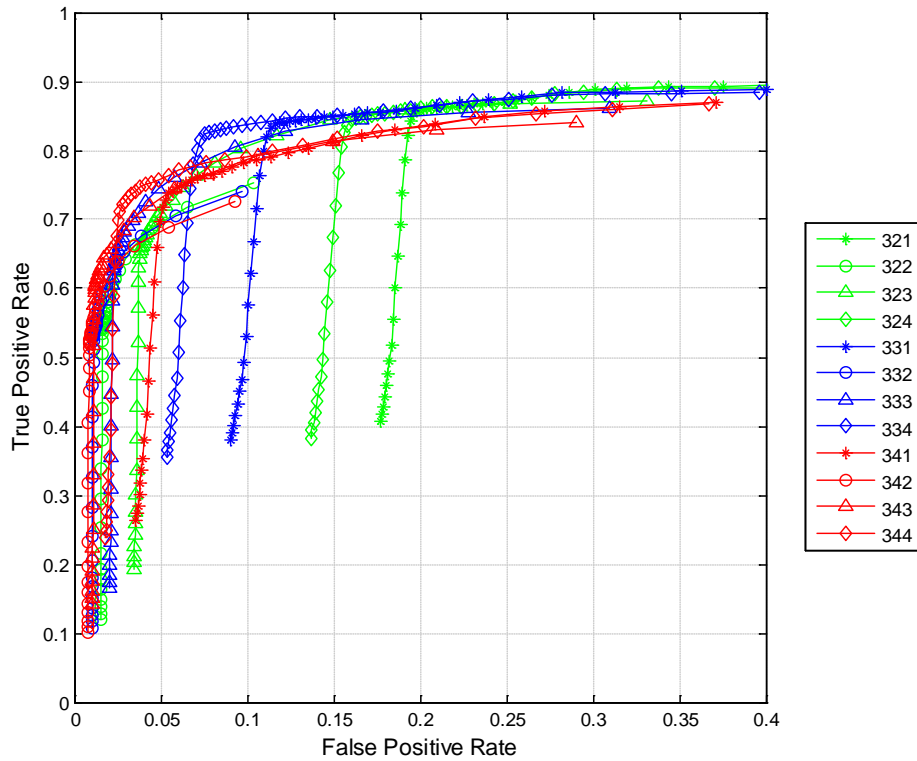


Figure 196 ROC curve for the 300 series algorithm family using a violation threshold of 10 mph.

ROC Curves for Signalized Intersections Using the 10-mph Violation Threshold

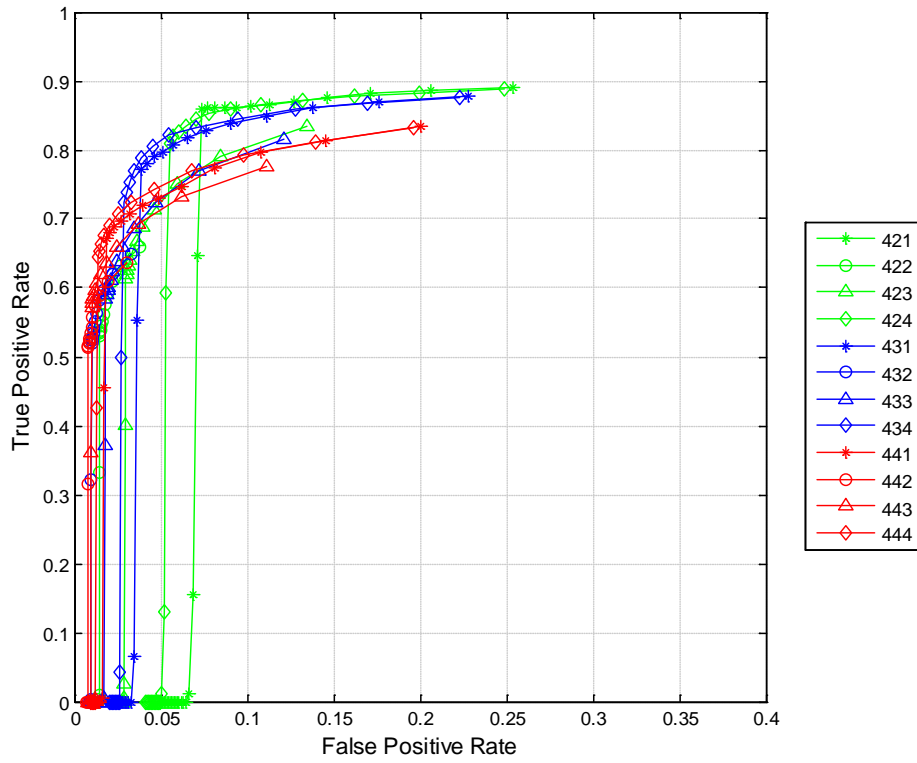


Figure 197 ROC curve for the 400 series algorithm family using a violation threshold of 10 mph.

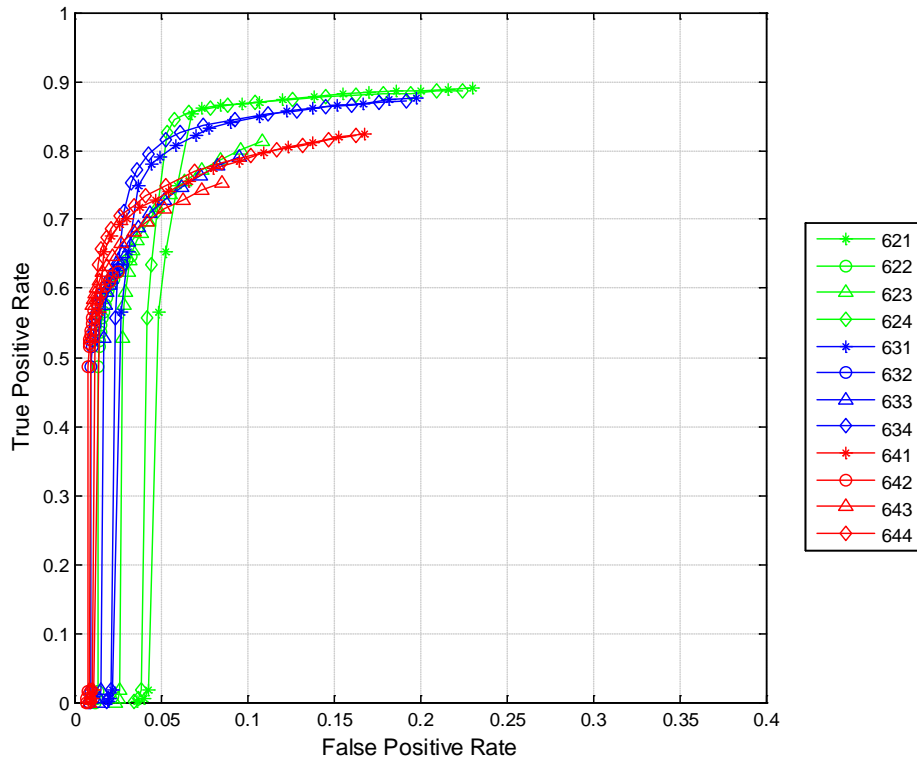


Figure 198 ROC curve for the 600 series algorithm family using a violation threshold of 10 mph.

ROC Curves for Signalized Intersections Using the 10-mph Violation Threshold

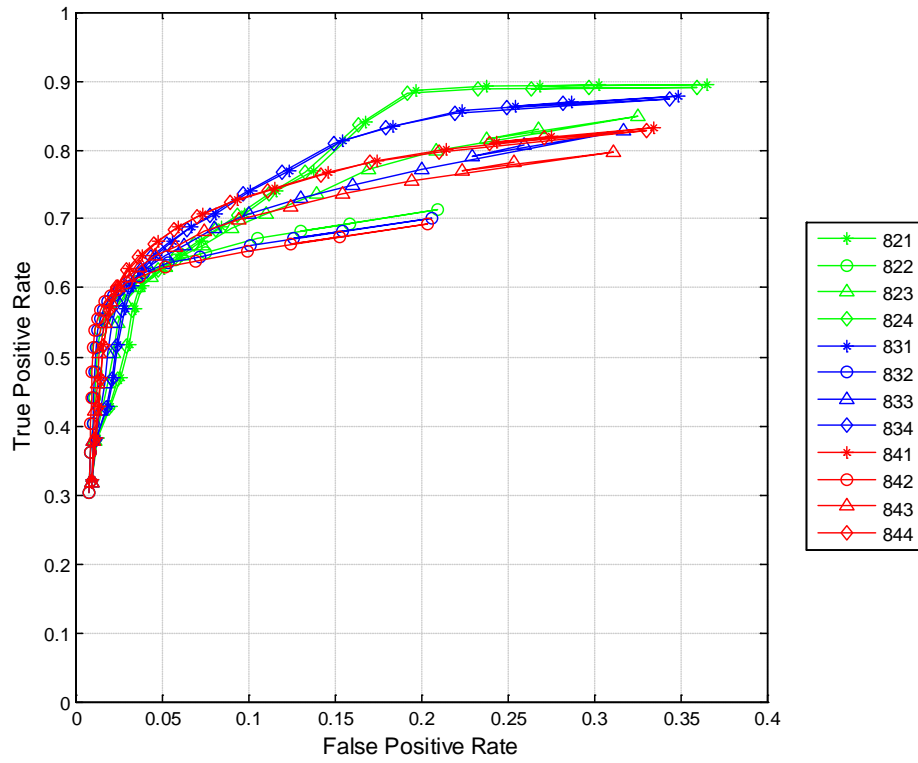


Figure 199 ROC curve for 800 series algorithm family using a violation threshold of 10 mph.

ROC Curves for Signalized Intersections Using the 15-mph Violation Threshold

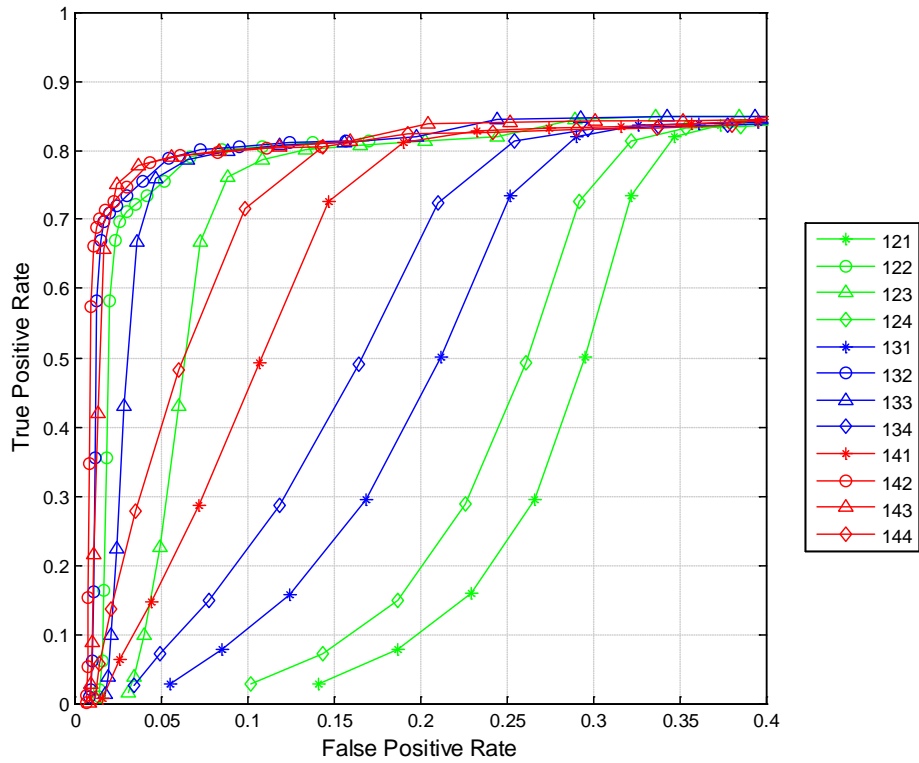


Figure 200 ROC curve for 100 series algorithm family using a violation threshold of 15 mph.

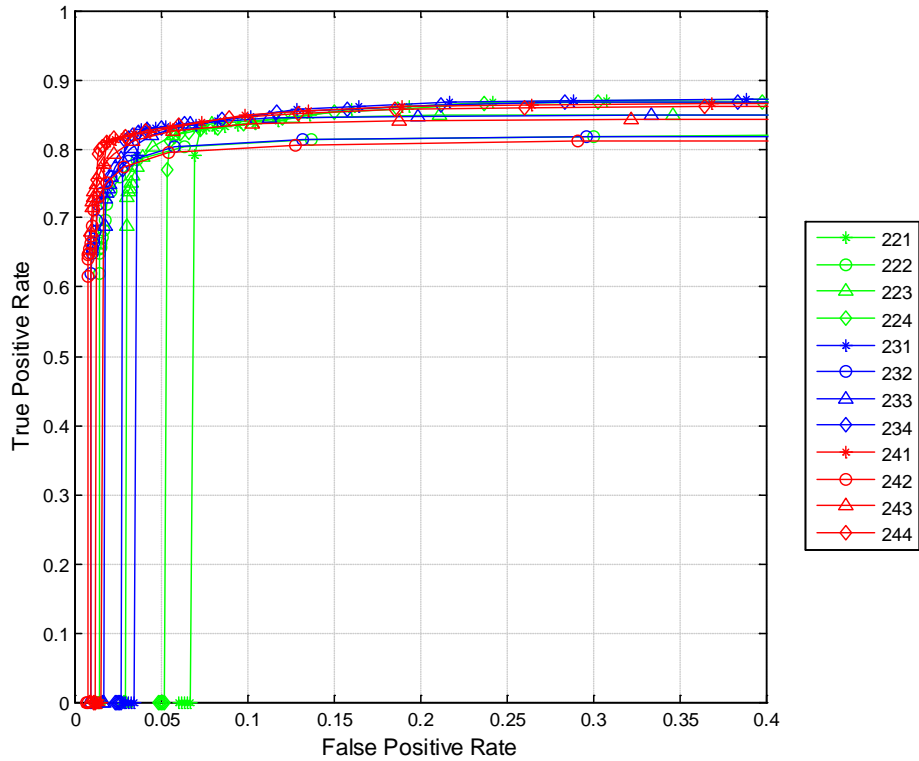


Figure 201 ROC curve for 200 series algorithm family using a violation threshold of 15 mph.

ROC Curves for Signalized Intersections Using the 15-mph Violation Threshold

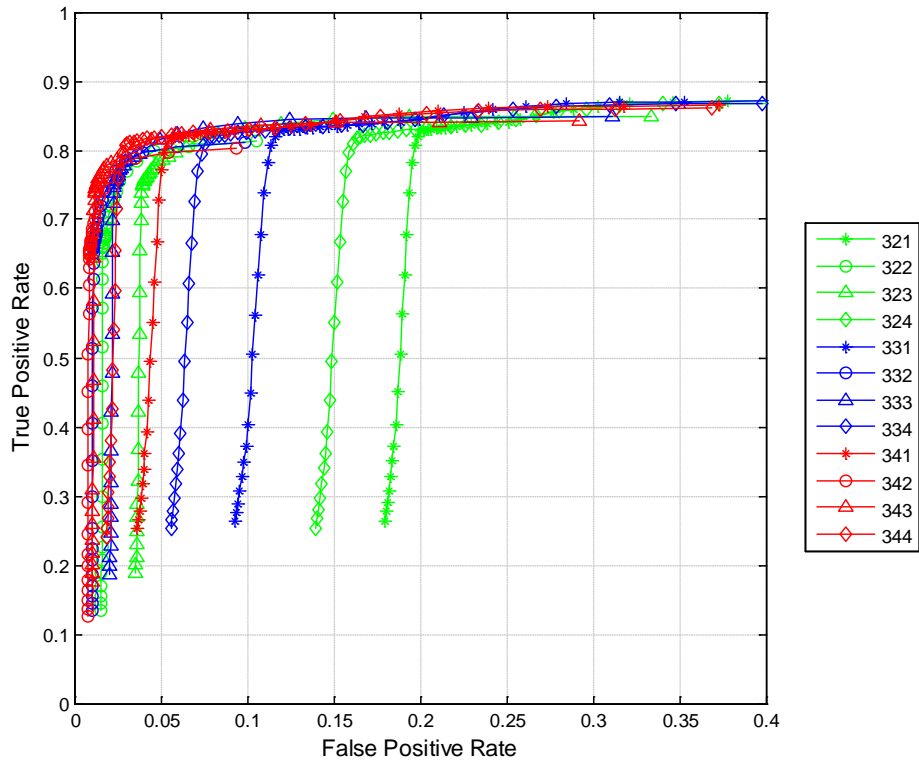


Figure 202 ROC curve for 300 series algorithm family using a violation threshold of 15 mph.

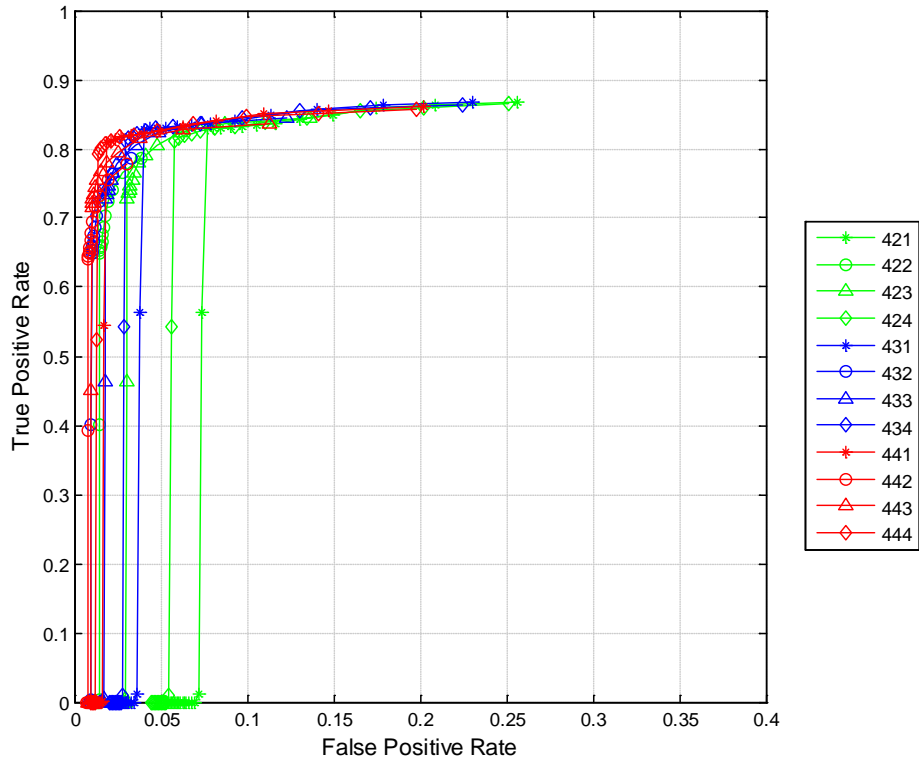


Figure 203 ROC curve for 400 series algorithm family using a violation threshold of 15 mph.

ROC Curves for Signalized Intersections Using the 15-mph Violation Threshold

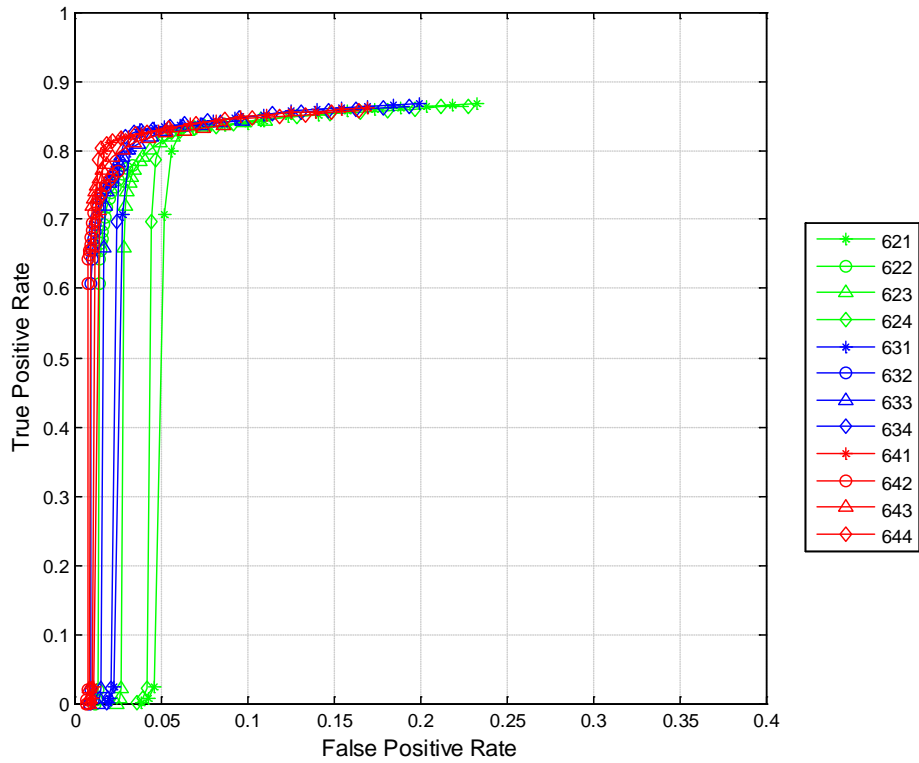


Figure 204 ROC curve for 600 series algorithm family using a violation threshold of 15 mph.

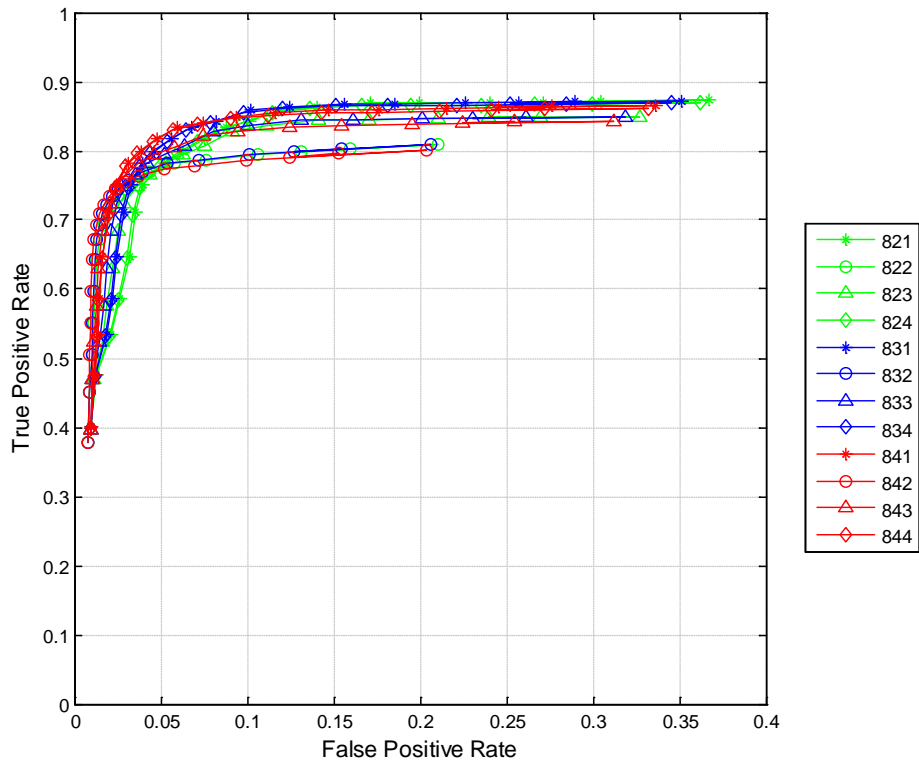


Figure 205 ROC curve for 800 series algorithm family using a violation threshold of 15 mph.

ROC Curves for Signalized Intersections Using the 20-mph Violation Threshold

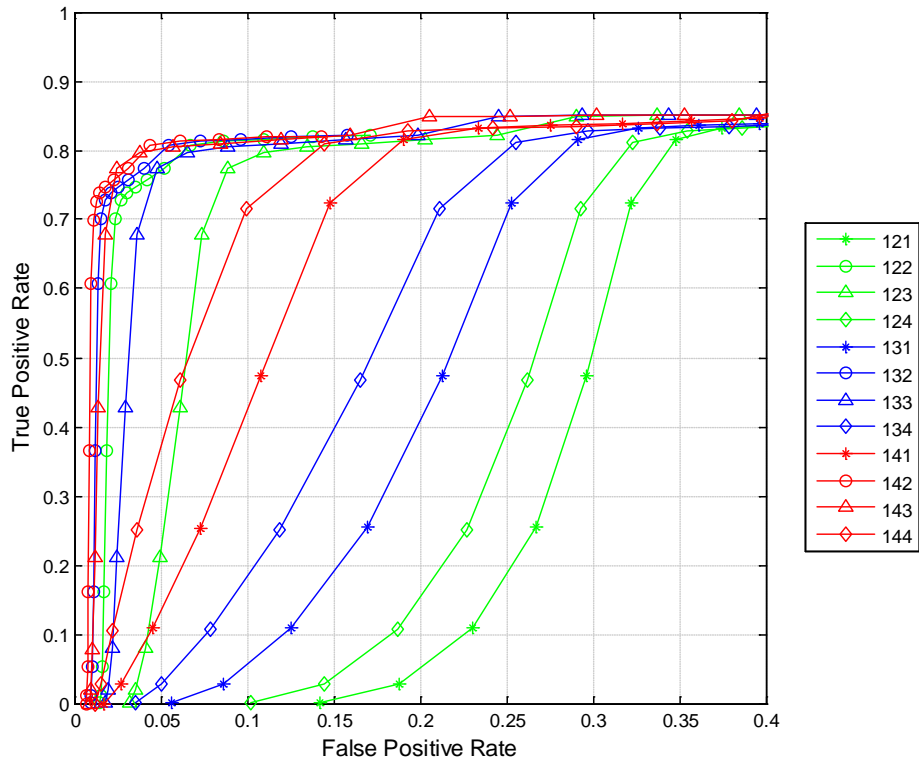


Figure 206 ROC curve for 100 series algorithm family using a violation threshold of 20 mph.

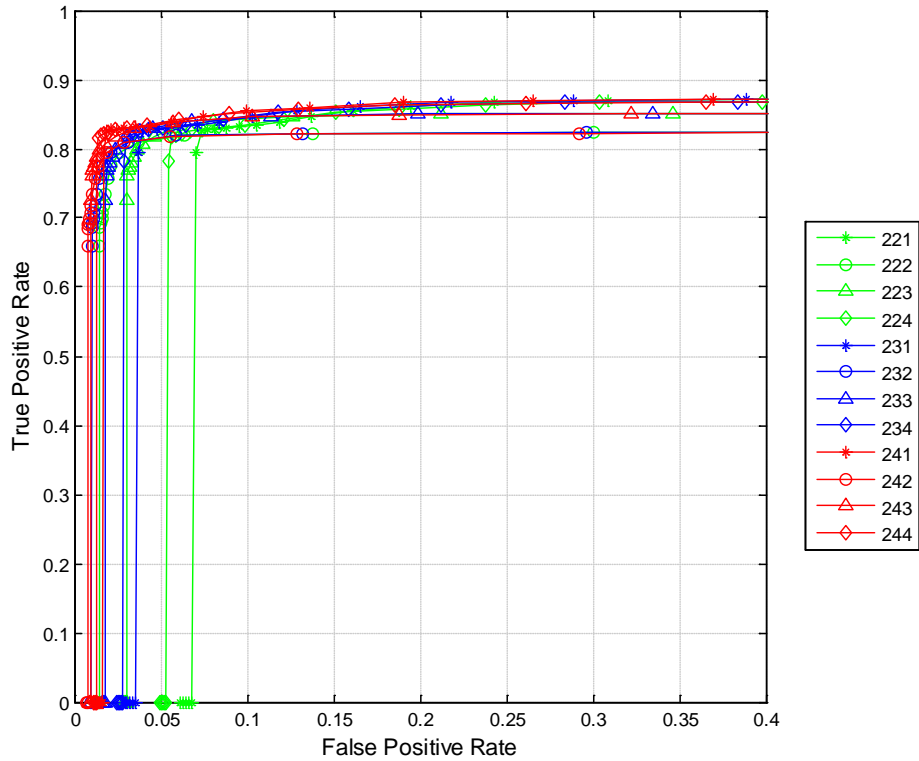


Figure 207 ROC curve for 200 series algorithm family using a violation threshold of 20 mph.

ROC Curves for Signalized Intersections Using the 20-mph Violation Threshold

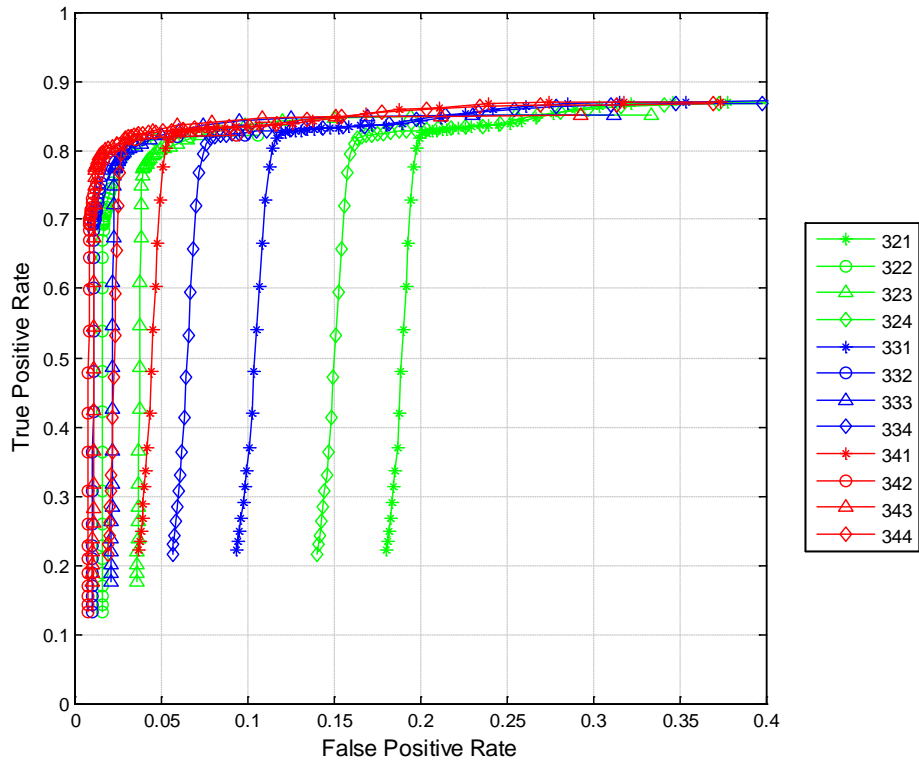


Figure 208 ROC curve for 300 series algorithm family using a violation threshold of 20 mph.

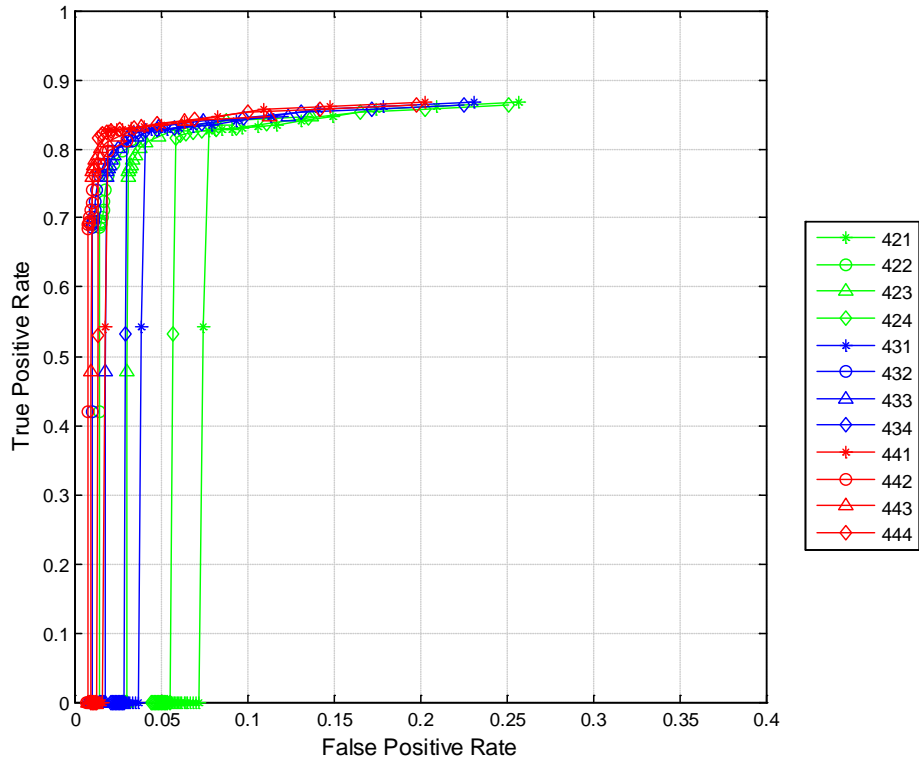


Figure 209 ROC curve for 400 series algorithm family using a violation threshold of 20 mph.



ROC Curves for Signalized Intersections Using the 20-mph Violation Threshold

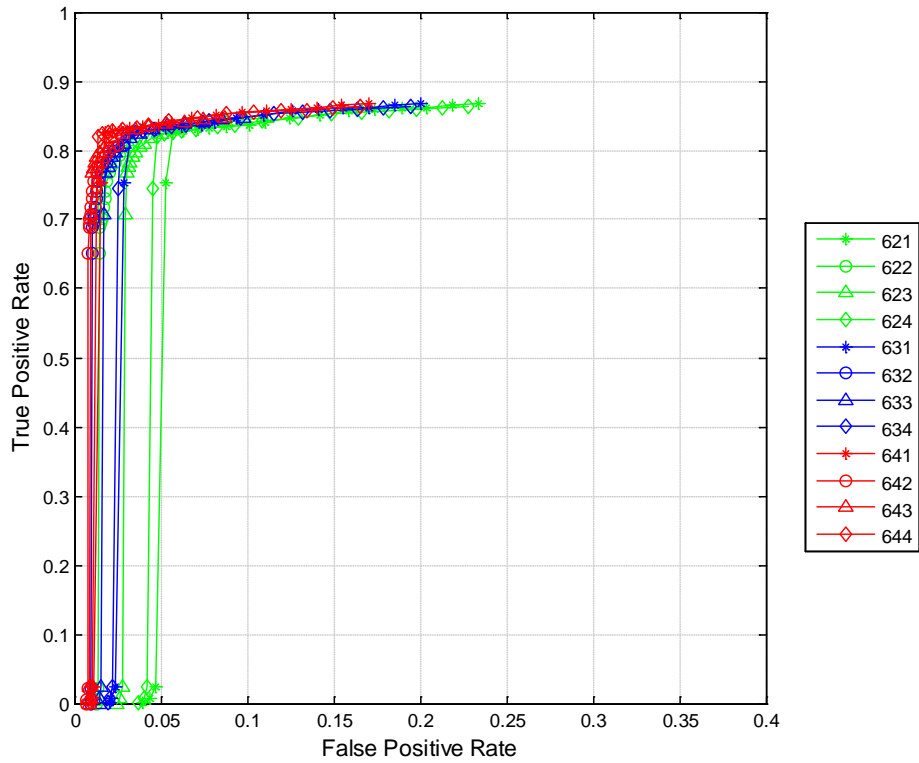


Figure 210 ROC curve for 600 series algorithm family using a violation threshold of 20 mph.

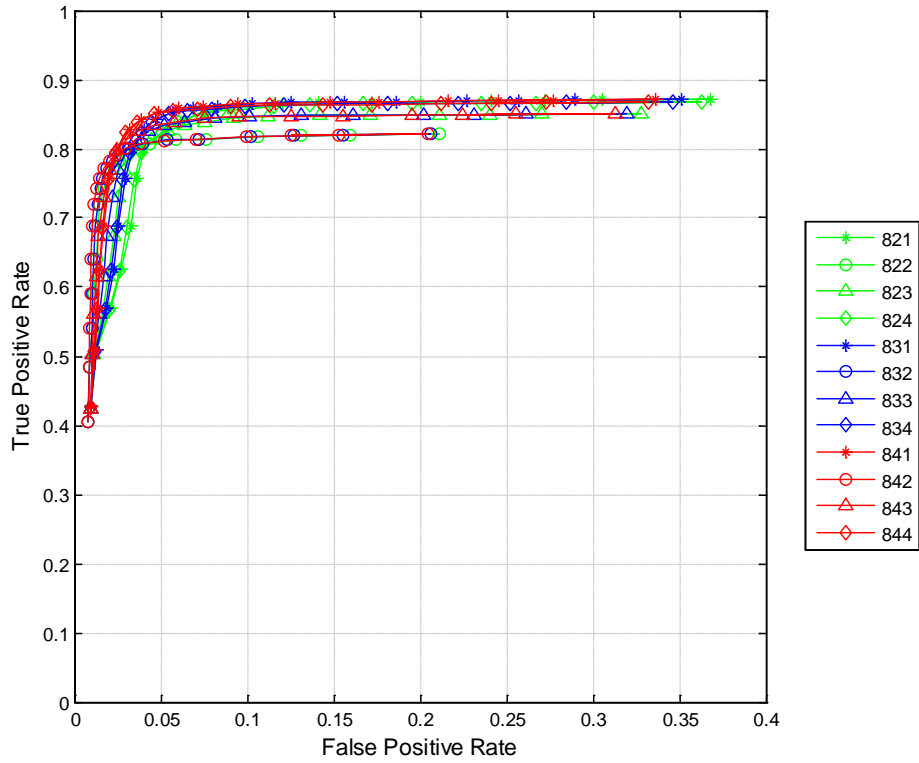


Figure 211 ROC curve for 800 series algorithm family using a violation threshold of 20 mph.

### 11.18 Appendix R: Signalized Warning Timing Distributions

Warning Timing Distributions for Signalized Intersections Using an FPR of 0.01 and a 10-mph Violation Threshold

(No warning was produced by the 100 series algorithm at a false positive rate of 0.01 using a violation threshold of 10 mph.)

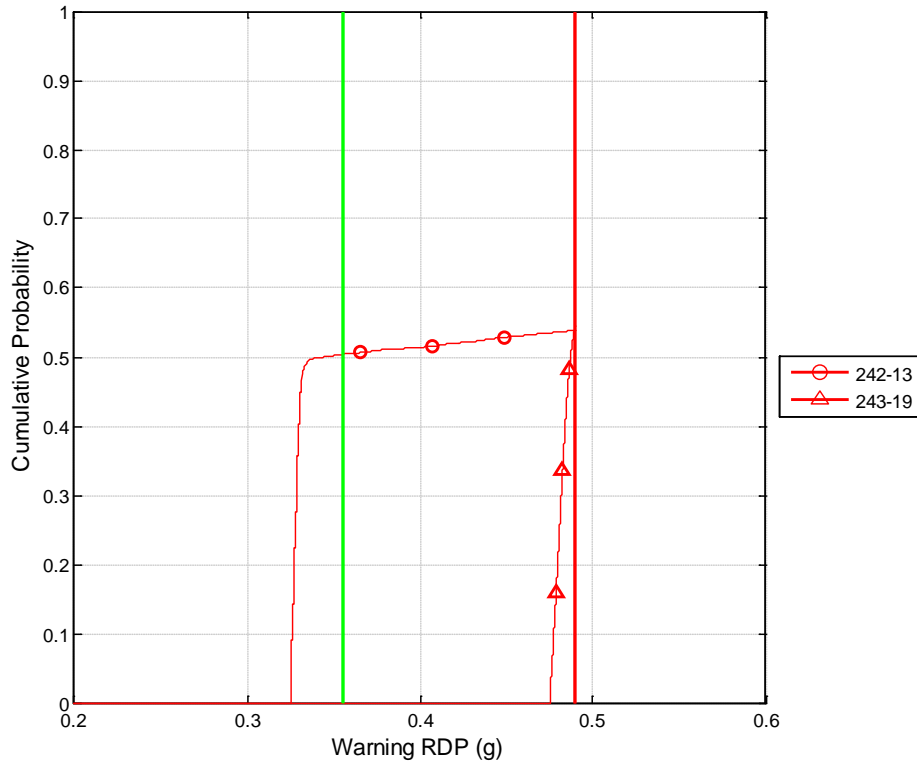


Figure 212 Cumulative distribution of the warning timing for true positives produced by the 200 series algorithm at a false positive rate of 0.01 using a violation threshold of 10 mph.

Warning Timing Distributions for Signalized Intersections Using an FPR of 0.01 and a 10-mph Violation Threshold

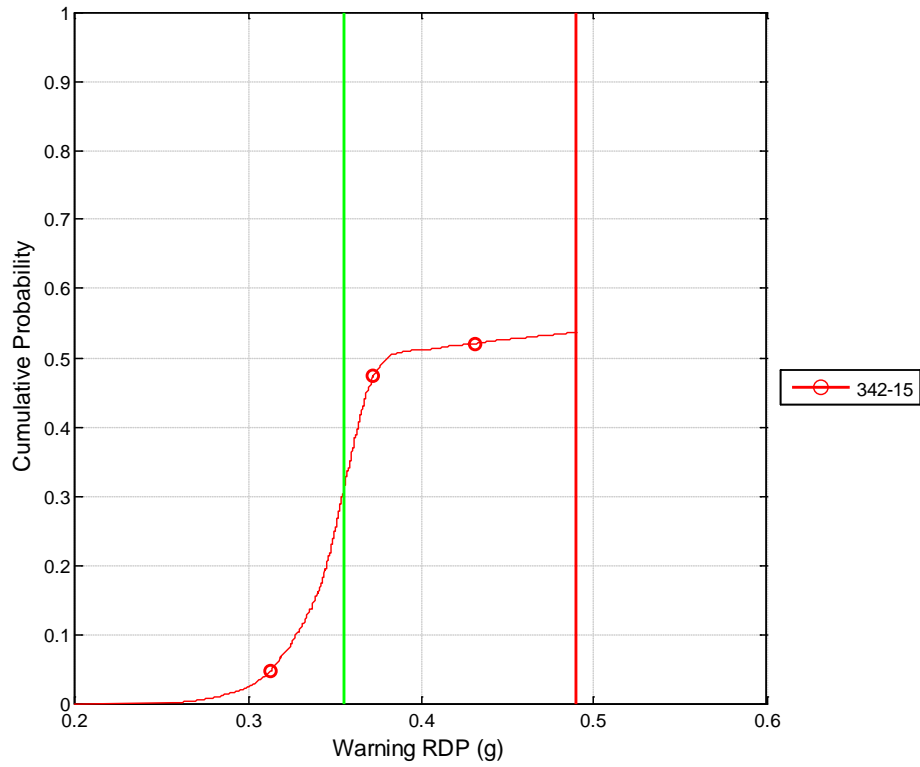


Figure 213 Cumulative distribution of the warning timing for true positives produced by the 300 series algorithm at a false positive rate of 0.01 using a violation threshold of 10 mph.

Warning Timing Distributions for Signalized Intersections Using an FPR of 0.01 and a 10-mph Violation Threshold

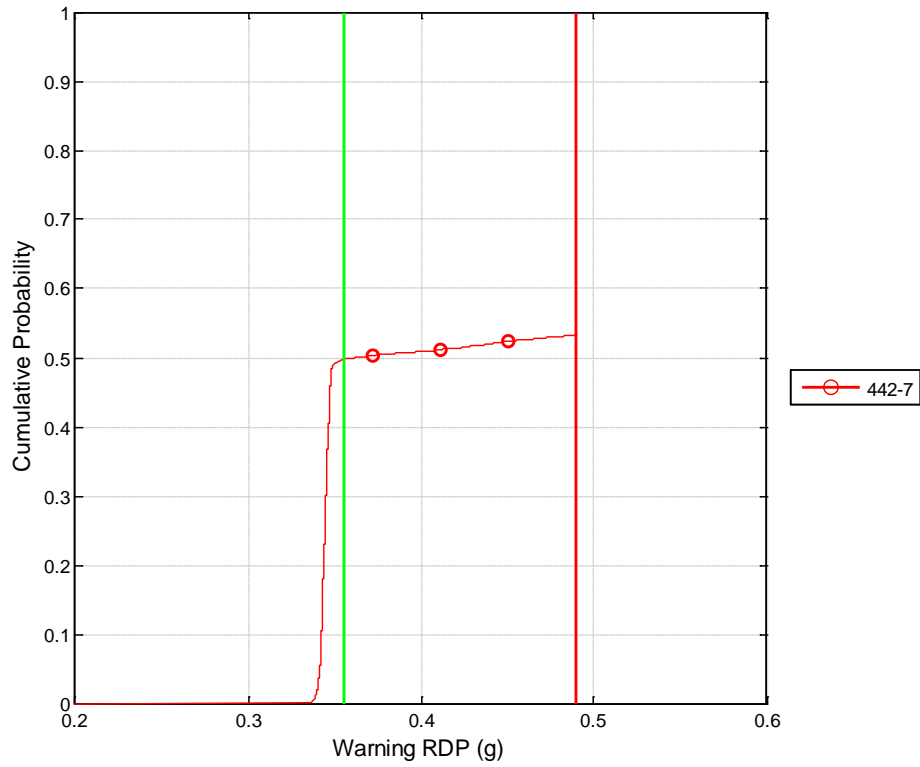


Figure 214 Cumulative distribution of the warning timing for true positives produced by the 400 series algorithm at a false positive rate of 0.01 using a violation threshold of 10 mph.

Warning Timing Distributions for Signalized Intersections Using an FPR of 0.01 and a 10-mph Violation Threshold

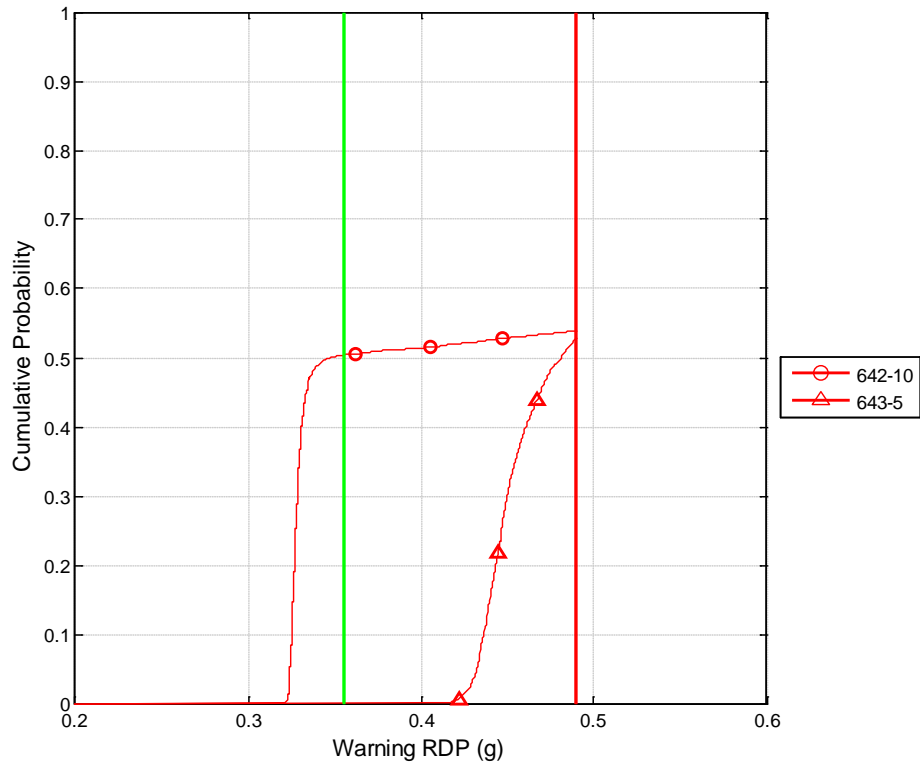


Figure 215 Cumulative distribution of the warning timing for true positives produced by the 600 series algorithm at a false positive rate of 0.01 using a violation threshold of 10 mph.

(No warning was produced by the 800 series algorithm at a true positive rate of 0.01 using a violation threshold of 10 mph.)

Warning Timing Distributions for Signalized Intersections Using an FPR of 0.01 and a 15-mph Violation Threshold

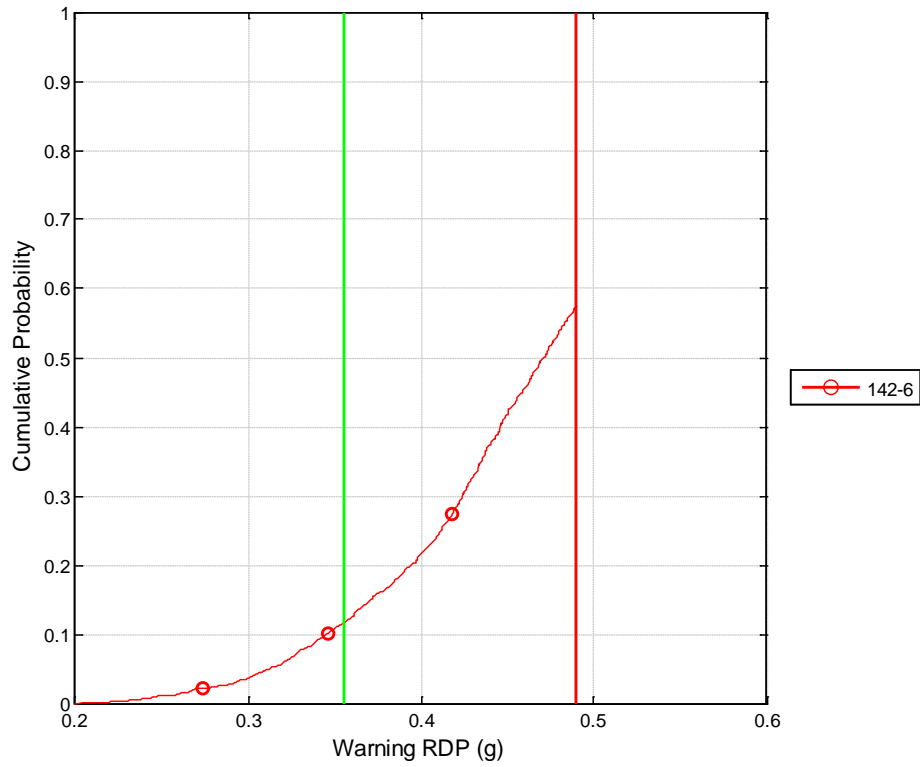


Figure 216 Cumulative distribution of the warning timing for true positives produced by the 100 series algorithm at a false positive rate of 0.01 using a violation threshold of 15 mph.

Warning Timing Distributions for Signalized Intersections Using an FPR of 0.01 and a 15-mph Violation Threshold

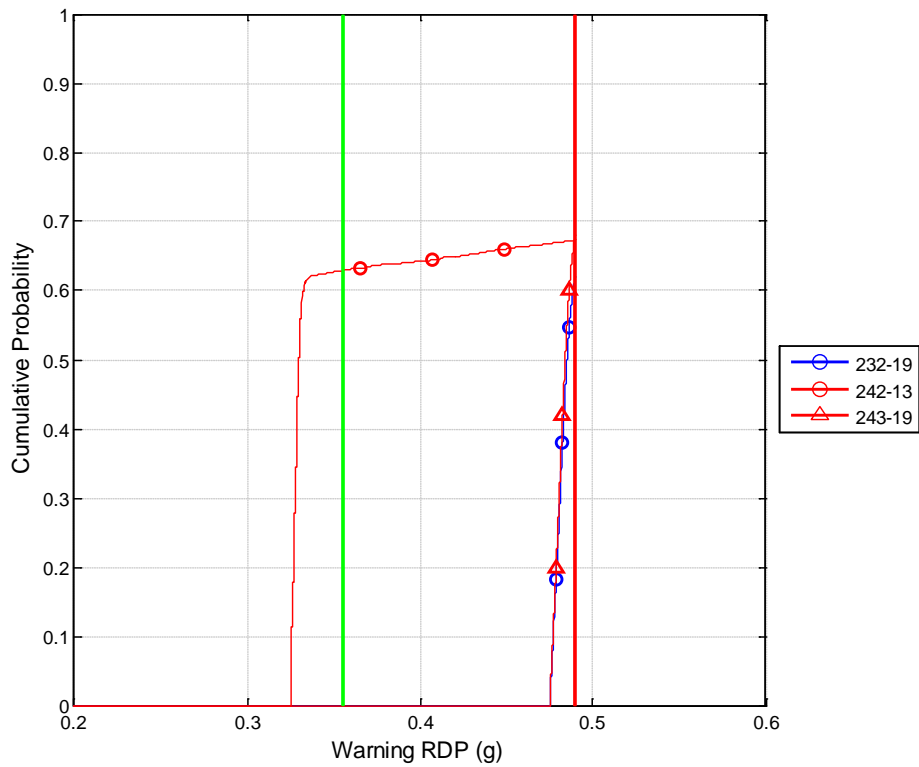


Figure 217 Cumulative distribution of the warning timing for true positives produced by the 200 series algorithm at a false positive rate of 0.01 using a violation threshold of 15 mph.

Warning Timing Distributions for Signalized Intersections Using an FPR of 0.01 and a 15-mph Violation Threshold

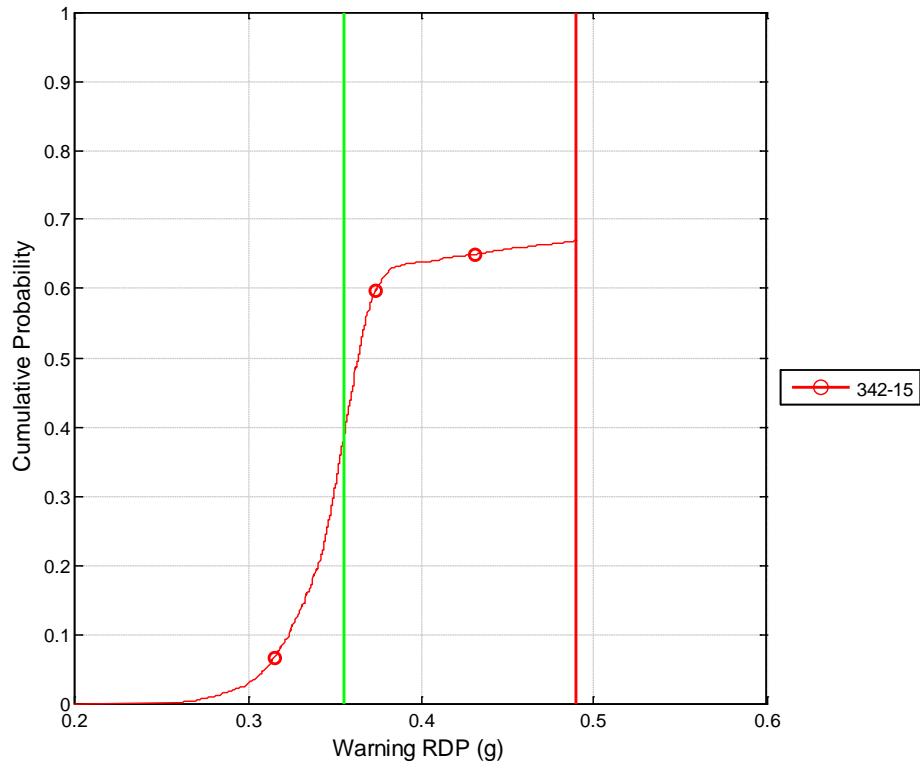


Figure 218 Cumulative distribution of the warning timing for true positives produced by the 300 series algorithm at a false positive rate of 0.01 using a violation threshold of 15 mph.



Warning Timing Distributions for Signalized Intersections Using an FPR of 0.01 and a 15-mph Violation Threshold

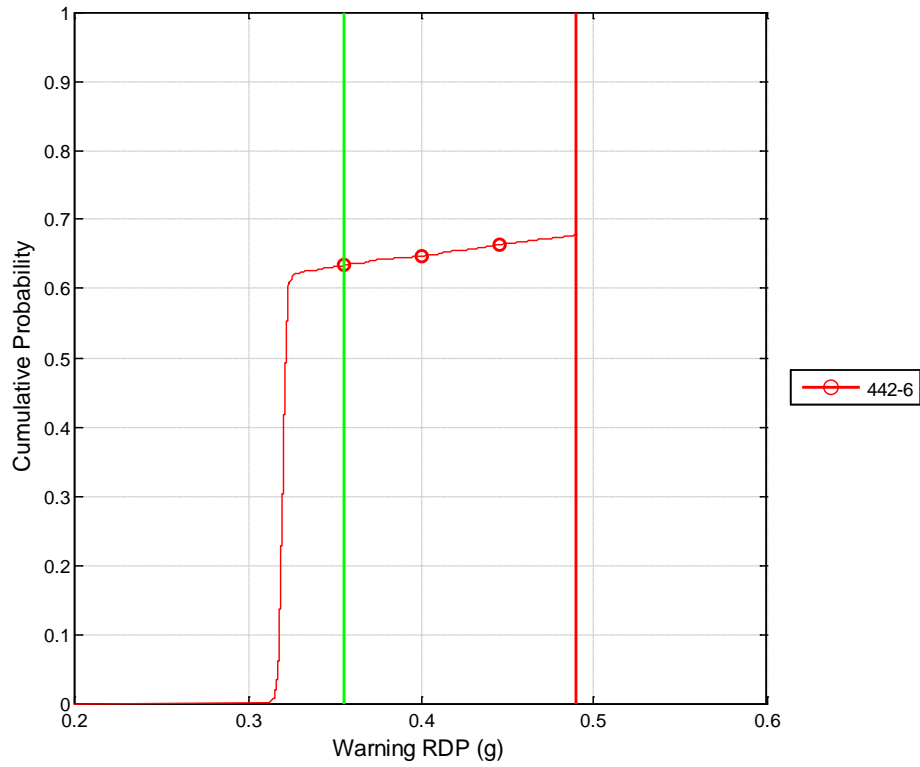


Figure 219 Cumulative distribution of the warning timing for true positives produced by the 400 series algorithm at a false positive rate of 0.01 using a violation threshold of 15 mph.

Warning Timing Distributions for Signalized Intersections Using an FPR of 0.01 and a 15-mph Violation Threshold

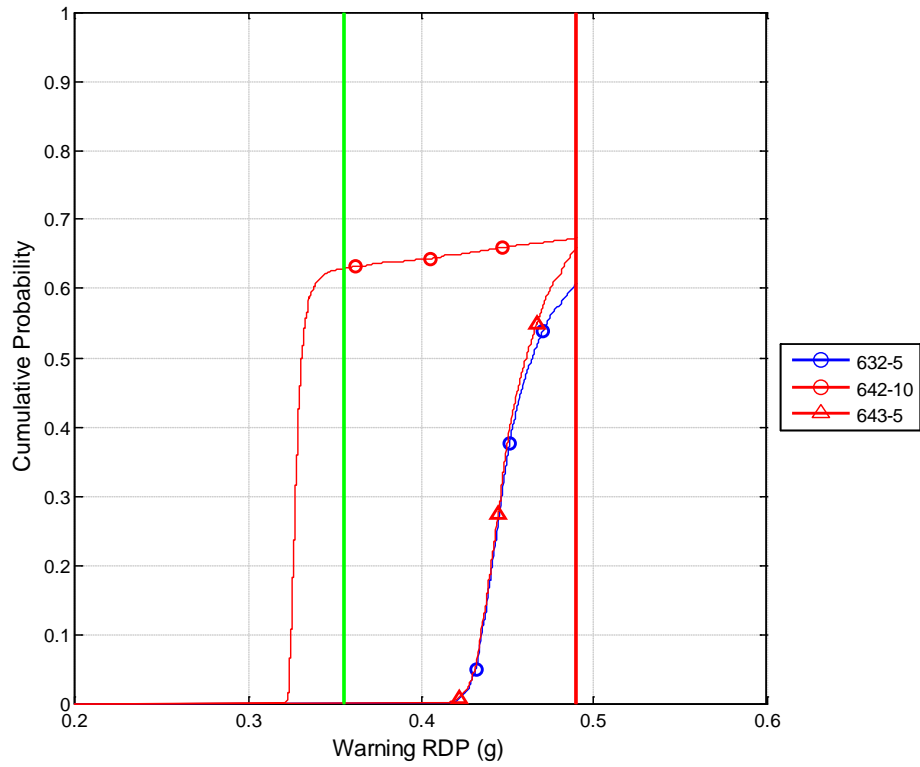


Figure 220 Cumulative distribution of the warning timing for true positives produced by the 600 series algorithm at a false positive rate of 0.01 using a violation threshold of 15 mph.

Warning Timing Distributions for Signalized Intersections Using an FPR of 0.01 and a 15-mph Violation Threshold

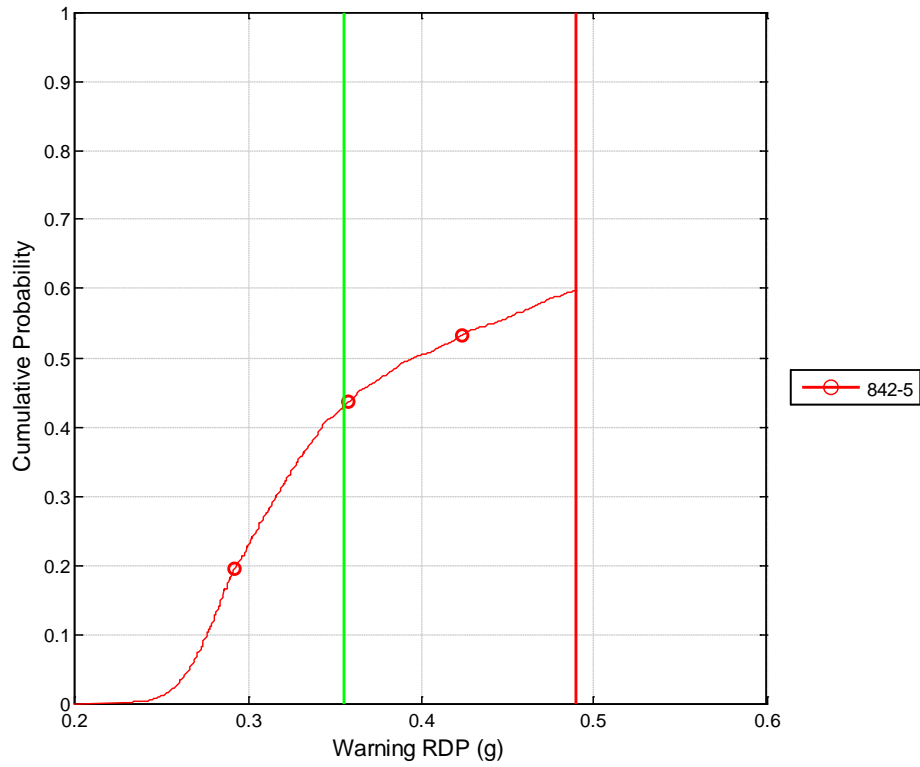


Figure 221 Cumulative distribution of the warning timing for true positives produced by the 800 series algorithm at a false positive rate of 0.01 using a violation threshold of 15 mph.

Warning Timing Distributions for Signalized Intersections Using an FPR of 0.01 and a 20-mph Violation Threshold

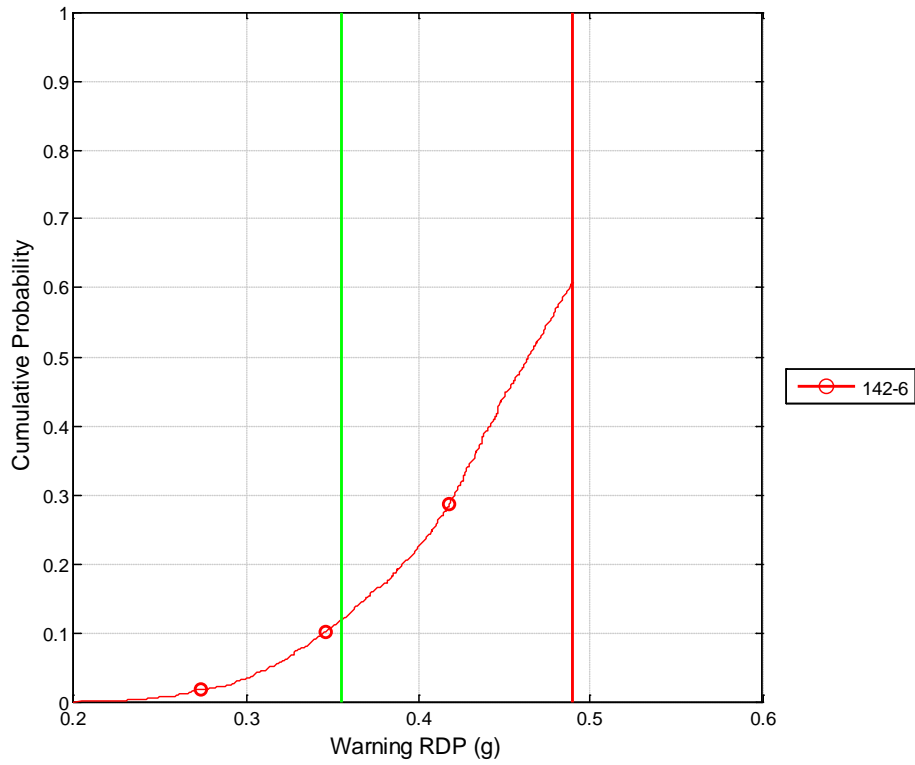


Figure 222 Cumulative distribution of the warning timing for true positives produced by the 100 series algorithm at a false positive rate of 0.01 using a violation threshold of 20 mph.

Warning Timing Distributions for Signalized Intersections Using an FPR of 0.01 and a 20-mph Violation Threshold

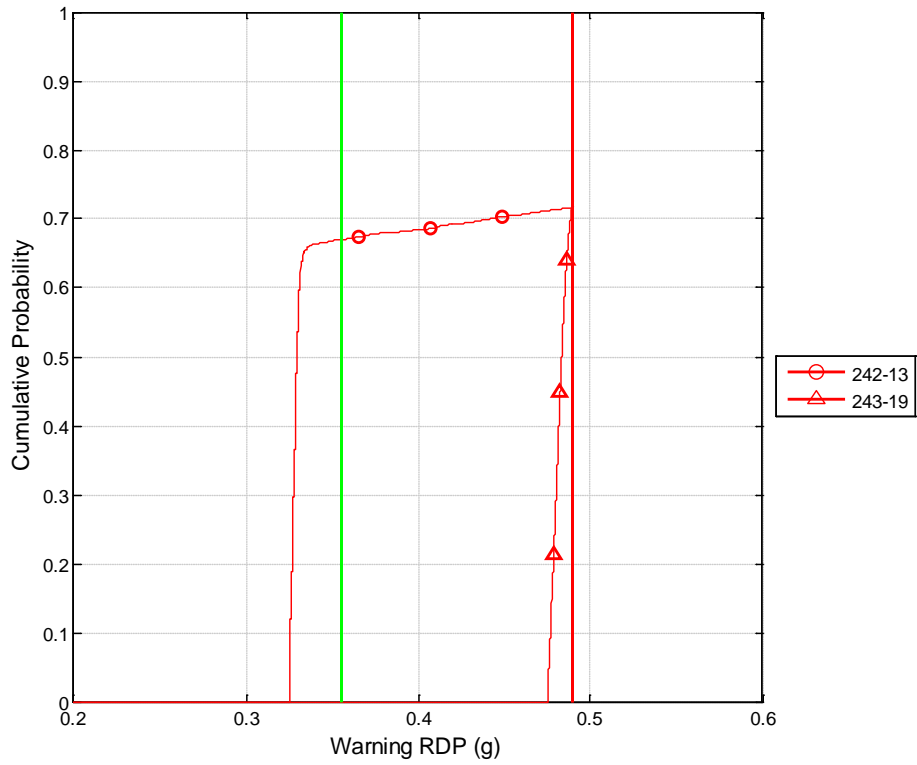


Figure 223 Cumulative distribution of the warning timing for true positives produced by the 200 series algorithm at a false positive rate of 0.01 using a violation threshold of 20 mph.

Warning Timing Distributions for Signalized Intersections Using an FPR of 0.01 and a 20-mph Violation Threshold

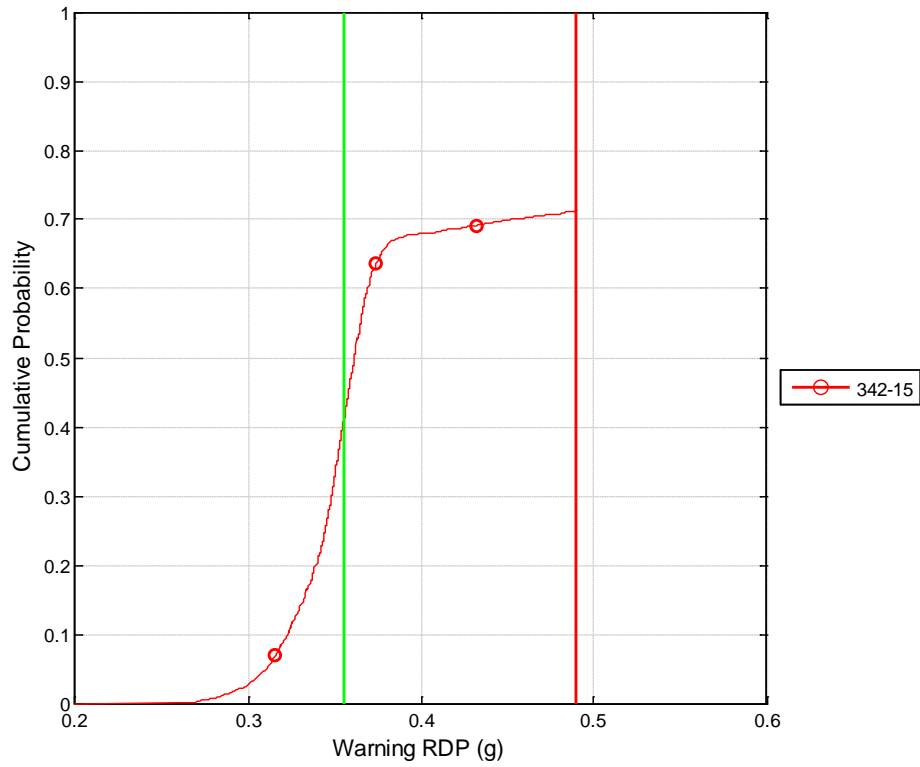


Figure 224 Cumulative distribution of the warning timing for true positives produced by the 300 series algorithm at a false positive rate of 0.01 using a violation threshold of 20 mph.

Warning Timing Distributions for Signalized Intersections Using an FPR of 0.01 and a 20-mph Violation Threshold

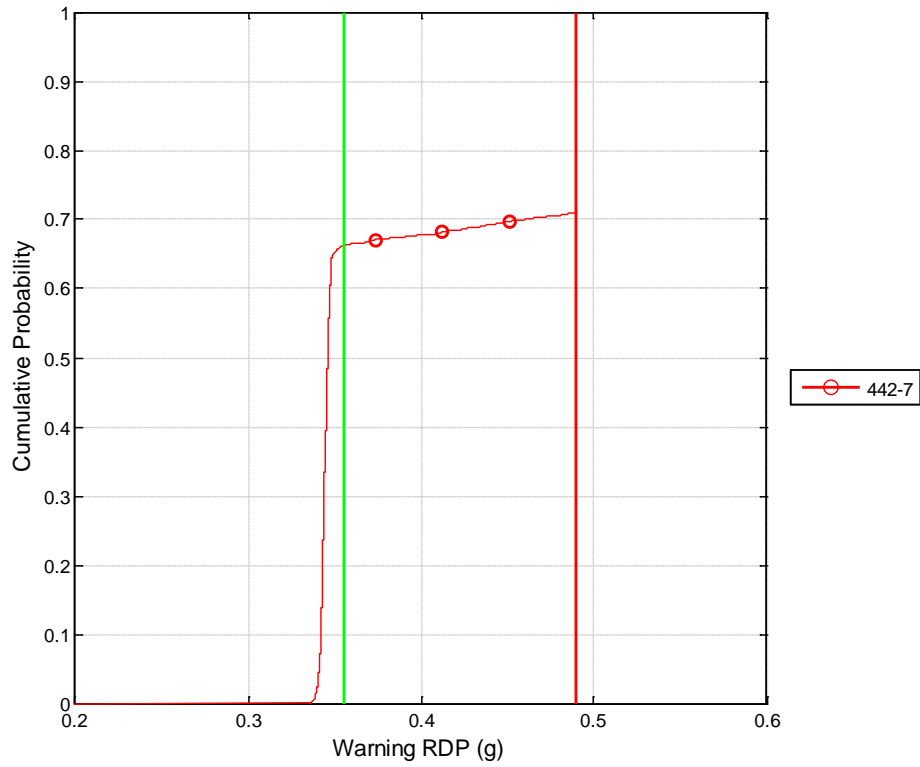


Figure 225 Cumulative distribution of the warning timing for true positives produced by the 400 series algorithm at a false positive rate of 0.01 using a violation threshold of 20 mph.

Warning Timing Distributions for Signalized Intersections Using an FPR of 0.01 and a 20-mph Violation Threshold

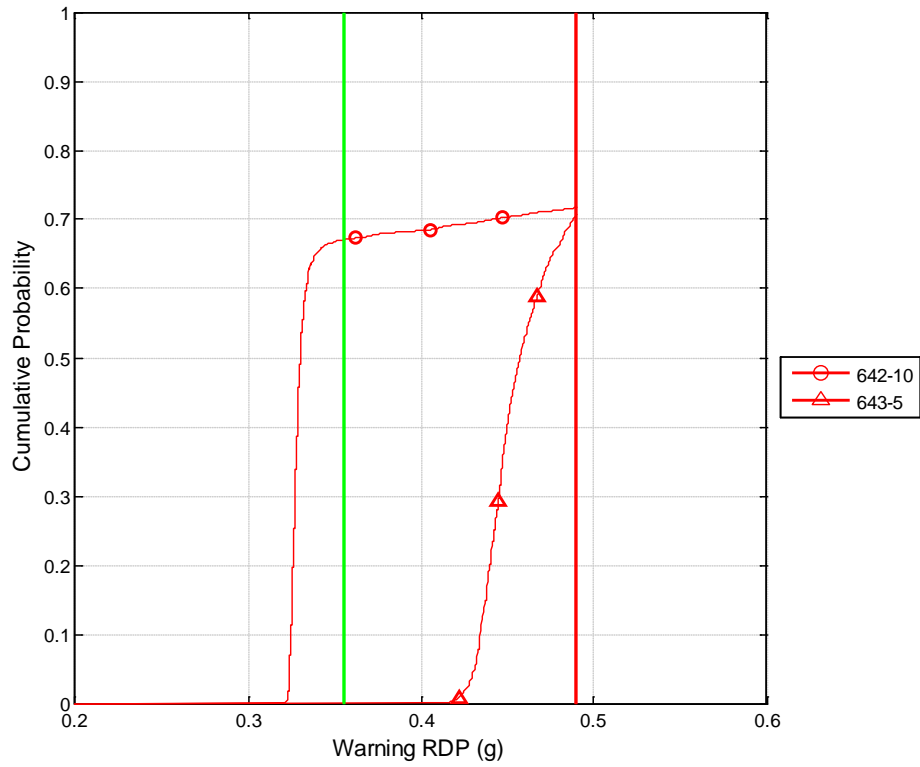


Figure 226 Cumulative distribution of the warning timing for true positives produced by the 600 series algorithm at a false positive rate of 0.01 using a violation threshold of 20 mph.



Warning Timing Distributions for Signalized Intersections Using an FPR of 0.01 and a 20-mph Violation Threshold

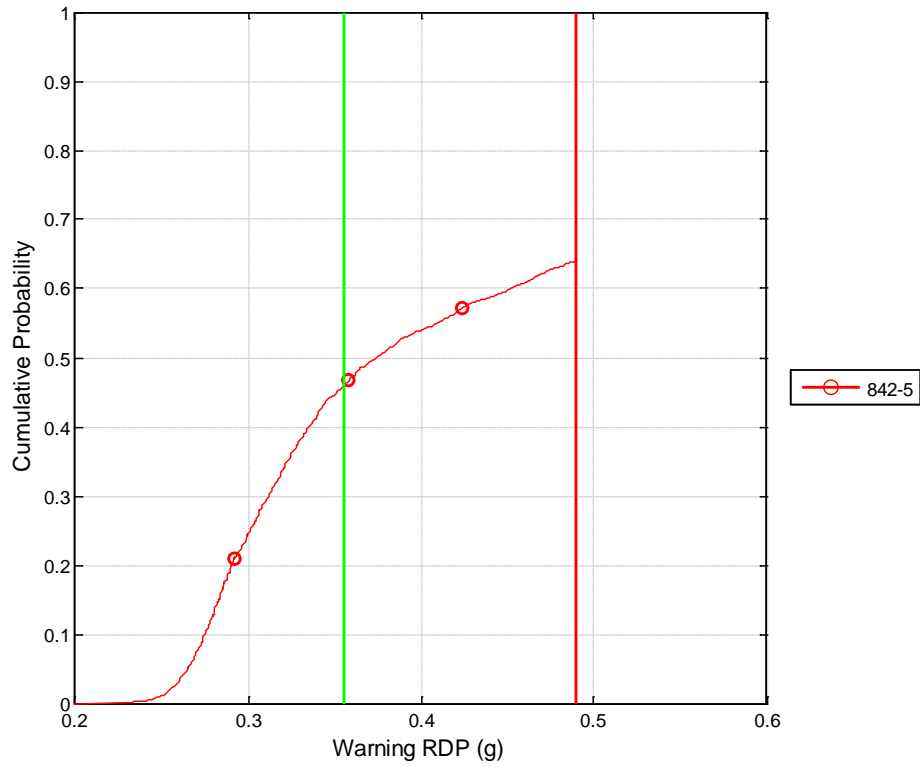


Figure 227 Cumulative distribution of the warning timing for true positives produced by the 800 series algorithm at a false positive rate of 0.01 using a violation threshold of 20 mph.

Warning Timing Distributions for Signalized Intersections Using an FPR of 0.05 and a 10-mph Violation Threshold

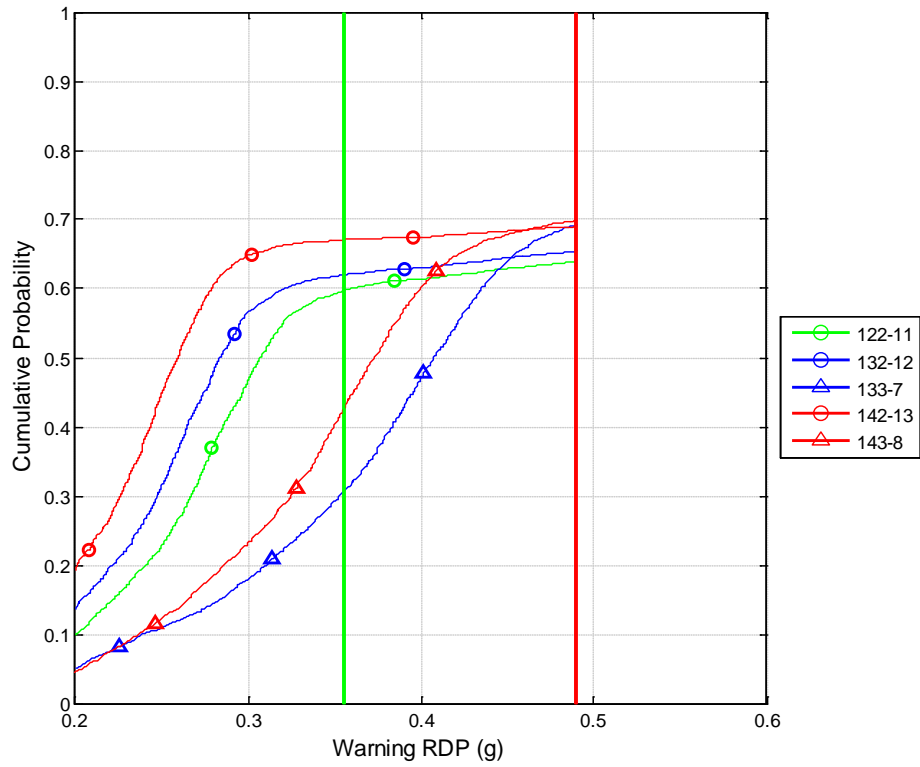


Figure 228 Cumulative distribution of the warning timing for true positives produced by the 100 series algorithm at a false positive rate of 0.05 using a violation threshold of 10 mph.

Warning Timing Distributions for Signalized Intersections Using an FPR of 0.05 and a 10-mph Violation Threshold

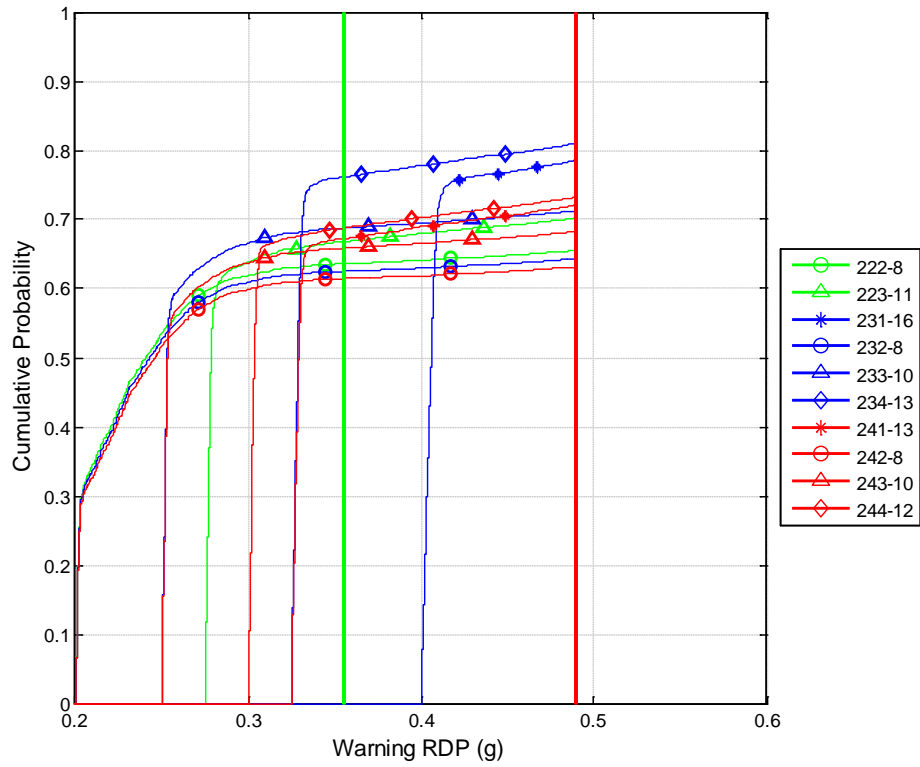


Figure 229 Cumulative distribution of the warning timing for true positives produced by the 200 series algorithm at a false positive rate of 0.05 using a violation threshold of 10 mph.

Warning Timing Distributions for Signalized Intersections Using an FPR of 0.05 and a 10-mph Violation Threshold

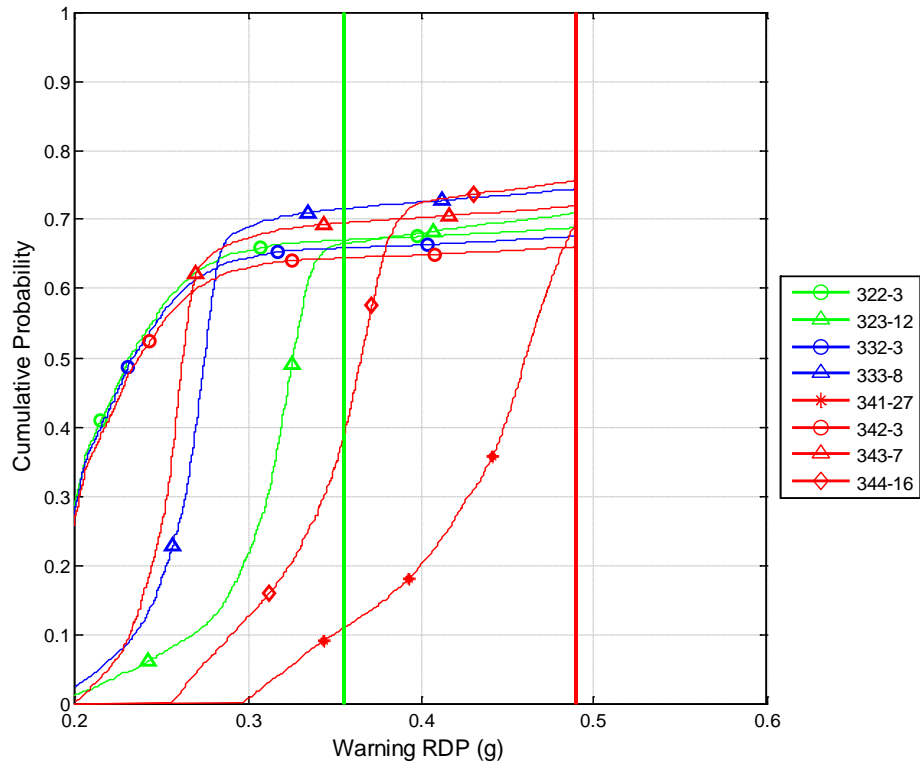


Figure 230 Cumulative distribution of the warning timing for true positives produced by the 300 series algorithm at a false positive rate of 0.05 using a violation threshold of 10 mph.

Warning Timing Distributions for Signalized Intersections Using an FPR of 0.05 and a 10-mph Violation Threshold

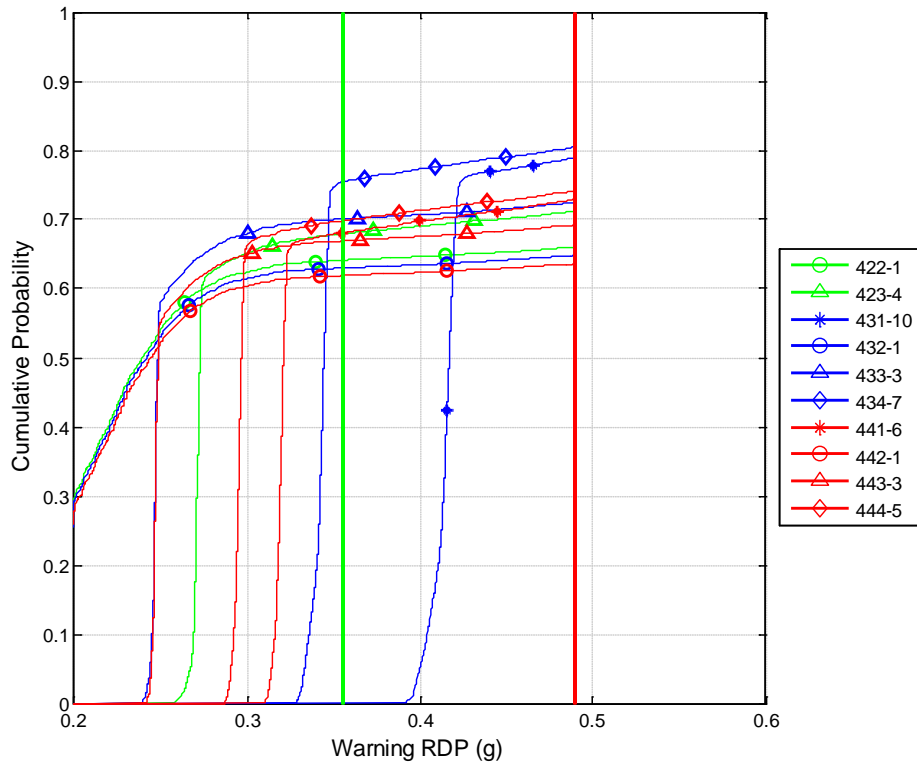


Figure 231 Cumulative distribution of the warning timing for true positives produced by the 400 series algorithm at a false positive rate of 0.05 using a violation threshold of 10 mph.

Warning Timing Distributions for Signalized Intersections Using an FPR of 0.05 and a 10-mph Violation Threshold

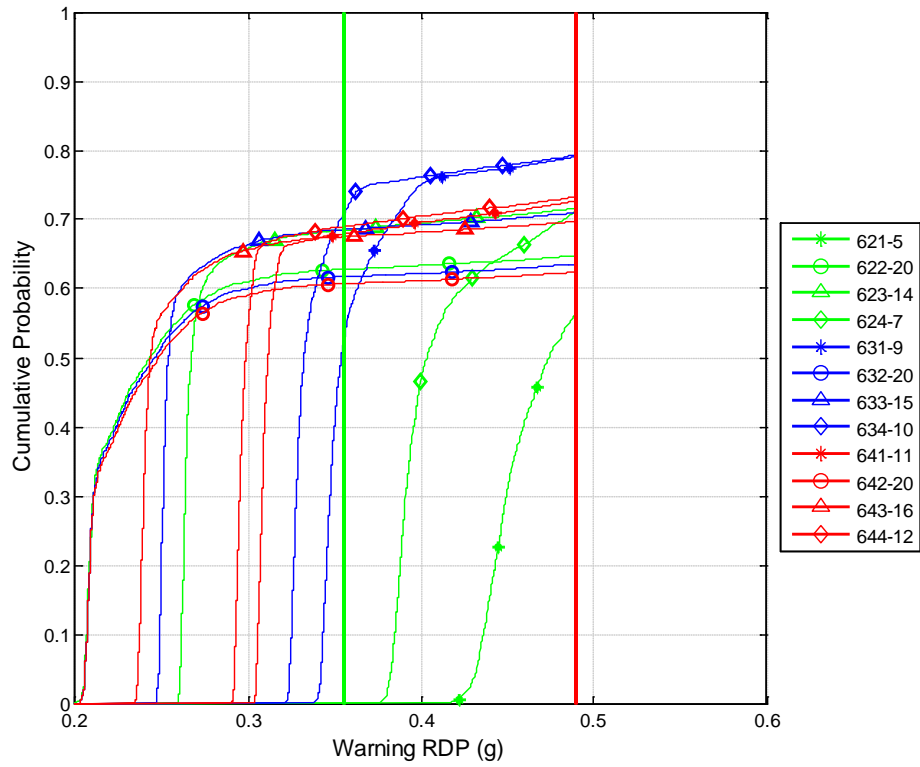


Figure 232 Cumulative distribution of the warning timing for true positives produced by the 600 series algorithm at a false positive rate of 0.05 using a violation threshold of 10 mph.

Warning Timing Distributions for Signalized Intersections Using an FPR of 0.05 and a 10-mph Violation Threshold

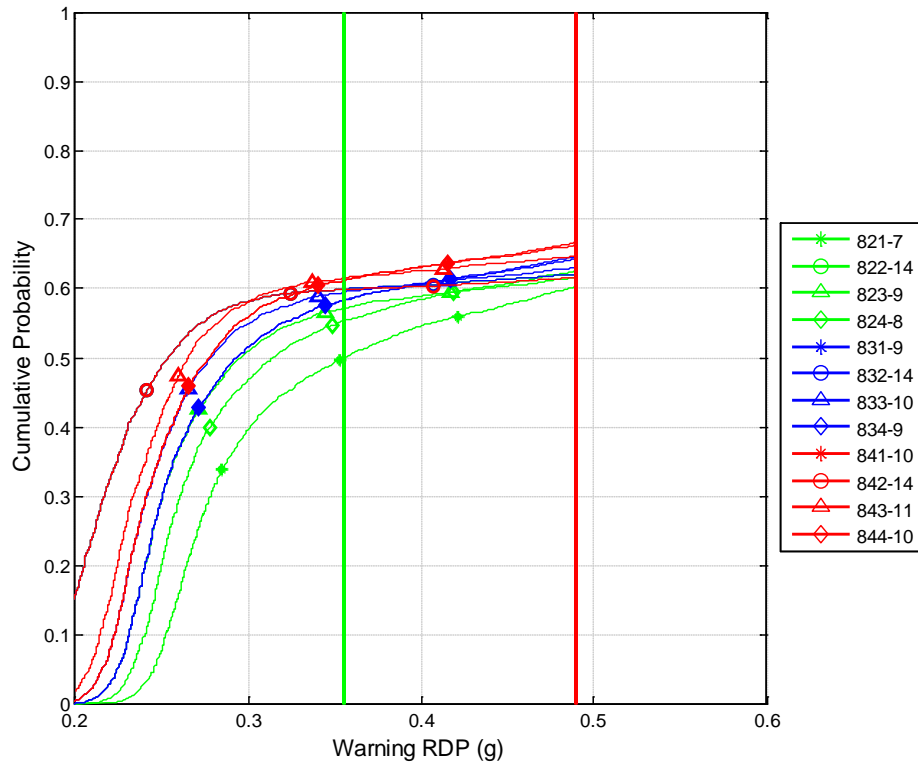


Figure 233 Cumulative distribution of the warning timing for true positives produced by the 800 series algorithm at a false positive rate of 0.05 using a violation threshold of 10 mph.

Warning Timing Distributions for Signalized Intersections Using an FPR of 0.05 and a 15-mph Violation Threshold

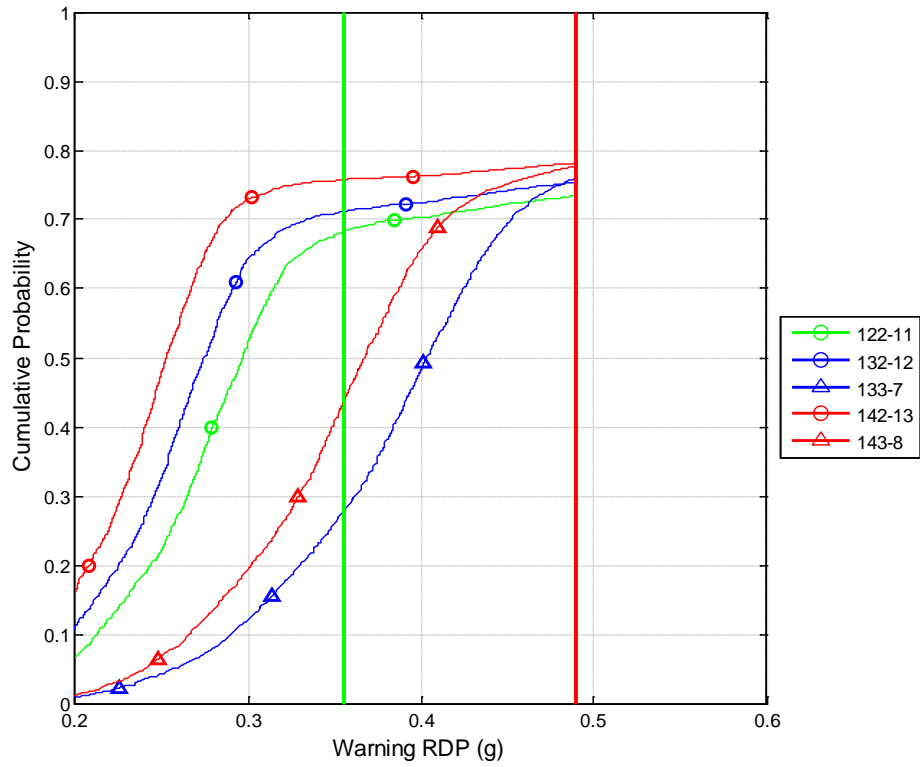


Figure 234 Cumulative distribution of the warning timing for true positives produced by the 100 series algorithm at a false positive rate of 0.05 using a violation threshold of 15 mph.



Warning Timing Distributions for Signalized Intersections Using an FPR of 0.05 and a 15-mph Violation Threshold

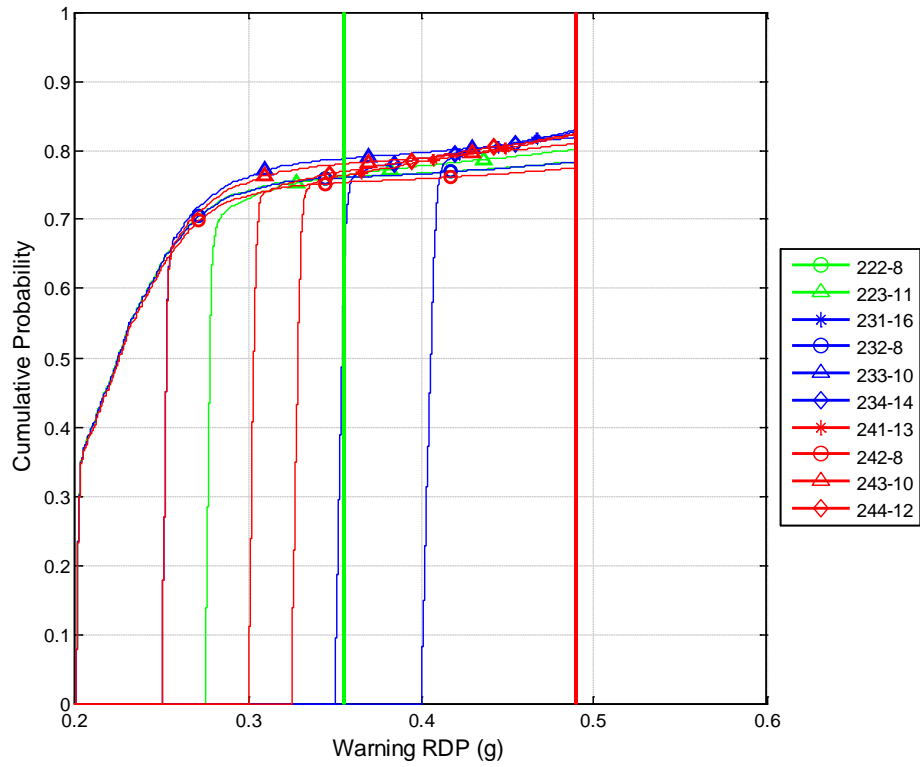


Figure 235 Cumulative distribution of the warning timing for true positives produced by the 200 series algorithm at a false positive rate of 0.05 using a violation threshold of 15 mph.

Warning Timing Distributions for Signalized Intersections Using an FPR of 0.05 and a 15-mph Violation Threshold

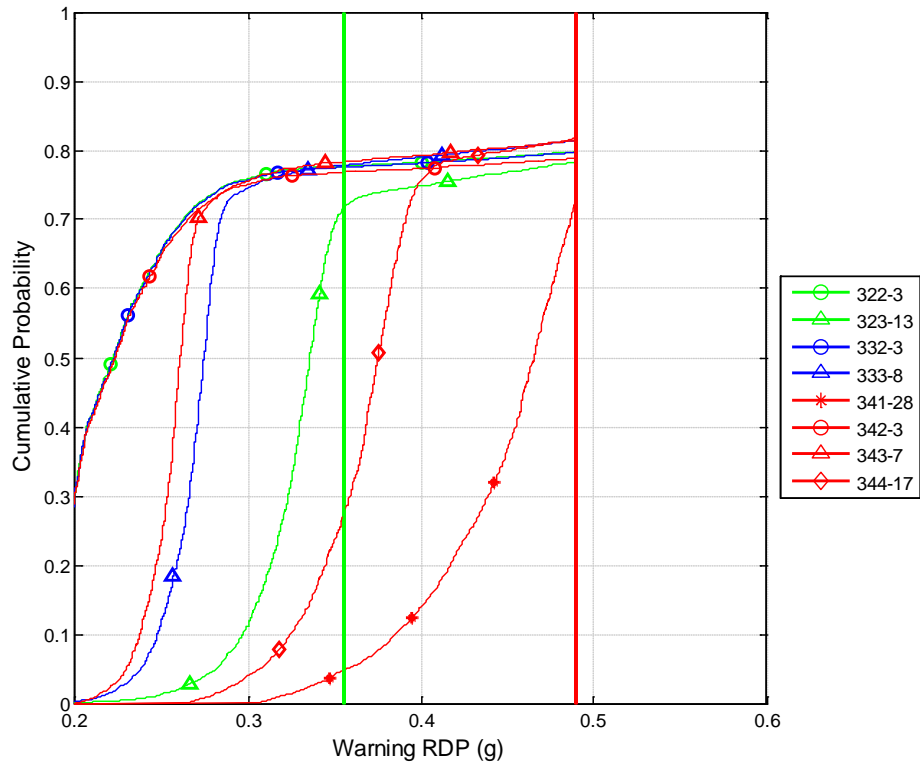


Figure 236 Cumulative distribution of the warning timing for true positives produced by the 300 series algorithm at a false positive rate of 0.05 using a violation threshold of 15 mph.

Warning Timing Distributions for Signalized Intersections Using an FPR of 0.05 and a 15-mph Violation Threshold

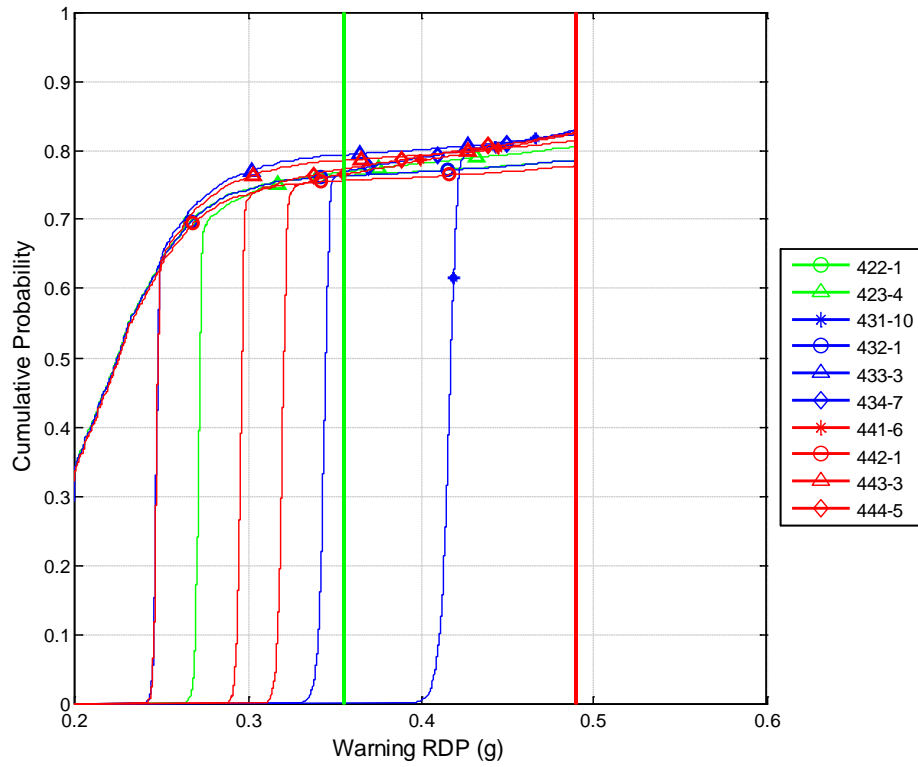


Figure 237 Cumulative distribution of the warning timing for true positives produced by the 400 series algorithm at a false positive rate of 0.05 using a violation threshold of 15 mph.

Warning Timing Distributions for Signalized Intersections Using an FPR of 0.05 and a 15-mph Violation Threshold

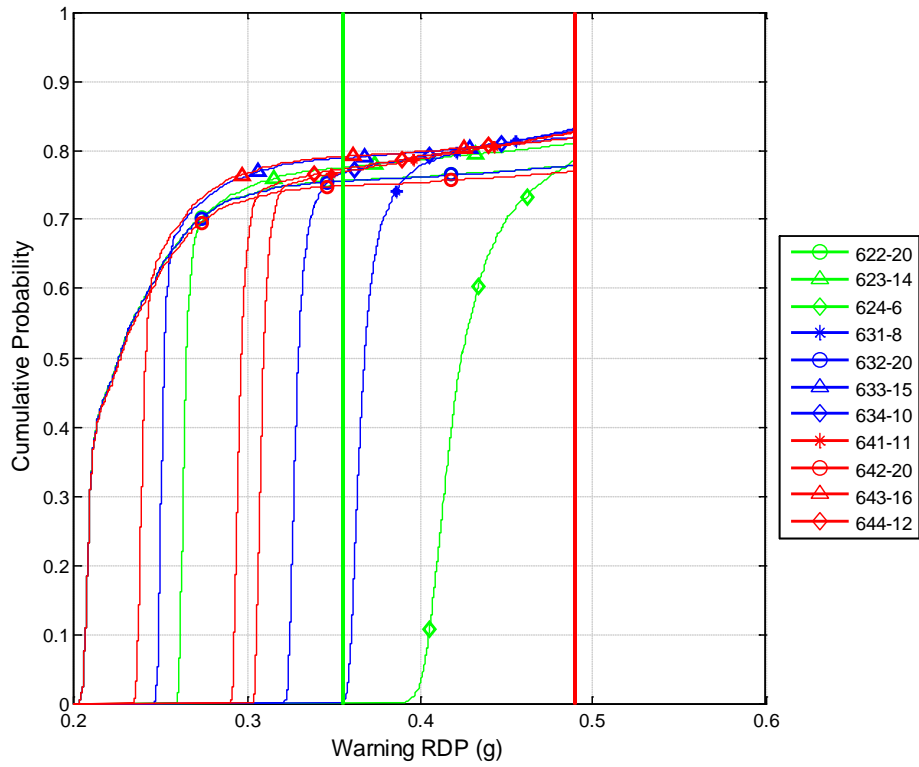


Figure 238 Cumulative distribution of the warning timing for true positives produced by the 600 series algorithm at a false positive rate of 0.05 using a violation threshold of 15 mph.

Warning Timing Distributions for Signalized Intersections Using an FPR of 0.05 and a 15-mph Violation Threshold

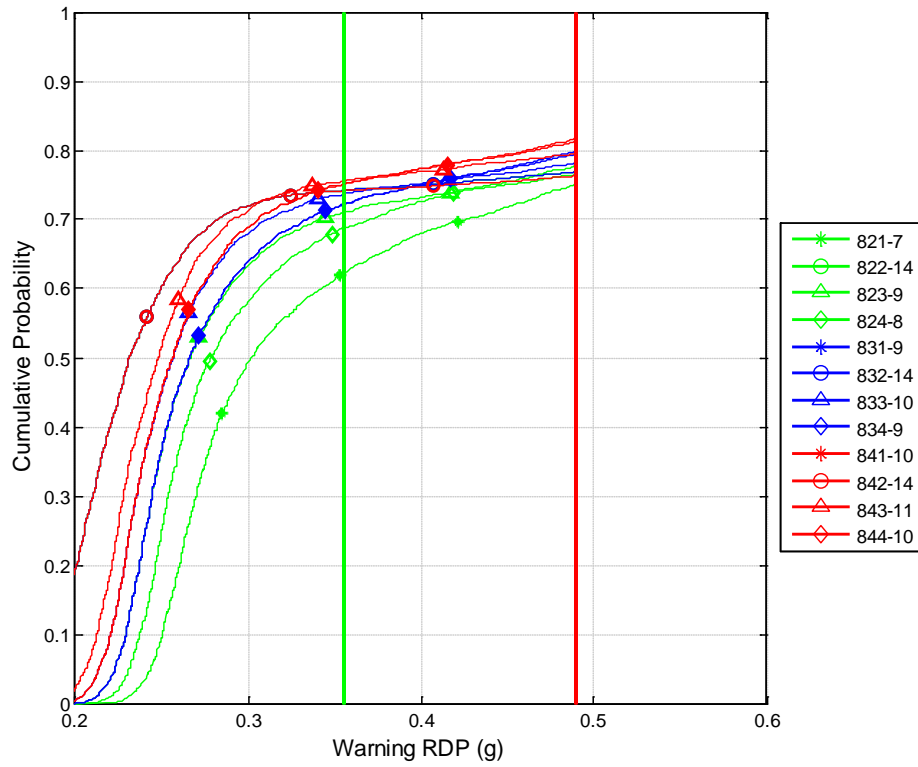


Figure 239 Cumulative distribution of the warning timing for true positives produced by the 800 series algorithm at a false positive rate of 0.05 using a violation threshold of 15 mph.

Warning Timing Distributions for Signalized Intersections Using an FPR of 0.05 and a 20-mph Violation Threshold

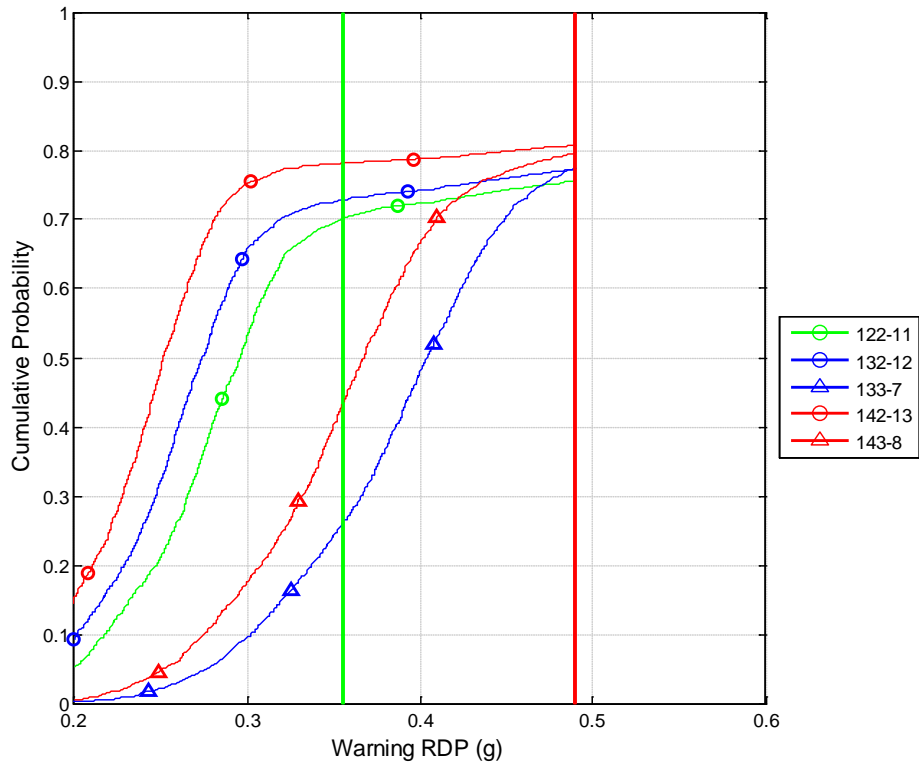


Figure 240 Cumulative distribution of the warning timing for true positives produced by the 100 series algorithm at a false positive rate of 0.05 using a violation threshold of 20 mph.

Warning Timing Distributions for Signalized Intersections Using an FPR of 0.05 and a 20-mph Violation Threshold

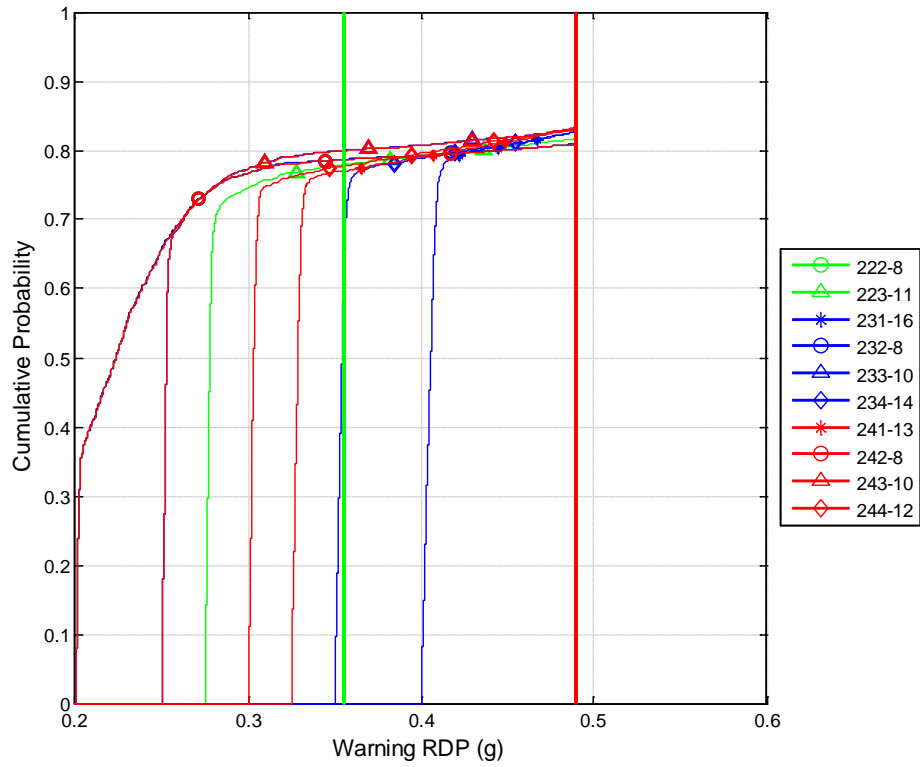


Figure 241 Cumulative distribution of the warning timing for true positives produced by the 200 series algorithm at a false positive rate of 0.05 using a violation threshold of 20 mph.

Warning Timing Distributions for Signalized Intersections Using an FPR of 0.05 and a 20-mph Violation Threshold

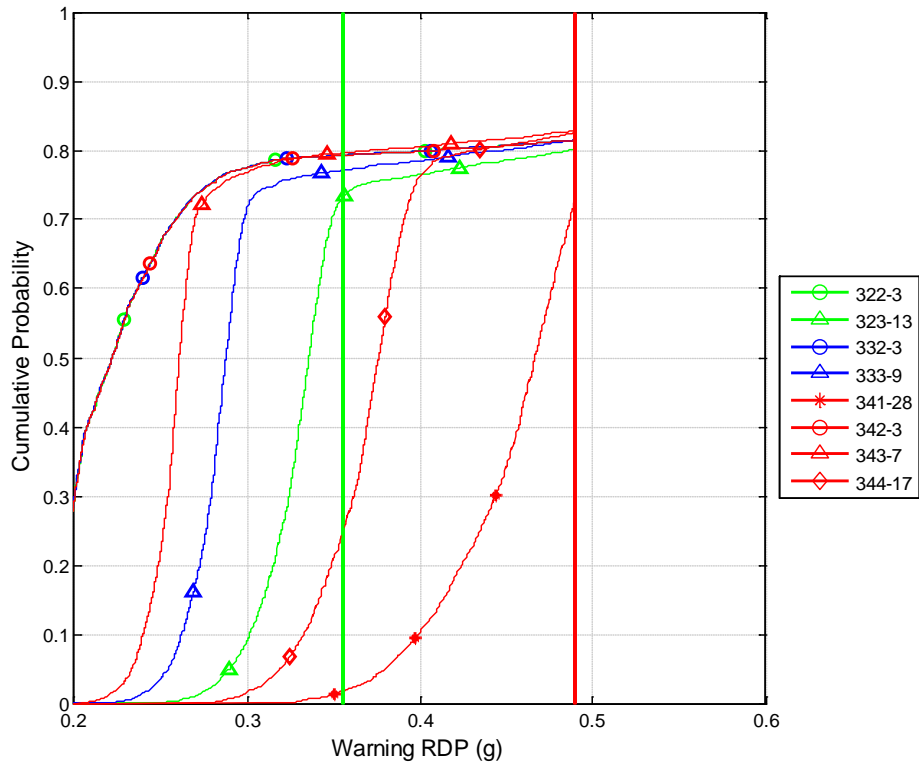


Figure 242 Cumulative distribution of the warning timing for true positives produced by the 300 series algorithm at a false positive rate of 0.05 using a violation threshold of 20 mph.



Warning Timing Distributions for Signalized Intersections Using an FPR of 0.05 and a 20-mph Violation Threshold

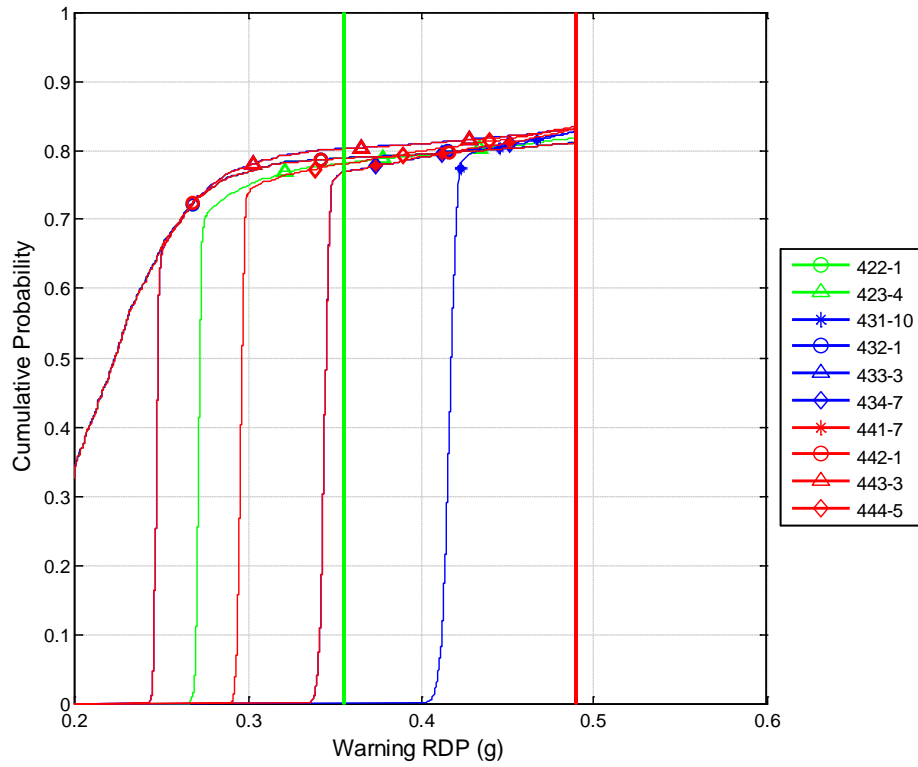


Figure 243 Cumulative distribution of the warning timing for true positives produced by the 400 series algorithm at a false positive rate of 0.05 using a violation threshold of 20 mph.

Warning Timing Distributions for Signalized Intersections Using an FPR of 0.05 and a 20-mph Violation Threshold

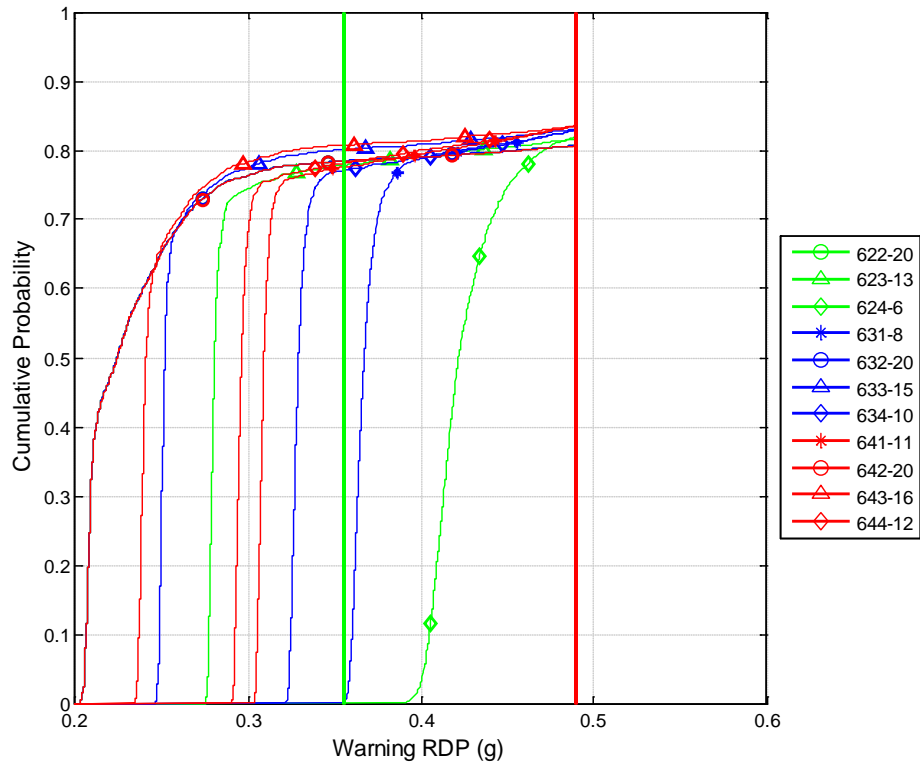


Figure 244 Cumulative distribution of the warning timing for true positives produced by the 600 series algorithm at a false positive rate of 0.05 using a violation threshold of 20 mph.

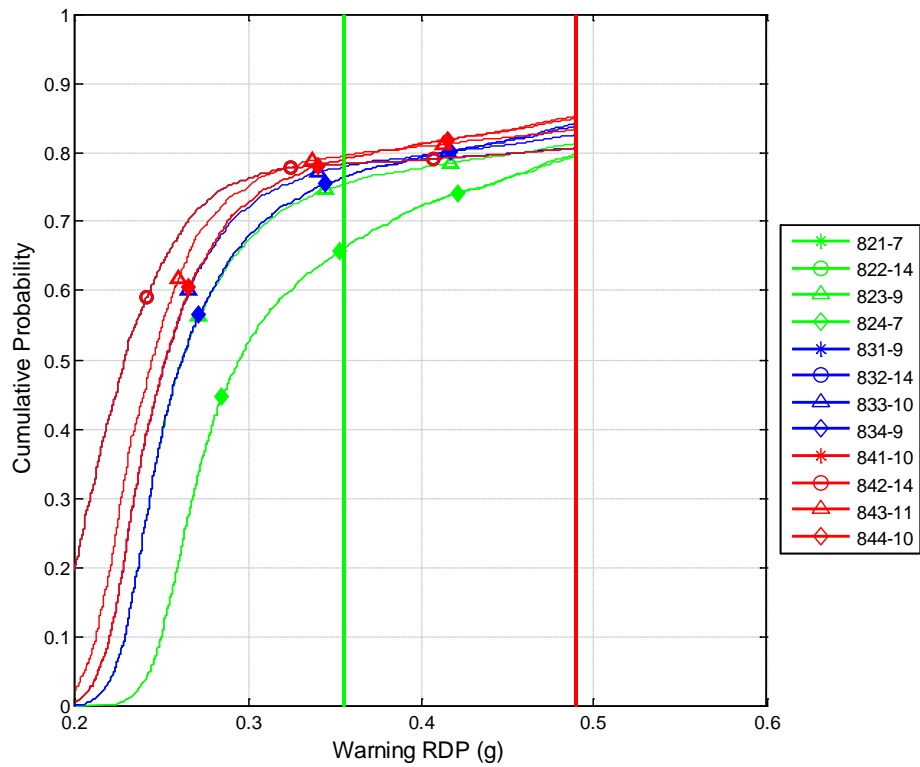


Figure 245 Cumulative distribution of the warning timing for true positives produced by the 800 series algorithm at a false positive rate of 0.05 using a violation threshold of 20 mph.

Warning Timing Distributions for Signalized Intersections Using an FPR of 0.05 and a 20-mph Violation Threshold

### 11.19 Appendix S: Signalized Nuisance Distributions

Stopbar Velocity Distributions for Signalized Intersections Using an FPR of 0.01 and a 10-mph Violation Threshold

(No warning produced for 100 series algorithm at a false positive rate of 0.01 using a violation threshold of 10 mph.)

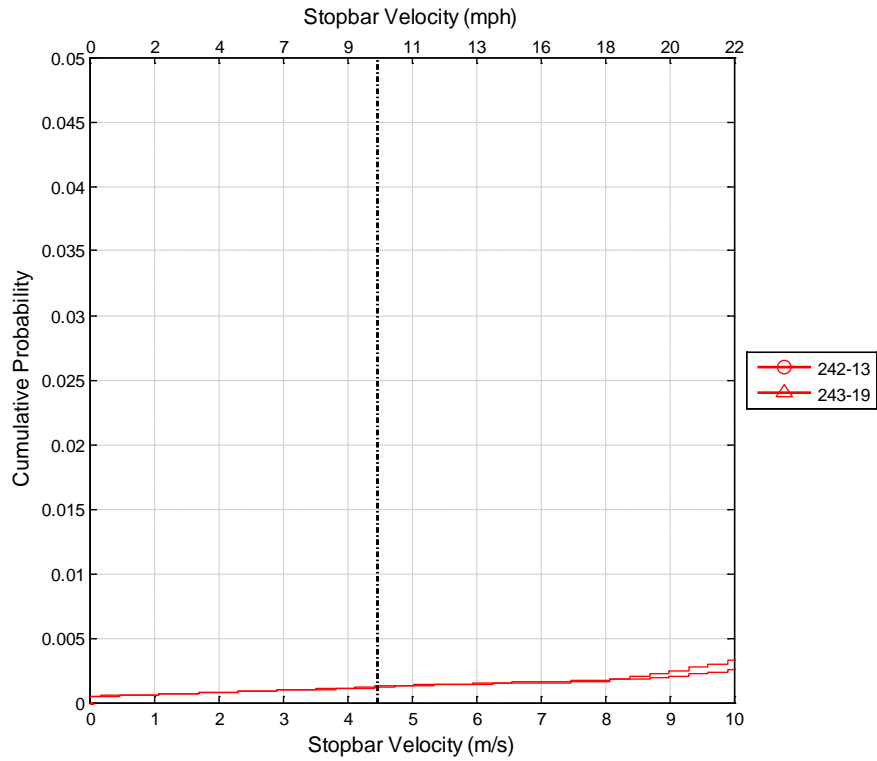


Figure 246 Cumulative distribution of the stop-bar speed for false positives produced by the 200 series algorithm at a false positive rate of 0.01 using a violation threshold of 10 mph.

Stopbar Velocity Distributions for Signalized Intersections Using an FPR of 0.01 and a 10-mph Violation Threshold

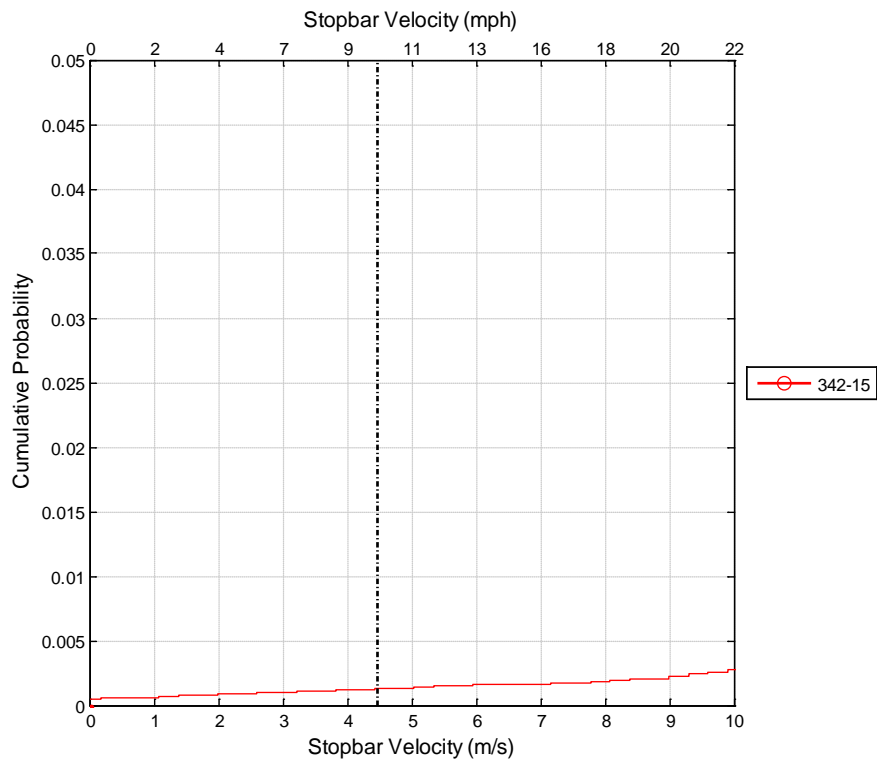


Figure 247 Cumulative distribution of the stop-bar speed for false positives produced by the 300 series algorithm at a false positive rate of 0.01 using a violation threshold of 10 mph.

Stopbar Velocity Distributions for Signalized Intersections Using an FPR of 0.01 and a 10-mph Violation Threshold

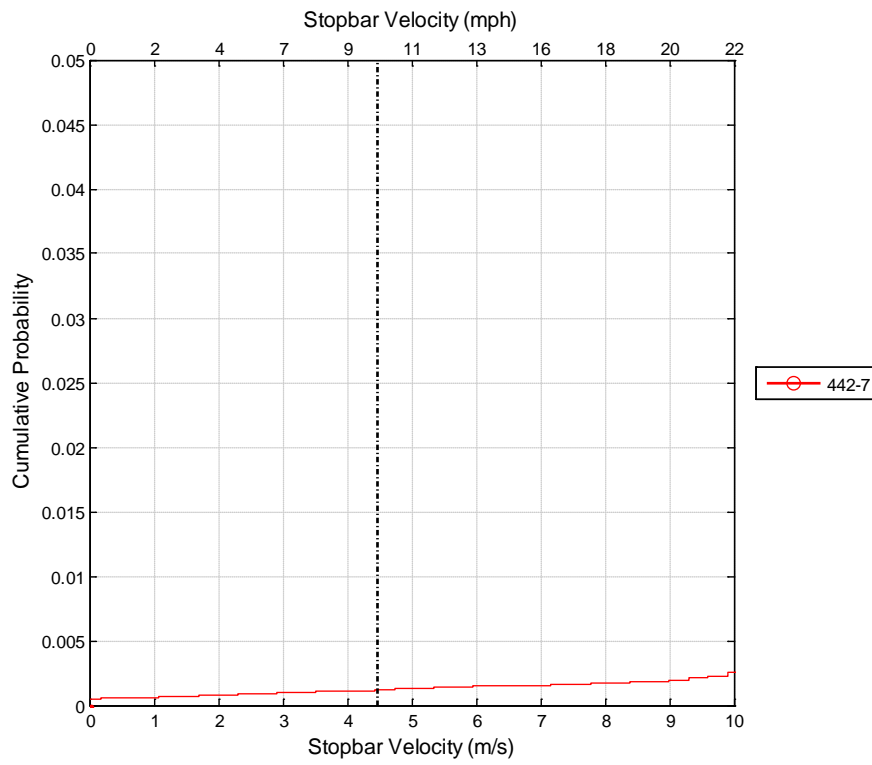


Figure 248 Cumulative distribution of the stop-bar speed for false positives produced by the 400 series algorithm at a false positive rate of 0.01 using a violation threshold of 10 mph.

Stopbar Velocity Distributions for Signalized Intersections Using an FPR of 0.01 and a 10-mph Violation Threshold

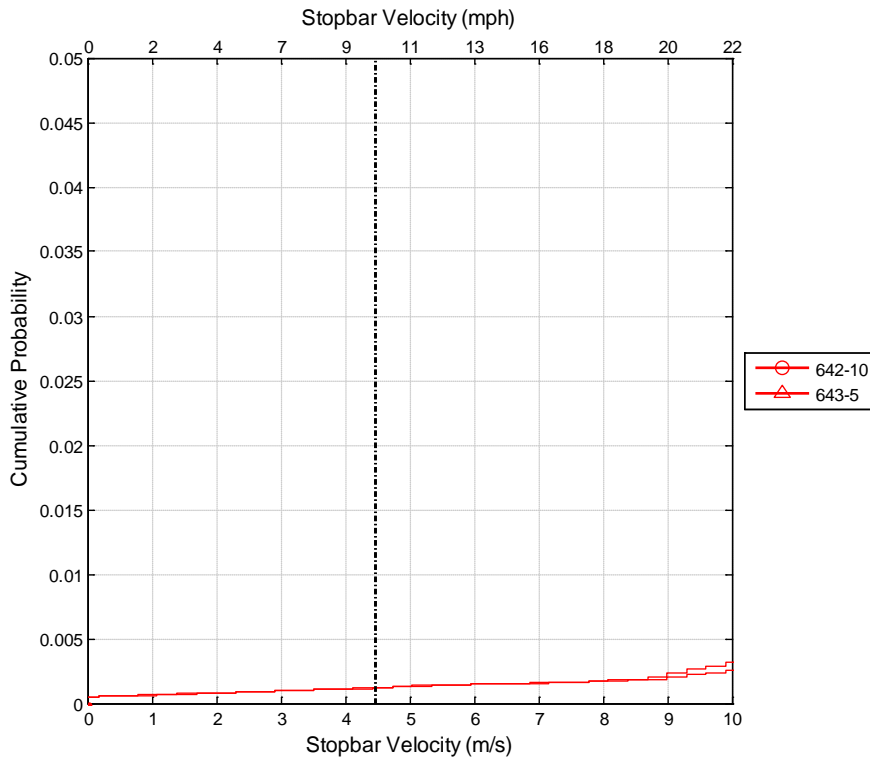


Figure 249 Cumulative distribution of the stop-bar speed for false positives produced by the 600 series algorithm at a false positive rate of 0.01 using a violation threshold of 10 mph.

(No warning produced for 800 series algorithm at a false positive rate of 0.01 using a violation threshold of 10 mph.)

Stopbar Velocity Distributions for Signalized Intersections Using an FPR of 0.01 and a 15-mph Violation Threshold

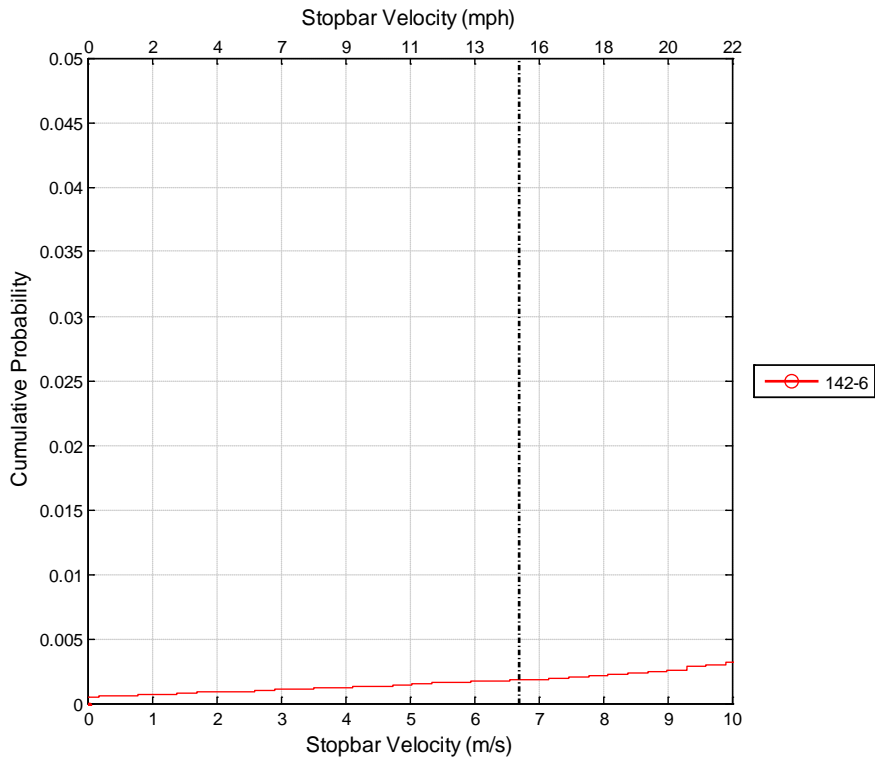


Figure 250 Cumulative distribution of the stop-bar speed for false positives produced by the 100 series algorithm at a false positive rate of 0.01 using a violation threshold of 15 mph.



Stopbar Velocity Distributions for Signalized Intersections Using an FPR of 0.01 and a 15-mph Violation Threshold

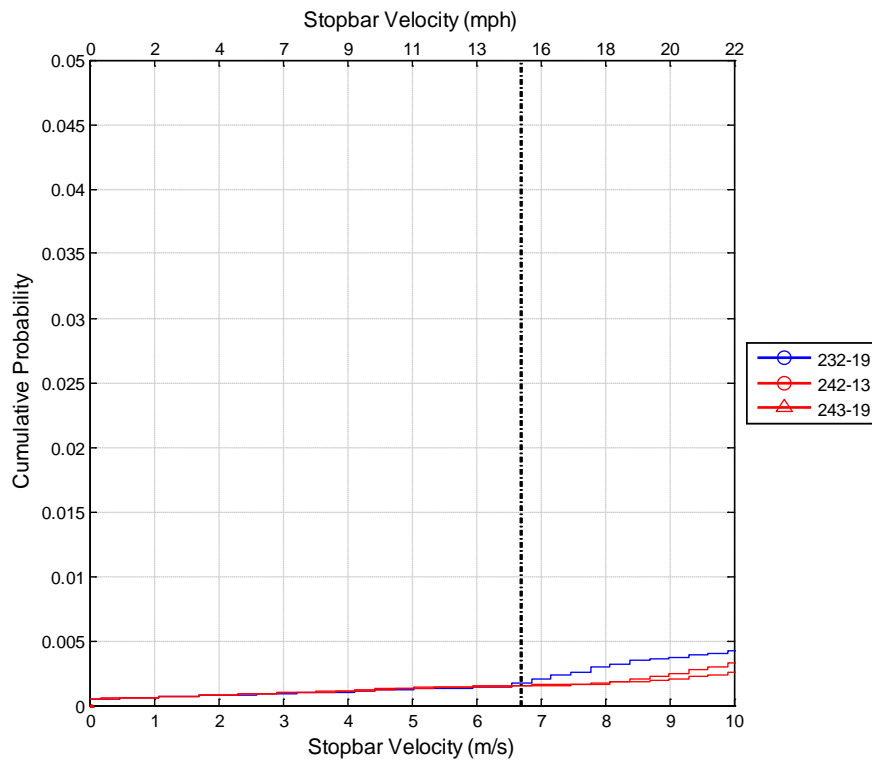


Figure 251 Cumulative distribution of the stop-bar speed for false positives produced by the 200 series algorithm at a false positive rate of 0.01 using a violation threshold of 15 mph.

Stopbar Velocity Distributions for Signalized Intersections Using an FPR of 0.01 and a 15-mph Violation Threshold

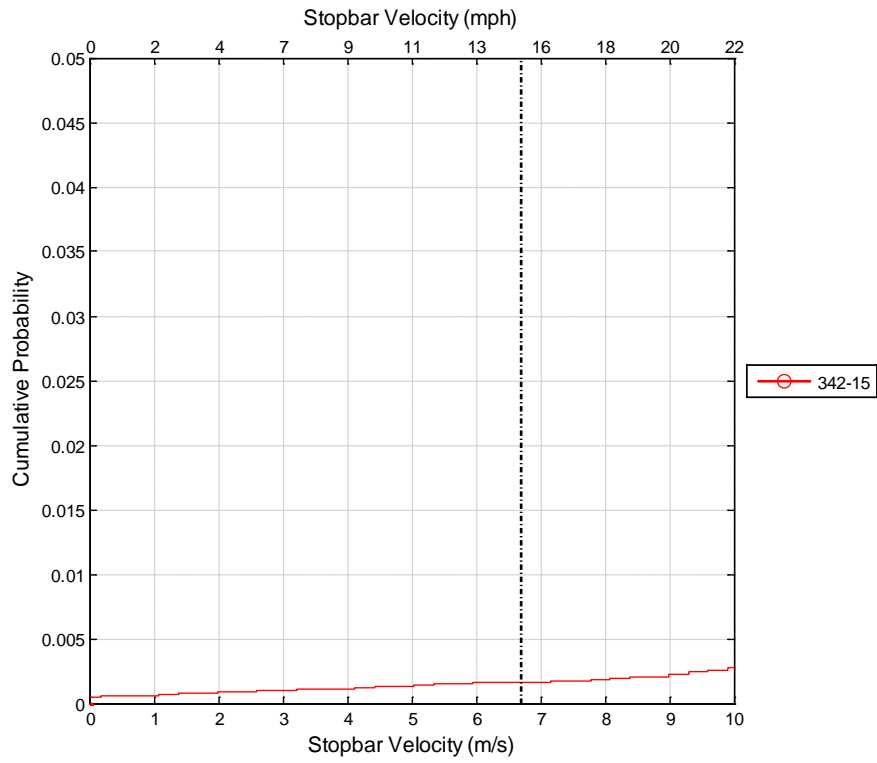


Figure 252 Cumulative distribution of the stop-bar speed for false positives produced by the 300 series algorithm at a false positive rate of 0.01 using a violation threshold of 15 mph.

Stopbar Velocity Distributions for Signalized Intersections Using an FPR of 0.01 and a 15-mph Violation Threshold

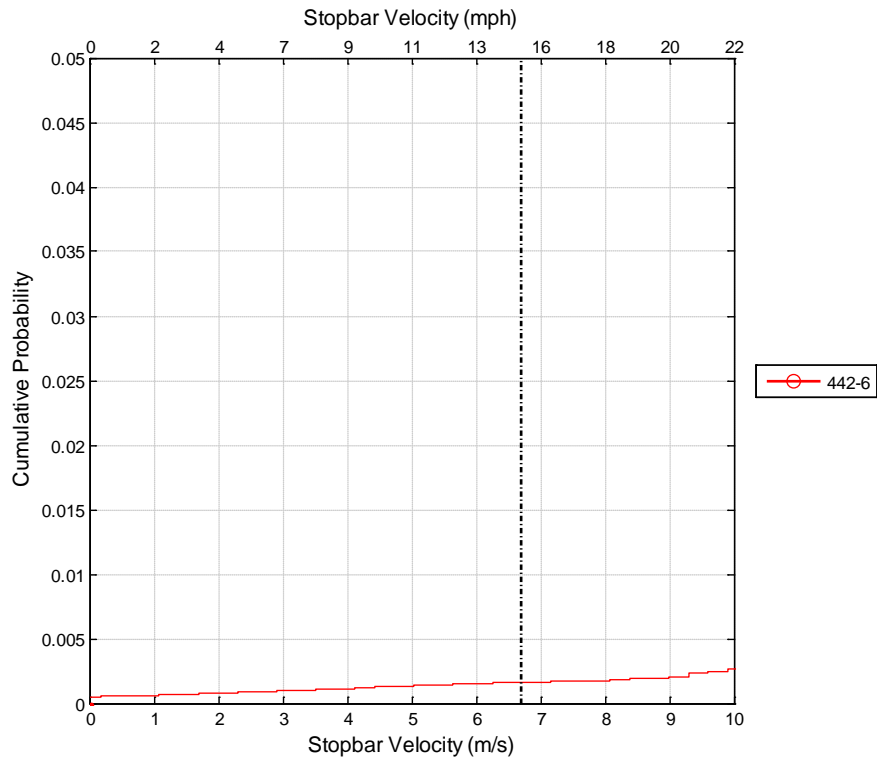


Figure 253 Cumulative distribution of the stop-bar speed for false positives produced by the 400 series algorithm at a false positive rate of 0.01 using a violation threshold of 15 mph.

Stopbar Velocity Distributions for Signalized Intersections Using an FPR of 0.01 and a 15-mph Violation Threshold

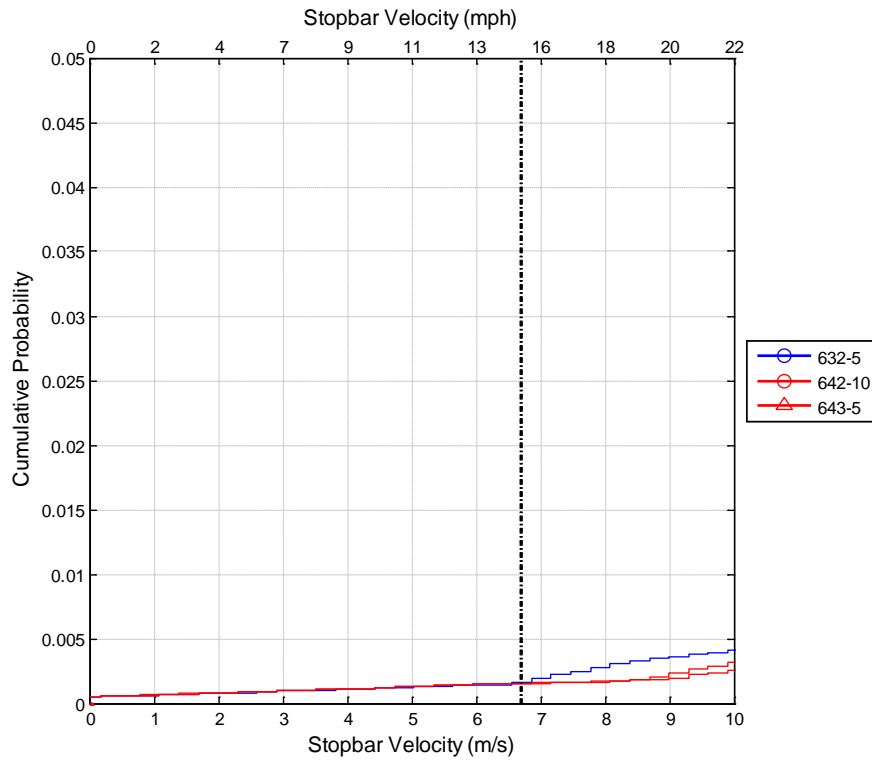


Figure 254 Cumulative distribution of the stop-bar speed for false positives produced by the 600 series algorithm at a false positive rate of 0.01 using a violation threshold of 15 mph.

Stopbar Velocity Distributions for Signalized Intersections Using an FPR of 0.01 and a 15-mph Violation Threshold

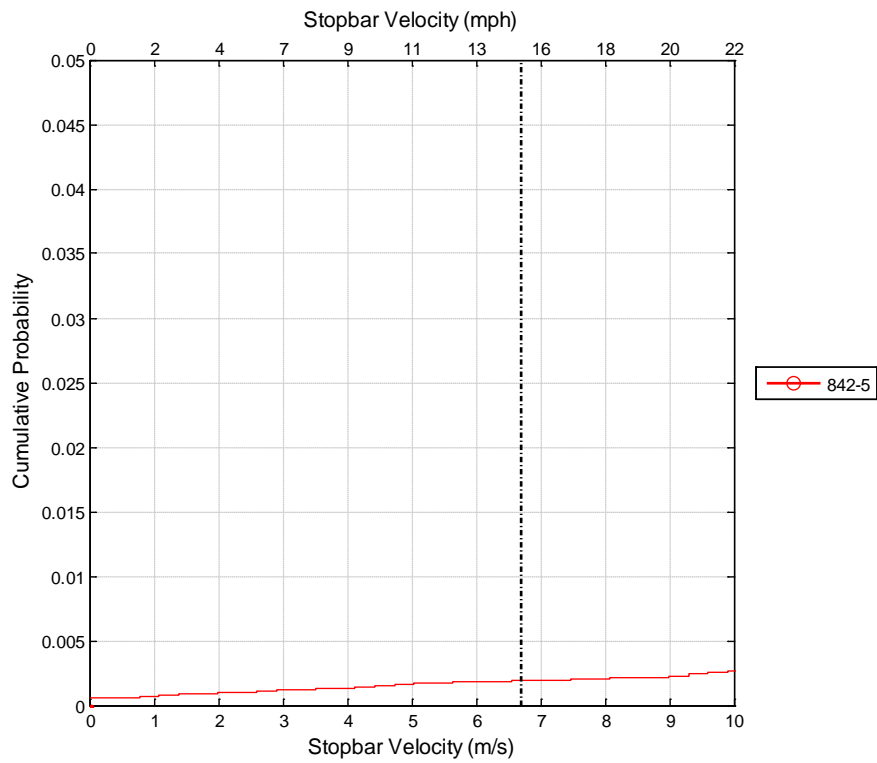


Figure 255 Cumulative distribution of the stop-bar speed for false positives produced by the 800 series algorithm at a false positive rate of 0.01 using a violation threshold of 15 mph.

Stopbar Velocity Distributions for Signalized Intersections Using an FPR of 0.01 and a 20-mph Violation Threshold

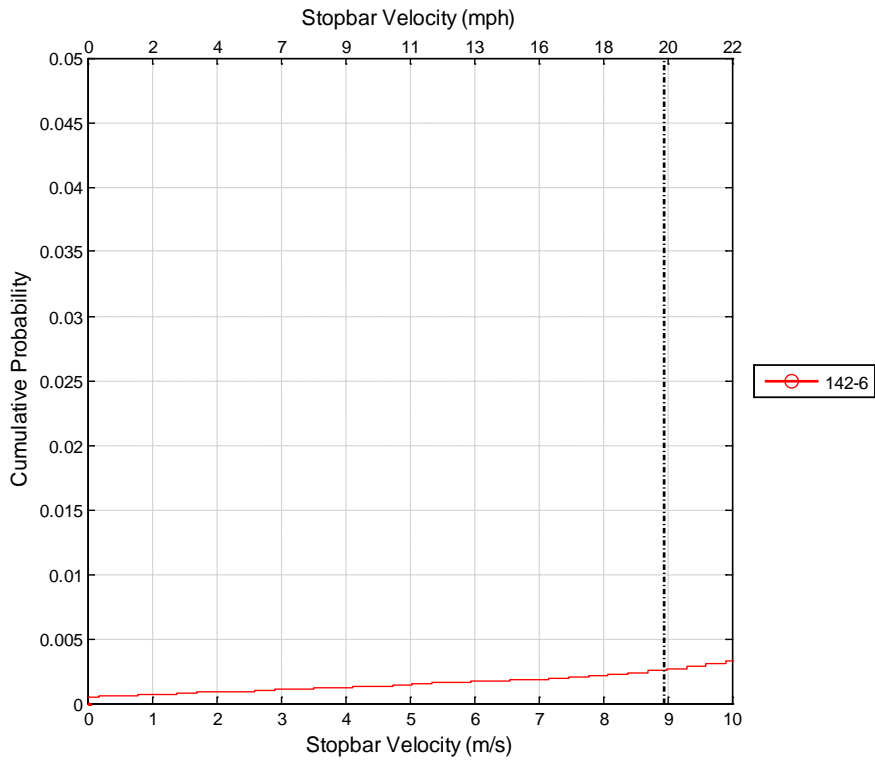


Figure 256 Cumulative distribution of the stop-bar speed for false positives produced by the 100 series algorithm at a false positive rate of 0.01 using a violation threshold of 20 mph.

Stopbar Velocity Distributions for Signalized Intersections Using an FPR of 0.01 and a 20-mph Violation Threshold

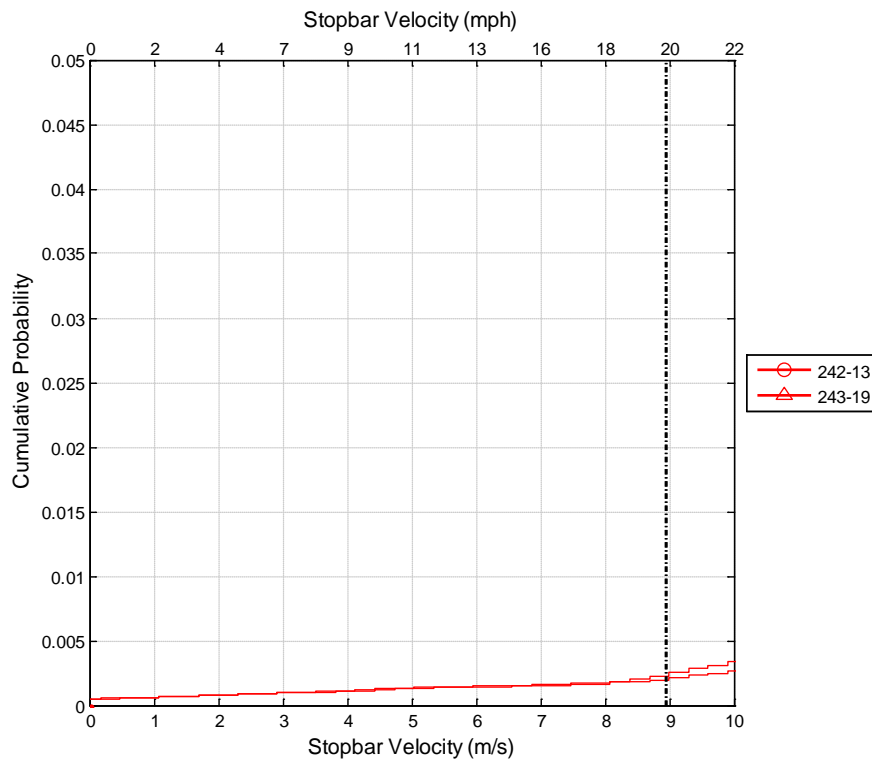


Figure 257 Cumulative distribution of the stop-bar speed for false positives produced by the 200 series algorithm at a false positive rate of 0.01 using a violation threshold of 20 mph.

Stopbar Velocity Distributions for Signalized Intersections Using an FPR of 0.01 and a 20-mph Violation Threshold

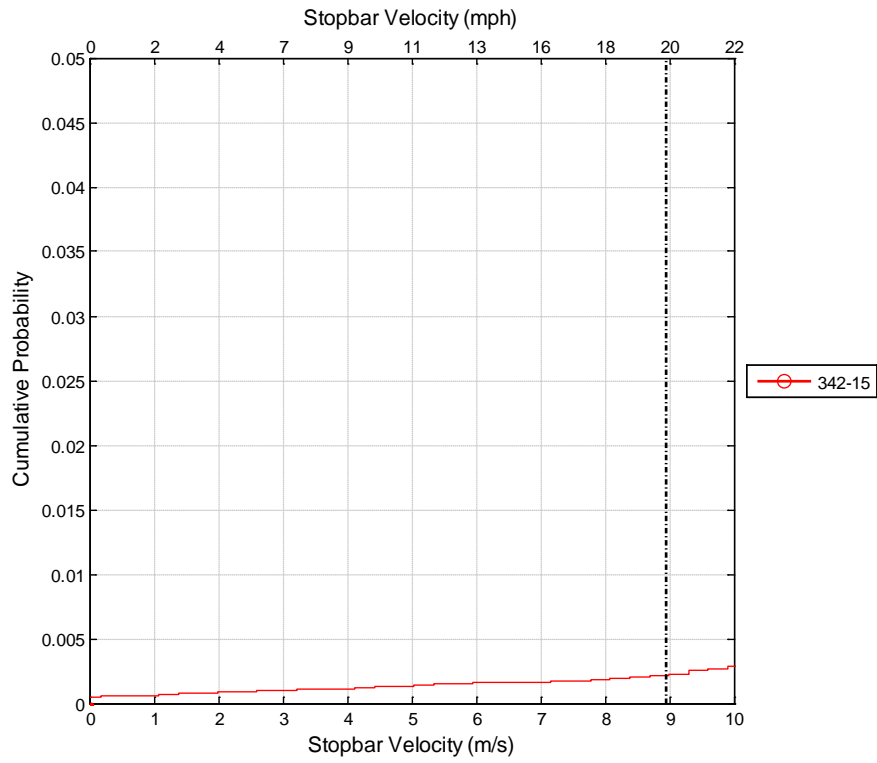


Figure 258 Cumulative distribution of the stop-bar speed for false positives produced by the 300 series algorithm at a false positive rate of 0.01 using a violation threshold of 20 mph.



Stopbar Velocity Distributions for Signalized Intersections Using an FPR of 0.01 and a 20-mph Violation Threshold

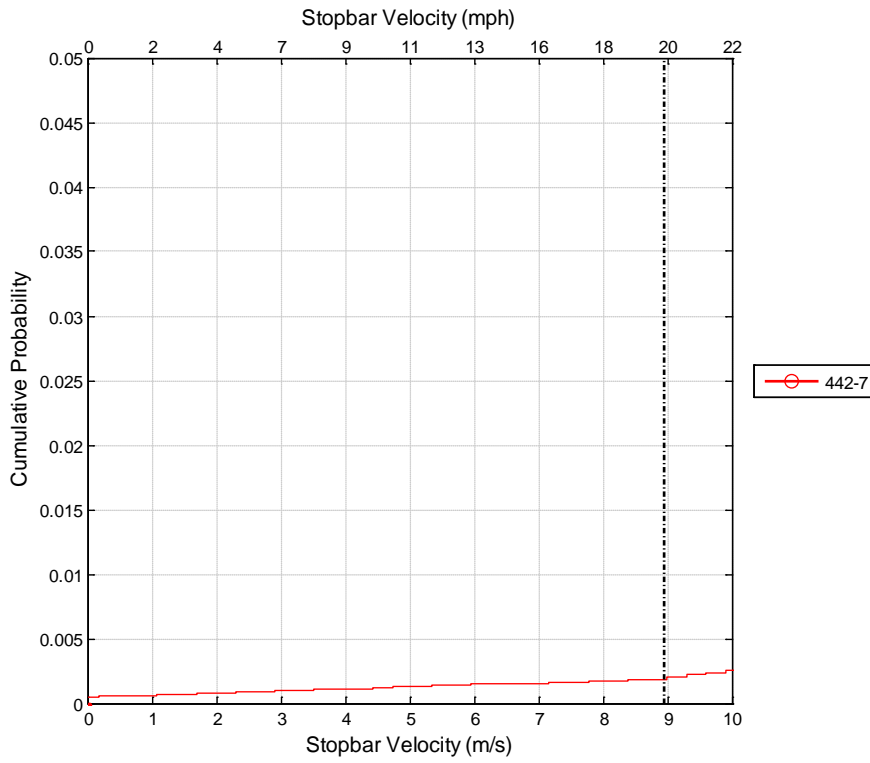


Figure 259 Cumulative distribution of the stop-bar speed for false positives produced by the 400 series algorithm at a false positive rate of 0.01 using a violation threshold of 20 mph.

Stopbar Velocity Distributions for Signalized Intersections Using an FPR of 0.01 and a 20-mph Violation Threshold

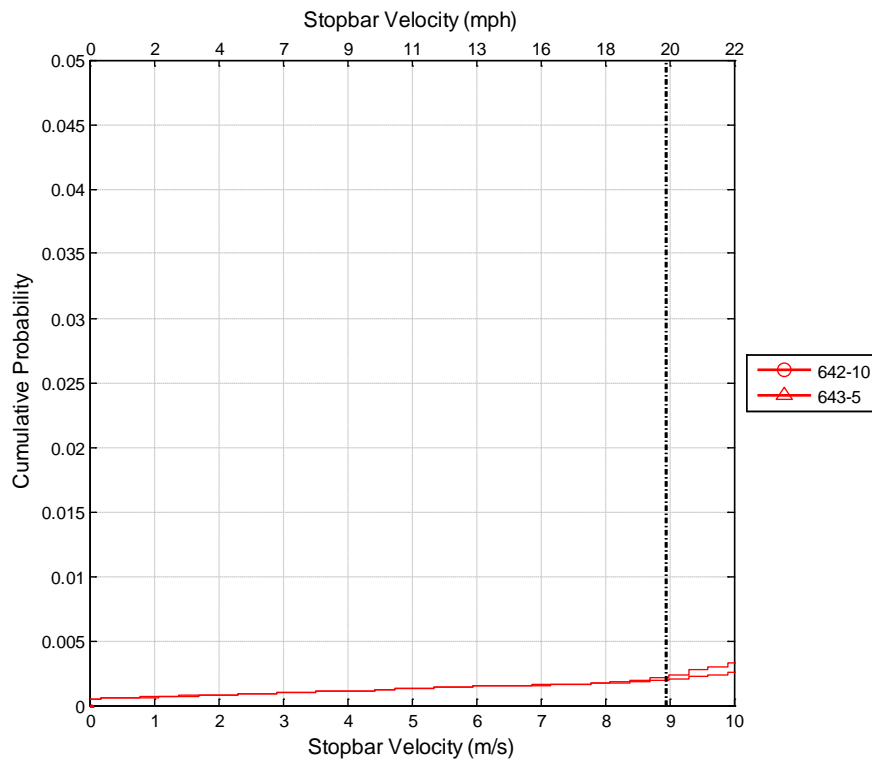


Figure 260 Cumulative distribution of the stop-bar speed for false positives produced by the 600 series algorithm at a false positive rate of 0.01 using a violation threshold of 20 mph.

Stopbar Velocity Distributions for Signalized Intersections Using an FPR of 0.01 and a 20-mph Violation Threshold

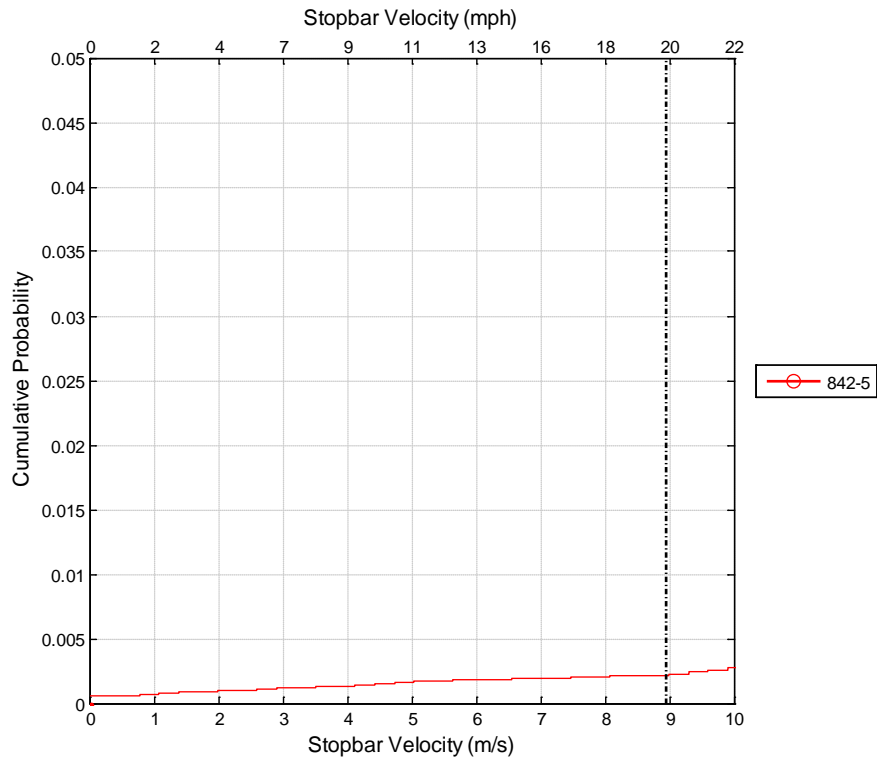


Figure 261 Cumulative distribution of the stop-bar speed for false positives produced by the 800 series algorithm at a false positive rate of 0.01 using a violation threshold of 20 mph.

Stopbar Velocity Distributions for Signalized Intersections Using an FPR of 0.05 and a 10-mph Violation Threshold

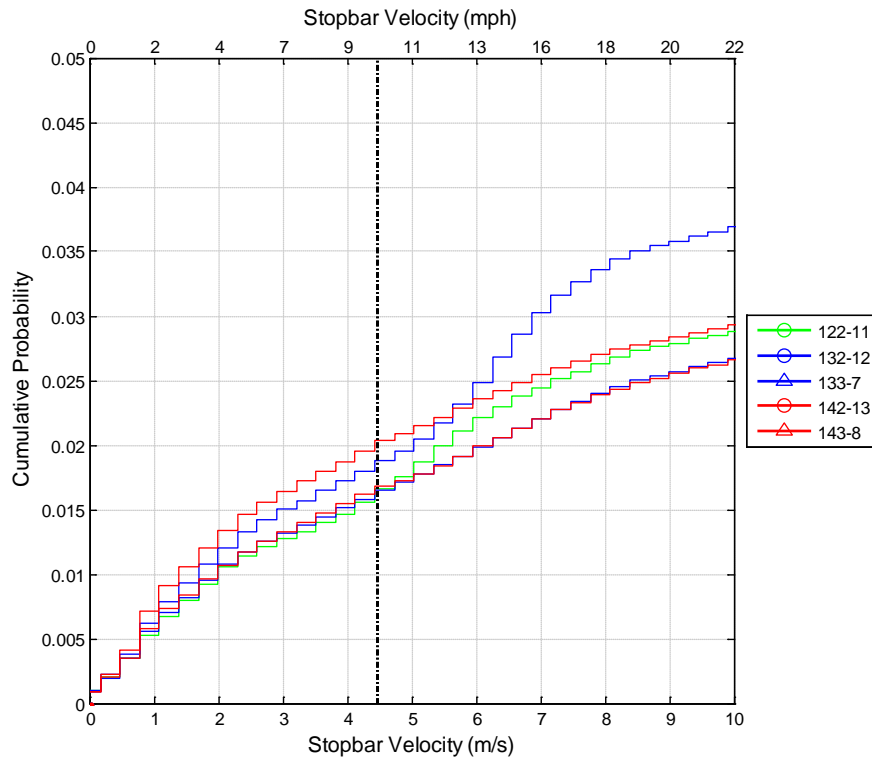


Figure 262 Cumulative distribution of the stop-bar speed for false positives produced by the 100 series algorithm at a false positive rate of 0.05 using a violation threshold of 10 mph.

Stopbar Velocity Distributions for Signalized Intersections Using an FPR of 0.05 and a 10-mph Violation Threshold

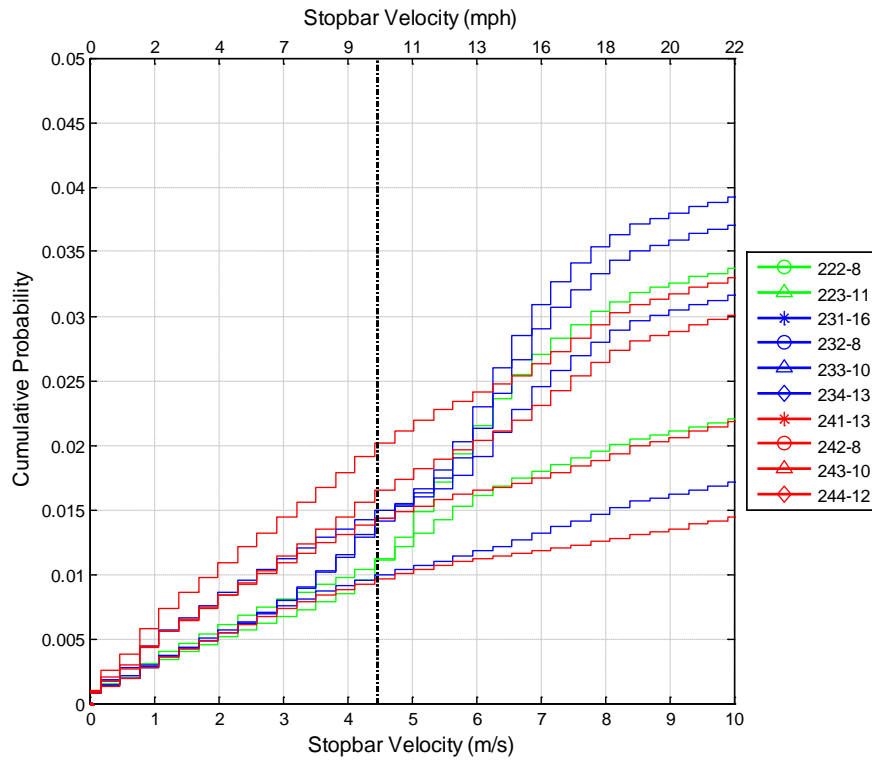


Figure 263 Cumulative distribution of the stop-bar speed for false positives produced by the 200 series algorithm at a false positive rate of 0.05 using a violation threshold of 10 mph.

Stopbar Velocity Distributions for Signalized Intersections Using an FPR of 0.05 and a 10-mph Violation Threshold

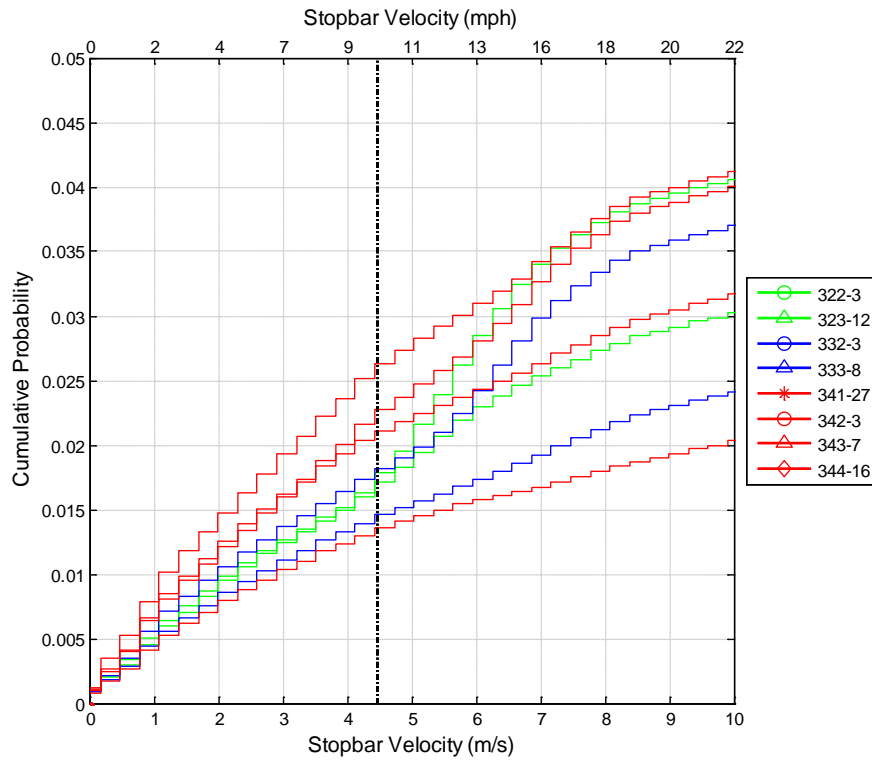


Figure 264 Cumulative distribution of the stop-bar speed for false positives produced by the 300 series algorithm at a false positive rate of 0.05 using a violation threshold of 10 mph.

Stopbar Velocity Distributions for Signalized Intersections Using an FPR of 0.05 and a 10-mph Violation Threshold

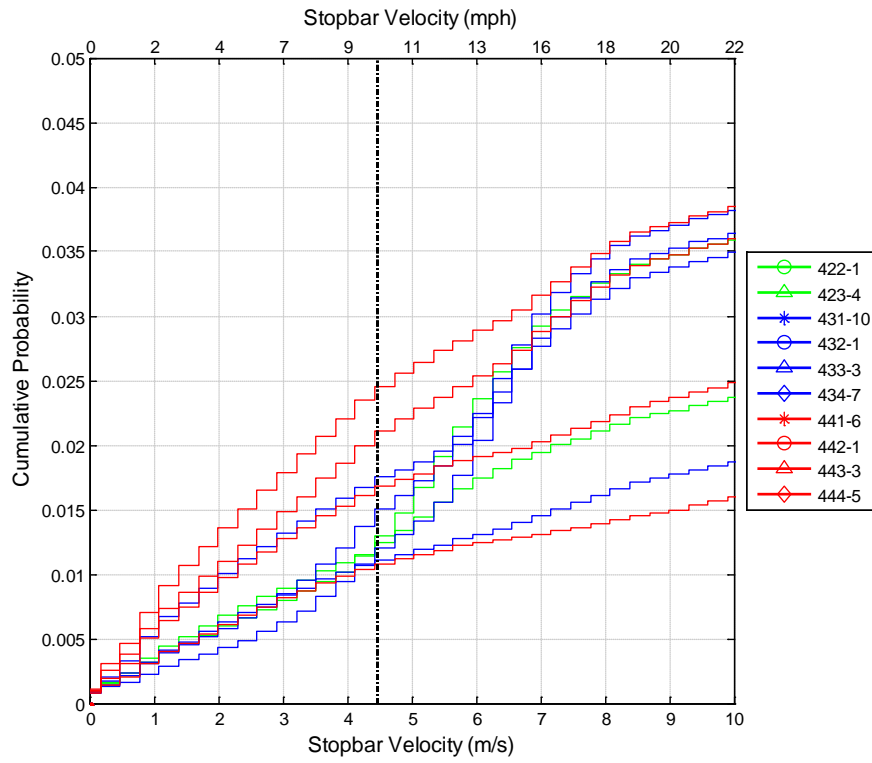


Figure 265 Cumulative distribution of the stop-bar speed for false positives produced by the 400 series algorithm at a false positive rate of 0.05 using a violation threshold of 10 mph.

Stopbar Velocity Distributions for Signalized Intersections Using an FPR of 0.05 and a 10-mph Violation Threshold

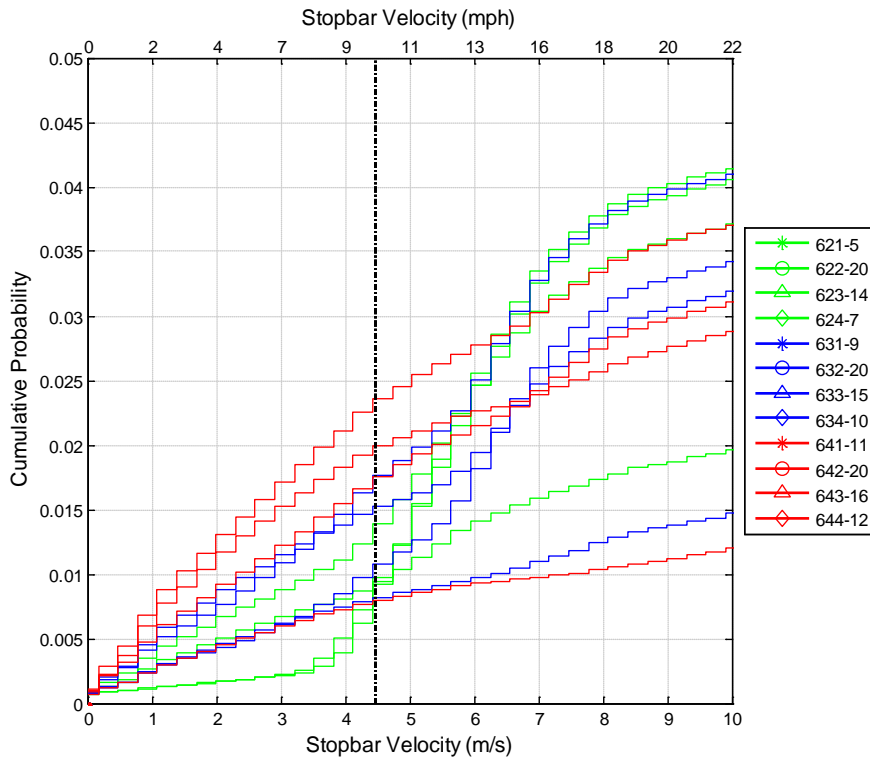


Figure 266 Cumulative distribution of the stop-bar speed for false positives produced by the 600 series algorithm at a false positive rate of 0.05 using a violation threshold of 10 mph.



Stopbar Velocity Distributions for Signalized Intersections Using an FPR of 0.05 and a 10-mph Violation Threshold

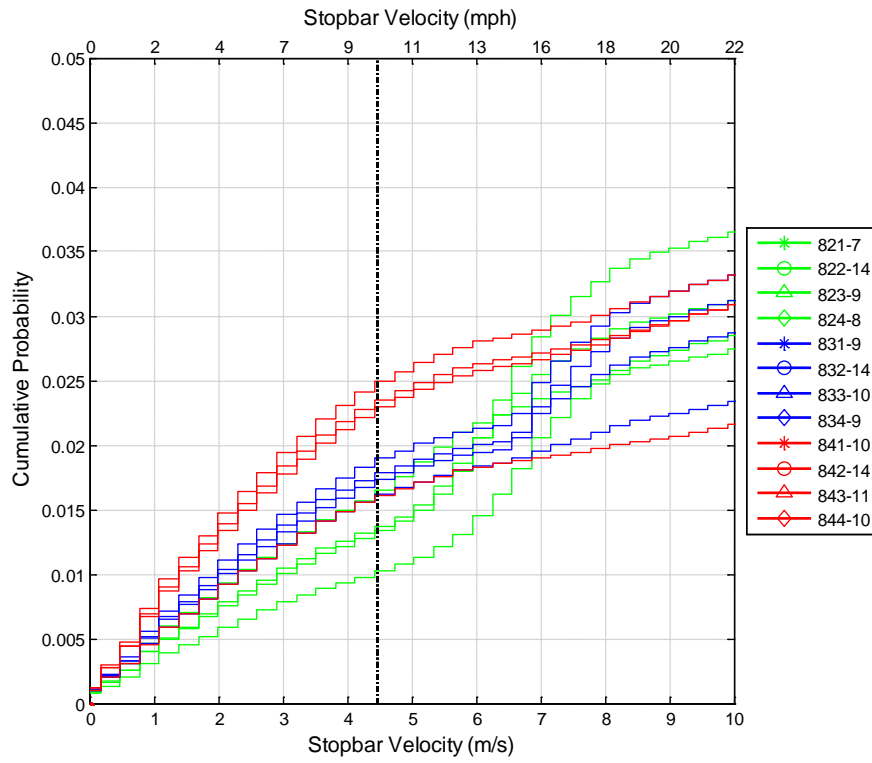


Figure 267 Cumulative distribution of the stop-bar speed for false positives produced by the 800 series algorithm at a false positive rate of 0.05 using a violation threshold of 10 mph.

Stopbar Velocity Distributions for Signalized Intersections Using an FPR of 0.05 and a 15-mph Violation Threshold

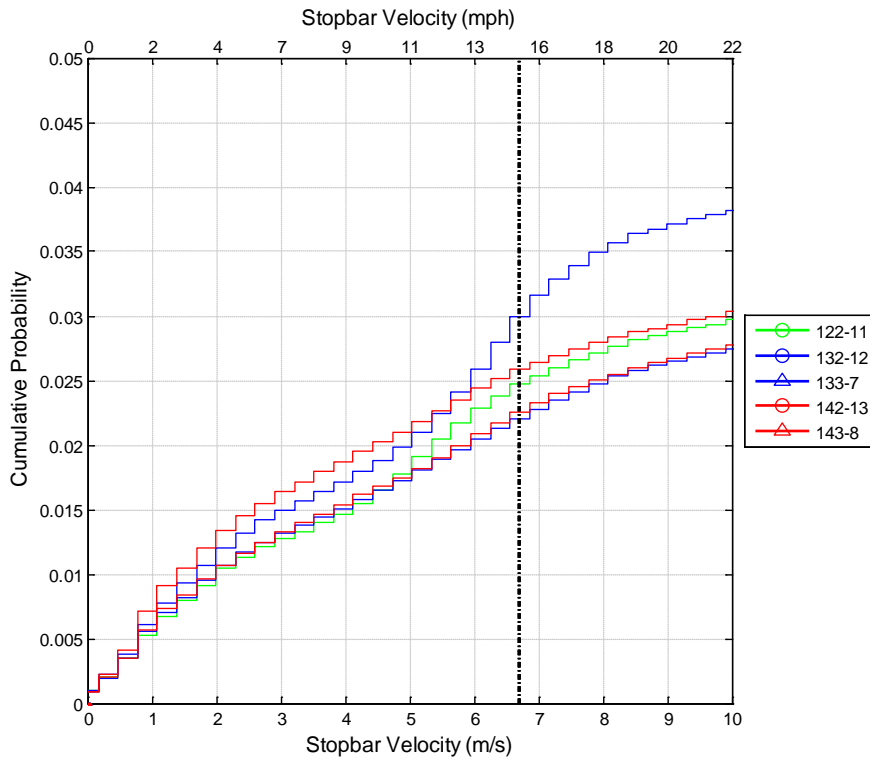


Figure 268 Cumulative distribution of the stop-bar speed for false positives produced by the 100 series algorithm at a false positive rate of 0.05 using a violation threshold of 15 mph.

Stopbar Velocity Distributions for Signalized Intersections Using an FPR of 0.05 and a 15-mph Violation Threshold

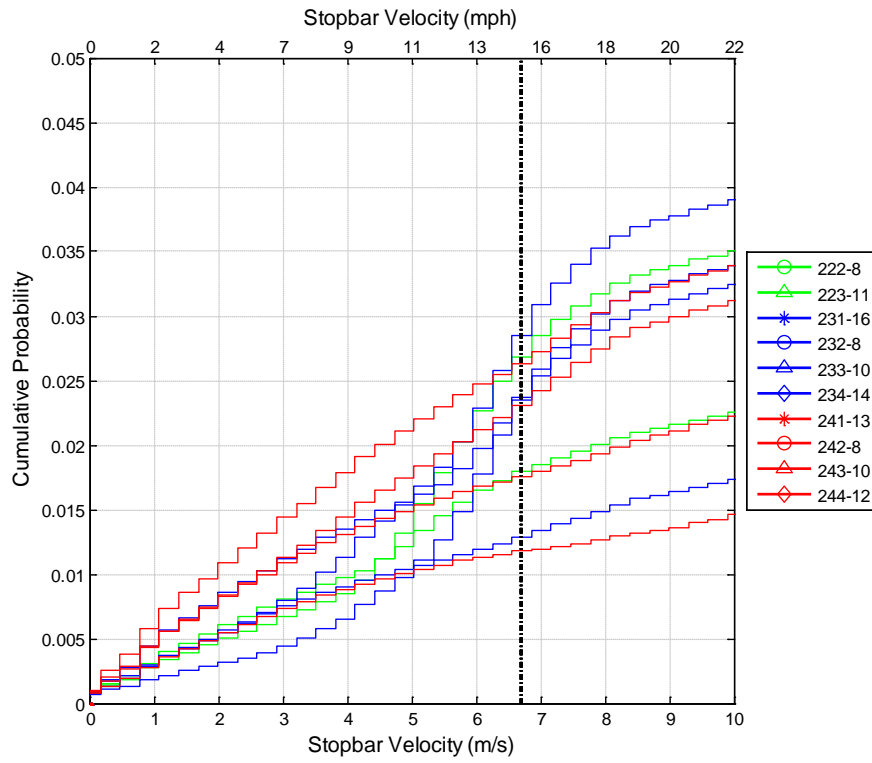


Figure 269 Cumulative distribution of the stop-bar speed for false positives produced by the 200 series algorithm at a false positive rate of 0.05 using a violation threshold of 15 mph.

Stopbar Velocity Distributions for Signalized Intersections Using an FPR of 0.05 and a 15-mph Violation Threshold

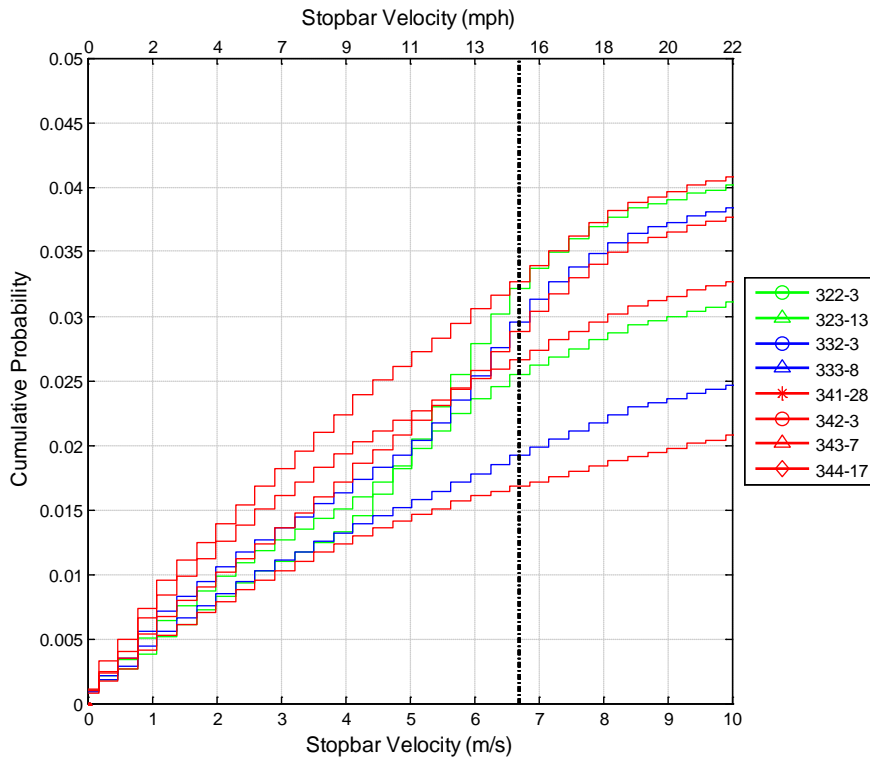


Figure 270 Cumulative distribution of the stop-bar speed for false positives produced by the 300 series algorithm at a false positive rate of 0.05 using a violation threshold of 15 mph.

Stopbar Velocity Distributions for Signalized Intersections Using an FPR of 0.05 and a 15-mph Violation Threshold

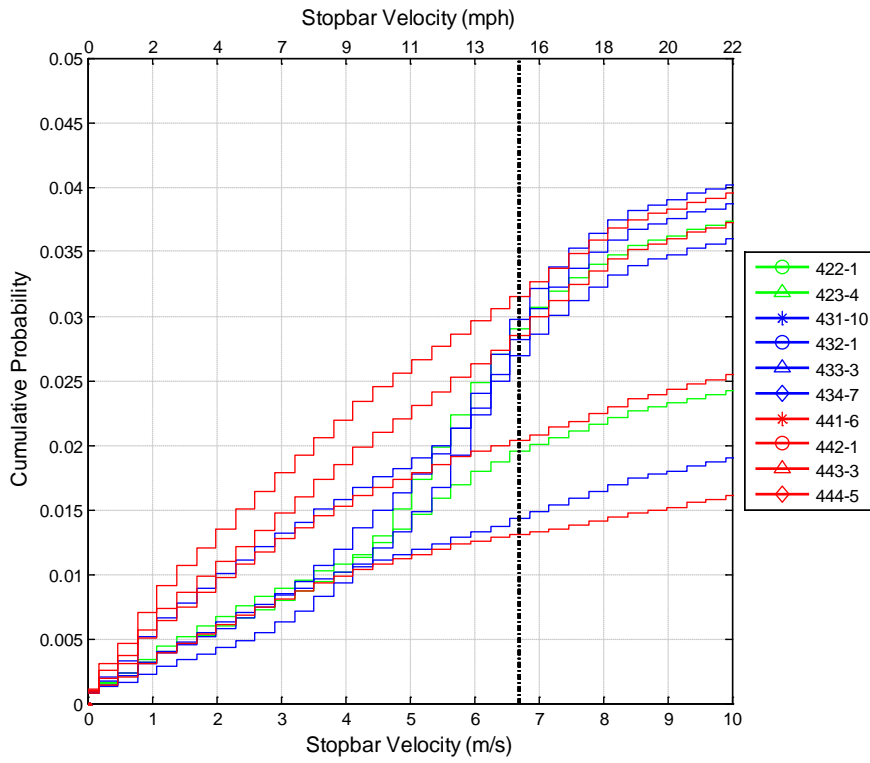


Figure 271 Cumulative distribution of the stop-bar speed for false positives produced by the 400 series algorithm at a false positive rate of 0.05 using a violation threshold of 15 mph.

Stopbar Velocity Distributions for Signalized Intersections Using an FPR of 0.05 and a 15-mph Violation Threshold

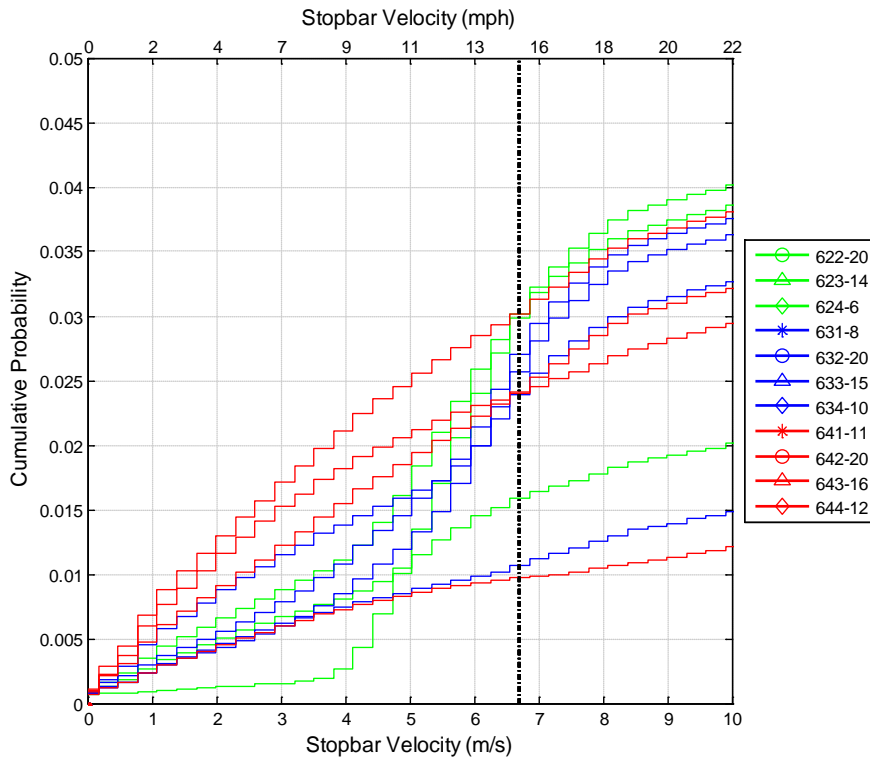


Figure 272 Cumulative distribution of the stop-bar speed for false positives produced by the 600 series algorithm at a false positive rate of 0.05 using a violation threshold of 15 mph.

Stopbar Velocity Distributions for Signalized Intersections Using an FPR of 0.05 and a 15-mph Violation Threshold

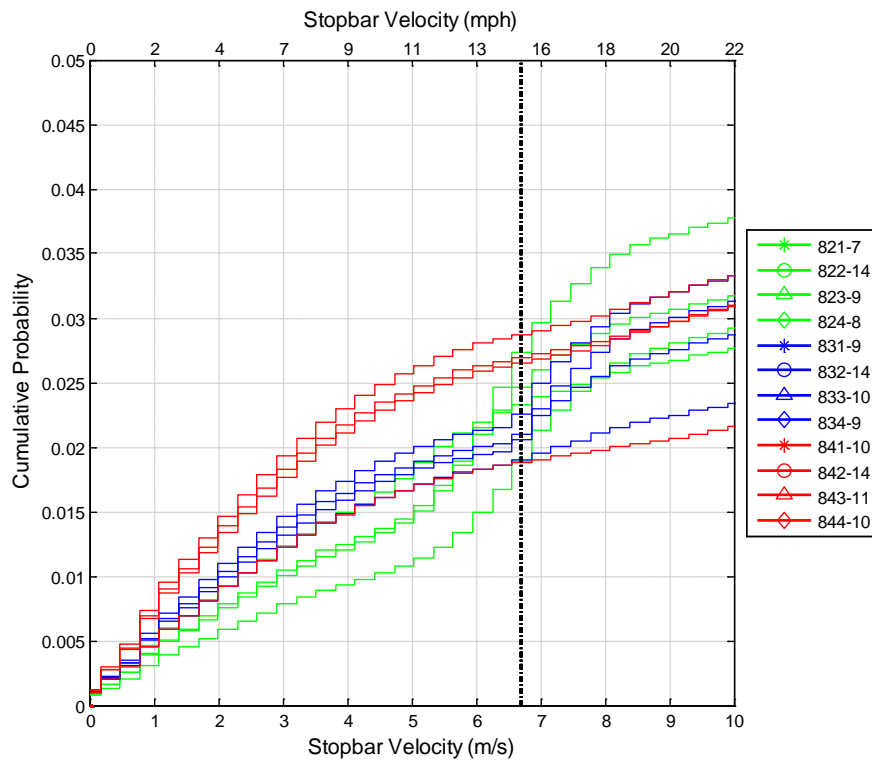


Figure 273 Cumulative distribution of the stop-bar speed for false positives produced by the 800 series algorithm at a false positive rate of 0.05 using a violation threshold of 15 mph.

Stopbar Velocity Distributions for Signalized Intersections Using an FPR of 0.05 and a 20-mph Violation Threshold

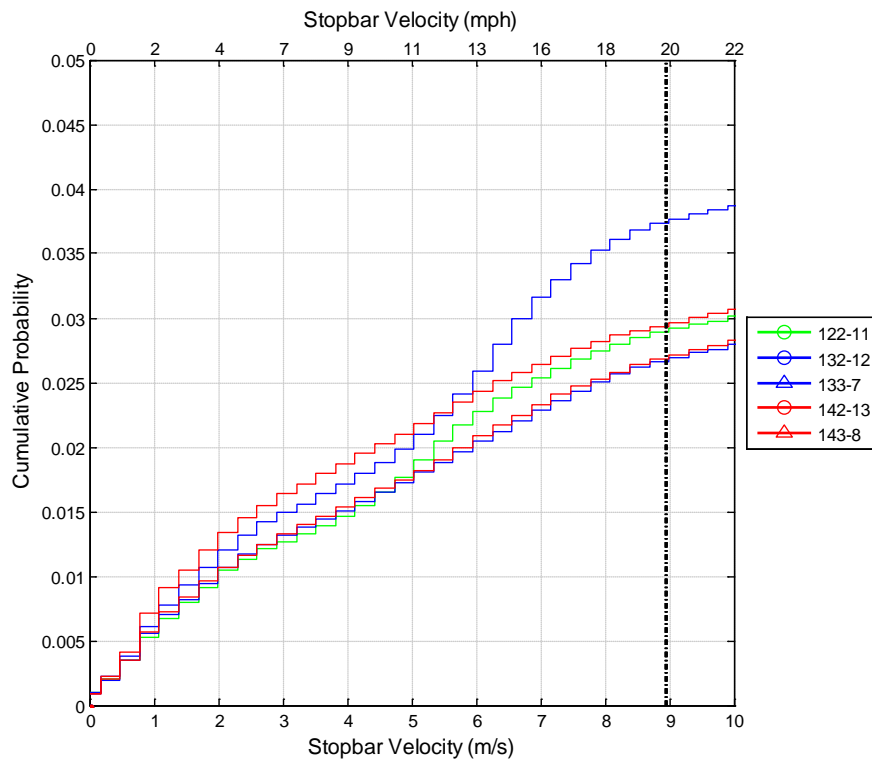


Figure 274 Cumulative distribution of the stop-bar speed for false positives produced by the 100 series algorithm at a false positive rate of 0.05 using a violation threshold of 20 mph.



Stopbar Velocity Distributions for Signalized Intersections Using an FPR of 0.05 and a 20-mph Violation Threshold

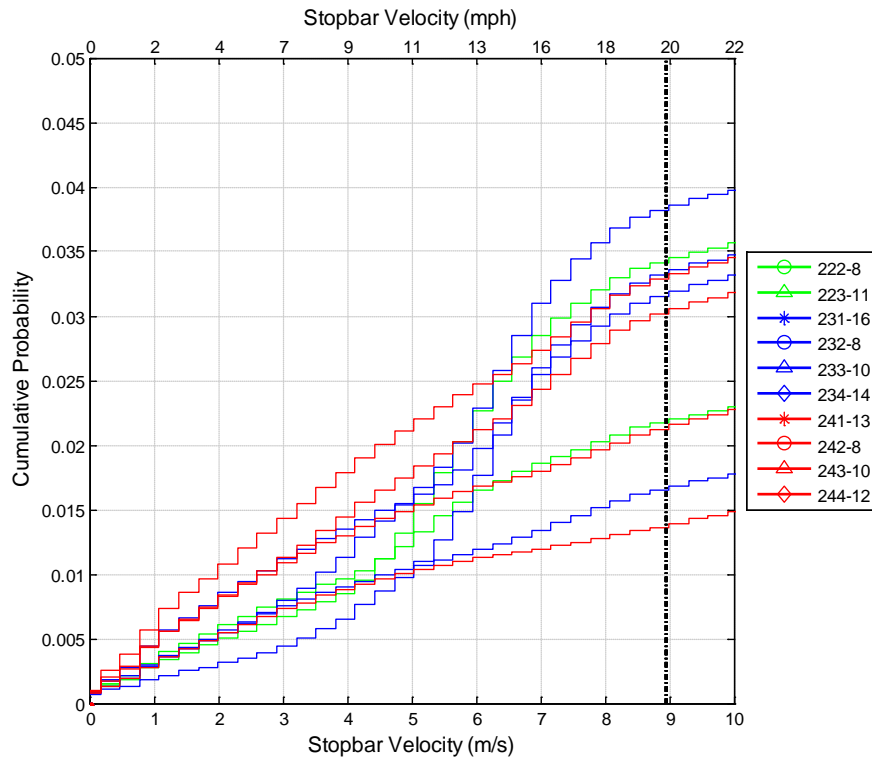


Figure 275 Cumulative distribution of the stop-bar speed for false positives produced by the 200 series algorithm at a false positive rate of 0.05 using a violation threshold of 20 mph.

Stopbar Velocity Distributions for Signalized Intersections Using an FPR of 0.05 and a 20-mph Violation Threshold

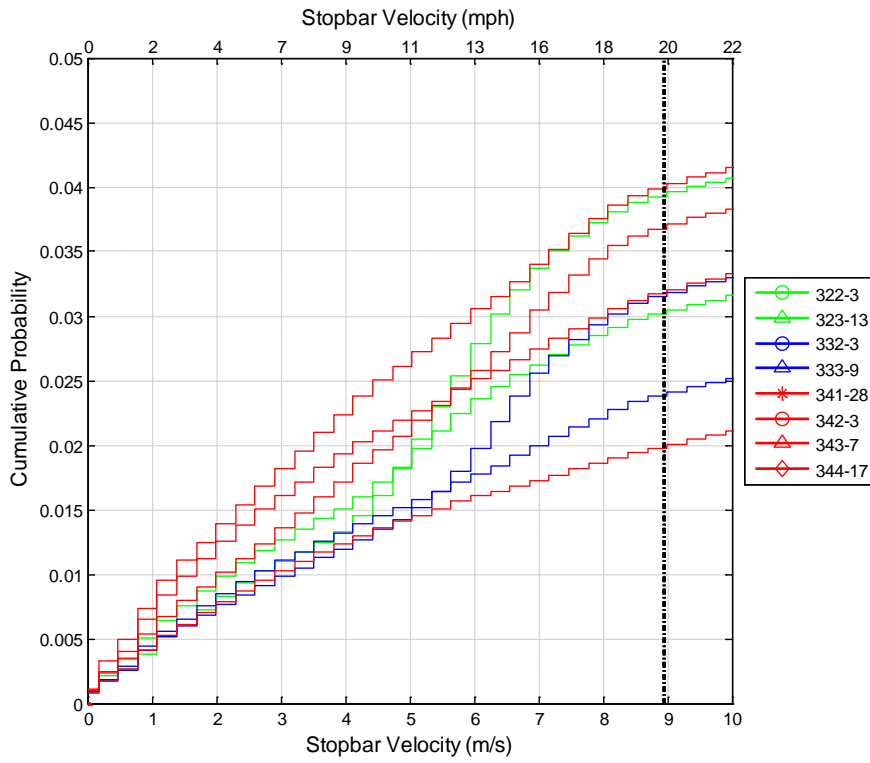


Figure 276 Cumulative distribution of the stop-bar speed for false positives produced by the 300 series algorithm at a false positive rate of 0.05 using a violation threshold of 20 mph.

Stopbar Velocity Distributions for Signalized Intersections Using an FPR of 0.05 and a 20-mph Violation Threshold

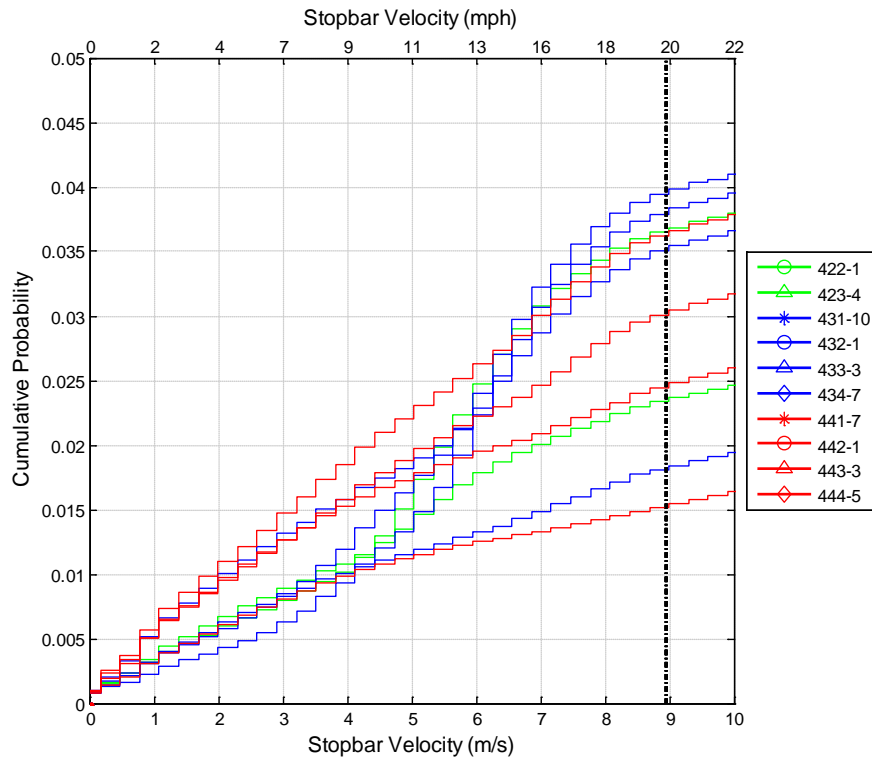


Figure 277 Cumulative distribution of the stop-bar speed for false positives produced by the 400 series algorithm at a false positive rate of 0.05 using a violation threshold of 20 mph.

Stopbar Velocity Distributions for Signalized Intersections Using an FPR of 0.05 and a 20-mph Violation Threshold

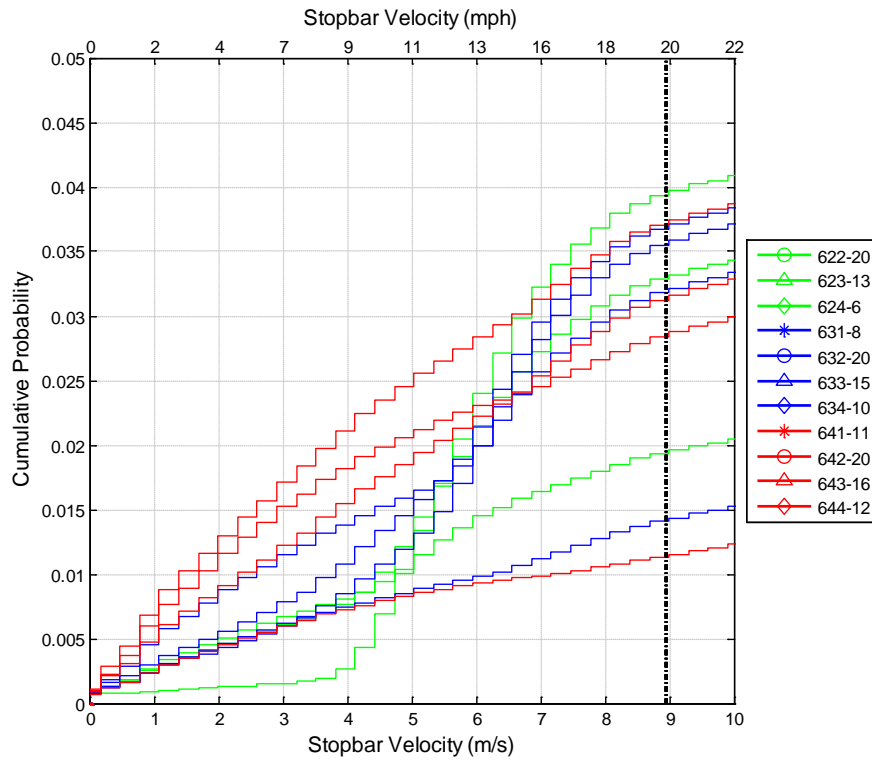


Figure 278 Cumulative distribution of the stop-bar speed for false positives produced by the 600 series algorithm at a false positive rate of 0.05 using a violation threshold of 20 mph.

Stopbar Velocity Distributions for Signalized Intersections Using an FPR of 0.05 and a 20-mph Violation Threshold

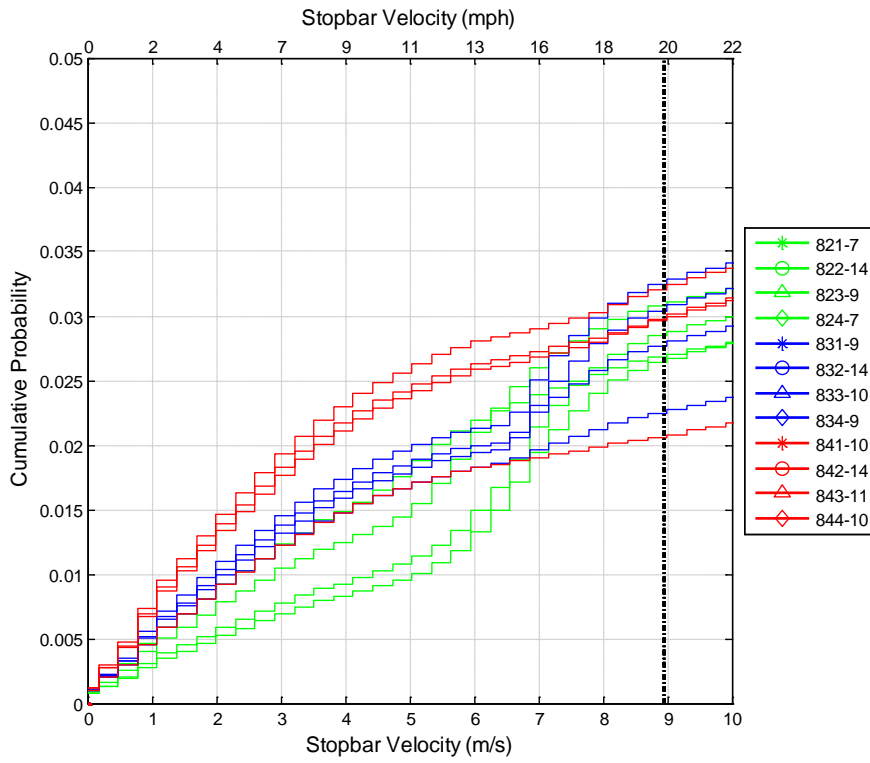


Figure 279 Cumulative distribution of the stop-bar speed for false positives produced by the 800 series algorithm at a false positive rate of 0.05 using a violation threshold of 20 mph.

### 11.20 Appendix T: Algorithm Simulation Results Summary

Table 40 Best stop-controlled algorithms for 10 mph.

Maximize True Positives									
	Algorithm	Point A	Point B	Point C	Point D	Point E	Point F	Point G	
Allowable FP=0.05	Best Overall	831 - 8	0.066	0.166	0.294	0.446	0.588	0.008	0.050
	Best Applicable	831 - 8	0.066	0.166	0.294	0.446	0.588	0.008	0.050
	Maximize Early Warnings								
		Algorithm	Point A	Point B	Point C	Point D	Point E	Point F	Point G
	Best Overall	831 - 8	0.066	0.166	0.294	0.446	0.588	0.008	0.050
	Best Applicable	831 - 8	0.066	0.166	0.294	0.446	0.588	0.008	0.050
Compromise between Early Warnings and Maximum True Positives									
	Algorithm	Point A	Point B	Point C	Point D	Point E	Point F	Point G	
Best Overall	831 - 8	0.066	0.166	0.294	0.446	0.588	0.008	0.050	
Best Applicable	831 - 8	0.066	0.166	0.294	0.446	0.588	0.008	0.050	

Table 41 Best stop-controlled algorithms for 20 mph.

<b>Allowable FP=0.05</b>	<b>Maximize True Positives</b>								
		Algorithm	Point A	Point B	Point C	Point D	Point E	Point F	Point G
	Best Overall	744 - 9	0.265	0.388	0.571	0.918	1.000	0.021	0.032
	Best Applicable	641 - 7	0.020	0.061	0.224	0.918	1.000	0.019	0.036
	<b>Maximize Early Warnings</b>								
		Algorithm	Point A	Point B	Point C	Point D	Point E	Point F	Point G
	Best Overall	244 - 13	0.918	0.939	0.959	0.959	0.980	0.026	0.039
	Best Applicable	242 - 8	0.633	0.755	0.816	0.878	0.918	0.036	0.046
	<b>Compromise between Early Warnings and Maximum True Positives</b>								
		Algorithm	Point A	Point B	Point C	Point D	Point E	Point F	Point G
Best Overall	244 - 13	0.918	0.939	0.959	0.959	0.980	0.026	0.039	
Best Applicable	841 - 4	0.041	0.102	0.286	0.796	1.000	0.017	0.033	

<b>Allowable FP=0.01</b>	<b>Maximize True Positives</b>								
		Algorithm	Point A	Point B	Point C	Point D	Point E	Point F	Point G
	Best Overall	844 - 9	0.122	0.245	0.816	0.959	0.980	0.005	0.009
	Best Applicable	742 - 14	0.531	0.653	0.714	0.776	0.837	0.006	0.009
	<b>Maximize Early Warnings</b>								
		Algorithm	Point A	Point B	Point C	Point D	Point E	Point F	Point G
	Best Overall	643 - 14	0.714	0.816	0.837	0.898	0.898	0.006	0.009
	Best Applicable	742 - 14	0.531	0.653	0.714	0.776	0.837	0.006	0.009
	<b>Compromise between Early Warnings and Maximum True Positives</b>								
		Algorithm	Point A	Point B	Point C	Point D	Point E	Point F	Point G
Best Overall	844 - 9	0.122	0.245	0.816	0.959	0.980	0.005	0.009	
Best Applicable	742 - 14	0.531	0.653	0.714	0.776	0.837	0.006	0.009	

**Table 42 Best signaled algorithms for 10 mph.**

Maximize True Positives									
	Algorithm	Point A	Point B	Point C	Point D	Point E	Point F	Point G	
Allowable FP=0.05	Best Overall	434 - 7	0.755	0.768	0.781	0.792	0.806	0.005	0.044
	Best Applicable	631 - 9	0.530	0.718	0.765	0.776	0.792	0.009	0.049
	Maximize Early Warnings								
		Algorithm	Point A	Point B	Point C	Point D	Point E	Point F	Point G
	Best Overall	434 - 7	0.755	0.768	0.781	0.792	0.806	0.005	0.044
	Best Applicable	641 - 11	0.679	0.691	0.702	0.713	0.727	0.014	0.046
	Compromise between Early Warnings and Maximum True Positives								
		Algorithm	Point A	Point B	Point C	Point D	Point E	Point F	Point G
	Best Overall	434 - 7	0.755	0.768	0.781	0.792	0.806	0.005	0.044
Best Applicable	631 - 9	0.530	0.718	0.765	0.776	0.792	0.009	0.049	

Maximize True Positives									
	Algorithm	Point A	Point B	Point C	Point D	Point E	Point F	Point G	
Allowable FP=0.01	Best Overall	243 - 19	0.001	0.001	0.001	0.001	0.545	0.001	0.010
	Best Applicable	242 - 13	0.504	0.512	0.520	0.530	0.539	0.001	0.010
	Maximize Early Warnings								
		Algorithm	Point A	Point B	Point C	Point D	Point E	Point F	Point G
	Best Overall	242 - 13	0.504	0.512	0.520	0.530	0.539	0.001	0.010
	Best Applicable	242 - 13	0.504	0.512	0.520	0.530	0.539	0.001	0.010
	Compromise between Early Warnings and Maximum True Positives								
		Algorithm	Point A	Point B	Point C	Point D	Point E	Point F	Point G
	Best Overall	243 - 19	0.001	0.001	0.001	0.001	0.545	0.001	0.010
Best Applicable	242 - 13	0.504	0.512	0.520	0.530	0.539	0.001	0.010	



Table 43 Best signaled algorithms for 20 mph.

Maximize True Positives									
	Algorithm	Point A	Point B	Point C	Point D	Point E	Point F	Point G	
Allowable FP=0.05	Best Overall	841 - 10	0.790	0.806	0.821	0.835	0.854	0.025	0.045
	Best Applicable	841 - 10	0.790	0.806	0.821	0.835	0.854	0.025	0.045
	Maximize Early Warnings								
		Algorithm	Point A	Point B	Point C	Point D	Point E	Point F	Point G
	Best Overall	643 - 16	0.808	0.811	0.819	0.826	0.835	0.020	0.041
	Best Applicable	342 - 3	0.793	0.796	0.802	0.808	0.815	0.014	0.034
	Compromise between Early Warnings and Maximum True Positives								
		Algorithm	Point A	Point B	Point C	Point D	Point E	Point F	Point G
	Best Overall	841 - 10	0.790	0.806	0.821	0.835	0.854	0.025	0.045
Best Applicable	841 - 10	0.790	0.806	0.821	0.835	0.854	0.025	0.045	

Maximize True Positives									
	Algorithm	Point A	Point B	Point C	Point D	Point E	Point F	Point G	
Allowable FP=0.01	Best Overall	243 - 19	0.001	0.001	0.001	0.001	0.725	0.001	0.010
	Best Applicable	642 - 10	0.670	0.681	0.692	0.706	0.718	0.001	0.009
	Maximize Early Warnings								
		Algorithm	Point A	Point B	Point C	Point D	Point E	Point F	Point G
	Best Overall	242 - 13	0.671	0.681	0.692	0.706	0.717	0.001	0.010
	Best Applicable	242 - 13	0.671	0.681	0.692	0.706	0.717	0.001	0.010
	Compromise between Early Warnings and Maximum True Positives								
		Algorithm	Point A	Point B	Point C	Point D	Point E	Point F	Point G
	Best Overall	642 - 10	0.670	0.681	0.692	0.706	0.718	0.001	0.009
Best Applicable	642 - 10	0.670	0.681	0.692	0.706	0.718	0.001	0.009	

### 11.21 Appendix U: Plots of the Best Overall Algorithms

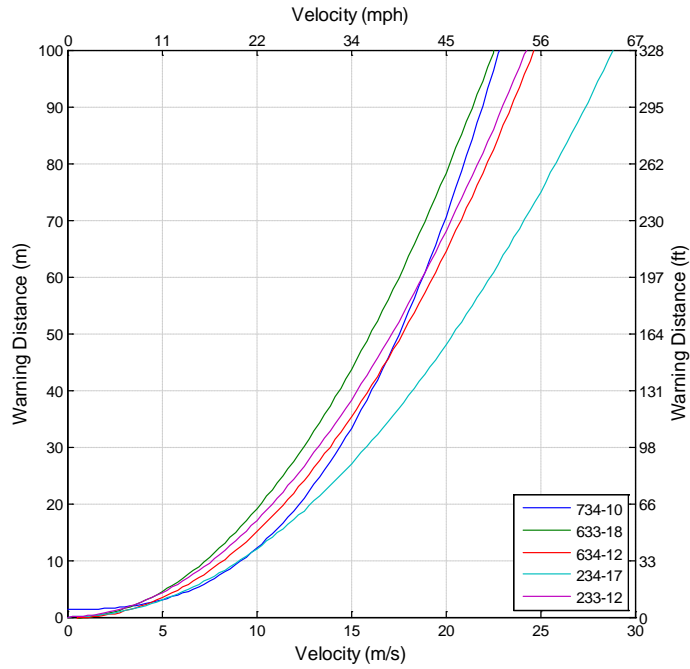


Figure 280 Stop bar velocity versus warning distance for the best overall algorithms identified in the stop-controlled intersection simulation.

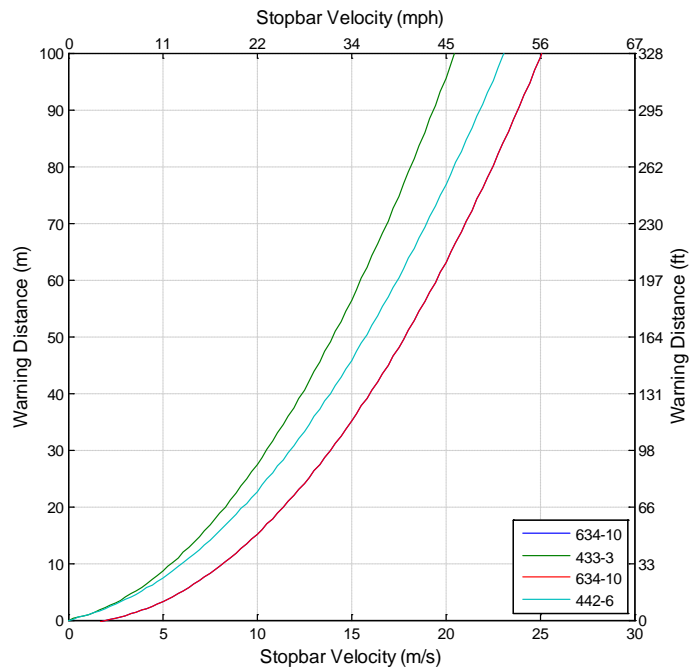


Figure 281 Stop bar velocity versus warning distance for the best overall algorithms identified in the signalized intersection simulation.

### 11.22 Appendix V: Base Rate Data for the Best Overall and Best Applicable Algorithms Across the Tested Violation Thresholds and Maximum False Positive Rates

Table 44 Stop-controlled data.

			Per 100,000 Crossings											
			Algorithm	TPR	FNR	FPR	TNR	TP	FN	FP	TN	FP : TP	TP : FN	
Maximum FPR=0.05	10 mph	Max True Positives	Best Overall	831 - 8	0.59	0.41	0.05	0.95	3,227	2,265	4,705	95,022	1 : 1	1 : 1
			Best Applicable	831 - 8	0.59	0.41	0.05	0.95	3,227	2,265	4,705	95,022	1 : 1	1 : 1
		Max Early Warnings	Best Overall	831 - 8	0.59	0.41	0.05	0.95	3,227	2,265	4,705	95,022	1 : 1	1 : 1
			Best Applicable	831 - 8	0.59	0.41	0.05	0.95	3,227	2,265	4,705	95,022	1 : 1	1 : 1
		Compromise b/w Early Warnings and Max True Positives	Best Overall	831 - 8	0.59	0.41	0.05	0.95	3,227	2,265	4,705	95,022	1 : 1	1 : 1
			Best Applicable	831 - 8	0.59	0.41	0.05	0.95	3,227	2,265	4,705	95,022	1 : 1	1 : 1
	15 mph	Max True Positives	Best Overall	734 - 10	0.90	0.10	0.05	0.95	545	62	4,633	95,339	8 : 1	9 : 1
			Best Applicable	532 - 12	0.70	0.30	0.04	0.96	424	184	4,097	95,878	10 : 1	2 : 1
		Max Early Warnings	Best Overall	633 - 18	0.74	0.26	0.04	0.96	450	158	3,881	96,096	9 : 1	3 : 1
			Best Applicable	232 - 8	0.68	0.32	0.05	0.95	410	197	4,757	95,214	12 : 1	2 : 1
		Compromise b/w Early Warnings and Max True Positives	Best Overall	634 - 12	0.86	0.14	0.05	0.95	525	82	4,853	95,118	9 : 1	6 : 1
			Best Applicable	232 - 8	0.68	0.32	0.05	0.95	410	197	4,757	95,214	12 : 1	2 : 1
20 mph	Max True Positives	Best Overall	744 - 9	1.00	0.00	0.03	0.97	161	0	3,211	96,784	20 : 1	na : 1	
		Best Applicable	641 - 7	1.00	0.00	0.04	0.96	161	0	3,592	96,402	22 : 1	na : 1	
	Max Early Warnings	Best Overall	244 - 13	0.98	0.02	0.04	0.96	158	3	3,845	96,149	24 : 1	48 : 1	
		Best Applicable	242 - 8	0.92	0.08	0.05	0.95	148	13	4,610	95,383	31 : 1	11 : 1	
	Compromise b/w Early Warnings and Max True Positives	Best Overall	244 - 13	0.98	0.02	0.04	0.96	158	3	3,845	96,149	24 : 1	48 : 1	
		Best Applicable	841 - 4	1.00	0.00	0.03	0.97	161	0	3,287	96,708	20 : 1	na : 1	
Maximum FPR=0.01	15 mph	Max True Positives	Best Overall	234 - 17	0.65	0.35	0.01	0.99	397	210	880	99,115	2 : 1	2 : 1
			Best Applicable	732 - 14	0.56	0.44	0.01	0.99	341	266	929	99,065	3 : 1	1 : 1
		Max Early Warnings	Best Overall	233 - 12	0.59	0.41	0.01	0.99	361	246	834	99,161	2 : 1	1 : 1
			Best Applicable	632 - 20	0.52	0.48	0.01	0.99	318	289	735	99,260	2 : 1	1 : 1
		Compromise b/w Early Warnings and Max True Positives	Best Overall	234 - 17	0.65	0.35	0.01	0.99	397	210	880	99,115	2 : 1	2 : 1
			Best Applicable	732 - 14	0.56	0.44	0.01	0.99	341	266	929	99,065	3 : 1	1 : 1
	20 mph	Max True Positives	Best Overall	844 - 9	0.98	0.02	0.01	0.99	158	3	946	99,053	6 : 1	48 : 1
			Best Applicable	742 - 14	0.84	0.16	0.01	0.99	135	26	877	99,122	7 : 1	5 : 1
		Max Early Warnings	Best Overall	643 - 14	0.90	0.10	0.01	0.99	144	16	906	99,092	6 : 1	9 : 1
			Best Applicable	742 - 14	0.84	0.16	0.01	0.99	135	26	877	99,122	7 : 1	5 : 1
		Compromise b/w Early Warnings and Max True Positives	Best Overall	844 - 9	0.98	0.02	0.01	0.99	158	3	946	99,053	6 : 1	48 : 1
			Best Applicable	742 - 14	0.84	0.16	0.01	0.99	135	26	877	99,122	7 : 1	5 : 1

Table 45 Signalized algorithm base rate results.

			Per 100,000 Crossings											
			Algorithm	TPR	FNR	FPR	TNR	TP	FN	FP	TN	FP : TP	TP : FN	
Maximum FPR=0.05	10 mph	Max True Positives	Best Overall	434 - 7	0.81	0.19	0.04	0.96	128	31	4,430	95,563	35 : 1	4 : 1
			Best Applicable	631 - 9	0.79	0.21	0.05	0.95	125	33	4,893	95,099	39 : 1	4 : 1
		Max Early Warnings	Best Overall	434 - 7	0.81	0.19	0.04	0.96	128	31	4,430	95,563	35 : 1	4 : 1
			Best Applicable	641 - 11	0.73	0.27	0.05	0.95	115	43	4,576	95,416	40 : 1	3 : 1
		Compromise b/w Early Warnings and Max True Positives	Best Overall	434 - 7	0.81	0.19	0.04	0.96	128	31	4,430	95,563	35 : 1	4 : 1
			Best Applicable	631 - 9	0.79	0.21	0.05	0.95	125	33	4,893	95,099	39 : 1	4 : 1
	15 mph	Max True Positives	Best Overall	634 - 10	0.83	0.17	0.04	0.96	105	21	4,445	95,549	42 : 1	5 : 1
			Best Applicable	631 - 8	0.83	0.17	0.05	0.95	106	21	4,525	95,469	43 : 1	5 : 1
		Max Early Warnings	Best Overall	433 - 3	0.82	0.18	0.05	0.95	104	22	4,628	95,366	44 : 1	5 : 1
			Best Applicable	322 - 3	0.80	0.20	0.04	0.96	101	26	4,377	95,617	43 : 1	4 : 1
		Compromise b/w Early Warnings and Max True Positives	Best Overall	634 - 10	0.83	0.17	0.04	0.96	105	21	4,445	95,549	42 : 1	5 : 1
			Best Applicable	641 - 11	0.83	0.17	0.05	0.95	105	22	4,671	95,323	44 : 1	5 : 1
20 mph	Max True Positives	Best Overall	841 - 10	0.85	0.15	0.05	0.95	101	17	4,538	95,457	45 : 1	6 : 1	
		Best Applicable	841 - 10	0.85	0.15	0.05	0.95	101	17	4,538	95,457	45 : 1	6 : 1	
	Max Early Warnings	Best Overall	643 - 16	0.84	0.16	0.04	0.96	99	19	4,077	95,918	41 : 1	5 : 1	
		Best Applicable	342 - 3	0.81	0.19	0.03	0.97	96	22	3,379	96,617	35 : 1	4 : 1	
	Compromise b/w Early Warnings and Max True Positives	Best Overall	841 - 10	0.85	0.15	0.05	0.95	101	17	4,538	95,457	45 : 1	6 : 1	
		Best Applicable	841 - 10	0.85	0.15	0.05	0.95	101	17	4,538	95,457	45 : 1	6 : 1	
Maximum FPR=0.01	10 mph	Max True Positives	Best Overall	243 - 19	0.55	0.45	0.01	0.99	64	54	974	99,025	15 : 1	1 : 1
			Best Applicable	242 - 13	0.54	0.46	0.01	0.99	64	55	953	99,046	15 : 1	1 : 1
		Max Early Warnings	Best Overall	242 - 13	0.54	0.46	0.01	0.99	64	55	953	99,046	15 : 1	1 : 1
			Best Applicable	242 - 13	0.54	0.46	0.01	0.99	64	55	953	99,046	15 : 1	1 : 1
		Compromise b/w Early Warnings and Max True Positives	Best Overall	243 - 19	0.81	0.19	0.01	0.99	95	23	974	99,025	10 : 1	4 : 1
			Best Applicable	242 - 13	0.54	0.46	0.01	0.99	64	55	953	99,046	15 : 1	1 : 1
	15 mph	Max True Positives	Best Overall	442 - 6	0.68	0.32	0.01	0.99	86	41	970	99,028	11 : 1	2 : 1
			Best Applicable	442 - 6	0.68	0.32	0.01	0.99	86	41	970	99,028	11 : 1	2 : 1
		Max Early Warnings	Best Overall	442 - 6	0.68	0.32	0.01	0.99	86	41	970	99,028	11 : 1	2 : 1
			Best Applicable	442 - 6	0.68	0.32	0.01	0.99	86	41	970	99,028	11 : 1	2 : 1
		Compromise b/w Early Warnings and Max True Positives	Best Overall	442 - 6	0.68	0.32	0.01	0.99	86	41	970	99,028	11 : 1	2 : 1
			Best Applicable	442 - 6	0.68	0.32	0.01	0.99	86	41	970	99,028	11 : 1	2 : 1
20 mph	Max True Positives	Best Overall	243 - 19	0.73	0.27	0.01	0.99	86	32	981	99,018	11 : 1	3 : 1	
		Best Applicable	642 - 10	0.72	0.28	0.01	0.99	85	33	948	99,051	11 : 1	3 : 1	
	Max Early Warnings	Best Overall	242 - 13	0.72	0.28	0.01	0.99	85	33	955	99,044	11 : 1	3 : 1	
		Best Applicable	242 - 13	0.72	0.28	0.01	0.99	85	33	955	99,044	11 : 1	3 : 1	
	Compromise b/w Early Warnings and Max True Positives	Best Overall	642 - 10	0.72	0.28	0.01	0.99	85	33	948	99,051	11 : 1	3 : 1	
		Best Applicable	642 - 10	0.72	0.28	0.01	0.99	85	33	948	99,051	11 : 1	3 : 1	

## **11.23 Appendix W: System Latency Investigation**

During the CICAS-V algorithm development, a concern was raised about potential latencies affecting threat assessment accuracy. A quick analysis of the available stop-controlled database was performed to provide the algorithm development team with data regarding the impact of system latencies on threat assessment performance. In particular, the brake pulse DVI required time to pre-pressure and initiate the brake pulse. The value of this latency could not be determined at this time, but it was estimated in the 100-ms to 300-ms region. The algorithm committee was concerned with the potential impact of the latency and would like some preliminary data to assist with system design.

To provide some initial data, a simulation was performed using the Subtask 3.2 stop-sign database to compare the relative effect of latency for one of the best performing algorithms at the time. The signalized database was not ready for a complimentary analysis at the time this was performed.

The stop-sign database and simulation method from Subtask 3.2 was used to model possible system latency. Three possible system latencies were tested, including 100, 300, and 500 milliseconds. The 634 algorithm was selected for this analysis. The 634 algorithm demonstrated the best performance from Table 16. The figure below provides the results of the simulation on an ROC curve. Each of the four latency scenarios is represented by a separate line plot.

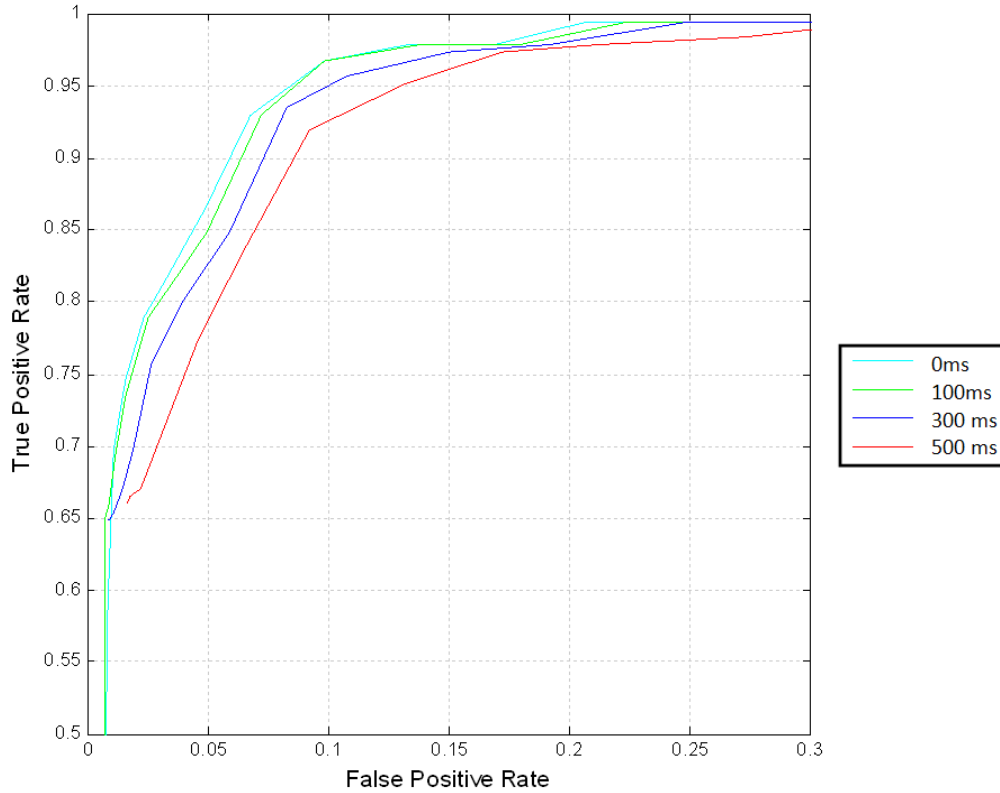


**Figure 282 The algorithm impact resulting from system latencies for the 634 algorithm.**

In general, as latency increases, fewer true positives will be achieved. For instance, assume the allowable false positive rate is set at 0.05. At zero latency approximately a 0.865 true positive rate will result. With latency increasing from 100 ms, 300 ms, and 500 ms the true positive rate will drop to 0.85, 0.825, and 0.785 respectively. From these results it appears that latency does have a negative impact on algorithm performance. The difference between the optimal case and a 500-ms latency results in ~8% loss in the number of true positives obtained.

These results should only be used to help guide the algorithm development process. Due to time constraints a thorough investigation of the impact of latency on all of the algorithms was not performed. As depicted in the figure, the impact of system latency

depended on the false positive rate selected. It was determined highly likely that some algorithms will have a different sensitivity to latency than the one evaluated above.

## 11.24 Appendix X: Approach Analysis of Violating and Nearly Violating Approaches at Stop-Controlled Intersections

While studying driver approaches to stop-controlled intersections, the data collected during the reduction was briefly considered. Recall that the primary purpose of the manual data reduction was to validate events captured by the automated violation detection triggers. While data reductionists had the files open for review, it was logical to collect some additional information regarding the event. The triggering scheme, described in detail in Appendix D, was designed to acquire intersection approaches to look for violations. During these approaches, a violation may or may not have occurred; however, the kinematic signature of their vehicle indicated a late or non-existent reaction from the driver in response to the stop sign.

This analysis is based only on the triggered vehicle approaches rather than on a comparison to a baseline sample; thus, it is essentially a comparison between near violations and violations at stop-controlled intersections. This investigation is not the main focus of this research project, but may provide insight into factors that differentiate violators from near violators. This information may be useful to future more-advanced ICAS-V systems that can use additional vehicle sensors to detect environmental conditions.

Logistic regression is a multivariate method that predicts the probability of a binary response, based on the values of a set of independent measures (Johnson, 1998). For the present analysis, the binary response variable represents whether or not the driver violated the stop sign. During data reduction, the stopping maneuver was subjectively coded for each driver. The coding initially included four levels: 1) no violation; 2) rolling violation; 3) violation with caution; and 4) violation without caution.

In Chapter 4, it was shown that rolling violations should not be the target violation for the ICAS-V system. For this reason, the four categories were collapsed into two categories: 1) *no violation* and *rolling violation* both represent the near violations category; and 2) *violation with caution* and *violation without caution* represent the violation category.

The logistic fit procedure was performed to fit the environmental data collected through reduction. Odds ratios were computed for each of the predictor variables to investigate the effects of the surrounding environment on violation likelihood. Table 46 provides the odds ratios computed through the logistic regression for all the predictors analyzed. If the confidence limits included a one, the effect was not significant.



**Table 46 Odds ratios for environmental variables.**

<b>Risk factor</b>	<b>Risk factor</b>	<b>Odds ratio</b>	<b>95% CI Low</b>	<b>95% CI High</b>
Turn Intent	Straight vs. Right	2.8197*	2.4298	3.2721
	Straight vs. Left	3.7384*	2.962	4.7183
	Right vs. Left	1.3258*	1.0669	1.6476
Conflict Vehicles	No-conflict vs. Conflict	2.4118*	1.8558	3.1344
Vehicle Type	Car vs. Minivan & Pickup	0.9544	0.8231	1.1067
Weather	Cloudy vs. Clear	1.3848*	1.1282	1.6997
	Inferior vs. Clear	1.152	0.8934	1.4854
	Cloudy vs. Inferior	1.2021	0.8835	1.6356
Time of Day	Daytime vs. Dawn/Dusk	1.0494	0.8509	1.2942
	Nighttime vs. Dawn/Dusk	2.6775*	1.9381	3.699
	Nighttime vs. Daytime	2.5515*	1.947	3.3437
Leading Vehicle	L.V. Violate vs. no-Violate	6.1388*	3.6489	10.3276

\*Odds ratio is significant

The likelihood of a violation versus a near violation depends on the turn intent of the driver. A driver is nearly three times more likely to violate if their intended maneuver is straight versus right, and nearly four times more likely if the intended maneuver is straight versus left.

Drivers are more than twice as likely to violate if there is no conflicting traffic present on the adjacent traffic lanes at the intersection. This effect is probably due to the subject vehicle yielding right of way to the conflicting vehicle.

Inferior weather was categorized as any form of precipitation, including fog. Interestingly, inferior weather did not influence the likelihood of a violation. There was a small effect noted for clear versus cloudy weather conditions. It remained unclear why violations were slightly more likely when clouds were present. One possible explanation may be the protection from glare which is afforded by the cloud cover. When the skies were clear, visibility may have been somewhat reduced by sun glare, which made drivers more cautious at the junction.

The time of day effect may also be attributed to visibility. There was not a significant difference between daytime and dawn/dusk; however, violations were more likely to occur at nighttime. The stop-controlled intersections investigated were not located in regions with street lighting. Lower visibility may have led to lower detection of the stop sign resulting in more violations. The other possibility is that headlights from other vehicles are highly visible at night, making drivers more willing to violate in the absence of adjacent headlamps.

Finally, the largest factor affecting the likelihood of violations is the presence of a lead vehicle that violates. When a lead vehicle violates, the subject vehicle is more than six times as likely to violate. It would be interesting to investigate whether these drivers are intentionally following the lead vehicle, or whether they blindly trust the lead to perform the correct traffic maneuvers. Unfortunately, such an investigation requires information from inside the vehicle and cannot be performed with the present data set.



U.S. Department of Transportation  
ITS Joint Program Office-HOIT  
1200 New Jersey Avenue, SE  
Washington, DC 20590

Toll-Free "Help Line" 866-367-7487  
[www.its.dot.gov](http://www.its.dot.gov)

FHWA-JPO-10-068



U.S. Department of Transportation  
**Research and Innovative Technology  
Administration**